frontiers | Research Topics

Bioactive compounds, functional ingredients, antioxidants, and health benefits of edible plants, volume II

Edited by
Eman. A. Mahmoud and Hosam O. Elansary

Published in
Frontiers in Plant Science

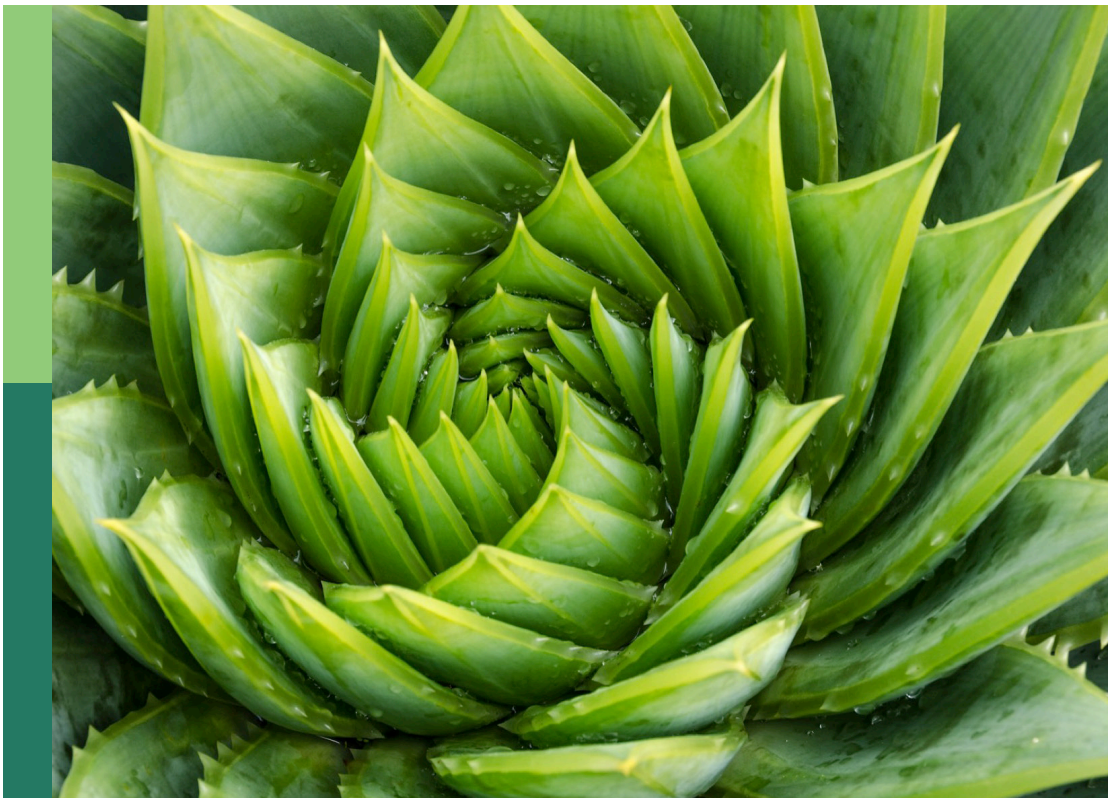

ISSN 1664-8714
ISBN 978-2-8325-6728-9
DOI 10.3389/978-2-8325-6728-9

Generative AI statement
Any alternative text (Alt text) provided alongside figures in the articles in this ebook has been generated by Frontiers with the support of artificial intelligence and reasonable efforts have been made to ensure accuracy, including review by the authors wherever possible. If you identify any issues, please contact us.

About Frontiers

Frontiers is more than just an open access publisher of scholarly articles: it is a pioneering approach to the world of academia, radically improving the way scholarly research is managed. The grand vision of Frontiers is a world where all people have an equal opportunity to seek, share and generate knowledge. Frontiers provides immediate and permanent online open access to all its publications, but this alone is not enough to realize our grand goals.

Frontiers journal series

The Frontiers journal series is a multi-tier and interdisciplinary set of open-access, online journals, promising a paradigm shift from the current review, selection and dissemination processes in academic publishing. All Frontiers journals are driven by researchers for researchers; therefore, they constitute a service to the scholarly community. At the same time, the *Frontiers journal series* operates on a revolutionary invention, the tiered publishing system, initially addressing specific communities of scholars, and gradually climbing up to broader public understanding, thus serving the interests of the lay society, too.

Dedication to quality

Each Frontiers article is a landmark of the highest quality, thanks to genuinely collaborative interactions between authors and review editors, who include some of the world's best academicians. Research must be certified by peers before entering a stream of knowledge that may eventually reach the public - and shape society; therefore, Frontiers only applies the most rigorous and unbiased reviews. Frontiers revolutionizes research publishing by freely delivering the most outstanding research, evaluated with no bias from both the academic and social point of view. By applying the most advanced information technologies, Frontiers is catapulting scholarly publishing into a new generation.

What are Frontiers Research Topics?

Frontiers Research Topics are very popular trademarks of the *Frontiers journals series*: they are collections of at least ten articles, all centered on a particular subject. With their unique mix of varied contributions from Original Research to Review Articles, Frontiers Research Topics unify the most influential researchers, the latest key findings and historical advances in a hot research area.

Find out more on how to host your own Frontiers Research Topic or contribute to one as an author by contacting the Frontiers editorial office: frontiersin.org/about/contact

Bioactive compounds, functional ingredients, antioxidants, and health benefits of edible plants, volume II

Topic editors

Eman. A. Mahmoud — Damietta University, Egypt

Hosam O. Elansary — King Saud University, Saudi Arabia

Citation

Mahmoud, E. A., Elansary, H. O., eds. (2025). *Bioactive compounds, functional ingredients, antioxidants, and health benefits of edible plants, volume II*. Lausanne: Frontiers Media SA. doi: 10.3389/978-2-8325-6728-9

Table of contents

frontiers | Frontiers in Plant Science

TYPE Editorial
PUBLISHED 06 August 2025
DOI 10.3389/fpls.2025.1666398

OPEN ACCESS

EDITED AND REVIEWED BY
Laigeng Li,
Chinese Academy of Sciences (CAS), China

*CORRESPONDENCE
Hosam O. Elansary
helansary@ksu.edu.sa

RECEIVED 15 July 2025
ACCEPTED 20 July 2025
PUBLISHED 06 August 2025

CITATION
Mahmoud EA and Elansary HO (2025) Editorial: Bioactive compounds, functional ingredients, antioxidants, and health benefits of edible plants, volume II. *Front. Plant Sci.* 16:1666398. doi: 10.3389/fpls.2025.1666398

Editorial: Bioactive compounds, functional ingredients, antioxidants, and health benefits of edible plants, volume II

Eman A. Mahmoud[1] and Hosam O. Elansary[2]*

[1]Department of Food Science, Faculty of Agriculture, Damietta University, Damietta, Egypt, [2]Department of Plant Production, College of Food & Agricultural Sciences, King Saud University, Riyadh, Saudi Arabia

KEYWORDS

bioactive compounds, natural products, medicinal plants, antioxidants, pharmaceutical

Editorial on the Research Topic

Bioactive compounds, functional ingredients, antioxidants, and health benefits of edible plants, volume II

Bioactive substances with physiological effects, including antibacterial, anti-inflammatory, antioxidant, and anticancer properties, are abundant in edible plants (Yousaf et al., 2024). In order to maintain the quality and safety of both fresh and processed foods, natural plant extracts are widely employed to extend their shelf life. In the food and human nutrition industries, phytochemical analyses of extracts and biological activities of different plant parts are also crucial. By creating new uses for the food industry, they could open the door for the commercialization of additional plants. A potential area of study for plant breeders, producers, and food processors is plant bioactive chemicals (Mazhar et al., 2025). The agriculture and food sectors around the world are very interested in developing new technical methods for the production and processing of edible plants. The goal of the producer and related food businesses is to increase the production of secondary metabolites (like polyphenols) and create new functions. The generation of particular secondary metabolites with significant uses is closely linked to the use of bioreactors in tissue cultures.

In the Research Topic, the work of Kumar et al. revealed that the Thiol-based redox sensing of 16 diverse genotypes of wheat grains affects various metabolic pathways. They found correlation between the accumulation of macro-/micronutrients such as iron and zinc inside the grains and the thiol and disulfide content. They proved a negative relationship between thiol content and nutrient-linked traits such as total protein, gluten, and phytic acid. In a related study, Xu et al. examined the metabolomic profiles and potential health benefits of Euchresta japonica tissues. They found 2,140 metabolites, including phenolic acids, flavonoids, alkaloids, lipids, and amino acids, which were concentrated in the plants' roots. The majority of these molecules are linked to active medicinal components that are resistant to nine human diseases.

Hou et al. used UPLC-MS/MS to identify 1929 distinct pharmacological compounds *in Dendrobium officinale* stems cultivated in various conditions. When compared to other habitats, they discovered that the stone epiphytic environment had higher levels of 58 primary and secondary metabolites. They came to the conclusion that growing

environment affects the amount and composition of metabolites in *D. officinale* stems. In the same context, the chemical and bioactive characteristics of Chinese peony flowers were investigated by Peng et al. Out of the 150 chemical components found in the study, over 50 were reported for the first time from this species, and there were also possible novel substances found. Four cultivars and flower sections were clearly distinguished by 67 quantified or semi-quantified targeted metabolomics analyses. CPF showed strong antioxidant properties and anti-inflammatory actions by lowering the release of nitric oxide, IL-6, and TNF-a in LPS-induced macrophages. They concluded the potential of these flowers to promote health by finding a link between total phenolic content and DPPH ABTS and FRAP antioxidant capabilities.

The effects of methyl jasmonate (MeJA) on blueberry ripening fruits were examined by Vasques-Rojas et al., with a focus on the antioxidant enzyme activity (APX, CAT, SOD, and POD), nutritional qualities, and cell wall composition. They discovered that MeJA increased the antioxidant enzymes' activities and that anthocyanin accumulation maximized in the blue stage. They came to the conclusion that MeJA reduces fruit softening during storage and preserves cell wall integrity. In the same context, Coban et al. investigated the bioactive substances in 31 genotypes of fenugreek (*Trigonella foenum-graecum*) cultivated in various conditions. They discovered that genotype, environment, and their combination had a substantial impact on the levels of diosgenin, trigonelline, and 4-hydroxyisoleucine measured under irrigated and non-irrigated conditions.

Amangeldinova et al. used the LC-MS/MS technology to quantitatively identify 53 phytochemicals in the roots of *Rheum tataricum* L. Cyranoside, epicatechin, catechin, and chlorogenic acid were all abundant in the extracts. Stronger antioxidant qualities were shown by extracts made using ultrasonic extraction. The UAE-M-4h extract has the highest total phenolic concentration (213.44 mg GAE/mL). For both Gram-positive and Gram-negative bacteria, the extracts made with UAE-MeOH-2h-4h, UAE-EtOH-2h-4h, Sbc-EtOH-E-140-60-80, Sc-90 atm, and Sc-400 atm exhibited antibacterial activity at different rates (MIC range: 31.25 to 250 μg/mL).

Cheng et al. used UPLC-QTOF-MS/MS to examine the seasonal variation and quality variations of flavonoids between *Scutellaria barbata* roots and aerial parts. They found 46 chemicals, mostly flavonoids, in *S. barbata*. They discovered that the root accumulates flavonoids lacking this 4′-hydroxyl group in a manner that is dependent on the season, but the aerial parts collect flavonoids with this group. While roots accumulated the majority of flavonoids in the fall, aerial portions accumulated the most in the spring. Viteri et al. investigated *Wigandia ecuadorensis* antimicrobial, enzymatic inhibitory, antioxidant, and phytochemical profile properties. With the ethyl acetate fraction being the most active, they discovered that the methanolic extract and its subfractions demonstrated a notable antioxidant activity. Its high total phenolic content (357.47 mg GAE/g) was associated with this antioxidant activities. Their Minimum Bactericidal Concentration (MBC) values for *S. aureus, E. faecalis*, and *E. coli* ranged from 1.56 to 6.25 mg/mL, indicating strong antibacterial activity against human pathogen strains. Forty chemicals, including phenolic acids, flavonoids, saponins, terpenes, and fatty acyls, were found using UHPLC-QTOF-MS analysis.

Gharzouli et al. studied Antifungal effect of Algerian essential oil of *Cymbopogon citratus* and *Citrus limon* nanoemulsions to control the fungal infections by *Penicillium digitatum* and *Penicillium expansum* in Thomson Navel oranges (*Citrus sinensis* L. Osbeck). They found that applying nanoemulsified *C. limon* and *C. citratus* as a coating on orange fruits reduced the spread of both fungi compared to the control and reduced the negative changes in quality parameters during storage, such as weight loss, firmness, TSS, TA, pH, and ascorbic acid content.

Jain et al. reviewed *Amorphophallus konjac* traditional uses, bioactive potential, and emerging health applications. They found remarkable health benefits, including improving metabolic health through weight management, blood glucose stabilization, and lipid profile enhancement. Additionally, they have anti-inflammatory, immune-regulatory, and gut-healthy properties. They can be used to treat colorectal cancer (CRC), hyperthyroidism, and inflammatory bowel disease. They also showed difficulties in preserving purity and molecular uniformity, as well as possible adverse effects such gastrointestinal distress and allergenicity.

Author contributions

HE: Conceptualization, Data curation, Formal Analysis, Funding acquisition, Investigation, Methodology, Project administration, Resources, Software, Supervision, Validation, Visualization, Writing – original draft, Writing – review & editing. EM: Conceptualization, Data curation, Formal Analysis, Funding acquisition, Investigation, Methodology, Project administration, Resources, Software, Supervision, Validation, Visualization, Writing – original draft, Writing – review & editing.

Conflict of interest

The authors declare that the research was conducted in the absence of any commercial or financial relationships that could be construed as a potential conflict of interest.

Generative AI statement

The author(s) declare that no Generative AI was used in the creation of this manuscript.

Publisher's note

References

Mazhar, M. W., Arshad, A., Parveen, A., Azeem, M., Ishtiaq, M., Thind, S., et al. (2025). Interaction of arsenic stress and graphene oxide nanoparticle seed priming modulates hormonal signalling to enhance soybean (Glycine max L.) growth and antioxidant defence. *Environ. Pollutants Bioavailability* 37, 1–17. doi: 10.1080/26395940.2025.2523548

Yousaf, M. J., Hussain, A., Hamayun, M., El-Sheikh, M. A., Elansary, H. O., and Kim, H. Y. (2024). Impact of cis-zeatin and lovastatin on antioxidant systems and growth parameters in Zea mays seedlings under phytohormonal crosstalks. *J. Plant Interact.* 19, 2327378. doi: 10.1080/17429145.2024.2327378

frontiers | Frontiers in Plant Science

TYPE Original Research
PUBLISHED 07 November 2024
DOI 10.3389/fpls.2024.1481447

OPEN ACCESS

EDITED BY
Eman A. Mahmoud,
Damietta University, Egypt

REVIEWED BY
Dong Pei,
Chinese Academy of Sciences (CAS), China
Viviana Maresca,
University of Naples Federico II, Italy

*CORRESPONDENCE
Rafael Viteri
raviteri@espol.edu.ec

RECEIVED 15 August 2024
ACCEPTED 14 October 2024
PUBLISHED 07 November 2024

CITATION
Viteri R, Espinoza F, Cornejo X, Simirgiotis MJ and Manzano P (2024) Phytochemical profiling, antioxidant, enzymatic inhibitory, and antibacterial activities of *Wigandia ecuadorensis*. *Front. Plant Sci.* 15:1481447. doi: 10.3389/fpls.2024.1481447

Phytochemical profiling, antioxidant, enzymatic inhibitory, and antibacterial activities of *Wigandia ecuadorensis*

Rafael Viteri[1]*, Fernando Espinoza[1], Xavier Cornejo[2], Mario J. Simirgiotis[3] and Patricia Manzano[1]

[1]Centro de Investigaciones Biotecnológicas del Ecuador, ESPOL, Polytechnic University, ESPOL, Guayaquil, Ecuador, [2]Herbario GUAY, Departamento de Botánica, Facultad de Ciencias Naturales, Universidad de Guayaquil, Guayaquil, Ecuador, [3]Instituto de Farmacia, Facultad de Ciencias, Universidad Austral de Chile, Valdivia, Chile

Wigandia ecuadoriensis, a member of the Namaceae family, is a source of metabolites and has been traditionally used as an anti-inflammatory. This work aimed to determine the total phenolic content (TPC), total flavonoid content (TFC), antioxidant effect, inhibition of α-glucosidase and cholinesterase enzymes (AChE, BChE), and antibacterial activity of the methanolic extract (ME) and subfractions of *Wigandia ecuadoriensis*. The findings revealed that ME and its subfractions exhibited significant antioxidant capacity, with the ethyl acetate fraction being the most active, displaying an IC_{50} of 17.66 µg/mL against the 1,1-diphenyl-2-picrylhydrazyl (DPPH) radical and 10.31 µg/mL against 2,2′-azinobis-(3-ethylbenzothiazoline-6-sulfonic acid) diammonium salt (ABTS). This activity was attributed to its high total phenolic content (357.47 mg GAE/g). Furthermore, *W. ecuadoriensis* fractions showed marked antimicrobial properties against human pathogen strains with Minimum Bactericidal Concentration (MBC) values of 1.56–6.25 mg/mL for *S. aureus*, *E. faecalis* and *E. coli*. Furthermore, aqueous fraction exhibited slight inhibition of acetylcholinesterase (IC_{50}: 915.98 µg/mL) and butyrylcholinesterase (IC_{50}: 380.42 µg/mL). Interestingly, EF showed the greatest inhibitory effect of α-glucosidase (IC_{50}: 38.44 µg/mL) which is more potent than the control used, acarbose (IC_{50}: 179.07 µg/mL). UHPLC-QTOF-MS analysis identified forty compounds, including phenolic acids, flavonoids, saponins, terpenes, and fatty acyls. As far as we know, this is the first study to evaluate the chemical composition and biological potential of *W. ecuadoriensis*. Our results provide the first evidence to the chemical knowledge of the species *W. ecuadoriensis* and demonstrate its bioactive potential as an interesting source of secondary metabolites with possible beneficial properties for health.

KEYWORDS

***Wigandia ecuadoriensis*, enzyme inhibition, antioxidant activity, antibacterial, phenols content, flavonoids**

1 Introduction

In recent years, there has been significant interest in using plant extracts. Indeed, it is recognized that plants harbor valuable bioactive compounds that can be beneficial both for promoting human well-being and for the formulation of supplements or nutraceuticals containing these enriching substances.

Antioxidant activity is essential to neutralize free radicals involved in aging and various chronic diseases, including cancer and cardiovascular diseases (Farhat et al., 2013). The study of inhibitors of enzymes such as α-glucosidase and cholinesterase is crucial in the search for valuable treatments for various diseases (Anand and Singh, 2013). Inhibition of α-glucosidase is an effective strategy in the management of type 2 diabetes mellitus, as it reduces blood glucose levels by slowing down carbohydrate digestion (Mustikasari et al., 2024). On the other hand, cholinesterase inhibitors play an important role in the treatment of Alzheimer's disease, improving the transmission of nerve signals by preventing the breakdown of acetylcholine (Anand and Singh, 2013). Together, these studies provide a solid foundation for the development of therapies that combat metabolic and neurodegenerative diseases.

In this sense, the Ecuadorian flora is known for its amazing diversity, hosting a unique wealth of plant species that arouse the interest of the scientific community. In this context, we focus on *Wigandia ecuadoriensis* (Figure 1), a new plant species botanically described in 2006 and which has captured the attention of botanists and ecologists due to its colonizing capacity and remarkable tolerance to reduced levels of precipitation, which could be used in the restoration of native vegetation in regions characterized by very dry tropical forests (Cornejo, 2006) and an interesting source of bioactive molecules. Although this species has been recognized locally, its detailed scientific study is still incipient.

Wigandia ecuadorensis is a shrub or small tree, up to 4 m tall, with large, shovel-shaped leaves and a terminal, branched inflorescence with pink flowers. It belongs to the Namaceae family and is endemic to the subtropical and tropical regions of the Ecuadorian coast (Cornejo, 2006; Vasile et al., 2020). In Ecuador, the Kichwa people used the leaves of the *Wigandia* Kunth genus as an anti-inflammatory (Torre et al., 2008). Other traditional uses of the *Wigandia urens* species are abortifacient, infections, epilepsy, psychological, skin, and immunological problems (Hitziger, 2016). The anti-inflammatory activity of different extracts of *Wigandia urens* has also been reported (Zavala-Sánchez et al., 2009). Some flavonoids and phacelioids have been isolated in the genus *Wigandia* (Gómez et al., 1980; Reynolds et al., 1989; Cao et al., 2003).

So far, there are no scientific studies in the literature on the plant species *W. ecuadorensis*, therefore, it represents an intriguing

FIGURE 1
Wigandia ecuadoriensis.

opportunity to discover new medicinal properties, unique chemical compounds, and possibly significant contributions to chemotaxonomy and natural medicine. This work aims to measure the content of phytochemicals (phenols and flavonoids) and evaluate the antioxidant, antibacterial, and enzymatic inhibition properties on cholinesterases and α-glucosidase of the methanolic extract and its subfractions from the leaves of *W. ecuadorensis*; and to analyze the metabolomic chemical profile by UHPLC-QTOF-MS of the fractions that presented the highest activity.

2 Materials and methods

2.1 Plant collection

The plant species *W. ecuadoriensis* was collected in Guayaquil, Guayas province, Ecuador (2°08'42.7"S 79°56'49.6"W) in October 2023. The species was identified by biologist Xavier Cornejo from the Faculty of Natural Sciences of the University of Guayaquil. A reference specimen (CIBE057) was deposited in the Herbarium of the Centro de Investigaciones Biotecnológicas del Ecuador, Guayaquil-Ecuador.

2.2 Extraction procedure and liquid–liquid fractionation

10 g of dried and powdered leaves of *W. ecuadoriensis* were macerated with methanol (three times with 100 mL each) under constant shaking using an orbital shaker (150 rpm) at 25°C for 24 h. Each extract was filtered through Whatman No. 1 filter paper and the solutions were concentrated under reduced pressure at 40°C to obtain the methanolic extract. Then, 2.9 g of the methanolic extract was suspended in 50 mL of a methanol-water mixture (1:3) and partitioned with *n*-hexane (HF), dichloromethane (DMF), ethyl acetate (EF), and a residual aqueous fraction (AqF). The extracts and subfractions were stored at -20°C until required for analysis.

2.3 Total phenolic content

Total phenolic content was determined according to the Folin-Ciocalteu (FC) assay (Ghareeb et al., 2017). 20 µL of the sample was mixed with 100 µL FC reagent (1:10 v/v) and 80 µL of a Na_2CO_3 solution (7.5%), incubated for 60 minutes at room temperature, and the absorbance of the resulting blue solution was measured at 760 nm in a microplate reader (Biotek Synergy HTX, Vermont, USA). The results of the total phenol content are expressed in mg of gallic acid equivalent per gram of dry extract (mg GAE/g DE). All measurements were carried out in triplicate.

2.4 Total flavonoid content

Total flavonoids were determined using the aluminum chloride method (Woster, 2003). 100 µL of sample was mixed with 100 µL of 2% $AlCl_3$ solution in ethanol. After 60 minutes at room temperature, absorbance at 420 nm was measured using a microplate reader (Biotek Synergy HTX, Vermont, USA). The results of the flavonoid content expressed in mg of quercetin equivalent per gram of dry extract (mg QE/g DE).

2.5 Antioxidant assays

2.5.1 DPPH radical scavenging assay

The antioxidant activity of extracts and subfractions was determined by the procedure described by (Thaipong et al., 2006). 50 µL of the sample was mixed with 150 µL of a DPPH solution (0.15 mM) dissolved in methanol in the dark for 30 minutes. Subsequently, the absorbance was measured at 517 nm in a microplate reader (Biotek Synergy HTX, Vermont, USA). A calibration curve with Trolox was used and the results were expressed in mg equivalent to Trolox/g DE.

2.5.2 ABTS

The antioxidant capacity was measured through the iron reduction method described by (van den Berg et al., 1999). The radical ABTS stock solution is diluted to a final concentration of 156 µM to obtain a final absorbance of 0.70 ± 0.02 at 732 nm. The radical discoloration was initiated by adding 50 µL of the sample solution with 150 µL of the ABTS solution. After 30 minutes of incubation in the dark, the absorbance was measured at 732 nm using a microplate reader (Biotek Synergy HTX, Vermont, USA). The calibration curve was constructed with Trolox, and the results were expressed in mg equivalent to Trolox/g DE.

2.5.3 Ferric-reducing antioxidant potential assay

The ferric reducing antioxidant power assay (FRAP) was determined according to the procedure described by (Ghareeb et al., 2017). In a 96-well microplate, 20 µl of each extract was mixed with 180 µl of FRAP reagent. The mixture remained for 30 minutes in the dark and the absorbance at 595 nm was measured in a microplate reader (BioTek Instrument, Inc., Winooski, VT, EE. UU.). The calibration curve was constructed with ferrous sulfate heptahydrate ($FeSO_4.7H_2O$), and the results were expressed in mmol Fe/g DE.

2.6 Cholinesterase inhibition

Acetylcholinesterase (AChE) and butyrylcholinesterase (BChE) inhibitions were performed *in vitro* according to the method of (Barrientos et al., 2023). The enzymes were dissolved in Tris-HCl buffer (50 mM, pH 8.0) and 5-dithiol-bis(2-nitrobenzoic) acid (DTNB) was prepared in buffer. *W. ecuadoriensis* fractions were prepared at a concentration of 20 mg per milliliter in buffer. 25 µL of the sample was mixed with 125 µL of DTNB and 25 µL of the enzyme (AChE 0.3 U/mL), incubated for 15 min at 37°C, then the substrates acetyl thiocholine iodide (15 mM) and butyryl thiocholine chloride (15 mM) were added, as appropriate, and the absorbance was measured at 412 nm at 37°C in a microplate reader

(BioTek Instrument, Inc., Winooski, VT, USA). The results were expressed as IC_{50} values (µg/mL). Galantamine was used as a positive control.

2.7 α-glucosidase inhibition assay

To determine the inhibitory activity of α-glucosidase, 600 µL of phosphate buffer (100 mM pH 6.9) was added with 250 µL of *p*-nitrophenyl-α-d-glucopyranoside (5 mM), 100 µL of sample (EF/AqF from *W. ecuadoriensis*) and incubated at 37°C for 5 min. After that, 50 µL of 0.5 U/mL α-glucosidase enzyme solution was added to start the reaction. After 15 min at 37°C, 1000 µL of Na_2CO_3 (200 mM) was added. The absorbance was measured at 400 nm (Biotek Synergy HTX, Vermont, USA). The results were expressed as IC_{50} values (µg/mL). Acarbose was used as a positive control (Coral Caycho et al., 2020).

2.8 Determination of the minimum bactericidal concentration

A widely accepted sensitive serial dilution microplate method was used to determine the minimum inhibitory concentration (MBC) (Elisha et al., 2017). Overnight bacterial cultures were adjusted to McFarland standard 1, equivalent to 3.0 x 10^8 CFU/mL (*Staphylococcus aureus*, *Enterococcus faecalis*, *Escherichia coli*, and *Pseudomonas aeruginosa*). The dried extract and subfractions were dissolved in 12.5% DMSO at a concentration of 25 mg/mL and 100 µL was added to the first well of a 96-well microtiter plate and serially diluted 1:1 with water. Bacterial cultures (100 µL) were added to each well. Starting with an extract concentration of 25 mg/mL, bacteria were therefore subjected to final concentrations of 6.25 to 0.05 mg/mL. Ampicillin was used as a positive control and DMSO (12.5%) as a solvent control. The highest concentration to which the bacteria were exposed was 12.5% DMSO in the first well and decreased two-fold in each subsequent well. Microplates were incubated overnight at 37°C. Finally, the solutions of the 96-well plates were subcultured in Petri dishes with 25 mL of soy agar. The MBC was defined as the lowest concentration of the extracts at which there was no sign of bacterial growth. The results are reported as mg/mL (Viteri et al., 2021). The antibiotic ampicillin was used as a positive control. For each bacteria and extract analyzed, a positive control (without plant extract) and a blank (without bacteria) were prepared.

2.9 UHPLC-QTOF-MS analysis

The separation and identification of the compounds present in the *W. ecuadoriensis* fractions was performed on a Compact QTOF MS + Elute UHPLC system, with the software Data Analysis 4.0 (all Bruker Daltonik GmbH, Bremen, Germany). Approximately 5 mg/mL of the fraction was dissolved in methanol and filtered through a 0.2 µm PTFE membrane and 3 µL was injected into the equipment. They were then measured in the chromatographic system consisting of a column temperature of 40°C; flow rate of 0.4 mL/min, mobile phase H_2O + 0.1% formic acid (A) and acetonitrile + 0.1% formic acid (B), and elution gradient, 0–0.5 min (12% B), 0.5–11 min (1–99% B), 11–14 min (99% B), and 14–16 min (12% B). Mass spectrometry conditions: electrospray ionization (ESI) source, scanning range 50–1300 m/z, the fragmentation pattern was obtained using the spectral libraries of the MassBank of North America (MoNA), obtained from https://mona.fiehnlab.ucdavis.edu/downloads.

2.10 Statistical analysis

All the assays were performed in triplicate and represented as median ± standard deviation (SD) using Microsoft Excel software (Microsoft 365, Microsoft Corporation, Redmond, WA, USA). Statistical significance between groups was set at $p < 0.05$ and determined by one-way ANOVA with Tukey's *post hoc* test using the commercial software Minitab 19.

3 Results and discussion

3.1 Extraction procedure

The total yield of the subfractions was performed after methanolic extraction and fractionation with *n*-hexane, dichloromethane, and ethyl acetate, resulting in four subfractions (hexane fraction, dichloromethane fraction, ethyl acetate fraction, and aqueous fraction). The results indicated that the methanolic extract (ME) yielded of 29.0%, followed by the aqueous fraction (AqF) which reached 15.5%. The dichloromethane fraction (DMF) had an intermediate yield of 8.5%, while the hexane fraction (HF) showed a much lower yield of 3.8%. Finally, the ethyl acetate fraction (EF) presented the lowest yield with only 1.0%.

3.2 Total phenolic and flavonoid content

The TPC and TFC of the extract and leaf fractions of *W. ecuadoriensis* were examined, and the results are presented in Table 1. The phenolic content was highest for the ethyl acetate fraction with 357.47 ± 12.78 mg GAE/g of dry extract. The flavonoid content was highest for the ethyl acetate fraction with 48.93 ± 6.32 mg QE/g of dry extract. Although this is the first report on *W. ecuadoriensis*, scientific information on the genus *Wigandia* and family Namaceae is scarce. However, there are some previous studies on other plants of the order Boraginales. The content of phenols and flavonoids in the ethanolic extract of *Eriodictyon californicum* leaves has been reported (Richards and Chaurasia, 2020). The authors report this species as a promising nutraceutical due to its healing properties against oxidative stress. Our results were superior to those reported for the species *Symphytum officinale* and *Anchusa ochroleuca*, with phenolic and flavonoid contents between 5.39-125.50 mg GAE/g of extract and 0.11-36.58 mg QE/g of extract, respectively (Trifan et al., 2021). In other species such as *Symphytum anatolicum* and *Cynoglottis barrelieri* the phenolic content was 32.7

TABLE 1 Content of phenols, flavonoids of the different fractions of leaves of *W. ecuadorensis*.

Extract and fractions	Total Phenolic content (mg GAE/g DE)	Total Flavonoid content (mg QE/g DE)
ME	176.29 ± 8.87 ^{b}	19.77 ± 4.53 ^{b,c}
HF	43.13 ± 0.79 ^{e}	26.89 ± 1.12 ^{b}
DMF	88.93 ± 0.79 ^{d}	9.51 ± 0.04 ^{c}
EF	357.47 ± 12.78 ^{a}	48.93 ± 6.32 ^{a}
AqF	113.44 ± 7.94 ^{c}	8.05 ± 0.07 ^{c}

TPC, Total phenolic content; TFC, Total flavonoid content; Different letters in the same column indicate significant differences: $p < 0.05$, $n= 3$.

and 52.8 mg GAE/g extract, respectively (Varvouni et al., 2020). In another study, it was determined that the phenolic and flavonoid content in the methanol extract of the *Onosma ambigens* species was lower with values of 51.19 mg GAE/g of extract and 45.39 mg QEs/g of extract, respectively (Sarikurkcu et al., 2020).

3.3 Antioxidant activity

The antioxidant activity of the extract and subfractions was analyzed by DPPH, ABTS, and FRAP methods and are presented in Table 2. These methods are widely used due to their simplicity, sensitivity, and ability to provide comparative antioxidant capacities of various extracts and compounds (Tabart et al., 2009).

The DPPH (2,2-diphenyl-1-picrylhydrazyl) assay measures the ability of antioxidants to scavenge free radicals by monitoring the color change from purple to yellow as the DPPH radical is reduced (Baliyan et al., 2022). The results of this assay ranged from 157.54 ± 0.49 to 187.32 ± 0.56 µmol TE/g of dry extract. *W. ecuadoriensis* ethyl acetate fraction scavenged DPPH in a concentration-dependent way with an IC_{50} of 17.66 µg/mL (Figure 2A). The hexane fraction had the highest value (IC_{50}: 97.30 µg/mL). The antioxidant activity (IC_{50}) decreased in descending order: EF > ME > AqF > DMF > HF. According to (Setha et al., 2013) IC_{50} values < 50 µg/mL are considered potent antioxidants. A study reported that the extract of the *Eriodictyon californicum* species showed a 93.39% inhibition of DPPH radicals at a concentration of 1.0 mg/mL (Richards and Chaurasia, 2020), similar to those obtained in our study evaluated at the same concentration (ME: 85.97%, EF: 76.12%, DMF: 81.78%, EF: 88.63%, AqF: 89.30%). Likewise, a study reported that the extract of the polar aerial part of *S. officinale* showed a DPPH radical scavenging activity similar to our study (138.41 µmol TE/g) (Trifan et al., 2021). In *Cordia gilletii*, an IC_{50} between 3.2 - 83.5 µg/mL is reported in different extracts (Okusa et al., 2007).

The ABTS, 2,2'-azino-bis(3-ethylbenzothiazoline-6-sulfonic acid) assay involves the generation of a blue-green ABTS radical cation, which is reduced by the antioxidants present in the sample, resulting in a decrease in absorbance. Similarly, the antioxidant activity evaluated against the ABTS radical, the extract, and all fractions had similar values in the range of 183.80 ± 0.37 and 184.12 ± 0.00 µmol TE/g extract. *W. ecuadoriensis* ethyl acetate fraction scavenged DPPH in a concentration-dependent way with an IC_{50} of 10.31 µg/mL (Figure 2B). The antioxidant activity (IC_{50}) decreased in descending order: EF > ME > DMF > AqF > HF. Likewise, the extract of the polar aerial part of *S. officinale* showed ABTS radical scavenging activity similar to our study (205.82 µmol TE/g extract) (Trifan et al., 2021). In another work it was observed that the Trolox equivalent antioxidant capacity (TEAC= IC_{50} Trolox/IC_{50} of the sample) ratio was 0.013, while in our study it was 0.18, concluding the antioxidant power of the methanolic extract of *W. ecuadoriensis* (Sarikurkcu et al., 2020).

The FRAP (ferric reducing antioxidant power) assay quantifies the antioxidant effect by evaluating the reduction of the ferric-tripyridyltriazine complex to its ferrous form, which has an intense blue color. FRAP values ranged from 0.65 ± 0.01 to 2.87 ± 0.01 mmol Fe/g of dry extract. The species of the genus *Eriodictyon* presented antioxidant activity with a concentration-dependent behavior comparable to the ascorbic acid standard (Richards and Chaurasia, 2022).

All these results demonstrate that the species *W. ecuadoriensis* and especially the ethyl acetate fraction present the highest antioxidant activity evaluated by the DPPH, ABTS, and FRAP methods, probably due to the higher total phenolic and flavonoid content compared to the other fractions tested (Table 1). In fact, the main compounds found in EF and AqF of *W. ecuadoriensis*, namely

TABLE 2 Antioxidant activity of the different fractions of leaves of *W. ecuadorensis*.

Extract and fractions	DPPH (µmol TE/g DE)	DPPH (IC_{50} µg/mL)	ABTS (µmol TE/g DE)	ABTS (IC_{50} µg/mL)	FRAP ($mmolFeSO_4 \cdot 7H_2O$/gDE)
ME	179.80 ± 1.22 ^{b}	35.70 ± 0.31 ^{d}	183.88 ± 0.24 ^{a}	30.19 ± 0.85 ^{d}	2.27 ± 0.07 ^{b}
HF	157.54 ± 0.49 ^{d}	97.30 ± 2.44 ^{a}	183.80 ± 0.37 ^{a}	65.69 ± 1.34 ^{a}	0.65 ± 0.01 ^{e}
DMF	170.33 ± 1.52 ^{c}	54.66 ± 1.28 ^{b}	183.88 ± 0.42 ^{a}	40.45 ± 0.57 ^{c}	0.99 ± 0.03 ^{d}
EF	185.82 ± 0.19 ^{a}	17.66 ± 0.58 ^{e}	183.96 ± 0.37 ^{a}	10.31 ± 0.08 ^{e}	2.87 ± 0.01 ^{a}
AqF	187.32 ± 0.56 ^{a}	41.14 ± 1.93 ^{c}	184.12 ± 0.00 ^{a}	62.36 ± 1.73 ^{b}	1.69 ± 0.11 ^{c}
Trolox *	n.a.	6.07 ± 0.46 ^{f}	n.a.	5.55 ± 0.50 ^{f}	n.a.
Ascorbic acid *	n.a.	3.06 ± 0.08 ^{f}	n.a.	7.35 ± 0.18 ^{e,f}	n.a.

*Used as standard antioxidant; DPPH, 2,2-diphenyl-1-picrylhydrazyl radical; ABTS, 2,2-azino-bis-3-ethylbenzothiazoline-6-sulfonic acid; FRAP, Ferric ion-reducing antioxidant power assay; Different letters in the same column indicate significant differences: $p < 0.05$, $n= 3$; n.a, Not applicable.

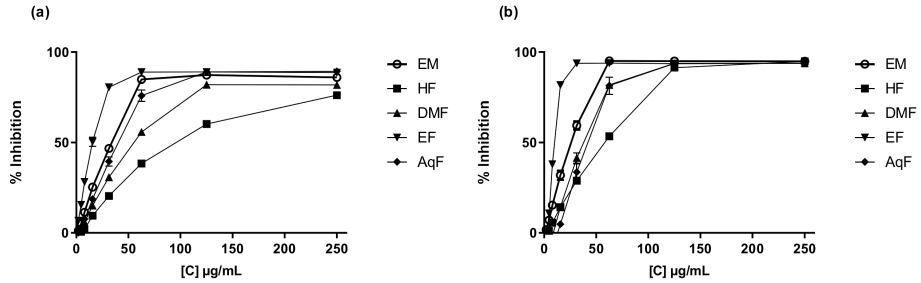

FIGURE 2
Antioxidant activity of *W. ecuadoriensis* extract and subfractions against DPPH **(A)** and ABTS **(B)**. Each point represents the average of three measurements.

caffeic acids, rosmarinic acid, cirsimaritin, luteolin-7-glycoside and apigenin-8-C-(6"acetyl)-β-D-glucopyranoside (Table 3), have already been reported as DPPH and ABTS scavengers. In this sense, these results indicate that the compounds present in the EF and DMF fractions have a strong capacity to neutralize free radicals, suggesting a high bioactive potential. This antioxidant activity highlights the *W. ecuadoriensis* species as a promising source of natural antioxidants, which may have therapeutic and preventive applications in diseases related to oxidative stress.

3.4 Antibacterial activity of *W. ecuadoriensis*

In the study of the antibacterial activity of the extract and subfractions of leaves of *W. ecuadoriensis* against *Staphylococcus aureus*, *Enterococcus faecalis*, *Escherichia coli*, and *Pseudomonas aeruginosa*, it was found that the crude extract and the different fractions presented varied effectiveness (Table 4). The crude extract showed remarkable activity against *S. aureus* (1.56 mg/mL) and *E. faecalis* (3.13 mg/mL), being less effective against *E. coli*. Curiously, the hexane fraction was the most effective against *S. aureus* and *E. faecalis* (1.56 mg/ml), while the dichloromethane and ethyl acetate fractions presented limited activity. No activity was detected in the aqueous fraction. Ampicillin was used as a control, showing high effectiveness against *S. aureus* and *E. coli*. The genus *Wigandia* has been reported to have antimicrobial activities. The activity of three extracts (*n*-hexane, ethanol, and acetone) of *W. caracasana* leaves has been reported against the strains *Streptococcus pneumoniae*, *S. pyogenes*, *E. coli*, *Salmonella typhi* and *Shigella flexneri* with zones of inhibition between 6 and 12 mm (Cáceresa et al., 1993). Another species, *Wigandia urens*, has reported the antimicrobial activity of

TABLE 3 UHPLC-QTOF-MS identification of ethyl acetate (a) and aqueous fraction (b) from *W. ecuadoriensis* leaves.

No	T_R(min)	Molecular formula	Major ion $[M-H]^-$ (m/z)	Calculated Molecular Weight	Tentative Compound	Fraction
1	0.11	$C_4H_2O_4$	112.9829	112.9856	Na formiate (internal standard)	EF, AqF
2	0.79	$C_9H_8O_4$	179,0363	180,0436	Caffeic acid	AqF
3	1.08	$C_{21}H_{20}O_{12}$	463,0859	464,0931	Hyperoside	EF, AqF
4	3.85	$C_{36}H_{32}O_{16}$	719,1564	720,1641	Sagerinic acid	EF, AqF
5	4.59	$C_{21}H_{20}O_{11}$	447,0928	448,1001	Luteolin-7-glucoside	EF
6	5.78	$C_{17}H_{12}O_9$	359.0408	360.0494	Acetyl miricetin	EF, AqF
7	5,82	$C_{18}H_{16}O_8$	359,0767	360,0832	Rosmarinic acid	EF
8	5.56	$C_{18}H_{32}O_5$	327,2173	328,2246	Corchorifatty acid F	EF
9	5.78	$C_{18}H_{32}O_5$	327,2173	328,2245	(10E,15Z)-9,12,13-trihydroxyoctadeca-10,15-dienoic acid	EF
10	6.19	$C_{17}H_{14}O_6$	313,0695	314,0767	Cirsimaritin	EF
11	6.33	$C_{29}H_{38}O_{12}$	577.2290	577.2574	Hydrangenoside C	EF, AqF
12	7.38	$C_{15}H_{22}O_4$	265,1481	266,1554	Strobilactone A	EF
13	7.59	$C_{17}H_{32}O_5$	315.2304	316.2329	Glyceryl-monomyristate	EF

(Continued)

10.3389/fpls.2024.1481447

TABLE 3 Continued

No	T_R(min)	Molecular formula	Major ion $[M-H]^-$ (m/z)	Calculated Molecular Weight	Tentative Compound	Fraction
14	7.77	$C_{28}H_{44}O_7$	491.2803	492.2873	Hirsutalin C	EF, AqF
15	8.38	$C_{16}H_{24}O_6$	311,1692	312,1765	Thymol-beta-D-glucoside	EF, AqF
16	8.81	$C_{18}H_{32}O_3$	295,2271	296,2344	Dimorphecolic acid	EF, AqF
17	9.05	$C_{19}H_{22}N_2O$	293,1784	294,185	Cinchonine	EF
18	9.22	$C_{23}H_{22}O_{12}$	489.2627	490.2628	Luteolin-8-C-(6"acetyl)-β-D-glucopyranoside	EF
19	9.33	$C_{17}H_{30}O_4$	297.2208	298.2223	Acaranoic acid	EF, AqF
20	9.47	$C_{17}H_{30}O_4$	297.2198	298.2223	Acaranoic acid isomer	EF, AqF
21	9.8	$C_{17}H_{28}O_4$	295.2054	296.1914	Acarenoic acid	EF, AqF
22	9.6	$C_{17}H_{32}O_4$	299.2265	300.2227	Heptadecanedioic acid isomer	EF, AqF
23	9.32	$C_{23}H_{22}O_{12}$	489.2802	490.2628	Luteolin-6-C-(6"acetyl)-β-D-glucopyranoside	EF, AqF
24	10.12	$C_{17}H_{28}O_4$	295.2056	296.1914	Acarenoic acid isomer	EF, AqF
25	10.72	$C_{21}H_{20}O_{11}$	447.0957	448.0933	Luteolin-6-C-β-D-glucopyranoside	EF
26	10.89	$C_{21}H_{20}O_{11}$	447.0921	448.0933	Luteolin-8-C-β-D-glucopyranoside	EF, AqF
27	10.97	$C_{23}H_{22}O_{11}$	473.2806	474.2797	Apigenin-6-C-(5"acetyl)-β-D-glucopyranoside	EF, AqF
28	11.14	$C_{23}H_{22}O_{11}$	473.2798	474.2797	Apigenin-8-C-(6"acetyl)-β-D-glucopyranoside	EF, AqF
29	11.26	$C_{39}H_{51}O_6$	615.3743	616.3691	Garcinol 13-O-methyl ether	EF, AqF
30	11.49	$C_{23}H_{22}O_{11}$	473.2603	474.2797	Apigenin-8-C-(5"acetyl)-β-D-glucopyranoside	EF, AqF
31	11.85	$C_{32}H_{54}O_{10}$	597.3644	597.3645	Kurilensoside G	EF
32	12.06	$C_{27}H_{42}O_7$	477.2857	477.3078	Erinacine D	EF, AqF
33	12.24	$C_{19}H_{27}$	255.2111	255.2138	Unknown	EF
34	12.57	$C_{21}H_{29}$	281.2274	282.2285	Unknown	EF, AqF
35	12.72	$C_{25}H_{39}O_4$	403.2853	403.2777	Uranediol diacetate	EF, AqF
36	13.45	$C_{32}H_{52}O_9$	579.3538	579.3638	Tokoronin	EF
37	13.63	$C_{40}H_{81}N_6O_{21}$	981.5527	981.5527	Unknown	EF
38	14.23	$C_{21}H_{40}O_7$	403.2701	403.2798	Aureosurfactin	EF
39	14.62	$C_{29}H_{38}O_{12}$	577.2290	577.2574	Hydrangenoside C	EF
40	15.51	$C_{21}H_{40}O_7$	403.2701	403.2798	Aureosurfactin	EF

the ethanolic extract of leaves against strains *S. aureus*, *E. coli*, and *P. aeruginosa* with diameters between 13-19 mm (Rojas et al., 2003). Another study reported the antimicrobial activity of *Cordia oncocalyx* (Boraginaceae) with MIC values <512 µg/mL (Thyalisson da Costa Silva et al., 2024). Our results were like those reported for the species *Echium humile*, who reported MCB values between 1.56 and 12.5 mg/mL against S. aureus, 0.19 and 12.5 against E. faecalis, 1.56 and 3.12 against E. coli, using different extraction solvents (Aouadi et al., 2022). Although the extract and subfractions showed low antibacterial activity, these results are interesting, considering that these come directly from a leaf extract.

3.5 Enzyme inhibitory activity

The inhibitory activity of the most polar fractions (EF and AqF) of *W. ecuadoriensis* leaves was determined by spectrophotometric assays against α-glucosidase and cholinesterases (AChE, BChE) (Table 5). Inhibition of α-glucosidase is seen as an effective strategy for the control of obesity and diabetes (Zengin et al., 2018). This enzyme, located at the edge of the small intestine, breaks down complex carbohydrates into glucose. By inhibiting α-glucosidase, the metabolism of complex carbohydrates is slowed down, which lowers blood glucose levels (Mustikasari et al., 2024). Figure 3 shows the

10.3389/fpls.2024.1481447

TABLE 4 Minimum bactericidal concentration (mg/mL) of leaf extracts against 4 pathogenic bacteria by microdilution assay.

Extract and fractions	*S. aureus*	*E. faecalis*	*E. coli*	*P. aeruginosa*
ME	1.56	3.13	6.25	–
HF	1.56	1.56	6.25	–
DMF	3.13	–	–	–
EF	6.25	6.25	–	–
AqF	–	–	–	–
Ampicillin *	2.06	–	0.26	–
Gentamicin *	0,19	1,56	0,39	6,25
Kanamycin *	0,78	6,25	1,56	–

*The antibiotic concentration is expressed as μg/mL (positive control). –, no inhibition.

effect of EF and acarbose on α-glucosidase enzyme activity. Figure 3 shows that increasing the concentration of EF (10–100 μg/mL) and acarbose (10–200 μg/mL) increased the inhibition of α-glucosidase activity. At the highest concentrations, EF and acarbose (100 and 200 μg/mL) achieved inhibitions of 73.58 ± 0.36% and 59.39 ± 0.45%, respectively. The IC_{50} values for α-glucosidase inhibition were 38.44 ± 0.75 μg/mL for EF (Figure 3A), which is approximately five times higher than the commercial standard, acarbose (179.07 ± 1.18 μg/mL, Figure 3B). These results indicate that the ethyl acetate (EF) fraction is more effective than acarbose in inhibiting α-glucosidase. According to (Benjamin et al., 2024) IC_{50} values lower than 50 μg/mL are indicators of a strong potential as an inhibitor of α-glucosidase activity. In this sense, it is important to highlight that our result was obtained from a fraction and not from an isolated compound, which highlights a promising bioactive potential for the species. The presence of several unpurified compounds within the fraction suggests that upon further purification, the inhibitory activity could even be enhanced, revealing individual compounds with even stronger properties. This observed enzyme inhibition could be related to the presence of phenolic compounds described in Table 1. On the other hand, the aqueous fraction showed low inhibition, reaching only 4.75 ± 0.16% at a concentration of 2 mg/mL, therefore, its IC_{50} value could not be determined. Several studies have investigated the inhibitory potential of α-glucosidase in species of the order Boraginales, showing promising results. Another medicinal herb that has been used for centuries to treat diabetes is *Symphytum*. The inhibitory effect of the whole plant extract of *Symphytum anatolicum* showed a potent inhibitory activity (IC_{50}: 18.28 ± 0.31 μg/mL), comparable to that exerted by acarbose (IC_{50}: 17.05 ± 0.25 μg/mL), used as a control (Kılınc et al., 2023). The methanolic extract of *Echium humile* presented a value of 60 μg/mL, indicating a strong effectiveness (Aouadi et al., 2022). An *in vitro* antidiabetic study revealed that ethyl acetate extract exhibits 60% inhibition, at a concentration of 500 μg/mL, with an IC_{50} value of 380 μg/mL and the IC_{50} value of standard acarbose was 250 μg/mL (Syed Akbar et al., 2023). The aqueous extract of *Glandora diffusa* showed a potent inhibitory effect on a-glucosidase with an IC_{50} value of 33.3 μg/mL, almost ten times lower than that described for acarbose 300 μg/mL. These authors attribute this activity to the compounds caffeic acid and rosmarinic acid, which have been reported as inhibitors of α-glucosidase, and which are also present in our study (Table 3) (Ferreres et al., 2013). According to these IC_{50} values, the ethyl acetate fraction studied in this work seems to show an enzyme inhibition capacity comparable to that reported in previous studies.

Cholinesterase inhibitors play a crucial role in the functioning of the nervous system and are related to the treatment of Alzheimer's disease. Over the past two decades, the search for natural products related to AChE and BChE inhibition has increased (Ortega de Oliveira et al., 2024). Figure 4 shows the inhibition of AChE and BChE enzymes in the presence of AqF and galantamine at increasing concentrations. The results revealed a dose-dependent behavior for the AChE enzyme with an IC_{50} value of 915.98 ± 7.25 μg/mL for AqF (Figure 4A). Regarding the effect on BChE, Figure 4C shows that the fraction inhibits the

TABLE 5 Enzyme inhibitory activity of *W. ecuadoriensis* fractions.

Fractions	α-glucoside		Cholinesterase inhibitory	
	% inhibition ± SD (2 mg/mL)	IC_{50} (μg/mL)	IC_{50} de AChE (μg/ml)	IC_{50} de BChE (μg/ml)
EF	85.83 ± 0.31 ^{a}	38.44 ± 0.75 ^{b}	–	–
AqF	4.75 ± 0.16 ^{b}	–	915.98 ± 7.25 ^{a}	380.42 ± 22.10 ^{a}
Acarbose *	59.39 ± 0.45 ^{c}	179.07 ± 1.18 ^{a}	-	-
Galantamine *	n.a.	n.a	0.53 ± 0.03 ^{b}	5.15 ± 0.44 ^{b}

AChE, acetylcholinesterase; BChE, butyrylcholinesterase. Different letters in the same column indicate significant differences: $p < 0.05$, $n = 3$. –, no inhibition; n.a, Not applicable. *Used as standard drug; Acarbose (0.2 mg/mL).

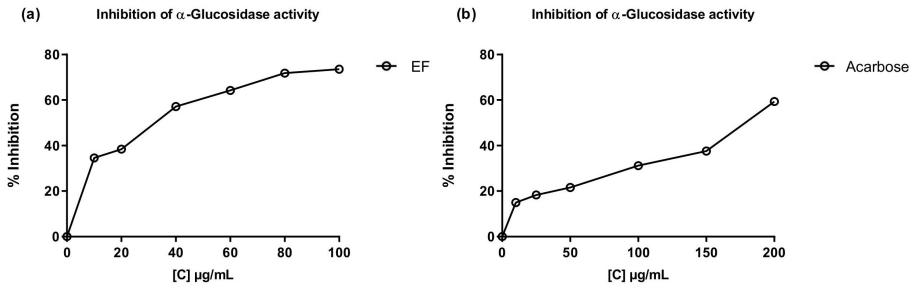

FIGURE 3
Inhibitory effects of EF from *W. ecuadoriensis* **(A)** and galantamine **(B)** on the enzyme α-glucosidase. Each point represents the average of three measurements.

butyrylcholinesterase enzyme depending on the concentration with an IC_{50} value of 380.42 ± 22.10 µg/mL for AqF (Figure 4C). The ethyl acetate fraction did not show any inhibitory activity. These results were higher compared to the positive control galantamine, which presented an IC_{50} of 0.53 ± 0.03 µg/mL for AChE and 5.15 ± 0.44 µg/mL for BChE, indicating that the standard drug, galantamine, is more effective in inhibiting these enzymes compared to the aqueous fraction of *W. ecuadoriensis*. However, this result is still encouraging, since we are evaluating a fraction and not an isolated compound. It is likely that the bioactive compounds responsible for the activity are found in low concentration within the fraction, suggesting that further purification could significantly increase the inhibitory activity. The results obtained for AChE are comparable to that reported for the methanolic extract of *Wigandia urens*, with an AChE inhibition of 43% evaluated at a concentration of 1 mg/mL (Ortiz et al., 2013). There is information on the traditional use of the *Wigandia urens* species in Guatemala for epilepsy and psychological problems (Hitziger, 2016). On the other hand, some extracts from the Boraginaceae family (*S. anatolicum*, *S. aintabicum*, *Cynoglossum creticum*, *C. barrelieri*, and *Alkanna sfikasiana*) have shown inhibitory effects on AChE, BChE, and α-glucosidase (Varvouni et al., 2020). Our results presented lower IC_{50} compared to other species of *Onosma trapezuntea* and *Onosma rigidum* with IC_{50} values of 1270 and 1180 µg/mL for AChE and 2550 and 2060 µg/mL for BChE, respectively (Kirkan et al., 2022). Another study reported that hexane, chloroform, ethyl acetate and methanol extracts of *Calophyllum gracilentum*, at a concentration of 1.0 mg/mL, inhibited AChE by 3.02 ± 0.998%, 12.30 ± 5.641%, 31.62 ± 2.057% and 4.61 ± 2.129%, respectively (Seruji et al., 2024). In our study, we evaluated at the same concentration reported an

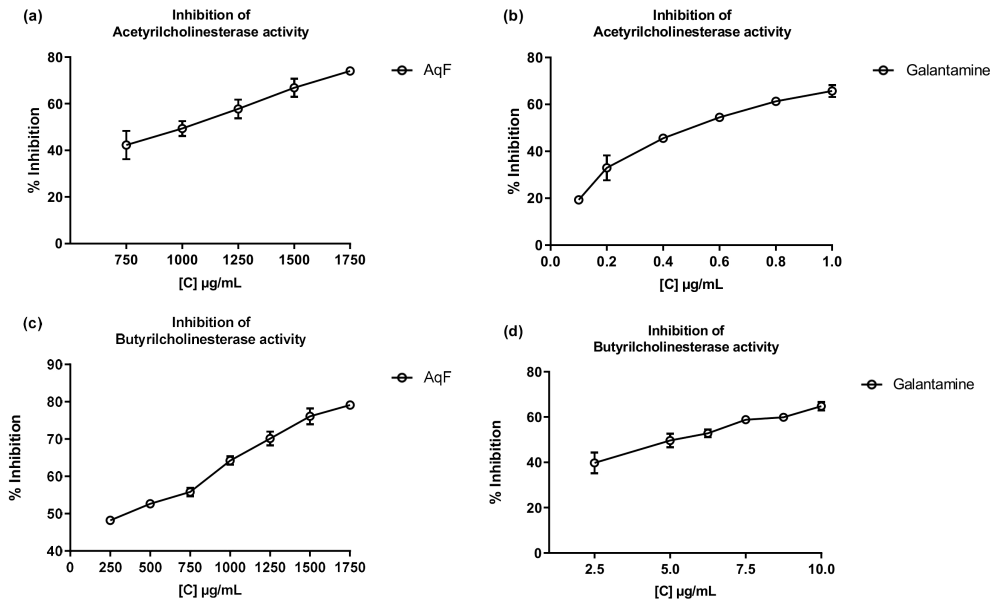

FIGURE 4
Inhibitory effects of AqF from *W. ecuadoriensis* and galantamine on cholinesterase enzymes. **(A, B)** Effect on AChE; **(C, D)** Effect on BChE. Each point represents the average of three measurements.

inhibition of 51.20 ± 0.60%. Based on these values, the fraction investigated in this study seems to be more effective in inhibiting this enzyme compared to previously reported results.

The results obtained in this study reveal that certain fractions of *W. ecuadoriensis* possess a strong antioxidant potential and a remarkable inhibitory activity of the enzyme α-glucosidase, suggesting that this species could be a promising source of bioactive compounds. However, extensive research should be carried out to isolate the main compounds and determine their activity, in order to understand their mechanism of action better. Furthermore, these observations provide a valuable scientific contribution to the chemical knowledge and biological properties of the plant species *Wigandia ecuadoriensis*.

3.6 UHPLC-QTOF-MS analysis

The compounds from the ethyl acetate and aqueous fractions of the methanolic extract of *W. ecuadoriensis* leaves were analyzed by UHPLC-QTOF-MS. The total ion current chromatogram in negative ESI mode is shown in Figure 5, and the tentatively detected compounds are summarized in Table 3. The UHPLC-QTOF-MS profile revealed the presence of 39 metabolites, belonging to the classes of phenolic acids, flavonoids, fatty acyls, naphthofuran, glycerolipids, terpene, alkaloid, prenol lipids. The tentative identification was performed in Metaboscape software, a proprietary Bruker software that allows the identification of metabolites based on their mass, fragmentation pattern, and isotopic pattern, subsequently compared with the MassBank of North America (MoNA) database. These compounds include two phenolic acids (peaks 2 and 7), eleven flavonoids (peaks 3, 5, 6, 10, 18, 23, 25, 26, 27, 28 and 30), one lignan (peak 4), four fatty acyls (peaks 8, 9, 16, 22 and 38), four prenol lipids (peaks 11, 29, 32 and 39), one naphthofuran (peak 12), one glycerolipids (peak 13), two terpenes (peaks 14 and 15), and one alkaloid (peak 17), four lactones (peaks 19, 20, 21 and 24), three steroidal (peaks 31, 35 and 36), three unknown compounds (peaks 33, 34 and 37).

The compounds identified in the subfractions of *W. ecuadoriensis* exhibit a wide range of biological activities. Quinic acid shows antioxidant, antidiabetic, anticancer, antimicrobial, antiviral, antiaging, protective, antinociceptive, and analgesic properties (Benali et al., 2022). 3,4-Dihydroxybenzeneacetic and caffeic acids possess antioxidant activity in rat plasma (Raneva et al., 2001). Citric acid, known for its antimicrobial and antioxidant properties (Søltoft-Jensen and Hansen, 2005). Other compounds such as 3-hydroxybenzaldehyde, *p*-hydroxybenzoic acid, and hyperoside exhibit multiple properties, from antioxidant and anti-inflammatory to anticancer and organ protective (Rohini et al., 2013; Chen et al., 2021; Wang et al., 2022). Luteolin-7-glucoside, rosmarinic acid, and cirsimaritin have antioxidant, antitumor, anti-inflammatory, and protective activities against various diseases (Cai et al., 2020; Silva et al., 2020; De Stefano et al., 2021). Strobilactone A is known for its antifungal activity (Cohen et al., 2011), while thymol-beta-D-glucoside and dimorpholicacid have antibacterial activity (Mundt et al., 2003; Anderson et al., 2021). Cinchonina, in addition to being an antimalarial agent, has anticancer, antiobesity, anti-inflammatory, antiparasitic, antimicrobial, and antiplatelet effects (Parveen et al., 2024). Derivatives of acaranoic acid exhibit potent antifungal action against *Botrytis cinerea*, *Septoria tritici* and *Pyricularia oryzae* (Hussain et al., 2012). Luteolin-8-C-β-D-glucopyranoside and apigenin-8-C-(6"acetyl)-β-D-glucopyranoside stand out for their antioxidant capacity to scavenge free radicals (Simirgiotis et al., 2013). Kurilensoside G shows moderate inhibition in sea urchin sperm tests (Stonik et al., 2008). Erinacine D promotes nerve growth factor synthesis (Kawagishi et al., 1996). Tokoronin inhibits α-MSH-induced melanogenesis with low cytotoxicity (Ukiya et al., 2020). Aureosurfactin, a biosurfactant with comparable activity to rhamnolipid, surfactin and sophorolipid (Kim et al., 2016).

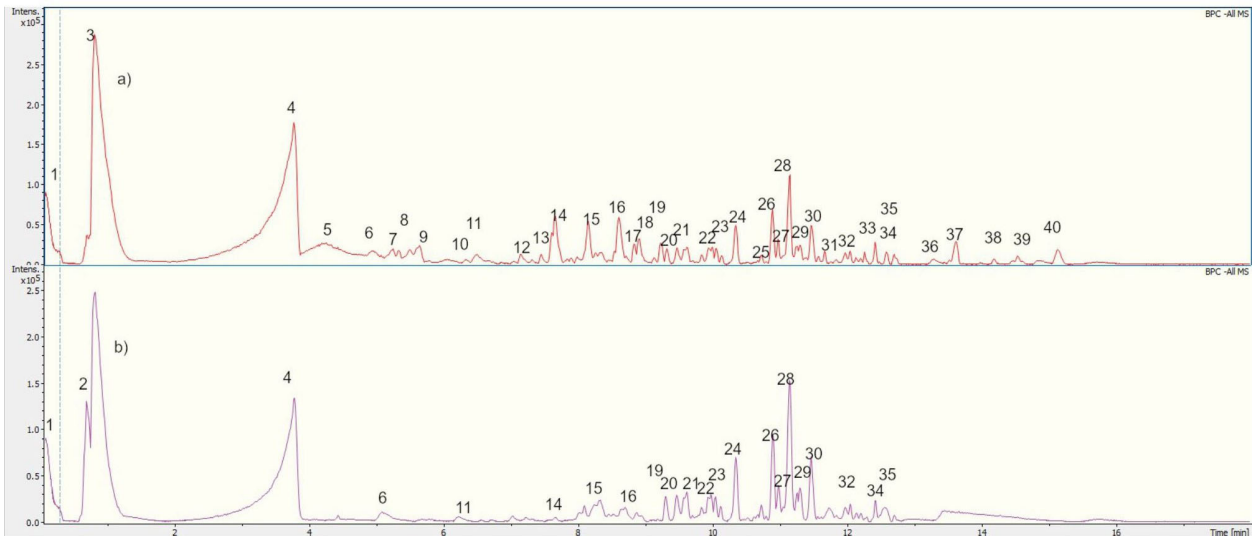

FIGURE 5
UHPLC-QTOF-MS Chromatogram of **(A)** EF and **(B)** AqF leaves *W. ecuadoriensis* in a negative ion mode.

Hydrogenoside C enhances cell viability and procollagen type I production in UVB-irradiated Hs68 cells (Shin et al., 2019).

4 Conclusion

This study is the first report of the *in vitro* activity of *W. ecuadoriensis* leaves. The ethyl acetate fraction was shown to have the highest content of phenols and flavonoids compared to the other fractions. This result elicited potent antioxidant activity. Furthermore, the ethyl acetate fraction was found to have strong potential as an inhibitor of α-glucosidase activity. On the other hand, the methanolic extract and its hexane fraction revealed antimicrobial activity. According to the UHPLC-MS results, the dominant compounds present in the fractions are caffeic acid, and hyperoside. These findings represent a valuable contribution to the knowledge of the species and suggest that *Wigandia* could be a promising source of bioactive compounds, creating new opportunities for the development of phytopharmaceuticals. Nevertheless, these initial results underline the need for further research to isolate the main compounds of the ethyl acetate fraction of *W. ecuadoriensis* to validate its antidiabetic effects.

Data availability statement

The datasets presented in this study can be found in online repositories. The names of the repository/repositories and accession number(s) can be found in the article/supplementary material.

Author contributions

RV: Conceptualization, Project administration, Visualization, Writing – original draft, Investigation. FE: Investigation, Methodology, Writing – review & editing. XC: Data curation, Methodology, Writing – review & editing. MS: Supervision, Writing – review & editing. PM: Writing – review & editing.

Funding

The author(s) declare financial support was received for the research, authorship, and/or publication of this article. The authors acknowledge the Biotechnology Research Center of Ecuador (CIBE) for supporting founding, Project CIBE-13-2023 and Fondecyt 1220075.

Acknowledgments

The authors acknowledge the Fondequip EQM170172.

Conflict of interest

The authors declare that the research was conducted in the absence of any commercial or financial relationships that could be construed as a potential conflict of interest.

Publisher's note

References

Anand, P., and Singh, B. (2013). A review on cholinesterase inhibitors for Alzheimer's disease. *Arch. Pharm. Res.* 36, 375–399. doi: 10.1007/s12272-013-0036-3

Anderson, R. C., Levent, G., Petrujkić, B. T., Harvey, R. B., Hume, M. E., He, H., et al. (2021). Antagonistic effects of lipids against the anti-*escherichia coli* and anti-*salmonella* activity of thymol and thymol-β-d-glucopyranoside in porcine gut and fecal cultures *in vitro*. *Front. Vet. Sci.* 8. doi: 10.3389/fvets.2021.751266

Aouadi, K., Hajlaoui, H., Arraouadi, S., Ghannay, S., Snoussi, M., and Kadri, A. (2022). Phytochemical profiling, antimicrobial and α-glucosidase inhibitory potential of phenolic-enriched extracts of the aerial parts from *echium humile* desf.: *in vitro* combined with in silico approach. *Plants* 11, 1131. doi: 10.3390/plants11091131

Baliyan, S., Mukherjee, R., Priyadarshini, A., Vibhuti, A., Gupta, A., Pandey, R. P., et al. (2022). Determination of antioxidants by DPPH radical scavenging activity and quantitative phytochemical analysis of *ficus religiosa*. *Molecules* 27, 1326. doi: 10.3390/molecules27041326

Barrientos, R. E., Romero-Parra, J., Cifuentes, F., Palacios, J., Romero-Jola, N. J., Paredes, A., et al. (2023). Chemical fingerprinting, aorta endothelium relaxation effect, and enzymatic inhibition of canelo (*Drimys winteri* J. R. Forst. & G. Forst, (D.C) A. Gray, family winteraceae) fruits. *Foods* 12, 2580. doi: 10.3390/foods12132580

Benali, T., Bakrim, S., Ghchime, R., Benkhaira, N., El Omari, N., Balahbib, A., et al. (2022). Pharmacological insights into the multifaceted biological properties of quinic acid. *Biotechnol. Genet. Eng. Rev.*, 1–30. doi: 10.1080/02648725.2022.2122303

Benjamin, M. A. Z., Mohd Mokhtar, R. A., Iqbal, M., Abdullah, A., Azizah, R., Sulistyorini, L., et al. (2024). Medicinal plants of Southeast Asia with anti-α-glucosidase activity as potential source for type-2 diabetes mellitus treatment. *J. Ethnopharmacol* 330, 118239. doi: 10.1016/j.jep.2024.118239

Cáceresa, A., Figueroa, L., Taracena, A. M., and Samayoa, B. (1993). Plants used in Guatemala for the treatment of respiratory diseases. 2: Evaluation of activity of 16 plants against Gram-positive bacteria. *J. Ethnopharmacol* 39, 77–82. doi: 10.1016/0378-8741(93)90053-8

Cai, Y., Zheng, Q., Sun, R., Wu, J., Li, X., and Liu, R. (2020). Recent progress in the study of *Artemisiae Scopariae* Herba (Yin Chen), a promising medicinal herb for liver diseases. *Biomedicine Pharmacotherapy* 130, 110513. doi: 10.1016/j.biopha.2020.110513

Cao, S., Rossant, C., Ng, S., Buss, A. D., and Butler, M. S. (2003). Phenolic derivatives from *Wigandia urens* with weak activity against the chemokine receptor CCR5. *Phytochemistry* 64, 987–990. doi: 10.1016/S0031-9422(03)00448-5

Chen, K.-Y., Chen, Y.-J., Cheng, C.-J., Jhan, K.-Y., Chiu, C.-H., and Wang, L.-C. (2021). 3-Hydroxybenzaldehyde and 4-Hydroxybenzaldehyde enhance survival of mouse astrocytes treated with *Angiostrongylus cantonensis* young adults excretory/secretory products. *BioMed. J.* 44, S258–S266. doi: 10.1016/j.bj.2020.11.008

Cohen, E., Koch, L., Thu, K. M., Rahamim, Y., Aluma, Y., Ilan, M., et al. (2011). Novel terpenoids of the fungus Aspergillus insuetus isolated from the Mediterranean sponge Psammocinia sp. collected along the coast of Israel. *Bioorg Med. Chem.* 19, 6587–6593. doi: 10.1016/j.bmc.2011.05.045

Coral Caycho, E. R., Calixto Cotos, M. R., and Soberón Lozano, M. M. (2020). Actividad inhibitoria in *vitro* de los extractos acuosos de los frutos de *Hylocereus megalanthus y Passiflora tripartita* var. mollisima sobre las enzimas α-amilasa y α-

glucosidasa. *Rev. la Sociedad Química del Perú* 86, 93–104. doi: 10.37761/rsqp.v86i2.279

Cornejo, X. (2006). *Wigandia Ecuadorensis* (Hydrophyllaceae), una Nueva Especie del Bosque Muy Seco Tropical al Occidente de Ecuador. *Novon* 16, 324–327. doi: 10.3417/1055-3177(2006)16[324:WEHUNE]2.0.CO;2

De Stefano, A., Caporali, S., Di Daniele, N., Rovella, V., Cardillo, C., Schinzari, F., et al. (2021). Anti-inflammatory and proliferative properties of luteolin-7-O-glucoside. *Int. J. Mol. Sci.* 22, 1321. doi: 10.3390/ijms22031321

Elisha, I. L., Botha, F. S., McGaw, L. J., and Eloff, J. N. (2017). The antibacterial activity of extracts of nine plant species with good activity against *Escherichia coli* against five other bacteria and cytotoxicity of extracts. *BMC Complement Altern. Med.* 17, 133. doi: 10.1186/s12906-017-1645-z

Farhat, M.B., Landoulsi, A., Chaouch-Hamada, R., Sotomayor, J. A., and Jordán, M. J. (2013). Characterization and quantification of phenolic compounds and antioxidant properties of *Salvia* species growing in different habitats. *Ind. Crops Prod* 49, 904–914. doi: 10.1016/j.indcrop.2013.06.047

Ferreres, F., Vinholes, J., Gil-Izquierdo, A., Valentão, P., Gonçalves, R. F., and Andrade, P. B. (2013). *In vitro* studies of α-glucosidase inhibitors and antiradical constituents of *Glandora diffusa* (Lag.) D.C. Thomas infusion. *Food Chem.* 136, 1390–1398. doi: 10.1016/j.foodchem.2012.09.089

Ghareeb, M. A., Mohamed, T., Saad, A. M., Refahy, L. A.-G., Sobeh, M., and Wink, M. (2017). HPLC-DAD-ESI-MS/MS analysis of fruits from *Firmiana simplex* (L.) and evaluation of their antioxidant and antigenotoxic properties. *J. Pharm. Pharmacol.* 70, 133–142. doi: 10.1111/jphp.12843

Gómez, F., Quijano, L., Calderón, J. S., and Ríos, T. (1980). Terpenoids isolated from *Wigandia kunthii*. *Phytochemistry* 19, 2202–2203. doi: 10.1016/S0031-9422(00)82225-6

Hitziger, M. (2016). *Mayan phytotherapy in Guatemala: a transdisciplinary study for ethnographic documentation and local empowerment*.

Hussain, H., Krohn, K., Schulz, B., Draeger, S., Nazir, M., and Saleem, M. (2012). Two new antimicrobial metabolites from the endophytic fungus, *seimatosporium* sp. *Nat. Prod Commun.* 7, 1934578X1200700. doi: 10.1177/1934578X1200700305

Kawagishi, H., Simada, A., Shizuki, K., Ojima, F., Mori, H., Okamoto, K., et al. (1996). Erinacine D, a stimulator of NGF-synthesis, from the mycelia of *Hericium erinaceum*. *Heterocycl Comm* 2. doi: 10.1515/HC.1996.2.1.51

Kim, J.-S., Lee, I.-K., Kim, D.-W., and Yun, B.-S. (2016). Aureosurfactin and 3-deoxyaureosurfactin, novel biosurfactants produced by *Aureobasidium pullulans* L3-GPY. *J. Antibiot (Tokyo)* 69, 759–761. doi: 10.1038/ja.2015.141

Kirkan, B., Sarikurkcu, C., and Zengin, G. (2022). Bioactive constituents, antioxidant effects and enzyme inhibitory properties of two *Onosma* species (*Onosma trapezuntea* and *O. rigidum*). *South Afr. J. Bot.* 145, 142–148. doi: 10.1016/j.sajb.2021.09.036

Kılınc, H., D'Urso, G., Paolillo, A., Alankus, O., Piacente, S., and Masullo, M. (2023). LC-MS and NMR based plant metabolomics: A comprehensive phytochemical investigation of *symphytum anatolicum*. *Metabolites* 13, 1051. doi: 10.3390/metabo13101051

Mundt, S., Kreitlow, S., and Jansen, R. (2003). Fatty acids with antibacterial activity from the cyanobacterium *Oscillatoria redekei* HUB 051. *J. Appl. Phycol* 15, 263–267. doi: 10.1023/A:1023889813697

Mustikasari, K., Santoso, M., Fadzelly Abu Bakar, M., and Fatmawati, S. (2024). Antioxidant, α-glucosidase inhibitory, and cytotoxic activities of *Mangifera rufocostata* extract and identification of its compounds by LC-MS/MS analysis. *Arabian J. Chem.* 17, 105391. doi: 10.1016/j.arabjc.2023.105391

Okusa, P. N., Penge, O., Devleeschouwer, M., and Duez, P. (2007). Direct and indirect antimicrobial effects and antioxidant activity of *Cordia gilletii* De Wild (Boraginaceae). *J. Ethnopharmacol* 112, 476–481. doi: 10.1016/j.jep.2007.04.003

Ortega de Oliveira, P. C., da Silva, G. M., Cass, Q. B., de Moraes, M. C., and Cardoso, C. L. (2024). Natural products as a source of cholinesterase inhibitors. *Pharmacol. Res. - Natural Products*, 100099. doi: 10.1016/j.prenap.2024.100099

Ortiz, D., Valdez, A., and Cáceres, A. (2013). Actividad inhibitoria de la acetilcolinesterasa por extractos de 18 especies vegetales nativas de Guatemala usadas en el tratamiento de afecciones nerviosas. *Rev. Cient. Fac. Cienc. Quim. Farm.* 22, 17–25. doi: 10.54495/Rev.Cientifica.v23i1.108

Parveen, S., Maurya, N., Meena, A., and Luqman, S. (2024). Cinchonine: A versatile pharmacological agent derived from natural cinchona alkaloids. *Curr. Top. Med. Chem.* 24, 343–363. doi: 10.2174/0115680266270796231109171808

Raneva, V., Shimasaki, H., Ishida, Y., Ueta, N., and Niki, E. (2001). Antioxidative activity of 3,4-dihydroxyphenylacetic acid and caffeic acid in rat plasma. *Lipids* 36. doi: 10.1007/s11745-001-0821-6

Reynolds, G. W., Gafner, F., and Rodriguez, E. (1989). Contact allergens of an urban shrub *Wigandia caracasana*. *Contact Dermatitis* 21, 65–68. doi: 10.1111/j.1600-0536.1989.tb04698.x

Richards, A., and Chaurasia, S. (2020). "A Promising Nutraceutical Eriodictyon californicum, a "Holy Herb," with its Healing Abilities against Oxidative Stress," in *The 1st International Electronic Conference on Food Science and Functional Foods* (MDPI, Basel Switzerland), 64. doi: 10.3390/foods_2020-07675

Richards, A., and Chaurasia, S. (2022). Antioxidant activity and reactive oxygen species (ROS) scavenging mechanism of *eriodictyon californium*, an edible herb of North America. *J. Chem.* 2022, 1–8. doi: 10.1155/2022/6980121

Rohini, M., Shikha, S., Akash, J., and Jasmine, C. (2013). A comprehensive review on biological activities of P-hydroxy benzoic acid and its derivatives. *Int. J. Pharm. Sci. Rev. Res.* 22, 109–115.

Rojas, R., Bustamante, B., Bauer, J., Fernández, I., Albán, J., and Lock, O. (2003). Antimicrobial activity of selected Peruvian medicinal plants. *J. Ethnopharmacol* 88, 199–204. doi: 10.1016/S0378-8741(03)00212-5

Sarikurkcu, C., Sahinler, S. S., Ceylan, O., and Tepe, B. (2020). *Onosma ambigens*: Phytochemical composition, antioxidant and enzyme inhibitory activity. *Ind. Crops Prod* 154, 112651. doi: 10.1016/j.indcrop.2020.112651

Seruji, N. M. U., Jong, V. Y. M., Karunakaran, T., Zamakshshari, N. H., Mah, S. H., Gunter, N. V., et al. (2024). Molecular docking studies and *in-vitro* cholinesterase inhibitory activities of chemical constituents of *Calophyllum gracilentum*. *Phytochem. Lett.* 63, 93–100. doi: 10.1016/j.phytol.2024.08.007

Setha, B., Gaspersz, F., Idris, A., Rahman, S., and Mailoa, M. (2013). Potential of seaweed *padina* sp. As A source of antioxidant. *Int. J. Sci. \& Technol. Res.* 2, 221–224.

Shin, J.-S., Han, H.-S., Lee, S.-B., Myung, D., Lee, K., Lee, S. H., et al. (2019). Chemical constituents from leaves of *hydrangea serrata* and their anti-photoaging effects on UVB-irradiated human fibroblasts. *Biol. Pharm. Bull.* 42, 424–431. doi: 10.1248/bpb.b18-00742

Silva, M., Caro, V., Guzmán, C., Perry, G., Areche, C., and Cornejo, A. (2020). *α-Synuclein and tau, two targets for dementia*. 1–25. doi: 10.1016/B978-0-12-819483-6.00001-1

Simirgiotis, M., Schmeda-Hirschmann, G., Bórquez, J., and Kennelly, E. (2013). The *passiflora tripartita* (Banana passion) fruit: A source of bioactive flavonoid C-glycosides isolated by HSCCC and characterized by HPLC–DAD–ESI/MS/MS. *Molecules* 18, 1672–1692. doi: 10.3390/molecules18021672

Søltoft-Jensen, J., and Hansen, F. (2005). "New chemical and biochemical hurdles," in *Emerging Technologies for Food Processing* (Elsevier), 387–416. doi: 10.1016/B978-012676757-5/50017-7

Stonik, V. A., IvanChina, N. V., and Kicha, A. A. (2008). New polar steroids from starfish. *Nat. Prod Commun.* 3, 1934578X0800301. doi: 10.1177/1934578X0800301005

Syed Akbar, W. A., Arokiarajan, M. S., John Christopher, J., Zaheer Ahmed, N., and Meena, R. (2023). Evaluation of bioactive compounds as antimicrobial and antidiabetic agent from the crude extract of *Heliotropium curassavicum* L. *Biocatal Agric. Biotechnol.* 50, 102745. doi: 10.1016/j.bcab.2023.102745

Tabart, J., Kevers, C., Pincemail, J., Defraigne, J.-O., and Dommes, J. (2009). Comparative antioxidant capacities of phenolic compounds measured by various tests. *Food Chem.* 113, 1226–1233. doi: 10.1016/j.foodchem.2008.08.013

Thaipong, K., Boonprakob, U., Crosby, K., Cisneros-Zevallos, L., and Hawkins Byrne, D. (2006). Comparison of ABTS, DPPH, FRAP, and ORAC assays for estimating antioxidant activity from guava fruit extracts. *J. Food Composition Anal.* 19, 669–675. doi: 10.1016/j.jfca.2006.01.003

Thyalisson da Costa Silva, J., Lima Bezerra, J. J., Moura, T. F., Pereira da Cruz, R., Gregorio de Oliveira, M., Costa, A. R., et al. (2024). Phytochemical analysis and evaluation of the antibacterial and antibiotic potentiation activities of the aqueous extract of *Cordia oncocalyx* Allemão (Boraginaceae). *Pharm. Sci. Adv.* 2, 100042. doi: 10.1016/j.pscia.2024.100042

Torre, L., Navarrete, H., Muriel M., P., Macía Barco, M. J., and Balslev, H. (2008). *Enciclopedia de las plantas útiles del Ecuador*.

Trifan, A., Zengin, G., Sinan, K. I., Wolfram, E., Skalicka-Woźniak, K., and Luca, S. V. (2021). LC-HRMS/MS phytochemical profiling of *Symphytum officinale* L. and Anchusa ochroleuca M. Bieb. (Boraginaceae): Unveiling their multi-biological potential via an integrated approach. *J. Pharm. BioMed. Anal.* 204, 114283. doi: 10.1016/j.jpba.2021.114283

Ukiya, M., Sato, D., Kimura, H., Hirai, Y., and Nishina, A. (2020). Tokoronin Contained in *Dioscorea tokoro* Makino ex Miyabe Suppressed α -MSH-Induced Melanogenesis in B16 Cells via Suppression of Classical MAPK Pathway Activation. *Chem. Biodivers* 17. doi: 10.1002/cbdv.202000077

van den Berg, R., Haenen, G. R. M. M., van den Berg, H., and Bast, A. (1999). Applicability of an improved Trolox equivalent antioxidant capacity (TEAC) assay for evaluation of antioxidant capacity measurements of mixtures. *Food Chem.* 66, 511–517. doi: 10.1016/S0308-8146(99)00089-8

Varvouni, E.-F., Zengin, G., Graikou, K., Ganos, C., Mroczek, T., and Chinou, I. (2020). Phytochemical analysis and biological evaluation of the aerial parts from *Symphytum anatolicum* Boiss. and *Cynoglottis barrelieri* (All.) Vural & Kit Tan (Boraginaceae). *Biochem. Syst. Ecol.* 92, 104128. doi: 10.1016/j.bse.2020.104128

Vasile, M.-A., Jeiter, J., Weigend, M., and Luebert, F. (2020). Phylogeny and historical biogeography of Hydrophyllaceae and Namaceae, with a special reference to *Phacelia* and *Wigandia*. *Syst. Biodivers* 18, 757–770. doi: 10.1080/14772000.2020.1771471

Viteri, R., Giordano, A., Montenegro, G., and Zacconi, F. (2021). *Eucryphia cordifolia* extracts: Phytochemical screening, antibacterial and antioxidant activities. *Nat. Prod Res.* 1–5. doi: 10.1080/14786419.2021.1960525

Wang, Q., Wei, H., Zhou, S., Li, Y., Zheng, T., Zhou, C., et al. (2022). Hyperoside: A review on its sources, biological activities, and molecular mechanisms. *Phytotherapy Res.* 36, 2779–2802. doi: 10.1002/ptr.7478

Woster, P. M. (2003), 203–211. doi: 10.1016/S0065-7743(03)38022-4

Zavala-Sánchez, M. A., Pérez-Gonzàlez, C., Arias-García, L., and Pérez-Gutiérrez, S. (2009). Anti-inflammatory activity of Wigandia urens and *Acalypha alopecuroides*. *Afr J. Biotechnol.* 8, 5901–5905. doi: 10.5897/AJB2009.000-9468

Zengin, G., Bulut, G., Mollica, A., Nancy Picot-Allain, C. M., and Mahomoodally, M. F. (2018). *In vitro* and in silico evaluation of Centaurea saligna (K.Koch) Wagenitz—An endemic folk medicinal plant. *Comput. Biol. Chem.* 73, 120–126. doi: 10.1016/j.compbiolchem.2018.02.010

frontiers | Frontiers in Plant Science

TYPE Original Research
PUBLISHED 21 November 2024
DOI 10.3389/fpls.2024.1491491

OPEN ACCESS

EDITED BY
Eman A. Mahmoud,
Damietta University, Egypt

REVIEWED BY
Porfirio Gutierrez-Martinez,
Instituto Tecnológico de Tepic, Mexico
Laura Santagostini,
University of Milan, Italy

*CORRESPONDENCE
Amr Farouk
af.mansour@nrc.sci.eg

RECEIVED 04 September 2024
ACCEPTED 29 October 2024
PUBLISHED 21 November 2024

CITATION
Gharzouli M, Aouf A, Mahmoud E, Ali H, Alsulami T, Badr AN, Ban Z and Farouk A (2024) Antifungal effect of Algerian essential oil nanoemulsions to control *Penicillium digitatum* and *Penicillium expansum* in Thomson Navel oranges (*Citrus sinensis* L. Osbeck). *Front. Plant Sci.* 15:1491491. doi: 10.3389/fpls.2024.1491491

Antifungal effect of Algerian essential oil nanoemulsions to control *Penicillium digitatum* and *Penicillium expansum* in Thomson Navel oranges (*Citrus sinensis* L. Osbeck)

Merihane Gharzouli[1], Abdelhakim Aouf[1], Engy Mahmoud[2], Hatem Ali[3], Tawfiq Alsulami[4], Ahmed Noah Badr[5], Zhaojun Ban[6] and Amr Farouk[2]*

[1]Laboratory of Applied Microbiology, Faculty of Natural and Life Sciences, University of Ferhat Abbas Setif1, Setif, Algeria, [2]Flavor and Aroma Chemistry Department, National Research Centre, Cairo, Egypt, [3]Food Technology Department, National Research Center, Cairo, Egypt, [4]Food Science and Nutrition Department, College of Food and Agricultural Sciences, King Saud University, Riyadh, Saudi Arabia, [5]Food Toxicology and Contaminants Department, National Research Centre, Cairo, Egypt, [6]Zhejiang Provincial Key Laboratory of Chemical and Biological Processing Technology of Farm Products, School of Biological and Chemical Engineering, Zhejiang University of Science and Technology, Hangzhou, China

Fungal infection is a potential issue in citrus fruits, while essential oils from *Cymbopogon citratus* and *Citrus limon* could be better alternatives to synthetic fungicides in orange preservation. The nanoparticles produced during ultrasonication exhibited a monomodal distribution of particle sizes with a mean zeta potential and a polydispersity index mean value of 74.12 nm, –38.4 mV, and 0.19 for *C. citratus* and 103 nm, –28.4 mV, and 0.22 for *C. limon*. The micrographs of the nanoemulsions exhibited spherical morphology with diverse nanometer-scale sizes. Nanoemulsification enhances the levels of neral and geranial in both oils while reducing the levels of limonene, γ-terpinene, and β-myrcene. The essential oils and their nanoemulsions exhibited good MIC values against Gram-positive and Gram-negative bacteria, ranging from 2% to 0.12%, while MBC was 4% to 0.25% (v/v) for both. The extended genetic investigation of the isolated fungal strains from Thomson Navel oranges through analysis of the ITS sequences and BLAST indicated 100% homology to those of *Penicillium digitatum* and *Penicillium expansum*. Both oils' MIC and MFC values and nanoemulsions ranged from 0.12% to 0.06% and 2% to 0.03% against *P. expansum* and *P. digitatum*, respectively. Applying nanoemulsified *C. limon* and *C. citratus* as a coating on orange fruits significantly reduced the spread of *P. expansum* and *P. digitatum* fungi compared to the control. Coating with

nanoemulsions reduced the negative changes in quality parameters during storage, such as weight loss, firmness, TSS, TA, pH, and ascorbic acid content. *Citrus limon* nanoemulsion did not alter the coated fruits' sensory attributes compared to *C. citratus* nanoemulsion.

KEYWORDS

Thomson Navel oranges, antimicrobial, lemongrass oil, lemon oil, *Penicillium digitatum*, *Penicillium expansum*

1 Introduction

Citrus fruits are one of the important crops economically for developing countries like Algeria and Egypt. In the 2023–2024 season, Egyptian orange production is expected to grow by 2.7% compared to the previous season, reaching 3.7 million tons, which accounts for 8% of the global production, according to the U.S. Department of Agriculture's Foreign Agricultural Service (USDA, 2024). On the other hand, in 2021, the total production of citrus fruits in Algeria exceeded 1.5 million tons, consumed domestically and exported (FAO, 2021). Citrus fruits rot due to mechanical injury, tissue senescence, and microbial infection during harvest, storage, and transit, causing major economic losses. The most destructive citrus fruit diseases are *Penicillium digitatum* and *Penicillium expansum* fungi (Vilanova et al., 2012). Fungi are a significant pathogenic factor for fruit infection, as they can secrete mycotoxins, which threaten the liver, immunological, neurological, and fertility systems (Lima et al., 2021). A previous investigation reported the presence of toxigenic fungi infection, with a prevalence of *P. digitatum* (Rovetto et al., 2023). Furthermore, patulin and rubratoxin B mycotoxins were found in fruits after being infected by such fungi.

Penicillium was a significant post-harvest infection reported to cause global decay in citrus fruits. Most *Penicillium* investigations have recently focused on treatments against infection symptoms, fungicide resistance, and antagonist microorganisms (Costa et al., 2019). Chemical fungicides are used for control, but long-term usage causes resistance, food safety, and environmental damage (Wuryatmo et al., 2014). Safe and natural antistaling treatments are needed to reduce citrus diseases and preserve fruit quality. Antifungal resistance is a concern in agriculture as there have been reports of resistance to the main fungicide groups (Brauer et al., 2019). In this context, investigations are focused on finding natural and safe antifungal alternatives to synthetic chemicals. Recently, neoteric peptides were reported to have a significant ability to limit fungal development and reduce their genetic capacity to produce harmful metabolites (Lima et al., 2021). Furthermore, anti-mycotoxigenic and anti-mycotoxin production was reported to be positively affected by essential oils as natural antifungals.

Essential oils of aromatic plants contain bioactive compounds with antibacterial and antioxidant properties and reduced toxicity, recommended as possible synthetic fungicide replacements (Maghenzani et al., 2018). For instance, essential thyme, savory, and oregano oils suppress the toxigenic fungal species of *P. expansum*-infected orange and lime (Buonsenso et al., 2023). Again, cinnamon and carvone-rich oils were found to be active in reducing *P. expansum* contamination during orange storage and were reported to have fungicidal activity (Combrinck et al., 2011; Lai et al., 2021). Also, a significant inhibition by cinnamon, dill, *Origanum*, ylang-ylang, patchouli, vetiver, and chamomile oils was reported against the toxigenic fungi of orange (Zulu et al., 2023). Finally, essential oils of biobased black caraway and anise possessed effective inhibition against toxigenic fungi in blood orange fruit (Aminifard and Bayat, 2018).

Lemongrass and lemon essential oils are safe extracts with practical food applications that could be recommended as alternatives to synthetic antifungal chemicals. They contain antifungal volatiles, recommended for their potential post-harvest decay controls. Lemongrass oil exhibited antibacterial, antifungal, and anti-aflatoxigenic properties (Boudechicha et al., 2023). A significant antifungal activity against *P. digitatum* using ponkan mandarin citral was reported (Fan et al., 2014). Also, an *in-vitro* investigation showed that lemon and lemongrass oils positively affected *P. expansum* (Kgang et al., 2022). However, the essential oils' short persistence, volatility, low solubility, and formulation difficulties restrict their use. Recent investigations are focused on their nanoemulsion applications to boost their utilization. Encapsulated essential oils in polymer matrixes inhibit *Aspergillus carbonarius*, increasing grape shelf life (Dhanasekaran et al., 2024). In the same line, *Citrus sinensis* L. oil nanoemulsion showed potential antifungal activity against *Aspergillus flavus*, *A. niger*, and *A. ochraceus* (Farouk et al., 2022), where its principal constituent, limonene, in collaboration with eugenol nanoemulsion, revealed the same on *Penicillium italicum* (Li et al., 2021).

Because of Egypt and Algeria's economic dependence on citrus crops, this study examined the antibacterial and antifungal properties of lemongrass and lemon essential oils and their nanoemulsions against *P. digitatum* and *P. expansum* from decaying orange fruits. A low-energy preparation of coarse emulsion was followed by ultrasonication to create a nanoemulsion with Tween 80. We measured physicochemical factors for fruit quality. The pilot investigations on Thomson Navel oranges suggest using these nanoemulsions in edible

coating films. In addition to the *in-vitro* nanoemulsion tests, the significant phytochemicals in both oils were docked with enzymes and target proteins involved in fungal metabolic processes to determine a possible mechanism of action for the antifungal effect.

2 Materials and methods

2.1 Chemicals and plants

All chemicals applied in this investigation were of HPLC grade and purchased from Sigma-Aldrich, Saint Louis, MO, USA. The lemon fruits, scientifically called *Citrus limon*, were supplied by a local market in Setif, Algeria. *Cymbopogon citratus* were collected from Bou Saada, 245 km south of Algiers, Algeria. Following identifications by a botanist at the Department of Biology and Plant Ecology, Setif-1 University, Algeria, a voucher specimen validating the plants' identity was placed in our laboratory herbarium, and the Algerian numbers CAS09/01/23 (for *C. limon*) and CAS28/06/21 (for *C. citratus*) were assigned. Then, the collected plant material was air-dried at ambient room temperature in shaded conditions. Thomson Sweet oranges were purchased from a local Setif, Algeria market in December 2023.

2.2 Essential oil extraction

Essential oils were extracted using hydrodistillation with a Clevenger apparatus. Fresh peels from *C. limon* and leaves of *C. citratus* (100 g each) were boiled separately with distilled water for 3 h. The oil phase was condensed, and the essential oils were extracted, dried with anhydrous sodium sulfate, and stored in airtight glass vials sealed with aluminum foil at −20°C until analysis. This process was repeated three times (Boudechicha et al., 2023).

2.3 Nanoemulsion formulation

The initial step involved preparing a coarse emulsion by mixing the organic phase of the essential oil and a surfactant (Tween 80) (4:1; v/v) using a stirrer (37°C/2 h). Next, the organic phase was added drop by drop to double-distilled water while continuously stirring it using a magnetic stirrer. Then, the formed emulsion was subjected to ultrasonic emulsification using a probe sonicator (Ultrasonic Microprocessor VCX 500, Fisher Scientific, Loughborough, UK) with a power of 250 W. Before the ultrasonic treatment, the samples were chilled to 4°C and kept on ice throughout the sonication process (Patel and Ghosh, 2020).

2.4 Nanoparticle characterization

The stability of the nanoemulsions was checked by centrifugation (3,500 rpm/30 min) to observe the separation phase (Sigma 3-18KS, Osterode am Harz, Germany). The separation percentage was calculated as:

$$\%\ Separation = (SAPW/TEW) \times 100$$

Where,

SAPW = separated aqueous phase weight and

TEW = total nanoemulsion weight.

The particle size distribution, polydispersity index (PDI), and ξ-potential of the nanoemulsion samples were measured using a Zetasizer Nano ZS (Nano-S90, Malvern Panalytical Ltd., UK) at a temperature of 25°C ± 0.1°C. Deionized water was used for dilution to prevent multiple scattering effects. The morphology of nanoemulsions was analyzed (Boudechicha et al., 2023) using transmission electron microscopy (TEM) at 160 kV operation (JEOL Ltd., Tokyo, Japan).

2.5 Gas chromatography-mass spectrometry

Gas chromatography-mass spectrometry (GC-MS) analysis reveals the effect of homogenization on the profile and constituents of essential oils. After mixing with diethyl ether, vortexing, and drying over anhydrous sodium sulfate, the nanoemulsion was transferred to a screw-cap vial for analysis. The extraction process was repeated thrice. Separation of the oils and nanoemulsion volatiles was carried out by using GC (Agilent 8890 System) coupled with an MS (Agilent 5977B GC/MSD) equipped with an HP-5MS capillary column (30 m, 0.25 mm i.d., 0.25 mm film thickness). The sample size injected was 1 µL at 230°C in a split mode (1:50). The oven was initially set at 50°C, raised at a rate of 5°C/min to 200°C and then from 200°C to 280°C at a rate of 10°C/min, and kept isothermal for 7 min. Mass spectra in electron EI mode were obtained at 70 eV, and the *m/z* ranged from 39 to 500 amu. Peaks were identified by comparing them to NIST, standards, and published data. Percentages of detected compounds were calculated using GC peak areas. Kovats index of each compound was determined using retention times of C_6–C_{26} n-alkanes and compared to literature values (Himed et al., 2016; Boudechicha et al., 2023).

2.6 *In vitro* antimicrobial activity of essential oils and their nanoemulsions

2.6.1 Microorganisms

The antibacterial activity was carried out on Gram-positive and Gram-negative bacterial strains procured from the Laboratory of Applied Microbiology at Ferhat Abbas University in Setif, Algeria. Gram-positive strains consisted of *Staphylococcus aureus* (ATCC 25923) and *Bacillus subtilis* (ATCC 6633). Gram-negative strains were *Escherichia coli* (ATCC 25922), *Salmonella typhimurium* (ATCC 14028), *Klebsiella pneumoniae* (ATCC 13883), and *Pseudomonas aeruginosa* (ATCC 27853). The evaluation of antifungal activity was performed on *A. niger* ATCC 16888, *A. flavus* ATIM 698, *Fusarium culmorum* KF91, and *Candida albicans* ATCC 10231 obtained from the National Research Centre, Egypt, in addition to isolated strains of *P. expansum* and *P. digitatum* retrieved from decaying orange fruits. The *Penicillium* strains

were cultured on potato dextrose agar (PDA) medium at a temperature of 25°C/5 days; after purification and macroscopic and microscopic identification at the Laboratory of Applied Microbiology, Algeria, the fungi were identified through molecular means by Gene Life Science in Algeria.

2.6.2 Molecular characterization

Genomic DNA was extracted from fungal mycelium using the NucleoSpin Plant II kit (Macherey-Nagel, Germany). PCR amplification targeted the ITS, Ef1, BT, and LSU rDNA regions. For ITS, primers ITS1 and ITS4 were used with an annealing temperature of 55°C to get fragments at the expected size of 600 bp (Gardes and Bruns, 1993). For Ef1, primers EF-728F and EF-2 were employed at a temperature of 52°C to amplify fragments at the predicted size of 450 bp (Carbone and Kohn, 1999). The PCR mixture included ultrapure water, Taq buffer (Promega, Madison, Wisconsin, USA), $MgCl_2$ (25 mM), dNTPs (25 mM), forward and reverse primers (10 µM each), and Taq polymerase (Promega), and genomic DNA was added. Thermal cycling comprised an initial denaturation at 95°C for 5 min, followed by 35 cycles of denaturation at 95°C for 30 s, annealing at 55°C–52°C for 30 s, and extension at 72° C for 45 s, with a final extension at 72°C for 7 min. PCR products were visualized on a 1.5% agarose gel stained with GelRed (Biotium, USA) and imaged under UV light using a Bio-Rad Gel Doc system (USA). Purification of the PCR products was done using the NucleoSpin Gel and PCR Clean-up kit (Macherey-Nagel, Germany) and sequenced via the Sanger method (Sanger et al., 1977) using the BigDye v3.1 kit, with sequences analyzed using the ChromasPro software and compared to the GenBank database using the NCBI BLAST program for identification.

2.6.3 Disk diffusion assay

The antimicrobial activity and nanoemulsions of the essential oils were evaluated using a slightly modified agar disk diffusion method (Micić et al., 2021). Bacterial and fungal suspensions were spread on agar plates. Paper disks soaked with essential oils and nanoemulsions were placed on the plates alongside positive controls (ceftriaxone and amphotericin B). After incubation, inhibition zones were measured. Each experiment was conducted in triplicate.

2.6.4 Determination of minimum inhibitory concentration

The minimum inhibitory concentration (MIC) was determined using the microdilution method on a 96-well microplate following the CLSI, C. S. M (2018). Essential oils and nanoemulsions were diluted to achieve 4% to 0.01% v/v concentrations. The MIC for bacteria and fungi was evaluated using serial dilutions in a 96-well microtiter plate. The microplates were then incubated, and MICs were determined using tetrazolium chloride as a viability indicator for bacteria.

2.6.5 Determination of minimum bactericidal and fungicidal concentrations

To determine minimum bactericidal (MBC) and minimum fungicidal (MFC) concentrations, an aseptic aliquot was collected from the cultures in wells with no visible turbidity, transferred to agar media, and incubated for 24 h at 37°C for bacteria and 5 days for fungi. All the tests were performed in triplicates (Boudechicha et al., 2023).

2.7 *In vivo* antifungal assay

With minor modifications, the technique of OuYang et al. (2020) was applied to disinfect fruits and artificially infect them with *P. digitatum* and *P. expansum* before the treatment with nanoemulsions. Orange fruits were selected based on size, color uniformity, and minimal surface injuries. These selected oranges were then subjected to disinfection using sodium hypochlorite solution (2%) for 2 min, followed by two washes with distilled water; the oranges were then left to air dry overnight. Subsequently, the oranges were divided into two treatment groups: T1 with *C. citratus* nanoemulsion and T2 with *C. limon* nanoemulsion, and a control group was treated with distilled water. Each treatment group was divided into four subgroups. In the first subgroup, oranges were treated with the respective nanoemulsions using the dipping method for 2 min.

In contrast, the second and the third subgroups were artificially infected with 15 µL of 10^5 (spores/mL) sporal suspension of *P. digitatm* and *P. expansum*, respectively. After inoculation, the second and third subgroups were left to air dry for 24 h before being immersed in nanoemulsions. The fourth subgroup served as the control and was also wounded with a similar spore suspension of *P. digitatum* and *P. expansum*, along with treatment with distilled water. All treated orange fruits were stored in clear plastic boxes at room temperature for 21 days.

2.8 Evaluation of fruit quality

Five fruits were weighed at the beginning of storage and labeled as W1 for each treatment. These same fruits were reweighed after 21 days and marked as W2. The weight loss as a percentage was calculated using the following formula (Motamedi et al., 2018):

$$\textbf{\textit{weight loss}}\ (\%) : \frac{\sum_{i=1}^{n} \frac{w1-w2}{w1}}{n} \times 100$$

The fruit samples were collected from each replicate and then juiced using a hand-press juicer. The total soluble solids (TSS, %), total acidity (TA, %), and pH were measured on both the first day (day 1) and the last day of 21 days of storage (Ncama et al., 2017). The TSS content of the juice was determined using a handheld manual refractometer, measuring in degrees Brix, and pH was measured using a pH meter. Simultaneously, TA was expressed as a percentage (%) of citric acid, measured via titration with 0.1 N of sodium hydroxide to reach pH 8.2, following the given formula:

$$\textit{TA}(\%) = \frac{(0.0064)(\textit{volume of NaOH in ml})}{10\textit{ml}\ (\textit{juice})} \times 100$$

Fruit firmness was determined for three fruits of each replication using a Brookfield CT3 Texture Analyzer (AMETEK

Brookfield, Middleboro, MA, USA) fitted with a 3R probe. The iodometric titration method was used to determine the ascorbic acid content of fruit juice, which was expressed as the amount of ascorbic acid (mg) per 100 mL of juice (Motamedi et al., 2018).

2.9 Sensory analysis

On both day 1 and day 21, four coated oranges from each treatment and oranges from the control group that showed no fungal growth were chosen and sliced into several pieces for sensory evaluation. A group of 12 panelists from the Faculty of Natural and Life Sciences, University of Ferhat Abbas Setif1 in Setif, Algeria (10 men and 10 women), were selected to evaluate the quality attributes of the fruits, including color, aroma, flavor, and overall acceptance. This assessment was conducted using a scale with endpoints at 0 and 5. For the color, the range was from pale yellow (0) to dark orange (5), while aroma and flavor were rated on a scale ranging from weak (0) to vigorous (5). Ultimately, a hedonic scale was implemented to evaluate overall preference, ranging from dislike extremely (0) to like extremely (5), as previously referenced (Radi et al., 2018).

2.10 Statistical analysis

GraphPad Prism (GraphPad Software Inc., San Diego, CA, USA) and Microsoft Excel were used for statistical analysis and graphing. Results are shown as means ± standard deviations (SD) from three replicates. ANOVA and Tukey's multiple range tests assessed differences between mean values, with $P \leq 0.05$ indicating significance.

3 Results

3.1 Effect of nanoformulations on the compositions of essential oils

The yields of the hydrodistilled essential oils were 1.45% ± 0.04% and 1.25% ± 0.03% for *C. citratus* and *C. limon*. The identification of chemical composition using GC-MS revealed the presence of 21 constituents in *C. citratus* oil, representing 99.56% of the total volatile content (Table 1; Figure 1A). Neral and geranial were the predominant compounds, with 27.97% and 31.7%,

TABLE 1 Volatile constituents' identification of *Cymbopogon citratus* and *Citrus limon* oils and their nanoemulsions using GC-MS.

S/N	Compound	RI[a]	LRI[b]	Area %				Identification[c]
				C. citratus oil	*C. citratus* nanoemulsion	*C. limon* oil	*C. limon* nanoemulsion	
1	α-Pinene	942	939	–	–	1.88	–	RI, MS, STD
2	Sabinene	978	975	–	–	0.92	–	RI, MS
3	6-Methyl-5-heptene-2-one	983	985	1.27	0.77	–	–	RI, MS
4	*β*-Myrcene	992	991	9.64	1.29	3.46	–	RI, MS, STD
5	Octanal	1,001	998	–	–	0.42	–	RI, MS
6	3-Carene	1,013	1,011	–	–	0.29	–	RI, MS
7	*Z*-*β*-Ocimene	1,040	1,037	0.25	–	–	–	RI, MS
8	*E*-*β*-Ocimene	1,051	1,050	0.57	–	–	–	RI, MS
9	Rose furan	1,063	1,065	0.42	–	–	–	RI, MS
10	*p*-Cymene	1,025	1,024	–	–	4.27	1.29	RI, MS, STD
11	D-Limonene	1,031	1,029	–	–	61.8	35.59	RI, MS, STD
12	γ-Terpinene	1,058	1,059	–	–	7.77	1.74	RI, MS, STD
13	Linalool	1,100	1,096	2.46	2.31	0.75	1.42	RI, MS, STD
14	*cis*-Limonene oxide	1,136	1,134	–	–	0.66	1.45	RI, MS
15	*trans*-Limonene oxide	1,143	1,142	–	–	0.33	0.63	RI, MS
16	Isocitral (exo-)	1,147	1,144	0.31	–	–	–	RI, MS
17	Isoneral	1,171	1,170	2.63	0.85	–	–	RI, MS
18	Rose furan oxide	1,180	1,177	1.64	1.48	–	–	RI, MS
19	Isogeranial	1,189	1,185	3.45	1.79	–	–	RI, MS, STD
20	Estragole	1,199	1,196	0.63	2.92	–	–	RI, MS, STD

(Continued)

10.3389/fpls.2024.1491491

TABLE 1 Continued

S/N	Compound	RI[a]	LRI[b]	Area %				Identification[c]
				C. citratus oil	*C. citratus* nanoemulsion	*C. limon* oil	*C. limon* nanoemulsion	
21	Decanal	1,203	1,201	–	–	0.38	–	RI, MS
22	Rose ether	1,221	1,223	–	1.79	–	3.81	RI, MS
23	Citronellol	1,228	1,225	0.64	0.63	–	–	RI, MS
24	Neral	1,240	1,238	27.97	33.58	7.89	24.77	RI, MS, STD
25	Carvone	1,245	1,243	–	–	–	1.43	RI, MS, STD
26	Geraniol	1,258	1,255	8.49	8.36	–		RI, MS, STD
27	Geranial	1,270	1,267	31.7	38.47	8.75	27.15	RI, MS, STD
28	Anethole	1,279	1,283	0.26	1.73	–	–	RI, MS, STD
29	Neryl formate	1,284	1,284	0.68	–	–	–	RI, MS
30	Nerolic acid	1,337	1,340	0.47	–	–	–	RI, MS
31	Geranyl acetate	1,384	1,383	5.25	4.03	–	–	RI, MS
32	Caryophyllene oxide	1,582	1,583	0.3	–	–	–	RI, MS
33	Selin-6-en-4α-ol	1,633	1,636	0.31	–	–	–	RI, MS
	Total	–	–	99.56	100	99.57	99.28	–

[a]RI, retention indices were calculated using the DB-5 column using alkane standards.
[b]LRI, retention indices according to the literature.
[c]Confirmed by comparison with the retention indices, the mass spectrum of the authentic compounds, and the NIST mass spectra library data.

respectively, followed by geraniol (8.49%), geranyl acetate (5.25%), and β-myrcene (9.64%). The nanoemulsion volatile pattern of the *C. citratus* oil showed the same trend with quantitative differences compared to the content of the raw oil (Table 1; Figure 1B). The same major components of the oil were identified as predominates in the nanoemulsion extract, except for β-myrcene, which dropped dramatically to 1.29%. The drop in the concentrations of many monoterpenes of the nanoemulsion like β-myrcene, linalool, isoneral, and isogeranial and the absence of others such as ocimene and rose furan were accompanied by an increase in neral (33.58%), geranial (38.47%), and estragole (2.92%), compared to the raw oil. The identified components in the nanoemulsion were represented in 100% of the total extract, with only 14 constituents.

On the other hand, only 14 compounds were identified in the *C. limon* oil, accounting for 99.57% of the total volatiles extracted. Limonene (61.8%), geranial (8.75%), neral (7.89%), and γ-terpinene (7.77%) were the main constituents of the oil (Table 1; Figure 1C). Increases were observed in the neral and geranial of the nanoemulsion (24.77% and 27.15%) at the expense of limonene and γ-terpinene, which showed a significant decline to 35.59% and 1.74%, with the absence of many monoterpenes identified in the oil like α-pinene, sabinene, β-myrcene, and 3-carene (Table 1; Figure 1D).

3.2 Nanoparticle characterizations

Table 2 presents the physical characteristics of the nanoemulsions formulated. The samples exhibited an average height ratio of 100%, indicating excellent stability with no apparent phase separation, creaming, or sedimentation. The nanoemulsions of *C. citratus* and *C. limon* had average particle sizes of 74.12 ± 2.33 nm and 103 ± 3.72 nm, respectively. They both exhibited a monomodal size distribution pattern, indicating their ultrafine sizes of less than 200 nm. The mean zeta potentials were −38.4 ± 1.45 mV and −28.4 ± 2.33 mV, as shown in Table 2. Additionally, the PDI demonstrated uniformity in dispersion, with mean values of 0.19 ± 0.04 and 0.22 ± 0.07 for both *C. citratus* and *C. limon* nanoemulsions (Supplementary Figure S1).

TEM was used to characterize the nanoemulsions of *C. citratus* and *C. limon*. The droplets were evenly distributed and appeared to darken, indicating a successful preparation. TEM micrographs revealed spherical nanoparticles with varying diameters in nanometers (Figures 2A, B).

3.3 Morphological and molecular identification of fungal isolates

A rigorous identification was undertaken upon macroscopic and microscopic examination of both fungal isolates obtained from orange fruits. It was found that both isolates belonged to the *Penicillium* genus based on their macroscopic features, such as color and consistency, along with microscopic observations of conidiophores and spores (Figures 3, 4). This process ensured the accuracy of our findings. The genetic investigation of the isolated fungal strains, designated as GY1 and GY2, involved examining the ITS and TEF1 sections, which had lengths of 660 bp and 450 bp,

10.3389/fpls.2024.1491491

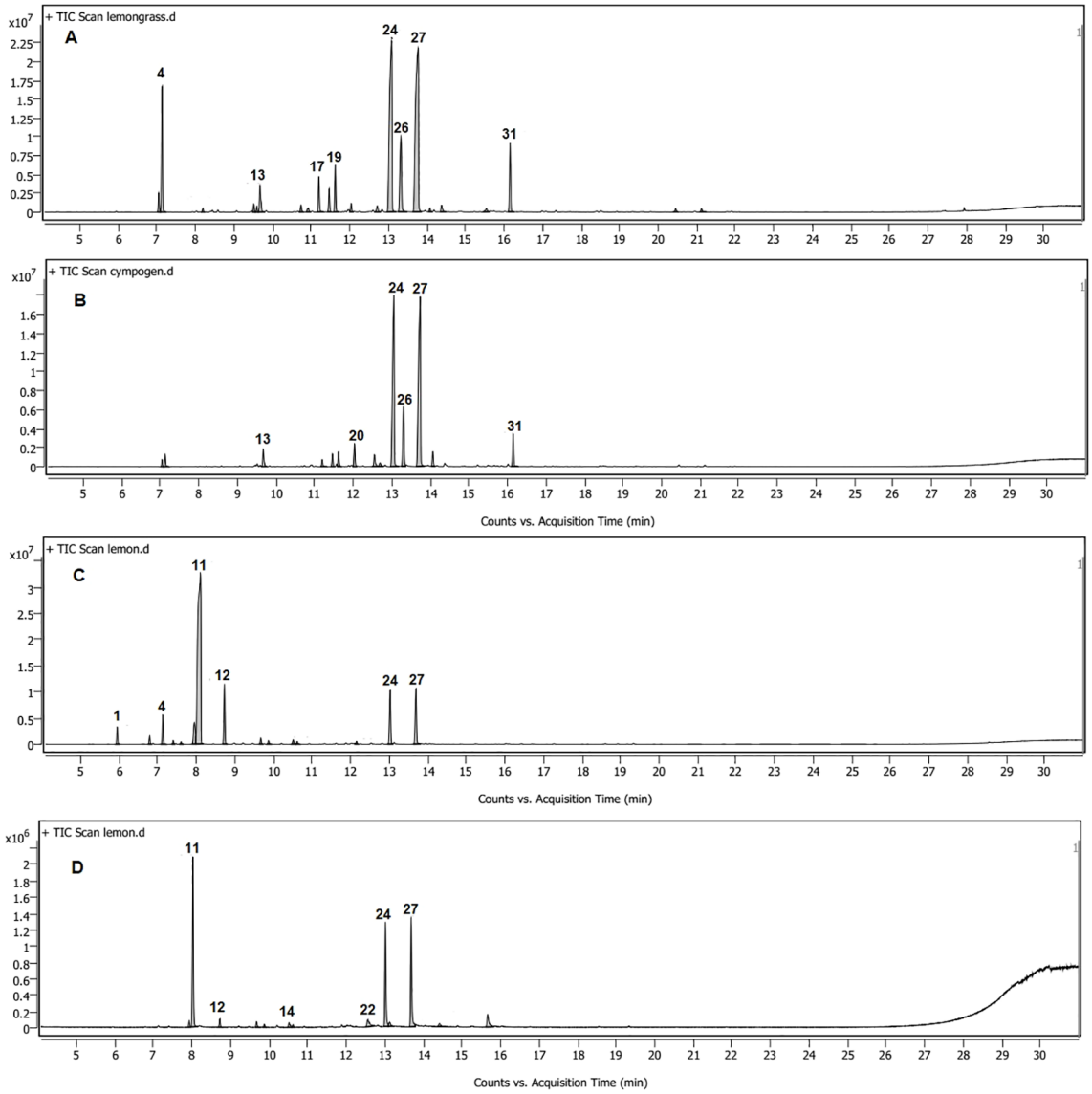

FIGURE 1
GC-MS chromatograms of *Cymbopogon citratus* oil **(A)** and its nanoemulsion **(B)** and *Citrus limon* oil **(C)** and its nanoemulsion **(D)**.

TABLE 2 Physical characterizations of the nanoemulsions.

Property	Value	
	C. citratus nanoemulsion	*C. limon* nanoemulsion
Refractive index	1.33 ± 0.004	1.472 ± 0.005
Density (g/mL)	0.96 ± 0.002	1.136 ± 0.005
pH	5.01 ± 0.008	5.47 ± 0.009
Stability (separation in mm)	ND	ND
Particle size (nm)	74.12 ± 2.33	103 ± 3.72
PDI	0.19 ± 0.04	0.22 ± 0.07
Zeta potential (mV)	−38.4 ± 1.45	−28.4 ± 2.33

ND, not detected.

respectively. The identification process involved doing a BLAST search against the GenBank database. The analysis of the ITS sequences indicated that strain GY1 displayed a 100% homology to both *P. italicum* and *P. expansum*, whereas strain GY2 showed a 99% similarity to *P. digitatum*. Further analysis using BLAST confirmed that GY1 corresponded to *P. expansum* (100% match), while GY2 was identified as *P. digitatum* (100% match).

3.4 *In vitro* antimicrobial activity of the oils and their nanoemulsions

3.4.1 Antibacterial effect

The antimicrobial activity of the essential oils and their nanoemulsions was tested using both disk diffusion and microdilution methods. The aforementioned disk diffusion method

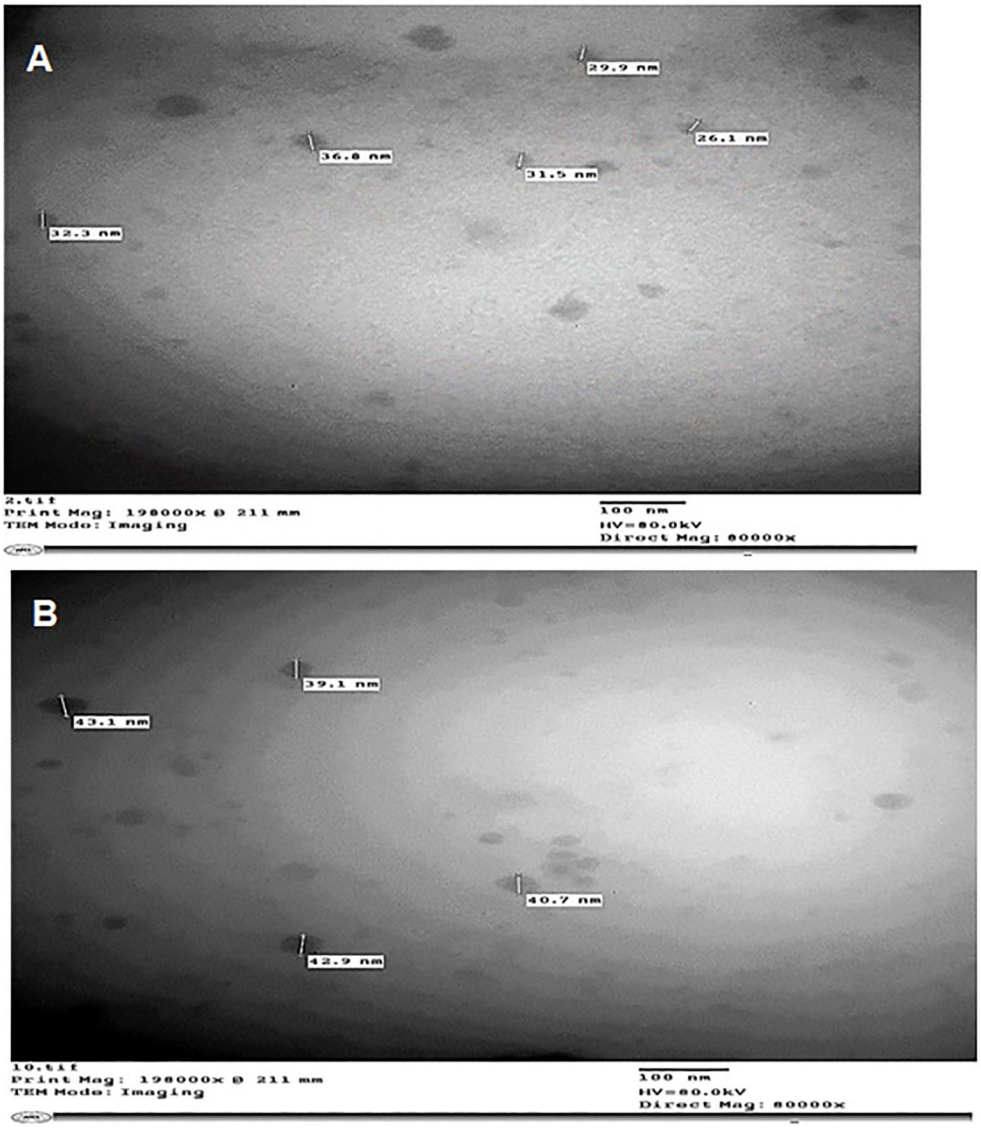

FIGURE 2
TEM micrograph of *C. citratus* **(A)** and *C. limon* **(B)** nanoemulsions.

showed that the tested essential oils and their nanoemulsions showed significant differences in antimicrobial activity against Gram-positive and Gram-negative bacteria (Figure 5).

The *C. limon* essential oil did not show activity against *P. aeruginosa* at 5 µL and 10 µL but exhibited moderate activity at 15 µL ($P \leq 0.05$), resulting in a 12.33 ± 2.08 mm inhibition zone. Its activity against *E. coli* was weak, with inhibition zones ranging from 8.67 ± 1.15 mm to 11.33 ± 0.57 mm. *Citrus limon* oil was not active against *S. typhimurium* or *B. subtilis* at 5 µL. However, it showed weak to moderate activity at 10 µL and 15 µL ($P \leq 0.05$) against *B. subtilis*, with inhibition zones of 10.66 ± 1.15 mm and 13 ± 1 mm. However, *C. limon* oil strongly affected *S. aureus*, with inhibition zones ranging from 25 ± 0 mm to 28.33 ± 2.88 mm (Figure 5). *Cymbopogon citratus* essential oil was the most active against all the tested strains in comparison with *C. limon*, especially against Gram-positive bacteria ($P \leq 0.05$), where it completely inhibits the growth of *S. aureus* and *B. subtilis*. In contrast, *C. citratus* oil showed weak to moderate activity against *P. aeruginosa*, with inhibition zone diameters ranging from 9 ± 1.73 mm to 11.67 ± 0.57 mm. For *K. pneumoniae* and *S. typhimurium*, the activity of *C. citratus* oil was moderate, with diameters of the inhibition zone spanning from 13.33 ± 1.53 mm to 15.33 ± 0.58 mm and 10.33 ± 0.57 mm to 14 ± 1.73 mm, respectively. Regarding *E. coli*, the activity was strong, with inhibition zone diameters varying from 17.67 ± 2.51 mm to 26.67 ± 2.89 mm (Figure 5).

The current study used the microdilution technique to determine the MIC and MBC of the oils and their nanoemulsions. The results are presented in Table 3. The essential oils exhibited good MIC values against both Gram-positive and Gram-negative bacteria, with MIC values ranging from 2% to 0.12%. The microdilution method showed better results than the disk diffusion method. Consistent with the previous results from the disk diffusion method, *C. citratus* oil displayed the best MIC values of 0.12% against *E. coli* and *K.*

10.3389/fpls.2024.1491491

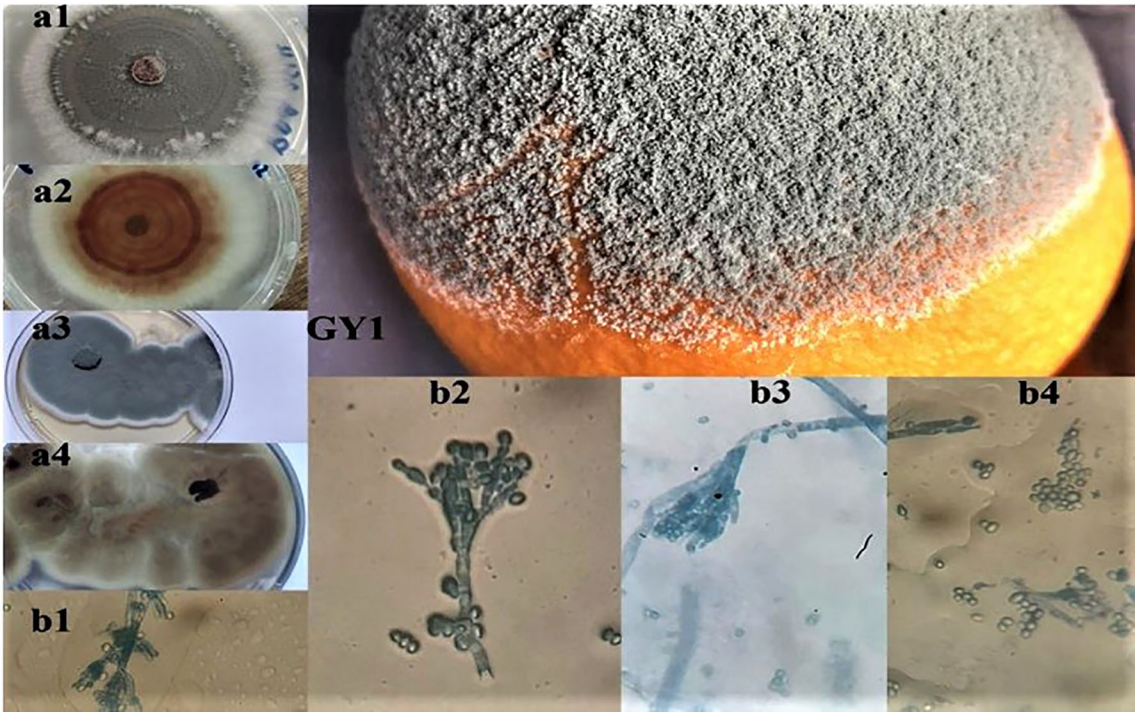

FIGURE 3
Macroscopic (a1, a2, a3, a4) and microscopic observations (b1, b2, b3, b4) of the isolated fungi (GY1) from decaying orange fruits, where (a1, a2) and (a3, a4) represent the aspect on PDA and Sabouraud media.

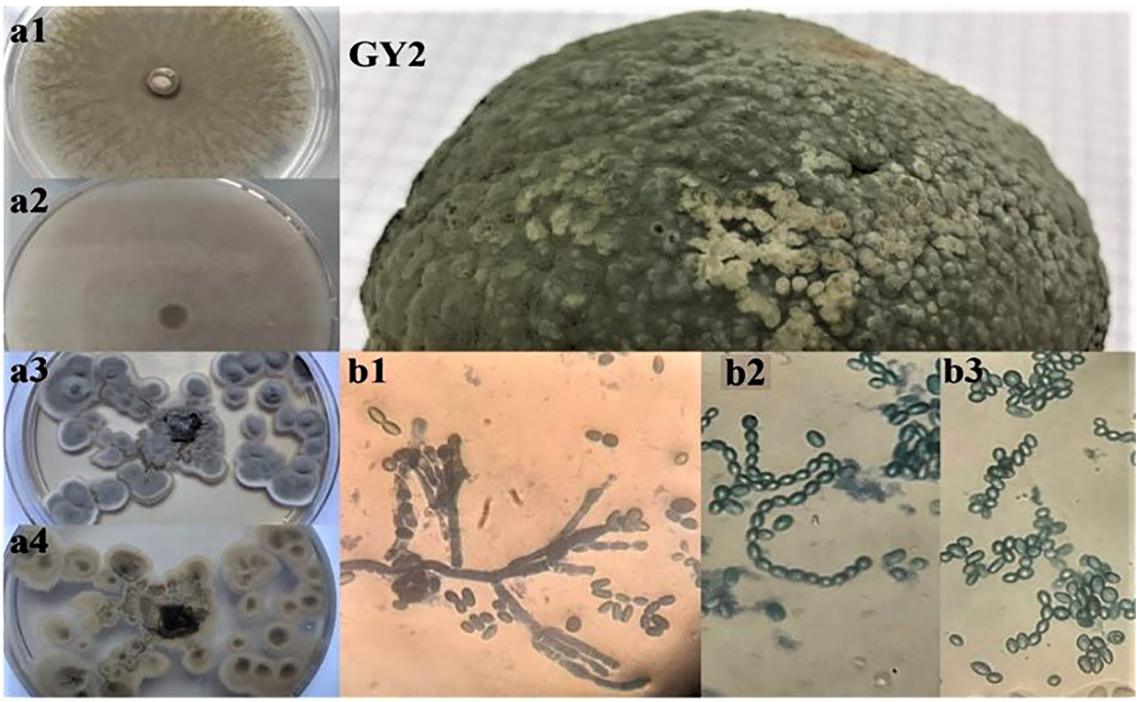

FIGURE 4
Macroscopic (a1, a2, a3, a4) and microscopic observations (b1, b2, b3) of the isolated fungi (GY2) from decaying orange fruits, where (a1, a2) and (a3, a4) represent the aspect on PDA and Sabouraud media.

10.3389/fpls.2024.1491491

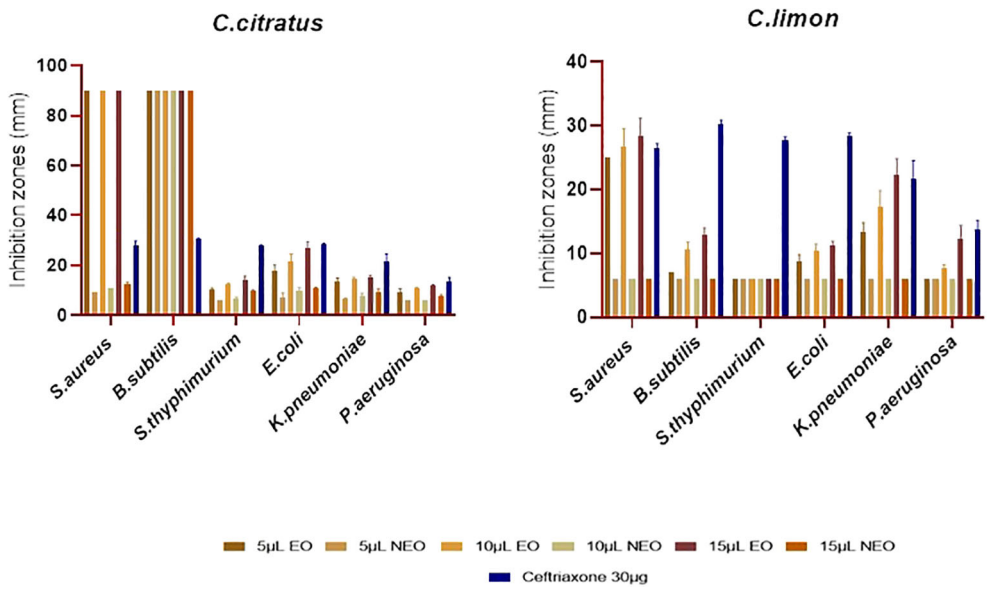

FIGURE 5
Antibacterial activity of *C. citratus* and *C. limon* essential oils and their nanoemulsions using disk diffusion assay, with ceftriaxone as the standard inhibitor, represented with error bars indicating ± standard deviation (n = 3).

pneumoniae and 0.25% against *S. aureus*, *B. subtilis*, and *P. aeruginosa*. The MIC values of *C. limon* oil were 0.5% against *S. aureus* and *P. aeruginosa*, 1% against *E. coli and K. pneumoniae*, and 2% against *B. subtilis* and *S. typhimurium* (Table 3).

Concerning the nanoemulsified essential oils, the antibacterial effectiveness was lower than essential oils, indicating that nanoemulsification does not necessarily improve the antimicrobial activity of essential oils (Figure 5). As previously mentioned, *C. citratus* essential oil was the most active; it was noted that the more highly effective the essential oil was, the more effective its nanoemulsion was; however, this does not necessarily apply to all the essential oils. It is worth shedding light on the resistance of *P. aeruginosa* to all the nanoemulsions. For *Salmonella*, *C. citratus* nanoemulsion was active only at 15 µL ($P > 0.05$), with inhibition zones of 9.67 ± 0.58 mm. For *E. coli*, the nanoemulsified *C. citratus* showed inhibition zones of 10 ± 1 mm and 10.67 ± 0.47 mm at 10 µL and 15 µL, respectively, and 9 ± 0 mm to 12.67 ± 0.58 mm against *S. aureus*. In contrast, it inhibits the growth of *B. subtilis* ($P \leq 0.05$). On the other hand, *C. limon* nanoemulsion was inefficient against all the bacterial strains. Regarding the outcomes of the microdilution method, *C. citratus* nanoemulsion exhibited strong activity compared to *C. limon* nanoemulsion, which was not active against all the strains (Table 3).

The MBC results ranged from 2% to 0.25% (v/v) for the free essential oils and from 4% to 0.5% (v/v) for *C. citrus* nanoemulsion (Table 3). These results demonstrated that the nanoemulsification process did not significantly enhance the bactericidal efficacy of the essential oils.

3.5 Antifungal effect

The antifungal activity of the previous essential oils and their nanoemulsions was evaluated against the most important pathogenic fungi, including *A. niger*, *A. flavus*, *P. digitatum*, *P. expansum*, *F. culmorum*, and *C. albicans* (Figure 6). Notably, the

TABLE 3 MIC and MBC determinations of *Cymbopogon citratus* and *Citrus limon* essential oils and their nanoemulsions against bacteria.

Strain	*C. citratus* oil		*C. limon* oil		*C. citratus* nanoemulsion		*C. limon* nanoemulsion	
	MIC (%)	MBC (%)	MIC (%)	MBC (%)	MIC (%)	MBC (%)	MIC (%)	MBC (%)
S. aureus ATCC 25923	0.25	0.25	0.5	0.5	0.25	0.5	–*	–
B. subtilis ATCC 6633	0.25	1	2	2	0.25	2	–	–
S. typhimurium ATCC 14028	0.5	2	2	2	2	4	–	–
E. coli ATCC 25922	0.12	0.25	1	1	0.25	2	–	–
K. pneumoniae ATCC 13883	0.12	0.25	1	1	0.25	2	–	–
P. aeruginosa ATCC 27853	0.25	2	0.5	2	0.25	4	–	–

*not detected.

10.3389/fpls.2024.1491491

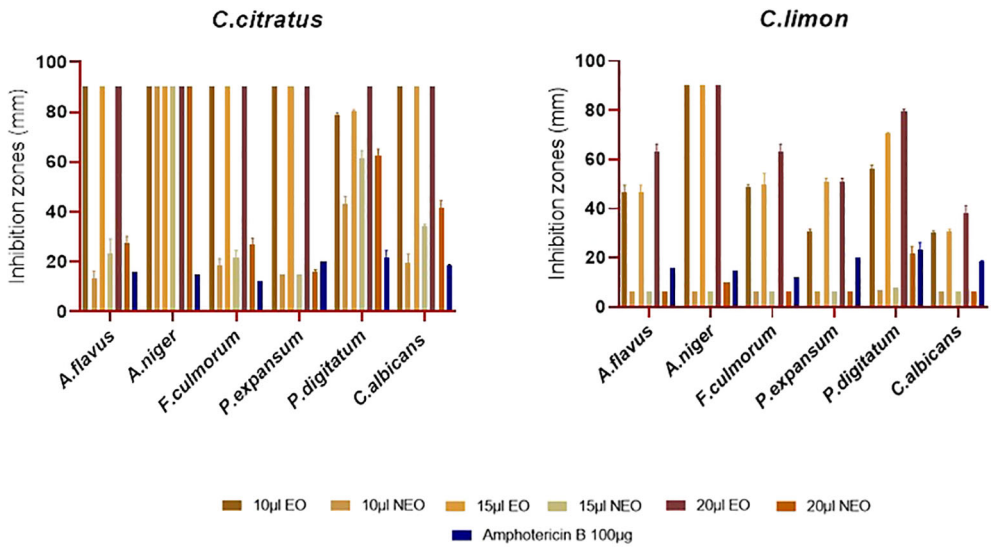

FIGURE 6
Antifungal activity of *C. citratus* and *C. limon* essential oils and their nanoemulsions using disk diffusion assay, with amphotericin B as the standard inhibitor, represented with error bars indicating ± standard deviation (n = 3).

essential oils and their nanoemulsions showed better antifungal activity than antibacterial activity. Consistent with the results obtained from the antibacterial assay, *C. citratus* essential oil had the highest level of potency, with complete inhibition of *A. niger*, *A. flavus*, *F. culmorum*, *P. expansum*, and *C. albicans*. Additionally, it showed very potent activity to total inhibition against *P. digitatum*, with inhibition zones ranging from 78.66 ± 1.15 mm to 90 ± 0.00 mm. Besides *C. citratus*, *C. limon* essential oil exhibited potential antifungal activity with inhibition zones spanning from 30.33 ± 0.57 mm to total inhibition (Figure 6).

The microdilution outcomes offered potent antifungal activity of the tested essential oils. *Cymbopogon citratus* displayed the highest activity, with MIC values of 0.03% (v/v) against both *P. digitatum* and *A. niger*. Meanwhile, it was 0.06% (v/v) against *F. culmorum*, *P. expansum*, and *C. albicans*. *Citrus limon* EO showed MIC values of 0.12% (v/v) against *P. expansum* and *C. albicans* and 0.25% (v/v) and 0.03% (v/v) against *A. flavus* and *P. digitatum*, respectively. The MIC value against *A. niger* and *F. culmorum* was 0.06% (v/v) (Table 4).

Concerning the results of the antifungal activity of the nanoemulsified essential oils, *C. citratus* displayed inhibition zones ranging from 15 ± 0 mm to 15.66 + 1.15 mm against *P. expansum*, the most resistant strain against the tested nanoemulsions. In addition, it showed inhibition zones ranging from 43.33 ± 2.88 mm to 62.66 ± 2.51 mm and from 19.66 ± 3.15 mm to 41.66 ± 2.88 mm against *P. digitatum* and *C. albicans*, respectively; additionally, it completely inhibited *A. niger*. The activity of the nanoemulsion of *C. limon* nanoemulsion was only active at 20 µL against *P. digitatum and A. niger* with inhibition zones of 21.66 ± 2.88 mm and 10 ± 0 mm, respectively. Notably, it was noted that the efficacy of *C. limon* nanoemulsion increased significantly with the increase in the dose ($P \leq 0.05$). In contrast, no activity was exercised by *C. limon* nanoemulsion against *P. expansum*, *F. culmorum*, *A. flavus*, and *C. albicans* (Figure 6). Regarding the MIC values, *C. citratus*

TABLE 4 MIC and MFC determination of *Cymbopogon citratus* and *Citrus limon* essential oils and their nanoemulsions against fungi.

Strain	*C. citratus* oil		*C. limon* oil		*C. citratus* nanoemulsion		*C. limon* nanoemulsion	
	MIC (%)	MFC (%)	MIC (%)	MFC (%)	MIC (%)	MFC (%)	MIC (%)	MFC (%)
A. flavus ATIM698	0.12	0.12	0.25	0.25	1	1	4	4
A. niger ATCC16888	0.03	0.06	0.06	0.06	0.25	0.25	4	4
F. culmorum KF91	0.06	0.06	0.06	0.06	0.12	0.12	4	4
P. expansum	0.06	0.06	0.12	0.12	0.12	0.12	0.12	0.12
P. digitatum	0.03	0.03	0.03	0.03	0.03	0.03	2	2
C. albicans ATCC 10231	0.06	0.06	0.12	0.12	0.12	0.12	–*	–

*not detected.

nanoemulsion was the most effective, showcasing MIC values of 0.12% (v/v) against *P. expansum*, *F. culmorum*, and *C. albicans*; values of 0.03% (v/v) and 0.25% (v/v) against *P. digitatum* and *A. niger*, respectively; and 1% (v/v) against *A. flavus*. *Citrus limon* nanoemulsion displayed a weaker activity against *A. flavus*, *A. niger*, and *F. culmorum*, showing values of 4% (v/v), with no activity against *C. albicans*. On the contrary, its activity was better against *P. expansum* and *P. digitatum*, with values of 0.12% (v/v) and 2% (v/v), respectively (Table 4).

On the other hand, the MFC outcomes were significantly varied, ranging from 0.25% to 0.03% (v/v) for the essential oils and from 4% to 0.03% (v/v) for their nanoemulsions (Table 4). This variation suggests that nanoemulsification might affect the fungicidal activity of the essential oils more than their bactericidal activity. Overall, the variability in MBC and MFC outcomes between free and nanoemulsified essential oils indicates that the nanoemulsification process may have differing impacts on their antimicrobial properties.

3.6 *In vivo* antifungal activity of the oil nanoemulsions

Our study demonstrated the effectiveness of nanoemulsified *C. limon* and *C. citratus* coatings in preventing fungal growth on orange fruits. On the 7th day, no fungal growth was observed in the coated fruits, while the control group displayed slight mold occurrence and dark spots on the orange peel. On the 15th day, no signs of fungal growth were observed within the coated samples, except for slight drying, color alterations, and darkening in *C. citratus*-coated fruits (Figure 7A). On day 7, inoculated fruits with *P. digitatum* showed fungal growth in wounded spots of the coated fruits, with the control group showing a higher occurrence. On day 15, the coated samples exhibited fungus spread in the same oranges, while the control group was infected entirely. On day 21, no considerable difference was observed compared to day 15, indicating that the fungal progression remained constant (Figure 7B). Regarding the samples inoculated with *P. expansum*, on day 7, no growth was observed in the coated samples, with moderate growth in the control group. However, slight drying and color alterations were noticed on the fruit's outer peel in samples coated with *C. citratus*. On day 15, the coated samples showed moderate *Penicillium* growth compared to the control. On day 21, the coated samples exhibited noticeable fungal proliferation within the fruit, with important dissemination in the control group (Figure 7C).

3.7 Assessment of fruit quality

After a storage period of 21 days, differences in physicochemical parameters were observed between the coated and control orange fruits, as seen in Figure 8. The weight loss analysis outcomes conducted over 3 weeks at room temperature revealed a weight reduction within all the treatments accompanied by notable dehydration, with no significant differences ($P > 0.05$). The highest loss (4.13% and 4.14%) was recorded in the control and the fruits coated with *C. citratus* nanoemulsion; however, fruits treated with *C. limon* nanoemulsions displayed a relatively moderate weight loss, with values of 3.52%, respectively (Figure 8A). The TSS percentage varied among treatments and the control group. After 21 days of storage, the TSS level increased for the coated oranges, with 13.66°Brix and 13.33°Brix for the *C. citratus* and C. *limon* nanoemulsion-coated samples, respectively. However, no significant difference existed between treatments ($P > 0.05$), as shown in Figure 8B. The pH values exhibited no significant difference ($P > 0.05$) in all treatments, indicating a minor increase, with the most notable decrease in uncoated fruits (Figure 8D). The TA percentage declined in the fruits treated with *C. citratus* nanoemulsion, in comparison to those coated with *C. limon* nanoemulsion and the control group. Overall, there was no significant difference ($P > 0.05$) in TA % in all the treatments (Figure 8C). In all treatments, fruit firmness decreased with the advancement of the storage period (Figure 8E). On the day of the experimental setup, fruit firmness was between 24.65 and 27.30 N. On the 21st day after storage, fruit firmness decreased, with the highest firmness observed in *C. limon* nanoemulsion-coated samples (20.83 N), followed by *C. citratus* nanoemulsion (18.01 N) and the control fruits (17.26 N). In agreement with the above findings, the ascorbic acid content decreased significantly after the storage period for both treated and untreated fruits (Figure 8F).

3.8 Sensory evaluation

The sensory evaluation of orange fruits was evaluated on the first day (day 1) and the last day of storage (day 21). The results revealed no significant differences between the coated samples and the control group on the first day of coating. In this study, the highest scores were achieved regarding color and aroma. On day 21, the control and coated samples with *C. limon* were the best, especially in texture, juiciness, and appearance, without significant differences, followed by fruits coated with *C. citratus* nanoemulsion. At the end of storage, all treatments slightly decreased the taste and flavor, especially in *C. citratus* nanoemulsion-coated samples, which displayed a darkening skin appearance, and an off-flavor, with alcoholic and fermented tastes. The nanoemulsions were acceptable except for *C. citratus* nanoemulsion (Figure 9; Supplementary Figure S2).

4 Discussion

Recent studies have found that aromatic plants like *C. citratus* and *C. limon* have antifungal effects in food, pharmaceutical, and other applications. Enhancing plant extracts using nanoformulations can improve their antifungal efficiency (Medeleanu et al., 2023). The yields of the current study agreed with previous research on *C. citratus* and *C. limon* essential oils (Himed et al., 2019; Medeleanu et al., 2023). The extraction method and environmental

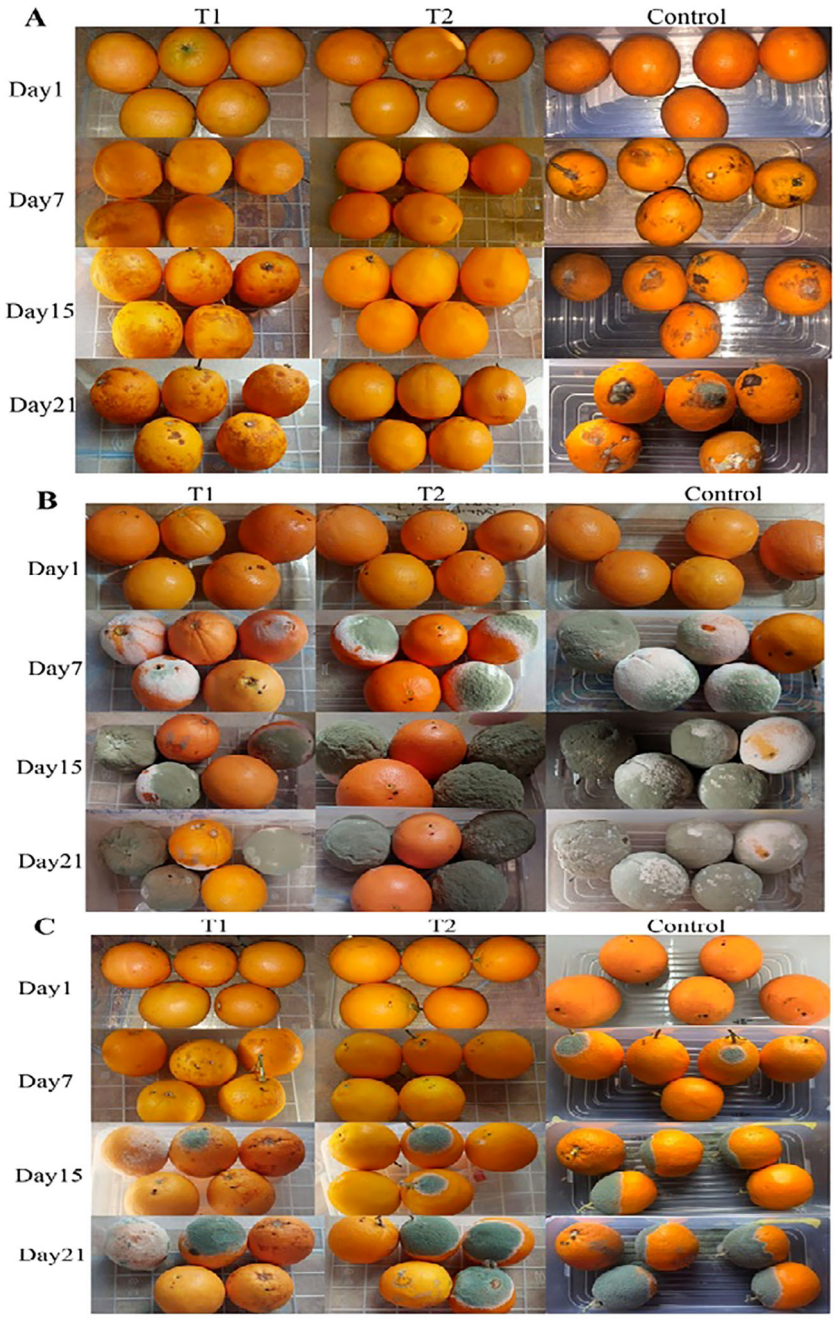

FIGURE 7
In-vivo antifungal activity of *C. citratus* (T1) and *C. limon* (T2) nanoemulsions during storage for 21 days **(A)**, after inoculating fruits with *P. digitatum* **(B)**, and after inoculating with *P. expansum* **(C)** compared to a control group.

factors can affect the oil's yield, quality, and composition. For example, *C. citratus* cultivated in Blida, Algeria, yielded 0.6% (Boukhatem et al., 2014), and the Lisbon variety of *C. limon* showed 0.81% (Himed et al., 2016).

The volatile profile of *C. citratus* oil in the current study is in line with Boudechicha et al. (2023), where neral, geranial, β-myrcene, geraniol, and geranyl acetate were the predominates but with some quantitative differences. For example, β-myrcene followed geranial and neral concentrations, which agreed with Blida oil (Benoudjit et al., 2022). On the other hand, limonene was the major component of *C. limon*, according to Himed et al. (2016) and Kehal et al. (2023). However, the dominance of neral, geranial, and γ-terpinene; the decline of β-pinene; and the presence of *p*-cymene represent the main differences for the first time in the literature (Table 1; Figure 1).

Despite the advantages of nanotechnology, the current study showed the effect of the intensive energy approach used as ultrasonication on the composition of essential oils investigated for the first time, which may change their volatile profile and, therefore, their bioactivity. In both oils, nanoemulsification leads to

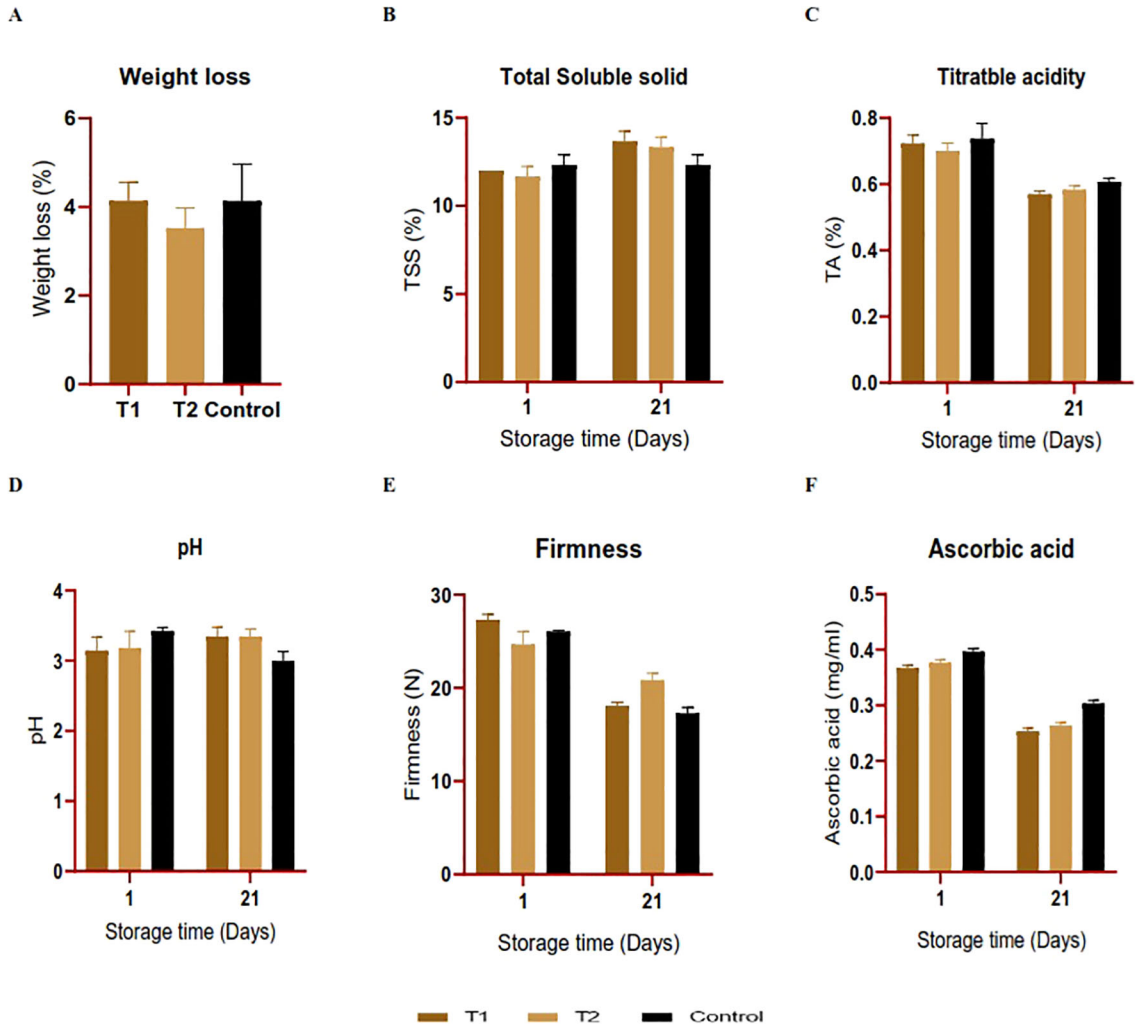

FIGURE 8
(A–F) The effect of nanoemulsions derived from *C. citratus* (T1) and *C. limon* (T2) on the quality parameters of orange fruits was studied over a 21-day storage period at room temperature. Error bars represent ± standard deviation (n = 3).

an increase of neral and geranial at the expense of monoterpenes, especially β-myrcene in *C. citratus* and limonene and γ-terpinene in *C. limon* (Table 1; Figure 1). The findings align with Boudechicha et al. (2023), who used microfluidization for homogenizing *C. citratus* oil with typical results. However, no information is available about the effect of homogenization on *C. limon* oil constituents. High-pressure homogenization of Algerian *Satureja hortensis* L. oil resulted in a significant increase in carvacrol content from 45.15% to 94.51%, along with a decline in γ-terpinene and *p*-cymene content (Boudechicha et al., 2024). It was found that γ-terpinene converts to carvacrol through aromatization and hydroxylation processes during storage of summer savory at different temperatures and times (Mohtashami et al., 2018).

The *C. citratus* and *C. limon* nanoemulsions have a mean particle size of 74.12 and 103 nm with a monomodal size distribution pattern, demonstrating an ultrafine size as it was less than 200 nm (Supplementary Figure S1). In a study by Dhanasekaran et al. (2024), the mean diameter of lemon oil–chitosan nanoemulsion was 130.01 nm, slightly higher than chitosan alone. The increase in diameter could be attributed to the concentration and encapsulation of lemon oil on the chitosan matrix. Similarly, the size of nanoemulsions could vary based on factors such as stabilizing agent, essential oil concentration, temperature, pH, agitation intensity, and ultrasonication time (Karimirad et al., 2019). Sabry et al. (2022) produced lemon oil emulsions ranging from 129 nm to 137 nm using Arabic gum and CMC as stabilizers. In another study, thyme oil nanoemulsion created by ultrasonically emulsifying with Tween80 showed a particle size of 83 nm (Patel and Ghosh, 2020). The PDI values ≤0.2 indicate uniformity among oil droplet sizes or monomodal distributions, as shown in Supplementary Figure S2, and therefore, better stability (Patel and Ghosh, 2020; Li et al., 2021). The ζ-potential is used to determine the electrical status of colloidal systems. In our study, the nanoemulsions showed a ζ-potential of ≥28 mV, indicating higher stability (Boudechicha et al., 2023). The non-ionic emulsifier Tween 80 gives oil droplets a negative charge,

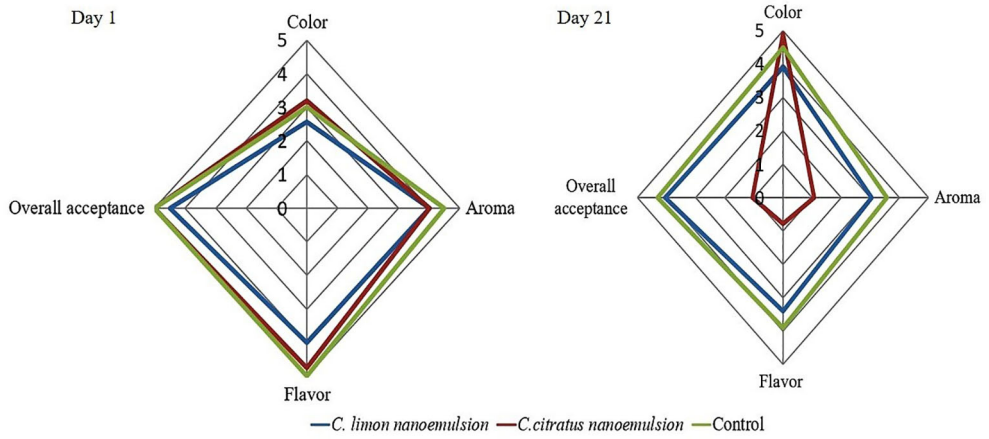

FIGURE 9
Radar chart illustrating the sensory characteristics of oranges on day 1 and after 21 days of storage. A rating system was employed, with color graded from pale yellow (0) to dark orange (5), aroma evaluated from weak (0) to strong (5), and overall acceptance rated from strong dislike (0) to strong liking (5).

affecting the ζ-potential of emulsions containing different essential oils (Guerra-Rosas et al., 2016).

TEM was used to image nanoemulsification samples to examine their morphology (Figure 2). It has been reported in the literature that the particle sizes determined by the TEM were expected to be smaller than those specified by the DLS instrument because of the emulsion drying out in the air during preparation (Filippov et al., 2023). The same result was obtained by Aouf et al. (2020), who used the same technique to encapsulate Algerian *Saccocalyx satureioides* Coss. et Durieu, with well-dispersed round nanoparticles having a narrow size distribution.

Both orange fruit fungal isolates were *Penicillium* based on their color, consistency, conidiophores, and spores (Figures 3, 4). For reliable fungal classification and identification, molecular biology methods must validate traditional findings (Yahya Allawi et al., 2022). The ITS sequence analysis showed that strain GY1 matched *P. expansum* (100% match), and GY2 matched *P. digitatum* (100% match). *Penicillium expansum* is not commonly found in citrus fruits. *Penicillium digitatum* and *P. italicum* are the main pathogens responsible for lesions on infected citrus fruits (Louw and Korsten, 2014). El-Dawy et al. (2021) showed the prevalence of *P. expansum* (38.2%) compared to other *Penicillium* species isolated from decaying citrus fruits. However, limited studies deal with the identification or resistance of such pathogens.

The antimicrobial activity of essential oils is influenced by their chemical composition and interactions between their constituents. Essential oils can impact membrane protein function and destroy bacterial structures, with higher doses having a greater effect on microorganisms (Khairan et al., 2024). The essential oil of *C. limon* exhibited weak to moderate activity against *P. aeruginosa*, *E. coli*, and *B. subtilis* and potential activity against *S. aureus*, in agreement with the literature (Aruna et al., 2022; Kehal et al., 2023). It also showed moderate to strong antibacterial activity against *K. pneumoniae*, in contrast to Louiza et al. (2018). This important activity is accepted due to the high percentage of oxygenated compounds and sesquiterpenes (Gupta, 2022). *Cymbopogon citratus* essential oil completely inhibited the growth of *S. aureus* and *B. subtilis* but exhibited weak to moderate activity against *P. aeruginosa*, in accordance with previous studies (Shendurse et al., 2021). Variations in the activity against Gram-negative bacteria may be related to their different thick outer membrane that can prevent the penetration of hydrophobic essential oils (Chao et al., 2000). It also showed lower activity against *K. pneumoniae* and *S. typhimurium* compared to a previous study (Mahmoud Mohamed et al., 2017). The activity against *E. coli* was good, similar to the study of Partovi et al. (2019). The strong antibacterial activity of *C. citratus* is expected due to its volatile components, including citral (Ujilestari et al., 2019).

With MIC values from 2% to 0.12%, the essential oils inhibited Gram-positive and Gram-negative bacteria (Table 3). This was more successful than disk diffusion, probably due to the essential oils' solubility and diffusion in culture fluids and their volatility impacting paper disk dosages (Mangalagiri et al., 2021). In agreement with Partovi et al. (2019), *C. citratus* essential oil showed the lowest MIC values and the highest activity against all tested bacteria. The MIC values of *C. limon* essential oil were 2% to 0.5% against the tested bacteria, which are better than those obtained by Galgano et al. (2022).

The antibacterial effectiveness of the nanoemulsified essential oils was lower than that of free essential oils, except for *C. citratus* oil nanoemulsion against *B. subtilis*. The present study's findings agreed with Jawaid et al. (2023), who reported good activity against *S. aureus* with a diameter of inhibition of 19.3 mm. Nanoemulsions can offer benefits like increased dispersion and stability. However, they may not always improve the antimicrobial activity of essential oils due to factors such as low oil concentration, physicochemical properties, and limited incubation time (Boudechicha et al., 2024). The results obtained in the current

study indicated that *C. limon* nanoemulsion was not active, contrary to those of Yazgan et al. (2019), who found moderate to good activity against *K. pneumoniae*, *Salmonella paratyphi*, and *S. aureus*, respectively. This dissimilitude in results could be attributed to many factors, including different strains tested and differences in the methodology used.

Essential oils can inhibit fungal growth and control mycotoxin production simultaneously (Boudechicha et al., 2023, 2024). The complete inhibition of the examined fungi by *C. citratus* oil is similar to previous results (Helal et al., 2006; Boukhatem et al., 2014). The microdilution outcomes offered potent antifungal activity of the tested essential oils. *Cymbopogon citratus* displayed the highest activity, which is similar to previous findings, where an MIC value of 0.06% (v/v) against *A. niger* was found (Bansod and Rai, 2008). The MIC value against *F. culmorum*, *P. expansum*, and *C. albicans* was 0.06% (v/v). *Citrus limon* oil also showed an intense activity toward the investigated fungi, more potent than recorded against *A. niger*, *A. flavus*, and *P. chrysogenum* (Viuda-Martos et al., 2008).

The nanoemulsion of *C. citratus* showed complete inhibition of *A. niger*, a potential activity against *P. digitatum* and *C. albicans*, and moderate activity against *P. expansum*. On the other hand, *C. limon* nanoemulsion exhibited moderate inhibition of *P. digitatum*, very weak activity against *A. niger*, and no activity toward the other tested fungi (Figure 6). Regarding the MIC, the essential oils and their nanoemulsions showed activity against *P. digitatum* and *P. expansum*. This opens prospects to use the investigated oils' nanoemulsions with all the encapsulation advantages as biopreservatives for citrus fruits. Some studies have shown contradictory results. In some cases, using a nanoemulsion seemed to lower the antimicrobial activity compared to the non-encapsulated compounds, while other studies showed higher antimicrobial activity of oils when using nanoemulsions (Cofelice et al., 2021).

The *P. expansum* and *P. digitatum* molds were greatly decreased by covering orange fruits with nanoemulsified *C. limon* and *C. citratus* (Figure 7). The control fruits showed dehydration, dryness during storage, and brown spots (Motamedi et al., 2018). Environmental variables pre- and post-harvest may darken and brown citrus fruit cells due to stress or injury. Finding the reasons for these defects might be challenging due to several considerations. Unlike coated samples, the control group had similar fungal development with minimal color changes (Zacarias et al., 2020). The control oranges infected with *P. digitatum* decayed the most after 7 days of storage compared to those treated with chitosan containing Denak, anise, and caraway essential oils (Aminifard and Bayat, 2018).

Current nanoemulsion coating research has shown considerable improvement in fruit quality (Figure 8). The barrier qualities of essential oils in coatings and their antioxidant activity decreased weight loss and gas and water interaction between fruit surfaces and the external environment (Shehata et al., 2020). After 21 days of storage, Khorram and Ramezanian (2021) found that cinnamon-oil-treated oranges lost more weight than controls. The research suggests that polysaccharide degradation into soluble sugars may impact TSS levels and fruit sweetness indicators during storage. Studies show that weight loss increases with sugar content, improving TSS, especially with particular essential oils (Aminifard and Bayat, 2018). The little rise in pH values, with the greatest reduction in uncoated fruits, corresponds with Radi et al. (2018), who found a slight increase in pH values during fresh-cut orange storage. The decreasing acidity and ascorbic acid concentration with time and increased fruit respiration may impact fruit acidity and pH (Wijewardane, 2022). Fruit respiration during lengthy storage has improved due to this organic acid decrease (Huang et al., 2021). *Cymbopogon citratus* nanoemulsion-coated fruits and the control group had a lower TA percentage than *C. limon*-coated samples, likely due to the interaction of the essential oil type and citrus fruit diversity, which significantly affect titratable acidity (Abdul-Rahaman et al., 2023). Nanoemulsions may postpone softening by improving pectin and enzyme activity and making the fruit resistant. Coating sweet oranges makes them firmer (Abdul-Rahaman et al., 2023).

Since essential oils are volatile compounds, their aroma will disappear with storage time. This study achieved the highest scores regarding color and aroma (Figure 9; Supplementary Figure S2). The choice of the appropriate dose of essential oil is a crucial factor since essential oils have a potent scent and flavor, which may negatively affect the organoleptic properties of the food product (Gurtler and Garner, 2022). On day 21, samples coated with *C. limon* nanoemulsion and the control were the same in texture, juiciness, and appearance, with no significant differences. These findings are similar to those of Gomes et al. (2017), who demonstrated that adding *C. limon* essential oil to the alginate coating did not affect the sensory properties of the fresh raspberries. At the end of storage, all treatments slightly decreased taste and flavor, especially in fruits coated with *C. citratus* nanoemulsion, which aligned with the findings of Khorram and Ramezanian (2021).

5 Conclusion

The Algerian essential oils of *Cymbopogon citratus* and *Citrus limon*, as well as their nanoemulsions prepared via ultrasonication, have shown promising results against both Gram-positive and Gram-negative bacteria as well as fungi identified in Thomson Navel oranges. When used as a coating on orange fruits inoculated with *P. expansum* and *P. digitatum* identified in fruits, the nanoemulsions significantly reduced fungal growth and minimized negative changes in fruit quality during storage. Intensive energy through ultrasonication successfully prepared particles on a nanoscale with good morphology and stability. However, it affects the oil constituents by increasing concentrations of oxygenated terpenes at the expense of non-oxygenated ones. The current study opens the perspective toward using available natural oils as preservatives for economic crops in developing countries like Egypt and Algeria.

Data availability statement

The datasets presented in this study can be found in online repositories. The names of the repository/repositories and accession number(s) can be found in the article/Supplementary Material.

Author contributions

AF: Conceptualization, Investigation, Methodology, Project administration, Supervision, Validation, Writing – original draft, Writing – review & editing. MG: Data curation, Formal analysis, Investigation, Methodology, Validation, Visualization, Writing – original draft. AA: Conceptualization, Investigation, Methodology, Supervision, Writing – review & editing. EM: Formal analysis, Methodology, Writing – review & editing. HA: Formal analysis, Funding acquisition, Methodology, Resources, Writing – review & editing. AB: Formal analysis, Methodology, Supervision, Validation, Visualization, Writing – review & editing. ZB: Formal analysis, Methodology, Writing – review & editing. TA: Formal analysis, Writing – review & editing, Funding acquisition, Resources.

Funding

The author(s) declare financial support was received for the research, authorship, and/or publication of this article. The authors thank the Researchers Supporting Project number (RSPD2024R641), King Saud University, Riyadh, Saudi Arabia, for funding this research.

Conflict of interest

The authors declare that the research was conducted in the absence of any commercial or financial relationships that could be construed as a potential conflict of interest.

Publisher's note

All claims expressed in this article are solely those of the authors and do not necessarily represent those of their affiliated organizations, or those of the publisher, the editors and the reviewers. Any product that may be evaluated in this article, or claim that may be made by its manufacturer, is not guaranteed or endorsed by the publisher.

Supplementary material

The Supplementary Material for this article can be found online at: https://www.frontiersin.org/articles/10.3389/fpls.2024.1491491/full#supplementary-material

References

Abdul-Rahaman, A., Irtwange, S. V., and Aloho, K. P. (2023). Preservative potential of biobased oils on the physiochemical quality of orange fruits during storage. *J. Food Process. Preservation* 2023, 9952788. doi: 10.1155/2023/9952788

Aminifard, M. H., and Bayat, H. (2018). Antifungal activity of black caraway and anise essential oils against penicillium digitatum on blood orange fruits. *Int. J. Fruit Sci.* 18, 307–319. doi: 10.1080/15538362.2017.1409682

Aouf, A., Ali, H., Al-Khalifa, A. R., Mahmoud, K. F., and Farouk, A. (2020). Influence of Nanoencapsulation Using High-Pressure Homogenization on the Volatile Constituents and Anticancer and Antioxidant Activities of Algerian Saccocalyx satureioides Coss. et Durieu. *Molecules* 25, 4756–4766. doi: 10.3390/molecules25204756

Aruna, T., Hemalatha, G., Kumutha, K., Kanchana, S., and Vellaikumar, S. (2022). Physicochemical, antioxidant and antimicrobial properties of citrus peel essential oils. *J. Appl. Natural Sci.* 14, 640–646. doi: 10.31018/jans.v14i2.3484

Bansod, S., and Rai, M. (2008). Antifungal activity of essential oils from Indian medicinal plants against human pathogenic Aspergillus fumigatus and A. Niger. *World J. Med. Sci.* 3, 81–88.

Benoudjit, F., Hamoudi, I., and Aboulouz, A. (2022). Extraction and characterization of Essential Oil and Hydrolate obtained from an Algerian Lemongrass (Cymbopogon citratus). *Algerian J. Environ. Sci. Technol.* 8, 2256–2263.

Boudechicha, A., Aouf, A., Ali, H., Alsulami, T., Badr, A. N., Ban, Z., et al. (2024). Effect of microfluidization on the volatiles and antibacterial, antifungal, and cytotoxic activities of Algerian satureja hortensis L. Oil-loaded nanoemulsions: *in vitro* and *in silico* study. *ACS Omega* 9, 27030–27046. doi: 10.1021/acsomega.4c00315

Boudechicha, A., Aouf, A., Farouk, A., Ali, H. S., Elkhadragy, M. F., Yehia, H. M., et al. (2023). Microfluidizing technique application for Algerian cymbopogon citratus (DC.) stapf effects enhanced volatile content, antimicrobial, and anti-mycotoxigenic properties. *Molecules* 28, 5367–5386. doi: 10.3390/molecules28145367

Boukhatem, M. N., Ferhat, M. A., Kameli, A., Saidi, F., and Kebir, H. T. (2014). Lemon grass (Cymbopogon citratus) essential oil as a potent anti-inflammatory and antifungal drugs. *Libyan J. Med.* 9, 25431–25440. doi: 10.3402/ljm.v9.25431

Brauer, V. S., Rezende, C. P., Pessoni, A. M., De Paula, R. G., Rangappa, K. S., Nayaka, S. C., et al. (2019). Antifungal agents in agriculture: friends and foes of public health. *Biomolecules* 9, 521–541. doi: 10.3390/biom9100521

Buonsenso, F., Schiavon, G., and Spadaro, D. (2023). Efficacy and Mechanisms of Action of Essential Oils' Vapours against Blue Mould on Apples Caused by Penicillium expansum. *Int. J. Mol. Sci.* 24, 2900–2914. doi: 10.3390/ijms24032900

Carbone, I., and Kohn, L. M. (1999). A method for designing primer sets for speciation studies in filamentous ascomycetes. *Mycologia* 91, 553–556. doi: 10.1080/00275514.1999.12061051

Chao, S. C., Young, D. G., and Oberg, C. J. (2000). Screening for inhibitory activity of essential oils on selected bacteria, fungi and viruses. *J. Essential Oil Res.* 12, 639–649. doi: 10.1080/10412905.2000.9712177

CLSI, C. S. M. (2018). *Methods for Dilution Antimicrobial Susceptibility Tests for Bacteria that Grow Aerobically. 11th. ed.* Ed. P. A. Wayne (Wayne, USA: Clinical Laboratory Standards Institute).

Cofelice, M., Cinelli, G., Lopez, F., Di Renzo, T., Coppola, R., and Reale, A. (2021). Alginate-assisted lemongrass (Cymbopogon nardus) essential oil dispersions for antifungal activity. *Foods* 10, 1528–1539. doi: 10.3390/foods10071528

Combrinck, S., Regnier, T., and Kamatou, G. P. P. (2011). *In vitro* activity of eighteen essential oils and some major components against common postharvest fungal pathogens of fruit. *Ind. Crops Products* 33, 344–349. doi: 10.1016/j.indcrop.2010.11.011

Costa, J. H., Bazioli, J. M., de Moraes Pontes, J. G., and Fill, T. P. (2019). Penicillium digitatum infection mechanisms in citrus: What do we know so far? *Fungal Biol.* 123, 584–593. doi: 10.1016/j.funbio.2019.05.004

Dhanasekaran, S., Liang, L., Gurusamy, S., Yang, Q., and Zhang, H. (2024). Chitosan stabilized lemon essential oil nanoemulsion controls black mold rot and maintains quality of table grapes. *Int. J. Biol. Macromolecules* 277, 134251. doi: 10.1016/j.ijbiomac.2024.134251

El-Dawy, E. G. A. E. M., Gherbawy, Y. A., Hassan, S., and Hussein, M. A. (2021). Molecular identification of penicillium sp. Isolated from citrus fruits. *Curr. Microbiol.* 78, 1981–1990. doi: 10.1007/s00284-021-02463-3

Fan, F., Tao, N., Jia, L., and He, X. (2014). Use of citral incorporated in postharvest wax of citrus fruit as a botanical fungicide against Penicillium digitatum. *Postharvest Biol. Technol.* 90, 52–55. doi: 10.1016/j.postharvbio.2013.12.005

FAO. (2021). *Citrus Fruit Statistical Compendium 2020* (Rome, Italy: Food and Agriculture Organization of the United Nations).

Farouk, A., Hathout, A. S., Amer, M. M., and Hussain, O. A. (2022). The impact of nanoencapsulation on volatile constituents of Citrus sinesis L. essential oil and their antifungal activity. *Egyptian J. Chem.* 65, 527–538. doi: 10.21608/ejchem.2021.95579.4485

Filippov, S. K., Khusnutdinov, R., Murmiliuk, A., Inam, W., Zakharova, L. Y., Zhang, H., et al. (2023). Dynamic light scattering and transmission electron microscopy in drug delivery: a roadmap for correct characterization of nanoparticles and interpretation of results. *Materials Horizons* 10, 5354–5370. doi: 10.1039/D3MH00717K

Galgano, M., Capozza, P., Pellegrini, F., Cordisco, M., Sposato, A., Sblano, S., et al. (2022). Antimicrobial activity of essential oils evaluated *In Vitro* against Escherichia coli and Staphylococcus aureus. *Antibiotics* 11, 979–981. doi: 10.3390/antibiotics11070979

Gardes, M., and Bruns, T. D. (1993). ITS primers with enhanced specificity for basidiomycetes - application to the identification of mycorrhizae and rusts. *Mol. Ecol.* 2, 113–118. doi: 10.1111/j.1365-294X.1993.tb00005.x

Gomes, M., d., S., d. G. Cardoso, M., Guimarães, A. C. G., Guerreiro, A. C., Gago, C. M. L., et al. (2017). Effect of edible coatings with essential oils on the quality of red raspberries over shelf-life. *J. Sci. Food Agric.* 97, 929–938. doi: 10.1002/jsfa.2017.97.issue-3

Guerra-Rosas, M. I., Morales-Castro, J., Ochoa-Martínez, L. A., Salvia-Trujillo, L., and Martín-Belloso, O. (2016). Long-term stability of food-grade nanoemulsions from high methoxyl pectin containing essential oils. *Food Hydrocolloids* 52, 438–446. doi: 10.1016/j.foodhyd.2015.07.017

Gupta, C. (2022). Chemical composition of fruit peels essential oil from citrus species and their antimicrobial efficacy as bio preservatives. *Adv. Food Technol. Nutr. Sci. Open J.* 8, 29–35. doi: 10.17140/AFTNSOJ-8-177

Gurtler, J. B., and Garner, C. M. (2022). A review of essential oils as antimicrobials in foods with special emphasis on fresh produce. *J. Food Prot.* 85, 1300–1319. doi: 10.4315/JFP-22-017

Helal, G. A., Sarhan, M. M., Shahla, A. N. K. A., and Ei-Khair, E. K. A. (2006). Antimicrobial activity of some essential oils against microorganisms deteriorating fruit juices. *Mycobiology* 34, 219–229. doi: 10.4489/MYCO.2006.34.4.219

Himed, L., Merniz, S., and Barkat, M. (2016). Evaluation of the chemical composition and antioxidant activity of Citrus limon essential oil and its application in margarine preservation. *J. Nat. Product* 4, 316–322.

Himed, L., Merniz, S., Monteagudo-Olivan, R., Barkat, M., and Coronas, J. (2019). Antioxidant activity of the essential oil of citrus limon before and after its encapsulation in amorphous SiO2. *Sci. Afr.* 6, e00181. doi: 10.1016/j.sciaf.2019.e00181

Huang, Q., Wan, C., Zhang, Y., Chen, C., and Chen, J. (2021). Gum arabic edible coating reduces postharvest decay and alleviates nutritional quality deterioration of ponkan fruit during cold storage. *Front. Nutr.* 8. doi: 10.3389/fnut.2021.717596

Jawaid, T., Alaseem, A. M., Khan, M. M., Mukhtar, B., Kamal, M., Anwer, R., et al. (2023). Preparation and evaluation of nanoemulsion of citronella essential oil with improved antimicrobial and anti-cancer properties. *Antibiotics* 12, 478–489. doi: 10.3390/antibiotics12030478

Karimirad, R., Behnamian, M., and Dezhsetan, S. (2019). Application of chitosan nanoparticles containing Cuminum cyminum oil as a delivery system for shelf life extension of Agaricus bisporus. *LWT* 106, 218–228. doi: 10.1016/j.lwt.2019.02.062

Kehal, F., Chemache, L., Himed, L., and Barkat, M. (2023). Antimicrobial and antioxidant activities of Citrus limon peel essential oils and their application as a natural preservative in fresh cream: effects on oxidative and sensory properties. *Acta Universitatis Cibiniensis. Ser. E: Food Technol.* 27, 1–14. doi: 10.2478/aucft-2023-0001

Kgang, I. E., Mathabe, P. M. K., Klein, A., Kalombo, L., Belay, Z. A., and Caleb, O. J. (2022). Effects of lemon (Citrus Limon L.), lemongrass (Cymbopogon citratus) and peppermint (Mentha piperita L.) essential oils against of Botrytis cinerea and Penicillium expansum. *JSFA Rep.* 2, 405–414. doi: 10.1002/jsf2.v2.8

Khairan, K., Marfu'ah, M., Idroes, R., Sriwati, R., and Diah, M. (2024). An overview of essential oil-based nanoemulsion and their biological activities against some microbial pathogenic. *IOP Conf. Series: Earth Environ. Sci.* 1297, 012083. doi: 10.1088/1755-1315/1297/1/012083

Khorram, F., and Ramezanian, A. (2021). Cinnamon essential oil incorporated in shellac, a novel bio-product to maintain quality of 'Thomson navel' orange fruit. *J. Food Sci. Technol.* 58, 2963–2972. doi: 10.1007/s13197-020-04798-4

Lai, T., Sun, Y., Liu, Y., Li, R., Chen, Y., and Zhou, T. (2021). Cinnamon oil inhibits penicillium expansum growth by disturbing the carbohydrate metabolic process. *J. Fungi* 7, 123–139. doi: 10.3390/jof7020123

Li, Y., Zhao, R., Li, Y., and Zhou, Z. (2021). Limonin enhances the antifungal activity of eugenol nanoemulsion against penicillium italicum *in vitro* and *in vivo* tests. *Microorganisms* 9, 969–982. doi: 10.3390/microorganisms9050969

Lima, P. G., Freitas, C. D. T., Oliveira, J. T. A., Neto, N. A. S., Amaral, J. L., Silva, A. F. B., et al. (2021). Synthetic antimicrobial peptides control Penicillium digitatum infection in orange fruits. *Food Res. Int.* 147, 110582. doi: 10.1016/j.foodres.2021.110582

Louiza, H., Salah, M., and Malika, B. (2018). Chemical composition of Citrus limon (Eureka variety) essential oil and evaluation of its antioxidant and antibacterial activities. *Afr. J. Biotechnol.* 17, 356–361. doi: 10.5897/AJB2016.15693

Louw, J. P., and Korsten, L. (2014). Pathogenicity and host susceptibility of penicillium spp. on citrus. *Plant Dis.* 99, 21–30. doi: 10.1094/PDIS-02-14-0122-RE

Maghenzani, M., Chiabrando, V., Santoro, K., Spadaro, D., and Giacalone, G. (2018). Effects of treatment by vapour of essential oil from Thymus vulgaris and Satureja montana on postharvest quality of sweet cherry (cv. Ferrovia). *J. Food Nutr. Res.* 57, 161–169.

Mahmoud Mohamed, A., Mohammad Abdi, Y., and Mohamed, N. A. (2017). GC-MS analysis and antimicrobial screening of essential oil from lemongrass (Cymbopogon citratus). *Int. J. Pharm. Chem.* 3, 72–76. doi: 10.11648/j.ijpc.20170306.11

Mangalagiri, N. P., Panditi, S. K., and Jeevigunta, N. L. L. (2021). Antimicrobial activity of essential plant oils and their major components. *Heliyon* 7, e06835-e06848. doi: 10.1016/j.heliyon.2021.e06835

Medeleanu, M. L., Fărcaș, A. C., Coman, C., Leopold, L., Diaconeasa, Z., and Socaci, S. A. (2023). Citrus essential oils – Based nano-emulsions: Functional properties and potential applications. *Food Chemistry: X* 20, 100960. doi: 10.1016/j.fochx.2023.100960

Micić, D., Đurović, S., Riabov, P., Tomić, A., Šovljanski, O., Filip, S., et al. (2021). Rosemary essential oils as a promising source of bioactive compounds: chemical composition, thermal properties, biological activity, and gastronomical perspectives. *Foods* 10, 2734–2749. doi: 10.3390/foods10112734

Mohtashami, S., Rowshan, V., Tabrizi, L., Babalar, M., and Ghani, A. (2018). Summer savory (Satureja hortensis L.) essential oil constituent oscillation at different storage conditions. *Ind. Crops Products* 111, 226–231. doi: 10.1016/j.indcrop.2017.09.055

Motamedi, E., Nasiri, J., Malidarreh, T. R., Kalantari, S., Naghavi, M. R., and Safari, M. (2018). Performance of carnauba wax-nanoclay emulsion coatings on postharvest quality of 'Valencia' orange fruit. *Scientia Hortic.* 240, 170–178. doi: 10.1016/j.scienta.2018.06.002

Ncama, K., Opara, U. L., Tesfay, S. Z., Fawole, O. A., and Magwaza, L. S. (2017). Application of Vis/NIR spectroscopy for predicting sweetness and flavour parameters of 'Valencia' orange (Citrus sinensis) and 'Star Ruby' grapefruit (Citrus x paradisi Macfad). *J. Food Eng.* 193, 86–94. doi: 10.1016/j.jfoodeng.2016.08.015

OuYang, Q., Okwong, R. O., Chen, Y., and Tao, N. (2020). Synergistic activity of cinnamaldehyde and citronellal against green mold in citrus fruit. *Postharvest Biol. Technol.* 162, 111095. doi: 10.1016/j.postharvbio.2019.111095

Partovi, R., Talebi, F., Boluki, Z., and Sharifzadeh, A. (2019). Evaluation of antimicrobial activity of Cymbopogon citratus essential oil alone and in combination with Origanum majorana and Caryophyllus aromaticus essential oils against some foodborne bacteria. *Int. J. Enteric Pathog.* 7, 60–67. doi: 10.15171/ijep.2019.14

Patel, A., and Ghosh, V. (2020). "Thyme (Thymus vulgaris) essential oil–based antimicrobial nanoemulsion formulation for fruit juice preservation," in *Biotechnological Applications in Human Health*. Eds. P. C. Sadhukhan and S. Premi (Springer Singapore, Singapore), 107–114.

Radi, M., Akhavan-Darabi, S., Akhavan, H.-R., and Amiri, S. (2018). The use of orange peel essential oil microemulsion and nanoemulsion in pectin-based coating to extend the shelf life of fresh-cut orange. *J. Food Process. Preservation* 42, e13441. doi: 10.1111/jfpp.13441

Rovetto, E. I., Luz, C., La Spada, F., Meca, G., Riolo, M., and Cacciola, S. O. (2023). Diversity of mycotoxins and other secondary metabolites recovered from blood oranges infected by colletotrichum, alternaria, and penicillium species. *Toxins* 15, 407–436. doi: 10.3390/toxins15070407

Sabry, B. A., Badr, A. N., Ahmed, K. A., Desoukey, M. A., and Mohammed, D. M. (2022). Utilizing lemon peel extract and its nano-emulsion to control aflatoxin toxicity in rats. *Food Bioscience* 50, 101998. doi: 10.1016/j.fbio.2022.101998

Sanger, F., Nicklen, S., and Coulson, A. R. (1977). DNA sequencing with chain-terminating inhibitors. *Proc. Natl. Acad. Sci.* 74, 5463–5467. doi: 10.1073/pnas.74.12.5463

Shehata, S. A., Abdeldaym, E. A., Ali, M. R., Mohamed, R. M., Bob, R. I., and Abdelgawad, K. F. (2020). Effect of some citrus essential oils on post-harvest shelf life and physicochemical quality of strawberries during cold storage. *Agronomy* 10, 1466–1494. doi: 10.3390/agronomy10101466

Shendurse, A. M., Sangwan, R. B., Amit, K., Ramesh, V., Patel, A. C., Gopikrishna, G., et al. (2021). Phytochemical screening and antibacterial activity of lemongrass (Cymbopogon citratus) leaves essential oil. *J. Pharmacogn Phytochem.* 10, 445–449.

Ujilestari, T., Martien, R., Ariyadi, B., Dono, N. D., and Zuprizal, (2019). Antibacterial effects of essential oils of Cymbopogon citratus and Amomum compactum under self-nanoemulsifying drug delivery system (SNEDDS). *IOP Conf. Series: Earth Environ. Sci.* 387, 012071. doi: 10.1088/1755-1315/387/1/012071

USDA, F. (2024). Available online at: https://fas.usda.gov/data/production/commodity/0571120 (Accessed 17-18-2024).

Vilanova, L., Viñas, I., Torres, R., Usall, J., Jauset, A. M., and Teixidó, N. (2012). Infection capacities in the orange-pathogen relationship: Compatible (Penicillium digitatum) and incompatible (Penicillium expansum) interactions. *Food Microbiol.* 29, 56–66. doi: 10.1016/j.fm.2011.08.016

Viuda-Martos, M., Ruiz-Navajas, Y., Fernández-López, J., and Pérez-Álvarez, J. (2008). Antifungal activity of lemon (Citrus lemon L.), mandarin (Citrus reticulata L.), grapefruit (Citrus paradisi L.) and orange (Citrus sinensis L.) essential oils. *Food Control* 19, 1130–1138. doi: 10.1016/j.foodcont.2007.12.003

Wijewardane, R. M. N. A. (2022). Evaluation of the effect of fruit coating on shelf life extension of lime (Citrus aurantifolia) under different storage condition. *J. Horticulture Postharvest Res.* 5, 337–348. doi: 10.22077/jhpr.2022.4949.1261

Wuryatmo, E., Able, A. J., Ford, C. M., and Scott, E. S. (2014). Effect of volatile citral on the development of blue mould, green mould and sour rot on navel orange. *Australas. Plant Pathol.* 43, 403–411. doi: 10.1007/s13313-014-0281-z

Yahya Allawi, M., Salim Al-Taie, B., and Hmoshi, R. M. (2022). Isolation and Identification of Penicillium rubens from the Local Strain in Mosul, Iraq, and Investigation of Potassium Phosphate Effect on its Growth. *Arch. Razi Institute* 77, 421–427. doi: 10.22092/ari.2021.356684.1896

Yazgan, H., Ozogul, Y., and Kuley, E. (2019). Antimicrobial influence of nanoemulsified lemon essential oil and pure lemon essential oil on food-borne pathogens and fish spoilage bacteria. *Int. J. Food Microbiol.* 306, 108266. doi: 10.1016/j.ijfoodmicro.2019.108266

Zacarias, L., Cronje, P. J. R., and Palou, L. (2020). "Chapter 21 - Postharvest technology of citrus fruits," in *The Genus Citrus*. Eds. M. Talon, M. Caruso and F. G. Gmitter (United Kingdom: Woodhead Publishing), 421–446.

Zulu, L., Gao, H., Zhu, Y., Wu, H., Xie, Y., Liu, X., et al. (2023). Antifungal effects of seven plant essential oils against Penicillium digitatum. *Chem. Biol. Technol. Agric.* 10, 82. doi: 10.1186/s40538-023-00434-3

frontiers | Frontiers in Plant Science

TYPE Original Research
PUBLISHED 02 December 2024
DOI 10.3389/fpls.2024.1497664

OPEN ACCESS

EDITED BY
Eman A. Mahmoud,
Damietta University, Egypt

REVIEWED BY
Mario Juan Simirgiotis,
Austral University of Chile, Chile
Jun Yuan,
Huaiyin Institute of Technology, China

*CORRESPONDENCE
Jingyuan Xu
xujingyuanxu@126.com
Da Qian
drqianda@hotmail.com

RECEIVED 17 September 2024
ACCEPTED 13 November 2024
PUBLISHED 02 December 2024

CITATION
Cheng Y, Cao W, Guo R, Chen R, Li X, Qian D and Xu J (2024) A comparative study of the quality differences and seasonal dynamics of flavonoids between the aerial parts and roots of *Scutellaria barbata*. *Front. Plant Sci.* 15:1497664. doi: 10.3389/fpls.2024.1497664

A comparative study of the quality differences and seasonal dynamics of flavonoids between the aerial parts and roots of *Scutellaria barbata*

Yijie Cheng[1,2,3], Wenxin Cao[3], Ru Guo[3], Ruihuan Chen[1], Xiaofan Li[4], Da Qian[2*] and Jingyuan Xu[2,3*]

[1]Pharmacy Department, Changshu Hospital Affiliated to Soochow University, Changshu No.1 People's Hospital, Changshu, China, [2]Central Laboratory, Changshu Hospital Affiliated to Soochow University, Changshu No.1 People's Hospital, Changshu, China, [3]School of Biology and Food Engineering, Changshu Institute of Technology, Changshu, China, [4]Suzhou Qifan Agricultural Technology Co., Ltd, Changshu, China

Introduction: *Scutellaria barbata* D. Don is a widely cultivated Chinese herbal medicine known for its medicinal properties. However, differences in the spatial distribution of metabolites, accumulation patterns of flavonoids, and pharmacological activities between the aerial parts and roots of *S. barbata* still remain unclear, posing challenges for its standardized cultivation and quality control. This study aimed to elucidate the quality differences between these plant parts and clarify their seasonal variations.

Methods: The chemical profiles were qualitatively analyzed by UPLC-QTOF-MS/MS. The accumulation patterns of total flavonoids, scutellarin and baicalin in different parts of *S. barbata* were quantitatively analyzed by UV and HPLC respectively. The differences of pharmacological efficacy were evaluated by antioxidant assays and CCK-8 assay.

Results: In this research, there were 46 compounds identified in *S. barbata* that included 44 flavonoids. The aerial parts primarily accumulate flavonoids with 4′-hydroxyl group, while the root mainly accumulate flavonoids without this group. Additionally, the accumulation and variation of flavonoid components were seasonally dependent, with the aerial parts reaching peak content in spring during vigorous vegetative growth and the roots accumulating most flavonoids in autumn. The extracts from both parts exhibited antioxidant activity and inhibitory effects on cancer cell proliferation, with notable differences between them.

Discussion: This study provides valuable insights into the quality differences and seasonal dynamics of the different parts of *S. barbata*, offering a reference for standardized harvesting and quality control.

KEYWORDS

***Scutellaria barbata*, quality differences, spatial distribution, seasonal dynamics, flavonoids**

1 Introduction

The therapeutic effects of medicinal plants are primarily attributed to the endogenous bioactive ingredients, most of which are secondary metabolites (Rogerio et al., 2010; Chen et al., 2024). The secondary metabolites in medicinal plants are diverse, accumulating in specific organs and exhibiting distinct distribution patterns. For instance, in *Astragalus membranaceus*, dihydroflavones, isoflavones, and flavones are predominantly found in the aerial parts, whereas saponins are primarily concentrated in the roots (Li et al., 2019; Gao et al., 2024). In addition, the accumulation of active ingredients in medicinal plants varies with the growth and development of the plants. For example, the young leaves of *Mitragyna speciosa* (Korth.) Havil. contain significantly higher levels of medicinally beneficial alkaloids, which decrease as the leaves mature (Kong et al., 2017; Veeramohan et al., 2023). Flavonoids, as active ingredients in many species of medicinal plants, exhibit organ-specific distribution, and their accumulation varies with the plant's development (del Baño et al., 2004; Xu et al., 2018b; Bouyahya et al., 2022; Ali Reza et al., 2023). Therefore, a comprehensive study of the distribution differences and accumulation patterns of flavonoids in medicinal plants can provide valuable insights for selecting medicinal parts and improving the quality control of medicinal materials.

Scutellaria barbata is a perennial herb belonging to the genus *Scutellaria* in the family Lamiaceae. Its dried whole herb, known as Ban-zhi-lian (BZL) in traditional Chinese medicine, is widely used in clinical practice. It is recognized for its properties of expelling toxins, cooling, dispersing blood stasis, and promoting diuresis. Clinically, it is used to treat throat swelling and pain, injuries from falls, and bite wounds from snakes or insects (Chinese Pharmacopoeia Commission, 2020). Pharmaceutical research indicates that BZL extract exhibits a range of activities, including anticancer, anti-inflammatory, and antibacterial effects (Sato et al., 2000; Xu et al., 2013; Wu et al., 2022). BZL extract is rich in flavonoids, and researchers have currently isolated more than 50 flavonoid compounds with diverse structures from the extract (Wang et al., 2020). Most of the flavonoids isolated from BZL exhibit significant bioactivity. For instance, scutellarin can inhibit the proliferation of breast cancer stem cells, while baicalin improves insulin resistance and regulates liver glucose metabolism (Xu et al., 2018a; Ma et al., 2024). Therefore, flavonoids are used as one of the key criteria for the quality evaluation of BZL in the Chinese Pharmacopoeia and other related studies (Chinese Pharmacopoeia Commission, 2020).

As the demand for BZL continues to increase year by year, the BZL currently available on the market is primarily sourced from artificial cultivation. Because the aboveground parts of *S. barbata* can regreen multiple times a year, the aboveground parts of artificially cultivated *S. barbata* are often harvested several times annually for use as medicinal materials. In addition, during artificial cultivation, the harvested parts of *S. barbata* are often inconsistent across different batches. For example, some batches only contain the aerial parts, while others contain both the aboveground parts and roots. Previous studies have shown that the harvest time can significantly impact the quality of Chinese medicinal materials. The types and accumulation of active ingredients also vary greatly among different plant organs (Zeng et al., 2017; Hazrati et al., 2024). Therefore, non-standard harvesting methods may result in quality differences between batches of BZL. To our knowledge, research on the distribution and accumulation patterns of flavonoids in the aerial parts and roots of *S. barbata* is lacking. Additionally, there is a lack of comprehensive bioactivity assessment for different parts of *S. barbata*. This gap hinders the effective quality control of *S. barbata* through standardized cultivation and harvesting practices.

This study first identified the chemical components of the aerial parts and roots of *S. barbata* using high-performance liquid chromatography (HPLC)–quadrupole time-of-flight (QTOF)–tandem mass spectrometry (MS/MS) to compare the chemical profiles of these two parts. After that, the metabolic change pattern of the total flavonoids and the key active flavonoids in both parts were investigated. Building on these findings, the study further detected the antioxidant properties and cancer cell proliferation inhibition of the aerial part extract and root extracts to gain preliminary insights into their quality differences. These insights provide a theoretical foundation for the standardized harvesting and quality control of artificially cultivated *S. barbata*.

2 Materials and methods

2.1 Plant materials

From March 9 to December 14, 2023, the entire *S. barbata* was collected biweekly from the Qi Fan Agricultural Technology Co., Ltd., planting base. The collected samples were washed and divided into aerial parts (mainly leaves and stems) and roots. These samples were then dried according to the methods outlined in the Chinese Pharmacopoeia (Chinese Pharmacopoeia Commission, 2020).

2.2 Chemicals and reagents

Baicalin and scutellarin, the reference standards, were obtained from Baoji Herbest Bio-Tech Co., Ltd. (Shannxi, China). The purity of each compound was determined to be over 98% through the HPLC analysis. Methanol for chromatography was obtained from Merck (Darmstadt, Germany). Chromatography-grade water was obtained from Watsons (Hong Kong, China). All other reagents were of analytical grade and obtained from Nanjing Chemical Regents Co., Ltd. (Nanjing, China).

2.3 Chemical profile qualitative analysis by UHPLC–QTOF–MS/MS

Chromatographic separation was performed using a Waters ACQUITY UPLC (Waters, Milford, MA, USA). An ACQUITY UPLC BEH-C18 column (2.1 × 150 mm, 1.7 µm; Waters, Wexford, Ireland) was utilized for analysis at 30°C. The mobile phase for chromatographic separation consisted of a mixture of 0.1% formic acid–water (A) and methanol (B). The flow rate was 0.3 mL/min,

with the following gradient conditions: 0–20 min, 5%–25% (B); 20–25 min, 25%–30% (B); 25–35 min, 30%–95%; 35–37 min, 95%–95%; and 37–40 min, 95%–5%. The injection volume was 5 µL. Qualitative analysis was conducted using the AB SCIEX Triple TOF 5600 system (AB SCIEX Technologies, Redwood City, CA, USA) in both negative and positive ion modes. The mass range was set from 100 to 2,000 *m*/*z*, and the electrospray ionization temperature was set to 50°C. The nebulizer gas pressure and ion spray voltage were 60 psi and 4.5 kV, respectively. The collision energy was −35 V for negative ion mode and 40 V for positive ion mode.

2.4 Quantitative analysis of total flavonoids by UV spectrophotometry

The standard curve of scutellarin and baicalin was established according to the Chinese Pharmacopoeia (2020 edition) for the quantitative analysis of total flavonoids in the aerial parts and roots of *S. barbata*, respectively. For sample preparation, approximately 1 g of powdered aerial parts of *S. barbata* (sieved through a No. 3 sieve) was placed in a Soxhlet extractor and extracted with petroleum ether (60°C–90°C) at a 1:100 material-to-liquid ratio. The mixture was refluxed at 82°C until colorless, after which the ether solution was discarded, and the residue was extracted with methanol until colorless. The extract was diluted to 100 mL with methanol, followed by further dilution of 1 mL of the solution to 50 mL. The absorbance was measured using an ultraviolet (UV) spectrophotometer at 335 nm. Root samples were directly extracted with methanol without prior treatment with petroleum ether, following the same procedure as for the aerial parts. The absorbance was measured at 278 nm.

2.5 Quantitative analysis of flavonoids by high-performance liquid chromatography

An HPLC method was developed to quantify scutellarin in the aerial parts and baicalin in the roots of *S. barbata*. All samples were analyzed using an Agilent Series 1260 LC system (Agilent Technologies, Cambridge, MA, USA). Chromatographic separation was performed with a mobile phase consisting of 0.1% formic acid in water (A) and methanol (B) under the following gradient conditions: 0–5 min, 15%–25% (B); 5–10 min, 25%–30% (B); 10–20 min, 30%–40% (B); 20–30 min, 40%–40% (B); 30–40 min, 40%–55% (B); 40–55 min, 55%–70% (B); 55–65 min, 70%–95% (B); 65–70 min, 95%–95% (B); 70–75 min, 95%–15% (B); and 75–78 min, 15%–15% (B). The detection wavelengths were set at 335 nm for the aerial parts and 278 nm for the roots. The column temperature was kept at 25°C, with a flow rate of 1 mL/min and an injection volume of 20 µL.

2.6 Method validation

Method validation was conducted following our previous research with slight modifications (Xu et al., 2018b). The validation process included analysis of the linear regression curve, limit of detection (LOD), limit of quantification (LOQ), repeatability, intra-day and inter-day stability, and recovery. Calibration curves were constructed using a series of standard solutions at appropriate concentrations. The LOD and LOQ were determined based on signal-to-noise (S/N) ratios of 3 and 10, respectively.

Precision was evaluated by analyzing standard solutions in six replicates for both intra-day and inter-day variability. To assess repeatability, six different sample solutions were prepared from the same root and aerial part samples collected on April 20, and the results were expressed as relative standard deviation (RSD). Stability was assessed by storing the sample solutions at 25°C and analyzing them at 0 hours, 2 hours, 4 hours, 6 hours, 8 hours, 12 hours, 24 hours, 48 hours, and 72 hours. For recovery validation, six replicates of root samples (collected on April 20) were added with baicalin for extraction and recovery assessment, while six replicates of aerial part samples (collected on April 20) were added with scutellarin. The results of method validation for HPLC and UV spectrophotometry are shown in Supplementary Table S1. The calibration curves are presented in Supplementary Figure S1.

2.7 Antioxidant assays

2.7.1 ABTS scavenging assay

The ABTS scavenging assay was performed to evaluate the antioxidant activity, following a previously reported method with modifications (Cheng et al., 2022). The ABTS stock solution was prepared and diluted to achieve an absorbance of approximately 0.7 at 734 nm. The BZL extracts were mixed with the diluted ABTS solution and incubated in the dark at 30°C for 30 min. The absorbance of the mixture was measured at 734 nm to determine the antioxidant activity. The ABTS radical scavenging activity was calculated as follows:

$$ABTS\ \ radical\ \ scavenging\ \ activity\ \ (\%) = \frac{A0-(A1-A2)}{A0} \times 100\,\%$$

where A_1, A_0, and A_2 are the absorbance values of the samples [or L-Ascorbic acid (Vc)], the control, and the blank without ABTS, respectively.

2.7.2 DPPH scavenging assay

The antioxidant activity was also assessed using the DPPH scavenging assay with slight modifications (Cheng et al., 2022). The sample extract (0.5 mL) was mixed with 6 mL of DPPH solution (0.1 mmol/L) and allowed to react at room temperature for 30 min. The reaction was protected from light. The absorbance of the mixture was measured at 517 nm to determine antioxidant activity. The DPPH radical scavenging activity was calculated as follows:

$$DPPH\ \ radical\ \ scavenging\ \ activity\ \ (\%) = \frac{A0-(A1-A2)}{A0} \times 100\,\%$$

where A_0 presents the absorbance of the control, A_1 presents the absorbance of samples (or Vc), and A_2 presents the absorbance of the blank without DPPH.

2.8 CCK-8 assay

Human colorectal cancer cell lines HT-29 and HCT116, as well as the human breast cancer cell line MDA-MB-468, were kindly provided by the Stem Cell Bank of the Chinese Academy of Sciences (Shanghai, China). The colorectal cancer cells were maintained in McCoy's 5A medium (Gibco^{TM}) supplemented with 10% fetal bovine serum (FBS; KM0502, Ozfan, Nanjing, Jiangsu, China) and 1% penicillin/streptomycin (Beyotime Biotechnology, Shanghai, China). The breast cancer cells were maintained in a dedicated cell culture medium (CM-0290B, Procell, Wuhan, Hubei, China).

Cancer cells in the exponential growth phase were seeded into 96-well plates at a density of 5×10^3 cells per well. After 24 hours, the cells were treated with *S. barbata* extracts at various concentrations: 0 μg/mL, 12.5 μg/mL, 25 μg/mL, 50 μg/mL, 100 μg/mL, 200 μg/mL, 400 μg/mL, 600 μg/mL, and 800 μg/mL. Each concentration had six replicates. Following the 72-hour incubation, 10 μL of Cell Counting Kit-8 (CCK-8) solution was added to each well, and the cells were incubated for an additional 2 hours. The IC_{50} of the extracts was determined by measuring the optical density at 450 nm using a microplate reader and plotting the dose–response curve.

3 Results and discussion

3.1 Phenotypic changes and biomass accumulation patterns of *S. barbata* at different growth stages

The phenotypic change in the aerial parts of *S. barbata* and the mass ratio of the aerial part to the root over 1 year are shown in Figures 1, 2, respectively. The aerial parts of *S. barbata* started to grow in early March. From March to early May, the biomass ratio of the aerial part to the root gradually increased, indicating vigorous growth and rapid biomass accumulation in the aerial parts during this time. However, from May onward, this ratio began to gradually decrease. Through observation, it was discovered that *S. barbata* entered the flowering period and began reproductive growth at this time, and after that, the aerial parts gradually withered. At the beginning of August, the aboveground parts underwent a second round of vigorous growth. By mid-October, they withered again. Although the aerial parts of *S. barbata* exhibited regrowth in November and December, the biomass accumulation during this time significantly slowed down compared to that in spring.

3.2 Comparative analysis of the spatial distribution of metabolites in *S. barbata*

Previous studies have isolated and identified various chemical components in *S. barbata*, but the differences in chemical composition between its aerial parts and roots remain unclear (Wang et al., 2020). In this study, UV–VIS spectroscopy was employed to scan the extract solutions of both parts. As illustrated in Figure 3, the aerial extract exhibited three distinct absorption peaks at 215 nm, 278 nm, and 335 nm, while the root extract showed only two prominent peaks at 218 nm and 278 nm. These differences in UV absorption spectra suggested that the chemical compositions of the aerial parts and roots of *S. barbata* were distinct.

HPLC–QTOF–MS/MS was also employed to elucidate the differences in chemical profiles between the aerial parts and roots of *S. barbata*. There were marked differences in the total ion

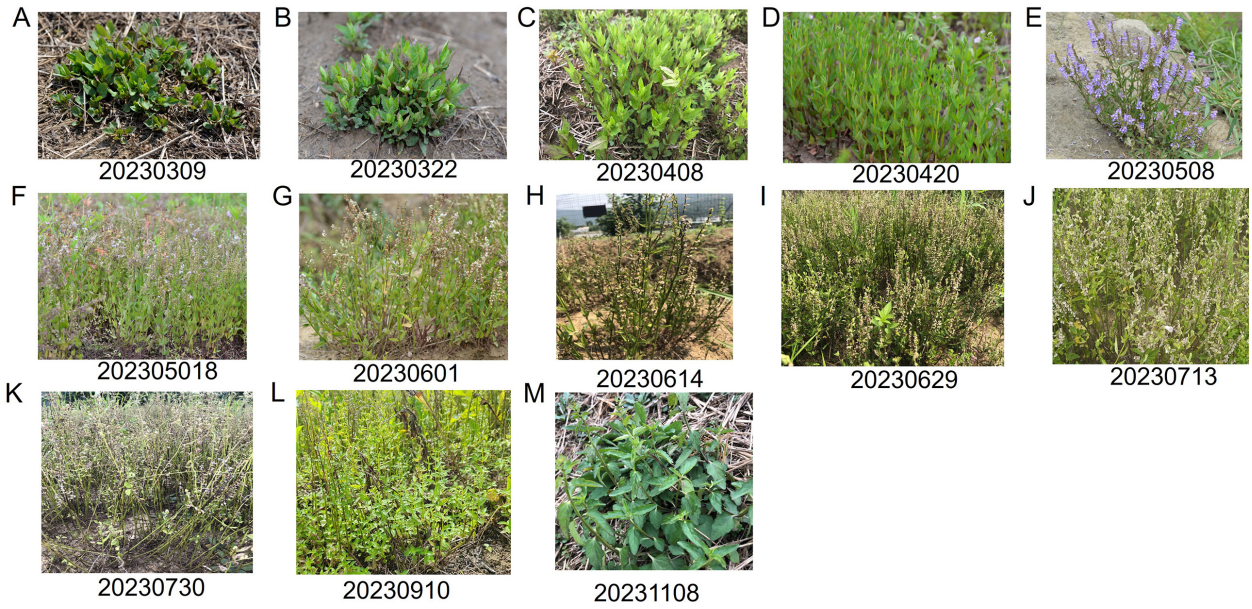

FIGURE 1
Morphology of the aerial parts of *Scutellaria barbata* at different stages over 1 year. **(A–K)** Morphological changes of the aerial parts of *S. barbata* from greening to withering during the first growth cycle (from March to July). **(L)** Morphology of the aerial parts during the second round of vigorous growth. **(M)** Morphology of the aerial parts during the third round of vigorous growth.

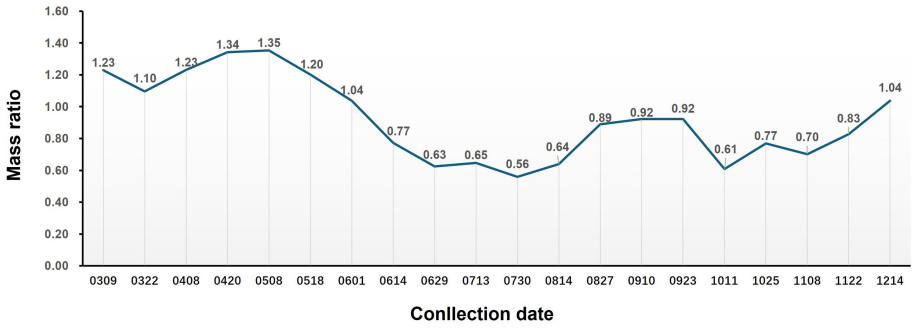

FIGURE 2
Changes in the mass ratio between the aerial parts and roots of *Scutellaria barbata* at different growth stages.

chromatograms (TICs) between the aerial parts and roots, indicating significant variations in their chemical compositions, consistent with the UV–VIS spectroscopy results (Figure 4). Upon analyzing the mass spectrometry data, a total of 46 compounds were identified in both parts of *S. barbata* (Table 1), mainly flavonoids and phenylethanol glycosides (Nos. 13 and 15). Among these, eight compounds were common to both the aerial parts and roots, including isocarthamidin-7-*O*-glucuronide, carthamidin-7-*O*-glucuronide, scutellarin, acteoside, 5,7,4′-trihydroxy-6-methoxy flavanone, 5,7,4′-trihydroxy-8-methoxy flavanone, isomer of isocarthamidin-7-*O*-glucuronide, and isomer of carthamidin-7-*O*-glucuronide. Fourteen compounds were found exclusively in the aerial parts, while 24 compounds were detected only in the roots of *S. barbata* (Figure 5A, Table 1). As depicted in Figures 5B, C, the aerial parts of *S. barbata* mainly accumulated 4′-hydroxyflavones such as scutellarin and luteolin 7-*O*-glucuronide, whereas the roots primarily accumulated specialized flavonoids lacking a 4′-OH group on their B-rings, such as baicalin and wogonoside. Similarly, our previous study revealed that the roots of *Scutellaria baicalensis* also accumulated large amounts of flavonoids without the 4′-OH group (Xu et al., 2018b). The flavonoid distribution in the aerial parts and roots of *S. barbata* is similar to the spatial distribution patterns of flavones in *S. baicalensis*. Research has shown that *S. baicalensis* possesses an evolved pathway for the biosynthesis of specific, bioactive 4′-deoxyflavones in its roots, involving enzymes such as flavone synthase II-2, cinnamic acid-specific coenzyme A ligase-7, and chalcone synthase-2 (Zhao et al., 2016). These genes are highly expressed in the roots of *S. baicalensis*, leading to the accumulation of flavonoids lacking hydroxylation at the 4′ position of the B-ring. Since *S. barbata* and *S. baicalensis* are

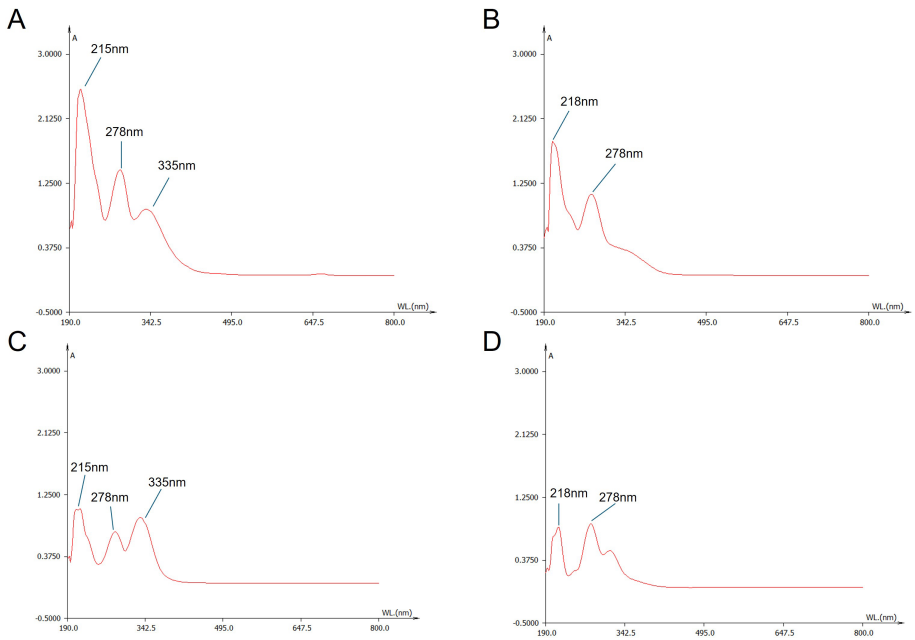

FIGURE 3
UV–Visible wavelength spectra of *Scutellaria barbata* extracts and representative flavonoid compounds. **(A)** Spectrum of the aerial part extract of *S. barbata*. **(B)** Spectrum of the root extract of *S. barbata*. **(C)** Spectrum of scutellarin. **(D)** Spectrum of baicalin.

10.3389/fpls.2024.1497664

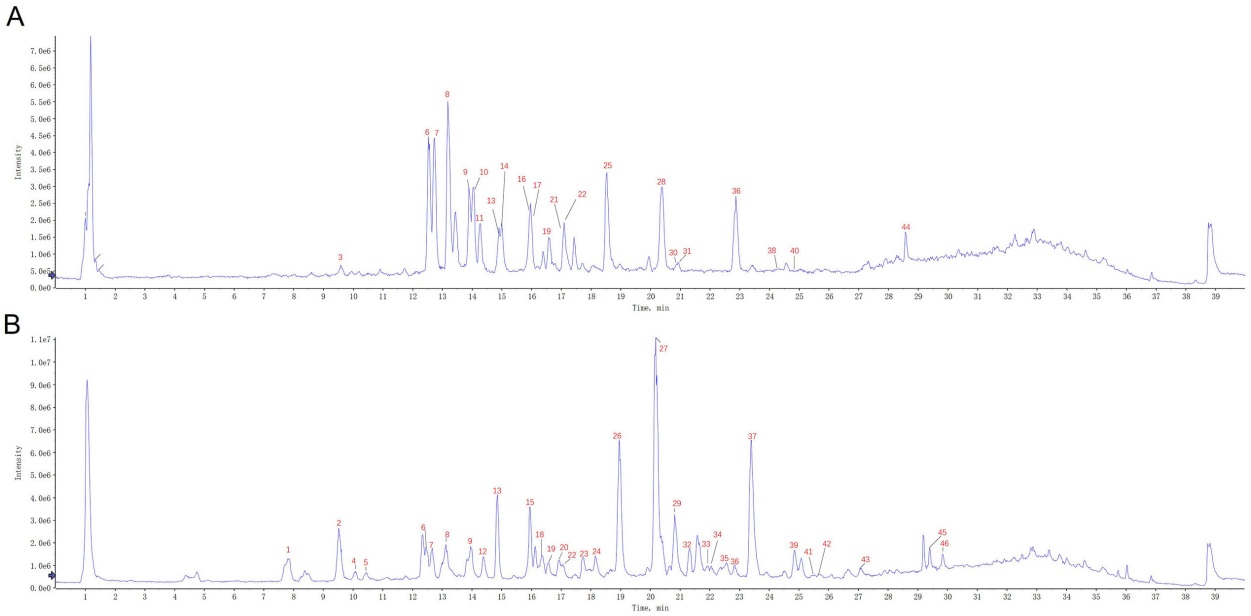

FIGURE 4
The representative TIC of *Scutellaria barbata* extracts on UHPLC–QTOF–MS. **(A)** Aerial part of *S. barbata*. **(B)** Root of *S. barbata*. The peak numbers in the TIC graph are consistent with those in Table 1. TIC, total ion chromatogram; UHPLC–QTOF–MS, ultra-high-performance liquid chromatography–quadrupole time-of-flight–mass spectrometry.

TABLE 1 Characterization of chemical constituents in *Scutellaria barbata* by UHPLC–QTOF–MS/MS.

No.	t_R (min)	Molecular formulas	[M−H] predicted	$[M-H]^-$ measured (error)	(−)-ESI–MS/MS (*m/z*)	$[M+H]^+$ measured (error)	Identification
1	7.79	$C_{21}H_{20}O_{13}$	479.0831	479.0809 (−4.6)	303.0499, 285.0389, 217.0498, 193.0352, 161.0250, 139.0050, 123.0107	481.0971 (−1.2)	5,6,7,3′,4′-Pentahydroxy flavanone-7-*O*-glucuronide [B]
2	9.421	$C_{21}H_{16}O_{13}$	475.0518	475.0495 (−4.9)	299.0192, 271.0237, 227.0361, 213.0227, 201.0202	477.0663 (−0.1)	5,6,7-Trihydroxy-8-methoxy flavone-7-*O*-β-D-glucuronide [B]
3	9.64	$C_{27}H_{30}O_{15}$	593.1512	593.149 (−3.7)	575.1407, 503.1181, 473.1066, 383.0751, 353.0652	595.1658 (0.1)	Vicenin-2 [A]
4	10.102	$C_{21}H_{20}O_{13}$	479.0831	479.0805 (−5.5)	303.0502, 285.0397, 217.0516, 193.0355, 161.0256, 139.0053, 123.0103	481.0973 (−0.8)	Isomer of 5,6,7,3′,4′-pentahydroxy flavanone-7-*O*-glucuronide [B]
5	10.458	$C_{21}H_{20}O_{13}$	479.0831	479.0805 (−5.5)	303.0501, 285.0378, 217.0439, 193.0348, 161.0249, 139.0053,	481.0975 (−0.3)	Isomer of 5,6,7,3′,4′-pentahydroxy flavanone-7-*O*-glucuronide [B]
6	12.44	$C_{21}H_{20}O_{12}$	463.0882	463.0868 (−3.0)	287.0551, 269.0453,259.0609,181.0152, 166.9997, 153.0210,139.0060, 119.0532,113.0284	465.1024 (−0.8)	Isocarthamidin-7-*O*-glucuronide [AB]
7	12.626	$C_{21}H_{20}O_{12}$	463.0882	463.087 (−2.6)	287.0550, 269.0458, 259.0610, 193.0166, 181.0154, 166.9998, 153.0210, 119.0535,113.0277	465.1026 (−0.3)	Isomer of isocarthamidin-7-*O*-glucuronide [AB]
8	13.167	$C_{21}H_{18}O_{12}$	461.0725	461.0716 (−2.1)	285.0401, 267.0301, 257.0386, 239.0342, 213.0551, 195.0455, 175.0261, 113.0279	463.0873 (0.4)	Scutellarin [AB]
9	13.909	$C_{21}H_{20}O_{12}$	463.0882	463.0865 (−3.7)	287.0548, 269.0452, 259.0615, 193.0141, 181.0147, 166.9990, 153.0202, 139.0052,119.0521, 113.0274	465.1027 (−0.1)	Carthamidin-7-*O*-glucuronide [AB]

(Continued)

10.3389/fpls.2024.1497664

TABLE 1 Continued

No.	t_R (min)	Molecular formulas	[M−H] predicted	$[M-H]^-$ measured (error)	(−)-ESI−MS/MS (*m/z*)	$[M+H]^+$ measured (error)	Identification
10	14.01	$C_{21}H_{20}O_{12}$	463.0882	463.0866 (−3.5)	287.0546, 269.0449, 259.0601, 193.0341, 181.0151, 166.9995, 153.0205, 139.0053, 119.0532, 113.0277	465.1026 (−0.3)	Isomer of carthamidin-7-*O*-glucuronide [A]
11	14.246	$C_{21}H_{20}O_{10}$	431.0984	431.0966 (−4.1)	26930446, 225.0561, 117.0372	433.1133 (0.9)	Apigenin-7-*O*-glucoside [A]
12	14.384	$C_{21}H_{18}O_{12}$	461.0725	461.0702 (−5.1)	285.0389, 267.0280, 223.0389, 185.0628, 139.0045, 113.0270	463.0873 (0.4)	Isomer of scutellarin [B]
13	14.883	$C_{29}H_{36}O_{15}$	623.1981	623.1958 (−3.6)	623.1942, 461.1644, 161.0255, 135.0495	625.2129 (0.3)	Acteoside [AB]
14	14.976	$C_{21}H_{18}O_{12}$	461.0725	461.0706 (−4.2)	285.0400, 257.0411, 241.0510, 229.0490, 213.0549, 185.0690, 113.0268	463.0871 (0)	Kaempferol-3-*O*-glucuronide [A]
15	15.942	$C_{29}H_{36}O_{15}$	623.1981	623.1955 (−4.2)	461.1645, 161.0265, 133.0310	625.2119 (−1.3)	Isomer of acteoside [B]
16	15.973	$C_{21}H_{20}O_{11}$	447.0933	447.0922 (−2.4)	271.0611, 175.0266, 151.0051, 113.0277	449.1077 (−0.3)	Naringenin-7-*O*-glucuronide [A]
17	15.973	$C_{21}H_{18}O_{11}$	445.0776	445.0762 (−3.2)	269.0455, 225.0572, 175.0254, 113.0278	447.0922 (0)	Apigenin-7-*O*-glucuronide [A]
18	16.37	$C_{21}H_{20}O_{12}$	463.0882	463.0862 (−4.3)	301.0349, 287.0549, 239.0369, 166.9981, 139.0052	465.1026 (−0.3)	Isomer of Isocarthamidin-7-*O*-glucuronide [B]
19	16.61	$C_{22}H_{20}O_{12}$	475.0882	475.087 (−2.5)	299.0556, 284.0323, 175.0253	477.1022 (−1.2)	5,7,8-Trihydroxy-6-methoxy flavone-7-*O*-glucuronide [AB]
20	16.899	$C_{21}H_{18}O_{12}$	461.0725	461.0704 (−4.7)	285.0395, 267.0280, 239.0351, 223.0410, 167.0008, 151.0055, 139.0050, 113.0260	463.0869 (−0.4)	Isoscutellarein-7-*O*-β-D-glucuronide [B]
21	17.101	$C_{22}H_{20}O_{12}$	475.0882	475.0866 (−3.4)	299.0548, 284.0318, 175.0249, 113.0271	477.1029 (0.3)	5,7,2′-Trihydroxy-6-methoxy flavone-7-*O*-glucuronide [A]
22	17.101	$C_{22}H_{22}O_{12}$	477.1039	477.1022 (−3.5)	301.0710, 286.0479, 181.0143, 175.0258, 165.9919, 113.0276	479.1180 (−0.8)	5,7,2′-Trihydroxy-8-methoxy flavanone-7-*O*-glucuronide [AB]
23	17.733	$C_{22}H_{22}O_{11}$	461.1089	461.1067 (−4.8)	299.0550, 284.0323, 165.9916	463.1237 (0.5)	5,7,2′-Trihydroxy-6-methoxy flavone 7-*O*-glucoside [B]
24	18.154	$C_{22}H_{20}O_{12}$	475.0882	475.0858 (−5.1)	299.0552, 284.0318, 175.0256, 165.9915, 113.0276	477.1021 (−1.4)	5,7,8-Trihydroxy-6-methoxy flavone 7-*O*-glucuronide [B]
25	18.549	$C_{21}H_{18}O_{12}$	461.0725	461.0705 (−4.4)	285.0397, 257.0448, 241.0498, 229.0489, 213.0570, 197.0616, 187.0407, 175.0261, 171.0465, 113.0267	463.0807 (−0.2)	Luteolin 7-*O*-glucuronide [A]
26	18.96	$C_{21}H_{18}O_{11}$	445.0776	445.0754 (−5.0)	269.0441, 251.0339, 241.0475, 223.0394, 195.0453, 113.0277	447.0923 (0.3)	Baicalin [B]
27	20.179	$C_{21}H_{20}O_{11}$	447.0933	447.0914 (−4.2)	271.0598, 253.0502, 243.0666, 113.0280	449.1075 (−0.8)	Dihydrobaicalin [B]
28	20.374	$C_{16}H_{14}O_6$	301.0718	301.0714 (−1.2)	286.0476, 258.0520, 181.0146, 165.9917, 137.9976, 119.0531, 110.0045	303.0864 (0.3)	5,7,4′-Trihydroxy-6-methoxy flavanone [A]
29	20.81	$C_{21}H_{18}O_{11}$	445.0776	445.0758 (−4.1)	269.0450, 241.0501, 225.0554, 213.0550, 197.0616, 171.0465, 113.0272	447.0922 (0)	Norwogonin 7-*O*-glucuronide [B]
30	20.9	$C_{15}H_{10}O_6$	285.0405	285.04 (−1.6)	257.0396, 241.0500, 217.0496, 199.0410, 175.0405, 151.0042, 133.0314	287.0549 (−0.4)	Luteolin [A]
31	20.938	$C_{31}H_{40}O_{15}$	651.2294	651.2285 (−1.5)	475.1829, 329.1212, 193.0497, 175.0400, 160.0157	653.2431 (−1.4)	Cistanoside D [A]

(Continued)

10.3389/fpls.2024.1497664

TABLE 1 Continued

No.	t_R (min)	Molecular formulas	[M−H] predicted	$[M-H]^-$ measured (error)	(−)-ESI−MS/MS (*m/z*)	$[M+H]^+$ measured (error)	Identification
32	21.276	$C_{21}H_{18}O_{11}$	445.0776	445.0757 (−4.3)	269.0443, 241.0496, 225.0538, 197.0606, 171.0456	447.0921 (−0.2)	Norwogonin 8-*O*-glucuronide [B]
33	21.925	$C_{21}H_{18}O_{10}$	429.0827	429.0809 (−4.2)	253.0500, 225.0543, 209.0611, 175.0254, 143.0530, 113.0278	431.0972 (−0.2)	Chrysin 7-*O*-glucuronide [B]
34	22.074	$C_{22}H_{20}O_{11}$	459.0933	459.0916 (−3.7)	283.0609, 268.0375, 175.0252, 113.0280	461.1077 (−0.3)	Oroxylin A 7-*O*-glucuronide [B]
35	22.578	$C_{23}H_{24}O_{11}$	475.12459	475.1224 (−4.6)	313.0702, 289.0467, 283.0236, 255.0299	477.1387 (−0.9)	Cirsimaritin 4′-glucoside [B]
36	22.88	$C_{16}H_{14}O_6$	301.0718	301.0714 (−1.2)	286.0475, 258.00513, 181.0147, 165.9918, 137.9979, 119.0536, 110.0052	303.0863 (0)	5,7,4′-Trihydroxy-8-methoxy flavanone [AB]
37	23.402	$C_{22}H_{20}O_{11}$	459.0933	459.0919 (−3.0)	283.0601, 268.0368, 175.0261, 113.0281	461.1074 (−1)	Wogonoside [B]
38	24.327	$C_{16}H_{12}O_6$	299.0561	299.0559 (−0.7)	284.0320, 256.0367, 227.0331, 212.0467, 136.9891	301.0712 (1.8)	4′-Hydroxywogonin [A]
39	24.844	$C_{23}H_{22}O_{12}$	489.1039	489.1022 (−3.4)	313.0711, 298.0474, 283.0240, 255.0306, 175.0252, 113.0280	491.1182 (−0.4)	5,7-Dihydroxy-8,2′-dimethoxy flavone 7-*O*-glucuronide [B]
40	24.928	$C_{16}H_{12}O_6$	299.0561	299.0557 (−1.4)	284.0316, 256.0349, 227.0334, 212.0468, 136.9899	301.0707 (0.1)	Hispidulin [A]
41	25.477	$C_{15}H_{10}O_5$	269.0456	269.0455 (0.2)	241.0508, 225.0548, 213.0562, 197.0611, 171.0463, 155.0519	271.0599 (−0.7)	Apigenin [B]
42	25.703	$C_{16}H_{14}O_6$	301.0718	301.0712 (−1.9)	286.0461, 195.0296, 181.0144, 165.9918, 155.0360, 140.0128, 119.0518, 110.0015	303.0862 (−0.4)	Isomer of 5,7,4′-trihydroxy-8-methoxy flavanone [B]
43	27.096	$C_{15}H_{10}O_5$	269.0456	269.045 (−2.0)	251.0325, 241.0492, 223.0401, 195.0444, 169.0667, 139.0043	271.0600 (−0.4)	Baicalin [B]
44	28.575	$C_{15}H_{12}O_5$	271.0612	271.0613 (0.4)	187.0413, 119.0534	273.0758 (0.2)	Naringenin [A]
45	29.405	$C_{16}H_{12}O_5$	283.0612	283.0611 (−0.3)	268.0366, 239.0349, 211.0394, 184.0534, 163.0051, 110.0041	285.0763 (1.9)	Wogonin [B]
46	29.838	$C_{17}H_{14}O_6$	313.0718	313.0715 (−0.8)	298.0482, 283.0245, 255.0301, 183.0454, 164.9840	315.0864 (0.3)	5,7-Dihydroxy-6,8-dimethoxy flavone [B]

UHPLC–QTOF–MS, ultra-high-performance liquid chromatography–quadrupole time-of-flight–mass spectrometry; ESI–MS/MS, electrospray ionization–tandem mass spectrometry.
[A]Compound identified in the aerial parts of *S. barbata*.
[B]Compound identified in the roots of *S. barbata*. The identification of compounds No. 3 and No. 40 were based on Li et al. (2015), and the other compounds were identified according to Xu et al. (2018b).

closely related species in the same genus, it is likely that a similar flavonoid without a 4′-OH group biosynthetic pathway exists in the roots of *S. barbata*. This pathway may run parallel to the classic flavone biosynthesis and specifically produce flavonoids that lack 4′-OH groups.

3.3 Seasonal dynamics of quality-related flavonoids in *S. barbata*

The accumulation of total flavonoids in the aerial parts and roots of *S. barbata* was quantitatively analyzed at different periods over 1 year, as shown in Figures 6A, B. The total flavonoid content in the aerial parts ranged from 10.99 ± 0.15 mg/g (collected on October 11) to 25.87 ± 0.91 mg/g (collected on March 22), while in the roots, it varied from 36.65 ± 1.12 mg/g (collected on December 14) to 73.38 ± 1.56 mg/g (collected on October 25). The accumulation of flavonoids in the aerial parts varied significantly across different growth stages. From early March to late April, when *S. barbata* primarily engaged in vegetative growth, the flavonoid content in the aerial parts was high and relatively stable. During May, the flowering period, there was a rapid decrease in flavonoid accumulation in the aerial parts. This may be due to the anthocyanidins and other flavonoids derived from the common biosynthetic pathway and share the same precursors (Li et al., 2016). The inhibition of flavonoid synthesis in vegetative organs leads to an increased accumulation of anthocyanidins in reproductive organs (Lim et al., 2016). From June to August, as the aboveground parts

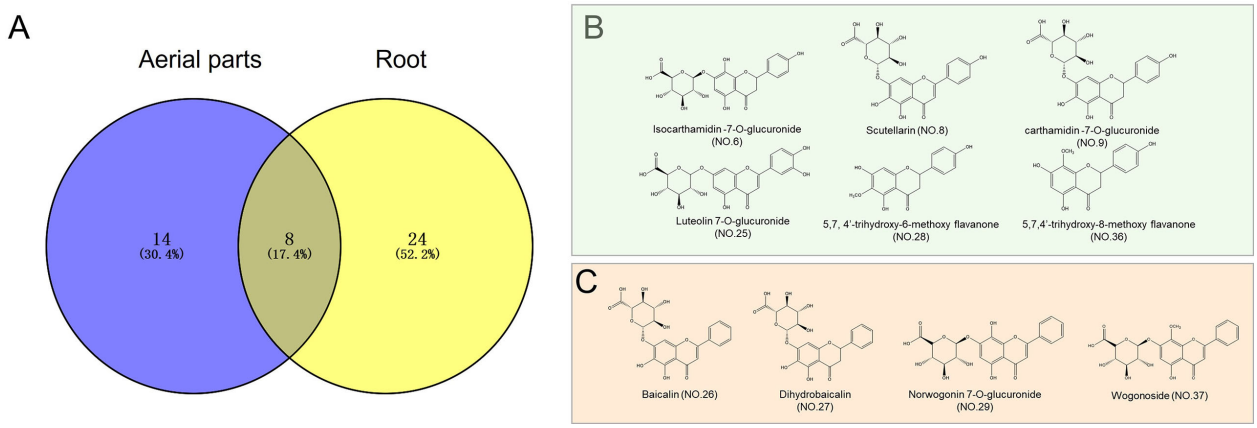

FIGURE 5
Distribution of the identified compounds in *Scutellaria barbata* and the chemical structures of representative compounds. **(A)** Venn diagram showing the distribution of identified compounds in *S. barbata*. **(B)** Chemical structures of the main flavonoids identified in the aerial parts of *S. barbata*. **(C)** Chemical structures of the main flavonoids identified in the roots of *S. barbata*.

began to wither, the contents of flavonoids initially increased and subsequently decreased. In early September and early November, the aboveground parts regrew, and flavonoid accumulation exhibited a similar pattern. However, the peak levels during these later stages (samples from September 10 and November 8) were lower than those observed during the initial vegetative growth phase (sample from March 22).

Changes in flavonoid accumulation may be related to the intensity and duration of daylight. Light, particularly UV radiation, can cause DNA damage and other cellular injuries in plants (Banerjee et al., 2024). Flavonoids act as effective UV filters, protecting plant cells by absorbing and dissipating UV radiation (Hichri et al., 2011; Ferreyra et al., 2021; Cao et al., 2024). Numerous studies have shown that UV radiation is a key environmental signal that triggers flavonoid synthesis in plants (Liu et al., 2015; Henry-Kirk et al., 2018; Xie et al., 2020). Plants grown under high-light conditions or longer daylight periods typically accumulated more flavonoids compared to those grown in shaded or low-light environments (Götz et al., 2010; Deng et al., 2012). *S. barbata* primarily grows from March to August, during the

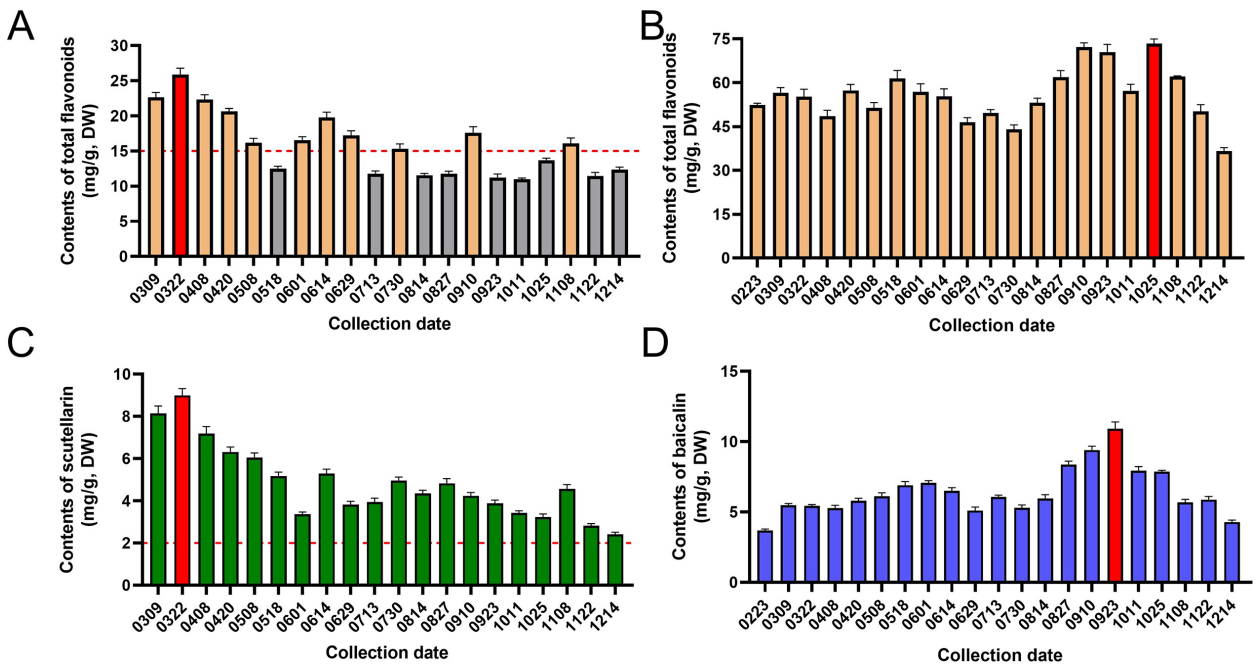

FIGURE 6
The accumulation patterns of quality-related flavonoids in *Scutellaria barbata*. **(A)** The contents of total flavonoids in aerial parts of *S. barbata* at different collection dates. **(B)** The contents of total flavonoids in roots of *S. barbata* at different collection dates. **(C)** The contents of scutellarin in aerial parts of *S. barbata* at different collection dates. **(D)** The contents of baicalin in roots of *S. barbata* at different collection dates.

spring and summer months. The high abundance of flavonoids during this period likely helps protect the leaves against the increasing light duration and UV intensity (Brunetti et al., 2013). In contrast, the subsequent greening periods in September and November, which occur during autumn and winter, coincide with shorter days and lower light intensity, reducing the need for UV protection. This seasonal variation may explain the differences in flavonoid accumulation observed during the vegetative growth stages of *S. barbata* at different times over 1 year.

Scutellarin is a quality marker for *S. barbata* as stipulated in the Chinese Pharmacopoeia. This study further analyzed the accumulation pattern of scutellarin in aerial parts of *S. barbata* across different growth stages. As shown in Figure 6C, the content of scutellarin in the aerial parts ranged from 2.41 ± 0.10 mg/g (collected on December 14) to 9.00 ± 0.32 mg/g (collected on March 22). The accumulation pattern of scutellarin in the aerial parts of *S. barbata* was consistent with that of total flavonoid. Scutellarin levels peaked in late March and gradually declined as the plant entered its flowering period. Following the end of reproductive growth, the content of scutellarin in *S. barbata* increased again, reaching another peak in August. The results indicated that the scutellarin content in the aerial parts of *S. barbata* exceeded the Chinese Pharmacopoeia's requirement (not less than 0.20%) at almost all development stages. However, the total flavonoid content in *S. barbata* meets the Chinese Pharmacopoeia standards (not less than 1.50%) only when the aerial parts grow vigorously.

This study found that the total flavonoid content in the roots of *S. barbata* ranged from 36.65 ± 1.12 mg/g (collected on December 14) to 73.38 ± 1.56 mg/g (collected on October 25). The accumulation pattern of total flavonoids in the roots differed significantly from that in the aerial parts. From February to July, while the total flavonoid content in the aerial parts underwent dramatic changes, the content in the roots only fluctuated slightly. However, from August to December, the accumulation of total flavonoids in the roots underwent two times distinct increases. This metabolic shift may be a response to environmental stress through nutrient reallocation. Reduced light hours, decreasing temperatures, and decreased water availability are common in autumn. In roots, flavonoids can stabilize cell membranes and mitigate oxidative stress induced by low temperatures, aiding in cold acclimation (Genzel et al., 2021; Song et al., 2023). The accumulated flavonoids may also improve drought resistance by maintaining cellular osmotic balance and protecting cells from dehydration (Nakabayashi et al., 2014; Zuo et al., 2024). Additionally, during the withering period, plants undergo metabolic reconstruction, leading to the accumulation of secondary metabolites in the roots (Zeng et al., 2017; Liu et al., 2020). These factors may contribute to the accumulation of total flavonoids in the roots of *S. barbata* in the fall.

The chemical profiles of *S. barbata* roots and aerial parts differ significantly, yet the Chinese Pharmacopoeia does not define specific chemical components for assessing the quality of roots. In this study, baicalin (No. 26 in Figure 4B) was identified as a major component in the roots of *S. barbata*. Previous studies have indicated that baicalin can exhibit significant pharmacological activity and serve as a quality marker for *S. baicalensis*, a root-based Chinese medicinal material (Zhang et al., 2023; Wang et al., 2024; Chinese Pharmacopoeia Commission, 2020). Therefore, the accumulation pattern of baicalin in the roots was examined to gain insights into the quality changes of *S. barbata*. The content of baicalin in *S. barbata* roots varied from 4.29 ± 0.14 mg/g (collected on December 14) to 10.92 ± 0.48 mg/g (collected on September 23). Figure 6D illustrates that the accumulation pattern of baicalin in the roots of *S. barbata* was inversely related to that of scutellarin in the aerial parts. The scutellarin was primarily accumulated during the vigorous growth of the aerial parts in spring, while baicalin in the roots of *S. barbata* reached the highest accumulation level when the aerial parts grew slowly in autumn.

The findings indicated that the aerial parts of *S. barbata* could be harvested several times annually. To enhance biomass accumulation and comply with the Chinese Pharmacopoeia's standards for total flavonoid and scutellarin content, it is recommended to harvest the aerial parts of *S. barbata* during the vigorous growth periods in March, April, June, early September, and early November. When roots are needed, harvesting should take place in the autumn season from August to November to maximize the flavonoid accumulation in the roots of *S. barbata*.

3.4 Comparative analysis of the pharmacodynamic activities of the aerial parts and roots of *S. barbata*

We observed distinct differences in the chemical profiles of the aerial and underground parts of *S. barbata*, but the variation in their pharmacodynamic activities remained unclear. Previous studies have demonstrated that *S. barbata* extracts exhibit strong antioxidant activity and inhibit cancer cell proliferation (Chen et al., 2020; Liu et al., 2022). Therefore, a functional analysis was performed to assess the *in vitro* antioxidant and cytotoxic activities of the different parts of *S. barbata*. Figures 7A, B illustrate that both the aerial parts extracts (DS) and root extracts (DX) of *S. barbata* exhibited good antioxidant activity. This activity was concentration-dependent with the total flavonoids in the extracts. The DX demonstrated stronger free radical scavenging activity than that of DS, regardless of whether assessed using the DPPH or ABTS method. To evaluate the differences in the effects of DS and DX on cancer cell proliferation, CCK-8 assays were performed. HT-29 and MDA-MB-468 cells were treated with DS and DX, respectively, resulting in a dose-dependent decrease in cell viability (Figures 7C, D). The IC_{50} of DX in MDA-MB-468 cells was lower than that of DS. However, DS exhibited a greater cytotoxic activity than DX in HT-29 cells.

The biological activity of a compound is closely linked to its structure. While flavonoids share a similar core structure, their activities differ due to variations in the types, numbers, and positions of functional groups on core structures. In this study, we found that although both the aerial parts and roots of *S. barbata* were rich in flavonoids, the type and concentration of these flavonoids differ significantly. The primary flavonoids in the aerial

parts were isocarthamidin-7-*O*-glucuronide, scutellarin, carthamidin-7-*O*-glucuronide, luteolin-7-*O*-glucuronide, 5,7,4′-trihydroxy-6-methoxy flavanone, 5,7,4′-trihydroxy-8-methoxy flavanone, while those in the roots were predominantly baicalin, dihydrobaicalin, norwogonin-7-*O*-glucuronide, and wogonoside. Research suggests that the hydroxyl group on the B-ring (C-4′) is more effective for enzyme inhibition, while the hydroxyl group on the A-ring (C-6) is more effective for antioxidant activity. Scutellarin and apigenin, which own the hydroxyl group on the B-ring (C-4′), contribute more to overall enzyme inhibition, while baicalin with no hydroxyl group on the B-ring (C-4′) is a key component to the antioxidant activity of *S. baicalensis* extracts (Li et al., 2018). Yang et al. found that, despite owned structural similarity, baicalin and scutellarin promoted glucose disposal in adipocytes through differential regulation of the AKT pathway, with scutellarin showing much more favorable binding energy to Akt (−29.81 kcal/mol) compared to baicalin (4.04 kcal/mol) (Yang et al., 2017). The IC_{50} of baicalin is approximately twice that of scutellarin, suggesting that the 4′-hydroxyl group plays a positive role in urease inhibition (Yu et al., 2015). While these studies do not completely clarify the differences in efficacy between the aerial parts and roots of *S. barbata*, it is evident that their distinct chemical compositions lead to varying biological activities and pharmacological mechanisms. This aligns with the multi-component, multi-target therapeutic mechanisms characteristic of traditional Chinese medicine. Therefore, it is essential to precisely specify the harvesting parts of *S. barbata* and control the proportion of different parts to ensure the quality and consistency of the medicinal material.

Conclusion

This study elucidated the distinct chemical profiles and accumulation patterns of flavonoids in the aerial parts and roots of *S. barbata*. The findings demonstrated that the aerial parts could be harvested during periods of vigorous growth in spring and early autumn to maximize flavonoid content, while the roots should be harvested in autumn to ensure high flavonoid accumulation. The study also highlighted significant differences in antioxidant and

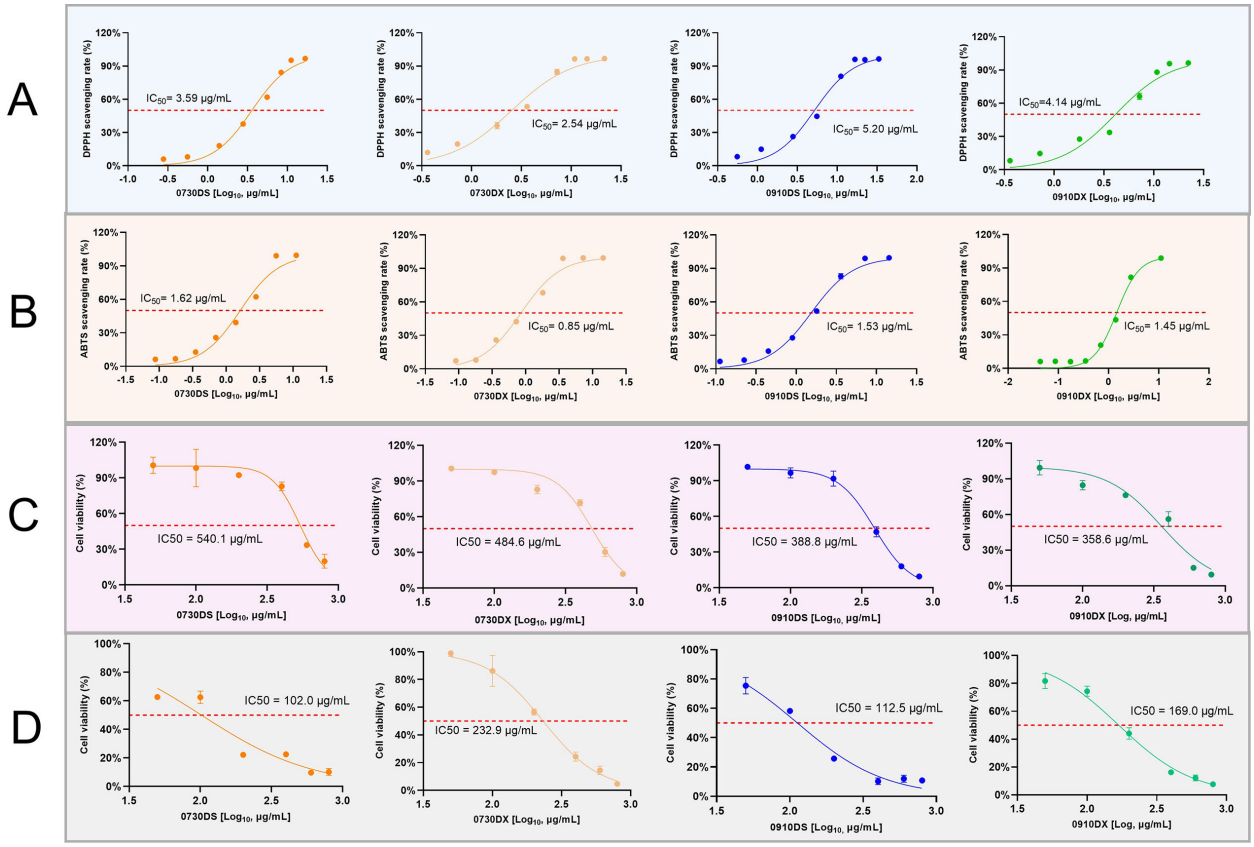

FIGURE 7
Comparative activities of extracts from the aerial parts and roots of *Scutellaria barbata*. **(A)** DPPH free radical scavenging activity. **(B)** ABTS free radical scavenging activity. **(C)** Inhibitory activity on breast cancer cell proliferation. **(D)** Inhibitory activity on colon cancer cell proliferation. 0730, sample collected on July 30; 0910, sample collected on September 10; DS, aerial part extract of *S. barbata*; DX, root extract of *S. barbata*.

anticancer activities between the aerial parts and roots, likely linked to their unique chemical compositions. These results underscore the importance of specifying harvesting periods and plant parts to ensure consistent quality in *S. barbata*. The insights would contribute to the development of standardized harvesting protocols and quality control measures for *S. barbata*.

Data availability statement

The original contributions presented in the study are included in the article/Supplementary Material. Further inquiries can be directed to the corresponding authors.

Author contributions

YC: Conceptualization, Formal analysis, Investigation, Validation, Visualization, Writing – original draft. WC: Data curation, Formal analysis, Investigation, Writing – original draft. RG: Data curation, Formal analysis, Investigation, Writing – original draft. RC: Data curation, Resources, Supervision, Writing – original draft. XL: Conceptualization, Resources, Supervision, Writing – original draft. DQ: Conceptualization, Project administration, Resources, Supervision, Writing – review & editing. JX: Conceptualization, Funding acquisition, Project administration, Resources, Writing – review & editing.

Funding

The author(s) declare financial support was received for the research, authorship, and/or publication of this article. This work was supported by the National Natural Science Foundation of China (82003885), the Suzhou science and technology plan project (SNG2022027) and Jiangsu Agricultural Science and Technology Innovation Funds (CX(23)3100).

Conflict of interest

Author XL was employed by the company Suzhou Qifan Agricultural Technology Co., Ltd.

The remaining authors declare that the research was conducted in the absence of any commercial or financial relationships that could be construed as a potential conflict of interest.

Publisher's note

Supplementary material

The Supplementary Material for this article can be found online at: https://www.frontiersin.org/articles/10.3389/fpls.2024.1497664/full#supplementary-material

SUPPLEMENTARY FIGURE 1
Calibration curves for the quantitative analysis of flavonoids in *S. barbata*. **(A)** Calibration curve for the quantification of total flavonoids in the aerial parts of *S. barbata* by UV spectrophotometry. **(B)** Calibration curve for the quantification of total flavonoids in the roots of S. barbata by UV spectrophotometry. **(C)** Calibration curve for the quantification of scutellarin in the aerial parts of *S. barbata* by HPLC. **(D)** Calibration curve for the quantification of baicalin in the roots of *S. barbata* by HPLC.

SUPPLEMENTARY FIGURE 2
The TIC chromatogram of *S. barbata* extracts on UHPLC-QTOF-MS in positive ion model. **(A)** Aerial part of *S. barbate*. **(B)** root of *S. barbate*.

SUPPLEMENTARY FIGURE 3
The representative TIC chromatogram of *S. barbata* collected at different date in negative ion model. **(A)** Aerial part of *S. barbate* collected on November 8. **(B)** Aerial part of *S. barbate* collected on April 20. **(C)** Root of *S. barbate* collected on April 20 or November 8. **(D)** Root of *S. barbate* collected on April 20.

References

Ali Reza, A. S. M., Nasrin, M. S., Hossen, M. A., Rahman, M. A., Jantan, I., Haque, M. A., et al. (2023). Mechanistic insight into immunomodulatory effects of food-functioned plant secondary metabolites. *Crit. Rev. Food Sci. Nutr.* 63, 5546–5576. doi: 10.1080/10408398.2021.2021138

Banerjee, S., Agarwal, P., Choudhury, S. R., and Roy, S. (2024). MYB4, a member of R2R3-subfamily of MYB transcription factor functions as a repressor of key genes involved in flavonoid biosynthesis and repair of UV-B induced DNA double strand breaks in Arabidopsis. *Plant Physiol. Biochem.* 211, 108698. doi: 10.1016/j.plaphy.2024.108698

Bouyahya, A., Guaouguaou, F.-E., El Omari, N., El Menyiy, N., Balahbib, A., El-Shazly, M., et al. (2022). Anti-inflammatory and analgesic properties of Moroccan medicinal plants: Phytochemistry, in *vitro* and in *vivo* investigations, mechanism insights, clinical evidences and perspectives. *J. Pharm. Anal.* 12, 35–57. doi: 10.1016/j.jpha.2021.07.004

Brunetti, C., Di Ferdinando, M., Fini, A., Pollastri, S., and Tattini, M. (2013). Flavonoids as antioxidants and developmental regulators: relative significance in plants and humans. *Int. J. Mol. Sci.* 14, 3540–3555. doi: 10.3390/ijms14023540

Cao, Y., Mei, Y., Zhang, R., Zhong, Z., Yang, X., Xu, C., et al. (2024). Transcriptional regulation of flavonol biosynthesis in plants. *Hortic. Res.* 11, uhae043. doi: 10.1093/hr/uhae043

Chen, X., Bahramimehr, F., Shahhamzehei, N., Fu, H., Lin, S., Wang, H., et al. (2024). Anti-aging effects of medicinal plants and their rapid screening using the nematode Caenorhabditis elegans. *Phytomedicine* 129, 155665. doi: 10.1016/j.phymed.2024.155665

Chen, Q., Rahman, K., Wang, S.-J., Zhou, S., and Zhang, H. (2020). Scutellaria barbata: A review on chemical constituents, pharmacological activities and clinical applications. *Curr. Pharm. Des.* 26, 160–175. doi: 10.2174/1381612825666191216124310

Cheng, Y., Zhang, Y., Sun, H., Huang, D., Jiang, B., and Xu, J. (2022). Optimization of ultrasonic-assisted total flavonoids extraction from flower of Albizia julibrissin durazz. by response surface methodology for characterization of chemical profile and evaluation of antioxidant and tyrosinase inhibitory activities. *AJBB* 18, 100–117. doi: 10.3844/ajbbsp.2022.100.117

Chinese Pharmacopoeia Commission. (2020). *Pharmacopoeia of the People's Republic of China. 2015th Edn* (Beijing: Chinese Medical Science and Technology Press).

del Baño, M. J., Lorente, J., Castillo, J., Benavente-García, O., Marín, M. P., Del Río, J. A., et al. (2004). Flavonoid distribution during the development of leaves, flowers, stems, and roots of Rosmarinus officinalis. postulation of a biosynthetic pathway. *J. Agric. Food Chem.* 52, 4987–4992. doi: 10.1021/jf040078p

Deng, B., Shang, X., Fang, S., Li, Q., Fu, X., and Su, J. (2012). Integrated effects of light intensity and fertilization on growth and flavonoid accumulation in Cyclocarya paliurus. *J. Agric. Food Chem.* 60, 6286–6292. doi: 10.1021/jf301525s

Ferreyra, M. L. F., Serra, P., and Casati, P. (2021). Recent advances on the roles of flavonoids as plant protective molecules after UV and high light exposure. *Physiol. Plant* 173, 736–749. doi: 10.1111/ppl.13543

Gao, Y., Huang, R., Qiu, Y., Liu, Y., and Chen, L. (2024). Characterization of the chemical composition of different parts of Dolichos lablab L. and revelation of its anti-ulcerative colitis effects by modulating the gut microbiota and host metabolism. *J. Ethnopharmacol* 322, 117629. doi: 10.1016/j.jep.2023.117629

Genzel, F., Dicke, M. D., Junker-Frohn, L. V., Neuwohner, A., Thiele, B., Putz, A., et al. (2021). Impact of moderate cold and salt stress on the accumulation of antioxidant flavonoids in the leaves of two capsicum cultivars. *J. Agric. Food Chem.* 69, 6431–6443. doi: 10.1021/acs.jafc.1c00908

Götz, M., Albert, A., Stich, S., Heller, W., Scherb, H., Krins, A., et al. (2010). PAR modulation of the UV-dependent levels of flavonoid metabolites in Arabidopsis thaliana (L.) Heynh. leaf rosettes: cumulative effects after a whole vegetative growth period. *Protoplasma* 243, 95–103. doi: 10.1007/s00709-009-0064-5

Hazrati, S., Mousavi, Z., and Nicola, S. (2024). Harvest time optimization for medicinal and aromatic plant secondary metabolites. *Plant Physiol. Biochem.* 212, 108735. doi: 10.1016/j.plaphy.2024.108735

Henry-Kirk, R. A., Plunkett, B., Hall, M., McGhie, T., Allan, A. C., Wargent, J. J., et al. (2018). Solar UV light regulates flavonoid metabolism in apple (Malus x domestica). *Plant Cell Environ.* 41, 675–688. doi: 10.1111/pce.13125

Hichri, I., Barrieu, F., Bogs, J., Kappel, C., Delrot, S., and Lauvergeat, V. (2011). Recent advances in the transcriptional regulation of the flavonoid biosynthetic pathway. *J. Exp. Bot.* 62, 2465–2483. doi: 10.1093/jxb/erq442

Kong, D., Li, Y., Bai, M., Deng, Y., Liang, G., and Wu, H. (2017). A comparative study of the dynamic accumulation of polyphenol components and the changes in their antioxidant activities in diploid and tetraploid Lonicera japonica. *Plant Physiol. Biochem.* 112, 87–96. doi: 10.1016/j.plaphy.2016.12.027

Li, P., Dong, Q., Ge, S., He, X., Verdier, J., Li, D., et al. (2016). Metabolic engineering of proanthocyanidin production by repressing the isoflavone pathways and redirecting anthocyanidin precursor flux in legume. *Plant Biotechnol. J.* 14, 1604–1618. doi: 10.1111/pbi.12524

Li, Y., Guo, S., Zhu, Y., Yan, H., Qian, D.-W., Wang, H.-Q., et al. (2019). Comparative analysis of twenty-five compounds in different parts of Astragalus membranaceus var. mongholicus and Astragalus membranaceus by UPLC-MS/MS. *J. Pharm. Anal.* 9, 392–399. doi: 10.1016/j.jpha.2019.06.002

Li, R., Song, W., Qiao, X., Liu, j., Liang, H., and Ye, M. (2015). Chemical profiling of Scutellaria barbata by ultra high performance liquid chromatography coupled with hybrid quadrupole-orbitrap mass spectrometry. *J. Chin. Pharm. Sci.* 24, 635–646. doi: 10.5246/jcps.2015.10.081

Li, K., Yao, F., Xue, Q., Fan, H., Yang, L., Li, X., et al. (2018). Inhibitory effects against α-glucosidase and α-amylase of the flavonoids-rich extract from Scutellaria baicalensis shoots and interpretation of structure-activity relationship of its eight flavonoids by a refined assign-score method. *Chem. Cent J.* 12, 82. doi: 10.1186/s13065-018-0445-y

Lim, S.-H., You, M.-K., Kim, D.-H., Kim, J. K., Lee, J.-Y., and Ha, S.-H. (2016). RNAi-mediated suppression of dihydroflavonol 4-reductase in tobacco allows fine-tuning of flower color and flux through the flavonoid biosynthetic pathway. *Plant Physiol. Biochem.* 109, 482–490. doi: 10.1016/j.plaphy.2016.10.028

Liu, L., Gregan, S., Winefield, C., and Jordan, B. (2015). From UVR8 to flavonol synthase: UV-B-induced gene expression in Sauvignon blanc grape berry. *Plant Cell Environ.* 38, 905–919. doi: 10.1111/pce.12349

Liu, L., Liu, T., Tao, W., Liao, N., Yan, Q., Li, L., et al. (2022). Flavonoids from Scutellaria barbata D. Don exert antitumor activity in colorectal cancer through inhibited autophagy and promoted apoptosis via ATF4/sestrin2 pathway. *Phytomedicine* 99, 154007. doi: 10.1016/j.phymed.2022.154007

Liu, P., Weng, R., Xu, Y., Feng, Y., He, L., Qian, Y., et al. (2020). Metabolic changes in different tissues of garlic plant during growth. *J. Agric. Food Chem.* 68, 12467–12475. doi: 10.1021/acs.jafc.0c04178

Ma, H., Yue, G. G.-L., Lee, J. K.-M., Gao, S., Yuen, K.-K., Cheng, W., et al. (2024). Scutellarin, a flavonoid compound from Scutellaria barbata, suppresses growth of breast cancer stem cells in *vitro* and in tumor-bearing mice. *Phytomedicine* 128, 155418. doi: 10.1016/j.phymed.2024.155418

Nakabayashi, R., Yonekura-Sakakibara, K., Urano, K., Suzuki, M., Yamada, Y., Nishizawa, T., et al. (2014). Enhancement of oxidative and drought tolerance in Arabidopsis by overaccumulation of antioxidant flavonoids. *Plant J.* 77, 367–379. doi: 10.1111/tpj.12388

Rogerio, A. P., Sá-Nunes, A., and Faccioli, L. H. (2010). The activity of medicinal plants and secondary metabolites on eosinophilic inflammation. *Pharmacol. Res.* 62, 298–307. doi: 10.1016/j.phrs.2010.04.005

Sato, Y., Suzaki, S., Nishikawa, T., Kihara, M., Shibata, H., and Higuti, T. (2000). Phytochemical flavones isolated from Scutellaria barbata and antibacterial activity against methicillin-resistant Staphylococcus aureus. *J. Ethnopharmacol* 72, 483–488. doi: 10.1016/s0378-8741(00)00265-8

Song, Z., Lai, X., Chen, H., Wang, L., Yao, Y., Chen, W., et al. (2023). MaC2H2-like regulates chilling stress response of "Fenjiao" banana by modulating flavonoid synthesis and fatty acid desaturation. *Food Chem.* 419, 136089. doi: 10.1016/j.foodchem.2023.136089

Veeramohan, R., Zamani, A. I., Azizan, K. A., Goh, H.-H., Aizat, W. M., Razak, M. F. A., et al. (2023). Comparative metabolomics analysis reveals alkaloid repertoires in young and mature Mitragyna speciosa (Korth.) Havil. Leaves. *PloS One* 18, e0283147. doi: 10.1371/journal.pone.0283147

Wang, L., Chen, W., Li, M., Zhang, F., Chen, K., and Chen, W. (2020). A review of the ethnopharmacology, phytochemistry, pharmacology, and quality control of Scutellaria barbata D. Don. *J. Ethnopharmacol* 254, 112260. doi: 10.1016/j.jep.2019.112260

Wang, R., Wang, C., Lu, L., Yuan, F., and He, F. (2024). Baicalin and baicalein in modulating tumor microenvironment for cancer treatment: A comprehensive review with future perspectives. *Pharmacol. Res.* 199, 107032. doi: 10.1016/j.phrs.2023.107032

Wu, X., Xu, N., Ye, Z., Zhao, Q., Liu, J., Li, J., et al. (2022). Polysaccharide from Scutellaria barbata D. Don attenuates inflammatory response and microbial dysbiosis in ulcerative colitis mice. *Int. J. Biol. Macromol* 206, 1–9. doi: 10.1016/j.ijbiomac.2022.02.119

Xie, L., Cao, Y., Zhao, Z., Ren, C., Xing, M., Wu, B., et al. (2020). Involvement of MdUGT75B1 and MdUGT71B1 in flavonol galactoside/glucoside biosynthesis in apple fruit. *Food Chem.* 312, 126124. doi: 10.1016/j.foodchem.2019.126124

Xu, J., Li, Y., Lou, M., Xia, W., Liu, Q., Xie, G., et al. (2018a). Baicalin regulates SirT1/STAT3 pathway and restrains excessive hepatic glucose production. *Pharmacol. Res.* 136, 62–73. doi: 10.1016/j.phrs.2018.08.018

Xu, J., Yu, Y., Shi, R., Xie, G., Zhu, Y., Wu, G., et al. (2018b). Organ-Specific Metabolic Shifts of Flavonoids in Scutellaria baicalensis at Different Growth and Development Stages. *Molecules* 23, 428. doi: 10.3390/molecules23020428

Xu, H., Yu, J., Sun, Y., Xu, X., Li, L., Xue, M., et al. (2013). Scutellaria barbata D. Don extract synergizes the antitumor effects of low dose 5-fluorouracil through induction of apoptosis and metabolism. *Phytomedicine* 20, 897–903. doi: 10.1016/j.phymed.2013.03.025

Yang, L.-L., Xiao, N., Liu, J., Liu, K., Liu, B., Li, P., et al. (2017). Differential regulation of baicalin and scutellarin on AMPK and Akt in promoting adipose cell glucose disposal. *Biochim. Biophys. Acta Mol. Basis Dis.* 1863, 598–606. doi: 10.1016/j.bbadis.2016.11.024

Yu, X.-D., Zheng, R.-B., Xie, J.-H., Su, J.-Y., Huang, X.-Q., Wang, Y.-H., et al. (2015). Biological evaluation and molecular docking of baicalin and scutellarin as Helicobacter pylori urease inhibitors. *J. Ethnopharmacol* 162, 69–78. doi: 10.1016/j.jep.2014.12.041

Zeng, H., Su, S., Xiang, X., Sha, X., Zhu, Z., Wang, Y., et al. (2017). Comparative Analysis of the Major Chemical Constituents in Salvia miltiorrhiza Roots, Stems, Leaves and Flowers during Different Growth Periods by UPLC-TQ-MS/MS and HPLC-ELSD Methods. *Molecules* 22, 771. doi: 10.3390/molecules22050771

Zhang, T., Deng, W., Deng, Y., Liu, Y., Xiao, S., Luo, Y., et al. (2023). Mechanisms of ferroptosis regulating oxidative stress and energy metabolism in myocardial ischemia-reperfusion injury and a novel perspective of natural plant active ingredients for its treatment. *BioMed. Pharmacother.* 165, 114706. doi: 10.1016/j.biopha.2023.114706

Zhao, Q., Zhang, Y., Wang, G., Hill, L., Weng, J.-K., Chen, X.-Y., et al. (2016). A specialized flavone biosynthetic pathway has evolved in the medicinal plant, Scutellaria baicalensis. *Sci. Adv.* 2, e1501780. doi: 10.1126/sciadv.1501780

Zuo, H., Chen, J., Lv, Z., Shao, C., Chen, Z., Zhou, Y., et al. (2024). Tea-derived polyphenols enhance drought resistance of tea plants (Camellia sinensis) by alleviating jasmonate-isoleucine pathway and flavonoid metabolism flow. *Int. J. Mol. Sci.* 25, 3817. doi: 10.3390/ijms25073817

frontiers | Frontiers in Plant Science

TYPE Original Research
PUBLISHED 06 December 2024
DOI 10.3389/fpls.2024.1513875

OPEN ACCESS

EDITED BY
Prof Eman. A. Mahmoud,
Damietta University, Egypt

REVIEWED BY
Ahmed Noah Badr,
National Research Centre, Egypt
Siniša Srečec,
Križevci University of Applied Sciences, Croatia
Mario Juan Simirgiotis,
Austral University of Chile, Chile

*CORRESPONDENCE
Metin Yildirim
metinyildirim4@gmail.com

RECEIVED 19 October 2024
ACCEPTED 13 November 2024
PUBLISHED 06 December 2024

CITATION
Amangeldinova M, Ersatır M, Necip A, Yilmaz MA, Cimentepe M, Kudrina N, Terletskaya NV, Ozturk Cimentepe O and Yildirim M (2024) Simultaneous quantitative screening of 53 phytochemicals from *Rheum tataricum* L. roots: a comparative study of supercritical CO_2, subcritical ethanol, and ultrasound-assisted extraction for enhanced antioxidant, antibacterial activities, and molecular docking study.
Front. Plant Sci. 15:1513875.
doi: 10.3389/fpls.2024.1513875

Simultaneous quantitative screening of 53 phytochemicals from *Rheum tataricum* L. roots: a comparative study of supercritical CO_2, subcritical ethanol, and ultrasound-assisted extraction for enhanced antioxidant, antibacterial activities, and molecular docking study

Madina Amangeldinova[1,2], Mehmet Ersatır[3], Adem Necip[4], Mustafa Abdullah Yilmaz[5,6], Mehmet Cimentepe[7], Nataliya Kudrina[1,2], Nina V. Terletskaya[1,2], Ozge Ozturk Cimentepe[8] and Metin Yildirim[9]*

[1]Faculty of Biology and Biotechnology, Al-Farabi Kazakh National University, Almaty, Kazakhstan, [2]Institute of Genetics and Physiology, Almaty, Kazakhstan, [3]Department of Chemistry, Faculty of Art and Science, Cukurova University, Adana, Türkiye, [4]Department of Pharmacy Services, Vocational School of Health Services, Harran University, Sanliurfa, Türkiye, [5]Dicle University Science and Technology Research and Application Center, Diyarbakir, Türkiye, [6]Department of Analytical Chemistry, Dicle University, Faculty of Pharmacy, Diyarbakir, Türkiye, [7]Department of Pharmaceutical Microbiology, Faculty of Pharmacy, Harran University, Sanliurfa, Türkiye, [8]Department of Pharmacology, Faculty of Pharmacy, Harran University, Sanliurfa, Türkiye, [9]Department of Biochemistry, Faculty of Pharmacy, Harran University, Sanliurfa, Türkiye

In this study, *Rheum tataricum* L. extracts were obtained using various green extraction techniques, including supercritical CO_2, subcritical ethanol, and ultrasound-assisted extraction, each performed under optimized parameters. The phytochemical content of the extracts was analyzed using the LC-MS/MS technique, quantifying 53 phytochemicals. Additionally, the *in vitro* antioxidant properties and antibacterial activities of the extracts were evaluated against *Staphylococcus aureus* and *Enterococcus faecalis* as gram-positive bacteria, and *Escherichia coli* and *Pseudomonas aeruginos*a as gram-negative bacteria. According to the results, the extracts were rich in catechin, epicatechin, cyranoside, and chlorogenic acid. Extracts obtained via ultrasonic extraction demonstrated stronger antioxidant properties. The IC_{50} values for the DPPH radical scavenging activity of obtained extracts ranged between 0.0173 mg/mL and 0.0400 mg/mL. The highest total phenolic content was found in the UAE-M-4h extract (213.44 mg GAE/mL). The extracts prepared with UAE-MeOH-2h-4h, UAE-EtOH-2h-4h, Sbc-EtOH-E-140-60-80, Sc-90 atm, and Sc-400 atm showed antibacterial activity against both Gram-positive and Gram-negative

bacteria at varying rates (MIC range: 31.25 to 250 µg/mL). Based on the all results, the ultrasound assisted extraction proved superior to the other techniques. This study, utilizing three different extraction methods with varying variables such as temperature, pressure, and extraction time, has provided significant insights into which extraction method should be employed for isolating specific phytochemicals or for therapeutic purposes, based on the differing antibacterial results observed. The findings highlight the importance of selecting the appropriate extraction method depending on the target phytochemical or desired antibacterial effect in treatment applications.

KEYWORDS

***Rheum tatarium* L., supercritical carbon dioxide, subcritical ethanol, ultrasound assisted extraction, biological activities**

1 Introduction

Tatar rhubarb (*Rheum tataricum* L.) is a widespread plant in the Republic of Kazakhstan, classified as an ephemeral species (Gemejiyeva and Grudzinskaya, 2018). Its distribution area includes plains, desert regions, and industrial zones in Russia, Xinjiang, and Afghanistan, where it is useful as a raw material source. The study of wild rhubarb species, such as *R. tataricum*, presents a significant scientific challenge due to their limited habitats within narrow strips of dry steppes and deserts in Central Asia, stretching from the northeast of the Astrakhan region in Russia to Lake Balkhash in Kazakhstan (Гемеджиева et al., 2017; Golubkina et al., 2022).

In recent years, rhubarb has become an increasingly promising research object due to its unique nutritional properties, high antioxidant levels, and wide range of applications in medicine and agriculture (Jiao and Du, 2000; Yildirim et al., 2021). It serves as a possible source of raw materials for creating herbal remedies with various properties, including anti-inflammatory, astringent, laxative, hemostatic, antitumor, and other properties (2014). Therefore, many researchers pay great attention to the use of *Rheum tataricum* for medical and food purposes (Dai et al., 2015; Shahrajabian et al., 2022). This plant contains anthocyanins and their derivatives, including cyanidin-3-glucoside, cyanidin-3-rutinoside, chrysanthemin, and cyanine (Agarwal et al., 2001).

Such secondary metabolites tend to decompose under the influence of various factors, such as temperature, pressure, and the solvent used to extract plant materials.

It should be noted that the method and conditions of extraction of biologically active compounds play an essential role in their wide application in medicine and pharmacology (Yıldırım et al., 2024). Numerous traditional extraction methods exist, such as hydrodistillation, which is often used for extracting essential oils. For the extraction of biologically active compounds (BACs) from plant materials, maceration has been traditionally employed, during which solvents are added in combination with heating or stirring to enhance the solubility of secondary metabolites (Ćujić et al., 2016; Cacique et al., 2020). Over the past decades, intensive research aimed at improving extraction methods has been driven by the growing public interest in using natural compounds and the increased awareness of the need for sustainable development and environmental protection (Picot-Allain et al., 2021). Traditional methods, such as percolation with organic solvents, Soxhlet extraction, rectification, and infusion, have certain drawbacks, including the use of hazardous solvents, lengthy processes, high resource consumption, and low efficiency in extracting secondary metabolites (Kubátová et al., 2001; Yıldırım et al., 2025b).

In order to improve the efficiency of the processes and enhance safety while maintaining high quality, various types of new green extraction methods have been developed such as ultrasound-assisted extraction (UAE), microwave-assisted extraction, supercritical CO_2 extraction and subcritical ethanol (sbcEtOH-E) (Chemat et al., 2012; Demirkol et al., 2022). Green extraction methods should fully comply with sustainable development strategies and the six principles of green extraction, such as using alternative solvents, reducing energy consumption, and striving for biodegradable extract (Li et al., 2004).

SC-CO_2 is one of the techniques developed from SFE technology. This method refers to the "green strategy" for efficiently extracting valuable chemical compounds from various plant materials by controlling the fluid density by changing the pressure and, less commonly, temperature (Demirkol et al., 2022).

UAE, known as a green method, involves the disruption of plant cell walls through the application of ultrasonic waves, resulting in the release of active compounds. It is relatively simple to use and does not require significant investment (Fu et al., 2021). Ultrasound can extract all known compounds produced by plants from plant raw materials, and it is not limited by the polarity or molecular weight of the component, making it suitable for extracting a wide range of BACs. In this method, ultrasound generates sound waves that create laminar or turbulent flow, enhancing the efficiency of the extraction process for biologically active substances (Rahaman et al.,

2019; Hadidi et al., 2020; Qin et al., 2021). It is worth noting that water serves as the primary medium for the propagation of ultrasonic waves during ultrasonic-assisted extraction (Panadare et al., 2020). Solvents commonly used in UAE include ethanol (for extracting phenols, aldehydes, and esters), chloroform (for extracting fatty acids, spices, and other fat-soluble substances), ether, and benzene (for extracting phenols and other aromatic compounds). When selecting an extraction solvent, it is important to adhere to the principles of green extraction and consider factors such as environmental safety, mass transfer, toxicity to the organism, financial feasibility, and the type of biologically active compound. For instance, in studies by Bellumori et al. (2016), it was demonstrated that the use of ethanol in the extraction of rosmarinic and carnosic acids from rosemary leaves resulted in a high yield of rosmarinic acid (6.8%), while the use of n-hexane as a solvent led to high yields of carnosic acids (13%) (Bellumori et al., 2016). Moreover, utilizing UAE significantly reduces the total solvent volume needed for the extraction process (Chemat et al., 2017).

sbcEtOH-E is considered a relatively new and green extraction method that does not require alternative energy sources, such as microwaves or ultrasound. Compared to subcritical water extraction, sbcEtOH-E does not require high temperatures to reach a subcritical state, which can be unsafe for thermolabile compounds (Wang et al., 2017; Marcus, 2018).

According to the literature, no studies have shown a comparative optimization of parameters for the best yield of biologically active compounds from the roots of *Rheum tataricum* L. This study aims to determine the optimal conditions for the extraction of biologically active compounds from the roots of *Rheum tataricum* L. using green extraction methods such as SC-CO_2, sbcEtOH-E, and UAE. Additionally, it seeks to analyze the composition of extracts prepared under different parameters using these methods through LC-MS/MS analysis, and to evaluate their *in silico*, antioxidant and antibacterial properties.

2 Materials and method

2.1 Plant material

The object of the study is *Rheum tataricum* L., collected on April 20, 2024, in the Sjugatinskaya Valley, located between the Charyn and Chilik rivers (coordinates: 43° 26′ 00″ N, 78° 59′ 00″ E). The collected *Rheum tataricum* L. sample was verified at the "Institute of Botany and Phytointroduction" in Almaty, Kazakhstan. The samples were dried in vacuum drying at 45-50°C and ground into powder. The dried plant material is stored at Harran University (Şanlıurfa, Turkey).

2.2 Extraction methods

2.2.1 sbcEtOH-E extraction

The experiments were conducted using a device designed for sub-critical solvent extraction. sbcEtOH-E was performed using 1 g of *Rheum tataricum* L. roots at a temperature of 140°C, a pressure of 60 and 80 atm, with a 30-minute static extraction time followed by a 20-minute dynamic extraction using ethyl alcohol at a flow rate of 2 mL per minute. All extractions were done in triplicate.

2.2.2 ScCO_2 extraction

Rheum tataricum L. roots extracts were prepared using a supercritical CO_2 extractor (Supercritical Extraction System SuperEx F series 500, Türkiye). Briefly, 25 grams of plant root (in a polyester pouch) was placed into the extractor vessel. The temperature values for the extractor, restrictor, and separator were set to 60°C, 120°C, and 60°C, respectively. The pressure was set to 90 and 400 atm. All extractions were performed at least three times.

2.2.3 UAE extraction

Ultrasound assisted extraction experiments of *Rheum tataricum* L. roots were performed using Elmasonic Select 150 device (19.9 in. x 11.8 in. surface area and 3.9 in. depth). For each experiment, 2 g of plant root and 30 ml of solvent were combined in a 50-ml capped sample tube. Experiments were performed at room temperature using two different solvents [methanol (MeOH) and ethanol (EtOH)] with two different extraction times (1 h and 4 h). All extractions were performed at least three times.

2.3 Mass spectrometer and chromatograph conditions for LC-MS/MS analysis

A Shimadzu-Nexera model ultrahigh performance liquid chromatograph (UHPLC) coupled with a tandem mass spectrometer was used for the identification of phytochemicals, and the detailed protocol is provided in the Supplementary Materials (Yilmaz, 2020).

2.3.1 Method validation studies for LC–MS/MS

The method validation study for LC/MSMS applied to the extracts of *Rheum tataricum* L. roots obtained under various extraction methods were conducted according to the procedure in the literature (Gemejiyeva and Grudzinskaya, 2018). The parameters related to the LC–MS/MS method validation studies given with table at Supplementary Materials.

2.4 Antioxidant activity

2.4.1 DPPH radical scavenging activity method

The DPPH free radical scavenging activity was determined using the DPPH˙ (1,1-diphenyl-2-picrylhydrazyl) method. Plant extracts were prepared at a concentration of 1.00 mg/mL. In this study, Trolox, BHA, and BHT were used as standard solutions at different concentrations. To 1 mL of an ethanol-water mixture, 0.5 mL of DPPH radical solution was added and vortexed, then incubated in the dark for half an hour. The absorbance was measured at 517 nm using a UV-VIS spectrophotometer. Results were expressed as IC_{50} (mg/mL) (Necip and Işık, 2019).

2.4.2 ABTS radical scavenging activity method

The ABTS free radical scavenging activity was described in detail in our previous study. Briefly, prepared ABTS radicals were mixed with standard and sample solutions and incubated in the dark for half an hour. After incubation, the absorbance values of the samples were measured at 734 nm using a UV spectrophotometer. Results were expressed as IC_{50} (mg/mL) (Necip et al., 2021).

2.4.3 Cu^{2+}-Cu^{+} reducing activity

Plant extracts and Trolox at different concentrations were mixed with neocuproine (7.5 mM), NH4Ac (1 M), and 0.25 mL $CuCl_2$ (0.01 M). The absorbance was measured at 450 nm using a UV-VIS spectrophotometer. The results were expressed as Trolox equivalent mg TE/mL.

2.4.4 Determination of total phenolic content

A 50 µL aliquot of the plant extract was taken, and 1.00 mL of distilled water was added to each sample, followed by 25 µL of Folin-Ciocalteu reagent, ensuring homogeneity through mixing. After 3 minutes, 40 µL of 20% sodium carbonate was added to the prepared samples, which were then vortexed and incubated at room temperature in the dark for two hours. The absorbance values were measured at a wavelength of 760 nm using a UV spectrophotometer. The corresponding amount of gallic acid equivalent was calculated based on the measured absorbance. The results were expressed as mg GAE/mg extract (Necip and Durgun, 2022).

2.5 Antibacterial activity

The broth microdilution test was studied according to our previous study (Weinstein and Lewis, 2020). *Staphylococcus aureus* ATCC 29213, *Enterococcus faecalis* ATCC 29212 as gram positive bacteria, *Escherichia coli* ATCC 35150 and *Pseudomonas aeruginosa* ATCC 27853 as gram negative bacteria, were used in this study.

Rheum tataricum L. extracts (3.91 to 2000 µg/mL) were added in each well of 96-well microtiter plate. The bacterial suspension, containing approximately 5×10^6 colony-forming units/mL, was incubated on plates at 37°C for 24 h. The absorbance values were determined using a microplate spectrophotometer (Thermo Fisher Scientific, USA) at 570 nm. The lowest concentration of *Rheum tataricum L. extract* that indicated no growth was determined as MIC. All studies were performed at least three times (Yildirim et al., 2025b). Minimum bactericidal concentration (MBC) was considered the lowest concentration of the *Rheum tataricum L.* different extract that results in the killing of 99.9% of the bacteria after the incubation period at 37°C for 24 h.

2.6 Molecular docking

The molecular docking studies were conducted based on our previous studies (Yildirim et al., 2025a; Yildirim et al., 2025b). Briefly, Molecular docking studies were carried out using the Maestro 13.8 Schrodinger ¨ 2023–3 program (https://www.schrodinger.com). Three dimensional crystal structures of the proteins were obtained from the RCSB Protein Data Bank (https://www.rcsb.org). Ligands and proteins were prepared using Wizard in the Maestro, Schrodinger packageCalculations were performed by docking the ligands to the proteins of *S. aureus*, *E. faecalis*, *P. aeruginosa*, and *E. coli*, using the proteins 1JIJ, 4WUB, 2UV0, and 6QXS, respectively. Docking studies were conducted using Schrödinger's Glide/XP module.

2.7 Statistical analysis

All statistical analyses were implemented with GraphPad Prism 9 (GraphPad Software Inc., USA) with one-way analysis of variance (ANOVA) followed by Tukey's multiple comparison test.

3 Results and discussion

3.1 Characterization

TIC (Total Ion Chromatogram) chromatogram of standard phenolic compounds analysed by the developed LC–MS/MS method. LC-MS/MS spectrums of *Rheum tataricum* L. root extracts obtained under different conditions are given in the Supplementary Materials.

The LC-MS/MS results regarding the presence of 53 phytochemicals in the extracts of *Rheum tataricum* L. roots are presented in Table 1. As shown in the Table 1, although 13 phytochemicals, including important ones such as quinic acid, gallic acid, tannic acid, rutin, hesperidin, catechin, and naringenin, were found in all extracts, 31 phytochemicals were not detected in any of the extracts (Figure 1). Phytochemicals such as epicatechin, vanillic acid, daidzin, salicylic acid, luteolin, kaempferol, and isoquercitrin were found in some extracts depending on the extraction conditions, while they were not detected in others.

Epicatechin was better extracted in ultrasonic-assisted extraction processes, while it could not be extracted using supercritical carbon dioxide extraction (Table 1. No: 15). Similarly, caffeic acid and astragalus were only extracted using subcritical ethanol extraction (Table 1. No: 17 and No: 42). Daidzin, epicatechin gallate, piceid, isoquercitrin, nicotiflorin, and kaempferol were present in all extracts but could not be extracted in the supercritical carbon dioxide extraction processes (Table 1).

In summary, based on these results. the extraction method, solvent, duration, temperature, and pressure can be adjusted to obtain extracts enriched with different phytochemicals. This approach can lead to the creation of extracts with a rich content that may influence biological activity. Quinic acid is found in the highest amount in the UAE-E-2h extract, while it is present in the lowest amount in the Sc-400 atm extract. One of the most significant antioxidants, epicatechin gallate, is found in concentrations ranging from 0.826 to 1.193 across the extracts;

10.3389/fpls.2024.1513875

TABLE 1 The LC-MS/MS results regarding the presence of 53 phytochemicals in the extracts of *Rheum tataricum* L. roots.

No	Analytes	UAE-E-2h	UAE-E-4h	UAE-M-2h	UAE-M-4h	Sc-90 atm	Sc-400 atm	Sbc-EtOH-140-60	Sbc-EtOH-140-80
1	**Quinic acid**	0.708	0.21	0.347	0.426	0.501	0.075	0.654	0.182
2	**Epicatechin gallate**	0.826	1.182	1.135	1.07	†	†	0.998	1.193
3	**Aconitic acid**	†	†	†	†	†	†	†	†
4	**Syringic aldehyde**	†	†	†	†	†	†	†	†
5	**Epigallocatechin**	†	†	†	†	†	†	†	†
6	**Protocatechuic acid**	1.078	1.118	0.837	0.9	0.088	0.055	2.934	1.971
7	**Catechin**	7.641	8.712	7.812	7.483	0.266	0.225	5.297	6.032
8	**Gentisic acid**	†	†	†	†	†	†	†	†
9	**Chlorogenic acid**	13.749	14.019	12.67	12.412	2.906	2.983	10.266	10.585
10	**Protocatechuic aldehyde**	0.152	0.153	0.13	0.141	0.095	0.061	0.527	0.347
11	**Tannic acid**	0.062	0.066	0.077	0.081	0.037	0.02	0.083	0.065
12	**Epigallocatechin gallate**	†	†	†	†	†	†	†	†
13	**Cynarin**	†	†	†	†	†	†	†	†
14	**4-OH Benzoic acid**	0.435	0.629	0.503	0.545	0.142	0.137	0.805	0.646
15	**Epicatechin**	10.307	11.936	11.744	11.799	†	†	9.158	10.273
16	**Vanilic acid**	†	†	†	†	†	†	†	†
17	**Caffeic acid**	†	†	†	†	†	†	0.022	0.014
18	**Syringic acid**	†	†	†	†	†	†	†	†
19	**Sinapic acid**	†	†	†	†	†	†	†	†
20	**Daidzin**	0.033	0.038	0.037	0.039	†	†	0.026	0.029
21	**Piceid**	†	†	†	†	†	†	†	†
22	**p-Coumaric acid**	0.12	0.115	0.109	0.114	0.062	0.038	0.209	0.166
23	**Ferulic acid-D3-IS**[h]	*	*	*	*	*	*	*	*
24	**isoquercitrin**	0.08	0.088	0.065	0.084	†	†	0.11	0.1
25	**Ferulic acid**	†	†	†	†	†	†	†	†
26	**Acacetin**	†	†	†	†	†	†	†	†
27	**Vanillin**	†	†	†	†	†	†	†	†
28	**Genistin**	†	†	†	†	†	†	†	†
29	**Coumarin**	†	†	†	†	†	†	†	†
30	**Chrysin**	†	†	†	†	†	†	†	†
31	**Cyranoside**	4.045	4.332	3.851	3.823	0.435	0.453	3.923	3.745
32	**Miquelianin**	†	†	†	†	†	†	†	†
33	**Rutin-D3-IS**	*	*	*	*	*	*	*	*
34	**Fisetin**	†	†	†	†	†	†	†	†
35	**Hesperidin**	0.315	0.366	0.295	0.291	0.024	0.021	0.466	0.431
36	**o-Coumaric acid**	†	†	†	†	†	†	†	†

(Continued)

TABLE 1 Continued

No	Analytes	UAE-E-2h	UAE-E-4h	UAE-M-2h	UAE-M-4h	Sc-90 atm	Sc-400 atm	Sbc-EtOH-140-60	Sbc-EtOH-140-80
37	**Astragalin**	†	†	†	†	†	†	0.009	†
38	**Rosmarinic acid**	†	†	†	†	†	†	†	†
39	**Ellagic acid**	†	†	†	†	†	†	†	†
40	**Rutin**	0.765	0.928	0.723	0.789	0.044	0.04	1.116	1.047
41	**Quercitrin**	†	†	†	†	†	†	†	†
42	**Amentoflavone**	†	†	†	†	†	†	†	†
43	**Nicotiflorin**	0.069	0.086	0.073	0.074	†	†	0.116	0.085
44	**Salicylic acid**	†	†	†	†	†	†	†	†
45	**Gallic acid**	0.449	0.607	0.5	0.542	0.033	0.014	1.53	0.917
46	**Quercetin-D3-IS**	*	*	*	*	*	*	*	*
47	**Quercetin**	†	†	†	†	†	†	†	†
48	**Luteolin**	†	0.003	†	†	†	†	0.007	0.004
49	**Hesperetin**	†	†	†	†	†	†	†	†
50	**Naringenin**	0.073	0.079	0.07	0.067	0.065	0.033	0.087	0.082
51	**Genistein**	†	†	†	†	†	†	†	†
52	**Kaempferol**	0.011	0.008	0.009	0.006	†	†	0.021	0.007
53	**Apigenin**	†	†	†	†	†	†	†	†
54	**Fumaric acid**	†	†	†	†	†	†	†	†
55	**Cosmosiin**	†	†	†	†	†	†	†	†
56	**Daidzein**	†	†	†	†	†	†	†	†

Bold values indicate the highest docking scores, representing the best binding energy for specific phytochemicals under various extraction methods.
†.: Not detected.
*.: Not applicable.

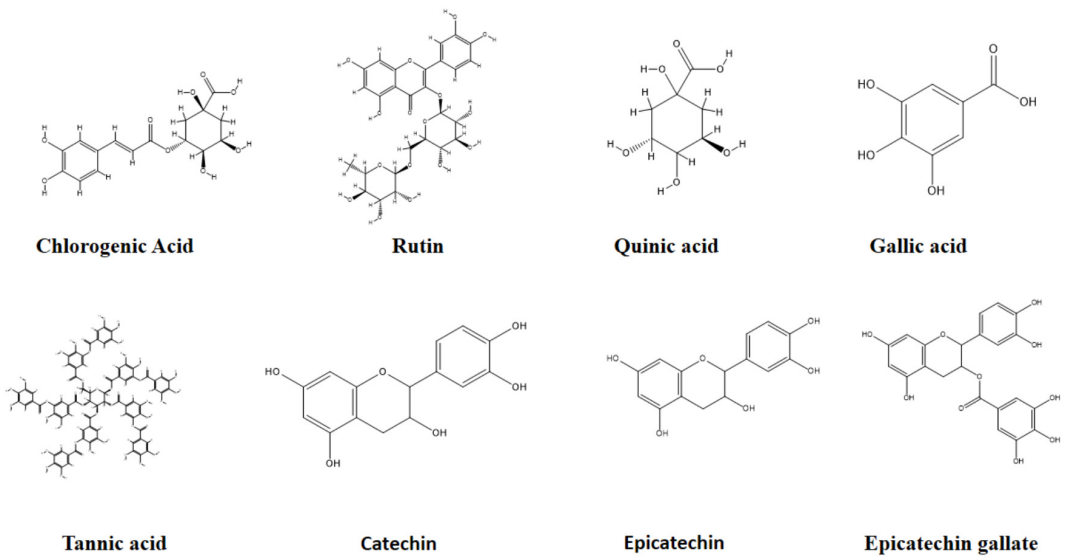

FIGURE 1
Representative compounds identified in *Rheum tataricum* L. extracts.

interestingly, it is absent in extracts obtained by the SC-CO_2 method. As for protocatechuic acid, the highest concentration is observed in the Sbc-EtOH-140-80 extract, while the lowest is found in extracts obtained via the SC-CO_2 method. Catechin and chlorogenic acid have their highest content in extracts produced by the UAE method. Epicatechin, daidzin, isoquercitrin, nicotiflorin, and kaempferol are present in all extracts except those obtained using the supercritical CO_2 method.

3.2 Antioxidant activity

There are various methods for determining antioxidant activities. Typically, the chemical complexity of extracts, which possess different functional groups, polarities, and chemical behaviors, produces varying results depending on the test used. Therefore, a multi-assay approach is considered more beneficial for evaluating the antioxidant potential of extracts. In this study, the DPPH radical scavenging activity, ABTS radical scavenging activity, and cupric ion reducing capacity (CUPRAC) were primarily employed. The total phenolic content, DPPH and ABTS radical scavenging activities, and Cu^{2+}-Cu^{+} reducing capacity of the extracts were calculated, and the results are presented in Table 2.

For the DPPH radical scavenging activity, the IC_{50} values of the standard antioxidants BHA, BHT, and Trolox were found to be 0.0021, 0.0033, and 0.0074 mg/mL, respectively. The IC_{50} values for the DPPH radical scavenging activity of obtained extracts ranged between 0.0173 mg/mL and 0.0400 mg/mL. The highest DPPH free radical scavenging activities were observed in the extracts Sbc-EtOH-140-80 and Sbc-EtOH-140-60, with IC_{50} values of 0.0173 mg/mL and 0.0182 mg/mL, respectively. Antioxidant activity increased with increasing extract concentration.

For the ABTS radical scavenging activity, the IC_{50} values of the standard antioxidants BHA, BHT, and Trolox were found to be 0.0023, 0.0032, and 0.0043 mg/mL, respectively. The IC_{50} values for the ABTS radical scavenging activity of Tartarium root plant extracts ranged from 0.0027 mg/mL to 0.0275 mg/mL. The Tartarium root plant extracts exhibited higher activity than BHT and Trolox and showed activity closer to that of BHA. Antioxidant activity also increased with the concentration of the extracts.

For the Cu^{2+}-Cu^{+} reducing activity, the Trolox equivalents of the plant extracts ranged between 0.0058 and 0.0138 mg TE/mL. The highest values were found in the extracts UAE-E-2h, UAE-M-2h, and UAE-M-4h, with values of 0.0138, 0.0125, and 0.0121 mg TE/mL, respectively. The total phenolic content in the plant extracts was calculated as gallic acid equivalents. The lowest total phenolic content was found in the Sbc-EtOH-140-80 plant extract (182.64 mg GAE/mL), while the highest was found in the UAE-M-4h extract (213.44 mg GAE/mL). According to the antioxidant data obtained, the UAE method showed superiority over other methods.

3.3 *In vitro* antimicrobial activity

The MIC and MBC values of test microorganisms against different extracts of *Rheum tataricum* L. are showed in Table 3.

TABLE 2 Radical Scavenging Activity (IC_{50} mg/mL) and Total Phenolic Content (mg GAE/g).

	DPPH (IC_{50} mg/mL)	ABTS (IC_{50} mg/mL)	CUPRAC (mg TE/mL)	Total Phenolic Content (mg GAE/g)
BHA	0.0021 ± 0.00015	0.0023 ± 0.00012		
BHT	0.0036 ± 0.00018	0.0032 ± 0.00015		
Trolox	0.0074 ± 0.0004	0.0043 ± 0.0002		
UAE-M-2h	0.0194± 0.00097^{a}	0.0027 ± 0.00014	0.0138 ± 0.00069	199.75 ± 5
UAE-E-2h	0.0188± 0.00099^{a}	0.0030 ± 0.00013	0.0125 ± 0.00061	192.42 ± 6
UAE-M-4h	0.0191± 0.001^{a}	0.0030 ± 0.00014	0.0121 ± 0.00058^{b,c}	213.44 ± 7^{c}
UAE-E-4h	0.0185± 0.00098^{a}	0.0049 ± 0.00018^{a,b}	0.0072 ± 0.00039^{b,c,d}	197.31 ± 5^{d}
Sbc-EtOH-140-60	0.0182± 0.00096^{a}	0.0050 ± 0.00014^{a,b,c,d}	0.0075 ± 0.0004^{c,d}	185.57 ± 4^{d}
Sbc-EtOH-140-80	0.0173± 0.00087^{a}	0.0049 ± 0.00015^{a,b,d}	0.0084 ± 0.00046^{c,d}	182.64 ± 5^{b,d,e}
Sc-90 atm	0.0356 ± 0.00178^{b,c,d,e,f,g}	0.0270 ± 0.00138	0.0088 ± 0.00045^{c,d}	167.27 ± 5^{b,c,d,e,f,g}
Sc-400 atm	0.0400 ± 0.002^{b,c,d,e,f,g}	0.0275 ± 0.00143	0.0058 ± 0.00025^{c,d,f,g,h}	137.09 ± 3^{b,c,d,e,f,g,h}

The data represent the means ± SD of three independent experiments.
a: Statistically significant at $p < 0.05$ compared to BHA
b: Statistically significant at $p < 0.05$ compared to UAE-M-2h
c: Statistically significant at $p < 0.05$ compared to UAE-E-2h
d: Statistically significant at $p < 0.05$ compared to UAE-M-4h
e: Statistically significant at $p < 0.05$ compared to UAE-E-4h
f: Statistically significant at $p < 0.05$ compared to Sbc-EtOH-140-60
g: Statistically significant at $p < 0.05$ compared to Sbc-EtOH-140-80
h: Statistically significant at $p < 0.05$ compared to Sc-90 atm
Bold text highlights values that are statistically significantly different from others, or key results that hold critical importance in the context of the experiment.

TABLE 3 Presents the MIC (μg/mL) and MBC (μg/mL) values of the extracts against Gram-positive and Gram-negative pathogenic bacteria.

	S. aureus		*E. faecalis*		*P. aeruginosa*		*E. coli*	
	MIC	MBC	MIC	MBC	MIC	MBC	MIC	MBC
UAE-EtOH-2h	250	250	125	125	125	1000	250	500
UAE-EtOH-4h	125	250	125	500	125	500	250	500
UAE-MeOH-2h	250	500	125	500	250	500	250	500
UAE-MeOH-4h	125	250	125	500	125	1000	250	500
sbcEtOH-E 140-60	125	500	31.25	31.25	125	1000	250	500
sbcEtOH-E 140-80	125	250	31.25	31.25	125	500	250	500
Sc-90 atm	250	500	250	500	1000	250	250	500
Sc-400 atm	125	500	31.25	125	125	500	125	125
Ampicillin	*		*		31.25		3.9	

Bold text emphasizes the minimum inhibitory concentrations (MIC) or minimum bactericidal concentrations (MBC) that demonstrate the highest antibacterial activity among the tested extracts. The symbol "*" indicates that the extract was effective at all tested concentrations against the specific bacteria.

The MIC values of the different extracts ranged from 31.25 μg/mL to 250 μg/mL. *E. faecalis* was one of the most sensitive bacteria to the extracts, with a MIC of 31.25 μg/mL. For the UAE-MeOH-2h extract, the MIC values were 125 μg/mL for *E. faecalis* and 250 μg/mL for *S. aureus*, *E. coli*, and *P. aeruginosa*. In the UAE-MeOH-4h extract, the MIC values were 125 μg/mL for *S. aureus*, *E. faecalis*, and *E. coli*, and 250 μg/mL for *P. aeruginosa*. In the UAE-EtOH-2h extract, the MIC values were 125 μg/mL for E. faecalis and P. aeruginosa, and 250 μg/mL for *S. aureus* and *E. coli*. Conversely, for the UAE-EtOH-4h extract, the MIC values were 125 μg/mL for *S. aureus*, *E. faecalis*, and *P. aeruginosa*, and 250 μg/mL for *E. coli*. The sbcEtOH-E 140-60 and 140-80 extracts exhibited similar antimicrobial activity against the tested microorganisms. The MIC values for these extracts were 31.25 μg/mL for *E. faecalis*, 125 μg/mL for *S. aureus* and P. *aeruginosa*, and 250 μg/mL for *E. coli*. The Sc-90 atm extract exhibited greater antibacterial activity than the Sc-400 atm extract. The MBC values for the different extracts of *Rheum tataricum* L. ranged from 31.5 μg/mL to 1000 μg/mL against the tested bacteria. Based on the MIC and MBC results, it can be concluded that these extracts can be considered potent antimicrobials, particularly against *E. faecalis*.

In this study, different extracts of *Rheum tataricum* L. were investigated for their antibacterial effects on some Gram-positive and Gram-negative bacteria. According to the results, it was determined that the extracts prepared with UAE-MeOH-2h-4h, UAE-EtOH-2h-4h, Sbc-EtOH-E-140-60-80, Sc-90 atm, and Sc-400 atm showed antibacterial activity against both Gram-positive and Gram-negative bacteria at varying rates (MIC range: 31.25 to 250 μg/mL). Among the Gram-negative bacteria tested, the green method (Sc-400) exhibited the strongest antibacterial effect on *E. coli* compared to the other extracts. The Sc-90 atm and Sc-400 atm extracts showed varying antibacterial activities due to changes in the pressure parameters during extraction, which affected the extract content. Except for UAE-MeOH-2h and Sc-90 atm (MIC value of 250 μg/mL), the other extracts (MIC value of 125 μg/mL) showed similar antibacterial effects against *P. aeruginosa*.

For the Gram-positive bacteria, the Sbc-EtOH-E 140-60, 140-80, and Sc-400 atm extracts (MIC value of 31.25 μg/mL) exhibited strong antibacterial effects on *E. faecalis* compared to the other extracts. The best antibacterial effect against *S. aureus* was observed in extracts other than UAE-MeOH-2h and UAE-EtOH-2h. The antibacterial activity of plant essential oils or extracts is generally stronger against Gram-positive bacteria than Gram-negative bacteria, which is attributed to the more complex cell wall structure of Gram-negative bacteria (Puupponen-Pimiä et al., 2001; Nazzaro et al., 2013).

The sbcEtOH-E 140-60 and sbcEtOH-E 140-80 extracts showed a notably strong antibacterial effect against *E. faecalis*. This effect, compared to other extracts, is attributed to their higher content of compounds such as protocatechuic acid, protocatechuic aldehyde, 4-OH benzoic acid, p-coumaric acid, hesperidin, rutin, and gallic acid, which are more abundant in these extracts than in those obtained by other extraction methods.

In a study by Onem et al (Önem et al., 2020), the methanolic, methanol-chloroform, and aqueous extracts of *Rheum ribes* L. were tested against S. aureus, methicillin-resistant *S. aureus* (MRSA), *Bacillus cereus*, *Enterococcus faecalis*, and *Listeria monocytogenes*. They found that the methanolic extract exhibited the most antibacterial activity against MRSA and B. cereus. Similarly, Alan et al. tested chloroform, hexane, acetone, ethanol, and methanol extracts from different parts of *Rheum ribes* L. against various microorganisms, with the most significant activity observed against *Bacillus subtilis* ATCC 6633 and *Enterobacter aerogenes* ATCC 13048 in ethanol and methanol extracts obtained from the root, stalk, and seed (Alan et al., 2013). Rolta et al. evaluated the antimicrobial effects of methanolic extracts and different solvent fractions (n-hexane, chloroform, ethyl acetate, and residual

aqueous) of *Rheum emodi* against *E. coli*, *S. aureus*, and *K. pneumoniae*. The MIC values of the chloroform sub-fraction were 1.95, 3.91, and 15.62 µg/mL against *S. aureus*, *K. pneumoniae*, and *E. coli*, respectively (Rolta et al., 2020). Additionally, another study found that ethanol and water extracts of *Rheum ribes* L. roots had antibacterial effects against *S. aureus* (Alaadin et al., 2007). Chen et al. demonstrated the antibacterial activity of different extracts of *Rheum palmatum* L. (Turkey rhubarb) roots. The liquid dilution MIC values of methanolic, aqueous, and ethyl acetate extracts inhibited the growth of A. baylyi at concentrations of 459, 1879, and 686 µg/mL, respectively, and *P. aeruginosa* at 230, 939, and 194 µg/mL, respectively. The chloroform and hexane extracts of *Rheum palmatum* L. also showed good antibacterial activity against *P. aeruginosa* (MIC values of 128 and 96 µg/mL, respectively) (Chen and Cock, 2022). The prepared extracts are rich in compounds such as catechin, chlorogenic acid, epicatechin, cyranoside, and gallic acid. According to the literature, these compounds are known to exhibit potent activity against *S. aureus*, *E. coli*, *P. aeruginosa*, and *E. faecalis* bacteria.

3.4 Molecular modelling

Molecular modeling studies provide significant insights into the interaction between compounds present in the prepared extracts and disease-associated proteins. In this study, interactions between the most abundant compounds in the plant extracts and proteins found in *S. aureus*, *E. coli*, *P. aeruginosa*, and *E. faecalis*—specifically, proteins 1JIJ, 4WUB, 2UV0, and 6QXS, respectively—were investigated.

Upon analyzing the molecular docking scores, it was found that rutin showed a docking score of -10.107 for the 1JIJ protein in *S. aureus*, hesperidin scored -8.746 for the 6QXS protein in *E. faecalis*, epicatechin gallate scored -10.031 for the 4WUB protein in *E. coli*, and epicatechin scored -8.176 for the 2UV0 protein in *P. aeruginosa* (Table 4). Figure 2 illustrates the 2D and 3D interaction images of the molecules with the highest molecular docking scores with their respective proteins.

TABLE 4 Molecular docking scores and binding modes of compounds with the 1JIJ, 4WUB, 2UV0, and 6QXS receptor.

Compound	1JIJ (*S. aureus*)	6QXS (*E. faecalis*)	4WUB (*E. coli*)	2UV0 (*P. aeruginosa*)
Cyranoside	-6.902	-7.052	-6.692	-6.904
Catechin	-8.330	-7.071	-7.638	**-8.176**
Quinic acid	-7.177	-7.068	**-10.500**	-6.455
Gallic acid	-7.069	-6.165	-9.856	-5.816
Protocatechuic acid	-6.890	-6.231	-9.697	-6.805
Chlorogenic acid	-8.241	-7.098	-10.691	-7.501
4-OH Benzoic acid	-6.495	-6.864	-9.934	-6.695
Epicatechin	-8.330	-7.071	-7.638	**-8.176**
Epicatechin gallate	-8.875	-7.546	**-10.031**	-6.124
Rutin	**-10.107**	-7.983	-8.779	-6.502
Hesperidin	-8.474	**-8.746**	-7.425	-5.932

Bold values indicate key statistical results, such as optimal extraction yields or the most significant biochemical activities among the methods tested.

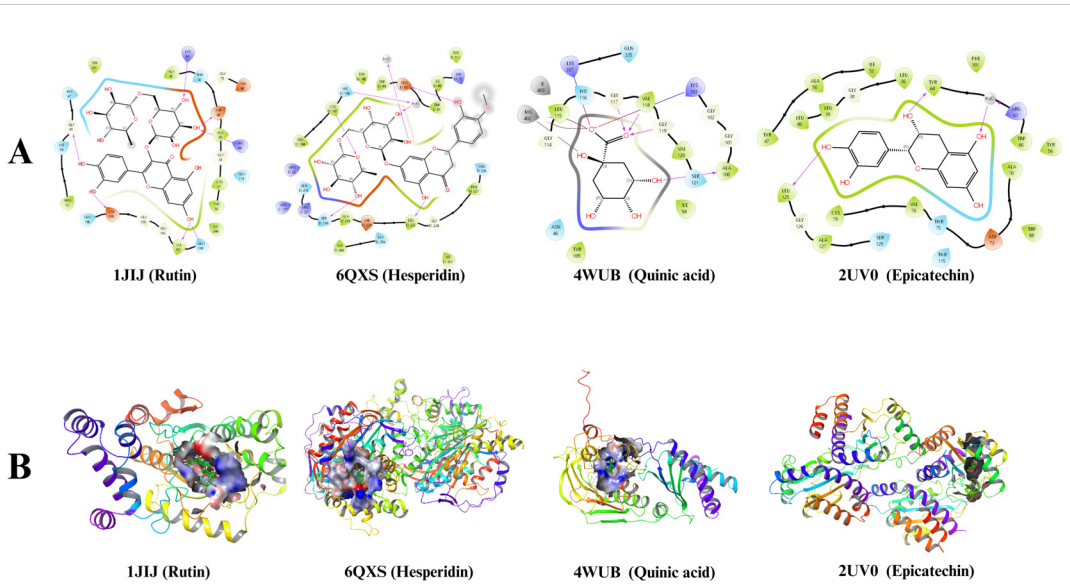

FIGURE 2
2D **(A)** and 3D **(B)** binding interactions of compounds in the active site of proteins.

4 Conclusion

In this study, extracts of *Rheum tataricum* L. were obtained using supercritical CO_2, subcritical ethanol, and ultrasound assisted extraction methods under varying temperatures and solvents. According to the LC-MS/MS data, catechin, epicatechin, cyranoside, and chlorogenic acid were identified as the predominant compounds among the 53 phytochemicals detected in the extracts. All extracts exhibited antibacterial activity against four different bacteria. Our results indicate the high antimicrobial potential of *Rheum tataricum* L. extracts, particularly against *E. faecalis* as a Gram-positive bacterium (with a MIC value of 31.25 µg/mL) when using the Sc-400 atm and Sbc-EtOH-E 140-60, 140-80 extraction methods. Upon analyzing all the data, the ultrasound assisted extraction method emerged as cheap and easy-to-apply technique, outperforming the other methods. Additionally, different methods may be preferred depending on the target compound to be isolated. Based on the obtained data, *Rheum tataricum L.* roots extract demonstrate a wide range of application potential, extending from the food industry to pharmaceutical applications. Among the extraction methods used, UAE stands out as a preferred technique due to its ease of application and cost-effectiveness. Additionally, the choice of extraction method can be tailored depending on the desired active compounds. Furthermore, given the strong antibacterial properties exhibited by the extracts, they may be considered as natural antimicrobial agents in pharmaceutical products.

Data availability statement

The datasets presented in this study can be found in online repositories. The names of the repository/repositories and accession number(s) can be found in the article/Supplementary Material.

Author contributions

MA: Data curation, Investigation, Methodology, Writing – original draft, Writing – review & editing. ME: Data curation, Formal analysis, Funding acquisition, Investigation, Methodology, Writing – original draft, Writing – review & editing. AN: Data curation, Formal analysis, Investigation, Methodology, Writing – original draft, Writing – review & editing. MY: Data curation, Formal analysis, Investigation, Methodology, Writing – original draft, Writing – review & editing. MC: Formal analysis, Investigation, Methodology, Validation, Writing – original draft, Writing – review & editing. NK: Conceptualization, Data curation, Formal analysis, Funding acquisition, Investigation, Methodology, Project administration, Resources, Software, Supervision, Validation, Visualization, Writing – original draft, Writing – review & editing. NT: Resources, Writing – original draft, Writing – review & editing. ÖÖ: Investigation, Methodology, Writing – original draft, Writing – review & editing. MY: Conceptualization, Data curation, Formal analysis, Funding acquisition, Investigation, Methodology, Project administration, Resources, Software, Supervision, Validation, Visualization, Writing – original draft, Writing – review & editing.

Funding

The author(s) declare financial support was received for the research, authorship, and/or publication of this article. This research was carried out within the framework of the Program BR21882180, "Strategy creation for conserving and developing medicinal and veterinary plant resources in Kazakhstan amid Climate Change," supported by the Science Committee of the Ministry of Science and Higher Education of the Republic of Kazakhstan. Additionally, the work was supported by the Scientific Research Committee of Çukurova University under the project number FAY-2023-15736.

Conflict of interest

The authors declare that the research was conducted in the absence of any commercial or financial relationships that could be construed as a potential conflict of interest.

Generative AI statement

The author(s) declare that no Generative AI was used in the creation of this manuscript.

Publisher's note

Supplementary material

The Supplementary Material for this article can be found online at: https://www.frontiersin.org/articles/10.3389/fpls.2024.1513875/full#supplementary-material

References

Гемеджиева, Н., Курбатова, Н., Музычкина, Р., and Корулькин, Д. (2017). К ботаническим и фитохимическим исследованиям Rheum tataricumL. из Южного Прибалхашья. *Bull. Karaganda Univ. Biol. Med. Geogr. Ser.* 86, 40–47. doi: 10.31489/2017bmg2/40-47

Agarwal, S. K., Singh, S. S., Lakshmi, V., Verma, S., and Kumar, S. (2001). Chemistry and pharmacology of rhubarb (Rheum species)-A review. *J. Sci. Ind. Res.* 60 (1), 1–9.

Alaadin, A. M., Al-Khateeb, E. H., and Jäger, A. K. (2007). Antibacterial activity of the Iraqi Rheum ribes. Root. *Pharm. Biol.* 45, 688–690. doi: 10.1080/13880200701575049

Alan, Y., Erbil, N., and Digrak, M. (2013). *In vivo* antimicrobial activity of Rheum ribes ekstracts obtained from various plant parts from Turkey. *J. Selcuk Univ. Natural Appl. Sci.* 1, 23–29.

(2014) 20, 200. список лекарственных растений Казахстана, А. Справочное издание/ ЛМ Грудзинская, НГ Гемеджиева, НВ Нелина, ЖЖ Каржаубекова. *Алма ты.*

Bellumori, M., Innocenti, M., Binello, A., Boffa, L., Mulinacci, N., and Cravotto, G. (2016). Selective recovery of rosmarinic and carnosic acids from rosemary leaves under ultrasound-and microwave-assisted extraction procedures. *Comptes Rendus. Chimie* 19, 699–706. doi: 10.1016/j.crci.2015.12.013

Cacique, A. P., Barbosa, É. S., de Pinho, G. P., and Silvério, F. O. (2020). Maceration extraction conditions for determining the phenolic compounds and the antioxidant activity of Catharanthus roseus (L.) G. Don. *Ciec. e Agrotecnologia* 44, e017420. doi: 10.1590/1413-7054202044017420

Chemat, F., Rombaut, N., Sicaire, A.-G., Meullemiestre, A., Fabiano-Tixier, A.-S., and Abert-Vian, M. (2017). Ultrasound assisted extraction of food and natural products. Mechanisms, techniques, combinations, protocols and applications. A review. *Ultrasonics sonochemistry* 34, 540–560. doi: 10.1016/j.ultsonch.2016.06.035

Chemat, F., Vian, M. A., and Cravotto, G. (2012). Green extraction of natural products: Concept and principles. *Int. J. Mol. Sci.* 13, 8615–8627. doi: 10.3390/ijms13078615

Chen, Y., and Cock, I. E. (2022). Rheum palmatum L. Root extracts inhibit the growth of bacterial triggers of selected autoimmune inflammatory diseases and potentiate the activity of conventional antibiotics. *Pharmacognosy Commun.* 12, 109–119. doi: 10.5530/pc.2022.3.22

Ćujić, N., Šavikin, K., Janković, T., Pljevljakušić, D., Zdunić, G., and Ibrić, S. (2016). Optimization of polyphenols extraction from dried chokeberry using maceration as traditional technique. *Food Chem.* 194, 135–142. doi: 10.1016/j.foodchem.2015.08.008

Dai, W., Robles, A., Rohena, C., Peng, J., Mooberry, S., Yan, X., et al. (2015). Cytotoxic effects of anthraquinones from the rhizome of Rheum tataricum on HeLa and MDA-MB-435 cells. *Planta Med.* 81, PG19. doi: 10.1055/s-00000058

Demirkol, O., Erşatır, M., Giray, E. S., and Kırıcı, S. (2022). Comparison of the effects of green and sustainable extraction methods on the extraction yield and chemical composition of Ruta chalepensis roots. *Sustain. Chem. Pharm.* 29, 100750. doi: 10.1016/j.scp.2022.100750

Fu, X., Wang, D., Belwal, T., Xie, J., Xu, Y., Li, L., et al. (2021). Natural deep eutectic solvent enhanced pulse-ultrasonication assisted extraction as a multi-stability protective and efficient green strategy to extract anthocyanin from blueberry pomace. *LWT* 144, 111220. doi: 10.1016/j.lwt.2021.111220

Gemejiyeva, N. G., and Grudzinskaya, L. M. (2018). "Current state and prospects for studies on the diversity of medicinal flora in Kazakhstan," in *Vegetation of Central Asia and Environs*. Eds. D. Egamberdieva and M. Öztürk (Almaty, Kazakhstan: Springer), 239–262. doi: 10.1007/978-3-319-99728-5_9

Golubkina, N., Kharchenko, V., Bogachuk, M., Koshevarov, A., Sheshnitsan, S., Kosheleva, O., et al. (2022). Biochemical characteristics and elemental composition peculiarities of Rheum tataricum L. @ in semi-desert conditions and of European garden rhubarb. *Int. J. Plant Biol.* 13, 368–380. doi: 10.3390/ijpb13030031

Hadidi, M., Ibarz, A., and Pagan, J. (2020). Optimisation and kinetic study of the ultrasonic-assisted extraction of total saponins from alfalfa (Medicago sativa) and its bioaccessibility using the response surface methodology. *Food Chem.* 309, 125786. doi: 10.1016/j.foodchem.2019.125786

Jiao, D., and Du, S. (2000). *The Study of Rhubarb* (Shanghai: Shanghai Science & Technology Press).

Kubátová, A., Lagadec, A. J., Miller, D. J., and Hawthorne, S. B. (2001). Selective extraction of oxygenates from savory and peppermint using subcritical water. *Flavour Fragrance J.* 16, 64–73. doi: 10.1002/1099-1026(200101/02)16:1<64::AID-FFJ949>3.0.CO;2-D

Li, H., Pordesimo, L., and Weiss, J. (2004). High intensity ultrasound-assisted extraction of oil from soybeans. *Food Res. Int.* 37, 731–738. doi: 10.1016/j.foodres.2004.02.016

Marcus, Y. (2018). Extraction by subcritical and supercritical water, methanol, ethanol and their mixtures. *Separations* 5, 4. doi: 10.3390/separations5010004

Nazzaro, F., Fratianni, F., De Martino, L., Coppola, R., and De Feo, V. (2013). Effect of essential oils on pathogenic bacteria. *Pharmaceuticals* 6, 1451–1474. doi: 10.3390/ph6121451

Necip, A., and Durgun, M. (2022). Antioxidant properties, total phenolic content and LC-MS/MS analysis of Mentha pulegium, Lepidium draba and Centaurea solstitialis. *J. Institute Sci. Technol.* 12, 2375–2385. doi: 10.21597/jist.1177585

Necip, A., and Işık, M. (2019). Bioactivities of Hypericum Perforatum L and Equisetum Arvense L fractions obtained with different solvents. *Int. J. Life Sci. Biotechnol.* 2, 221–230. doi: 10.38001/ijlsb.636502

Necip, A., Mesut, I., Güzel, A., Takim, K., and Kaygisiz, F. (2021). LC-MS/MS analysis, antioxidant properties and inhibition effect on some important metabolic enzymes of Nicotiana rustica L. *Kahramanmaraş Sütçü İmam Üniversitesi Tarım ve Doğa Dergisi* 24, 930–938. doi: 10.18016/ksutarimdoga.vi.856514

Önem, E., Sarısu, H. C., and Ibrahım, B. (2020). The effect of Rheum ribes L. extracts on bacterial communication and antibacterial activity. *Süleyman Demirel Üniversitesi Sağlık Bilimleri Dergisi* 11, 436–442. doi: 10.22312/sdusbed.757976

Panadare, D. C., Gondaliya, A., and Rathod, V. K. (2020). Comparative study of ultrasonic pretreatment and ultrasound assisted three phase partitioning for extraction of custard apple seed oil. *Ultrasonics Sonochemistry* 61, 104821. doi: 10.1016/j.ultsonch.2019.104821

Picot-Allain, C., Mahomoodally, M. F., Ak, G., and Zengin, G. (2021). Conventional versus green extraction techniques—A comparative perspective. *Curr. Opin. Food Sci.* 40, 144–156. doi: 10.1016/j.cofs.2021.02.009

Puupponen-Pimiä, R., Nohynek, L., Meier, C., Kähkönen, M., Heinonen, M., Hopia, A., et al. (2001). Antimicrobial properties of phenolic compounds from berries. *J. Appl. Microbiol.* 90, 494–507. doi: 10.1046/j.1365-2672.2001.01271.x

Qin, L., Yu, J., Zhu, J., Kong, B., and Chen, Q. (2021). Ultrasonic-assisted extraction of polyphenol from the seeds of Allium senescens L. and its antioxidative role in Harbin dry sausage. *Meat Sci.* 172, 108351. doi: 10.1016/j.meatsci.2020.108351

Rahaman, A., Zeng, X.-A., Kumari, A., Rafiq, M., Siddeeg, A., Manzoor, M. F., et al. (2019). Influence of ultrasound-assisted osmotic dehydration on texture, bioactive compounds and metabolites analysis of plum. *Ultrasonics sonochemistry* 58, 104643. doi: 10.1016/j.ultsonch.2019.104643

Rolta, R., Kumar, V., Sourirajan, A., Upadhyay, N. K., and Dev, K. (2020). Bioassay guided fractionation of rhizome extract of Rheum emodi wall as bio-availability enhancer of antibiotics against bacterial and fungal pathogens. *J. ethnopharmacology* 257, 112867. doi: 10.1016/j.jep.2020.112867

Shahrajabian, M. H., Cheng, Q., and Sun, W. (2022). Wonderful natural drugs with surprising nutritional values, Rheum species, gifts of the nature. *Lett. Organic Chem.* 19, 818–826. doi: 10.2174/1570178619666220112115918

Wang, Y., Gao, Y., Ding, H., Liu, S., Han, X., Gui, J., et al. (2017). Subcritical ethanol extraction of flavonoids from Moringa oleifera leaf and evaluation of antioxidant activity. *Food Chem.* 218, 152–158. doi: 10.1016/j.foodchem.2016.09.058

Weinstein, M. P., and Lewis, J. S. (2020). The clinical and laboratory standards institute subcommittee on antimicrobial susceptibility testing: background, organization, functions, and processes. *J. Clin. Microbiol.* 58 (3), e01864-19. doi: 10.1128/jcm.01864-19

Yildirim, M., Cimentepe, M., Dogan, K., Necip, A., and Karakoc, V. (2025a). Advancing drug delivery and antimicrobial activity: Development and molecular docking analysis of quercetin-loaded pHEMA cryogel membranes. *J. Mol. Structure* 1319, 139271. doi: 10.1016/j.molstruc.2024.139271

Yildirim, M., Degirmenci, U., Akkapulu, M., Comelekoglu, U., Balli, E., Metin Ozcan, T., et al. (2021). The effect of Rheum ribes L. @ on oxidative stress in diabetic rats. *J. Basic Clin. Physiol. Pharmacol.* 32, 20200058. doi: 10.1515/jbcpp-2020-0058

Yildirim, M., Kilic, A., Cimentepe, M., Necip, A., and Turedi, S. (2025b). Synthesis of bioactive quercetin-boronate esters as a novel biological agent: Enzyme inhibition, antimicrobial properties, computational insights and anti-cancer activity. *J. Mol. Structure* 1321, 140216. doi: 10.1016/j.molstruc.2024.140216

Yilmaz, M. A. (2020). Simultaneous quantitative screening of 53 phytochemicals in 33 species of medicinal and aromatic plants: A detailed, robust and comprehensive LC–MS/MS method validation. *Ind. Crops Products* 149 (16), 112347. doi: 10.1016/j.indcrop.2020.112347

Yıldırım, M., Erşatır, M., Poyraz, S., Amangeldinova, M., Kudrina, N. O., and Terletskaya, N. V. (2024). Green extraction of plant materials using supercritical CO2: insights into methods, analysis, and bioactivity. *Plants* 13, 2295. doi: 10.3390/plants13162295

frontiers | Frontiers in Plant Science

TYPE Original Research
PUBLISHED 27 January 2025
DOI 10.3389/fpls.2024.1501966

OPEN ACCESS

EDITED BY
Eman. A. Mahmoud,
Damietta University, Egypt

REVIEWED BY
Wanpeng Xi,
Southwest University, China
Mario Juan Simirgiotis,
Austral University of Chile, Chile

*CORRESPONDENCE
Wen Xu
fantacy@gzucm.edu.cn

†These authors have contributed equally to this work

RECEIVED 26 September 2024
ACCEPTED 02 December 2024
PUBLISHED 27 January 2025

CITATION
Peng M-l, Gong M-J, Zhang J, Gadetskaya AV, Liang Q-W, He P-W, Qiu X-H, Huang Z-H and Xu W (2025) Comprehensive chemical and bioactive investigation of Chinese peony flower: a case of valorization of by-products as a new food ingredient from Chinese herb. *Front. Plant Sci.* 15:1501966. doi: 10.3389/fpls.2024.1501966

Comprehensive chemical and bioactive investigation of Chinese peony flower: a case of valorization of by-products as a new food ingredient from Chinese herb

Meng-ling Peng[1†], Ming-Jiong Gong[1†], Jing Zhang[1†], Anastassiya V. Gadetskaya[2], Qian-Wen Liang[1], Pei-Wen He[1], Xiao-Hui Qiu[1], Zhi-Hai Huang[1] and Wen Xu[1,3*]

[1]State Key Laboratory of Traditional Chinese Medicine Syndrome, The Second Affiliated Hospital of Guangzhou University of Chinese Medicine, Guangzhou, China, [2]School of Chemistry and Chemical Technology, Al-Farabi Kazakh National University, Almaty, Kazakhstan, [3]Chinese Medicine Guangdong Laboratory, Hengqin, China

Introduction: In the present study, the flower of Chinese peony (CPF), major waste by-product of Chinese Herb *Radix paeoniae*, was comprehensively investigated for the first time.

Methods: A validated UHPLC Orbitrap Mass spectrometry combined a three-levels characterization strategy were used to analyze CPF samples from four representative cultivars. The anti-inflammatory and antioxidant activities were analyzed using RAW264.7 cells, and DPPH, ABTS, FRAP, and ORAC antioxidant assays.

Results: A total of 150 chemical components were identified in CPF, among them, more than 50 components were reported from this species for the first time, with potential new chemicals reported. 67 quantified or semi-quantified targeted metabolomics analysis indicated a clear distinction between flower parts and four cultivars. CPF demonstrated significant antioxidant activities and displayed anti-inflammatory effects by reducing nitric oxide, IL-6, and TNF-a release in LPS-induced macrophages. Correlation analysis highlighted a strong positive correlation between total phenolic content and DPPH ABTS, and FRAP antioxidant activities.

Discussion: The present study is the first to comprehensively investigate the chemical profile and bioactivities of CPF, which provide insights into further understanding of its health-promoting potential.

KEYWORDS

***Paeonia lactiflora*, Orbitrap, flavonoids, antioxidants, biowaste valorization**

1 Introduction

Chinese peony (*Paeonia lactiflora* Pall.), is the most common herbaceous peony species in China, and is renowned worldwide as a time-honored ornamental and medicinal herb (Yang et al., 2023). The root of Chinese peony, known as *Radix Paeoniae*, has been commonly used as a traditional medicine in East Asia for over 1200 years for treatment of rheumatoid arthritis, systemic lupus erythematosus, hepatitis, dysmenorrhea, muscle spasms, and so on (Han et al., 2022; Xu et al., 2022; Sang et al., 2023; Wu et al., 2023).

Due to the high clinical demand for *Radix Paeoniae* in Traditional Chinese Medicine (TCM), Chinese peony is usually grown for 3-5 years to obtain the roots. However, the aerial parts are often discarded. Especially, the flowers and buds must be removed during the annual flowering period to promote root growth, causing huge waste that could be potentially valorized.

The Chinese peony flowers (CPF), also known as the 'minister of flowers', is one of the popular ornamental flowers, offering a rich array of colors. Beyond that, CPF is also appreciated for its potential health-promoting effects (Kang et al., 2020). In western countries, the petals of Chinese peony are parboiled with a pinch of sugar and then used in desserts or home baking, or as a dressing for fruit salads. Additionally, CPF can be utilized in the creation of cocktails and lemonades (Liu et al., 2023). In China, CPF is used as a flavorful ingredient in traditional Chinese cuisine (Yuan, 2011). However, these applications are primarily limited to small-scale usage. Recently, scented tea and its related beverage products have been attracted enormous attentions and have become very popular around the world due to not only its natural and flavorful properties, but also receiving potential health benefits (Yuan, 2011; Zhao et al., 2023). Scented tea (An et al., 2022) is a kind of tea made by brewing flowers, leaves, or herbs, and is a kind of reprocessed tea endemic to China (Yun-Jie et al., 2019). Being rich in flavonoids and anthocyanins, scented tea is claimed to have anti-aging, cardiovascular protection, and metabolism promotion effects. CPF tea is currently available on the market sporadically. Its petals, stamens, whole flowers and sprouts, individually or commonly can be made into teas with multiple production processes.

For a long time, the chemical and pharmacological research on Chinese peony has mostly been restricted to the roots, yet rarely addressed to the aerial parts. A few studies have been made focusing on the analysis of certain components of CPF, which showed that it contains large portions of polyphenols (Shu et al., 2014; Ogawa et al., 2015) and flavonoids with potential antioxidant activity. In a recent study from Liu et al (Liu et al., 2022)., a total 1102 metabolites were preliminarily annotated using Kyoto Encyclopedia of Genes and Genomes (KEGG) and compared in different parts of *P. lactiflora* flower. Li et al (Li et al., 2023) compared peony petals from 12 different varieties using LC-MS-based fingerprints and metabolomics technology. Regarding its bio-activities, studies also demonstrated CPF has anti-melanin production activity (Liu et al., 2022), and inhibits H_2O_2-induced cell damage (Liu et al., 2023) by upregulating the expression of nuclear Factor E2-related factor (Nrf2).

Liquid chromatography coupled with high-resolution mass spectrometer (LC-HR MS) has been proven as an effective and desirable tool to explore and profile chemical constituents from complex materials such as natural products. A comprehensive chemical profiling strategy was established in our previous studies based on the combination of LC Q-exactive™ Orbitrap MS with metabolomics analysis, which has been successfully applied to global analysis for a variety of natural resources such as *Citrus reticulata* (Chachi) (Zhang et al., 2020a), *Citrus medica* (Zhang et al., 2022)and Ganpu tea (Xu et al., 2021). In the present study, we collected four representative cultivars of Chinese peonies that grow in the same experimental field under the same conditions. The global chemical identification was carried out firstly by LC-Q Orbitrap MS based on our established LC-HR MS identification strategy (Qiu et al., 2013). Then a validated quantitative and semi-quantitative analysis of multiple targets in CPF combined with untargeted and targeted metabolomics method was used to further compare the variations of different cultivars and different parts of CPF. Moreover, the correlation analysis between the chemical indexes and the anti-inflammatory/anti-oxidative activities was performed to indicate potential components that are responsible for the bioactivities. The present study could be a great instance in terms of the valorization of by-products as a new functional food from Chinese herb.

2 Materials and methods

2.1 Chemicals and reagents

Liquid chromatography (LC)-grade methanol, acetonitrile, and formic acid were purchased from Merck (Darmstadt, Germany). Ultra-pure water (18.2MΩ·cm) was pre-pared using a Milli-Q system (Millipore, Bedford, MA, USA). Reference standards of kaempferol, quercetin, taxifolin, apigenin, naringenin, peonidin-3-O-glucoside, cya-nidin-3-O-rutinoside, malvidin-3-O-glucoside, petunidin-3-O-glucoside, cyanidin 3-glucoside, cyanidin 3-(6''-malonylglucoside), pelargonidin-3-O-glucoside, del-phinidin-3-O-Glucoside were purchased from Wuhan Zbsci Co., Ltd (Wuhan, China). The purity of the above references was higher than 98% (HPLC).

Griess reagent, Total Antioxidant Capacity Assay Kits with the DPPH, ABTS, and FRAP methods were from (eyotime Biotechnology (Shanghai, China). Tumor necrosis factor-α (TNF-α) and interleukin-6 (IL-6) by enzyme-linked immunosorbent assay (ELISA) kits were bought from Boster Biological Technology (Wuhan, China). Total Antioxidant Capacity Assay Kit for ORAC method was from Congyi Bio (Shanghai, China). All other reagents used were of analytical grade.

2.2 Plant materials

Four cultivars of CPF from Anhui (AH), Sichuan (SC), Shandong (SD), and Shanxi (SX), were grown in separate areas of the same experimental field in Hezhe County, Shangdong province of China for five years. The cultivars names are 1# Xinshaofeng (AH), Guifeichacui (AH), Dafugui (SD), and Shuangchonglou (SX), respectively. The CPF samples were harvested at the same time in

April 2021 when the flowers were in full bloom. The plants were authenticated by Prof. G.X., Zhou (Pharmacognosy Department, Jinnan University, Guangzhou, China), and a voucher specimen (2021SYH01) was stored at the Guangdong Provincial Academy of Chinese Medical Sciences. Samples were separated into three parts: stamens, petals, and calyx (Figure 1), except SC cultivar, of which the stamens were not separated from the petals. Samples were placed in a freeze-dryer at -80°C for 48 hours and then grounded, sealed, and stored at 4°C before use.

2.3 Preparation of sample solutions

0.1 g of each powder sample was accurately weighed and then extracted with 3 mL methanol-water (70:30, v/v) containing 0.1% hydrochloric acid for 24 hours at room temperature. The extract was centrifuged at 5,000 rpm for 15 minutes. The supernatants were collected and filtered through a 0.22 μm filter (JinTeng, Tianjin, China). Quality control (QC) sample was made by assembling the same amount of each sample solution. In the LC-MS run, samples were analyzed in random order and a QC sample was inserted in every six testing samples to monitor the reproducibility and stability of the method.

2.4 UHPLC-Q-Orbitrap MS analysis

LC-MS experiments were performed on a U3000 UHPLC (Thermo Fisher Scientific, Waltham, MA, USA) coupled with a Q-Exactive Orbitrap hybrid MS system (Thermo Fisher Scientific, Rockford, IL, USA). The chromatographic separation was performed on a Waters HSS T3 column at a flow rate of 200 μL/min. The mobile phase consisted of water (A) and acetonitrile (B), both containing 0.1% formic acid. The elution gradient was set as follows: 90% A (0-1 min), 90-82% (1-3 min), 82-68% A (3-6 min), 68-54% A (6-8.5 min), 54-50% A (8.5-10 min), 50-10% A (10-13 min), 10% A (13-15min), 10-90% A (15-17min), 90% A (17-19min). The column temperature was 30°C and the injection volume was 2 μL.

The MS data were acquired using an Electron Spray Ionization (ESI) source both in negative and positive modes. The parameters were as follows: Ion spray voltage, 3,500 V in positive mode and 3,700 V in negative mode; capillary temperature, 350 °C; aux gas, 15 arb; sheath gas, 40 arb; MS resolutions for survey scanning and data-dependent acquisition were 35,000 and 17,500, respectively; scan range, m/z 100 ~ 1,200; and the normalized collision energy for DDA, 35 eV. Xcalibur software (version 3.1, Thermo Fisher Scientific, Waltham, MA, USA) was used for data acquisition.

FIGURE 1
Morphological characteristics of four kinds of herbaceous peony flower samples.

2.5 Qualitative analysis

The identification procedure of the chemical components of CPF was summarized as the following three levels of strategy. Level one, components are directly and accurately identified by comparing the retention time, quasi-molecular and fragment ions with reference standards analyzed under the same condition. Level two, components were identified by comparing their orthogonal MS features (precursor ion and characteristic fragment ions) to those known compounds from *P. lactiflora* and related species. Relative retention time would be considered as well. Level three, identification was conducted based on the fragmentation patterns and diagnostic fragment ions and/or neutral losses patterns summarized from the analysis of standards and known compounds. For these unknown compounds, highly accurate diagnostic fragment ion filtering and characteristic neutral loss filtering strategies were used to classify them into specific chemical subfamilies. In most cases, two or more common MS/MS product ions of the components with the same core substructures were selected as the characteristic fragment ions. Typical characteristic neutral losses of moieties such as C_2H_2O (acetyl), $C_7H_6O_5$ (galloyl), $C_3H_2O_3$ (malonyl), $C_6H_{10}O_5$ (hexosyl, hex), and their combinations, which can be deduced from the common fragmentation behaviors of the same type, were used to characterize these derivatives of known compounds.

2.6 Quantitative analysis

Among all identified compounds, 69 compounds with high peak intensities, as well as good peak shapes and resolution were selected for quantitative analysis. The methodology was evaluated firstly by testing the linearity, limit of detection (LOD), limit of quantification (LOQ), and inter-day and intra-day precision of the 14 standard compounds. The calibration curves were obtained by plotting the peak area versus concentration, while the LOD and LOQ were determined by signal-to-noise ratios greater than 3 and 10. The intra-day and inter-day precision were evaluated by preparing three different concentration levels (low, medium, and high) of reference samples in one day and re-peated for three consecutive days, respectively. The Intermediate precision was tested using medium reference samples by two experimenters at the same lab. The recovery rates of the fourteen analytes were determined at one level and calculated % recovery of known amounts of added to samples.

The results were expressed as relative standard deviation (RSD%). Since only 14 references were used for quantification, the quantities of these 14 components were calculated by calibration curves directly, while the rest of the components were quantified by using standard curves of those references that shared similar core structures with the target components. For example, the quantification of quercetin glucoside was determined by the standard curve of quercetin; the quantification of centaureidin di-glucoside was determined by the standard curve of centaureidin glucoside.

2.7 Evaluation of antioxidant activity

1,1-Diphenyl-2-picrylhydrazyl (DPPH) radical scavenging activity was assayed by the Total Antioxidant Capacity Assay Kit with the DPPH method 30μL calibration solution (Trolox), sample or blank (70% methanol) was added to 270 μL of DPPH (6×10-2 mM in 80% methanol) in different wells of a 96-well microplate, which was instantly kept in the dark for 30 min. The absorbance of the reaction mixture was then measured at 517 nm. The standard curve was established using Trolox ranging from 0.02 to 0.24 mM. The results were calculated from the linear calibration curve and expressed as μM Trolox equivalent (TE)/g dry weight of the sample.

2,2′-Azinobis-(3-ethylbenzthiazolin-6-sulfonic acid) (ABTS) radical cation scavenging activity was assayed by the Total Antioxidant Capacity Assay Kit with ABTS method. A stock solution was made by mixing the ABTS solution and oxidizing agent in equal volumes and kept in the dark for 16 hours. Then it was diluted in 80% methanol to obtain a working solution with absorbance of 0.7 ± 0.05 at 734 nm. 10 μL calibration solution (Trolox), sample or blank solution (80% methanol) were added to 200 μL of work solution in a 96-well microplate, which was incubated in the dark for 10 min. The absorbance of the reaction mixture was then measured at 734 nm. The standard curve was established using Trolox ranging from 0.1 to 0.9 mM. The results were calculated from the linear calibration curve and expressed as μM Trolox equivalent (TE)/g dry weight of the sample.

Ferric ion-reducing antioxidant power (FRAP) was assayed by the Total Antioxidant Capacity Assay Kit with the FRAP method. A working solution was prepared by mixing the tripyridyltriazine (TPTZ) solution, TPTZ dilution, and detective buffer at a ratio of 10:1:1 (v/v). The working solution was warmed in a water bath at 37°C and should be used within 2 hours. 5 μL calibration solution (Trolox), sample, or blank (70% methanol) was added to 180 μL of work solution in different wells of a 96-well microplate, then the mixture was incubated in the dark for 6 min at 37°C. The absorbance of the reaction mixture was then measured at 593 nm. The standard curve was established using $FeSO_4$ solution ranging from 0.15 to 1.5 mM. Results were calculated from the linear curve.

Oxygen radical absorbance capacity (ORAC) was tested by the Total Antioxidant Capacity Assay Kit with the ORAC method. The assay was conducted in a 96-well microplate with black opaque. Reagent 1 working solution was prepared by adding 10 mL dilution to 100 μL reagent 1. Reagent 2 working solution was prepared by adding 15 mL dilution to reagent 2. Briefly, 50 μL of calibration solution (Trolox), sample, or blank solution were added to 50 μL of reagent 1 working solution in each well of the microplate and the mixture was kept for 30 min at 37°C in the dark, then 100 μL of reagent 2 working solution was added immediately, and the microplate was placed into a micro-plate reader with the parameters set as follows: shaking time, 5 s; incubation temperature, 37°C; excitation wavelength, 485 nm; excitation wavelength, 520 nm. The fluorescence was read every 2 min for 90 min. The standard curve was established using Trolox ranging from 2.5 to 60 μM. The final ORAC results were calculated based on the differences in areas under the fluorescence quenching

curve (AUC) between a sample and blank and expressed as μM Trolox equivalent (TE)/g dry weight of the sample. The AUC was calculated by Eq.

$$AUC = \frac{f_0}{f_0} + \frac{f_1}{f_0} + \frac{f_2}{f_0} + \ldots + \frac{f_{n-1}}{f_0} + \frac{f_n}{f_0} \quad (1)$$

where f_0 indicated initial fluorescence reading at 0 min and fn indicated fluorescence reading at the nth detection.

2.8 Anti-inflammatory activity assay

RAW264.7 cells (2×10^5 cells/well) were seeded into 24-well plates and induced by 1 μg/mL LPS, with or without CPF for 24 h. Then the cell supernatant was collected and the content of NO was determined with Griess reagent at 540 nm with a microplate reader. Meanwhile, the supernatant was used to measure the levels of proinflammatory cytokines including tumor necrosis factor-α (TNF-α) and interleukin-6 (IL-6) by enzyme-linked immunosorbent assay (ELISA) kits in strict accordance with the manufacturers' instructions.

2.9 Determination of total phenolic, flavonoid, and anthocyanin contents

The total phenolic contents (TPC) of different parts of CPF were measured according to the previous protocol (Duan et al., 2006). Briefly, 0.5 mL of 0.2 N Folin-Ciocalteu reagent was added to 0.1 mL of sample extract solution. After 5 min of incubation, 0.4 mL of 7.5% Na_2CO_3 solution was sequentially added, followed by a two-hour incubation in the dark. The absorbance of each mixture was read at 760 nm in a microplate reader. Gallic acid solutions with a series of concentrations were measured at the same condition for drawing the regression curve. The TFC result was expressed as gram gallic acid equivalents (GE)/100 g sample in dry weight.

The total flavonoid contents (TFC) of different parts of CPF were measured according to the previous protocol with slight modifications (Bai et al., 2021). In brief, 0.5 mL of sample extract solution was added with 0.15 mL of 5% $NaNO_2$ solution and 0.15 mL of Al $(NO_3)_3$ solution (0.3 M). After incubation for 6 min, 2 mL of NaOH solution (4%, w/v) was sequentially added and the absorbance of the mixture was read at 510 nm. Series concentrations of rutin solutions were measured at the same condition for drawing the regression curve. The TFC result of each sample was expressed as gram rutin equivalents (RE)/100 g sample in dry weight.

Total anthocyanins content (TAC) was determined using a modification of the pH differential method (Moldovan et al., 2016). Aqueous buffer solutions at pH 1 and 4.5 were prepared from 0.025 M potassium chloride/hydrochloric acid buffer and 0.4 M sodium acetate/acetic acid buffer, respectively. Each sample (300 μL) was mixed with 2.7 mL of buffer. After equilibrating at room temperature in the darkness for 15 min, the absorbance at 515 and 700 nm was read using a UV-visible spectrophotometer and extraction solvent as the blank. The total anthocyanins content was calculated as equivalents of cyanidin-3-glucoside per gram of CPF sample using the previous equation (Moldovan et al., 2016).

2.10 Data preprocessing and statistical analysis

Data acquisition was achieved by Xcalibur software (version 3.1, Thermo Fisher, Waltham, MA, U.S.A.). The quantitative data were processed with the LC-Quan module (Thermo Fisher, Waltham, MA, U.S.A.). For untargeted metabolomics analysis, raw LC-MS data were processed by Compound Discovery, version 3.2, including feature detection, alignment, and normalization. The mass window for feature detection and alignment was set at 5 ppm. The retention time (RT) window was set at 0.2 min. The normalized data matrix was exported into SIMCA-P 14.1 (Umetrics, Sweden) for principal component analysis (PCA). The established models were assessed by calculating the R2 and Q2 values, which represented the goodness and predictability of the models, respectively. A one-way analysis of variance (ANOVA) statistical test was performed to analyze statistical significance between groups using SPSS software (version 25.0). Heat map analysis was conducted by R-Studio and Metware Cloud (https://cloud.metware.cn/) to display the quantitative changes in the chemical constituents.

For antioxidant activity, total phenolic, total flavonoid, and anthocyanin contents assays, all the samples were tested in triplicates. Statistical analysis was conducted by using the one-way analysis of variance and $p<0.05$ was considered to be significant.

3 Results

The typical base peak chromatograms (BPC) of each part are illustrated in Figure 2, where the disparity in the relative peak height and peak area can be drawn by visual in-spection. In order to obtain detailed knowledge concerning the changes of individual chemical constituents, a systematic chemical investigation was conducted first.

3.1 Identification of chemical components

According to the qualitative Analysis strategy, 150 components were characterized, of which the retention times, molecular formulae, and the high-resolution precursor and characteristic fragment ions are listed in Supplementary Table S3. Except those major and representative components, more than 50 compounds were detected from *Paeonia lactiflora* for the first time. In addition, the fragmentation behaviors and characteristic fragments of those new detected components were elaborated.

10.3389/fpls.2024.1501966

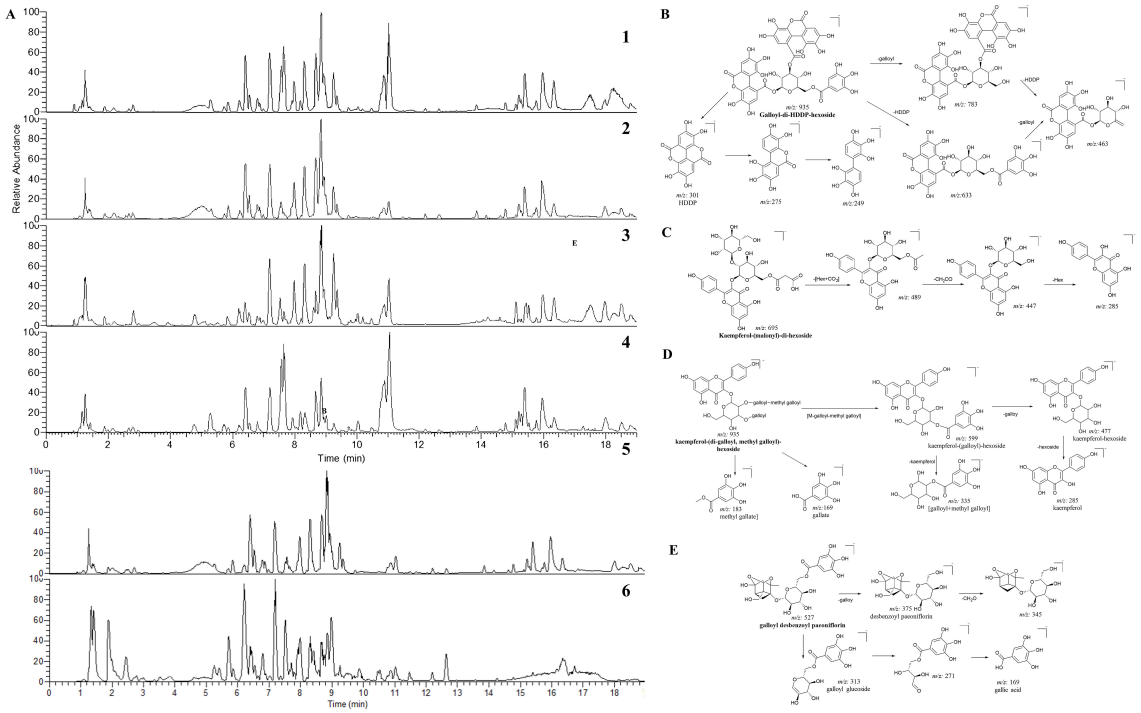

FIGURE 2
The LC-MS chromatograms of CPF and the fragmentation pathways of selected compounds. **(A)** The base peak chromatograms (BPC) of whole flower (A1), petals (A2), calyx (A3) and stamens (A4); The BPC of petals in positive (A5) and negative (A6) ion modes of mass spectrometry. The proposed fragmentation pathways of galloyl-di-HDDP-hexoside **(B)**, kaempferol-(malonyl)-di-hexoside **(C)**, kaempferol-(di-galloyl, methyl galloyl)-hexoside **(D)**, and galloyl desbenzoyl paeoniflorin **(E)**.

3.1.1 Identification of hydrolysable tannins

Previous reports showed that the fruit of *Paeonia lactiflora* possess considerable number of tannins (Li et al., 2021). Hydrolysable tannins are an important group of secondary metabolites that exhibit anti-angiogenic, antioxidant, anti-inflammatory, and anti-ulcerative properties. For the first time, the present LC-MS study indicated that CPF is rich in hydrolysable tannins but not condensed tannin. Herein thirty-one compounds were rapidly characterized as hydrolysable tannins based on their characteristic fragment ions in Orbitrap MS.

Simple gallotannins included di-gallic acid, tri-gallic acid, tetra-gallic acid and their isomers. They all showed common characteristic ions at *m/z* 169.0131 and 125.0230, referring to [gallic acid] and [gallic acid - CO_2] residues, respectively. Compound 18 exhibited a precursor ion at *m/z* 183.0298 $[M\text{-}H]^-$ ion, yielding two odd-electron fragments at *m/z* 168.0052 $[M -\cdot CH_3]$ and 124.0152 $[M - CO_2 -\cdot CH_3]^-$, indicating a methyl gallic acid (Qiu et al., 2022). In addition, compounds 25 and 31, with their $[M–H]^-$ ion at *m/z* 335.0408 $[M–H]^-$ ion and main fragments at *m/z* 183, 168, and 124, were identified as methyl di-gallate. Another common type of gallic acid derivatives found in CPF were galloyl hexosides. Those precursor ions showed fragments of *m/z* 169 $[M–H–162\ Da]^-$ and 125 $[M–H–162\ Da–44\ Da]^-$, corresponding to the characteristic neutral loss of a hexoside unit. Accordingly, these two characteristic fragments facilitated the identification of galloyl hexoside analogs such as di-galloyl hexoside, tri-galloyl hexoside, tetra-galloyl hexoside, and penta-galloyl hexoside.

Compounds 26 and 30 were identified from Chinese peony for the first time. Notably, their common fragmentation behaviors on Orbitrap MS were characterized by characteristic fragment ions due to successive losses of $C_7H_4O_4$ and $C_7H_6O_5$ units, indicating they were gallotannins. Take compound 26 as an example. It produced $[M–H]^-$ ion at *m/z* 801.1159 ($C_{35}H_{30}O_{22}$), and further fragmented into *m/z* 649.1077 ($C_{28}H_{25}O_{18}$), 631.0933 ($C_{28}H_{23}O_{17}$), 479.0836 ($C_{21}H_{19}O_{13}$), and 327.0718($C_{14}H_{15}O_9$), representing the neutral losses of $[C_7H_4O_4]$, $[C_7H_6O_5]$, $[C_7H_6O + C_7H_4O_4]$, and $[C_7H_6O + 2\times C_7H_4O_4]$, respectively. The final fragment product ion at *m/z* 193.0133 represented methyl glucoside, thus, compound 26 was deduced to be methyl-tetra-galloyl hexoside (Supplementary Figure S1).

Ellagitannins and its major components ellagic acid present in some fruits and seeds. Their structures are characterized by the distinct hexahydroxydiphenol (HHDP) group. Herein, we reported five HHDP hexosides from CPF for the first time. Peak 21 displayed $[M–H]^-$ ion at *m/z* 935.0800 and produced major fragments at *m/z* 300.9988, 275.0199, 249.0400, 169.0129, indicating a hexahydroxydiphenol (HHDP) group (Qiu et al., 2022). Other fragments such as 783.0720, 633.0732, and 463.0501 referred to the losses of galloyl, HHDP, and [galloyl+HHDP] units, respectively (Figure 2B). Thus, it was tentatively identified as galloyl-di-HDDP-hexoside. By using the fragment ions filtering of 300.9988, 275.0199, 249.0400, several HDDP-hexoside (7, 10, 15, and 19) derivatives were also detected.

3.1.2 Identification of flavonoids

A total of 70 compounds were identified as flavonoid derivatives. Five flavonoid aglycones, taxifolin, quercetin, apigenin, naringenin, and kaempferol, were unambiguously identified by comparing their retention times and mass spectrometry features with those standard compounds. As described in previous studies (Bai et al., 2021), the MS fragmentation of flavone/flavanone *O*-glycosides in both positive and negative ion modes is featured by producing the prominent base fragment ion of [M-glycosides]. Generally, neutral losses of these glycosides refer to rutinoside (308 Da), hexoside (162 Da), deoxyhexoside (146 Da), and pentoside (132 Da).

Notably, a series of modified flavonoid glycosides, where the glycoside residue is acylated with aromatic or aliphatic acids (malonic, gallic, and acetic acids, to name a few), were identified. For instance, several malonyl-substituted flavonoid glycosides, including isorhamnetin-malonyl dihexoside, isorhamnetin-malonylhexoside, kaempferol-malonyl dihexoside, kaempferol-malonyl hexoside, and so on were reported. Those malonyl derivatives showed [F+$C_3H_2O_3$ (86 Da)] precursor ions (herein, F denotes the corresponding flavonoid glycoside) in the survey scan. Specifically, when it was modified by malonyl on the glycoside part, prominent fragment ions referring to neutral losses of malonyl residue (86 Da, CHO) and/or malonyl glucoside residue (162 + 86 Da) would present in MS/MS spectra, while other fragment ions were identical to those prototypical compounds. Take kaempferol-(malonyl)-di-hexoside as an example. It produced precursor ion at *m/z* 695.1464, which further fragmented into the base fragment peak at *m/z* 447.0911 [M-(162 + 86 Da)-H]. In addition, another characteristic fragmentation ion at *m/z* 489.1005 was resulted from the cleavage of the malonyl group, which shows neutral loss of [162(glu)+44 Da (CO_2)]. The proposed fragmentation pattern is illustrated in Figure 2C. As natural derivatives, malonyl glycosides were reported from many plant species and their content may be associated with antioxidant capacities (Kwak et al., 2007). To our knowledge, this is the first time for the detection of malonyl-substituted flavonoids in CPF.

Likewise, acetyl, gallic acyl, and *p*-coumaroyl-substituted flavonoid glycosides were also detected and characterized by applying the same strategy (Supplementary Figure S1). In general, they showed the characteristic precursor ions such as [F+C_2H_2O (42 Da)], [F+$C_7H_4O_4$ (152 Da)] or [F+$C_9H_6O_2$ (146 Da)] in survey scans, respectively, and exhibit the same prominent aglycone ions in their MS/MS spectra with their prototype components.

For compound 77, it showed a $[M-H]^-$ at *m/z* 935.1528 ($C_{43}H_{36}O_{24}$), which further produced as same fragments at *m/z* 599.1040, 447.0919, 313.0559, 285.0400, 169.0129, 151.0028 as kaempferol-(galloyl)-hexoside, indicating it was kaempferol-(galloyl)-hexoside derivative. The base fragment ion at *m/z* 183.0289 was deduced to be a methyl gallate module. Both the fragment at *m/z* 335.0399 and the neutral loss for *m/z* 599.1040 further indicated the [methyl gallate + gallate] unit. The fragmentation pathway is illustrated in Figure 2D. Thus it was tentatively identified as kaempferol-(di-galloyl, methyl galloyl)-hexoside, which is a potential new component.

3.1.3 Identification of anthocyanins

Anthocyanins are natural pigments belonging to the flavonoid group. So far, more than 25 natural anthocyanins have been identified, of which 95% are derived from six aglycone porotypes, namely cyanidin (Cy), paeonidin (Pn), pelargonidine (Pg), malvidin (Mv), delphinidin (Dp), and petunidin (Pt) (Chen et al., 2022). In the present study, 16 compounds were identified as anthocyanins. Cy-diglu, Pn-diglu, Dp-glu, Cy-glu, Pt-glu, Cy-rutin, Pg-glu, Pn-glu, Mv-glu, Cy-malglu, Dp, Cy, Pt, Pg, and Mv were unambiguously identified by comparison the retention time and mass spectrometric information with the standard compounds. Other anthocyanins were tentatively identified based on level 3 strategy.

3.1.4 Identification of monoterpene glycosides

Pinane monoterpene glycosides are the characteristic components of *P. lactiflora*. Two prominent peaks (peaks 125 and 127) were identified as albiflorin and paeoniflorin, according to their distinctive fragmentation patterns (Nie et al., 2021). As the type of benzoate ester of monoterpene lactone glycosides, their typical characteristic fragment ions in negative mode are at [M- CH_2O (30 Da)], [[M-CH_2O-benzoate], *m/z* 327.1077[M-2× CH_2O-benzoate], and *m/z* 121.0280[benzoyl-H] (Supplementary Figure S1).

Compounds 119, 120, 122 - 128, 130, and 131 were determined to share the same pinane monoterpene skeleton as paeoniflorin. In general, these compounds can also form a characteristic fragment ion of $[M-H-CH_2O]^-$, as well as fragments referring to the loss of the benzoyl group. For instance, compound 124 generated characteristic fragment ions of *m/z* 489.1611 $[M-H-CH_2O$-benzoate$]^-$ and *m/z* 121.0281 [benzoate -H]$^-$, and a characteristic pinane monoterpene ($C_{10}H_9O_3$) fragment ion at *m/z* 177.0546. Thus, it was deduced to be albiflorin hexoside.

Herein two potential new monoterpene glycosides were tentatively identified. Compound 135 and 136 showed their $[M-H]^-$ ion at *m/z* 527.1409, producing fragment ion at *m/z* 375.1293 due to the neutral loss of galloyl (152 Da), which further loss 30 Da [CH_2O] to produce characteristic ion at *m/z* 345.1187. The rest characteristic fragments such as 313.0565, 271.0462, and 169.0132 are the same as galloylpaeoniflorin (130). Based on this information, they were tentatively identified as galloyl desbenzoyl paeoniflorin or galloyl desbenzoyl albiflorin. The fragmentation pathway was proposed in Figure 2E.

3.1.5 Identification of other phenolics

Fourteen compounds in the samples were tentatively identified as phenolic acids. To our knowledge, 15 of these compounds were identified for the first time from this genus. In this study, we identified protocatechuic acid hexoside (137,139), *p*-hydroxybenzoic acid hexoside (138), *p*-coumaryl glucarate (140,142,143), benzoic acid glucarate (141,144,145,147) and their isomers. They showed the characteristic fragment ions in their product ion spectra by elimination of hexoside (162Da) and glucarate (192 Da) moieties.

3.2 Metabolomics profiling analysis of CPF from different parts and cultivars

To capture an overall picture of the primary distinction of CPF in different parts and cultivars, an untargeted PCA and Hierarchical Cluster Analysis (HCA) models were created firstly. The clear chemical variation between three flower parts could be seen from the PCA score plot (Figure 3A) and HCA plot (Figure 4A) of all the 66 samples, while the QC group gathered together at the origin of the orthogonal coordinate. Samples from the same plant part were selected to further PCA analysis (Figures 3B–D). They explicitly showed the distinct chemical compositions among those cultivars even though they were grown at the same place. Previous studies indicated (Li et al., 2023; Yang et al., 2023) significant chemical differences between Chinese Peony cultivars. Although both genetic and environmental factors can affect the chemical phenotype, our result showed that the chemical distinctions between those cultivars could be solely attributed to the intrinsic cause.

3.3 Quantitative comparison and multivariate analysis

Subsequently, targeted multivariate analysis and comparison between those samples, based on quantifying the contents of individual compounds in CPF, were constructed to get a more precise picture of chemical differences. Previously, we set up a simi-quantification data-based targeted metabolomics strategy, which had been successfully applied for fast analysis and comparison of plant-derived food resources, such as tangerine (Zhang et al., 2020a), Ganpu tea (Xu et al., 2021) and citron (Zhang et al., 2022). Herein, we used similar strategy to address the CPF samples from different flower parts and cultivars.

Firstly, 14 reference compounds, covering anthocyanins and flavonoids, were used to construct and validate the quantitative methodology. The selection of the 14 quantitative targets is based on the content in CPF implied by previous chemical investigation (Zhang et al., 2020b; Liu et al., 2023). Also, the commercial availability of those reference standards was considered. Validation of the quantification method in terms of linearity, LOD, LOQ, intra-day, inter-day precision, Intermediate precision and recovery rate was conducted by using 14 standards, which covered the main anthocyanins, flavonoids, and monoterpenoids in CPF. As shown in Supplementary Table S1, all 14 standards showed good linearity between concentrations and corresponding MS peak areas with correlation coefficients >0.995. The intra-day and inter-day of most standards at low, medium, and high concentration levels were<10%, and the Intermediate precision RSDs were less than 12%, indicating acceptable precision of the method. The recovery rates of 14 analytes were between 85.71% to 112.09% with RSDs less than 10.62%. The LODs and LOQs for 14 analytes were between 0.2–1.0 and 0.4– 4.0 ng/mL, respectively, suggesting good sensitivity of the method. Other than the 14 reference compounds, components with high peak intensities (above 1 ×

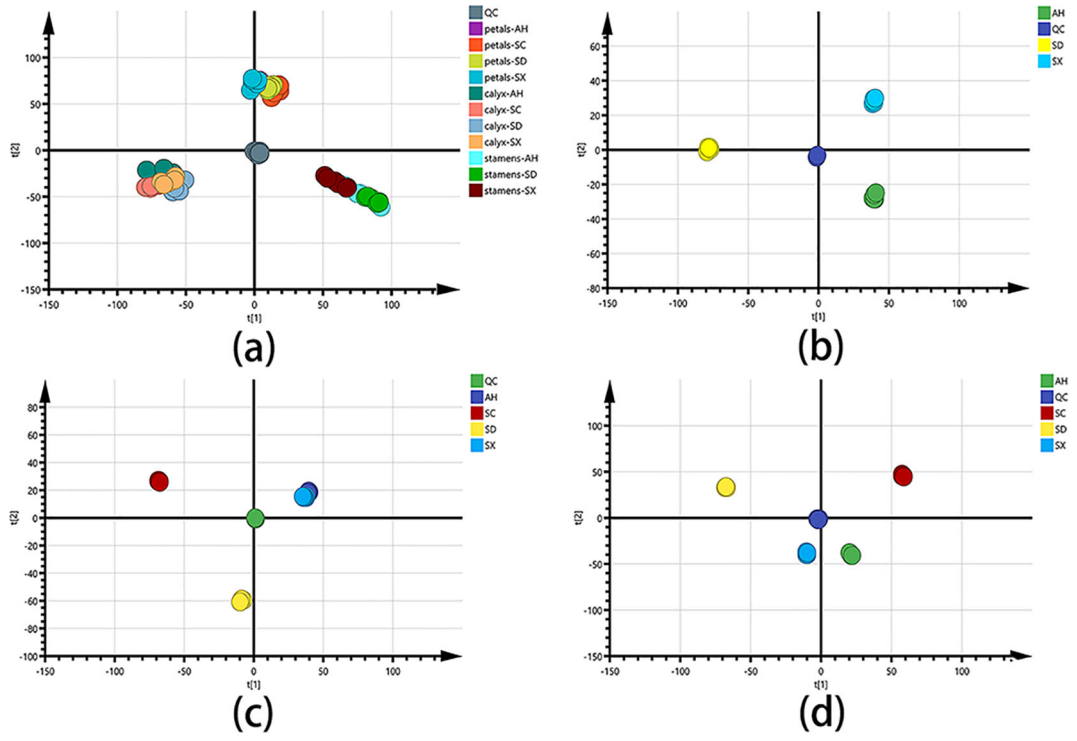

FIGURE 3
PCA score charts for different group settings: **(A)** PCA score plot of all CPF samples (n = 6), with R^2X and Q^2 of 0.836 and 0.747, respectively. **(B)** PCA score plot of stamen samples. **(C)** PCA score plot of petal samples. **(D)** PCA score plot of calyx samples. SC, AH, SD, and SX denote cultivars from Sichuan, Anhui, Shandong, and Shanxi, respectively.

10.3389/fpls.2024.1501966

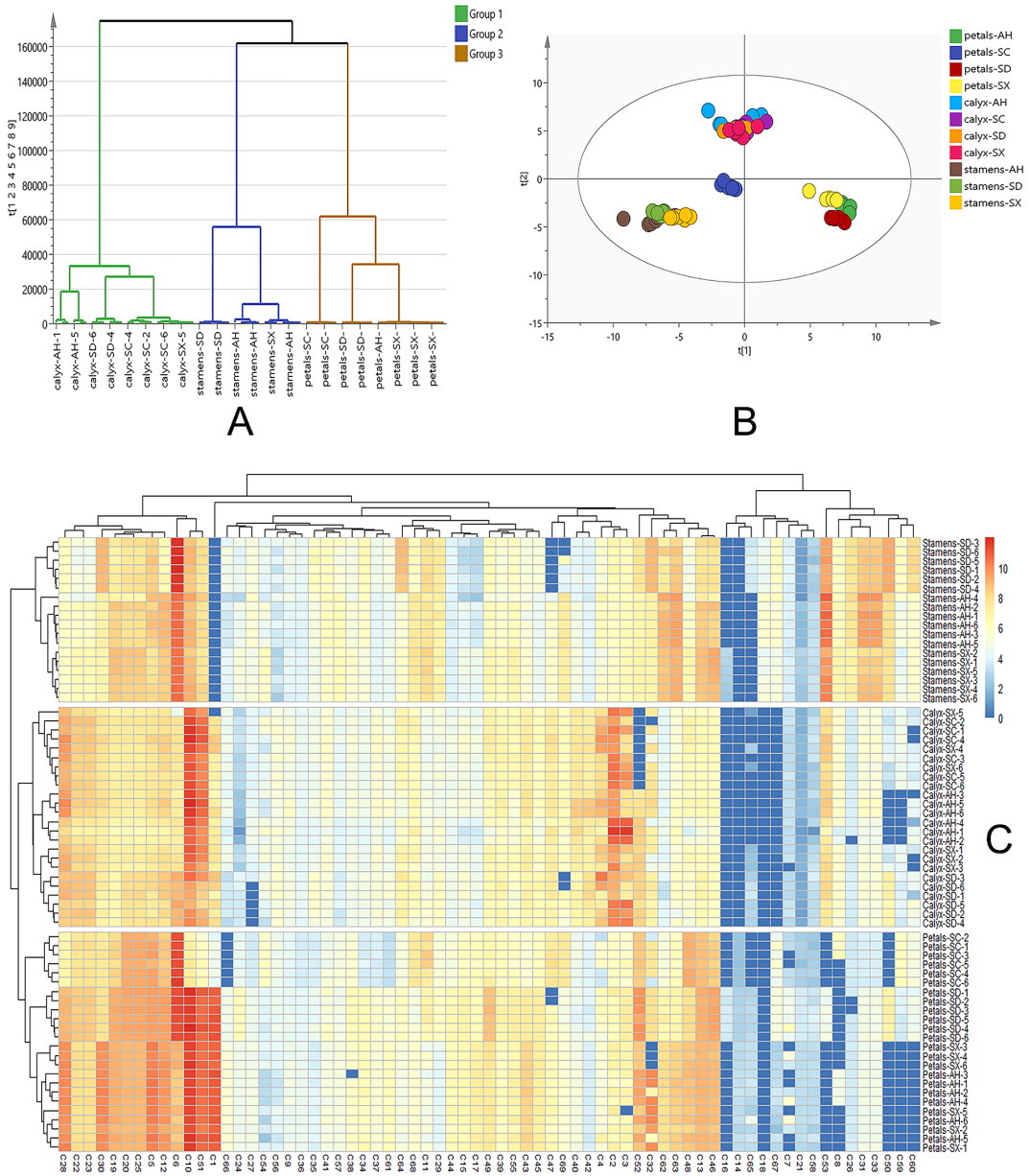

FIGURE 4
(A) Clustering analysis of all the CPF samples. Group 1 in green represents 24 calyx samples, group 2 in blue represents 18 stamen samples and group 3 in brown represents 24 petal samples. **(B)** Targeted PCA analysis of 69 quantification data. R^2X = 0.901, Q^2 = 0.830. **(C)** Heatmap constructed from quantification data. The abscissa represents the quantified components and the ordinate represents samples. SC, AH, SD, and SX denote cultivars from Sichuan, Anhui, Shandong, and Shanxi, respectively.

10^6 in the QC sample) and good separation were selected for further quantitative comparison. Those targets would be quantified by using the standard curve of reference compounds from the same structure prototype. Thus, a total of 69 targets were selected and they were quantified or semi-quantified (Table 1; Supplementary Table S2).

Multivariate statistical analysis based on the quantification data was further carried out. As shown in Figure 4B, the PCA score plot shows three distinct clusters (R^2X = 0.901 and Q^2 = 0.830). The detailed content of each target among the 66 samples was for hierarchical cluster analysis using the Ward chain algorithm. In the heat map and dendrogram (Figure 4C), it graphically showed that all the samples could be divided into three major clusters (stamen, calyx, and petal). each major cluster can be roughly separated into cultivars sub-clusters (SD, AH, SX and SC). Given the fact that there is conceptual disparity between targeted and untargeted metabolomics analysis, our data showed very consistency between these two methods. Within the petal group, SC samples were clustered separately, while AH, SD, and SX samples were clustered together, which is perfectly fit into the color discrepancies of the four cultivar petals (Figure 1). This finding suggested a clear correlation between those 69 major components and petal color.

As one of major natural colorants, anthocyanins play important role in color formation during plant blooming. Our subsequent

TABLE 1 The contents or relative contents of 69 targets quantified by LC-MS.

No.	compounds	petal-AH	petal-SC	petal-SD	petal-SX	petal	calyx-AH	calyx-SC	calyx-SD	calyx-SX	calyx	stamen-AH	stamen-SD	stamen-SX	stamen
C1	Cyanidin-3,5-O-diglucoside	2016.09 ± 171.93	22.21 ± 4.3	2019.61 ± 170.59	1767.45 ± 117.59	1456.34	168.8 ± 62.47	214.92 ± 95.46	261.57 ± 115.32	180.71 ± 123.4	206.50	N.D.	N.D.	N.D.	N.D.
C2*	Delphinidol-3-O-glucoside	82.18 ± 24.19	62.18 ± 3.05	97.05 ± 33.65	143.59 ± 24.93	96.25	1530.61 ± 944.34	1132.72 ± 246.66	843.15 ± 329.47	1017.1 ± 295.26	1130.90	62.85 ± 10.75	91.57 ± 18.24	56.46 ± 4.48	70.29
C3	Delphinidin	108.55 ± 24.3	61.02 ± 17.87	162.19 ± 13.11	95.23 ± 48.39	106.74	1171.81 ± 1121.39	586.7 ± 332.59	708.5 ± 553.06	492.14 ± 318.12	739.79	81.42 ± 9.48	84.28 ± 11.43	87.82 ± 9.54	84.51
C4*	Cyanidin-3-O-glucoside	55.44 ± 40.11	31.55 ± 23.87	65.34 ± 19.55	42.96 ± 3.79	48.82	342.37 ± 194.14	466.18 ± 258.9	508.72 ± 447.06	357.74 ± 185.43	418.75	82.23 ± 21	46.6 ± 7.31	46.39 ± 14.39	58.41
C5	Cyanidin	1251.17 ± 46.79	635.9 ± 91.87	720.82 ± 11.89	1131.46 ± 93.4	934.84	185.29 ± 74.06	223.89 ± 53.86	228.5 ± 61.76	198.38 ± 34.12	209.01	381.32 ± 61.18	342.26 ± 29.4	249.42 ± 36.08	324.33
C6*	Petunidin-3-O-glucoside	364.34 ± 17.92	2532.6 ± 285.86	2412.18 ± 104.34	512.43 ± 52.32	1455.39	169.87 ± 25.04	217.22 ± 29.5	532.78 ± 68.83	172.9 ± 76.73	273.19	1573.36 ± 58.9	3634.04 ± 224.8	1478.57 ± 76.86	2228.66
C7* C8*	Cyanidin-3-O-rutinoside	16.48 ± 22.1	4.83 ± 3.77	31.32 ± 19.5	8.82 ± 12.41	15.36	8.15 ± 0.59	8.48 ± 1.46	7.7 ± 1.12	6.55 ± 3.29	7.72	13.48 ± 0.74	14.23 ± 1.94	12.12 ± 1.25	13.28
	Pelargonidin-3-O-glucoside	17.92 ± 13.9	35.88 ± 40.14	N.D.	N.D.	13.45	40.55 ± 18.76	54.72 ± 5.04	51.07 ± 3.39	52.28 ± 2.32	49.65	83.31 ± 9.36	66.28 ± 2.95	115.46 ± 12.18	88.35
C9	Pelargonidin	25.59 ± 3.95	17.4 ± 1.25	20.27 ± 2.11	23.99 ± 2.96	21.81	40.36 ± 12.84	34.61 ± 6.68	29.58 ± 3.05	26.65 ± 4.37	32.80	17.15 ± 5.21	23.21 ± 3.43	15.84 ± 1.96	18.73
C10*	Peonidin-3-O-glucoside	2843.22 ± 286.11	155.8 ± 38.1	3221.15 ± 510.57	2783.51 ± 303.97	2250.92	2545.34 ± 813.06	2610.63 ± 780.38	903.46 ± 394.03	1912.69 ± 485.31	1993.03	528.84 ± 98.22	446.28 ± 65.22	492.73 ± 91.93	489.28
C11*	Malvidin-3-O-glucoside	28.72 ± 5.37	265.29 ± 87.03	123.94 ± 29.59	37.65 ± 10.7	113.90	29.68 ± 2.85	23.99 ± 2.53	39.26 ± 10.57	28.75 ± 3.12	30.42	212.58 ± 38.42	265 ± 28.05	285.66 ± 24.27	254.41
C12*	Cyanidin-3-(6”-malonylglucoside)	859.45 ± 46.09	383.67 ± 33.06	718.99 ± 38.73	731.46 ± 100.81	673.39	234.71 ± 101.99	269.17 ± 52.41	315.98 ± 72.21	264.18 ± 56.71	271.01	470.47 ± 31.75	89.93 ± 14.61	357.7 ± 22.06	306.03
C13	Kaempferol-dihexoside	522.02 ± 11.48	429.34 ± 17.21	557.16 ± 15.72	478.85 ± 23.05	496.84	63.51 ± 28.08	83.84 ± 15.13	104.31 ± 19.16	73.84 ± 13.12	81.37	335.35 ± 87.32	225.21 ± 33.87	429.18 ± 29.96	329.91
C14	Dihydrokaempferol-hexoside	8.18 ± 0.25	3.57 ± 0.12	5.62 ± 0.18	6.98 ± 0.54	6.09	N.D.	N.D.	N.D.	N.D.	N.D.	N.D.	N.D.	N.D.	N.D.
C15	Kaempferol-(malonyl)-dihexoside	94.89 ± 3.37	63.9 ± 4.45	117.44 ± 3.45	90.1 ± 8.79	91.58	25.57 ± 14.6	37.3 ± 8.65	39.21 ± 9.01	32.21 ± 7.64	33.57	16.64 ± 6.94	9.38 ± 2.32	24.47 ± 4.35	16.83
C16	Kaempferol-(galloylhexoside)-hexoside	N.D.	N.D.	11 ± 0.71	N.D.	2.75	N.D.	N.D.	N.D.	N.D.	N.D.	N.D.	N.D.	5.31 ± 0.95	1.77
C17	Kaempferol-hexoside-deoxyhexoside II	161.24 ± 4.9	76.88 ± 10.33	83.26 ± 1.96	142.54 ± 11.81	115.98	20.53 ± 8.33	26.62 ± 5.11	21.66 ± 4.63	23.14 ± 4.32	22.99	10.9 ± 4.31	7.3 ± 0.98	21.52 ± 4	13.24
C18	Kaempferol-rutinoside-hexoside	N.D.	N.D.	N.D.	N.D.	N.D.	N.D.	N.D.	N.D.	N.D.	N.D.	46.5 ± 7.37	21.92 ± 2.23	28.97 ± 7.1	32.46

(Continued)

10.3389/fpls.2024.1501966

TABLE 1 Continued

No.	compounds	petal-AH	petal-SC	petal-SD	petal-SX	petal	calyx-AH	calyx-SC	calyx-SD	calyx-SX	calyx	stamen-AH	stamen-SD	stamen-SX	stamen
C19	Kaempferol-hexoside	600.85 ± 9.2	296.91 ± 27.92	596.85 ± 15.93	541.8 ± 31.36	509.10	140.87 ± 50.59	165.57 ± 19.74	107.77 ± 11.66	143.01 ± 15.74	139.31	296.08 ± 92.14	152.75 ± 24.37	410.04 ± 43.89	286.29
C20	Kaempferol-hexoside II	502.67 ± 12.35	615.48 ± 29.92	648.55 ± 18.3	483.43 ± 22.92	562.53	124.52 ± 37.23	182.36 ± 24.96	253.4 ± 28.14	155.54 ± 22.47	178.95	252.15 ± 78.91	237.25 ± 36.35	360.41 ± 36.63	283.27
C21	Kaempferol or Luteolin-(galloylhexoside)-gallic a	7.98 ± 0.26	4.8 ± 0.77	11.61 ± 0.37	7.2 ± 0.31	7.90	2.09 ± 0.66	2.27 ± 0.17	1.78 ± 0.27	2.32 ± 0.2	2.11	2.68 ± 0.95	1.44 ± 0.2	4.73 ± 0.89	2.95
C22	Kaempferol-malonyl-hexoside I	256.97 ± 7	236.27 ± 18.67	363.32 ± 14.4	260.49 ± 22.57	279.26	248.94 ± 82.84	360.49 ± 42.62	387.15 ± 51.52	313.9 ± 39.74	327.62	60.17 ± 22.62	32.13 ± 7.21	87.52 ± 13.76	59.94
C23	Kaempferol-malonyl-hexoside II	256.97 ± 7	236.27 ± 18.67	363.32 ± 14.4	260.49 ± 22.57	279.26	248.94 ± 82.84	360.49 ± 42.62	387.15 ± 51.52	313.9 ± 39.74	327.62	60.17 ± 22.62	32.13 ± 7.21	87.52 ± 13.76	59.94
C24*	Kaempferol	25.25 ± 1.19	19.87 ± 2.78	78.98 ± 3.27	25.24 ± 2.58	37.33	2.8 ± 1.16	7.71 ± 1.76	11.98 ± 2.35	6.38 ± 1.32	7.22	20.59 ± 8.18	19.32 ± 4.12	33.83 ± 4.03	24.58
C25	Astragalin	502.67 ± 12.35	615.48 ± 29.92	648.55 ± 18.3	483.43 ± 22.92	562.53	124.52 ± 37.23	182.36 ± 24.96	253.4 ± 28.14	155.54 ± 22.47	178.95	252.15 ± 78.91	237.25 ± 36.35	360.41 ± 36.63	283.27
C26	Isorhamnetin-trihexoside	11.35 ± 0.24	11.1 ± 0.2	7.31 ± 5.66	11.15 ± 0.52	10.23	10.55 ± 5.18	11.51 ± 0.46	11.91 ± 0.77	11.68 ± 0.55	11.41	231.45 ± 42.07	231.85 ± 18.81	135.42 ± 20.72	199.57
C27	Isorhamnetin-trihexoside II	30.23 ± 1.67	11.43 ± 0.3	23.45 ± 1.06	25.81 ± 2.41	22.73	21.68 ± 4.23	16.16 ± 1.82	2.1 ± 5.15	16.22 ± 2.07	14.04	44.77 ± 6.98	35.64 ± 2.17	30.45 ± 4.81	36.95
C28	Isorhamnetin-(malonyl)-hexoside- hexoside	1003.63 ± 53.94	113 ± 10.51	502.95 ± 22.5	954.84 ± 110.39	643.61	617.3 ± 327.52	660.79 ± 157.32	413.32 ± 89.95	563.76 ± 119.77	563.79	54.76 ± 11.05	67.98 ± 2.75	53.55 ± 5.22	58.76
C29	Isorhamnetin-trihexoside III	16.35 ± 0.97	39.18 ± 1.38	60.27 ± 3.07	19.16 ± 1.73	33.74	33.58 ± 10.54	33.73 ± 4.1	58.6 ± 2.86	31.39 ± 4.22	39.33	141.37 ± 29.32	181.53 ± 5.96	126.15 ± 23.75	149.68
C30	Isorhamnetin-deoxyhexoside_-hexoside	1067 ± 47.7	195.38 ± 13.79	249.08 ± 11.12	920.44 ± 97.03	607.97	203.72 ± 60.13	232.51 ± 34.84	144.78 ± 29.79	195.83 ± 34.01	194.21	138.41 ± 8.73	482.66 ± 14.83	118.72 ± 8.89	246.60
C31	Isorhamnetin-(malonyl)-dihexoside	27.78 ± 1.01	12.41 ± 0.31	28.39 ± 1.92	24.83 ± 1.6	23.35	42.16 ± 18.7	40.96 ± 4.76	37.73 ± 4.33	38.13 ± 5.64	39.75	717.76 ± 117.99	385.8 ± 19.82	387.93 ± 82.8	497.16
C32	Isorhamnetin-deoxyhexoside-hexoside II	733.38 ± 499.45	137.91 ± 98.24	249.08 ± 11.12	459.81 ± 511.18	395.04	178.09 ± 96.99	113.9 ± 106.19	139.07 ± 27.19	140.09 ± 96.69	142.79	138.41 ± 8.73	482.67 ± 14.83	118.72 ± 8.89	246.60
C33	Isorhamnetin-digallic acid-benzoic acid	27.77 ± 1.02	12.41 ± 0.31	28.38 ± 1.92	24.82 ± 1.62	23.35	42.17 ± 18.72	40.97 ± 4.76	37.74 ± 4.33	38.13 ± 5.64	39.75	717.76 ± 117.99	385.8 ± 19.82	387.91 ± 82.78	497.15
C34	Isorhamnetin-deoxyhexoside_-hexoside III	79.95 ± 15.4	12.15 ± 1.53	84.83 ± 4.65	77.45 ± 13.83	63.60	21.88 ± 4.98	23.95 ± 2.69	27.14 ± 2.73	21.72 ± 2.42	23.67	55.28 ± 6.28	88.21 ± 7.94	36.34 ± 4.4	59.94
C35	Isorhamnetin-(p-coumaroyl)-hexoside	15.56 ± 1.89	12.39 ± 0.35	21.2 ± 3.41	13.31 ± 1.48	15.62	23.57 ± 7	26.23 ± 3.03	46.43 ± 8.08	23.63 ± 2.51	29.96	34.66 ± 4.45	76.22 ± 21.94	26.85 ± 2.53	45.91
C36	Quercetin-(galloyl)-dihexoside I	22.49 ± 0.89	12.03 ± 0.37	16.98 ± 0.39	21.11 ± 0.69	18.15	17.25 ± 2.04	20.63 ± 1.5	18.16 ± 2.18	19.28 ± 1.42	18.83	14.49 ± 0.18	19.03 ± 0.42	14.55 ± 0.44	16.03

(Continued)

10.3389/fpls.2024.1501966

TABLE 1 Continued

No.	compounds	petal-AH	petal-SC	petal-SD	petal-SX	petal	calyx-AH	calyx-SC	calyx-SD	calyx-SX	calyx	stamen-AH	stamen-SD	stamen-SX	stamen
C37	Quercetin-(galloyl)-dihexoside II	44.07 ± 1.13	12.61 ± 0.72	50.98 ± 2.39	41.88 ± 2.67	37.38	39.02 ± 10.82	47.92 ± 6.16	37.22 ± 3.79	43.69 ± 5.55	41.96	16.68 ± 0.75	25.07 ± 0.89	18.19 ± 1.04	19.98
C38	Quercetin-pentoside I	51.55 ± 25.52	44.22 ± 3.21	87.22 ± 4.82	50.28 ± 4.49	58.32	29.42 ± 8.53	34.42 ± 4.4	26.17 ± 2.01	31.17 ± 3.57	30.30	34.63 ± 8.75	32.73 ± 3.92	50.35 ± 5.98	39.24
C39	Quercetin-hexoside-deoxyhexoside	79.78 ± 6.29	71.01 ± 9.73	125.35 ± 18.3	64.21 ± 5.19	85.09	91.76 ± 39.69	106.48 ± 14.32	111.69 ± 20.39	95.7 ± 14.3	101.41	50.79 ± 11.09	42.74 ± 5.22	70.49 ± 8.02	54.67
C40	Quercetin-(galloyl)-hexoside	35.92 ± 2.82	23.94 ± 3.22	22.55 ± 6.07	31.13 ± 1.92	28.39	271.87 ± 78.13	185.93 ± 16.87	123.57 ± 15.8	179.81 ± 24.84	190.29	27.38 ± 6.17	17.79 ± 2.92	31.33 ± 5.18	25.50
C41	Quercetin-deoxyhexoside-hexoside II	33.42 ± 5.91	29.07 ± 5.59	44.89 ± 13.04	30.41 ± 3.21	34.45	41.5 ± 13.29	47.93 ± 6.78	36.43 ± 3.59	43.76 ± 5.59	42.41	70.96 ± 6.13	69.25 ± 1.71	53.56 ± 4.34	64.59
C42	Quercetin-(malonyl)-hexoside	11.84 ± 0.67	13.98 ± 0.74	16.12 ± 5.57	12.69 ± 0.3	13.66	236.81 ± 118.06	164.98 ± 21.53	209.57 ± 62.43	154.23 ± 31.16	191.40	14.6 ± 1.93	14.55 ± 1.55	15.33 ± 1.16	14.82
C43	Quercetin-(digalloyl)-hexoside	333.01 ± 17.6	44.45 ± 3.23	173.77 ± 6.67	294.46 ± 16.73	211.42	169.8 ± 69.94	163.69 ± 18.99	123.99 ± 13.92	159.73 ± 19.34	154.30	37.56 ± 8.44	36.41 ± 3.37	48.02 ± 3.22	40.66
C44	Quercetin-pentoside II	96.6 ± 7.5	38.33 ± 5.44	98.12 ± 7.41	83.29 ± 12.57	79.09	25.27 ± 5.81	26.4 ± 4.22	24.63 ± 3.9	25.26 ± 4.11	25.39	13.58 ± 0.78	15.48 ± 0.65	13.31 ± 0.48	14.12
C45*	Quercetin	154.67 ± 9.36	66.93 ± 4.23	153.63 ± 5.29	156.86 ± 11.89	133.02	47.58 ± 17.3	76.52 ± 9.72	95.16 ± 18.56	63.91 ± 9.63	70.79	20.73 ± 1.17	38.21 ± 1.91	21.2 ± 0.31	26.71
C46	Luteolin-(galloylhenxoside)-hexoside	484.53 ± 13.28	343.17 ± 30.57	665.13 ± 30.83	448.46 ± 41.59	485.32	64.2 ± 17.48	80.06 ± 13.72	68.22 ± 18.77	69.81 ± 10.03	70.57	305.2 ± 112.71	238.34 ± 34.3	541.59 ± 79.99	361.71
C47*	Luteoloside	86.72 ± 9.77	204.38 ± 46.92	55.57 ± 43.67	85.27 ± 15.5	107.98	173.26 ± 42.84	187.51 ± 42.05	151.65 ± 36.22	153.99 ± 29.23	166.60	47.39 ± 14.48	N.D.	50.8 ± 5.78	32.73
C48	Luteolin-deoxyhexoside I	454.69 ± 37.46	566.42 ± 49.41	258.46 ± 21.26	384.18 ± 50.82	415.94	53.81 ± 33.48	106.04 ± 26.34	49.27 ± 10.11	82.55 ± 23.02	72.92	64.97 ± 22.16	38.24 ± 5.92	108.69 ± 14.58	70.63
C49	Luteolin-deoxyhexoside II	173.28 ± 7.8	110.47 ± 27.26	425.55 ± 35.67	207.09 ± 26.63	229.10	64.19 ± 24.5	125.33 ± 23.21	93.02 ± 16.17	114.03 ± 21.19	99.14	64.88 ± 14.86	74.45 ± 3.55	99.94 ± 11.1	79.76
C50	Laricitrin-trihenxoside	N.D.	N.D.	130.62 ± 5.84	N.D.	32.65	N.D.	12.23 ± 5.56	129.61 ± 21.8	12.8 ± 4.85	38.66	254.62 ± 28.39	617.1 ± 25.87	242.47 ± 14.75	371.40
C51	Chrysoeriol-hexoside	1540.02 ± 156.79	67.46 ± 20.85	1747.28 ± 279.68	1507.3 ± 166.58	1215.51	1376.78 ± 445.56	1412.56 ± 427.65	477.03 ± 215.93	1030.09 ± 265.95	1074.11	271.72 ± 53.85	226.46 ± 35.78	251.95 ± 50.38	250.04
C52	Chrysoerio-hexoside	647.89 ± 33.68	375.73 ± 15.8	871.4 ± 108.62	362.98 ± 34.61	564.50	278.28 ± 67.45	N.D.	306.7 ± 33.06	167.36 ± 184.2	188.08	110.9 ± 6	220.23 ± 17.12	123.34 ± 6.82	151.49
C53	Syringetin-(malonyl)-hexoside	N.D.	N.D.	26.52 ± 4.89	N.D.	6.63	247.96 ± 117.64	320.23 ± 58.21	239.8 ± 55.15	273.73 ± 51.81	270.43	1480.79 ± 240.42	698.29 ± 54.15	893.85 ± 226.54	1024.31
C54	Hydroxy-dimethoxy-flavanone-O-hexoside	6.14 ± 1.28	58.2 ± 3.88	15.33 ± 2.43	14.6 ± 3.19	23.57	25.69 ± 15.18	27.96 ± 12.78	20.85 ± 10.52	22.1 ± 11	24.15	25.14 ± 10.48	19.23 ± 3.26	61.38 ± 9.89	35.25

(Continued)

10.3389/fpls.2024.1501966

TABLE 1 Continued

No.	compounds	petal-AH	petal-SC	petal-SD	petal-SX	petal	calyx-AH	calyx-SC	calyx-SD	calyx-SX	calyx	stamen-AH	stamen-SD	stamen-SX	stamen
C55	Naringenin	141.81 ± 6.21	64.53 ± 11.24	154.9 ± 8.82	101.82 ± 13.06	115.77	39.72 ± 3.3	96.87 ± 3.93	49.42 ± 12.06	84.11 ± 3.39	67.53	72.89 ± 18.62	60.81 ± 5.84	116.34 ± 15.36	83.35
C56*	Taxifolin	11.35 ± 2.42	24.57 ± 3.52	21.6 ± 2.59	16.73 ± 2.46	18.56	35 ± 5.74	44.67 ± 6.35	44.81 ± 5.75	37.14 ± 5.26	40.40	13.36 ± 4.76	13.43 ± 4.74	7.46 ± 2.84	11.42
C57	Apigenin hexoside	33.33 ± 1.7	34.02 ± 4.22	27.39 ± 3.06	31.92 ± 3.33	31.67	17.63 ± 3.4	21.87 ± 2.83	12.61 ± 2.08	17.35 ± 1.82	17.36	83.05 ± 6.97	43.35 ± 10.26	75.88 ± 5.06	67.43
C58*	Apigenin	7.86 ± 1.55	4.69 ± 0.93	11.07 ± 2.16	6.83 ± 1.23	7.61	4.57 ± 2.46	8.12 ± 2.43	8.51 ± 2.01	6.75 ± 2	6.99	7.67 ± 1.25	5.34 ± 1.51	8.37 ± 0.68	7.13
C59	Aucubin	N.D.	70.12 ± 6.09	12.34 ± 1.47	N.D.	20.62	N.D.	26.3 ± 3.54	13.34 ± 1.97	20.36 ± 3.44	15.00	35.07 ± 8.49	66.26 ± 4.56	22.36 ± 5.92	41.23
C60	Mudanpioside E	N.D.	34.51 ± 5.54	23.42 ± 5.55	N.D.	14.48	14.51 ± 10.74	9.62 ± 8.01	23.56 ± 11.96	8.14 ± 6.61	13.96	50.92 ± 3.61	277.21 ± 20.59	50.13 ± 3.84	126.09
C61	Isomaltopaeoniflorin	74.81 ± 5.13	8.13 ± 0.62	43.48 ± 2.9	69.22 ± 3.82	48.91	29.59 ± 15.7	29.77 ± 5.75	33.33 ± 7.75	27.4 ± 5.89	30.02	20.98 ± 1.42	32.66 ± 0.97	21.36 ± 1.68	25.00
C62	Oxypaeoniflora III	275.9 ± 17.7	37.52 ± 2.47	112.89 ± 27.89	251.77 ± 23.69	169.52	20.48 ± 4.17	17.76 ± 1.6	13.12 ± 3.73	18.14 ± 2.89	17.37	504.18 ± 89.61	199.38 ± 79.91	407.55 ± 15.51	370.37
C63	Oxypaeoniflora IV	362.77 ± 26.5	73.95 ± 10.92	120.3 ± 6.61	315.43 ± 19.41	218.11	65.38 ± 8.87	45.25 ± 6.34	51.54 ± 16.32	44.81 ± 6.82	51.75	664.3 ± 79.49	371.63 ± 46.59	565.9 ± 21.7	533.94
C64*	Galloylpaeoniflorin I	28.58 ± 1.91	35.06 ± 2.41	64.81 ± 5.67	37.05 ± 1.75	41.38	45.61 ± 12.58	101.89 ± 19.66	133.32 ± 31.02	113.69 ± 19.06	98.63	40.67 ± 3.4	438.37 ± 43.43	53.39 ± 4.67	177.48
C65	Mudanpioside H	11.27 ± 6.43	N.D.	6.66 ± 0.66	7.18 ± 1.15	6.28	N.D.	N.D.	7.2 ± 2.25	2.94 ± 1.23	2.54	N.D.	11.76 ± 1.22	N.D.	3.92
C66	Galloylpaeoniflorin II	45.49 ± 1.52	N.D.	25.69 ± 1.61	39.93 ± 3.05	27.78	18.63 ± 4.93	20.9 ± 2.01	9.98 ± 2.08	25.27 ± 2.41	18.70	10.82 ± 2.04	25.69 ± 5.28	15.8 ± 2.5	17.44
C67	Benzoyloxypaeoniflflorin	8.38 ± 1.76	33.1 ± 12.08	34.67 ± 2.26	5.84 ± 1.38	20.50	N.D.	N.D.	N.D.	0.06 ± 0.16	0.02	49.26 ± 14.09	62.52 ± 7.91	31.08 ± 3.91	47.62
C68	Mudanpioside J	46.08 ± 2.39	185.35 ± 4.9	34.69 ± 6.09	49.86 ± 4.97	78.99	93.98 ± 31.07	93.99 ± 27.95	78.42 ± 29.61	81.66 ± 24.48	87.01	189.15 ± 28.94	68.04 ± 15.36	189.94 ± 37.83	149.04
C69	Mudanpioside B	46.08 ± 2.39	185.35 ± 4.9	34.69 ± 6.09	46.07 ± 3.78	78.05	70.81 ± 20.58	78.5 ± 12.52	43.75 ± 39.32	67.4 ± 8.61	65.11	189.15 ± 28.94	21.09 ± 30.29	154.93 ± 9.67	121.73

*Targets were quantified by using reference compounds.

10.3389/fpls.2024.1501966

quantitative analysis of individual components showed that the total content of 12 major anthocyanins individuals was in line with the total anthocyanins content (TAC). Among all petals of the four cultivars, the SC samples contained fewer anthocyanins than the other cultivars. For individual anthocyanins, the contents were lower in SC petals than other cultivars. For instance, the content of Cy-di-glu, one of the main anthocyanins in petals, were nearly 100 times lower in SC petals than others. However, the content of Pt-glu was relative higher in SC petals (2.53 ± 0.28 μg/mL) than AH (0.36 ± 0.02 μg/mL) and SX (0.51 ± 0.05 μg/mL). Wang et al's research (Yue et al., 2023) suggested that Pg-glu was responsible for red color in CPF petal. From our data, however, the contents of Pg-glu (0~0.084 μg/mL) were too low to be detected in most of samples. The major anthocyanins among four cultivar petal samples are Cy-di-glu, Cy, Pn-glu and Cy- malonyl glu, of which the contents are significant lower in SC petals than others. It's suggested that Cy and its glucosides mainly contributed to the color discrepancy. In addition, our quantification data suggested that some of the major flavonoid glycoside may contribute to the lighter color of SC petals as well, as those flavonoid compounds were significant lower that other three cultivar petals (Supplementary Table S2).

We also quantified the relative contents of ten monoterpenoids. It was found that the content of mudanpioside in the petals of the SC cultivar was much higher than that of other cultivars, while other terpenoids contents were the opposite. In addition, the content of galloylpaeoniflorin in SD cultivars was overall higher than those cultivars, especially in the stamen part.

3.4 Antioxidant activities and total phenolic, flavonoid, and anthocyanin contents

Reactive oxygen species (ROS) are widely present in cells. Excess ROS usually causes oxidative stress, leading to various diseases such as inflammation, cancer, and aging. The antioxidant activity of different parts of CPF is measured by ABTS, DPPH, FRAP, and ORAC methods, respectively. Among them, ABTS, DPPH, and FRAP are used to obtain antioxidant capacity through the single electron transfer (SET) reaction mechanism, while the ORAC method is used to obtain antioxidant capacity through the hydrogen atom transfer (HAT) reaction mechanism. HAT is the key step in the free radical chain reaction. Therefore, those reacting with hydrogen atom transfer are more effective in terms of free radical-breaking antioxidant capacity (Huang et al., 2005; Brewer, 2011). In general, all the samples showed good antioxidant activities. Although the data obtained differed, the three SET antioxidant assays (ABTS, DPPH, and FRAP) showed a parallel trend (Figures 5A–D). For SET mechanism antioxidant assays, petals samples showed relative stronger activity than other

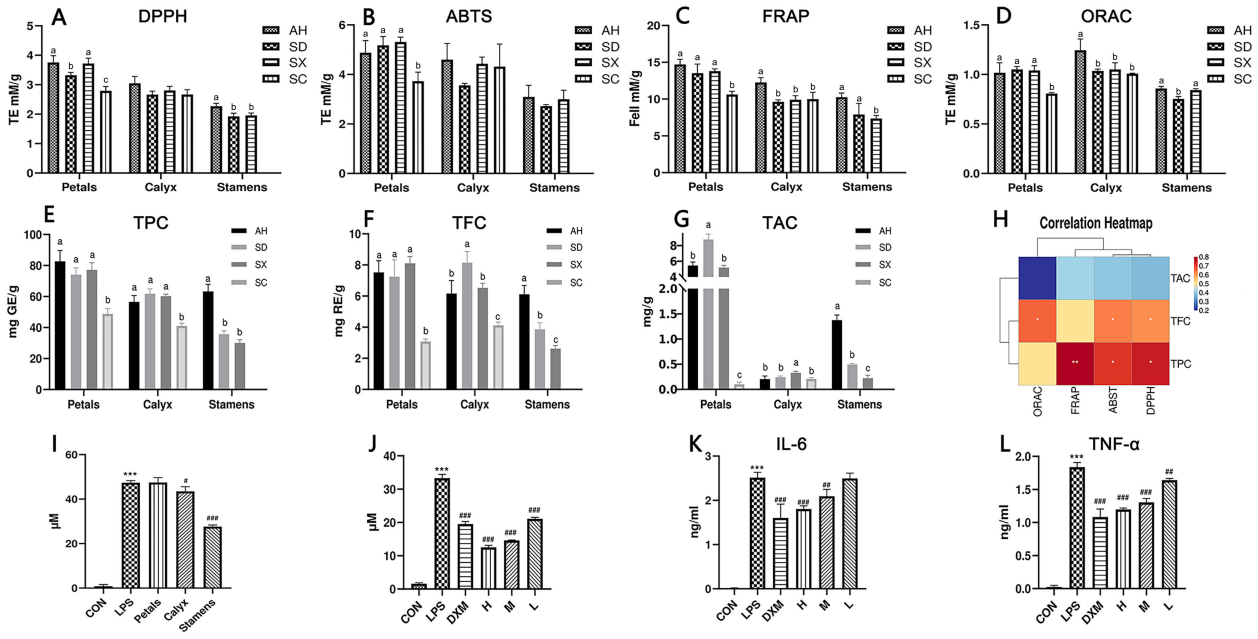

FIGURE 5
(A–D) Antioxidant capacity results, data are presented as mean ± SD (n = 3). Different superscript letters in each row indicate significant differences. Using one-way ANOVA or Tamhane T^2, $^{abc}p<0.05$. **(E–G)** Total polyphenol, total flavonoid, and total anthocyanin contents of different species and parts (n = 3), Using one-way ANOVA, $^{abc}p<0.05$. **(H)** Correlation heat map between total polyphenols, total flavonoids, total anthocyanins content, and antioxidant capacity. correlation coefficients present as the color. **(I)** Effects of the petals, calyx, and stamens of CPF on inflammatory extracellular NO release (n = 3). Effects of CPF stamen extracts at 93.75, 46.88, and 23.44 μg/mL concentrations on the release of extracellular NO **(J)**, secretion of IL-6 **(K)** and TNF-α **(L)** (n = 3). $^{\#}$, $^{\#\#}$, and $^{\#\#\#}$ denote $p< 0.05$, 0.01, and 0.001, respectively compared with the LPS group. $^{***}p<$ 0.001 compared with control group.

two parts. Among petal samples, SC cultivars showed the weakest antioxidant activities, regardless of the method applied, while other three cultivars were at same levels. It indicated a significant correlation between the petal colors and the antioxidant activities.

As shown in Figures 5E–G, the TPC content ranged from 30.01 to 82.74 mg (RE)/g. The TFC contents in CPF petals, calyx, and stamens ranged from 3.08 - 8.10 mg (RE)/g, 4.11 - 8.14 mg (RE)/g, and 0.22 - 1.37 mg (RE)/g, respectively. TAC ranges from 0.10 mg/g DW to 8.78 mg/g DW. The TAC content results indicated that most anthocyanins exist in petals other than in calyx and stamens. Overall, the TPC, TAC, and TFC of SC samples were significantly lower than other cultivars, which strongly correlated with their shade of color. The different distribution patterns of TPC, TFC, and TAC in CPF may be due to interspecific biodiversity.

The correlation between TPC, TAC, and TFC and antioxidant capacity in CPF was also analyzed (Figure 5H). It showed that the contents of anthocyanins, phenolics and flavonoids had a positive correlation with three all the antioxidant capacity tests (FRAP, ABST, ORAC), however there is no significant relation between the contents and the DPPH test. In general, our correlation analysis suggests that the TAC, TPC and TFC had positive but not negative correlation with the antioxidant activity.

3.5 Anti-inflammatory activity

The anti-inflammatory activity of the petals, calyx, and stamens of Anhui CPF was assessed using the LPS-induced RAW264.7 inflammation model. As shown in Figure 5I, only the stamens samples significantly reduced NO release from macrophages in a dose-dependent manner (Figure 5J). Further ELISA tests showed that it had a significant dose-dependent inhibitive effect on LPS-induced release of inflammatory factors IL-6 and TNF-α (Figures 5K, L). To our knowledge, this the first report of the anti-inflammation activity of CPF.

4 Discussion

Anthocyanins are major components in CPF petals. The correlation analysis among chemical quantification, petal color and antioxidant assays suggested a notion that the deeper the color is, the better antioxidant activity. For instance, the anthocyanins contents in SC cultivars (light pink and white) were much lower than other deep-color cultivars (deep purple or reddish purple), Correspondingly, their antioxidant activities (Figure 5) were also the lowest in all the four petals. For individual anthocyanins, cyanidin (cy)-type (C1, C4, C5, C7 and C12) and peonidin (pn)-type anthocyanins (C10) had positive relation with antioxidant activities, while pelargonidin (C6), petunidin (C8) and malvidin (C11) types has negative impact on antioxidant activities.

The stamens samples consist of lower phenolics, flavonoids and anthocyanins contents. However, our quantification data showed that their contents of monoterpenoid such as oxypaeoniflora, galloylpaeoniflorin, mudanpioside J and mudanpioside B were significantly higher than other parts. This clearly indicates that its superior anti-inflammatory effects are more attributed to these monoterpenoid components other than polyphenolic compounds.

In this paper, we explored the potential applications of Chinese peony flowers, particularly focusing on their chemical and biological properties. According to our experiment design, environment factors were managed to avoid by using vigorous sample collection protocol, by which sample were harvested at same experimental field and same time. It dramatically increased the sampling homogeneity, reduced in-sample chemical variations, and hence facilitated our understanding about the inherent chemical variation among those commonly grown cultivars in China. It, however, may not accurately represent the variability of peony species and their uses in different climates and cultures.

In summary, our comprehensive chemical and biological investigation indicated that CPF is rich in bioactive phytochemicals, and possess potential health benefits, including anti-inflammatory, and antioxidant effects. Previous *in vivo* studies also indicated *Paeonia* petals could alleviate oxidative stress and restore gut microbiota (Liu et al., 2021), and exert skin-beneficial effects (Cutovic et al., 2022) by antioxidant, antimicrobial and antibiofilm activities. Combining those findings, it supports the potential use of CPF as a functional bioactive ingredient. Moreover, the revalorization of CPF could be diversified with different application purpose.

Data availability statement

The original contributions presented in the study are included in the article/Supplementary Material. Further inquiries can be directed to the corresponding author.

Ethics statement

Ethical approval was not required for the studies on animals in accordance with the local legislation and institutional requirements because only commercially available established cell lines were used.

Author contributions

MP: Visualization, Writing – original draft. MG: Data curation, Writing – original draft. JZ: Data curation, Project administration, Writing – review & editing. AG: Conceptualization, Investigation, Writing – review & editing. QL: Software, Validation, Writing – original draft. PH: Software, Writing – original draft, Visualization. XQ: Conceptualization, Supervision, Writing – review & editing. ZH: Supervision, Writing – review & editing, Resources. WX: Writing – review & editing, Funding acquisition.

Funding

The author(s) declare financial support was received for the research, authorship, and/or publication of this article. This research was funded by Special funds for International Cooperation from Guangdong Provincial Hospital of Chinese Medicine, grant number YN2024RD01.

Acknowledgments

The authors wish to express their gratitude to Ms. Ling Yao and Ms. Li-E Cheng (ShenZhen Tsumura Co., Ltd) for assistance in sample collection.

Conflict of interest

The authors declare that the research was conducted in the absence of any commercial or financial relationships that could be construed as a potential conflict of interest.

Generative AI statement

The author(s) declare that no Generative AI was used in the creation of this manuscript.

Publisher's note

All claims expressed in this article are solely those of the authors and do not necessarily represent those of their affiliated organizations, or those of the publisher, the editors and the reviewers. Any product that may be evaluated in this article, or claim that may be made by its manufacturer, is not guaranteed or endorsed by the publisher.

Supplementary material

The Supplementary Material for this article can be found online at: https://www.frontiersin.org/articles/10.3389/fpls.2024.1501966/full#supplementary-material

References

An, H. M., Ou, X. C., Zhang, Y. B., Li, S., Xiong, Y. F., Li, Q., et al. (2022). Study on the key volatile compounds and aroma quality of jasmine tea with different scenting technology (vol 385, 132718, 2022). *Food Chem.* 385, 132718. doi: 10.1016/j.foodchem.2022.133172

Bai, Z. Z., Tang, J. M., Ni, J., Zheng, T. T., Zhou, Y., Sun, D. Y., et al. (2021). Comprehensive metabolite profile of multi-bioactive extract from tree peony (Paeonia ostii and Paeonia rockii) fruits based on MS/MS molecular networking. *Food Res. Int.* 148, 110609. doi: 10.1016/j.foodres.2021.110609

Brewer, M. S. (2011). Natural antioxidants: sources, compounds, mechanisms of action, and potential applications. *Compr. Rev. Food Sci. Food Saf.* 10, 221–247. doi: 10.1111/j.1541-4337.2011.00156.x

Chen, J., Liu, F., Wu, R. A., Chen, J., Wang, W., Ye, X., et al. (2022). An up-to-date review: differential biosynthesis mechanisms and enrichment methods for health-promoting anthocyanins of citrus fruits during processing and storage. *Crit. Rev. Food Sci. Nutr.* 64, 3989–4015. doi: 10.1080/10408398.2022.2137778

Cutovic, N., Markovic, T., Kostic, M., Gasic, U., Prijic, Z., Ren, X., et al. (2022). Chemical profile and skin-beneficial activities of the petal extracts of Paeonia tenuifolia L. from Serbia. *Pharm. (Basel)* 15, 1537. doi: 10.3390/ph15121537

Duan, X.-J., Zhang, W.-W., Li, X.-M., and Wang, B.-G. (2006). Evaluation of antioxidant property of extract and fractions obtained from a red alga, Polysiphonia urceolata. *Food Chem.* 95, 37–43. doi: 10.1016/j.foodchem.2004.12.015

Han, X., Hu, S., Yang, Q., Sang, X., Tang, D., and Cao, G. (2022). Paeoniflorin ameliorates airway inflammation and immune response in ovalbumin induced asthmatic mice: From oxidative stress to autophagy. *Phytomedicine* 96, 153835. doi: 10.1016/j.phymed.2021.153835

Huang, D., Ou, B., and Prior, R. L. (2005). The chemistry behind antioxidant capacity assays. *J. Agric. Food Chem.* 53, 1841–1856. doi: 10.1021/jf030723c

Kang, L., Miao, J. X., Cao, L. H., Miao, Y. Y., Miao, M. S., Liu, H. J., et al. (2020). Total glucosides of herbaceous peony (Paeonia lactiflora Pall.) flower attenuate adenine- and ethambutol-induced hyperuricaemia in rats. *J. Ethnopharmacol.* 261, 113054. doi: 10.1016/j.jep.2020.113054

Kwak, C. S., Lee, M. S., and Park, S. C. (2007). Higher antioxidant properties of Chungkookjang, a fermented soybean paste, may be due to increased aglycone and malonylglyco side isoflavone during fermentation. *Nutr. Res.* 27, 719–727. doi: 10.1016/j.nutres.2007.09.004

Li, P., Shen, J., Wang, Z., Liu, S., Liu, Q., Li, Y., et al. (2021). Genus Paeonia: A comprehensive review on traditional uses, phytochemistry, pharmacological activities, clinical application, and toxicology. *J. Ethnopharmacol.* 269, 113708. doi: 10.1016/j.jep.2020.113708

Li, Z., Ma, Y., Li, F., Wei, Y., Zhang, L., Yu, L., et al. (2023). Quality evaluation of peony petals based on the chromatographic fingerprints and simultaneous determination of sixteen bioactive constituents using UPLC-DAD-MS/MS. *Molecules* 28, 7741. doi: 10.3390/molecules28237741

Liu, X., Chen, Y., Zhang, J., He, Y., Ya, H., Gao, K., et al. (2022). Widely targeted metabolomics reveals stamen petaloid tissue of Paeonia lactiflora Pall. being a potential pharmacological resource. *PloS One* 17, e0274013. doi: 10.1371/journal.pone.0274013

Liu, L., Yuan, Y., and Tao, J. (2021). Flavonoid-Rich Extract of Paeonia lactiflora Petals Alleviate d-Galactose-Induced Oxidative Stress and Restore Gut Microbiota in ICR Mice. *Antioxidants* 10, 1889. doi: 10.3390/antiox10121889

Liu, L., Yuan, Y., Zuo, J., and Tao, J. (2023). Composition and antioxidant activity of Paeonia lactiflora petal flavonoid extract and underlying mechanisms of the protective effect on H2O2-induced oxidative damage in BRL3A cells. *Hortic. Plant J.* 9, 335–344. doi: 10.1016/j.hpj.2022.06.001

Moldovan, B., Hosu, A., David, L., and Cimpoiu, C. (2016). Total phenolics, total anthocyanins, antioxidant and pro-oxidant activity of some red fruits teas. *Acta Chim. Slov.* 63, 213–219. doi: 10.17344/acsi.2015.1421

Nie, R., Zhang, Y., Jin, Q., Zhang, S., Wu, G., Chen, L., et al. (2021). Identification and characterisation of bioactive compounds from the seed kernels and hulls of Paeonia lactiflora Pall by UPLC-QTOF-MS. *Food Res. Int.* 139, 109916. doi: 10.1016/j.foodres.2020.109916

Ogawa, K., Nakamura, S., Sugimoto, S., Tsukioka, J., Hinomaru, F., Nakashima, S., et al. (2015). Constituents of flowers of Paeoniaceae plants, Paeonia suffruticosa and Paeonia lactiflora. *Phytochem. Lett.* 12, 98–104. doi: 10.1016/j.phytol.2015.03.002

Qiu, J., Chen, X., Liang, P., Zhang, L., Xu, Y., Gong, M., et al. (2022). Integrating approach to discover novel bergenin derivatives and phenolics with antioxidant and anti-inflammatory activities from bio-active fraction of Syzygium brachythyrsum. *Arabian J. Chem.* 15, 103507. doi: 10.1016/j.arabjc.2021.103507

Qiu, X., Zhang, J., Huang, Z., Zhu, D., and Xu, W. (2013). Profiling of phenolic constituents in Polygonum multiflorum Thunb. by combination of ultra-high-pressure liquid chromatography with linear ion trap-Orbitrap mass spectrometry. *J. Chromatogr A* 1292, 121–131. doi: 10.1016/j.chroma.2012.11.051

Sang, X., Wan, X., Zhang, H., Ying, J., Wang, L., Yang, Q., et al. (2023). The most bioactive fraction of stir-fried Radix Paeoniae Alba regulating IL-6/STAT3 signaling pathway in allergic asthma mouse. *J. Ethnopharmacol.* 301, 115821. doi: 10.1016/j.jep.2022.115821

Shu, X. K., Duan, W. J., Liu, F., Shi, X. G., Geng, Y. L., Wang, X., et al. (2014). Preparative separation of polyphenols from the flowers of Paeonia lactiflora Pall. by high-speed counter-current chromatography. *J. Chromatogr. B Anal. Technol. Biomed. Life Sci.* 947, 62–67. doi: 10.1016/j.jchromb.2013.12.004

Wu, F., Wu, G., Li, T., Lu, W., Fu, T., and Zhang, Z. (2023). Exploring the target and mechanism of radix Paeoniae alba on Sjogren's syndrome. *Comb. Chem. High Throughput Screen* 26, 1224–1232. doi: 10.2174/1386207325666220823144054

Xu, Y., Liang, P. L., Chen, X. L., Gong, M. J., Zhang, L., Qiu, X. H., et al. (2021). The impact of citrus-tea cofermentation process on chemical composition and contents of Pu-Erh tea: an integrated metabolomics study. *Front. Nutr.* 8. doi: 10.3389/fnut.2021.737539

Xu, J. J., Xu, F., Wang, W., Wang, P. P., Xian, J., Han, X., et al. (2022). Paeoniae Radix Rubra can enhance fatty acid beta-oxidation and alleviate gut microbiota disorder in alpha-naphthyl isothiocyanate induced cholestatic model rats. *Front. Pharmacol.* 13. doi: 10.3389/fphar.2022.1002922

Yang, S., Du, Q. Q., Yue, Q. X., Sun, Y. F., Jin, C. S., Zhang, W., et al. (2023). Analysis and evaluation on Paeoniae Radix Alba from different cultivars by UPLC-Q-TOF-MS and HPLC. *Zhongguo Zhong Yao Za Zhi* 48, 715–724. doi: 10.19540/j.cnki.cjcmm.20220618.201

Yuan, Q. L. (2011). *The culture of Chinese herbaceouspeony* (Beijing: Beijing Forestry University).

Yue, F., Zhang, F., Qu, Q., Wang, C., Qin, Y., Ma, L., et al. (2023). Effects of ageing time on the properties of polysaccharide in tangerine peel and its bacterial community. *Food Chem.* 417, 135812. doi: 10.1016/j.foodchem.2023.135812

Yun-Jie, L. I., Hua-Jun, F. U., Bo, Y. U., Chen, W., and Wang, Y. K. (2019). Nutritional function analysis of Chinese scented tea and research progress on its main processing technology. *Storage Process*. 19, 207-210.

Zhang, J., Wu, X., Qiu, J., Zhang, L., Zhang, Y., Qiu, X., et al. (2020a). Comprehensive comparison on the chemical profile of Guang Chen Pi at different ripeness stages using untargeted and pseudotargeted metabolomics. *J. Agric. Food Chem.* 68, 8483–8495. doi: 10.1021/acs.jafc.0c02904

Zhang, J., Xu, Y., Ho, C. T., Qiu, J. Q., Qiu, X. H., Huang, Z. H., et al. (2022). Phytochemical profile of Tibetan native fruit "Medog lemon" and its comparison with other cultivated species in China. *Food Chem.* 372, 131255. doi: 10.1016/j.foodchem.2021.131255

Zhang, Y., Zhang, Y., Duan, X., Liu, X., Yuan, S., Han, J., et al. (2020b). Anthocyanins in tree peony (Paeonia suffruticosa) and their relationship with flower color. *Hortic. Sci. Technol.* 38, 776–784. doi: 10.7235/hort.20200070

Zhao, Q., Gu, L., Li, Y. Q., Zhi, H., Luo, J. R., and Zhang, Y. L. (2023). Volatile composition and classification of Paeonia lactiflora flower aroma types and identification of the fragrance-related genes. *Int. J. Mol. Sci.* 24, 9410. doi: 10.3390/ijms24119410

frontiers | Frontiers in Plant Science

TYPE Review
PUBLISHED 21 February 2025
DOI 10.3389/fpls.2025.1530814

OPEN ACCESS

EDITED BY
Eman A. Mahmoud,
Damietta University, Egypt

REVIEWED BY
Devesh U. Kapoor,
Gujarat Technological University, India
Da Sun,
Wenzhou University, China

*CORRESPONDENCE
Jingshan Shi
shijs@zmu.edu.cn

†These authors share first authorship

RECEIVED 19 November 2024
ACCEPTED 27 January 2025
PUBLISHED 21 February 2025

CITATION
Jain A, Sarsaiya S, Gong Q, Wu Q and Shi J (2025) *Amorphophallus konjac*: traditional uses, bioactive potential, and emerging health applications. *Front. Plant Sci.* 16:1530814. doi: 10.3389/fpls.2025.1530814

Amorphophallus konjac: traditional uses, bioactive potential, and emerging health applications

Archana Jain[1†], Surendra Sarsaiya[1,2†], Qihai Gong[1], Qin Wu[1] and Jingshan Shi[1,2*]

[1]Key Laboratory of Basic Pharmacology and Joint International Research Laboratory of Ethnomedicine of Ministry of Education, Zunyi Medical University, Zunyi, China, [2]Bioresource Institute for Healthy Utilization, Zunyi Medical University, Zunyi, China

Amorphophallus konjac is a perennial plant native to Southeast Asia, renowned for its edible corms and rich nutritional value. The bioactive component, konjac glucomannan (KGM), has garnered significant attention due to its broad applications. This review aims to provide a comprehensive overview of the traditional uses, chemical and physical properties, and modern health applications of KGM. It highlights cutting-edge research, discusses challenges and limitations, and identifies future directions for advancing the utility of KGM in health and nutrition. KGM demonstrates remarkable health benefits, including improving metabolic health through weight management, blood glucose stabilization, and lipid profile enhancement. It also plays a vital role in gut health. Emerging evidence highlights its anti-inflammatory and immune-regulatory effects, with applications in managing inflammatory bowel disease, hyperthyroidism, and colorectal cancer (CRC). Recent advancements in multi-omics analyses and high-throughput screening (HTS) approaches have improved KGM extraction, characterization, and evaluation. However, potential side effects such as gastrointestinal discomfort and allergenicity, along with challenges in maintaining purity and molecular consistency, require careful consideration. KGM is a versatile dietary fiber with extensive applications in functional foods, nutraceuticals, and therapeutic interventions. Future research should focus on enhancing KGM's bioavailability, developing targeted delivery systems, and formulating novel applications.

KEYWORDS

***Amorphophallus konjac*, konjac glucomannan, dietary fiber, health benefits, antiinflammatory, multi-omics**

1 Introduction

Amorphophallus konjac, commonly known for its edible corm and the production of KGM, has a rich cultural and medical history, particularly in East Asia (Pedrosa L de and Fabi, 2024). Traditionally, KGM has been utilized in Chinese medicine for over 2000 years, serving various health purposes such as detoxification, tumor suppression, and treatment of respiratory and skin disorders (Islam et al., 2023). This historical context underscores the significance of konjac in both dietary and medicinal practices, highlighting its role as a staple food source in countries like China and Japan (Ye et al., 2021). The chemical and physical properties of KGM contribute to its health benefits. KGM is a soluble dietary fiber that exhibits unique gel-forming capabilities, which are essential for its applications in food and health products (Sun et al., 2023). Modern research has revealed that KGM can significantly lower plasma cholesterol levels, improve carbohydrate metabolism, and enhance bowel movement, thereby promoting gut health (Du et al., 2021). As a prebiotic, KGM supports the regulation of gut microbiota, which is crucial for maintaining digestive health and overall metabolic function (Xia et al., 2024).

In terms of metabolic health, KGM has shown promise in weight management and blood sugar regulation, making it a valuable component in diabetes management strategies (Fang et al., 2023a). Additionally, its anti-inflammatory properties have been studied for their potential to manage chronic diseases and improve immune function, further expanding its therapeutic applications (Liu et al., 2025). Emerging research is increasingly focused on the diverse biological activities of KGM, exploring its potential in treating lifestyle-related diseases such as obesity and diabetes (Dai et al., 2019). Advanced methodologies, including multi-omics analysis and HTS, are being employed to enhance the extraction, purification, and functional evaluation of KGM, paving the way for innovative health applications (Liu et al., 2023). Emerging research has begun to uncover the broader potential of konjac in addressing metabolic disorders, particularly in combating rising global rates of obesity and type 2 diabetes (Au-Yeung et al., 2018). Its ability to low-density lipoprotein cholesterol (LDL-C) levels and improve blood lipid profiles has positioned it as a promising natural intervention for cardiovascular health. Moreover, the prebiotic properties of glucomannan foster a healthy gut microbiome, offering therapeutic possibilities for managing conditions such as irritable bowel syndrome (IBS) and other digestive disorders (Lasrado and Rai, 2022). This growing body of evidence underscores the need for further research on the mechanisms of action of konjac and its full spectrum of health benefits (Wilianto et al., 2024). As the world increasingly turns to plant-based and natural solutions for health management, *A. konjac* stands out as a traditional remedy with vast modern relevance, offering both preventative and therapeutic potential in the context of contemporary health challenges (Pan et al., 2024). Despite the promising benefits of KGM, challenges remain in standardizing its commercial production and ensuring quality control across different markets. Future research should address these limitations while exploring the full spectrum of KGM's health benefits and applications. This review was aimed to provide a comprehensive overview of the traditional uses, modern health applications, and cutting-edge research surrounding KGM, ultimately contributing to a deeper understanding of its potential in health and nutrition. This review article stands out by offering a holistic view of *A. konjac*, from its traditional uses to its modern health applications, supported by scientific research and innovative approaches like multi-omics analysis and HTS.

2 Traditional uses and historical background: an overview of the cultural and medical background of KGM

A. konjac, commonly known as konjac, is a perennial plant native to Southeast Asia, particularly valued for its edible corms and traditional applications in food and medicine. This plant has been cultivated for thousands of years, not only as a food source but also for its medicinal properties in traditional Chinese medicine (TCM) (Derosa et al., 2024). The cultivation practices of *A. konjac* involve planting corms, where factors such as corm size and plant density play a crucial role in determining the yield (Xu et al., 2024). Globally, *A. konjac* is produced in significant quantities, with major cultivation occurring in China and Japan, and its production is expanding into other Southeast Asian countries (Luo et al., 2024). The plant prefers warm subtropical to tropical climates, requiring well-drained, nutrient-rich soils that retain moisture without becoming waterlogged (Srzednicki and Borompichaichartkul, 2020). Additionally, moderate shading (50%-70%) is beneficial as it enhances photosynthesis and increases corm weight, making it an essential factor in cultivation (Qin et al., 2019; Nurshanti et al., 2023). The economic importance of *A. konjac* cannot be overstated, as it is in high demand within the food and health industries, primarily due to its glucomannan content, which is valued for its health benefits (Chua et al., 2010). The extraction of KGM from the corms is a key aspect of its commercial processing. This process typically involves washing, slicing, and drying the corms to obtain the soluble fiber used in various applications, including food products and dietary supplements (Kapoor et al., 2024; Widjanarko et al., 2024). The nutritional composition of *A. konjac* corms is noteworthy, as they are rich in glucomannan, starch, and various inorganic elements, contributing to their value as a dietary component (Kulkarni et al., 2024). Despite its benefits, the cultivation of *A. konjac* faces several challenges, including environmental factors, disease management, and the need to optimize growth conditions to enhance yields (Niu et al., 2024; Rahman et al., 2024). These challenges can impact the overall production and availability of *A. konjac* in the global market.

Its historical significance is underscored by its first documentation in the *'Shen Nong Materia Medica'* during the Western Han Dynasty, which highlights its longstanding role in ancient Chinese medicine (Chua et al., 2010). Over the centuries, konjac has been integrated into

various cultural practices, especially in China and Japan, where it has been consumed for its health benefits (Qi et al., 2024). The primary component of konjac is KGM, a water-soluble dietary fiber extracted from its corm. KGM has been utilized in TCM for thousands of years, often for detoxification and tumor suppression (Lin and Rezaei, 2024). The health benefits associated with KGM are well-documented, including its roles in weight management, cholesterol reduction, and digestive health (Devaraj et al., 2019a). Research indicates that KGM can enhance satiety, reduce body weight, and improve metabolic parameters by increasing the transit time of food and prolonging gastric emptying (Shang et al., 2020; Guo et al., 2021). Culinary applications of konjac are also significant, as it is used to create various dishes such as noodles, tofu, and snacks, showcasing its versatility as a food ingredient (Chua et al., 2010; Zhang et al., 2020). The refined konjac flour, which contains a high percentage of KGM, has been introduced into Western markets as a food additive and dietary supplement, reflecting its growing global appeal (Zhu, 2018). Modern research has focused on the extraction, characterization, and health benefits of KGM, expanding its applications in nutrition and medicine (Devaraj et al., 2019a). Studies have demonstrated that KGM possesses pharmacological properties, including anti-obesity and cholesterol-lowering effects, making it a valuable component in health-related products (Table 1; Figure 1) (Behera and Ray, 2016).

3 Chemical and physical properties of *Amorphophallus konjac*

A. konjac is rich in various bioactive compounds, making it both nutritionally and pharmacologically valuable. The predominant compound in these corms is glucomannan, which accounts for approximately 49–60% of the corm weight (Alamgir, 2018). Additionally, corms contain 10–30% starch and 2.6–7% inorganic elements, including key minerals such as calcium,

TABLE 1 Overview of Konjac: cultivation, historical significance, and applications.

Aspect	Details	Citations
Plant Origin and Cultivation		
Native Region	Perennial plant native to Southeast Asia, valued for edible corms and medicinal use.	(Derosa et al., 2024)
Cultivation Areas	Primarily cultivated in China, Japan, and other Southeast Asian countries.	(Luo et al., 2024)
Optimal Growth Conditions	Warm subtropical to tropical climates, nutrient-rich soils, and moderate shading.	(Mekkerdchoo et al., 2016; Qin et al., 2019; Nurshanti et al., 2023)
Yield Factors	Corm size and plant density significantly affect yield.	(Xu et al., 2024)
Cultivation Challenges	Environmental factors, disease management, and optimizing growth conditions.	(Niu et al., 2024; Rahman et al., 2024)
Historical Significance		
Ancient Documentation	Mentioned in *Shen Nong Materia Medica* during the Western Han Dynasty.	(Chua et al., 2010)
Cultural Integration	Incorporated into traditional Chinese and Japanese practices for food and health benefits.	(Qi et al., 2024)
Nutritional and Economic Value		
Nutritional Composition	Rich in glucomannan, starch, and inorganic elements.	(Kulkarni et al., 2024)
Economic Demand	High demand in food and health industries due to glucomannan content.	(Chua et al., 2010)
Food Applications	Used in various food products, including noodles, tofu, and snacks.	(Chua et al., 2010; Zhang et al., 2020)
Market Expansion	Refined konjac flour introduced into Western markets as a food additive and dietary supplement.	(Zhu, 2018)
Konjac Glucomannan (KGM)		
Description	Water-soluble dietary fiber with applications in food, medicine, and health products.	(Devaraj et al., 2019b)
Traditional Uses	Utilized in TCM for detoxification and tumor suppression.	(Lin and Rezaei, 2024)
Health Benefits	Weight management, cholesterol reduction, and improved digestive health.	(Shang et al., 2020; Guo et al., 2021)
Pharmacological Properties	Includes anti-obesity and cholesterol-lowering effects.	(Behera and Ray, 2016)
Processing and Applications		
Extraction Process	Involves washing, slicing, and drying corms to obtain soluble fiber.	(Kapoor et al., 2024; Widjanarko et al., 2024)
Research Focus	Modern studies focus on extraction, characterization, and expanded applications.	(Devaraj et al., 2019b)

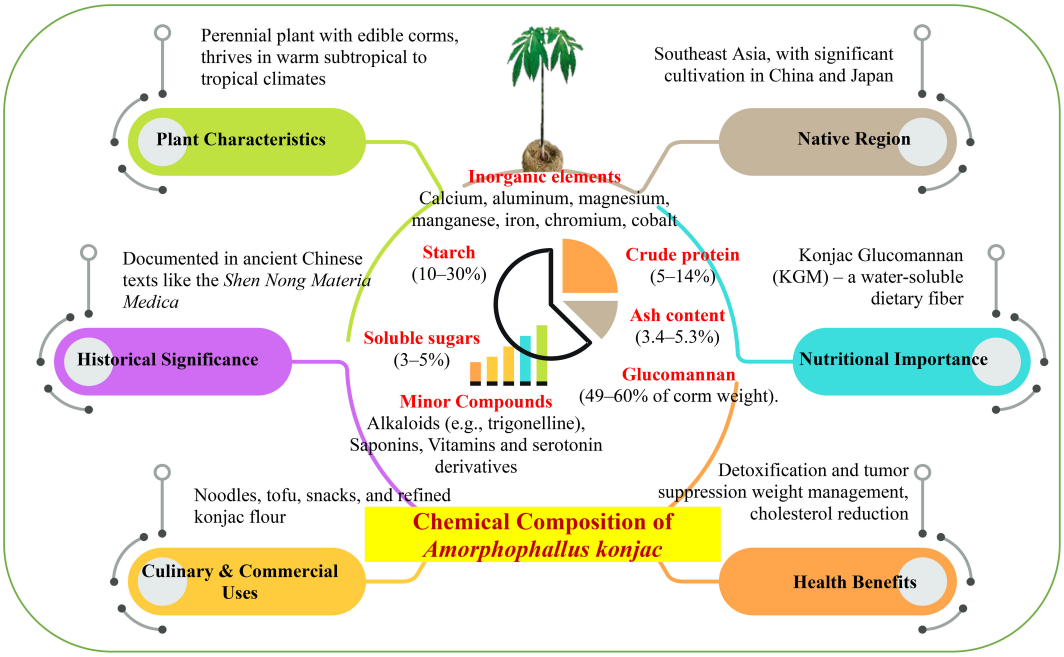

FIGURE 1
Amorphophallus konjac: a plant of culinary, medicinal, and commercial potential.

aluminum, magnesium, manganese, iron, chromium, and cobalt (Gómez et al., 2017). These corms also possess crude protein content ranging from 5% to 14%, 3% to 5% soluble sugars, and 3.4–5.3% ash. Furthermore, small quantities of bioactive compounds, such as alkaloids (such as trigonelline) and saponins, are present, particularly near the stem base (Sengupta et al., 2022). In addition to the essential organic and inorganic compounds, *A. konjac* corms are abundant in vitamins and other bioactive components. Corms are notable for their content of some organic compounds, which enhance their nutritional value. Furthermore, fresh corm tissue contains serotonin and its derivatives. These serotonin derivatives are interesting because of their potential therapeutic properties (Shi et al., 2019). The precise chemical composition of mature Amorphophallus corms can vary depending on species, geographic region, and environmental factors during cultivation. Among the nine species of Amorphophallus grown in China, *A. konjac* and *A. albus* are especially important for storing glucomannan as their primary carbohydrate, making them important for both traditional and modern applications (Mekkerdchoo et al., 2016). This variation in composition highlights the importance of understanding the specific growth conditions and species characteristics when utilizing these corms for their health benefits and industrial applications. The study of these variations can lead to optimized cultivation practices, potentially enhancing the yield of desired compounds, such as glucomannan and other bioactive constituents (Gao et al., 2023).

The chemical structure of polysaccharides plays a significant role in determining their functional and nutritional properties as well as their biological activities (Yu et al., 2018). The primary structure of KGM consists of repeating units of D-glucose and D-mannose in a molar ratio of 1:1.6–1.7, connected by β-1,4-glycosidic bonds. Some side chains may branch from the main mannose backbone at the C-3 position or from the sugar unit at the C-6 position through acetyl-group linkages. KGM exists in two native conformations, alpha (amorphous) and beta (crystalline), which affect its physical and functional properties, respectively. The molecular weight of KGM is relatively homogenous and normally distributed, although it can vary depending on factors such as origin, processing methods, and storage conditions. KGM is reported to have an average molecular weight of 5.83×10^5 g/mol, contributing to its unique functional properties in both food and health applications. The unique internal structure of the two-year-old KGM provides insight into the tissue composition of the plant. As the size and quantity of these idioblasts increase toward the center of the corm, the central region contains idioblasts that can reach up to 650 μm in diameter. This branching was relatively minimal, with approximately three branches for each of the 32 sugar units (Felix da Silva et al., 2020). In addition, these calcium oxalate formations are located within KGM-containing idioblasts and in the surrounding parenchyma. The dual presence of KGM and calcium oxalate within the corm tissue highlights the complex structure of *A. konjac* corms. KGM and calcium oxalate are deposited within corms, forming needle-shaped raphide crystals and multi-crystal druses, also known as cluster crystals (Chua et al., 2013). The molecular configuration of KGM includes a mannose-to-glucose ratio of approximately 1.6:1. These acetyl groups are crucial for enhancing the solubility of KGM (Kulkarni et al., 2024). The molecular weight of KGM varies widely, ranging from 200 to 2000 kDa, and is influenced by factors such as the specific cultivar, growing region, and processing and storage techniques used (Liu et al., 2021a). One of KGM's distinctive properties of KGM is its ability to dissolve in hot and cold water. The solubility of KGM can

be further enhanced by applying heat and mechanical agitation, which makes it versatile for various applications across the food and industrial sectors (Shi et al., 2019). KGM solutions may decrease over time, possibly because of bacterial contamination or enzymatic hydrolysis, particularly by β-mannanase. When mild alkali is added to KGM solutions, a thermostable gel is formed, which has applications in food and industrial products (Liu et al., 2021a). This unique combination of structural and physicochemical properties renders KGM a valuable compound for various applications (Table 2).

4 Modern health applications

KGM is a soluble fiber derived from the konjac plant, known for its potential health benefits, particularly in managing metabolic disorders. One of the primary advantages of KGM is its ability to ameliorate conditions such as diabetes and hypercholesteremia, suggesting its role as a functional food in metabolic health (Jian et al., 2024). KGM is recognized as an effective weight loss aid, promoting satiety and reducing overall caloric intake. This is largely due to its capacity to form a gel-like substance in the stomach, which enhances feelings of fullness and helps control hunger (Jin et al., 2024). Consequently, individuals may experience reduced food intake, contributing to weight management efforts. Moreover, KGM supports digestive health by slowing down the digestive process, which can improve bowel movements and overall gut function (Deng et al., 2024). This property not only aids digestion but also plays a role in regulating blood sugar levels by slowing the absorption of glucose in the bloodstream after meals, thereby helping to maintain stable blood sugar levels (Fang et al., 2023a). The health benefits of KGM encompass weight loss support, appetite suppression, improved digestive health, and blood sugar regulation, making it a valuable addition to a balanced diet aimed at enhancing overall well-being (Table 3).

TABLE 2 Chemical composition, structural properties, and applications of konjac glucomannan (KGM).

Aspect	Details	Citations
Main Component	Glucomannan (49–60% of corm weight).	(Alamgir, 2018)
Additional Components		
	Starch (10–30%), inorganic elements (e.g., calcium, magnesium, iron, cobalt).	(Gómez et al., 2017)
	Crude protein (5–14%), soluble sugars (3–5%), and ash (3.4–5.3%).	(Sengupta et al., 2022)
	Bioactive compounds such as alkaloids (e.g., trigonelline), saponins, and serotonin derivatives.	(Shi et al., 2019)
	Vitamins and other bioactive components vary based on growth conditions.	(Gao et al., 2023)
Species Variability		
	A. konjac and *A. albus* are key species for glucomannan storage.	(Mekkerdchoo et al., 2016)
	Chemical composition varies with species, region, and environment.	(Gao et al., 2023)
Polysaccharide Structure		
	Repeating units of D-glucose and D-mannose in a 1:1.6–1.7 molar ratio, linked by β-1,4 bonds.	(Yu et al., 2018)
	Side chains branch at C-3 and C-6 positions with acetyl-group linkages.	(Kulkarni et al., 2024)
	Alpha (amorphous) and beta (crystalline) conformations affect physical properties.	(Felix da Silva et al., 2020)
Molecular Properties		
	Molecular weight ranges from 200–2000 kDa; average weight ~5.83×10^5 g/mol.	(Liu et al., 2021b)
	Solubility in hot and cold water, enhanced by heat and mechanical agitation.	(Shi et al., 2019)
	Acetyl groups improve solubility.	(Kulkarni et al., 2024)
	Forms thermostable gel with mild alkali; useful in food and industrial products.	(Liu et al., 2021b)
Corm Tissue Structure		
	Contains KGM and calcium oxalate in needle-shaped raphides and cluster-shaped druses.	(Chua et al., 2013)
	Idioblasts in corms increase in size toward the center; central region ~650 μm diameter.	(Felix da Silva et al., 2020)
Physical Properties		
	KGM solutions degrade over time due to bacterial contamination or enzymatic hydrolysis.	(Shi et al., 2019)
	Unique gelation and functional properties for food, health, and industrial applications.	(Liu et al., 2021b)

4.1 Metabolic health (e.g., diabetes, weight loss)

KGM, derived from the tubers of *A. konjac*, has gained attention for its multifaceted health benefits, particularly in the realm of metabolic health (Behera and Ray, 2016; Devaraj et al., 2019a). Its role in weight management, blood glucose regulation, and lipid profile improvement positions it as a valuable dietary intervention for conditions such as obesity and diabetes (Fang et al., 2023a). One of the primary applications of KGM is its effectiveness in promoting weight loss. Research indicates that incorporating glucomannan into a low-calorie diet significantly enhances weight loss outcomes compared to a diet alone (Jian et al., 2024). In a study involving 30 patients, those who consumed glucomannan alongside a 1,200 kcal

TABLE 3 Health benefits and mechanisms of konjac glucomannan (KGM).

Health Aspect	Mechanism of Action	Findings	Advantages	Citations
Metabolic health (e.g., diabetes, weight loss)				
Weight Management	Forms a gel-like substance in the stomach, increasing satiety and reducing caloric intake.	5.5 lbs weight loss in 8 weeks with a low-calorie diet.	Aids adherence to dietary regimens and promotes healthy weight loss.	(Behera and Ray, 2016; Hasbay, 2019; Mah et al., 2022)
		8.5% reduction in body fat among overweight children in 2 months.	Effective in children and adults for weight and fat reduction.	(Ngondi et al., 2005; Behera and Ray, 2016)
		51 ± 16% reduction in excess weight among obese children over 4 months.	Supports pediatric obesity management.	(Behera and Ray, 2016)
Blood Glucose Regulation	Slows glucose absorption, stabilizing blood sugar levels and enhancing insulin sensitivity.	Fasting glucose reduction by 23.2% in type 2 diabetics.	Improves long-term glycemic control (HbA1c).	(Shah et al., 2015b; Behera and Ray, 2016)
		Glucose levels decreased by 55.37% with 1.5 g/kg dose in studies.	Helps manage diabetes and prediabetes.	(Ling et al., 2013)
Lipid Profile Improvement	Binds bile acids, promoting cholesterol excretion, reducing LDL-C and triglycerides.	LDL-C reduction by 5.45%; TC decreased by 3.24%.	Reduces cardiovascular risk factors like LDL-C and TC.	(Reimer et al., 2013; Li et al., 2021)
		More pronounced cholesterol reduction in females (LDL-C 9%, TC -6.1%).	Gender-specific benefits observed in lipid improvements.	(Vuorio et al., 2017; Ding et al., 2020)
		Cholesterol reduced by 7.3% in hypercholesterolemic children.	Safe and effective for managing lipid profiles in children.	(Santos et al., 2011)
Digestive Health	Acts as a soluble fiber, slowing digestion and enhancing gut function.	Promotes regular bowel movements and improved gut microbiota composition.	Supports overall digestive well-being.	(Kapoor et al., 2024)
Childhood Health	Combats obesity and hypercholesterolemia through a low-fat, fiber-rich diet.	Significant weight and cholesterol reductions observed in pediatric studies.	Offers a safe approach to improving metabolic health in children.	(Santos et al., 2011; Behera and Ray, 2016)
Dosage Variability	Dosages ranging from 0.7 g to 15 g/day show varying efficacy based on BMI and health conditions.	Higher dosages yield more pronounced effects on weight, glucose, and cholesterol management.	Customizable dosages for individual health needs.	(Devaraj et al., 2019b; Fang et al., 2023b)
Additional Benefits	Biocompatible, biodegradable polysaccharides support cardiovascular health and metabolic regulation.	Reduced risk factors like cholesterol, blood sugar, and obesity.	Suitable for functional foods and supplements.	(Watanabe et al., 2020; Kapoor et al., 2024)
Gut Health (e.g., prebiotics, microbiota regulation)				
Gut Microbiota Modulation	Enhances growth of beneficial bacteria like Bifidobacterium and Lactobacillus; increases microbiota diversity.	Promotes a balanced gut environment and reduces CRC risk through microbiome modulation.	Supports gut health and reduces risks of colorectal diseases.	(Wu et al., 2011; Gómez et al., 2017; Li et al., 2024)

(Continued)

TABLE 3 Continued

Health Aspect	Mechanism of Action	Findings	Advantages	Citations
Gut Health (e.g., prebiotics, microbiota regulation)				
Bowel Health and Regularity	Adds stool bulk and regulates bowel movements; dose-dependent effects.	3 g/day increases frequency by 3 evacuations/week; 4 g/day increases by 6 evacuations/week.	Relieves constipation, supports regularity, and improves overall bowel health.	(Hayeeawaema et al., 2020)
Prebiotic Properties	Supports beneficial gut bacteria and balances the gut environment.	Alleviates inflammation and promotes a healthy intestinal barrier.	Acts as a natural prebiotic with anti-inflammatory benefits.	(Du et al., 2021)
SCFAs	Enhances SCFA production, maintaining gut barrier integrity and modulating immune responses.	SCFAs reduce inflammation, improve gut health, and lower CRC risk.	Reduces inflammation and strengthens gut barrier.	(Zhang et al., 2023; Jin et al., 2025)
Colorectal Cancer Prevention	Reduces β-glucuronidase activity and secondary bile acids, minimizing genotoxic risks.	High-fiber diets including KGM lower CRC risk and enhance the efficacy of therapies like immunochemotherapy.	Prevents CRC and supports cancer treatments.	(Sawai et al., 2019; Yan et al., 2024)
IBD Symptom Alleviation	Improves stool consistency, fosters beneficial bacteria, and reduces gut inflammation.	Alleviates diarrhea and constipation symptoms in IBD patients.	Promotes intestinal health and symptom relief in IBD.	(Guarino et al., 2020; Du et al., 2021)
Hyperthyroidism Management	Supports nutrient absorption and regulates gastrointestinal symptoms like diarrhea.	Mitigates malabsorption and diarrhea symptoms while managing weight.	Improves gut health and nutritional balance in hyperthyroid patients.	(Kalra et al., 2021; Gan et al., 2024)
DNA Protection	Reduces harmful metabolites like β-glucuronidase and secondary bile acids that lead to DNA damage.	Protects against DNA damage and cancer development in the colon.	May reduce cancer risks and improve cellular health.	(Deng et al., 2024; Yan et al., 2024)
Therapeutic Role in CRC	Enhances the effectiveness of CRC treatments (e.g., polysaccharide K in immunochemotherapy).	Adjuvant therapies improve survival rates and reduce treatment side effects.	Complements CRC treatment, enhancing outcomes and reducing toxicity.	(Sawai et al., 2019)
Anti-inflammatory and immune regulation				
Skin Inflammation Relief	Lowers IL-4/IFN-γ ratio and suppresses hyper-IgE production.	Reduces symptoms of atopic dermatitis, allergic reactions, and eczema.	Effective in managing atopic dermatitis and other skin allergies.	(Devaraj et al., 2019b; Tian et al., 2023; Pan et al., 2024)
Colitis Management	Reduces cytokines (e.g., IL-4, IL-13, TNF-α, IL-1β) and modulates immune responses.	Improves symptoms of OXA by lowering inflammatory markers.	Supports treatment of inflammatory bowel conditions like colitis.	(Handa et al., 2015; Onitake et al., 2015; Fang et al., 2023b)
Gut Inflammation Modulation	Regulates gut inflammation through cytokine reduction and microbiome modulation.	Potential to manage conditions like Irritable Bowel Disease (IBD).	Improves gut health and reduces inflammation in IBD patients.	(Changchien et al., 2021)
Wound Healing	Maintains moisture at the wound site, absorbs exudates, and promotes tissue repair.	Accelerates healing and reduces risk of infection; effective for biocompatible wound care applications.	Provides safe and effective wound management for various skin conditions.	(Alven et al., 2022; Zhou et al., 2022; Borbolla-Jiménez et al., 2023)
Gut Microbiota and Immune Support	Enhances growth of beneficial bacteria (e.g., Bifidobacteria, Lactobacilli) and GALT function.	Improves immune system resilience and enhances GALT activity.	Supports a healthy gut microbiome, which benefits systemic immunity.	(Devaraj et al., 2019b; Ye et al., 2021)
SCFAs Production	Increases SCFAs (e.g., acetate, propionate, butyrate) essential for gut integrity and inflammation control.	Reduces systemic inflammation, strengthens gut barrier, and supports immune tolerance.	Promotes gut health and reduces risks of autoimmune and inflammatory disorders.	(Elshaghabee and Rokana, 2021; Zhang et al., 2022a)
Allergy and Atopic Dermatitis	Suppresses OVA-specific IgE response; reduces hyper-IgE production.	Ameliorates eczema and allergic responses, highlighting its potential for atopic disease management.	Helps manage allergies and atopic conditions like dermatitis and rhinitis.	(Suzuki et al., 2010; Mao et al., 2022; Guerreiro et al., 2023)

(Continued)

TABLE 3 Continued

Health Aspect	Mechanism of Action	Findings	Advantages	Citations
Anti-inflammatory and immune regulation				
Immune Cell Regulation	Supports T-cell and macrophage activity through gut health and beneficial metabolite production.	Enhances immune defense and promotes systemic immune resilience.	Contributes to stronger immunity and balanced immune responses.	(Pan et al., 2024; Srividya et al., 2024)
Anti-inflammatory Mechanisms	Downregulates pro-inflammatory cytokines (e.g., TNF-α, IL-1β) and reduces NK1.1+ T cells.	Reduces systemic and localized inflammation, especially in conditions like colitis.	Effective for immune modulation and controlling chronic inflammatory diseases.	(Handa et al., 2015; Fang et al., 2023b)
Individual Variability	Immune and anti-inflammatory effects depend on individual health conditions and genetic factors.	Benefits vary; consultation with healthcare providers is advised for safe dietary integration in immune-related cases.	Tailored application ensures safety and effectiveness for diverse populations.	(Srividya et al., 2024)

diet experienced greater reductions in body weight and fat mass, alongside improved satiety and adherence to dietary regimens (Koncz et al., 2021; Mah et al., 2022). This is particularly relevant given the rising prevalence of obesity in many populations. In an 8-week study, participants who added KGM to a hypocaloric diet lost an average of 5.5 lbs, with a notable reduction in body fat, compared to the diet-only group (Hasbay, 2019; Xu et al., 2023). Regular consumption of KGM has been shown to significantly decrease body fat, particularly in individuals with a higher body mass index (BMI). In a clinical trial involving children, the glucomannan treatment group experienced a notable reduction in mean overweight from 49.5% to 41%, indicating a substantial decrease in body fat over the course of the study (Ngondi et al., 2005). Additionally, another study reported that treated obese patients exhibited a significant decrease in excess weight of 51 ± 16% compared to controls after four months, further supporting the effectiveness of KGM in weight reduction (Behera and Ray, 2016).

In addition to weight loss, KGM has demonstrated positive effects on metabolic health by regulating blood glucose levels. The consumption of glucomannan has been associated with improved insulin sensitivity and lower blood sugar levels, which are crucial for managing diabetes (Shah et al., 2015a). This regulation of blood glucose is complemented by KGM's ability to enhance carbohydrate tolerance, further supporting its role in diabetes management (Devaraj et al., 2019a). Research has shown that KGM has demonstrated significant efficacy in reducing glucose levels by 55.37% when administered at a dose of 1.5 g/kg in both animal models and clinical settings (Ling et al., 2013). Additionally, konjac flour, which contains glucomannan, resulted in a 40.9% reduction in blood sugar levels under similar experimental conditions. In clinical trials involving type 2 diabetic patients, KGM supplementation has been associated with a reduction in fasting glucose levels by 23.2% compared to placebo (Shah et al., 2015a; Behera and Ray, 2016). Dosage differences also play a crucial role in the effectiveness of KGM. Studies have reported a wide range of KGM dosages, from 0.7 g to 15 g per day, which can significantly influence the outcomes related to blood sugar regulation and cholesterol reduction (Devaraj et al., 2019a; Fang et al., 2023a). Higher dosages may yield more pronounced effects, while lower dosages might not be sufficient to achieve significant results. Furthermore, the demographic and health characteristics of study participants can affect KGM's efficacy. Factors such as age, BMI, and pre-existing health conditions can lead to variations in how individuals respond to KGM supplementation (Devaraj et al., 2019a; Colantonio et al., 2020). By forming a gel-like substance in the stomach, KGM not only slows the absorption of sugars but also helps regulate the release of insulin (Xia et al., 2024). Improved insulin sensitivity indicates that cells become more responsive to insulin, facilitating better regulation of blood glucose levels (Kapoor et al., 2024). Additionally, some studies suggest that KGM may help lower HbA1c levels, which are indicators of long-term blood sugar control and are vital for preventing diabetes-related complications. In addition to these direct effects, KGM also supports metabolic health through its impact on weight. Additional weight is a main risk factor for Type 2 diabetes, and the ability of KGM to induce satiety can help with weight management and reduce overall caloric intake. This weight-lowering effect can further enhance insulin sensitivity and glycemic control (Watanabe et al., 2020). Additionally, KGM, a soluble dietary fiber derived from the konjac plant, has demonstrated significant potential in improving cholesterol levels, particularly by lowering LDL-C and triglycerides, which are crucial for cardiovascular health. In a controlled study, subjects taking glucomannan experienced a notable reduction in serum cholesterol by −32.0 mg/dl and LDL-C by −28.7 mg/dl, indicating its effectiveness in managing lipid profiles (Behera and Ray, 2016). The mechanism behind KGM's cholesterol-lowering effects is attributed to its ability to bind bile acids in the intestine, promoting their excretion and subsequently leading to a reduction in cholesterol levels as the body utilizes cholesterol to replenish bile acids (Kapoor et al., 2024). Meta-analyses of KGM studies suggest overall benefits in lowering cholesterol and blood glucose, but they also highlight the need for standardized methodologies to improve reliability and comparability of results (Ho et al., 2017). Clinical trials have reported significant reductions in fasting glucose and cholesterol levels with KGM supplementation, yet these results can vary based on trial conditions (Chen et al., 2003; Xia et al., 2024).

Moreover, KGM contributes to the improvement of lipid profiles, particularly in lowering total serum cholesterol and enhancing overall lipid status. The same study that highlighted weight loss also reported

significant improvements in lipid parameters for participants consuming glucomannan, indicating its potential for cholesterol management (Zhu et al., 2024). This is particularly important as elevated cholesterol levels are a major risk factor for cardiovascular diseases. The health benefits of KGM extend beyond individual metrics; its soluble fiber content aids in the maintenance of normal blood cholesterol levels, making it a promising candidate for dietary interventions aimed at improving metabolic health (Kapoor et al., 2024). In a study involving 110 elderly individuals with hyperlipidemia, those who consumed refined konjac meal experienced notable decreases in triglyceride (TG), total cholesterol (TC), and LDL-C levels, along with increases in HDL-C and apoprotein (AI) levels. In contrast, the control group, which did not consume KGM, showed no changes in blood lipid and cholesterol (Mah et al., 2022). In a study assessing the efficacy of Minolest, which contains KGM, participants experienced a significant decrease in TC by 3.24%. Additionally, the study highlighted a more pronounced reduction in LDL-C, which decreased by 5.45% (Reimer et al., 2013; Li et al., 2021). These findings suggest that KGM supplementation can be beneficial for individuals with mild hypercholesterolemia, particularly those at a lower risk for coronary artery disease (Koyama, 2017). KGM has been shown to be effective in managing childhood obesity, particularly in reducing excess weight among obese children. In a clinical study involving 23 obese children aged between 5.2 and 15.8 years, those treated with highly purified glucomannan fibers experienced a significant reduction in excess weight, averaging 51 ± 16% compared to controls. This treatment involved administering 2-3 capsules of glucomannan twice daily, alongside a balanced diet, which ensured adequate caloric intake for all participants (Behera and Ray, 2016). Moreover, another study indicated that children under glucomannan treatment demonstrated a decrease in mean overweight from 49.5% to 41% over a two-month period, highlighting its effectiveness in weight management (Behera and Ray, 2016). In hypercholesterolemic children, the incorporation of KGM into a low-fat, fiber-rich diet has demonstrated significant efficacy in reducing cholesterol levels. Specifically, the treatment resulted in a 5.1% reduction in TC levels and a 7.3% decrease in LDL-C levels (Santos et al., 2011). These findings highlight the potential of KGM as a beneficial dietary intervention for managing cholesterol levels in this population. Moreover, gender differences were observed in the effectiveness of KGM treatment. In females, the reduction in TC was reported at 6.1%, while the decrease in LDL-C was even more pronounced at 9% (Vuorio et al., 2017; Ding et al., 2020). The ability of KGM to act as a natural polysaccharide with excellent biocompatibility and biodegradability further enhances its appeal for use in functional foods and supplements (Chandarana et al., 2024). KGM serves as a powerful tool in modern health applications, particularly for metabolic health. Its efficacy in weight loss, blood glucose regulation, and lipid profile improvement underscores its potential as a dietary intervention for managing obesity and diabetes, making it a significant focus for future research and public health initiatives (Figure 2) (Liu et al., 2025).

4.2 Gut health (e.g., prebiotics, microbiota regulation)

KGM is a soluble fiber that has garnered attention for its potential to modulate the gut microbiome, which may play a

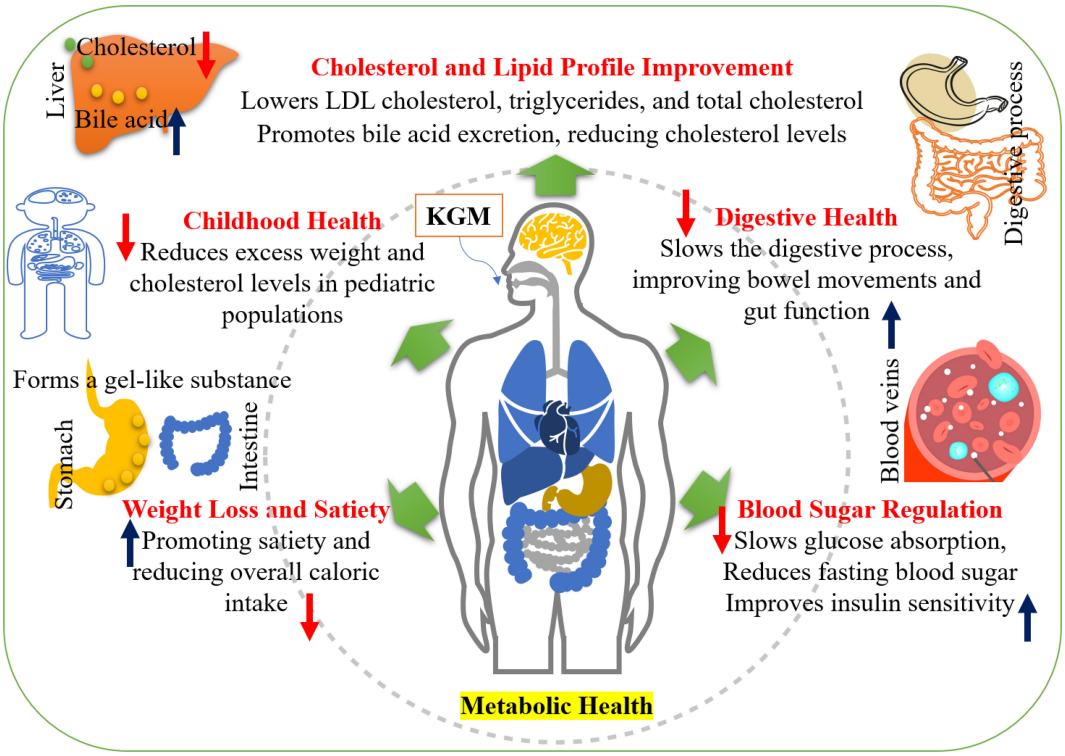

FIGURE 2
Metabolic health benefits of konjac glucomannan (KGM).

significant role in CRC prevention. One of the primary mechanisms by which KGM exerts its effects is through the enhancement of beneficial gut bacteria, particularly the Bifidobacterium genus and the Lactobacillus–Enterococcus group (Li et al., 2024). These populations significantly increase following the fermentation of KGM, suggesting a favorable modulation of gut microbiota that could contribute to protective effects against CRC (Gómez et al., 2017; Wu et al., 2011). Data from studies indicate that a daily intake of 3 grams of KGM results in an increase of 0.5 times per day and 3 additional evacuations per week compared to baseline values. When the dosage is increased to 4 grams per day, the effect is even more pronounced, with an increase of 0.9 times per day and 6 more evacuations per week. This demonstrates a clear dose-response relationship, where higher doses of KGM correlate with greater improvements in stool bulk and frequency of bowel movements (Hayeeawaema et al., 2020). KGM, a soluble dietary fiber, forms a gel-like substance when it enters the digestive tract. This gel can improve stool consistency, which is particularly beneficial for individuals with digestive disorders such as irritable bowel disease (IBD). KGM's ability to regulate stool consistency may help alleviate symptoms associated with IBD, such as diarrhea and constipation, thus contributing to better overall bowel health and comfort (Guarino et al., 2020).

KGM also acts as a prebiotic that fosters the growth of beneficial gut bacteria. The healthy gut microbiome plays a critical role in maintaining intestinal health and reducing inflammation. By supporting the proliferation of beneficial bacteria, KGM may contribute to a balanced gut environment, which is essential for managing IBD and promoting overall gut health (Du et al., 2021). Maintaining a healthy weight can be a challenge for patients due of symptoms such as malabsorption, reduced appetite, and dietary restrictions. KGM has been shown to induce a feeling of fullness, help manage appetite, and support weight control. This could be particularly beneficial for IBD patients striving to maintain a healthy weight, as proper weight management is linked to better overall well-being and could positively influence the management of IBD symptoms (Shah et al., 2020). Despite its potential benefits, there are some considerations when incorporating KGM into the diet of IBD patients. Tolerance to KGM can vary, and some individuals may experience gastrointestinal discomfort when introducing new fibers. It is recommended to start with small amounts of KGM and gradually increase intake while monitoring for any adverse effects (Zhang et al., 2021b). Additionally, KGM may affect the absorption of certain medications; therefore, it is crucial for patients to consult their healthcare provider before incorporating KGM into their diet to ensure that it does not interfere with their treatment plan (Pan et al., 2024).

KGM also promotes the production of short-chain fatty acids (SCFAs), which are crucial for gut health. The increase in cecal SCFA contents observed with KGM supplementation indicates that it not only supports beneficial bacteria but also enhances the metabolic byproducts that these bacteria produce. SCFAs are known to have anti-inflammatory properties and may help in reducing the risk of CRC by maintaining gut barrier integrity and modulating immune responses (Zhang et al., 2023; Jin et al., 2025). Research indicates that a diet rich in dietary fiber, including KGM, is associated with a lower risk of developing CRC. This protective effect is thought to arise from the fermentation of dietary fibers in the gut, leading to the production of SCFAs, which may exert chemopreventive properties on colonocytes (Devaraj et al., 2019a). Clinical trials have demonstrated that adjuvant therapies incorporating KGM, such as immunochemotherapy with polysaccharide K (PSK), can lead to improved survival rates and disease-free survival in patients with curatively resected CRC (Sawai et al., 2019). These findings highlight KGM's potential not only as a dietary supplement but also as a therapeutic agent that may mitigate the adverse effects of cancer treatments and enhance overall efficacy. High-fiber diets, particularly those rich in whole grains and vegetables, are consistently associated with a lower risk of CRC (Shah et al., 2015a).

The application of KGM to hyperthyroidism treatment is a novel area of research. Hyperthyroidism, characterized by an overactive thyroid gland, leads to the excessive production of thyroid hormones, causing symptoms such as weight loss, rapid heartbeat, and increased metabolism (Behera and Ray, 2016). Hyperthyroidism can affect digestive health, leading to diarrhea or malabsorption. KGM, with its fiber and prebiotic properties, can help manage gastrointestinal symptoms by improving gut health and regularity (Kalra et al., 2021). KGM's appetite-suppressing effects of KGM and its role in promoting satiety could potentially aid in managing weight changes associated with hyperthyroidism. By reducing appetite and caloric intake, KGM may help balance metabolic changes caused by these conditions (Gan et al., 2024). In hyperthyroidism, absorption of certain nutrients may be disrupted. KGM's role in improving overall digestive health could support better nutrient absorption and help manage deficiencies commonly seen in thyroid disorders (Devaraj et al., 2019b). Although the use of KGM in wound dressings has already been established and has clinical support, its application in hyperthyroidism treatment is less well documented and requires further investigation. Research on KGM's potential benefits of KGM for hyperthyroidism is ongoing, and more studies are needed to validate its effectiveness and safety in this context.

Moreover, KGM has demonstrated anti-genotoxic effects, which are vital in preventing DNA damage that can lead to cancer. Studies have shown that KGM supplementation reduces fecal β-glucuronidase activity and secondary bile acid levels, both of which are associated with increased cancer risk. This reduction in harmful metabolites may lower the precancerous risk factors in the colon (Yan et al., 2024). The prebiotic potential of KGM is further supported by its ability to stimulate the growth of beneficial gut bacteria, thereby enhancing gut microbiome diversity and activity (Deng et al., 2024). This modulation of the gut microbiome not only contributes to improved gut health but also plays a role in the prevention of CRC by potentially influencing metabolic pathways related to cancer development. KGM's mechanisms for modulating the gut microbiome include enhancing beneficial bacterial populations, increasing SCFA production, and exerting anti-genotoxic effects (Zhang et al., 2024). These actions collectively contribute to a healthier gut environment, which is crucial for reducing the risk of CRC. Future research, particularly *in vivo* studies involving human subjects, is necessary to further elucidate

these mechanisms and confirm the beneficial effects of KGM on gut health and cancer prevention (Ye et al., 2021).

4.3 Anti-inflammatory and immune regulation

Regular consumption of KGM has been shown to significantly alleviate skin inflammation, particularly in models of atopic dermatitis. KGM, a dietary fiber derived from the konjac plant, possesses notable anti-inflammatory properties that contribute to its effectiveness in managing skin conditions (Pan et al., 2024). Specifically, pulverized konjac glucomannan (PKGM) has been demonstrated to reduce the frequency of skin inflammation and associated symptoms in murine models. In studies involving PKGM, mice exhibited a marked decrease in the IL-4/IFN-γ ratio in the colonic lamina propria, indicating an improvement in immune response and a reduction in inflammation (Tian et al., 2023). Furthermore, the administration of PKGM not only mitigated skin inflammation but also suppressed hyper-IgE production, which is often linked to allergic reactions and dermatitis (Devaraj et al., 2019b). The anti-inflammatory activity of KGM is prominently demonstrated through its effects in a mouse model of oxazolone-induced colitis (OXA), where it significantly ameliorated the symptoms associated with this condition. In the context of OXA-induced colitis, KGM administration resulted in a marked reduction in the levels of critical inflammatory cytokines, specifically interleukin-4 (IL-4) and interleukin-13 (IL-13) (Onitake et al., 2015). These cytokines are pivotal in mediating inflammatory responses, and their suppression indicates a robust anti-inflammatory effect of KGM. The study revealed that PKGM not only improved histological markers of colonic inflammation but also led to a decrease in the population of NK1.1+ T cells in the liver, which is associated with the induction of Th1-polarized immune responses. The mechanism underlying KGM's anti-inflammatory activity appears to involve cytokine regulation, as it influences the levels of pro-inflammatory cytokines such as TNF-α and IL-1β, which are crucial in inflammatory processes (Handa et al., 2015). By modulating these cytokines, KGM can effectively reduce inflammation and enhance immune responses, showcasing its potential therapeutic applications in inflammatory diseases. Moreover, the study highlights that the preventive role of KGM in OXA-induced colitis was not observed in invariant natural killer T cell-deficient mice, further emphasizing the importance of immune modulation in its mechanism of action (Ye et al., 2021; Fang et al., 2023b).

Emerging research suggests that dietary fibers such as KGM may have anti-inflammatory properties. This fiber has the potential to modulate the inflammatory response in the gut, which is a key aspect in managing irritable bowel disease (IBD). Although preliminary findings are promising, more studies are required to fully understand the extent of KGM's anti-inflammatory effects of KGM and its practical applications for reducing inflammation in individuals with IBD (Changchien et al., 2021). KGM has shown significant potential in wound care due to its unique physical and chemical properties, making it an effective component in modern wound dressings. The primary benefit of KGM-based wound dressings is their ability to form gel-like substances when hydrated, which offers several advantages in wound management. One of the key features of KGM in wound dressings is its ability to maintain a moist environment around the wound. A moist environment is critical to promote faster and more efficient wound healing. This moisture prevents the wound from drying out and forms a crust, which can impede the healing process. KGM dressings help keep the wound bed hydrated, facilitating cell migration and tissue repair, ultimately accelerating the healing process (Zhou et al., 2022). Another important benefit of KGM is its ability to absorb wound exudates. As the gel formed by KGM absorbs excess wound fluid, it helps to manage the moisture levels at the wound site, reducing the risk of maceration. Maceration, which occurs when the skin becomes soft and breaks down owing to prolonged exposure to moisture, can lead to further complications in wound healing. By effectively managing the exudate, KGM dressings contribute to a more stable and controlled healing environment (Borbolla-Jiménez et al., 2023). KGM is highly biocompatible and non-toxic, making it particularly suitable for use in medical applications, such as wound care. It does not cause irritation or allergic reactions, thereby ensuring patient comfort and safety during the healing process. The non-reactive nature of KGM allows its use in a wide range of patients, including those with sensitive skin or allergies, making it a versatile and safe option for wound management (Veerasubramanian et al., 2018). In some formulations, KGM wound dressings are combined with antimicrobial agents to prevent infections, which can be a major complication of wound care. These antimicrobial KGM dressings help reduce the risk of bacterial infections at the wound site, support optimal healing, and minimize the chances of further complications. This combination of antimicrobial properties and KGM's natural benefits enhances the efficacy of these dressings in clinical settings (Alven et al., 2022).

KGM may influence the immune system primarily through its positive effects on gut health and its ability to modulate inflammation. One of the key mechanisms by which KGM supports immune function is through the modulation of the gut microbiota. Acting as a prebiotic, KGM promotes the growth of beneficial gut bacteria, such as Bifidobacteria and Lactobacilli, which are crucial for maintaining a balanced gut microbiome (Ye et al., 2021). Because a significant portion of the immune system is located in the gut-associated lymphoid tissue (GALT), the health of the gut microbiome directly affects immune responses. By promoting a healthy microbiome, KGM plays a role in strengthening immune defenses (Devaraj et al., 2019b). Another important way to support the immune system is through the production of SCFAs during fermentation by gut bacteria. SCFAs, including acetate, propionate, and butyrate, are essential for maintaining gut integrity and reducing inflammation, which can influence systemic immune responses (Zhang et al., 2022b). By promoting immune tolerance, KGM can help prevent excessive or inappropriate immune reactions, potentially reducing the risk of autoimmune disorders (Elshaghabee and Rokana, 2021). Additionally, a healthy gut microbiome is key to the development and activity of immune cells, such as T-cells and macrophages,

which are central to immune defense mechanisms (Pan et al., 2024). Specifically, PKGM supplementation has been reported to suppress the OVA-specific IgE response, which is a critical marker of allergic reactions, without adversely affecting other immune responses such as IgG1 and IgG2a production (Suzuki et al., 2010). In addition to its effects on allergic rhinitis, KGM has demonstrated efficacy in preventing skin inflammation associated with atopic dermatitis (Guerreiro et al., 2023). Studies have shown that PKGM can ameliorate eczema and hyper-IgE production in mouse models, suggesting its potential as a dietary intervention for managing atopic diseases (Mao et al., 2022). However, it is important to note that the effects of KGM on the immune system vary among individuals. Those with immune-related disorders should consult healthcare professionals before incorporating KGM into their diet to ensure their safety and efficacy in specific health conditions (Srividya et al., 2024). Overall, KGM's ability to support gut health and produce beneficial metabolites, such as SCFAs, positions it as a potential modulator of immune function (Figure 3).

5 Emerging cutting-edge research

KGM is emerging as a significant player in cutting-edge research within the fields of drug delivery and biological materials. KGM, derived from the corms of *A. konjac*, exhibits unique properties that make it an attractive candidate for various applications, particularly in the pharmaceutical sector due to its biocompatibility and biodegradability (Kulkarni et al., 2024; Zhuang et al., 2024). Recent studies have focused on the development of KGM-based microcapsules, which serve as innovative carriers for drug delivery. These microcapsules are prepared using a piercing method, where KGM forms the main membrane, encapsulating active ingredients such as N-Methyl-2-pyrrolidone (NMP) (Spirk, 2018; Khodadadi Yazdi et al., 2020). The preparation process involves blending KGM with Xanthan gum to create a gel that enhances the viscosity and tenacity of the microcapsules, thereby improving their drug delivery characteristics (Lin et al., 2024). The resulting konjac micro-balls (KMBs) demonstrate sustained-release properties, with delivery times exceeding 24 hours, indicating their potential for long-term therapeutic applications (Zhang et al., 2014). Key performance metrics such as embedding rate and encapsulation yield are critical in assessing the effectiveness of these KGM-based microcapsules. The embedding rate reflects the efficiency of drug loading, while encapsulation yield quantifies the success of the microcapsule formation process (Zhang et al., 2024). These metrics are essential for optimizing drug delivery systems, ensuring that therapeutic agents are effectively delivered to target sites within the body. Moreover, the preparation of KGM gel through alkali catalysis has opened new avenues for research in material science. The gel's properties, influenced by factors such as concentration, pH, and temperature, contribute to its potential applications in drug delivery systems (Sun et al., 2023). The molecular structure of KGM gel, characterized by advanced techniques like Fourier transform infrared spectroscopy and wide-angle X-ray diffraction, reveals a more regular arrangement

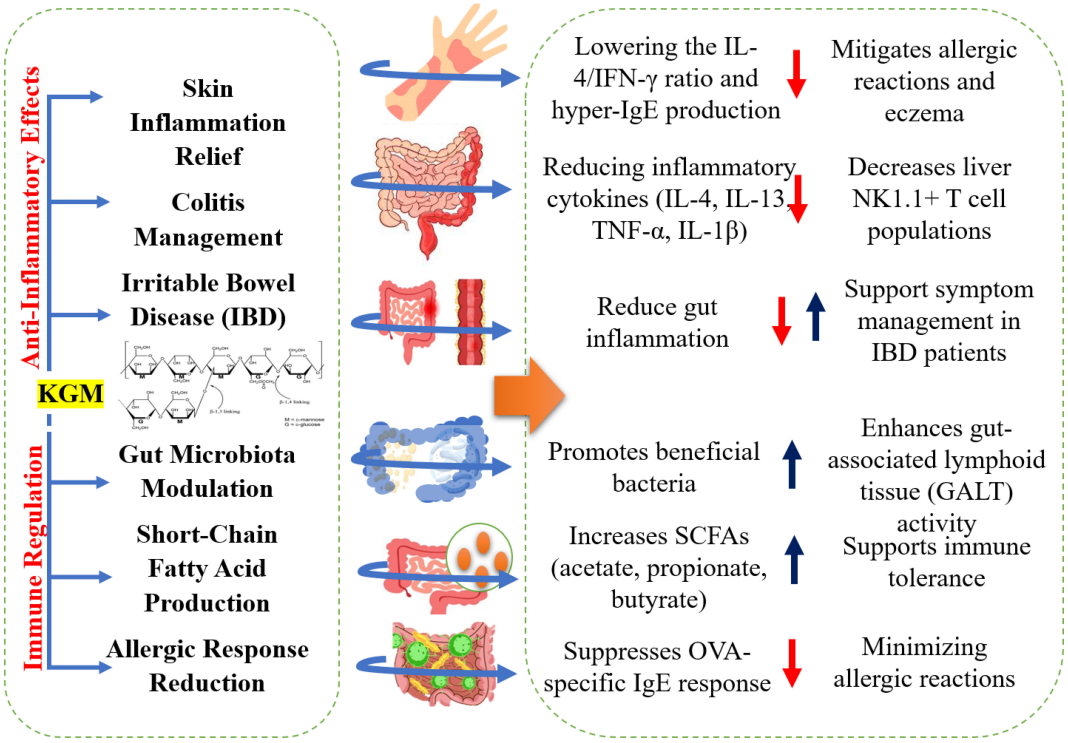

FIGURE 3
Anti-inflammatory and immune-regulating properties of konjac glucomannan (KGM).

compared to pure KGM, enhancing its functional capabilities in biological applications (Yang et al., 2017). The integration of KGM in drug delivery and biological materials research highlights its versatility and potential. The ongoing exploration of KGM-based systems promises to yield innovative solutions for effective drug delivery, addressing critical challenges in the pharmaceutical industry and paving the way for future advancements in health care (Zhou et al., 2022; Zhuang et al., 2024).

Furthermore, KGM serves as the primary membrane in the formation of microcapsules, which are designed to enhance drug delivery through their ability to control release and target specific sites within the body (Zhang et al., 2024). The encapsulation yield, which measures the effectiveness of KGM in encapsulating therapeutic agents, is a critical factor that underscores its potential in targeted delivery systems (Kapoor et al., 2024; Madawi et al., 2024). The structural integrity of KGM is significantly influenced by its hydrogen bonding network, particularly at the O (Xia et al., 2024) and O (Islam et al., 2023) positions on the KGM ring. These key linking points contribute to the stability of the hydrogen bonding network, which is essential for maintaining the functionality of KGM in drug delivery applications (Sun et al., 2023; Zheng et al., 2024a). The stability of this network is further enhanced through the process of deacetylation, which not only improves the hydrogen bonding structures but also increases the overall performance of KGM in drug delivery systems (Sun et al., 2023; Ye et al., 2021). Moreover, the gelation performance of KGM is crucial for its application in drug delivery. The ability of KGM to form gels allows it to encapsulate and release drugs in a controlled manner, thereby improving the therapeutic efficacy of the delivered agents (Lafarge and Cayot, 2018; Kapoor et al., 2024). The drug loading capacity of KGM-based microcapsules demonstrates how its unique structure can effectively accommodate and deliver therapeutic agents, ensuring that the drugs are released at the desired rate and location (Shen et al., 2024). The embedding rate of the microcapsules, which reflects the efficiency of KGM's structure in encapsulating the core substance, is another important aspect that enhances targeted drug delivery (Cui et al., 2021). The combination of these structural features—hydrogen bonding stability, gelation properties, and effective encapsulation—positions KGM as a promising candidate for developing advanced drug delivery systems (Table 4).

6 Multi-omics analysis and high-throughput screening approaches

Multi-omics analysis and HTS are pivotal methodologies that enhance the functional evaluation of KGM, a polysaccharide known for its health benefits and applications in food and pharmaceuticals. Multi-omics analysis integrates data from various biological layers, including genomics, proteomics, and metabolomics, to provide a comprehensive understanding of KGM's biological functions and interactions within biological systems (Wang and Li, 2021). This integrative approach allows researchers to identify the molecular mechanisms through which KGM exerts its health benefits, such as its antioxidant properties and cellular protection capabilities (Zhang et al., 2021a). On the other hand, HTS facilitates the rapid assessment of KGM's biological activity by enabling the

TABLE 4 Pharmaceutical applications and drug delivery potential of konjac glucomannan (KGM).

Aspect	Findings	Citations
Biocompatibility and Biodegradability	KGM's natural origin and compatibility with biological systems make it ideal for pharmaceutical applications, including drug delivery systems.	(Kulkarni et al., 2024; Zhuang et al., 2024)
Microcapsule Development	KGM-based microcapsules prepared using piercing methods exhibit sustained-release properties, making them suitable for long-term therapeutic applications.	(Spirk, 2018; Khodadadi Yazdi et al., 2020)
Sustained-Release Capabilities	KMBs can deliver drugs over 24 hours, showcasing potential for extended-release drug formulations.	(Zhang et al., 2014)
Encapsulation Yield and Embedding Rate	Metrics like encapsulation yield and embedding rate are critical for optimizing drug delivery systems, ensuring efficient and targeted delivery.	(Kapoor et al., 2024; Zhang et al., 2024)
Gelation Properties	Gelation performance of KGM enables encapsulation and controlled drug release, improving therapeutic efficacy in drug delivery applications.	(Lafarge and Cayot, 2018; Kapoor et al., 2024)
Hydrogen Bonding Stability	Stability at O (Xia et al., 2024) and O (Islam et al., 2023) positions contributes to KGM's structural integrity, crucial for maintaining functionality in drug delivery systems.	(Sun et al., 2023; Zheng et al., 2024a)
Deacetylation Benefits	Deacetylation improves KGM's hydrogen bonding network, enhancing its stability and performance in drug delivery applications.	(Ye et al., 2021; Sun et al., 2023)
Structural Characterization	Advanced techniques such as FTIR and X-ray diffraction reveal a more regular molecular structure in KGM gels, enhancing biological application potential.	(Sun et al., 2023; Yang et al., 2017)
Integration with Xanthan Gum	Blending KGM with xanthan gum enhances gel viscosity and tenacity, improving the drug encapsulation and release performance of the microcapsules.	(Lin et al., 2024)
Drug Loading Capacity	KGM-based systems demonstrate effective drug loading and targeted delivery, ensuring controlled release at specific sites within the body.	(Cui et al., 2021; Shen et al., 2024)
Material Science Applications	KGM gel preparation via alkali catalysis opens avenues for broader applications in biological materials and drug delivery systems.	(Sun et al., 2023)

testing of numerous compounds and their effects on specific biological pathways. This method is crucial in drug discovery and functional evaluation, as it allows for the identification of active compounds that can enhance the extraction and purification processes of KGM (Zhang et al., 2021b; Shen et al., 2024). By employing HTS, researchers can efficiently screen various extraction methods and purification techniques, optimizing conditions to isolate pure KGM or its derivatives for further study (Franková and Fry, 2015; Qi and Chen, 2024). The functional evaluation of KGM is further supported by the assessment of its antioxidant activity, which can be measured through various assays that evaluate its ability to scavenge free radicals (Zhu, 2018). This evaluation is essential for understanding how KGM can protect cells from oxidative stress, a significant factor in many diseases. Additionally, the purification techniques employed to isolate KGM are critical, as they ensure that the final product retains its functional properties, including its viscosity and health benefits (Widjanarko et al., 2024). Moreover, enzymatic hydrolysis and γ-irradiation are techniques that can modify KGM to enhance its functional properties. Enzymatic hydrolysis breaks down KGM into oligo-glucomannan, which may exhibit improved bioactivity (Zhu, 2018; Zheng et al., 2024a). Similarly, γ-irradiation can induce structural changes that enhance the extraction efficiency and functional characteristics of KGM (Zheng et al., 2024b).

However, both techniques come with their own set of advantages and disadvantages. The advantages of multi-omics include comprehensive data integration and improved understanding of biological processes, which can lead to enhanced identification of therapeutic targets (Chen et al., 2021; Li et al., 2024). Conversely, the disadvantages of HTS may include high costs, the potential for false positives, and the necessity for extensive validation of results (Misra et al., 2019). These challenges can complicate the interpretation of data and may require additional resources to ensure reliability. The integration of multi-omics and HTS in KGM research holds significant potential for future studies. By combining the strengths of both approaches, researchers can gain deeper insights into KGM's properties and interactions, ultimately leading to improved applications in food preservation and drug delivery systems. For instance, understanding the gel formation mechanism of KGM, which involves molecular interactions such as hydrogen bonding and hydrophilic group interactions, can be enhanced through multi-omics data (Song et al., 2024). Additionally, chemical modifications of KGM can be systematically evaluated using HTS to optimize its properties for specific applications (Tsurumaki et al., 2015). The synergistic use of multi-omics analysis and HTS can significantly advance the functional evaluation of KGM, paving the way for innovative applications and improved product formulations in both the food and pharmaceutical industries (Table 5).

7 Limitation, challenges and future directions

The quality of KGM products is influenced by several critical factors that play a significant role in their formulation and performance. Understanding these factors is essential for optimizing the efficacy of KGM-based applications, particularly in

TABLE 5 Advanced analytical techniques and functional insights of konjac glucomannan (KGM).

Aspect	Findings	Citations
Multi-omics Analysis	Integrates genomics, proteomics, and metabolomics data to elucidate KGM's molecular mechanisms, including antioxidant properties and cellular protection capabilities.	(Wang and Li, 2021; Zhang et al., 2021b)
High-Throughput Screening (HTS)	Facilitates rapid assessment of KGM's biological activity, enabling efficient testing of extraction and purification techniques for isolating pure KGM or its derivatives.	(Zhang et al., 2021b; Shen et al., 2024)
Antioxidant Activity	KGM's ability to scavenge free radicals and protect cells from oxidative stress is essential for understanding its health benefits.	(Zhu, 2018)
Purification Techniques	Critical for preserving KGM's functional properties, including viscosity and bioactivity, during extraction and processing.	(Widjanarko et al., 2024)
Enzymatic Hydrolysis	Converts KGM into oligo-glucomannan, enhancing bioactivity and functional properties.	(Zhu, 2018; Zheng et al., 2024a)
γ-Irradiation	Induces structural changes in KGM, improving extraction efficiency and functional characteristics.	(Zheng et al., 2024a)
Advantages of Multi-omics	Comprehensive data integration improves understanding of biological processes and facilitates the identification of therapeutic targets.	(Chen et al., 2021; Li et al., 2024)
Disadvantages of HTS	High costs, potential false positives, and the need for extensive result validation pose challenges in HTS applications.	(Misra et al., 2019)
Synergistic Integration	Combining multi-omics and HTS enhances understanding of KGM properties and molecular interactions, advancing applications in food preservation and drug delivery.	(Tsurumaki et al., 2015; Song et al., 2024)
Gel Formation Mechanism	Multi-omics data improves understanding of KGM gelation through molecular interactions such as hydrogen bonding and hydrophilic group interactions.	(Song et al., 2024)
Chemical Modifications	HTS enables systematic evaluation of KGM modifications to optimize properties for specific applications.	(Tsurumaki et al., 2015)

drug delivery systems. One of the primary factors is the concentration of KGM itself. The concentration directly affects the release degree of encapsulated drugs, such as cap, which is crucial for ensuring that the active ingredients are delivered effectively. Optimal conditions have been identified, with a concentration of 2.5% (w/v) KGM yielding a predicted release degree of 92.258% for cap (Chao et al., 2012). This highlights the importance of selecting the right concentration to achieve desired release profiles. Another significant factor is the embedding rate, which determines how efficiently active ingredients are incorporated into the KGM matrix. A higher embedding rate typically correlates with better delivery of the active compounds, thereby enhancing the overall quality of the KGM product (Sun et al., 2023). Additionally, the drug loading capacity is a direct measure of how well the KGM microcapsules can incorporate and deliver these active compounds, further influencing product quality (Shen et al., 2024). The encapsulation yield is also a critical parameter, reflecting the effectiveness of the microencapsulation process. A higher encapsulation yield indicates a more successful process, which is vital for the functionality of KGM products (Zhang et al., 2024). Furthermore, the physical properties of the microcapsules, such as particle size and distribution, are essential for understanding their performance. These characteristics can significantly impact the release behavior and stability of the KGM products (Halahlah et al., 2023). The preparation parameters, including mixing time, laying-time, and drying temperature, are crucial for ensuring the quality of KGM membranes. For instance, the duration of mixing affects the uniformity of the membrane, while the laying-time is important for proper formation (Yuan et al., 2017). The drying temperature, specifically at 65°C, has been shown to influence the final quality and release characteristics of the product (Ni et al., 2021). Lastly, the morphology of the KGM products provides insights into their structural characteristics, which are critical for assessing quality. Analyzing the morphology can help identify any potential issues in the formulation process that may affect performance (Sun et al., 2023; Kapoor et al., 2024). The safety and efficacy of KGM products are significantly influenced by the dosage forms and dosages used in clinical studies. A notable example is the specific dosage of 3.9 g of KGM administered daily, which was shown to effectively lower TC levels by 10% in a controlled study involving 63 healthy men (Behera and Ray, 2016; Jian et al., 2024). This dosage not only demonstrated a significant reduction in TC but also led to a 7.2% decrease in LDL-C and a 23% reduction in triglycerides, indicating a robust lipid-lowering effect (Nie and Luo, 2021; Cheung et al., 2023). This variability in dosage highlights the importance of tailoring KGM products to individual needs and health conditions to optimize safety and efficacy. In addition to dosage, the physiochemical properties of KGM can also be altered through processes such as γ-irradiation. Studies have shown that different doses of γ-irradiation (5, 20, 50, and 100 kGy) can affect the weight-average molecular weight (M_w) and apparent viscosity of KGM, which are critical factors influencing its functional properties and, consequently, its safety and efficacy (Xu et al., 2007; Jian et al., 2016).

The extraction and purification of KGM on a large scale presents significant sustainability challenges that must be addressed to minimize environmental impact. One of the primary difficulties lies in maintaining ecological balance during these processes, which often leads to adverse effects on local ecosystems (Behera and Ray, 2017; Pan et al., 2024). Resource efficiency is a crucial aspect of sustainable KGM production. The extraction and purification processes must be optimized to minimize waste and maximize the use of available resources. This involves not only improving the efficiency of the extraction methods but also considering the trade-offs between different resource efficiency objectives, such as reducing environmental impacts while ensuring cost-effectiveness (He et al., 2024). The complexity of these trade-offs highlights the need for a comprehensive approach to resource management in KGM production. Technological innovations present a promising avenue for addressing these sustainability challenges. Advancements in extraction techniques could lead to more sustainable practices that reduce environmental impacts and enhance resource efficiency (Mathura et al., 2024). However, the adoption of such technologies must be coupled with strict regulatory compliance to ensure that environmental standards are met throughout the production process. Additionally, the impact of climate change on the availability and quality of raw materials for KGM extraction cannot be overlooked. Fluctuations in climate conditions can affect the growth of konjac plants, thereby influencing the sustainability of KGM supply chains (Srzednicki and Borompichaichartkul, 2020). This underscores the importance of supply chain coordination among producers, suppliers, and manufacturers to enhance the overall sustainability of KGM production. Addressing the sustainability challenges associated with large-scale KGM extraction and purification requires a multifaceted approach that includes improved waste management, resource efficiency, technological innovations, regulatory compliance, and effective supply chain coordination. By tackling these limitations, the industry can move towards a more sustainable future for KGM production.

To enhance the future outlook for research on KGM, strategic recommendations can be made focusing on improving extraction efficiency and developing more effective functional food and drug delivery systems. Firstly, leveraging biotechnological methods to enhance the extraction efficiency of KGM from konjac tubers is crucial. Current extraction processes can be optimized through innovative biotechnological approaches, which may lead to higher yields and better quality of KGM. This aligns with the need for improved extraction techniques that can support the growing demand for KGM in various applications. Secondly, the development of KGM-based functional food and drug delivery systems should be prioritized. Research indicates that KGM can be effectively utilized in creating microcapsules that enhance the delivery of active ingredients, such as vitamins and drugs. The preparation of KGM-based microcapsules has shown promising results in terms of morphology, particle size distribution, and encapsulation efficiency, which are critical for ensuring the stability and bioavailability of the encapsulated substances. Moreover, optimizing the release properties of these systems is essential. Studies have identified key factors affecting the release degree of encapsulated compounds, such as concentration of KGM, mixing time, and drying conditions. For instance, optimal

conditions for the release of a model drug were determined to be 2.5% (w/v) KGM mixed with specific parameters, achieving a predicted release degree of 92.258%. Future research should continue to explore these parameters using response surface analysis to refine the formulation processes further. Additionally, the synergistic effects of KGM with other polysaccharides, such as xanthan gum, should be investigated. This combination has demonstrated potential in creating sustained release systems, which can significantly improve the efficacy of drug delivery. Lastly, the development of innovative functional food products incorporating KGM can address health concerns such as weight management and cholesterol control. By focusing on these health benefits, researchers can create products that not only meet consumer demand but also contribute positively to public health. In conclusion, by enhancing extraction methods, optimizing drug delivery systems, and developing functional foods, future research can significantly advance the applications of KGM, making it a valuable component in health and nutrition sectors (Table 6).

8 Conclusions

A. konjac, particularly its bioactive component KGM, stands as a promising dietary fiber with extensive health benefits and industrial applications. Its unique physicochemical properties, such as high viscosity and gel-forming ability, enable its use in various health and nutritional applications, including blood glucose regulation, weight management, lipid metabolism improvement, and gastrointestinal health. KGM's prebiotic and anti-inflammatory properties further enhance its therapeutic potential, with emerging applications in

TABLE 6 Key factors and innovations in konjac glucomannan (KGM) applications.

Aspect	Key Factors	Findings/Recommendations	Citations
KGM Concentration	Drug Release Degree	Optimal concentration: 2.5% (w/v) KGM achieves 92.258% drug release.	(Chao et al., 2012)
	Embedding Rate	Higher embedding rates improve delivery efficiency of active ingredients.	(Sun et al., 2023; Shen et al., 2024)
	Drug Loading Capacity	Higher drug loading enhances the incorporation and release of active compounds.	(Sun et al., 2023)
	Encapsulation Yield	High yield indicates successful microencapsulation and product functionality.	(Zhang et al., 2024)
Physical Properties	Particle Size & Distribution	Influences release behavior and stability, requiring precise formulation.	(Halahlah et al., 2023)
Preparation Parameters	Mixing Time, Laying-Time, Drying Temperature	Uniformity of KGM membranes and product quality depend on optimized mixing, laying-time, and drying (e.g., 65°C).	(Yuan et al., 2017; Ni et al., 2021)
Morphology Analysis	Structural Quality	Morphology analysis helps identify issues in structural quality and formulation.	(Sun et al., 2023; Kapoor et al., 2024)
Dosage and Clinical Efficacy	Specific Dosage	A daily dose of 3.9 g KGM reduces cholesterol levels (10% TC, 7.2% LDL-C, 23% triglycerides).	(Behera and Ray, 2016; Cheung et al., 2023)
	Physicochemical Modifications	γ-Irradiation modifies molecular weight and viscosity, affecting KGM's functional properties.	(Xu et al., 2007; Jian et al., 2016)
Sustainability Challenges	Environmental Impact	Address ecological challenges in extraction and purification processes.	(Behera and Ray, 2017; Pan et al., 2024)
	Resource Efficiency	Optimize extraction methods and minimize waste for cost-effective production.	(He et al., 2024)
	Climate Change Impact	Fluctuating climate affects raw material supply, requiring robust supply chain management.	(Mekkerdchoo et al., 2016)
Technological Innovations	Extraction Techniques	Advanced methods improve sustainability and reduce environmental impact.	(Mathura et al., 2024)
	Regulatory Compliance	Adhere to environmental standards to ensure sustainable production practices.	(He et al., 2024)
Extraction Efficiency	Biotechnological Approaches	Enhanced extraction efficiency and yield through biotechnological innovations.	(He et al., 2024)
Drug Delivery Systems	Encapsulation Techniques	Improve encapsulation efficiency for enhanced stability and bioavailability.	(Sun et al., 2023)
	Synergistic Effects with Other Polysaccharides	Combining KGM with xanthan gum shows potential for sustained-release drug systems.	(Tsurumaki et al., 2015)
Functional Food Innovations	Weight Management and Cholesterol Control	Develop KGM-based functional food products to address growing consumer demand for health benefits.	(Behera and Ray, 2017; Cheung et al., 2023)
Release Optimization	Formulation Refinements	Optimize key factors like KGM concentration, mixing, and drying for controlled release systems.	(Chao et al., 2012)

wound care, hyperthyroidism management, and CRC prevention. Despite its established benefits, the continued growth of KGM-based products requires rigorous quality control measures to ensure purity, molecular consistency, and safety. Addressing potential side effects, such as gastrointestinal discomfort and allergenicity, is essential for consumer safety. Future research focusing on bioavailability, targeted delivery systems, and novel formulations can significantly enhance KGM's therapeutic efficacy. Innovations in sustainable cultivation and ethical sourcing practices will ensure the environmental and economic viability of KGM production. Expanding applications beyond current uses, particularly in pharmaceuticals, cosmetics, and medical devices, presents an exciting avenue for KGM research. Detailed mechanistic studies on KGM's interaction with gut microbiota and metabolic pathways will deepen understanding of its health impacts and foster the development of targeted interventions. Population-based clinical trials and epidemiological studies are critical to establishing evidence-based guidelines for KGM consumption, ensuring its long-term safety and efficacy. In conclusion, KGM represents a versatile and beneficial component in functional foods, nutraceuticals, and therapeutic applications. With advancements in research, innovation, and sustainability, KGM holds immense potential to contribute significantly to global health and wellness, supporting diverse populations while promoting sustainable and ethical practices in its production and use.

Author contributions

AJ: Conceptualization, Data curation, Formal Analysis, Funding acquisition, Investigation, Methodology, Project administration, Resources, Software, Supervision, Validation, Visualization, Writing – original draft, Writing – review & editing. SS: Conceptualization, Data curation, Formal Analysis, Funding acquisition, Investigation, Methodology, Project administration, Resources, Software, Supervision, Validation, Visualization, Writing – original draft, Writing – review & editing. QG: Project administration, Resources, Supervision, Writing – review & editing. QW: Funding acquisition, Project administration, Resources, Software, Supervision, Writing – review & editing. J-SS: Conceptualization, Funding acquisition, Project administration, Resources, Software, Supervision, Visualization, Writing – review & editing.

Funding

The author(s) declare that financial support was received for the research, authorship, and/or publication of this article. Guizhou Science and Technology Corporation Platform Talents Fund (Grant No (2017).:5733-001 and CK-1130-002), the National Natural Science Foundation of China (U1812403, 82373981 and 82060750), 2011 Collaborative Innovation Centre of Traditional Chinese Medicine in Guizhou Province (No. (2022)026).

Acknowledgments

The authors express their gratitude for the financial support received through the Distinguished High-Level Talents Research Grant from the Guizhou Science and Technology Corporation Platform Talents Fund (Grant No.: [2017]5733-001 and CK-1130-002), the National Natural Science Foundation of China (U1812403, 82373981 and 82060750), 2011 Collaborative Innovation Centre of Traditional Chinese Medicine in Guizhou Province (No. [2022]026) and the support provided by the Zunyi Medical University, China. Special appreciation is extended to all laboratory colleagues and research staff members for their valuable insights, constructive guidance, and assistance throughout this study.

Conflict of interest

The authors declare that the research was conducted in the absence of any commercial or financial relationships that could be construed as a potential conflict of interest.

The author(s) declared that they were an editorial board member of Frontiers, at the time of submission. This had no impact on the peer review process and the final decision.

Generative AI statement

The author(s) declare that no Generative AI was used in the creation of this manuscript.

Publisher's note

References

Alamgir, A. N. M. (2018). Phytoconstituents–Active and inert constituents, metabolic pathways, chemistry and application of phytoconstituents, primary metabolic products, and bioactive compounds of primary metabolic origin. In: *Therapeutic Use of Medicinal Plants and their Extracts: Volume 2. Progress in Drug Research*, vol 74. (Cham: Springer), 25–164. doi: 10.1007/978-3-319-92387-1

Alven, S., Peter, S., Mbese, Z., and Aderibigbe, B. A. (2022). Polymer-based wound dressing materials loaded with bioactive agents: potential materials for the treatment of diabetic wounds. *Polymers (Basel).* 14, 724. doi: 10.3390/polym14040724

Au-Yeung, F., Jovanovski, E., Jenkins, A. L., Zurbau, A., Ho, H. V. T., and Vuksan, V. (2018). The effects of gelled konjac glucomannan fibre on appetite and energy intake in

healthy individuals: a randomised cross-over trial. *Br. J. Nutr.* 119, 109–116. doi: 10.1017/S0007114517003233

Behera, S. S., and Ray, R. C. (2016). Konjac glucomannan, a promising polysaccharide of Amorphophallus konjac K. *Koch Health Care Int. J. Biol. Macromol.* 92, 942–956. doi: 10.1016/j.ijbiomac.2016.07.098

Behera, S. S., and Ray, R. C. (2017). Nutritional and potential health benefits of konjac glucomannan, a promising polysaccharide of elephant foot yam, Amorphophallus konjac K. Koch: A review. *Food Rev. Int.* 33, 22–43. doi: 10.1080/87559129.2015.1137310

Borbolla-Jiménez, F. V., Peña-Corona, S. I., Farah, S. J., Jiménez-Valdés, M. T., Pineda-Pérez, E., Romero-Montero, A., et al. (2023). Films for wound healing fabricated using a solvent casting technique. *Pharmaceutics.* 15, 1914. doi: 10.3390/pharmaceutics15071914

Chandarana, C., Bonde, S., Vashi, V., Akhter, M. S., and Prajapati, B. (2024). Konjac glucomannan-based edible films: method, properties, and applications. *J. Food Process Eng.* 47 (12), e70009. doi: 10.1111/jfpe.v47.12

Changchien, C. H., Wang, C. H., and ling, C. H. (2021). Konjac glucomannan polysaccharide and inulin oligosaccharide ameliorate dextran sodium sulfate-induced colitis and alterations in fecal microbiota and short-chain fatty acids in C57BL/6J mice. *Biomedicine (Taipei).* 11, 23–30. doi: 10.37796/2211-8039.1191

Chao, W., Mei, X., Yu-peng, Z., Yang, X., Wei-hua, Z., and Dong-sheng, L. (2012). Study on preparation and optimization of konjac glucomannan coated soluble drug. In: G. Lee (ed) *Advances in Computational Environment Science. Advances in Intelligent and Soft Computing*, vol 142. (Berlin, Heidelberg: Springer), 335–341. doi: 10.1007/978-3-642-27957-7_41

Chen, H., Nie, Q., Hu, J., Huang, X., Yin, J., and Nie, S. (2021). Multiomics approach to explore the amelioration mechanisms of glucomannans on the metabolic disorder of type 2 diabetic rats. *J. Agric. Food Chem.* 69, 2632–2645. doi: 10.1021/acs.jafc.0c07871

Chen, H. L., Sheu, W. H. H., Tai, T. S., Liaw, Y. P., and Chen, Y. C. (2003). Konjac supplement alleviated hypercholesterolemia and hyperglycemia in type 2 diabetic subjects—A randomized double-blind trial. *J. Am. Coll. Nutr.* 22, 36–42. doi: 10.1080/07315724.2003.10719273

Cheung, B., Sikand, G., Dineen, E. H., Malik, S., and Barseghian-El-Farra, A. (2023). Lipid-lowering nutraceuticals for an integrative approach to dyslipidemia. *J. Clin. Med.* 12, 3414. doi: 10.3390/jcm12103414

Chua, M., Baldwin, T. C., Hocking, T. J., and Chan, K. (2010). Traditional uses and potential health benefits of Amorphophallus konjac K. *Koch ex N.E.Br. J. Ethnopharmacol.* 128, 268–278. doi: 10.1016/j.jep.2010.01.021

Chua, M., Hocking, T. J., Chan, K., and Baldwin, T. C. (2013). Temporal and spatial regulation of glucomannan deposition and mobilization in corms of Amorphophallus konjac (Araceae). *Am. J. Bot.* 100, 337–345. doi: 10.3732/ajb.1200547

Colantonio, A. G., Werner, S. L., and Brown, M. (2020). The effects of prebiotics and substances with prebiotic properties on metabolic and inflammatory biomarkers in individuals with type 2 diabetes mellitus: A systematic review. *J. Acad. Nutr. Diet.* 120, 587–607.e2. doi: 10.1016/j.jand.2018.12.013

Cui, T., Chen, C., Jia, A., Li, D., Shi, Y., Zhang, M., et al. (2021). Characterization and human microfold cell assay of fish oil microcapsules: Effect of spray drying and freeze-drying using konjac glucomannan (KGM)-soybean protein isolate (SPI) as wall materials. *J. Funct. Foods.* 83, 104542. doi: 10.1016/j.jff.2021.104542

Dai, S., Jiang, F., Shah, N. P., and Corke, H. (2019). Functional and pizza bake properties of Mozzarella cheese made with konjac glucomannan as a fat replacer. *Food Hydrocoll.* 92, 125–134. doi: 10.1016/j.foodhyd.2019.01.045

Deng, L., Zhong, G., Zhang, D., Zhu, Z., and Peng, Y. (2024). Effects of konjac glucomannan and its oligosaccharides on improvement of lactose intolerance as gut prebiotics. *ACS Omega.* 9, 29609–29619. doi: 10.1021/acsomega.4c02768

Derosa, G., D'Angelo, A., and Maffioli, P. (2024). The role of selected nutraceuticals in management of prediabetes and diabetes: An updated review of the literature. Part II. *Phytotherapy Res.* 38, 5490–5532. doi: 10.1002/ptr.v38.11

Devaraj, R. D., Reddy, C. K., and Xu, B. (2019a). Health-promoting effects of konjac glucomannan and its practical applications: A critical review. *Int. J. Biol. Macromol.* 126, 273–281. doi: 10.1016/j.ijbiomac.2018.12.203

Devaraj, R. D., Reddy, C. K., and Xu, B. (2019b). Health-promoting effects of konjac glucomannan and its practical applications: A critical review. *Int. J. Biol. Macromol.* 126, 273–281. doi: 10.1016/j.ijbiomac.2018.12.203

Ding, Y. F., Sun, T., Li, S., Huang, Q., Yue, L., Zhu, L., et al. (2020). Oral colon-targeted konjac glucomannan hydrogel constructed through noncovalent cross-linking by cucurbit[8]uril for ulcerative colitis therapy. *ACS Appl. Bio Mater.* 3, 10–19. doi: 10.1021/acsabm.9b00676

Du, Q., Liu, J., and Ding, Y. (2021). Recent progress in biological activities and health benefits of konjac glucomannan and its derivatives. *Bioactive Carbohydrates Dietary Fibre.* 26, 100270. doi: 10.1016/j.bcdf.2021.100270

Elshaghabee, F. M. F., and Rokana, N. (2021). Dietary management by probiotics, prebiotics and synbiotics for the prevention of antimicrobial resistance. In: H. Panwar, C. Sharma and E. Lichtfouse (eds) *Sustainable Agriculture Reviews 49. Sustainable Agriculture Reviews*, vol 49. (Cham: Springer). doi: 10.1007/978-3-030-58259-3_2 33–56

Fang, Y., Ma, J., Lei, P., Wang, L., Qu, J., Zhao, J., et al. (2023a). Konjac glucomannan: an emerging specialty medical food to aid in the treatment of type 2 diabetes mellitus. *Foods.* 12, 363. doi: 10.3390/foods12020363

Fang, Y., Ma, J., Lei, P., Wang, L., Qu, J., Zhao, J., et al. (2023b). Konjac glucomannan: an emerging specialty medical food to aid in the treatment of type 2 diabetes mellitus. *Foods.* 12, 363. doi: 10.3390/foods12020363

Felix da Silva, D., Ogawa, C. Y. L., Sato, F., Neto, A. M., Larsen, F. H., and Matumoto-Pintro, P. T. (2020). Chemical and physical characterization of Konjac glucomannan-based powders by FTIR and 13C MAS NMR. *Powder Technol.* 361, 610–616. doi: 10.1016/j.powtec.2019.11.071

Franková, L., and Fry, S. C. (2015). A general method for assaying homo- and hetero-transglycanase activities that act on plant cell-wall polysaccharides. *J. Integr. Plant Biol.* 57, 411–428. doi: 10.1111/jipb.12337

Gan, H. W., Cerbone, M., and Dattani, M. T. (2024). Appetite- and weight-regulating neuroendocrine circuitry in hypothalamic obesity. *Endocr. Rev.* 45, 309–342. doi: 10.1210/endrev/bnad033

Gao, L., Xia, X., Shuai, Y., Zhang, H., Jin, W., Zhang, X., et al. (2023). Gut microbiota, a hidden protagonist of traditional Chinese medicine for acute ischemic stroke. *Front. Pharmacol.* 14. doi: 10.3389/fphar.2023.1164150

Gómez, B., Míguez, B., Yáñez, R., and Alonso, J. L. (2017). Manufacture and properties of glucomannans and glucomannooligosaccharides derived from konjac and other sources. *J. Agric. Food Chem.* 65 (10), 2019–2031. doi: 10.1021/acs.jafc.6b05409

Gómez, B., Míguez, B., Yáñez, R., and Alonso, J. L. (2017). Manufacture and properties of glucomannans and glucomannooligosaccharides derived from konjac and other sources. *J. Agric. Food Chem.* 65, 2019–2031. doi: 10.1021/acs.jafc.6b05409

Guarino, M., Altomare, A., Emerenziani, S., Di Rosa, C., Ribolsi, M., Balestrieri, P., et al. (2020). Mechanisms of action of prebiotics and their effects on gastro-intestinal disorders in adults. *Nutrients.* 12, 1037. doi: 10.3390/nu12041037

Guerreiro, F., Pontes, J. F., Gaspar, M. M., Rosa da Costa, A. M., Faleiro, M. L., and Grenha, A. (2023). Respirable konjac glucomannan microparticles as antitubercular drug carriers: Effects of *in vitro* and *in vivo* interactions. *Int. J. Biol. Macromol.* 248, 125838. doi: 10.1016/j.ijbiomac.2023.125838

Guo, L., Yokoyama, W., Chen, M., and Zhong, F. (2021). Konjac glucomannan molecular and rheological properties that delay gastric emptying and improve the regulation of appetite. *Food Hydrocoll.* 120, 106894. doi: 10.1016/j.foodhyd.2021.106894

Halahlah, A., Piironen, V., Mikkonen, K. S., and Ho, T. M. (2023). Polysaccharides as wall materials in spray-dried microencapsulation of bioactive compounds: Physicochemical properties and characterization. *Crit. Rev. Food Sci. Nutr.* 63, 6983–7015. doi: 10.1080/10408398.2022.2038080

Handa, H., Saitoh, T., and Murakami, H. (2015). Immunomodulatory effects of lenalidomide. *Nihon Rinsho.* 73, 156–161.

Hasbay, İ. (2019). "Dietary fiber and nutrition," in *Dietary fiber: properties, recovery, and applications* (Netherlands: Elsevier), 79–123.

Hayeeawaema, F., Wichienchot, S., and Khuituan, P. (2020). Amelioration of gut dysbiosis and gastrointestinal motility by konjac oligo-glucomannan on loperamide-induced constipation in mice. *Nutrition.* 73, 110715. doi: 10.1016/j.nut.2019.110715

He, Y., Liu, Y., and Zhang, M. (2024). Hemicellulose and unlocking potential for sustainable applications in biomedical, packaging, and material sciences: A narrative review. *Int. J. Biol. Macromol.* 280, 135657. doi: 10.1016/j.ijbiomac.2024.135657

Ho, H. V. T., Jovanovski, E., Zurbau, A., Blanco Mejia, S., Sievenpiper, J. L., Au-Yeung, F., et al. (2017). A systematic review and meta-analysis of randomized controlled trials of the effect of konjac glucomannan, a viscous soluble fiber, on LDL cholesterol and the new lipid targets non-HDL cholesterol and apolipoprotein B. *Am. J. Clin. Nutr.* 105, 1239–1247. doi: 10.3945/ajcn.116.142158

Islam, F., Labib, R. K., Zehravi, M., Lami, M. S., Das, R., Singh, L. P., et al. (2023). Genus amorphophallus: A comprehensive overview on phytochemistry, ethnomedicinal uses, and pharmacological activities. *Plants.* 12, 3945. doi: 10.3390/plants12233945

Jian, X., Jian, S., and Deng, B. (2024). Konjac Glucomannan: A functional food additive for preventing metabolic syndrome. *J. Funct. Foods.* 115, 106108. doi: 10.1016/j.jff.2024.106108

Jian, W., Wu, H., Wu, L., Wu, Y., Jia, L., Pang, J., et al. (2016). Effect of molecular characteristics of Konjac glucomannan on gelling and rheological properties of Tilapia myofibrillar protein. *Carbohydr Polym.* 150, 21–31. doi: 10.1016/j.carbpol.2016.05.001

Jin, H., Wang, S., Sheng, J., Yang, X., Li, J., and Li, B. (2025). Konjac glucomannan and its degradation products inhibit intestinal lipid absorption by regulating gut microbiota and the production of short-chain fatty acids. *J. Agric. Food Chem.* 73 (2), 1203–1218. doi: 10.1021/acs.jafc.4c06280

Jin, H., Yao, L., Wang, S., Xia, P., Hou, T., Li, B., et al. (2024). Effects of KGM and degradation products on appetite regulation and energy expenditure in high-fat-diet mice via the adipocyte–hypothalamus axis. *J. Agric. Food Chem.* 72, 15765–15777. doi: 10.1021/acs.jafc.4c03819

Kalra, S., Aggarwal, S., and Khandelwal, D. (2021). Thyroid dysfunction and dysmetabolic syndrome: the need for enhanced thyrovigilance strategies. *Int. J. Endocrinol.* 2021, 1–11. doi: 10.1155/2021/9641846

Kapoor, D. U., Sharma, H., Maheshwari, R., Pareek, A., Gaur, M., Prajapati, B. G., et al. (2024). Konjac glucomannan: A comprehensive review of its extraction, health benefits, and pharmaceutical applications. *Carbohydr Polym.* 339, 122266. doi: 10.1016/j.carbpol.2024.122266

Khodadadi Yazdi, M., Taghizadeh, A., Taghizadeh, M., Stadler, F. J., Farokhi, M., Mottaghitalab, F., et al. (2020). Agarose-based biomaterials for advanced drug delivery. *J. Controlled Release.* 326, 523–543. doi: 10.1016/j.jconrel.2020.07.028

Koncz, D., Tóth, B., Roza, O., and Csupor, D. (2021). A systematic review of the european rapid alert system for food and feed: tendencies in illegal food supplements for weight loss. *Front. Pharmacol.* 11, 611361. doi: 10.3389/fphar.2020.611361

Koyama, T. (2017). 18. Bioactive foods and herbs in prevention and treatment of cardiovascular disease. In: *Handbook of nutrition in heart health*, vol 14. (Brill), 373–398. doi: 10.3920/978-90-8686-853-7_18

Kulkarni, D., Agnihotri, V., Bhinge, S., Ban, M., Bari, D., and Pardeshi, C. V. (2024). Konjac glucomannan: A functional biopolymer for multifaceted drug delivery applications. *Polym Adv. Technol.* 35, 119–141. doi: 10.1002/pat.v35.7

Lafarge, C., and Cayot, N. (2018). Potential use of mixed gels from konjac glucomannan and native starch for encapsulation and delivery of aroma compounds: A review. *Starch - Stärke* 70 (9–10), 1700159. doi: 10.1002/star.201700159

Lasrado, L. D., and Rai, A. K. (2022). Use of prebiotics for addressing gut dysbiosis and achieving healthy gut–brain axis. In: K. Chopra, M. Bishnoi and K. K. Kondepudi (eds) *Probiotic Research in Therapeutics*. (Singapore: Springer), 5, 207–239. doi: 10.1007/978-981-16-8444-9_11

Li, Y., Liang, S., Shao, Y., Li, Y., Chen, C., You, C., et al. (2021). Impacts of dietary konjac glucomannan supplementation on growth, antioxidant capacity, hepatic lipid metabolism and inflammatory response in golden pompano (Trachinotus ovatus) fed a high fat diet. *Aquaculture.* 545, 737113. doi: 10.1016/j.aquaculture.2021.737113

Li, Y., Lu, H., Liao, C., and Liu, X. (2024). Oxidized konjac glucomannan: A safe dietary fiber influencing mouse gut microbiota. *Food Chem. X.* 21, 101089. doi: 10.1016/j.fochx.2023.101089

Li, W., Xu, P., Qian, C., Zhao, X., Xu, H., and Li, K. (2024). The combined analysis of the transcriptome and metabolome revealed the possible mechanism of flower bud formation in amorphophallus bulbifer. *Agronomy.* 14, 519. doi: 10.3390/agronomy14030519

Lin, D., and Rezaei, M. J. (2024). Plant polysaccharides and antioxidant benefits for exercise performance and gut health: from molecular pathways to clinic. *Mol. Cell Biochem.* doi: 10.1007/s11010-024-05178-8

Lin, Y., Zhang, L., Li, X., Zhai, C., Liu, J., and Zhang, R. (2024). Effect and characterization of konjac glucomannan on xanthan gum/κ-carrageenan/agar system. *Int. J. Biol. Macromol.* 257, 128639. doi: 10.1016/j.ijbiomac.2023.128639

Ling, L., Hua, D. R., Chen, N., Pan, J., and Pang, J. (2013). Review of konjac glucomannan: isolation, structure, chain conformation and bioactivities. *J. Single Molecule Res.* 1, 7. doi: 10.12966/jsmr.07.03.2013

Liu, Q., Fang, J., Huang, W., Liu, S., Zhang, X., Gong, G., et al. (2023). The intervention effects of konjac glucomannan with different molecular weights on high-fat and high-fructose diet-fed obese mice based on the regulation of gut microbiota. *Food Res. Int.* 165, 112498. doi: 10.1016/j.foodres.2023.112498

Liu, Z., Ren, X., Cheng, Y., Zhao, G., and Zhou, Y. (2021a). Gelation mechanism of alkali induced heat-set konjac glucomannan gel. *Trends Food Sci. Technol.* 116, 244–254. doi: 10.1016/j.tifs.2021.07.025

Liu, Z., Ren, X., Cheng, Y., Zhao, G., and Zhou, Y. (2021b). Gelation mechanism of alkali induced heat-set konjac glucomannan gel. *Trends Food Sci. Technol.* 116, 244–254. doi: 10.1016/j.tifs.2021.07.025

Liu, F., Wan, H., Fan, H., Zhang, Z., Dai, H., and He, H. (2025). Complexation of starch and konjac glucomannan during screw extrusion exhibits obesity-reducing effects by modulating the intestinal microbiome and its metabolites. *Food Funct.* 16, 232–248. doi: 10.1039/D4FO04275A

Luo, C., Luo, S., Chen, Z., Yang, R., He, X., Chu, H., et al. (2024). Genome-wide analysis of the Amorphophallus konjac AkCSLA gene family and its functional characterization in drought tolerance of transgenic arabidopsis. *BMC Plant Biol.* 24, 1033. doi: 10.1186/s12870-024-05747-5

Madawi, E. A., Manaa, H. M., Alattrach, D. G., Al Mogharbel, Z. A., Hussain, Z., and Ahmed, I. S. (2024). Dry emulsions as a promising adaptation in pharmaceutical dosage formulations: A review of recent developments and biopharmaceutical significance. *J. Drug Delivery Sci. Technol.* 96, 105712. doi: 10.1016/j.jddst.2024.105712

Mah, E., Chen, O., Liska, D. J., and Blumberg, J. B. (2022). Dietary supplements for weight management: A narrative review of safety and metabolic health benefits. *Nutrients.* 14, 1787. doi: 10.3390/nu14091787

Mao, Y. H., Xu, Y., Song, F., Wang, Z. M., Li, Y. H., Zhao, M., et al. (2022). Protective effects of konjac glucomannan on gut microbiome with antibiotic perturbation in mice. *Carbohydr Polym.* 290, 119476. doi: 10.1016/j.carbpol.2022.119476

Mathura, S. R., Landázuri, A. C., Mathura, F., Andrade Sosa, A. G., and Orejuela-Escobar, L. M. (2024). Hemicelluloses from bioresidues and their applications in the food industry – towards an advanced bioeconomy and a sustainable global value chain of chemicals and materials. *Sustain. Food Technology.* 2, 1183–1205. doi: 10.1039/D4FB00035H

Mekkerdchoo, O., Borompichaichartkul, C., Perrigo, A., Srzednicki, G., Prakitchaiwattana, C., and Antonelli, A. (2016). Tracing the Evolution and Economic Potential of Konjac Glucomannan in Amorphophallus species (Araceae) using Molecular Phylogeny and RAPD Markers. *Phytotaxa.* 282 (2), 81–106. doi: 10.11646/phytotaxa.282.2.1

Misra, B. B., Langefeld, C., Olivier, M., and Cox, L. A. (2019). Integrated omics: tools, advances and future approaches. *J. Mol. Endocrinol.* 62, R21–R45. doi: 10.1530/JME-18-0055

Ngondi, J. L., Oben, J. E., and Minka, S. R. (2005). The effect of Irvingia Gabonensis seeds on body weight and blood lipids of obese subjects in Cameroon. *Lipids Health Dis.* 4, 12. doi: 10.1186/1476-511X-4-12

Ni, Y., Liu, Y., Zhang, W., Shi, S., Zhu, W., Wang, R., et al. (2021). Advanced konjac glucomannan-based films in food packaging: Classification, preparation, formation mechanism and function. *LWT.* 152, 112338. doi: 10.1016/j.lwt.2021.112338

Nie, Y., and Luo, F. (2021). Dietary fiber: an opportunity for a global control of hyperlipidemia. *Oxid. Med. Cell Longev.* 8, 5542342. doi: 10.1155/2021/5542342

Niu, L., Xia, T., Ren, Z., Tang, Z., Cao, Z., Jia, B., et al. (2024). Growth Promoting Characteristics of Bacillus amyloliquefaciens GZA69 and Its Biocontrol Potential Against Soft Rot of Amorphophallus konjac. *J. Biobased Mater Bioenergy.* 18, 819–826. doi: 10.1166/jbmb.2024.2442

Nurshanti, D. F., Lakitan, B., Hasmeda, M., and Ferlinahayati, F. (2023). Shoot emergence, leaf expansion, and corm growth in amorphophallus muelleri blume treated with hydropriming and shading. *AGRIVITA J. Agric. Sci.* 45 (1), 98–109. doi: 10.17503/agrivita.v45i1.3837

Onitake, T., Ueno, Y., Tanaka, S., Sagami, S., Hayashi, R., Nagai, K., et al. (2015). Pulverized konjac glucomannan ameliorates oxazolone-induced colitis in mice. *Eur. J. Nutr.* 54, 959–969. doi: 10.1007/s00394-014-0772-2

Pan, X., Zong, Q., Liu, C., Wu, H., Fu, B., Wang, Y., et al. (2024). Konjac glucomannan exerts regulatory effects on macrophages and its applications in biomedical engineering. *Carbohydr Polym.* 345, 122571. doi: 10.1016/j.carbpol.2024.122571

Pedrosa L de, F., and Fabi, J. P. (2024). Polysaccharides from medicinal plants: bridging ancestral knowledge with contemporary science. *Plants.* 13, 1721. doi: 10.3390/plants13131721

Qi, C., and Chen, L. (2024). Progress of ligand-modified agarose microspheres for protein isolation and purification. *Microchimica Acta* 191, 149. doi: 10.1007/s00604-024-06224-4

Qi, Y., Gao, P., Yang, S., Li, L., Ke, Y., Zhao, Y., et al. (2024). Unveiling the impact of nitrogen deficiency on alkaloid synthesis in konjac corms (Amorphophallus muelleri Blume). *BMC Plant Biol.* 24, 923. doi: 10.1186/s12870-024-05642-z

Qin, Y., Yan, Z., Gu, H., Wang, Z., Jiang, X., Chen, Z., et al. (2019). Effects of different shading rates on the photosynthesis and corm weight of konjac plant. *Not Bot. Horti Agrobot Cluj Napoca* 47 (3), 716–721. doi: 10.15835/nbha47311437

Rahman, W., Cahyaningsih, R., Herawati, H., Aminah, A., Risliawati, A., Diantina, S., et al. (2024). Harnessing plant genetic diversity in research on industrial crop plants for environmental conservation concerns. In: N. Kumar (ed) *Industrial Crop Plants. Interdisciplinary Biotechnological Advances*. (Singapore: Springer), 293–313. doi: 10.1007/978-981-97-1003-4_11

Reimer, R. A., Yamaguchi, H., Eller, L. K., Lyon, M. R., Gahler, R. J., Kacinik, V., et al. (2013). Changes in visceral adiposity and serum cholesterol with a novel viscous polysaccharide in Japanese adults with abdominal obesity. *Obesity.* 21 (9), E379–87. doi: 10.1002/oby.20435

Santos, R. D., Nasir, K., and Blumenthal, R. S. (2011). "LDL targeted therapies," in *Asymptomatic atherosclerosis. Totowa* (Humana Press;, NJ), 605–619.

Sawai, S., Mohktar, M. S., Safwani, W. K. Z. W., and Ramasamy, T. S. (2019). Suppression of the viability and proliferation of hepG2 hepatocellular carcinoma cell line by konjac glucomannan. *Anticancer Agents Med. Chem.* 18, 1258–1266. doi: 10.2174/1871520618666180307143229

Sengupta, P., Tiwari, N., Bhatt, T., and Paul, A. T. (2022). Mechanistically acting anti-obesity compositions/formulations of natural origin: a patent review (2010–2021). *Expert Opin. Ther. Pat.* 32, 29–46. doi: 10.1080/13543776.2021.1954161

Shah, B. R., Li, B., Al Sabbah, H., Xu, W., and Mráz, J. (2020). Effects of prebiotic dietary fibers and probiotics on human health: With special focus on recent advancement in their encapsulated formulations. *Trends Food Sci. Technol.* 102, 178–192. doi: 10.1016/j.tifs.2020.06.010

Shah, B. R., Li, B., Wang, L., Liu, S., Li, Y., Wei, X., et al. (2015a). Health benefits of konjac glucomannan with special focus on diabetes. *Bioactive Carbohydrates Dietary Fibre.* 5, 179–187. doi: 10.1016/j.bcdf.2015.03.007

Shah, B. R., Li, B., Wang, L., Liu, S., Li, Y., Wei, X., et al. (2015b). Health benefits of konjac glucomannan with special focus on diabetes. *Bioactive Carbohydrates Dietary Fibre.* 5, 179–187. doi: 10.1016/j.bcdf.2015.03.007

Shang, L., Wang, Y., Ren, Y., Ai, T., Zhou, P., Hu, L., et al. (2020). *In vitro* gastric emptying characteristics of konjac glucomannan with different viscosity and its effects on appetite regulation. *Food Funct.* 11, 7596–7610. doi: 10.1039/D0FO01104E

Shen, C., Li, X., Qin, J., and Duan, L. (2024). Characterization of miRNA profiling in konjac-derived exosome-like nanoparticles and elucidation of their multifaceted roles in human health. *Front. Plant Sci.* 15, 1444683. doi: 10.3389/fpls.2024.1444683

Shen, J., Li, Y., Yong, D., Tang, Y., and Wang, Y. (2024). Research and functionalization of konjac glucomannan and its hydrogel in wound dressing. *J. Polymer Eng.* 2024 (10), 58–72. doi: 10.1515/polyeng-2024-0132

Shi, X. D., Yin, J. Y., Zhang, L. J., Huang, X. J., and Nie, S. P. (2019). Studies on O-acetyl-glucomannans from Amorphophallus species: Comparison of physicochemical

properties and primary structures. *Food Hydrocoll.* 89, 503–511. doi: 10.1016/j.foodhyd.2018.11.013

Song, H., Guo, R., Sun, X., Kou, Y., Ma, X., Chen, Y., et al. (2024). Integrated metabolomics and transcriptomics revealed the anti-constipation mechanisms of xylooligosaccharides from corn cobs. *Food Funct.* 15, 894–905. doi: 10.1039/D3FO04366E

Spirk, S. (2018). *Polysaccharides in batteries*. (Cham: Springer), 1, 9–57. doi: 10.1007/978-3-319-65969-5

Srividya, N., Haldipur, A. C., and Yerra, H. (2024). Lifestyle modifications and nutritional modulation of immune system for prevention and management of diabetes mellitus: Current perspectives. In: *Biochem. Immunol. Diabetes Associated Complications*. Elsevier, 313–330. doi: 10.1016/B978-0-443-13195-0.00016-8

Srzednicki, G., and Borompichaichartkul, C. (2020). *Konjac glucomannan* (Boca Raton: CRC Press).

Sun, Y., Xu, X., Wu, Z., Zhou, H., Xie, X., Zhang, Q., et al. (2023). Structure, merits, gel formation, gel preparation and functions of konjac glucomannan and its application in aquatic food preservation. *Foods.* 12, 1215. doi: 10.3390/foods12061215

Sun, Y., Xu, X., Zhang, Q., Zhang, D., Xie, X., Zhou, H., et al. (2023). Review of konjac glucomannan structure, properties, gelation mechanism, and application in medical biology. *Polymers (Basel).* 15 (8), 1852. doi: 10.3390/polym15081852

Suzuki, H., Oomizu, S., Yanase, Y., Onishi, N., Uchida, K., Mihara, S., et al. (2010). Hydrolyzed konjac glucomannan suppresses igE production in mice B cells. *Int. Arch. Allergy Immunol.* 152, 122–130. doi: 10.1159/000265533

Tian, Y., Li, C., Xue, W., Huang, L., and Wang, Z. (2023). Natural immunomodulating substances used for alleviating food allergy. *Crit. Rev. Food Sci. Nutr.* 63, 2407–2425. doi: 10.1080/10408398.2021.1975257

Tsurumaki, M., Kotake, M., Iwasaki, M., Saito, M., Tanaka, K., Aw, W., et al. (2015). The application of omics technologies in the functional evaluation of inulin and inulin-containing prebiotics dietary supplementation. *Nutr. Diabetes.* 5, e185–e185. doi: 10.1038/nutd.2015.35

Veerasubramanian, P. K., Thangavel, P., Kannan, R., Chakraborty, S., Ramachandran, B., Suguna, L., et al. (2018). An investigation of konjac glucomannan-keratin hydrogel scaffold loaded with Avena sativa extracts for diabetic wound healing. *Colloids Surf B Biointerfaces.* 165, 92–102. doi: 10.1016/j.colsurfb.2018.02.022

Vuorio, A., Kuoppala, J., Kovanen, P. T., Humphries, S. E., Tonstad, S., Wiegman, A., et al. (2017). Statins for children with familial hypercholesterolemia. *Cochrane Database Syst. Rev.* 2017 (7), CD006401. doi: 10.1002/14651858.CD006401.pub4

Wang, H., and Li, K. (2021). Research status and prospect in molecular biology of amorphophallus. *Medicinal Plant Res.* 11 (2), 1–7. doi: 10.5376/mpr.2021.11.0002

Watanabe, M., Risi, R., Masi, D., Caputi, A., Balena, A., Rossini, G., et al. (2020). Current evidence to propose different food supplements for weight loss: A comprehensive review. *Nutrients.* 12, 2873. doi: 10.3390/nu12092873

Widjanarko, S. B., Mubarok, A. Z., Hermanto, M. B., Nuriyanto, A. F. P., and Sianturi, M. T. (2024). Comparative analysis of glucomannan properties from wet and dry-extractions of porang (Amorphophallus muelleri blume) and commercial konjac glucomannan. *Trends Sci.* 22 (2), 8278. doi: 10.48048/tis.2025.8278

Wilianto, Y. R., Tjahjono, Y., Foe, K., Wijaya, S., Ervina, M., Setiadi, D. A., et al. (2024). A novel konjac rice formula with glucomannan and tapioca starch improve postprandial glycemic response – a randomized single-blind clinical trial. *Nutr. Food Sci.* 54, 1437–1450. doi: 10.1108/NFS-12-2023-0290

Wu, W. T., Cheng, H. C., and Chen, H. L. (2011). Ameliorative effects of konjac glucomannan on human faecal β-glucuronidase activity, secondary bile acid levels and faecal water toxicity towards Caco-2 cells. *Br. J. Nutr.* 105, 593–600. doi: 10.1017/S0007114510004009

Xia, P., Zheng, Y., Sun, L., Chen, W., Shang, L., Li, J., et al. (2024). Regulation of glycose and lipid metabolism and application based on the colloidal nutrition science properties of konjac glucomannan: A comprehensive review. *Carbohydr Polym.* 331, 121849. doi: 10.1016/j.carbpol.2024.121849

Xu, Z., Sun, Y., Yang, Y., Ding, J., and Pang, J. (2007). Effect of γ-irradiation on some physiochemical properties of konjac glucomannan. *Carbohydr Polym.* 70, 444–450. doi: 10.1016/j.carbpol.2007.05.011

Xu, C., Yu, C., Yang, S., Deng, L., Zhang, C., Xiang, J., et al. (2023). Effects of physical properties of konjac glucomannan on appetite response of rats. *Foods.* 12, 743. doi: 10.3390/foods12040743

Xu, R., Zheng, X., Chen, C., Li, M., Li, J., Zhou, H., et al. (2024). Effects of different substrates on the growth and yield of Amorphophallus muelleri. *Heliyon.* 10, e31501. doi: 10.1016/j.heliyon.2024.e31501

Yan, Q., Wang, W., Fan, Z., Li, B., Wei, Y., Yu, R., et al. (2024). Gut microbes mediate prebiotic-like effects of resistant starch. *Food Biosci.* 61, 104627. doi: 10.1016/j.fbio.2024.104627

Yang, D., Yuan, Y., Wang, L., Wang, X., Mu, R., Pang, J., et al. (2017). A review on konjac glucomannan gels: microstructure and application. *Int. J. Mol. Sci.* 18, 2250. doi: 10.3390/ijms18112250

Ye, S., Zongo, A. W. S., Shah, B. R., Li, J., and Li, B. (2021). Konjac glucomannan (KGM), deacetylated KGM (Da-KGM), and degraded KGM derivatives: A special focus on colloidal nutrition. *J. Agric. Food Chem.* 69, 12921–12932. doi: 10.1021/acs.jafc.1c03647

Yu, Y., Shen, M., Song, Q., and Xie, J. (2018). Biological activities and pharmaceutical applications of polysaccharide from natural resources: A review. *Carbohydr Polym.* 183, 91–101. doi: 10.1016/j.carbpol.2017.12.009

Yuan, Y., Hong, X., Mu, R., Gong, J., Wang, L., Huang, R., et al. (2017). Structure and properties of konjac glucomannan/galactoglucomannan nanofiber membrane. *Macromol Res.* 25, 963–970. doi: 10.1007/s13233-017-5125-6

Zhang, Y., Aldamarany, W. A. S., Deng, L., and Zhong, G. (2023). Carbohydrate supplementation retains intestinal barrier and ameliorates bacterial translocation in an antibiotic-induced mouse model. *Food Funct.* 14, 8186–8200. doi: 10.1039/D3FO01343J

Zhang, C., da, C. J., and qing, Y. F. (2014). Konjac glucomannan, a promising polysaccharide for OCDDS. *Carbohydr Polym.* 104, 175–181. doi: 10.1016/j.carbpol.2013.12.081

Zhang, Y., Huo, W., Hou, J., Liu, L., Yu, X., and Xu, L. (2022a). Effects and benefits of orchid mycorrhizal symbionts on dendrobium officinale. *Horticulturae.* 8 (10), 861. doi: 10.3390/horticulturae8100861

Zhang, Y., Tong, C., Chen, Y., Xia, X., Jiang, S., Qiu, C., et al. (2024). Advances in the construction and application of konjac glucomannan-based delivery systems. *Int. J. Biol. Macromol.* 262, 129940. doi: 10.1016/j.ijbiomac.2024.129940

Zhang, B., Zhang, M., Tian, J., Zhang, X., Zhang, D., Li, J., et al. (2024). Advances in the regulation of radiation-induced apoptosis by polysaccharides: A review. *Int. J. Biol. Macromol.* 263, 130173. doi: 10.1016/j.ijbiomac.2024.130173

Zhang, H., Zhang, F., and Yuan, R. (2020). Applications of natural polymer-based hydrogels in the food industry. *In: Hydrogels Based Natural Polymers. Elsevier;*, 357–410. doi: 10.1016/B978-0-12-816421-1.00015-X

Zhang, Y., Zhao, Y., Yang, W., Song, G., Zhong, P., Ren, Y., et al. (2022b). Structural complexity of Konjac glucomannan and its derivatives governs the diversity and outputs of gut microbiota. *Carbohydr Polym.* 292, 119639. doi: 10.1016/j.carbpol.2022.119639

Zhang, Q., Zhong, D., Ren, Y. Y., kuan, M. Z., Pegg, R. B., and Zhong, G. (2021a). Effect of konjac glucomannan on metabolites in the stomach, small intestine and large intestine of constipated mice and prediction of the KEGG pathway. *Food Funct.* 12, 3044–3056. doi: 10.1039/D0FO02682D

Zhang, Q., Zhong, D., Sun, R., Zhang, Y., Pegg, R. B., and Zhong, G. (2021b). Prevention of loperamide induced constipation in mice by KGM and the mechanisms of different gastrointestinal tract microbiota regulation. *Carbohydr Polym.* 256, 117418. doi: 10.1016/j.carbpol.2020.117418

Zheng, Y., Liu, Q., Luo, H., Zheng, J., and Li, W. (2024a). Effect of pretreatment with electron beam irradiation on the deacetylation efficiency of konjac glucomannan and its structural, physicochemical and gel properties. *Int. J. Biol. Macromol.* 276 (1), 133887. doi: 10.1016/j.ijbiomac.2024.133887

Zheng, Y., Luo, H., Liu, Q., Zheng, J., and Li, W. (2024b). Electron beam irradiation-assisted preparation of oxidized konjac glucomannan and its structural and physicochemical properties. *Food Hydrocoll.* 154, 110088. doi: 10.1016/j.foodhyd.2024.110088

Zhou, N., Zheng, S., Xie, W., Cao, G., Wang, L., and Pang, J. (2022). Konjac glucomannan: A review of structure, physicochemical properties, and wound dressing applications. *J. Appl. Polym Sci.* 139 (11), 51780. doi: 10.1002/app.v139.11

Zhu, F. (2018). Modifications of konjac glucomannan for diverse applications. *Food Chem.* 256, 419–426. doi: 10.1016/j.foodchem.2018.02.151

Zhu, S., Yang, J., Xia, P., Li, S., Wang, Q., Li, K., et al. (2024). Effects of konjac glucomannan intake patterns on glucose and lipid metabolism of obese mice induced by a high fat diet. *Food Funct.* 15, 9116–9135. doi: 10.1039/D4FO02442G

Zhuang, K., Shu, X., and Xie, W. (2024). Konjac glucomannan-based composite materials: Construction, biomedical applications, and prospects. *Carbohydr Polym.* 344, 122503. doi: 10.1016/j.carbpol.2024.122503

frontiers | Frontiers in Plant Science

TYPE Original Research
PUBLISHED 24 March 2025
DOI 10.3389/fpls.2025.1562931

OPEN ACCESS

EDITED BY
Eman A. Mahmoud,
Damietta University, Egypt

REVIEWED BY
Cassandra Terry,
London Metropolitan University,
United Kingdom
Rohit Jain,
Manipal University Jaipur, India

*CORRESPONDENCE
Furkan Coban
furkan.coban@slu.se

RECEIVED 20 January 2025
ACCEPTED 05 March 2025
PUBLISHED 24 March 2025

CITATION
Coban F, Ozer H, Yilmaz B and Lan Y (2025) Characterization of bioactive compounds in fenugreek genotypes in varying environments: diosgenin, trigonelline, and 4-hydroxyisoleucine.
Front. Plant Sci. 16:1562931.
doi: 10.3389/fpls.2025.1562931

Characterization of bioactive compounds in fenugreek genotypes in varying environments: diosgenin, trigonelline, and 4-hydroxyisoleucine

Furkan Coban[1,2]*, Hakan Ozer[2], Bilal Yilmaz[3] and Yuzhou Lan[1]

[1]Department of Plant Breeding, The Swedish University of Agricultural Sciences, Lomma, Sweden, [2]Department of Field Crops, Faculty of Agriculture, Ataturk University, Erzurum, Türkiye, [3]Department of Analytical Chemistry, Faculty of Pharmacy, Ataturk University, Erzurum, Türkiye

This study investigates the effects of irrigated and non-irrigated conditions on the bioactive compound content in fenugreek (*Trigonella foenum-graecum*) across 31 diverse genotypes from various geographical regions. The study was conducted at Atatürk University Research and Extension Center, Türkiye (N 39° 55'59.9", E 41°14'10.6", altitude 1789 m) during the 2021 and 2022 growing seasons. The levels of diosgenin, trigonelline, and 4-hydroxyisoleucine analyzed under irrigated and non-irrigated conditions were found to be significantly influenced by genotype, environment, and their interaction (Genotype × Environment), with a highly significant effect observed at the $p < 0.001$ level. The compounds analyzed included diosgenin (0.50-0.93%), trigonelline (5.22-13.65 mg g^{-1}), and 4-hydroxyisoleucine (0.41-1.90%). Notably, genotypes such as Sivas/TR, Amasya/TR, Konya/TR and Samsun/TR exhibited higher diosgenin content across all conditions, while Spain, Malaysia, France, and India showed higher trigonelline content under irrigation. Variability in 4-hydroxyisoleucine content was observed, with some genotypes showing stability across different environmental conditions. A negative correlation between diosgenin and trigonelline was observed in fenugreek. Furthermore, Principal Component Analysis (PCA) and cluster analysis were found to be effective in revealing genetic diversity, morphological differences, and genotype adaptability. The findings highlight the potential for selecting superior genotypes for breeding programs focused on enhancing bioactive compound yields, especially under varying irrigation and non-irrigated conditions. This research emphasizes the critical role of environmental and genetic factors in optimizing the production of health-benefiting compounds in fenugreek.

KEYWORDS

diosgenin, trigonelline, 4-hydroxyisoleucine, fenugreek, genetic background

1 Introduction

Fenugreek (*Trigonella foenum-graecum*), widely recognized for its culinary and medicinal applications, is an annual herb belonging to the family Leguminosae (Zandi et al., 2015; Maloo et al., 2023). Fenugreek is a rich source of bioactive compounds beyond its traditional uses, particularly diosgenin, trigonelline, and 4-hydroxyisoleucine, which have demonstrated significant health benefits (Figure 1). Diosgenin has been recognized for its positive effects on glucose metabolism and diabetes management (Narender et al., 2006). Trigonelline plays a crucial role in reducing oxidative stress, which is a key factor in the development of cardiovascular diseases and neurodegenerative disorders (Mohammad-Sadeghipour et al., 2021). Additionally, 4-hydroxyisoleucine has been identified as a key amino acid that enhances insulin secretion, making it a promising candidate for type 2 diabetes treatment (Faisal et al., 2024). Given these bioactive compounds, fenugreek has been increasingly studied for its potential role in managing chronic diseases such as diabetes, cardiovascular diseases, and metabolic syndrome (Khorshidian et al., 2016; Nguyen et al., 2024; Tak et al., 2024).

Bioactive compounds in plants are significantly influenced by various environmental factors, including temperature, light, soil nutrients, water availability, and interactions with other organisms (Qaderi et al., 2023; Tsipinana et al., 2023). These environmental conditions lead to noticeable differences in the production of secondary metabolites (Khare et al., 2020; Fouad et al., 2023). Irrigation plays a critical role in promoting optimal plant growth, biomass production, and overall yield. Adequate water supply ensures the proper maintenance of plant physiological processes and photosynthesis, resulting in significant growth improvements (Prinsloo and Nogemane, 2018). Under sufficient irrigation (defined as 100% of the crop water requirement, ETc), plants effectively synthesize primary metabolites and, under favorable conditions, produce secondary metabolites at notable levels. In contrast, non-irrigated conditions rely solely on natural precipitation, which may not fully meet the water demands of plants, potentially limiting growth and metabolism (Isah, 2019). However, secondary metabolite levels in plants may be lower under drought stress due to the adequate water supply reducing environmental stress and suppressing the metabolic signals that trigger the production of defense-related secondary metabolites (Zarinkamar et al., 2022; Camlica and Yaldiz, 2024). On the other hand, the increase in secondary metabolites in plants irrigated before drought reaches a critical level suggests that the production of these compounds is not solely a response to stress but is also linked to the plant's optimal metabolic functioning (Erb and Kliebenstein, 2020; Afrouz et al., 2023). Additionally, irrigation enhances primary metabolite production, thereby supporting the formation of precursor molecules required for the synthesis of secondary metabolites (Al Kashgry et al., 2024). Agricultural management practices must integrate strategies that balance irrigation and environmental stress conditions, such as drought, heat stress, and salinity, to achieve both resilience and high productivity. Climate change, characterized by rising temperatures, irregular rainfall, and prolonged droughts, directly impacts plant metabolism, emphasizing the need for robust stress tolerance mechanisms. Managing genetic and environmental factors harmoniously is crucial, especially for regulating secondary metabolite production under varying environmental conditions (Gadanakis et al., 2015; Yoon et al., 2020).

Diosgenin is a bioactive compound found in fenugreek seeds, possessing significant potential for diabetes treatment. Diosgenin mitigates the harmful effects of diabetes in rodents by reducing insulin resistance, lowering plasma glucose levels, and promoting pancreatic beta cell regeneration (Tharaheswari et al., 2014). Its antioxidant properties help reduce oxidative stress and provide cellular protection. Studies have demonstrated that diosgenin significantly decreases plasma glucose levels, increases insulin levels in diabetic rats, and inhibits cancer cell growth while inducing apoptosis (Pari et al., 2012; Hao et al., 2015; Tak et al., 2024). This compound stands out as a promising bioactive ingredient in the treatment of chronic diseases like diabetes and cancer.

Another remarkable compound, trigonelline (TRG) is a naturally occurring alkaloid with promising therapeutic potential due to its multifaceted pharmacological properties. TRG has been recognized for its potential in managing metabolic, inflammatory, and oxidative stress-related conditions; (Nguyen et al., 2024). TRG can modulate glucose and lipid metabolism, making it beneficial for patients with diabetes and obesity (Hamden et al., 2013; Yoshinari et al., 2013; Ilavenil et al., 2015). Moreover, it exhibits anti-inflammatory and antioxidant properties, which are crucial in mitigating chronic inflammatory diseases and oxidative stress (Hamadi, 2012; Zhou et al., 2013; Li et al., 2019). TRG also shows neuroprotective effects, offering potential benefits in treating neurodegenerative disorders like Alzheimer's and Parkinson's diseases, as well as cognitive impairments and diabetic neuropathy (Makowska et al., 2014; Fahanik-Babaei et al., 2019; Farid et al., 2020; Liang et al., 2023);. Additionally, TRG has been observed to protect against liver and kidney injuries, cardiovascular diseases, and certain cancers by inhibiting tumor cell proliferation and inducing apoptosis (Afifi et al., 2017; Peerapen et al., 2023)e;. These broad-spectrum therapeutic effects underline TRG's potential as a valuable natural compound in developing treatments for various pathological conditions (Yoshinari and Igarashi, 2010; Costa et al., 2020).

Also, another compound found in the fenugreek seed is 4-Hydroxyisoleucine (4-HIL). This amino acid exhibits notable antihyperglycemic and antihyperlipidemic properties (Narender et al., 2006). It enhances insulin secretion, thereby lowering blood glucose levels, and reduces plasma triglycerides, total cholesterol, and free fatty acids while increasing the HDL-C/TC ratio. Studies have shown that 4-HIL regulates key genes involved in lipid metabolism, in human colorectal cancer cells, indicating its potential therapeutic role in managing metabolic disorders like diabetes and dyslipidemia (Mohammad-Sadeghipour et al., 2021).

In recent years, research on the adaptation of fenugreek genotypes to environmental conditions has increased both in Türkiye and globally (Beyzi et al., 2021; Maloo et al., 2023;

Camlica and Yaldiz, 2024; Camlica et al., 2024; Coban et al., 2024; Ghosaliya et al., 2024; Haliloğlu et al., 2024). Changing climate conditions, particularly drought and irregular rainfall patterns, are significant stress factors that negatively impact the growth and yield potential of fenugreek (Abd-El-Wahab et al., 2023; Dobeie et al., 2024). However, fenugreek stands out not only for its agricultural use but also for its bioactive compounds, which have important applications in the health sector. Additionally, due to its suitability for mechanization, short vegetation period, and low production cost, fenugreek is considered a more suitable alternative to plants from the Dioscorea family, traditionally used for diosgenin production (Coban, 2021). These characteristics make fenugreek a valuable resource for both sustainable agriculture and the pharmaceutical and food industries.

This study aims to provide a novel perspective on the production of significant bioactive compounds in fenugreek by investigating the impact of irrigated and non-irrigated conditions on 31 diverse genotypes collected from different regions worldwide. By combining multivariate statistical approaches, this research uniquely elucidates the complex genotype-environment interactions that influence the production of diosgenin, trigonelline, and 4-hydroxyisoleucine. Furthermore, it identifies the regions and genotypes with the highest bioactive compound content, offering valuable insights for the selection of superior genotypes in future breeding programs. This comprehensive evaluation not only highlights the genetic and environmental factors driving metabolite variability but also addresses the increasing demand for bioactive compound-rich crops in the context of climate change and sustainable agriculture.

2 Materials and methods

2.1 Plant materials

In this research, 31 distinct fenugreek seed genotypes were obtained from diverse locations, including Iran (IR), Türkiye (TR), Egypt, Germany, South Sudan, France, Australia, Spain, Morocco, Ukraine, China, Serbia, Israel, Malaysia, Pakistan, and India (Table 1). Berkem, Çiftçi, and Güraslan are genotypes that were previously registered by the Seed Registration and Certification Center Directorate of Türkiye. The seeds were obtained from research centers, international seed banks, field projects, local vendors, and local producers. The classification of fenugreek seed genotypes into Group A and Group B was primarily based on observable phenotypic and genotypic differences. These differences were particularly prominent in genotypes originating from Iran (IR) and Türkiye (TR). During preliminary analyses, these genotypes exhibited significantly distinct results in several key traits, such as germination rates and environmental adaptability. These remarkable regional variations led to the inclusion of genotypes from Iran and Türkiye in Group B to facilitate a more detailed analysis of their unique characteristics. In contrast, genotypes obtained from other regions (Group A) displayed more homogeneous traits, aligning with broader global patterns. In this context, the classification of genotypes in this manner aimed not only to highlight the distinctiveness of Iranian and Turkish genotypes but also to provide a clearer framework for comparing regional and global trends observed in the study. Accession numbers are also listed in Table 1.

TABLE 1 Origin, accession numbers and group classification of fenugreek genotypes.

Origin	Accessions	Group	Accession Type
Urmia/IR	ZFTB0001	B	Population
Yozgat/TR	ZFTB0002	B	Population
Samsun/TR	ZFTB0003	B	Population
Sanliurfa/TR	ZFTB0004	B	Population
Sivas/TR	ZFTB0005	B	Population
Corum/TR	ZFTB0006	B	Population
Egypt	ZFTB0007	A	Population
Germany	ZFTB0009	A	Population
Kermanshah/IR	ZFTB0010	B	Population
Berkem/TR	ZFTB0011	B	Cultivar
South Sudan	ZFTB0012	A	Population
Güraslan/TR	ZFTB0013	B	Cultivar
France	ZFTB0014	A	Population
Australia	ZFTB0015	A	Population
Spain	ZFTB0016	A	Population
Morocco	ZFTB0017	A	Population
Ukraine	ZFTB0018	A	Population
China	ZFTB0019	A	Population
Salmas/IR	ZFTB0020	B	Population
Kayseri/TR	ZFTB0021	B	Population
Serbia	ZFTB0022	A	Population
Israel	ZFTB0023	A	Population
Tokat/TR	ZFTB0024	B	Population
Malaysia	ZFTB0026	A	Population
Konya/TR	ZFTB0027	B	Population
Karaman/TR	ZFTB0028	B	Population
Ahvaz/IR	ZFTB0029	B	Population
Amasya/TR	ZFTB0030	B	Population
Pakistan	ZFTB0031	A	Population
India	ZFTB0034	A	Population
Çiftçi/TR	ZFTB0035	B	Cultivar

"TR" represents Türkiye, and "IR" represents Iran.

2.2 Site and experiment description

The field experiment was conducted at Ataturk University Research and Extension Center (39°55'59.9"N, 41°14'10.6"E) in Türkiye, located at an altitude of 1789 m. The study was laid out in a Randomized Complete Block Design (RCBD) with three replications. The experimental plots, measuring 5.0 m x 1.2 m, were sown with spring wheat as the previous crop in both years. Fenugreek seeds were sown at a rate of 40 kg ha^{-1} with a row spacing of 30 cm. Fenugreek seeds were sown at a rate of 40 kgha-1 with a row spacing of 30 cm (Supplementary Video 1). Irrigation was performed during the flowering and seed formation stages, when the water demand of fenugreek plants increases, using the furrow irrigation method. Groundwater was used for irrigation, supplied from an irrigation pond located near the experimental area. The irrigation water was classified as high-quality water with no salinity or sodium-related issues. A total of five irrigation applications were carried out in 2021, whereas four irrigation applications were performed in 2022 to fulfill the water requirements of fenugreek. After harvesting, the seeds were stored under appropriate conditions to maintain their quality. To prevent the deterioration of genetic material, the seeds were preserved at 4°C with a moisture content of 8-10%. These conditions are considered ideal for ensuring the homogeneity of the genotypes and the accuracy of subsequent analyses. Table 2 presents detailed information about the research. Field trials were established as separate experiments under irrigated and non-irrigated conditions.

It was observed that the total rainfall in the first year was lower than the average of the second year and long-term average. In 2021, the lowest rainfall was recorded in May and June (3.8 mm and 2.4 mm, respectively), which are critical months for plant emergence and growth, while rainfall increased in July and August. In contrast, in 2022, rainfall in May and June (41.0 mm and 65.2 mm, respectively) was significantly higher, but it dropped to very low levels in July and August. The average temperatures in 2021 and 2022 were similar. Particularly in 2021, the combination of low rainfall during critical growth periods and high temperatures highlighted an increased risk of drought (Table 3). Indeed, 2021 was recorded as the driest year in Türkiye in the last 20 years (Soylu Pekpostalci et al., 2023). Due to germination and emergence problems in trials conducted under non-irrigated conditions, data could not be collected homogeneously, and reliable results could not be obtained. Therefore, the dry conditions of 2021 were excluded from the study. Based on this, the research continued under the following conditions: 2021-irrigated, 2022-non-irrigated, and 2022-irrigated. It has been determined that the soils have a slightly alkaline character, with low levels of total nitrogen, available phosphorus, and lime, very low levels of organic matter, and, on the other hand, are rich in plant-available potassium.

TABLE 2 Site and experimental design details.

Site Coordinates	N 39°55'59.9" E 41°14'10.6"	
Location	Ataturk University Research and Extension Center/Türkiye	
Altitude (m)	1789	
Study design	Randomized Complete Blok Design (RCBD-three replications)	
Previous crop	Spring wheat (both year)	
Plot size	5.0 m x 1.2 m	
Rows space	30 cm	
Sowing rate	40 kg ha^{-1}	
Sowing method	Plot drill (Pocta, Model CP-1 SR-1)	
Nitrogen fertilezer, IR	40 kg N ha^{-1} (AS*)	
Phosphor fertilezer, IR	60 kg N ha^{-1} (TSP**)	
Nitrogen fertilezer, Non-IR	20 kg N ha^{-1} (AS)	
Phosphor fertilezer, Non-IR	30 kg N ha^{-1} (TSP)	
*Soil texture****	Clay-loam	
Soil pH (0-30 cm depth)	7.45	
$CaCO_3$ (%)	0.795	
Organic matter (%)	1.29	
P_2O_5 (kg/ha)	77.3	
K_2O (kg/ha)	1633.3	
	2021	2022
Irrigation Management [&]	5x	4x
Sowing Date	6 May	6 May
Vegetation Day	108-132	101-138

*AS, ammonium sulfate; **TSP, triple superphosphate; ***The soil properties are provided according to the average of the years. [&]Specified for irrigated conditions.

2.3 Determination of bioactive compounds

2.3.1 Determination of diosgenin (%)

Diosgenin content was quantified using a modified version of the method reported by Taylor et al. (2000). In this process, 10 g of dried and powdered fenugreek seeds were first defatted using petroleum ether (Merck, Darmstadt, Germany) in a Soxhlet apparatus (Isolab, Wertheim, Germany) for 6 hours. After filtering and drying the material, an extract was obtained with 300 mL of 80% ethanol (Sigma-Aldrich) using a rotary evaporator (Heidolph Instruments GmbH and Co.KG, Schwabach, Germany) at 80°C. After evaporating the solvent, the remaining extract was hydrolyzed with 120 mL of 70% isopropanol (Thermo Fisher Scientific, Bridgewater, NJ, USA) containing 1M H_2SO_4 (Merck) at 100°C for 2 hours. The solvent was evaporated again, and 90 mL of hexane (Sigma-Aldrich) was added to the remaining extract. The resulting extract was washed 3 times with 30 mL of 4N NaOH (Merck) and then 3 times with 30 mL of distilled water, after which the hexane was evaporated. The extracts were dissolved in 1 mL of methanol (Merck) and injected into a GC-MS system. For GC-MS analysis, an Agilent 6890N Gas Chromatography system (Agilent Technologies, Palo Alto, CA, USA) equipped with an Agilent 5973N CI/EI MS Detector and an Agilent 7673 Autosampler was used. Quantitative analysis of the prepared extracts was performed

TABLE 3 Climate data (temperature, precipitation, and relative humidity) for the vegetation period in the research area, encompassing long-term averages (1990–2020) along with sowing and harvest times for the years 2021 and 2022.

Years	Months					Annual precipitation (mm)/ Average temperature (°C) and humidity (%)
	May	June	July	August	September	
Precipitation (mm)						
1990–2020	52,3	41,0	25,2	16,7	4,32	139,5
2021	3,8	7,4	30,3	38,6	5,85	86,0
2022	41,0	65,2	3,10	8,10	0,30	117,7
Temperature (°C)						
1990-2020	10,5	14,9	19,2	19,4	14,1	15,6
2021	18,0	17,6	20,7	19,9	13,2	17,9
2022	10,9	16,7	20,5	23,3	21,6	18,6
Humidity (%)						
1990-2020	64,1	58,9	53,3	49,8	52,6	55,7
2021	36,3	43,3	47,7	48,6	45,6	44,3
2022	60,4	60,8	48,6	39,8	38,7	49,6

The data covers the months of May (May 6-31), June, July, August, and September (September 1-10).

using standard diosgenin (D1634 Sigma-Aldrich Diosgenin ≥93%) to construct a calibration curve to determine the diosgenin content in the extracts. A HP-5 MS column (Agilent Technologies, dimensions: 30 m x 0.250 mm ID and 0.25 µm film thickness) was employed for separation. The splitless injection sample technique (1 µL) and a helium carrier gas at a flow rate of 1 mL/min were used. The GC oven temperature program was set to start at 200°C, held for 1.0 minutes, then increased at a rate of 10°C per minute to 290°C, and held for 1.0 minute.

In the National Institute of Standards and Technology Library Version (2005), Software, Turbomass 5.2, the range of the obscure segment was compared with the range of the part stored identification of diosgenin. By comparing direct kovats maintenance list and mass spectra with those obtained from the MS library, the pieces could be separated. Every component relative rate measure was calculated by comparing its typical pinnacle region to the total areas. The test materials component names, atomic weights, and structures were uncovered. The purity and specificity of the method was investigated by observing interferences between diosgenin and the excipients. For GC-MS, electron impact mode with selected ion monitoring (SIM) was used for quantitative analysis (m/z 139 for diosgenin).

2.3.2 Determination of trigonelline (mg g^{-1})

To determine the TRG content in fenugreek seeds, we followed the method described by Shailajan et al. (2011) with slight modifications. Specifically, 10g of ground dry seed samples were diluted with 200 mL ethanol (Sigma-Aldrich) at a 1:10 ratio, mixed for 60 seconds on a vortex mixer (IKA, Staufen, Germany), and then placed on an orbital shaker (Heidolph Instruments GmbH and Co.KG, Schwabach, Germany) at 150 rpm for 12 hours. The mixture was filtered through Whatman No. 1 filter paper and stored at +4°C prior to analysis. For the standard solution (CAS Number: 6138-41-6; EC Number: 228-119-5; Sigma-Aldrich, USA), TRG (10 mg) was dissolved in 10 mL of methanol (Merck) to prepare a 1000 µg/mL stock solution. The high-performance liquid chromatography (HPLC) system (FRC-10A, Shimadzu Scientific Instruments, Japan) consisted of a diode-array detector (DAD, SPD-M20A), system control unit (LC-20ADXR), degassing unit (DGU-20ASR), pump (LC-20ADXR), column oven (CTO-10ASVP), and autosampler (SIL-20AXR). The TRG content in fenugreek seeds was quantified using a reverse-phase Inertsil ODS-3 column (5 µm, 250×4.6 mm, GL Sciences, Japan). The mobile phase consisted of methanol and ultrapure water (Milli-Q system, Millipore, Burlington, USA) at a ratio of 95:5 (v/v), adjusted to a pH of 3.5 with hydrochloric acid (HCl, Sigma-Aldrich). The analysis was carried out at 267 nm with a flow rate of 1.0 mL/min at room temperature (27 ± 1°C), and an injection volume of 10 µL was used.

2.3.3 Determination of 4-hydroxyisoleucine (%)

The 4-HIL content was determined by the method used by Abd-El Mawla and Osman (2011) with slight modifications. 10g of fenugreek seeds were placed in a centrifuge tube, and 5 mL of 1.0 M sulfuric acid was added. The mixture was homogenized and incubated in a water bath at 30°C for 2 hours. Then, 5 mL of ethyl acetate was added, mixed for 10 seconds using a vortex mixer, and centrifuged (5000 rpm, 5 minutes). The organic phase was collected and evaporated under a nitrogen gas stream. Finally, the residue was dissolved in 1.0 mL methanol and 20 µL was injected into the HPLC system. The 4-HIL content was expressed as a percentage of dry matter. The analysis was performed using an HPLC system with a DAD detector. A C18 reverse-phase column (5 µm, 250×4.6 mm i.d.) was used. The mobile phase consisted of

0.1 M ammonium hydroxide (A) and acetonitrile (B), and the analysis was conducted using a gradient elution technique with a gradient of 10-30% (B) over 30 minutes. The column flow rate was set at 1.0 mL/min, and detection was performed at a wavelength of 265 nm. The injection volume was 30 µL.

2.4 Data analysis

Statistical analyses were conducted in Microsoft Excel (2016) and RStudio (Team, 2015). To evaluate the interaction effect of genotype and environment, a two-way analysis of variance (ANOVA) was performed., Due to the lack of normal distribution of Diosgenin and 4-Hydroxyisoleucine content among genotypes, a permutation-based approach with a permutation number of 5000 was performed to assess the statistical significance of ANOVA outcome using the R package 'RVAideMemoire'. A pair-wise mean comparison was conducted between different environments using the posthoc LSD test with the R package 'agricolae'. A hierarchical clustering was conducted and visualized in the form of a heatmap using the R package 'pheatmap'. The relationship between diosgenin, TRG and 4-HIL was examined by linear regression. Principal component analysis (PCA) was conducted separately in each environment using the R package 'ggfortify'. To assess the stability of each genotype across three environments (2021irrigated, 2022-irrigated, 2022 non-irrigated), the additive main effects and multiplicative interaction (AMMI) were computed using the R package 'metan'.

3 Results

3.1 Genotypic variations in bioactive compounds in relation to environments

Basically, all three bioactive compounds i.e. Diosgenin, TRG and 4-HIL varied significantly among genotypes (Table 4), indicating promising genetic diversity of the genotypes used in this study. The hierarchical clustering based on three bioactive compounds divided 31 genotypes into two clusters, which matched our regional grouping method (group A and B) well with only two genotypes i.e. Germany and Ukraine allocated to the cluster dominated by Iran and Türkiye genotypes (Figure 2). Further, the changing environments, interacting with genotypic variations showed significant impacts ($p < 0.001$) on these bioactive compounds (Table 4).

TABLE 4 ANOVA table in the form of mean square values for Diosgenin, TRG and 4-HIL investigated in different environments (***sig. < 0.001).

	Genotype	Environment	Genotype * Environment
Degree of freedom	30	2	60
Diosgenin	0.085***	0.54***	0.0033***
TRG	6.29***	64.05***	8.23***
4-HIL	0.95***	2.66***	0.16***

Across the three environments, the content of diosgenin, TRG and 4-HIL ranged between 0.42 - 0.93%, 5.22 - 13.65 mg g^{-1} and 0.41 - 1.90%, respectively (Figure 3). Under 2021-irrigated conditions, the Samsun genotype (0.90%) exhibited the highest diosgenin content, while India (0.50%) had the lowest. In 2022-non-irrigated conditions, the Konya genotype (0.77%) showed the highest diosgenin content, followed by Samsun/TR (0.73%), Urmia/IR (0.72%), and Sivas/TR (0.69%), with India again having the lowest (0.42%). Under 2022-irrigated conditions, Samsun/TR (0.93%) consistently maintained the highest diosgenin content. For 4-hydroxyisoleucine (4-HIL), under 2021-irrigated conditions, the Amasya/TR genotype (1.63%) had the highest level, while under 2022-irrigated conditions, India (1.90%) and Malaysia (1.66%) genotypes led. Trigonelline content under 2021-irrigated conditions, with South Sudan (13.65 mg g^{-1}) showing the highest, while under 2022 -irrigated conditions, India recorded the highest (13.02 mg g^{-1}). Across both years, genotypes grown under irrigated conditions generally exhibited higher diosgenin, 4-HIL, and trigonelline contents, highlighting the significant influence of environmental conditions on bioactive compound production. Clearly, all the Group-B genotypes exhibited close values in diosgenin and TRG while the other Group-A genotypes varied more drastically. The 4-HIL showed a larger variation among both Group-B and Group-A genotypes, indicating a strong genetic diversity in this compound (Supplementary Table 1).

Therefore, a mean comparison was performed between Group-A and Group-B genotypes. Interestingly, the Group-B genotypes showed significantly higher content of diosgenin than the Group-A genotypes across three environments while Group-A genotypes were found with higher content of TRG than Group-B genotypes in 2021-irrigated environment. These trends implied a clear regional pattern of the diosgenin and TRG contained in fenugreek seeds. No difference was found in average 4-HIL content between Group A and Group B genotypes.

Genotypes grown in 2022-irrigated condition exhibited the significantly highest average content of diosgenin, TRG and 4-HIL across three environments (Figure 4). The 2022-non-irrigated environment resulted in the lowest average diosgenin content (Figure 4A) while no difference was found between 2022-non-irrigated and 2021-irrigated genotypes in TRG and 4-HIL content (Figures 4B, C).

3.2 Relationships between genotype and bioactive compounds in each environment

The Group-A genotypes, except for Germany and Ukraine, were all located with negative values on PC1, which primarily reflects the distribution of TRG content among genotypes with eigenvectors of -0.69 and -0.14 on PC1 and PC2 respectively. This negative assignment arises because TRG content was strongly correlated with the negative direction of PC1, as determined by

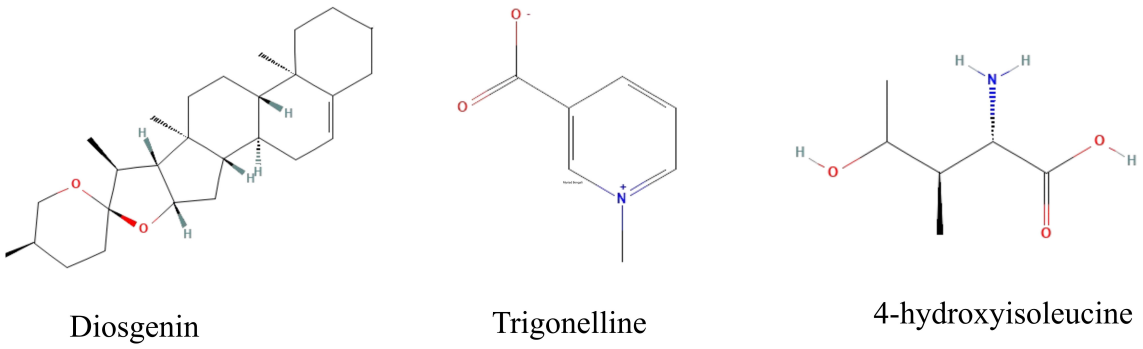

FIGURE 1
Chemical structures of diosgenin, trigonelline, and 4-hydroxyisoleucine.

the biplot analysis. PCA separates groups by maximizing variance along the first principal component (PC1), which explained 55.4% of the total variation in this analysis. In this case, the high TRG content of Group-A genotypes contributed significantly to the variation captured in the negative region of the PC1 axis. Thus, the positioning of Group-A genotypes along the negative PC1 axis clearly differentiates them from Group-B genotypes, which exhibited higher diosgenin content associated with positive PC1 values. This contrast highlights the primary traits defining each genotype group under the 2021-irrigated environment.

The second principal component (PC2) accounting for 31.5% of the total variation mainly differentiated the variation of 4-HIL,

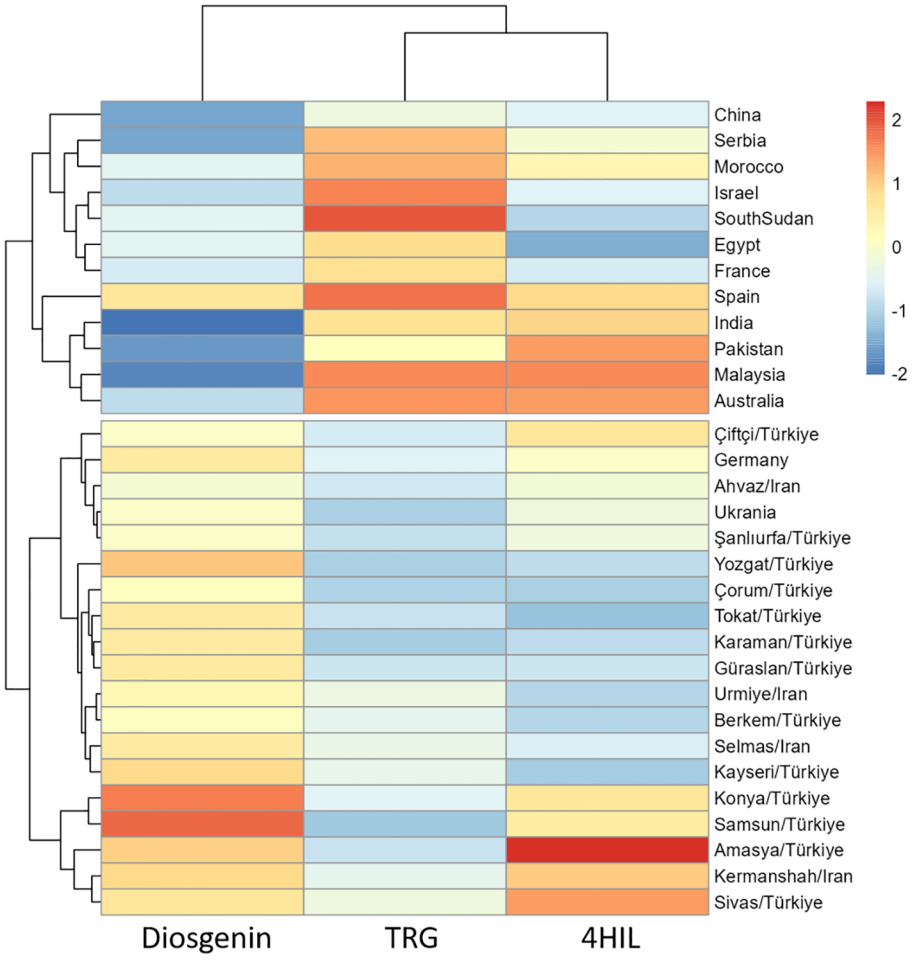

FIGURE 2
Cluster analysis of fenugreek genotypes based on diosgenin, TRG, 4-HIL.

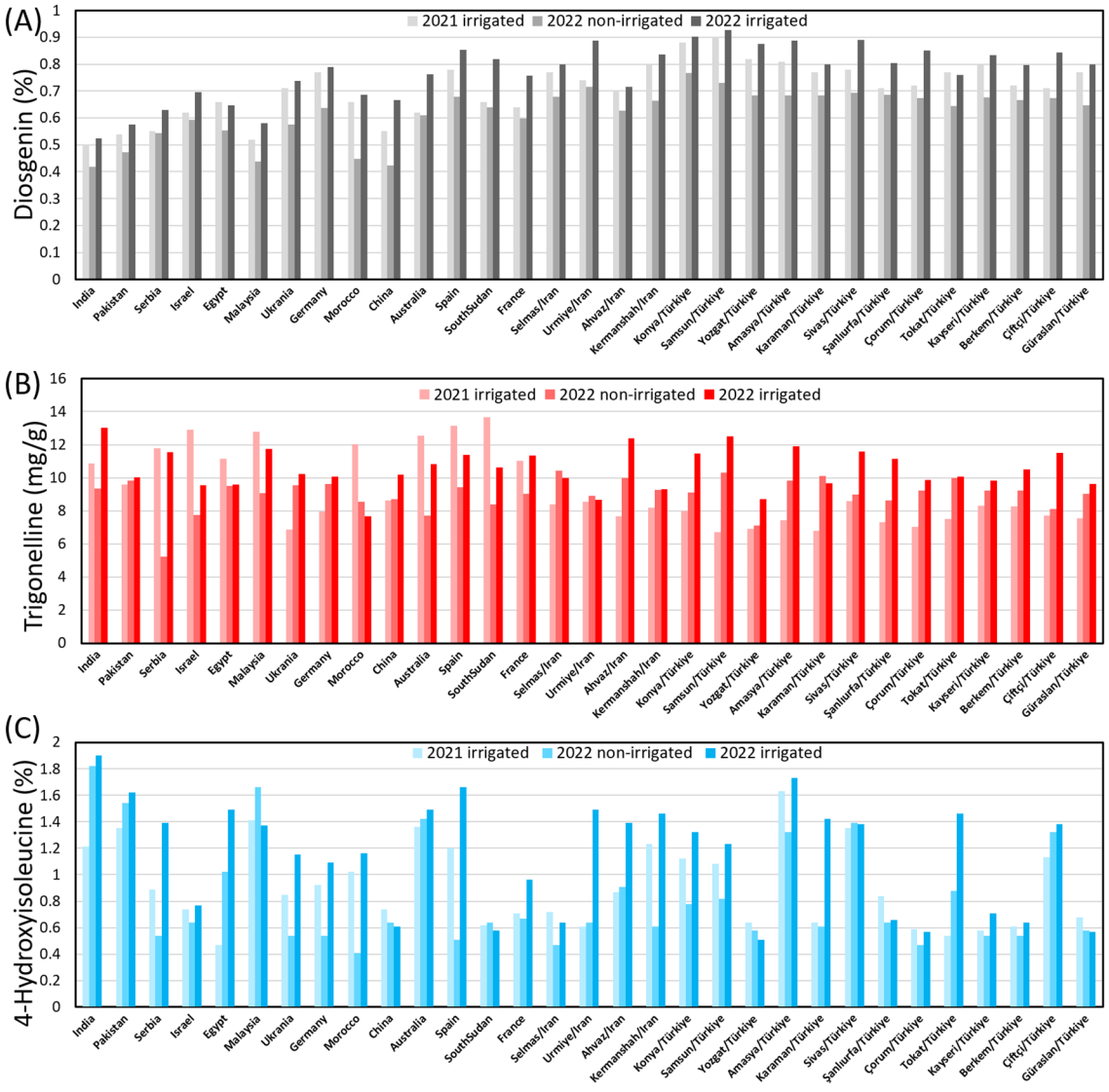

FIGURE 3
Genotypic variation in the content of **(A)** diosgenin, **(B)** TRG and **(C)** 4-HIL under three environments.

with eigenvectors of -0.29 and 0.95 on PC1 and PC2 respectively (Figure 5A). Under 2022-non-irrigated environment, the Group-B genotypes maintained a relatively high diosgenin content while several Group-A genotypes e.g. India, Pakistan and Malaysia exhibited a high 4-HIL (eigenvectors on PC1 and PC2: -0.67 and 0.37) (Figure 5B). Under 2022-irrigated environment, two genotype groups were separated along the PC2 axis, explaining 30.9% of the variation. Most Group-A genotypes distributed in the positive direction of PC2, indicating low values of TRG (eigenvectors on PC1 and PC2: -0.60 and -0.52) and diosgenin content (eigenvectors on PC1 and PC2: 0.43 and -0.85) in these genotypes, while Group-B genotypes such as Çiftçi/TR, Sivas/TR, Konya/TR, Amasya/TR and Samsun/TR showed positive correlations with high TRG and diosgenin (Figure 5C). Furthermore, among these three studied bioactive compounds, diosgenin displayed a significant negative correlation with TRG and 4-HIL under 2021-irrigated (Figure 6A) and 2022-non-irrigated (Figure 6B), respectively while TRG was found to be positively correlated with 4-HIL under 2022-irrigated environment (Figure 6C). This indicated that the changing climate and irrigation pattern influenced these compounds differently. Thus, they are likely to be controlled by separate genetic mechanisms.

3.3 Stability of genotypes in bioactive compounds across environments

The additive main effects and multiplicative interaction (AMMI) results showed a contrasting adaptability pattern of the 31 genotypes in diosgenin, TRG and 4-HIL. The high and stable diosgenin contents were found in Group B genotypes i.e. Sivas/TR, Amasya/TR, Konya/TR, Yozgat/TR and Samsun/TR (Figure 7A), while all the high and stable TRG contents were identified in Group

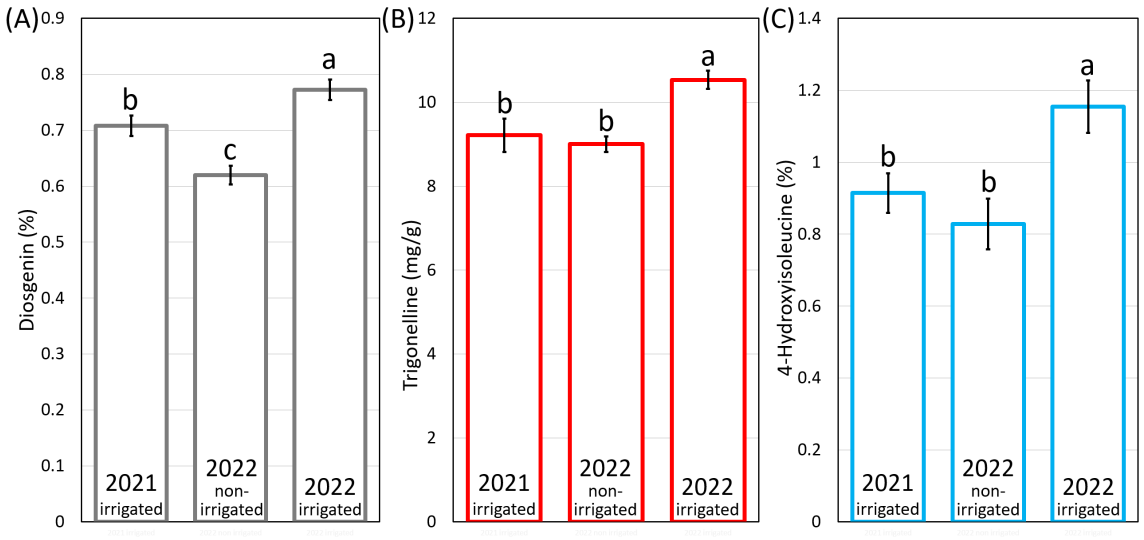

FIGURE 4
The average content of **(A)** diosgenin, **(B)** TRG and **(C)** 4-HIL under three environments. Means marked by the same letter do not differ significantly (LSD *post hoc* test at $p < 0.05$).

A genotypes i.e. Spain, Malaysia, France and India (Figure 7B). No clear regional pattern was found for genotypes with high and stable 4-HIL content (Figure 7C).

4 Discussion

The genetic structure of a plant is a fundamental factor in determining the synthesis and quantity of bioactive compounds. Different genotypes, owing to their unique metabolic pathways, can significantly influence the concentrations of these compounds, even within the same species. However, the regulation of bioactive compound synthesis is not solely dictated by genetics; environmental factors also play a crucial role. Temperature, rainfall, and light availability can substantially impact the levels of these compounds, either promoting or inhibiting their production (Khare et al., 2020; Mansinhos et al., 2024). While the genetic makeup establishes baseline production potential, environmental factors can modulate this potential, either enhancing or reducing the content of these compounds. Therefore, the interaction between genotype and environment is crucial, as it integrates these factors to shape the biosynthetic outcomes, determining which bioactive compounds are more prominently produced under a specific condition.

The impact of genotype-environment interactions becomes particularly evident when comparing fenugreek genotypes across

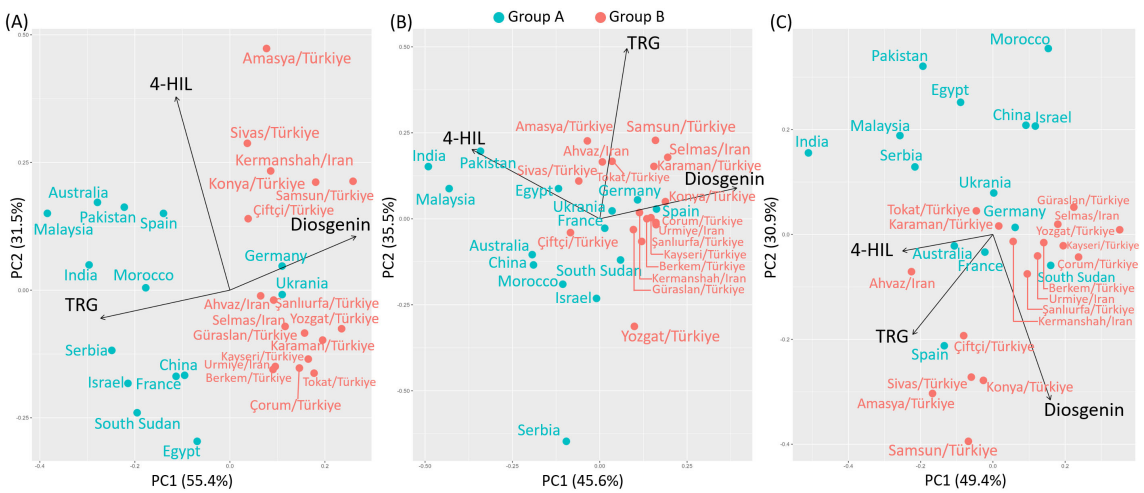

FIGURE 5
Principal component analysis (PCA) for the content of diosgenin, TRG and 4-HIL in Group A and Group B genotypes under **(A)** 2021-irrigated, **(B)** 2022-non-irrigated and **(C)** 2022-irrigated environments.

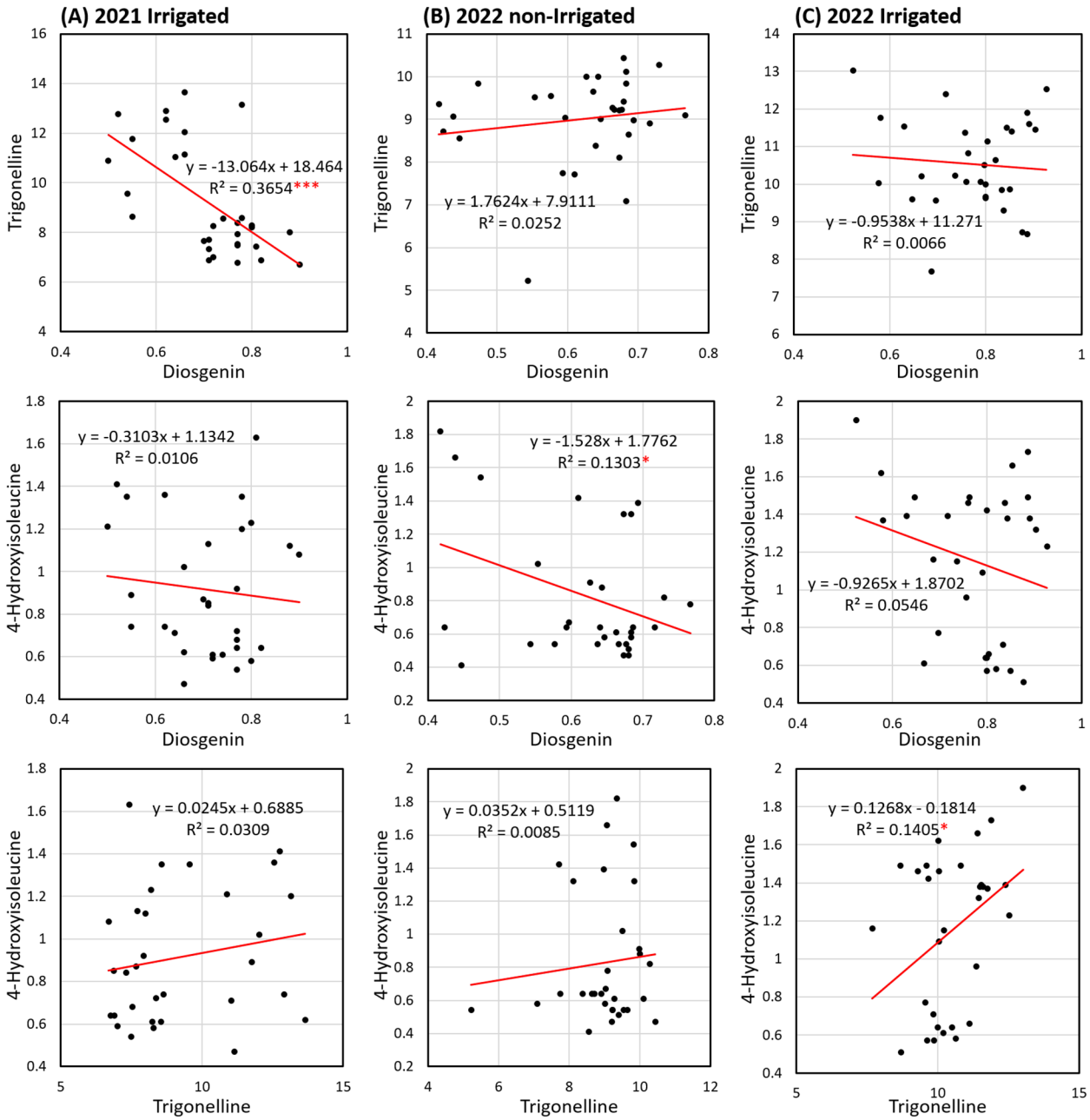

FIGURE 6
Linear regression (R2 = the coefficient of determination) of diosgenin versus TRG, diosgenin versus 4-HIL and TRG versus 4-HIL in 31 genotypes under three environments including **(A)** 2021-irrigated, **(B)** 2022-non-irrigated and **(C)** 2022-irrigated (*sig. < 0.05; ***sig. < 0.001).

different environmental conditions. The significant variations in compound concentrations observed among different fenugreek genotypes under varying environmental conditions can be attributed to genetic factors, environmental influences, and interactions. Genetic variability plays a critical role, with some genotypes exhibiting resilience to environmental stress, maintaining stable levels of bioactive compounds such as phenolics and antioxidants despite fluctuations in temperature, soil quality, and moisture (Singh et al., 2013). This genetic stability is often associated with specific alleles that enhance the synthesis of beneficial compounds under stress (Zandi et al., 2015). Conversely, other genotypes show significant variations in their chemical profiles due to their sensitivity to environmental changes, which may trigger or inhibit the biosynthetic pathways responsible for producing key phytochemicals (Güzel and Özyazıcı, 2021). For example, some genotypes increase polyphenol production under high temperatures or limited light, while others do not respond similarly. Additionally, genotype-environment interactions (G×E) significantly impact the phenotypic expression of compounds, as certain genotypes thrive in specific climatic and soil conditions while others perform poorly (Maurya et al., 2023; Camlica and Yaldiz, 2024; Coban et al., 2024). This interaction underscores the importance of selecting genotypes with favorable traits for specific

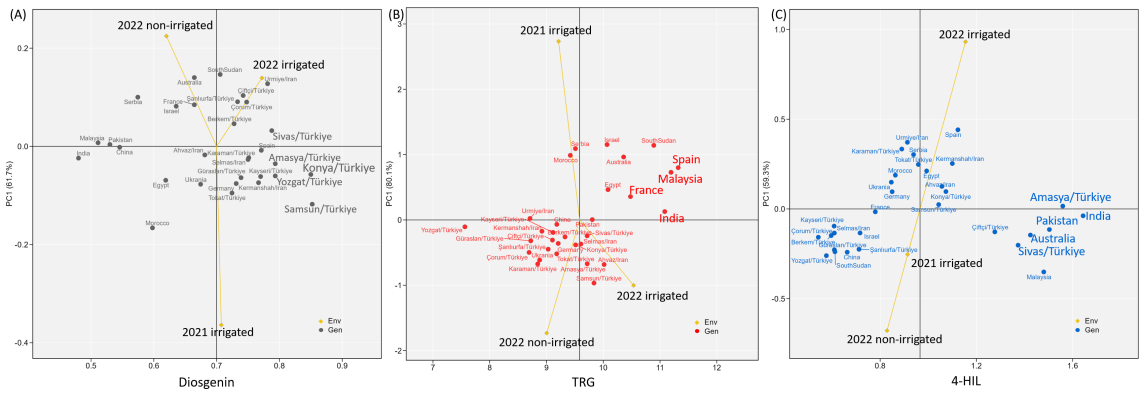

FIGURE 7
Additive main effects and multiplicative interaction (AMMI) biplots showing **(A)** diosgenin, **(B)** TRG and **(C)** 4-HIL versus the first principal component (PC1) score of 31 genotypes and three environments including 2021-irrigated, 2022-non-irrigated and 2022-irrigated. Genotypes located closer to the horizontal axis have higher stability across three environments while the vertical axis indicates the mean value of the 31 genotypes.

growing conditions to optimize fenugreeks nutritional and medicinal potential. For instance, genotypes adapted to semiarid climates may yield higher quality and quantity of bioactive compounds compared to those grown in humid environments, where they may be more susceptible to stress and disease (Zandi et al., 2015).

4.1 Diosgenin shows significant variability due to both genetic and environmental differences

Diosgenin, a steroidal saponin, has been extensively studied for its pharmacological applications, especially due to its cholesterol-lowering and anti-inflammatory properties (Pari et al., 2012; Tak et al., 2024). However, research on how agronomic practices affect diosgenin content in fenugreek remains relatively scarce. Several studies have documented significant variability in diosgenin levels among different genotypes, underscoring the impact of genetic differences on its content.

Indeed, previous studies have reported a wide range of diosgenin concentrations across various fenugreek genotypes, further highlighting the genetic influence on its accumulation. Provorov et al. (1996) reported diosgenin concentrations across 31 different fenugreek genotypes, with the lowest level found in a Ukrainian genotype at 1.14% and the highest in a Polish genotype at 1.64%. In contrast, Król-Kogus et al. (2018) reported lower diosgenin levels of 0.18% in a Polish genotype and 0.13% in an Algerian genotype, values significantly below those observed in our study. Other research has also highlighted variability in diosgenin content: Taylor et al. (2000) found levels ranging from 0.38 to 0.79%, while Taylor et al. (2002) reported a range of 0.32 to 0.64%. Similarly, Lee (2009) documented diosgenin concentrations between 0.50 and 0.81%, Kaufmann et al. (2007) reported values from 0.097 to 0.159%, and Laila et al. (2014) observed levels ranging from 0.113 to 0.135%. Additional studies by Giridhar et al. (2016) and Saxena et al. (2017) reported diosgenin contents between 0.52 to 0.97% and 0.35 to 0.78%, respectively. On the other hand, Beyzi et al. (2021), in their study involving the Güraslan, which is also included in our research, reported that the diosgenin content ranged between 0.43 and 0.52%. These findings are consistent with the results of our study, suggesting that genetic differences among fenugreek genotypes play a crucial role in determining diosgenin content. This variability highlights the importance of selecting appropriate genotypes for optimizing diosgenin production, especially in the context of breeding and cultivation strategies aimed at enhancing the medicinal value of fenugreek.

Beyond genetic factors, environmental conditions also play a crucial role in diosgenin accumulation, particularly under stress conditions such as drought. In our study, a significant decrease in diosgenin levels was observed under drought stress (2022-irrigated: 0.77% *vs.* 2022-non-irrigated: 0.62%), attributed to the combined effects of multiple factors, including alterations in gene expression and enzyme activity, disruptions in cellular osmotic balance, energy metabolism changes, and oxidative stress (Javan et al., 2024). Under drought conditions, the expression levels of certain key genes involved in diosgenin biosynthesis may be reduced, negatively impacting the biosynthetic process. Key genes such as CYP90B, CYP94, and CYP72A, which are part of the cytochrome P450 enzyme family, play critical roles in diosgenin production. Additionally, genes like HMGCS (hydroxymethylglutaric acid CoA synthetase), MVK (mevalonate kinase), and squalene epoxidase (SE) are essential for converting precursors into diosgenin. The downregulation of these genes under drought stress may significantly hinder diosgenin accumulation (Sun et al., 2017; Li et al., 2022).

Furthermore, specific enzymes that facilitate diosgenin biosynthesis are also affected by drought stress, contributing to reduced accumulation. Cycloartenol synthase (CAS) and beta-glucosidase (BG) play essential roles in diosgenin biosynthesis. CAS catalyzes a critical step by converting squalene epoxide into cycloartenol, which is a precursor for steroidal saponins, including diosgenin. BG, on the other hand, is necessary for converting diosgenin from its glycosidic form into free diosgenin. Under drought stress, decreased expression levels of these enzymes can

lead to a reduction in diosgenin production. Studies on fenugreek have indeed shown that drought stress lowers the expression of these genes involved in diosgenin biosynthesis (Javan et al., 2024; Maleki et al., 2024).

Conversely, under irrigated conditions, diosgenin production appears to be more favorable due to improved plant growth and metabolic efficiency. Irrigation conditions provide a more favorable environment for plant growth and development. Therefore, higher yield and improved yield components are expected outcomes (Ali et al., 2023; Guo et al., 2023). Lee (2009) reported that steroidal saponins in fenugreek are localized as furostanol glycosides within the cell walls of the embryo, and smaller seeds generally have lower diosgenin levels. In line with this, the higher diosgenin content observed in seeds grown under irrigated conditions in our study is related to these findings.

A similar pattern was observed for TRG biosynthesis, which also exhibited a decline under drought stress. TRG biosynthesis and accumulation also showed a decline under drought stress, reflecting the complex metabolic and physiological adaptations of plants. During drought stress, plants reorganize their metabolic priorities to survive, leading to reduced production of certain secondary metabolites (Farooq et al., 2009). Since the synthesis of secondary metabolites requires substantial energy, limited energy availability under drought conditions forces plants to deprioritize these energy-intensive processes, resulting in a decrease in some bioactive compounds (Chaves et al., 2003; Jaleel et al., 2009).

4.2 Trigonelline synthesis is restricted under drought, and it may be competing with diosgenin

TRG, a nitrogenous compound, plays a role in amino acid metabolism, but under drought stress, its synthesis may be restricted as plants channel energy and resources toward more critical processes, such as the production of compatible solutes (e.g., proline, glycinebetaine, and trigonelline), maintaining osmotic balance, and preventing water loss (Ashihara et al., 2015). Although the need to maintain osmotic balance promotes the synthesis of osmoregulators like proline and betaine, TRG production may be deprioritized. Furthermore, increased levels of abscisic acid (ABA) during drought stress cause stomata to close to reduce water loss, which can also inhibit the synthesis of secondary metabolites, thereby reducing TRG levels (Salvi et al., 2021).

Indeed, variations in TRG content depending on ecological conditions and crop years have been reported (Baghbani-Arani et al., 2017; Salehi et al., 2019). In our study, a wide variation in total TRG content (5.2–13.0 mg/g) was detected. These values are generally consistent with findings from previous research; however, significant differences were observed based on genotype, cultivation practices, and ecological factors. Such variability underscores the strong influence of environmental conditions on TRG accumulation, as reported in multiple studies. For example, Camlica and Yaldiz (2024) reported TRG content for fenugreek genotypes grown under two distinct environmental conditions in Northwestern Türkiye. Under irrigated conditions, TRG content ranged from 2.3 to 4.6 mg/g, while under dryland conditions, it ranged from 2.4 to 4.8 mg/g. Beyzi et al. (2021) conducted their study in Central Anatolia, Türkiye, under irrigated conditions with varying phosphorus fertilizer levels, documenting TRG values between 7.4 and 9.7 mg/g. Similarly, Güzel and Özyazıcı (2021) explored fenugreek grown in semiarid Southeastern Anatolia, Türkiye, noting TRG levels between 7.1 and 13.2 mg/g. On the other hand, Bakhtiar et al. (2024) studied wild fenugreek species under uniform cultivation conditions at Iran, and reported TRG levels ranging from 4.26 to 6.78 mg/g.

Beyond environmental influences, metabolic trade-offs may also explain fluctuations in TRG content, particularly in relation to diosgenin levels. The negative correlation observed between diosgenin and trigonelline in fenugreek likely arises from the interplay of competing biosynthetic pathways and adaptive responses to environmental stress. Diosgenin, a steroidal saponin synthesized via the mevalonate pathway, and trigonelline, an alkaloid derived from the shikimic acid pathway, may compete for shared substrates or enzymatic resources within the plant, leading to a trade-off in their synthesis (Naika et al., 2022). This trade-off is a common phenomenon in plants, where metabolic resources are allocated dynamically based on environmental and physiological needs. Additionally, this negative correlation may reflect an adaptive response to stress, as both compounds play crucial roles in plant defense mechanisms. Diosgenin has been linked to the regulation of oxidative stress through pathways such as Nrf2 and AMPK, while trigonelline has shown protective effects against oxidative damage and improved insulin sensitivity in diabetic models (Li et al., 2019; Tang et al., 2024). Under specific stress conditions, the plant may prioritize the synthesis of one compound over the other depending on the type of stress encountered, leading to variations in their concentrations (Mahmoudi et al., 2021).

Furthermore, genetic variability among fenugreek genotypes can significantly influence this relationship, as certain genotypes may exhibit regulatory mechanisms that favor the production of one compound over the other under environmental conditions (Naika et al., 2022). This highlights the importance of genotype selection in optimizing bioactive compound production, particularly in breeding programs aimed at enhancing fenugreek's medicinal and nutritional potential. Understanding these interactions provides valuable insights into the metabolic regulation of fenugreek and offers opportunities to optimize its nutritional and medicinal potential.

4.3 Fenugreek produces higher 4-hydroxyisoleucine levels under irrigated conditions

The analysis also revealed that the amount of 4-HIL in fenugreek genotypes was higher under irrigated conditions compared to non-irrigated conditions. 4-HIL is synthesized

through the modification of L-isoleucine, a process influenced by various enzymes whose activity can vary based on the plant's physiological state and environmental factors (Yang et al., 2021). This compound plays a significant role in carbon and nitrogen metabolism and can influence energy production pathways and protein synthesis, thereby supporting overall plant growth and development (Lai et al., 2022).

However, drought stress significantly alters the metabolic priorities of plants, which in turn affects 4-HIL biosynthesis. During drought stress, as a survival and stress management strategy, plants redirect their energy and resources toward essential metabolic processes. This reallocation results in decreased synthesis of secondary metabolites, particularly nitrogenous compounds. The biosynthesis of 4-HIL is thought to be diminished as a result of this metabolic shift (Hura et al., 2022).

These variations in 4-HIL content across different environmental conditions have also been observed among various fenugreek genotypes. Fenugreek seeds contain varying levels of 4-HIL, an amino acid derivative known for its antidiabetic properties. In our study, the highest 4-HIL levels were observed in 2022 under both irrigated (1.90%) and rainfed (1.82%) conditions in the Indian genotype. Previous research highlights the significant influence of different genotypes and environmental conditions on the concentration of this compound. For instance, a wide range of 4-HIL levels has been reported across different studies, emphasizing the role of genetic and environmental factors. Haeri et al. (2011) reported 0.27% 4-HIL in Iranian genotypes, while Gopu et al. (2008) found concentrations ranging between 0.207% and 0.259% in Indian genotypes. Similarly, Singh et al. (2025) reported 0.55% in yellow-seeded fenugreek and 0.81% in green-seeded fenugreek in an Indian genotype, while Haxhiraj et al. (2024) indicated that the 4-HIL levels could vary between 1% and 2% in certain samples.

Beyond genetic and environmental influences, post-harvest factors also play a crucial role in determining the final 4-HIL content in fenugreek. The 4-HIL content in fenugreek seeds is influenced not only by genetic factors but also by environmental conditions such as the growth environment, soil composition, climate, and agricultural practices (Gopu et al., 2008; Haeri et al., 2011). Additionally, post-harvest drying and storage conditions play a crucial role in the stability and concentration of this compound (Al Mosawi, 2021). Notably, certain cultivars selected for medicinal purposes are known to have higher levels of 4-HIL (Gopu et al., 2008). Therefore, optimizing both cultivation and post-harvest strategies is essential to ensure consistent and high-quality 4-HIL production in fenugreek. Considering these factors, the selection of fenugreek varieties for medicinal or industrial purposes should carefully account for genetic makeup, cultivation conditions, and post-harvest processes to ensure the desired levels of bioactive compounds.

To further refine genotype selection, statistical tools such as PCA and cluster analysis have been widely employed to assess genetic diversity and adaptability. Many studies conducted under different environmental conditions have shown that PCA effectively reveals morphological differences among genotypes and guides the selection of superior genotypes. Complementing this, cluster analysis groups genotypes based on similar characteristics, facilitating the identification of genetic diversity and playing an integral role in understanding G×E interactions. The integration of PCA and cluster analysis has been widely employed to reveal morphological differences, genetic diversity, and adaptability among the fenugreek genotypes. Studies by Maleki et al. (2021), Hasaroeih et al. (2023), and Alqathama et al. (2024) highlighted the role of PCA and cluster analysis in identifying superior genotypes. This approach has been particularly useful in research, as demonstrated by Camlica and Yaldiz (2024), who found significant differences in morphology, yield, and bioactive properties among genotypes, emphasizing their adaptability to diverse environmental conditions.

5 Conclusion

The study has revealed significant findings on diosgenin, TRG, and 4-HIL; these compounds exhibited notable variations across genotypes under both irrigated and non-irrigated conditions. The diosgenin content in Group B genotypes was generally higher than in other genotypes, highlighting its potential in the development of pharmaceutical products due to its cholesterol-lowering and anti-inflammatory properties. The results demonstrated that variations in bioactive compound levels were more pronounced under different environmental conditions, and higher yields were typically observed under irrigated conditions. Due to its suitability for mechanization, short growing season, and lower costs, fenugreek cultivation is regarded as a more suitable alternative for diosgenin production compared to traditional methods involving plants from the Dioscorea family. These advantages present the potential to further increase the agricultural and pharmacological value of fenugreek.

In terms of breeding, selecting bioactive compound-stable genotypes is of great interest, especially in the context of climate change. The broad genetic background of genotypes studied here allowed the search for superior genetic resources in these bioactive compounds. Interestingly, a clear genotype group pattern was identified for high and stable bioactive compounds. Genotypes with high and stable diosgenin were all group-B genotypes. The high and stable TRG was only found in group-A genotypes while the high and stable 4-HIL was found in genotypes from both groups. This trend further confirmed the different genetic mechanisms underlying these three bioactive compounds. The Turkish genotypes such as Sivas, Amasya, Konya, Yozgat and Samsun can be used as high-diosgenin germplasms in future breeding, while the genotypes Spain, Malaysia, France and India were screened out with promising potential for high TRG content. More studies are needed to dissect the genetic background of high 4-HIL content.

Future studies should also incorporate transcriptomic and metabolomic approaches to validate the observed trends in bioactive compound synthesis and identify the genetic and molecular pathways regulating these compounds. Such integrative analyses will help refine breeding strategies for fenugreek and enhance its value as a pharmacological and agricultural crop.

Data availability statement

The raw data supporting the conclusions of this article will be made available by the authors, without undue reservation.

Author contributions

FC: Conceptualization, Data curation, Formal Analysis, Validation, Writing – original draft, Writing – review & editing. HO: Conceptualization, Investigation, Methodology, Project administration, Resources, Supervision, Writing – review & editing. BY: Conceptualization, Methodology, Supervision, Writing – review & editing. YL: Conceptualization, Data curation, Formal Analysis, Methodology, Writing – review & editing.

Funding

The author(s) declare that financial support was received for the research and/or publication of this article. This research was funded by 1001 -The Scientific and Technological Research Projects Funding Program (No: TOVAG 220O003)' of TUBITAK (The Scientific and Technological Research Council of Türkiye). The funders did not participate in the design of the study, data collection and analysis, the decision to publish, or the preparation of the manuscript.

Acknowledgments

Special thanks to Atatürk University East Anatolia High Technology Application and Research Center (DAYTAM) for the significant technical support they provided during this study. The authors also wish to extend their gratitude to TÜBİTAK (The Scientific and Technological Research Council of Türkiye) for their financial support.

Conflict of interest

The authors declare that the research was conducted in the absence of any commercial or financial relationships that could be construed as a potential conflict of interest.

Generative AI statement

The author(s) declare that no Generative AI was used in the creation of this manuscript.

Publisher's note

Supplementary material

The Supplementary Material for this article can be found online at: https://www.frontiersin.org/articles/10.3389/fpls.2025.1562931/full#supplementary-material

References

Abd-El Mawla, M. A., and Osman, E. H. (2011). Elicitation of trigonelline and 4-hydroxyisoleucine with hypoglycemic activity in cell suspension cultures of *Trigonella foenum-graecum* L. *Open Conf. Proc.* 2, 80–84. doi: 10.2174/2210289201102010080

Abd-El-Wahab, M. M., Abdel-Lattif, H., Emara, K. S., Mosalam, M., Aljabri, M., and El-Soda, M. (2023). Identifying SNP markers associated with distinctness, uniformity, and stability testing in Egyptian fenugreek genotypes. *PloS One* 18, e0291527. doi: 10.1371/journal.pone.0291527

Afifi, N. A., Ramadan, A., Erian, E. Y., Saleh, D. O., Sedik, A. A., Badawi, M., et al. (2017). Trigonelline attenuates hepatic complications and molecular alterations in high-fat high-fructose diet-induced insulin resistance in rats. *Can. J. Physiol. Pharmacol.* 95, 427–436. doi: 10.1139/cjpp-2016-0269

Afrouz, M., Ahmadi-Nouraldinvand, F., Elias, S. G., Alebrahim, M. T., Tseng, T. M., and Zahedian, H. (2023). Green synthesis of spermine coated iron nanoparticles and its effect on biochemical properties of *Rosmarinus officinalis*. *Sci. Rep.* 13, 775. doi: 10.1038/s41598-023-27844-5

Ali, M., Ahmed, I., and Bibi, H. (2023). Impact of irrigation schedules on yield-related traits of wheat under semi-arid region. *Gesunde. Pflanzen.* 75, 2413–2422. doi: 10.1007/s10343-023-00888-3

Al Kashgry, N. A. T., Darwish, H., Aljomiha, N. A., Alharthi, S., Alayafi, A. A. M., Fallatah, A. M., et al. (2024). Silver nanoparticles alleviate the impact of soil contamination and wastewater irrigation on rosemary plants: modulating of gene expression and secondary metabolites. *Mater. Res. Express.* 11, 065009. doi: 10.1088/2053-1591/ad5788

Al Mosawi, A. J. (2021). The use of fenugreek supplementation in diabetes. *Glob J Obes Diabetes Metab Syndr.* 8 (2), 010–013. doi: 10.17352/2455-8583.000051

Alqathama, A., Bader, A., Pieracci, Y., Ahmad, R., Ascrizzi, R., and Flamini, G. (2024). Headspace analysis of volatiles from commercial seeds of *Trigonella foenum-graecum* L. obtained from four Middle Eastern countries. *J. Essent. Oil Res.* 36, 387–394. doi: 10.1080/10412905.2024.2371823

Ashihara, H., Ludwig, I. A., Katahira, R., Yokota, T., Fujimura, T., and Crozier, A. (2015). Trigonelline and related nicotinic acid metabolites: Occurrence, biosynthesis, taxonomic considerations, and their roles in planta and in human health. *Phytochem. Rev.* 14, 765–798. doi: 10.1007/s11101-014-9375-z

Baghbani-Arani, A., Modarres-Sanavy, S. A. M., Mashhadi-Akbar-Boojar, M., and Mokhtassi-Bidgoli, A. (2017). Towards improving the agronomic performance, chlorophyll fluorescence parameters and pigments in fenugreek using zeolite and

vermicompost under deficit water stress. *Ind. Crops Prod.* 109, 346–357. doi: 10.1016/j.indcrop.2017.08.049

Bakhtiar, Z., Hassandokht, M., Naghavi, M. R., Rezadoost, H., and Mirjalili, M. H. (2024). Fatty acid and nutrient profiles, diosgenin and trigonelline contents, mineral composition, and antioxidant activity of the seed of some Iranian *Trigonella* L. species. *BMC Plant Biol.* 24, 669. doi: 10.1186/s12870-024-05341-9

Beyzi, E., Köngül Şafak, E., Gürbüz, P., Koşar, M., and Gürbüz, B. (2021). Fatty acid composition, diosgenin and trigonelline contents of fenugreek (*Trigonella foenum-graecum*): effects of phosphorus fertilizer. *Plant Biosyst.* 155, 663–667. doi: 10.1080/11263504.2020.1769216

Camlica, M., and Yaldiz, G. (2024). Comparison of twenty selected fenugreek genotypes grown under irrigated and dryland conditions: morphology, yield, quality properties and antioxidant activities. *Agronomy* 14, 713. doi: 10.3390/agronomy14040713

Camlica, M., Yaldiz, G., and Askın, H. (2024). Deciphering the genetic diversity of different fenugreek genotypes based on the morphology, yield, UPOV criteria and some quality properties. *Genet. Resour. Crop Evol.*, 1–20. doi: 10.1007/s10722-024-02207-9

Chaves, M. M., Maroco, J. P., and Pereira, J. S. (2003). Understanding plant responses to drought—from genes to the whole plant. *Funct. Plant Biol.* 30, 239–264. doi: 10.1071/FP02076

Coban, F. (2021). *Effect of different sowing norms and nitrogen rates on the yield, yield component and quality of fenugreek (*Trigonella foenum-graecum *L.)* (University of Atatürk).

Coban, F., Ozer, H., and Lan, Y. (2024). Genetic and environmental influences on fatty acid composition in different fenugreek genotypes. *Ind. Crops Prod.* 222, 119774. doi: 10.1016/j.indcrop.2024.119774

Costa, M. C., Lima, T. F. O., Arcaro, C. A., Inacio, M. D., Batista-Duharte, A., Carlos, I. Z., et al. (2020). Trigonelline and curcumin alone, but not in combination, counteract oxidative stress and inflammation and increase glycation product detoxification in the liver and kidney of mice with high-fat diet-induced obesity. *J. Nutr. Biochem.* 76, 108303. doi: 10.1016/j.jnutbio.2019.108303

Dobeie, A. M., Nemr, R. A., Abd-El-Wahab, M. M., Shahba, M., and El-Soda, M. (2024). Mapping single nucleotide polymorphism markers associated with the pre-flowering morphological performance of fenugreek under different levels of salt stress. *Stresses* 4, 282–292. doi: 10.3390/stresses4020017

Erb, M., and Kliebenstein, D. J. (2020). Plant secondary metabolites as defenses, regulators, and primary metabolites: the blurred functional trichotomy. *Plant Physiol.* 184, 39–52. doi: 10.1104/pp.20.00433

Fahanik-Babaei, J., Baluchnejadmojarad, T., Nikbakht, F., and Roghani, M. (2019). Trigonelline protects hippocampus against intracerebral Aβ (1–40) as a model of Alzheimer's disease in the rat: Insights into underlying mechanisms. *Metab. Brain Dis.* 34, 191–201. doi: 10.1007/s11011-018-0338-8

Faisal, Z., Irfan, R., Akram, N., Manzoor, H. M. I., Aabdi, M. A., Anwar, M. J., et al. (2024). The multifaceted potential of fenugreek seeds: From health benefits to food and nanotechnology applications. *Food Sci. Nutr.* 12, 2294–2310. doi: 10.1002/fsn3.3959

Farid, M. M., Yang, X., Kuboyama, T., and Tohda, C. (2020). Trigonelline recovers memory function in Alzheimer's disease model mice: evidence of brain penetration and target molecule. *Sci. Rep.* 10, 16424. doi: 10.1038/s41598-020-73514-1

Farooq, M., Wahid, A., Kobayashi, N., Fujita, D., and Basra, S. M. A. (2009). "Plant drought stress: Effects, mechanisms and management," in *Sustainable agriculture*. Eds. E. Lichtfouse, M. Navarrete, P. Debaeke, S. Véronique and C. Alberola (Springer, Dordrecht), 153–188. doi: 10.1007/978-90-481-2666-8_12

Fouad, R., Fouad, H., El-Desoky, A. H., and Omer, E. A. (2023). "Secondary metabolism and its role in enhancing drought stress tolerance," in *Climate-Resilient Agriculture, Vol 2: Agro-Biotechnological Advancement for Crop Production*. Ed. M. Hasanuzzaman (Springer, Cham), 603–640. doi: 10.1007/978-3-031-37428-9_26

Gadanakis, Y., Bennett, R., Park, J., and Areal, F. J. (2015). Evaluating the sustainable intensification of arable farms. *J. Environ. Manage.* 150, 288–298. doi: 10.1016/j.jenvman.2014.10.005

Ghosaliya, B. K., Mittal, G. K., Shivran, A. C., Sharma, S. K., Saxena, S. N., and Jain, S. K. (2024). Water stress induced changes in seed quality of Fenugreek (*Trigonella foenum-graecum* L.) Genotypes. *Legume. Res.* 47, 20–26. doi: 10.18805/LR-4493

Giridhar, K., Kumari, S. S., Rajani, A., Sarada, C., and Naidu, L. (2016). Identification of potential genotypes of fenugreek in rainfed vertisols for yield and diosgenin content. *Indian J. Agric. Res.* 50, 311–317. doi: 10.18805/ijare.v0iOF.8603

Guo, J., Zheng, L., Ma, J., Li, X., and Chen, R. (2023). Meta-analysis of the effect of subsurface irrigation on crop yield and water productivity. *Sustainability* 15, 15716. doi: 10.3390/su152215716

Gupo, C. L., Gilda, S. S., Paradkar, A. R., and Mahadik, K. R. (2008). Development and validation of a densitometric TLC method for analysis of trigonelline and 4-hydroxyisoleucine in fenugreek seeds. *Acta Chromatogr* 20 (4), 709–719. doi: 10.1556/achrom.20.2008.4.15

Güzel, Y., and Özyazıcı, G. (2021). Adoption of promising fenugreek (*Trigonella foenum-graceum* L.) genotypes for yield and quality characteristics in the semiarid climate of Turkey. *Atmosphere* 12, 1199. doi: 10.3390/atmos12091199

Haeri, M. R., Izaddoost, M., Ardekani, M. R. S., and White, K. (2011). Improved isolation of 4-hydroxyisoleucine from Trigonella foenum graecum seeds. *Chem Nat Compd.* 47, 157–158. doi: 10.1007/s10600-011-9867-7

Haliloğlu, K., Özer, H., Melik, S., Çoban, F., and Türkoğlu, A. (2024). Exploring the genetic diversity and population structure of fenugreek (*Trigonella foenum-graecum* L.) genotypes through inter-primer binding site (iPBS)-retrotransposon marker system. *Genet. Resour. Crop Evol.* 71 (7), 3253–3266. doi: 10.1007/s10722-023-01849-5

Hamadi, S. A. (2012). Effect of trigonelline and ethanol extract of Iraqi Fenugreek seeds on oxidative stress in alloxan diabetic rabbits. *J. Assoc. Arab. Univ. Basic. Appl. Sci.* 12, 23–26. doi: 10.1016/j.jaubas.2012.02.003

Hamden, K., Bengara, A., Amri, Z., and Elfeki, A. (2013). Experimental diabetes treated with trigonelline: effect on key enzymes related to diabetes and hypertension, β-cell and liver function. *Mol. Cell. Biochem.* 381, 85–94. doi: 10.1007/s11010-013-1690-y

Hao, S., Xu, R., Li, D., Zhu, Z., Wang, T., and Liu, K. (2015). Attenuation of streptozotocin-induced lipid profile anomalies in the heart, brain, and mRNA expression of HMG-CoA reductase by diosgenin in rats. *Cell Biochem. Biophys.* 72, 741–749. doi: 10.1007/s12013-015-0525-8

Hasaroeih, N. E., Ghanavati, F., Moradi, F., Kohpalkani, J. A., and Rahimizadeh, M. (2023). Multivariate analysis of seed chemical diversity among wild fenugreek (*Trigonella monantha* CA Mey.) ecotypes. *BMC Plant Biol.* 23, 324. doi: 10.1186/s12870-023-04327-3

Haxhiraj, M., White, K., and Terry, C. (2024). The Role of Fenugreek in the Management of Type 2 Diabetes. *Int. J. Mol. Sci.* 25, 6987. doi: 10.3390/ijms25136987

Hura, T., Hura, K., and Ostrowska, A. (2022). Drought-stress induced physiological and molecular changes in plants. *Int. J. Mol. Sci.* 23, 4698. doi: 10.3390/ijms23094698

Ilavenil, S., Kim, D. H., Jeong, Y. I., Arasu, M. V., Vijayakumar, M., Prabhu, P. N., et al. (2015). Trigonelline protects the cardiocyte from hydrogen peroxide-induced apoptosis in H9c2 cells. *Asian Pac. J. Trop. Med.* 8, 263–268. doi: 10.1016/S1995-7645(14)60328-X

Isah, T. (2019). Stress and defense responses in plant secondary metabolites production. *Biol. Res.* 52, 1–25. doi: 10.1186/s40659-019-0246-3

Jaleel, C. A., Manivannan, P., Wahid, A., Farooq, M., Al-Juburi, H. J., Somasundaram, R., et al. (2009). Drought stress in plants: A review on morphological characteristics and pigments composition. *Int. J. Agric. Biol.* 11, 100–105.

Javan, S. L., Kashkooli, A. B., Shojaeiyan, A., and Majidian, S. (2024). Transcriptomic data reveals the dynamics of terpenoids biosynthetic pathway of fenugreek. *BMC Genomics* 25, 390. doi: 10.1186/s12864-024-10253-x

Kaufmann, B., Rudaz, S., Cherkaoui, S., Veuthey, J. L., and Christen, P. (2007). Influence of plant matrix on microwave-assisted extraction process: The case of diosgenin extracted from fenugreek (*Trigonella foenum-graecum* L.). *Phytochem. Anal.* 18, 70–76. doi: 10.1002/pca.954

Khare, S., Singh, N. B., Singh, A., Hussain, I., Niharika, K. M., Yadav, V., et al. (2020). Plant secondary metabolites synthesis and their regulations under biotic and abiotic constraints. *J. Plant Biol.* 63, 203–216. doi: 10.1007/s12374-020-09245-7

Khorshidian, N., Yousefi Asli, M., Arab, M., Adeli Mirzaie, A., and Mortazavian, A. M. (2016). Fenugreek: potential applications as a functional food and nutraceutical. *Nutr. Food Sci. Res.* 3, 5–16. doi: 10.18869/acadpub.nfsr.3.1.5

Król-Kogus, B., Lamine, K. M., Migas, P., Boudjeniba, M., and Krauze-Baranowska, M. (2018). HPTLC determination of diosgenin in fenugreek seeds. *Acta Pharm.* 68, 97–107. doi: 10.2478/acph-2018-0002

Lai, W., Shi, F., and Tan, S. (2022). Dynamic control of 4-hydroxyisoleucine biosynthesis by multi-biosensor in Corynebacterium glutamicum. *Appl. Microbiol. Biotechnol.* 106, 5105–5112. doi: 10.1007/s00253-022-12034-6

Laila, O., Murtaza, I., Abdin, M. Z., Ahmad, S., Ganai, N. A., and Jehangir, M. (2014). Development and validation of HPTLC method for simultaneous estimation of diosgenin and quercetin in fenugreek seeds (*Trigonella foenum-graecum*). *Int. Sch. Res. Not.* 2014, 583047. doi: 10.1155/2014/583047

Lee, E. L. (2009). *Genotype X environment impact on selected bioactive compound content of fenugreek (*Trigonella foenum-graecum *L.)* (Canada: University of Saskatchewan).

Li, Y., Li, Q., Wang, C., Lou, Z., and Li, Q. (2019). Trigonelline reduced diabetic nephropathy and insulin resistance in type 2 diabetic rats through peroxisome proliferator-activated receptor-γ. *Exp. Ther. Med.* 18, 1331–1337. doi: 10.3892/etm.2019.7698

Li, Y., Tan, C., Li, Z., Guo, J., Li, S., Chen, X., et al. (2022). The genome of *Dioscorea zingiberensis* sheds light on the biosynthesis, origin and evolution of the medicinally important diosgenin saponins. *Hortic. Res.* 9, uhac165. doi: 10.1093/hr/uhac165

Liang, Y., Dai, X., Cao, Y., Wang, X., Lu, J., Xie, L., et al. (2023). The neuroprotective and antidiabetic effects of trigonelline: A review of signaling pathways and molecular mechanisms. *Biochimie* 206, 93–104. doi: 10.1016/j.biochi.2022.10.009

Mahmoudi, N., Kiasalari, Z., Rahmani, T., Sanaierad, A., Afshin-Majd, S., Naderi, G., et al. (2021). Diosgenin attenuates cognitive impairment in streptozotocin-induced diabetic rats: underlying mechanisms. *Neuropsychobiology* 80, 25–35. doi: 10.1159/000507398

Makowska, J., Szczesny, D., Lichucka, A., Giełdoń, A., Chmurzyński, L., and Kaliszan, R. (2014). Preliminary studies on trigonelline as potential anti-Alzheimer disease agent: Determination by hydrophilic interaction liquid chromatography and modeling of interactions with beta-amyloid. *J. Chromatogr. B.* 968, 101–104. doi: 10.1016/j.jchromb.2013.12.001

Maleki, M., Shojaeiyan, A., and Mokhtassi-Bidgoli, A. (2024). Differential responses of two fenugreek (*Trigonella foenum-graecum* L.) landraces pretreated with melatonin to prolonged drought stress and subsequent recovery. *BMC Plant Biol.* 24, 161. doi: 10.1186/s12870-024-04835-w

Maleki, M., Shojaeiyan, A., and Mokhtassi-Bidgoli, A. (2021). Genotypic variation in biochemical and physiological responses of fenugreek (*Trigonella foenum-graecum* L.) landraces to prolonged drought stress and subsequent rewatering. *Sci. Hortic.* 287, 1110224. doi: 10.1016/j.scienta.2021.110224

Maloo, S. R., Sharma, R., and Soan, H. (2023). SSR based genetic diversity analysis in fenugreek (*Trigonella foenum-graecum* L.) genotypes. *Legume. Res.* 46, 307–311. doi: 10.18805/LR-4787

Mansinhos, I., Gonçalves, S., and Romano, A. (2024). How climate change-related abiotic factors affect the production of industrial valuable compounds in *Lamiaceae* plant species: a review. *Front. Plant Sci.* 15. doi: 10.3389/fpls.2024.1370810

Maurya, H. K., Mishra, D. P., Singh, H., Singh, A. V., and Maurya, B. K. (2023). An experimental study of genetic divergence in fenugreek (*Trigonella foenum-graecum* L.). *Int. J. Plant Soil Sci.* 35, 23–30. doi: 10.9734/ijpss/2023/v35i173177

Mohammad-Sadeghipour, M., Mahmoodi, M., Karimabad, M. N., Mirzaei, M. R., and Hajizadeh, M. R. (2021). Diosgenin and 4-hydroxyisoleucine from fenugreek are regulators of genes involved in lipid metabolism in the human colorectal cancer cell line SW480. *Cell J.* 22, 514–521. doi: 10.22074/cellj.2021.6751

Naika, M. B., Sathyanarayanan, N., Sajeevan, R. S., Bhattacharyya, T., Ghosh, P., Iyer, M. S., et al. (2022). Exploring the medicinally important secondary metabolites landscape through the lens of transcriptome data in fenugreek (*Trigonella foenum graecum* L.). *Sci. Rep.* 12, 13534. doi: 10.1038/s41598-022-17779-8

Narender, T., Puri, A., Khaliq, T., Saxena, R., Bhatia, G., and Chandra, R. (2006). 4-Hydroxyisoleucine an unusual amino acid as antidyslipidemic and antihyperglycemic agent. *Bioorg. Med. Chem. Lett.* 16, 293–296. doi: 10.1016/j.bmcl.2005.10.003

Nguyen, V., Taine, E. G., Meng, D., Cui, T., and Tan, W. (2024). Pharmacological activities, therapeutic effects, and mechanistic actions of trigonelline. *Int. J. Mol. Sci.* 25, 3385. doi: 10.3390/ijms25063385

Pari, L., Monisha, P., and Jalaludeen, A. M. (2012). Beneficial role of diosgenin on oxidative stress in aorta of streptozotocin-induced diabetic rats. *Eur. J. Pharmacol.* 691, 143–150. doi: 10.1016/j.ejphar.2012.06.038

Peerapen, P., Chanthick, C., and Thongboonkerd, V. (2023). Quantitative proteomics reveals common and unique molecular mechanisms underlying beneficial effects of caffeine and trigonelline on human hepatocytes. *Biomed. Pharmacother.* 158, 114124. doi: 10.1016/j.biopha.2022.114124

Prinsloo, G., and Nogemane, N. (2018). The effects of season and water availability on chemical composition, secondary metabolites and biological activity in plants. *Phytochem. Rev.* 17, 889–902. doi: 10.1007/s11101-018-9567-z

Provorov, N. A., Soskov, Y. D., Lutova, L. A., Sokolova, O. A., and Bairamov, S. S. (1996). Investigation of the fenugreek (*Trigonella foenum-graecum* L.) genotypes for fresh weight, seed productivity, symbiotic activity, callus formation and accumulation of steroids. *Euphytica* 88, 129–138. doi: 10.1007/BF00032444

Qaderi, M. M., Martel, A. B., and Strugnell, C. A. (2023). Environmental factors regulate plant secondary metabolites. *Plants* 12, 447. doi: 10.3390/plants12030447

Salehi, A., Fallah, S., Zitterl-Eglseer, K., Kaul, H. P., Abbasi Surki, A., and Mehdi, B. (2019). Effect of organic fertilizers on antioxidant activity and bioactive compounds of fenugreek seeds in intercropped systems with buckwheat. *Agronomy* 9, 367. doi: 10.3390/agronomy9070367

Salvi, P., Manna, M., Kaur, H., Thakur, T., Gandass, N., Bhatt, D., et al. (2021). Phytohormone signaling and crosstalk in regulating drought stress response in plants. *Plant Cell Rep.* 40, 1305–1329. doi: 10.1007/s00299-021-02683-8

Saxena, S. N., Kakani, R. K., Sharma, L. K., Agarwal, D., John, S., and Sharma, Y. (2017). Genetic variation in seed quality and fatty acid composition of fenugreek (*Trigonella foenum-graecum* L.) genotypes grown under limited moisture conditions. *Acta Physiol. Plant* 39, 1–10. doi: 10.1007/s11738-017-2522-6

Shailajan, S., Sayed, N., Menon, S., Singh, A., and Mhatre, M. (2011). A validated RP-HPLC method for quantitation of trigonelline from herbal formulations containing *Trigonella foenum-graecum* (L.) seeds. *Pharm. Methods* 2, 157–160. doi: 10.4103/2229-4708.90354

Singh, K. P., Nair, B., Jain, P. K., Naidu, A. K., and Paroha, S. (2013). Variability in the nutraceutical properties of fenugreek (*Trigonella foenum-graecum* L.) seeds. *Rev. Colomb. Cienc. Hortic.* 7, 228–239. doi: 10.17584/rcch.2013v7i2.2237

Singh, R., Meena, R. S., Choudhary, S., Meena, N. K., Meena, R. D., Verma, A. K., et al. (2025). Deciphering agronomic traits, biochemical components, and color in unique green-seeded fenugreek (*Trigonella foenum-graecum* L.) genotypes. *Front. Nutr.* 12, 1542211. doi: 10.3389/fnut.2025.1542211

Soylu Pekpostalci, D., Tur, R., Danandeh Mehr, A., Vazifekhah Ghaffari, M. A., Dąbrowska, D., and Nourani, V. (2023). Drought monitoring and forecasting across Turkey: A contemporary review. *Sustainability* 15, 6080. doi: 10.3390/su15076080

Sun, W., Wang, B., Yang, J., Wang, W., Liu, A., Leng, L., et al. (2017). Weighted gene co-expression network analysis of the dioscin rich medicinal plant *Dioscorea nipponica*. *Front. Plant Sci.* 8. doi: 10.3389/fpls.2017.00789

Tak, Y., Kaur, M., Chitranashi, A., Samota, M. K., Verma, P., Bali, M., et al. (2024). Fenugreek derived diosgenin as an emerging source for diabetic therapy. *Front. Nutr.* 11. doi: 10.3389/fnut.2024.1280100

Tang, Y., Hu, W., Peng, Y., and Ling, X. (2024). Diosgenin inhibited podocyte pyroptosis in diabetic kidney disease by regulating the Nrf2/NLRP3 pathway. *Biocell* 48 (10), 1503–1516. doi: 10.32604/biocell.2024.052692

Taylor, W. G., Elder, J. L., Chang, P. R., and Richards, K. W. (2000). Microdetermination of diosgenin from fenugreek (*Trigonella foenum-graecum*) seeds. *J. Agric. Food Chem.* 48, 5206–5210. doi: 10.1021/jf000467t

Taylor, W. G., Zulyniak, H. J., Richards, K. W., Acharya, S. N., Bittman, S., and Elder, J. L. (2002). Variation in diosgenin levels among 10 accessions of fenugreek seeds produced in western Canada. *J. Agric. Food Chem.* 50, 5994–5997. doi: 10.1021/jf020486y

Team, R. (2015). *RStudio*. (Boston, MA: Integrated Development for R. RStudio Inc), 700. Available online at: https://posit.co/download/rstudio-desktop/ (Accessed June 23, 2024).

Tharaheswari, M., Jayachandra Reddy, N., Kumar, R., Varshney, K. C., Kannan, M., and Sudha Rani, S. (2014). Trigonelline and diosgenin attenuate ER stress, oxidative stress-mediated damage in pancreas and enhance adipose tissue PPARγ activity in type 2 diabetic rats. *Mol. Cell. Biochem.* 396, 161–174. doi: 10.1007/s11010-014-2152-x

Tsipinana, S., Husseiny, S., Alayande, K. A., Raslan, M., Amoo, S., and Adeleke, R. (2023). Contribution of endophytes towards improving plant bioactive metabolites: a rescue option against red-taping of medicinal plants. *Front. Plant Sci.* 14. doi: 10.3389/fpls.2023.1248319

Yang, J., Ran, Y., Yang, Y., Song, S., Wu, Y., Qi, Y., et al. (2021). 4-Hydroxyisoleucine alleviates macrophage-related chronic inflammation and metabolic syndrome in mice fed a high-fat diet. *Front. Pharmacol.* 11. doi: 10.3389/fphar.2020.606514

Yoon, Y., Seo, D. H., Shin, H., Kim, H. J., Kim, C. M., and Jang, G. (2020). The role of stress-responsive transcription factors in modulating abiotic stress tolerance in plants. *Agronomy* 10, 788. doi: 10.3390/agronomy10060788

Yoshinari, O., and Igarashi, K. (2010). Anti-diabetic effect of trigonelline and nicotinic acid on KK-Ay mice. *Curr. Med. Chem.* 17, 2196–2202. doi: 10.2174/092986710791299902

Yoshinari, O., Takenake, A., and Igarashi, K. (2013). Trigonelline ameliorates oxidative stress in type 2 diabetic Goto-Kakizaki rats. *J. Med. Food.* 16, 34–41. doi: 10.1089/jmf.2012.2311

Zandi, P., Basu, S. K., Khatibani, L. B., Balogun, M. O., Aremu, M. O., Sharma, M., et al. (2015). Fenugreek (*Trigonella foenum-graecum* L.) seed: a review of physiological and biochemical properties and their genetic improvement. *Acta Physiol. Plant* 37, 1–14. doi: 10.1007/s11738-014-1714-6

Zarinkamar, F., Rezayian, M., and Medhat, R. (2022). Increase of Trigonelline in Trigonella persica Plant under Drought Stress. *J. Bot. Res.* 4, 19–25. doi: 10.30564/jbr.v4i2.4512

Zhou, J., Zhou, S., and Zeng, S. (2013). Experimental diabetes treated with trigonelline: effect on β cell and pancreatic oxidative parameters. *Fundam. Clin. Pharmacol.* 27, 279–287. doi: 10.1111/j.1472-8206.2011.01022.x

frontiers | Frontiers in Plant Science

TYPE Original Research
PUBLISHED 27 March 2025
DOI 10.3389/fpls.2025.1550131

OPEN ACCESS

EDITED BY
Eman. A. Mahmoud,
Damietta University, Egypt

REVIEWED BY
Ahmed Noah Badr,
National Research Centre, Egypt
Archana Jain,
Zunyi Medical University, China

*CORRESPONDENCE
Carolina Parra-Palma
carolina.parra@uautonoma.cl
Luis Morales-Quintana
luis.morales@uautonoma.cl

RECEIVED 22 December 2024
ACCEPTED 05 March 2025
PUBLISHED 27 March 2025

CITATION
Vasquez-Rojas C, Muñoz-Vera M, Flores S, Betancourt M, Castro RI, Ramos P, Laporte D, Parra-Palma C and Morales-Quintana L (2025) Impact of methyl Jasmonate on blueberry ripening fruits: assessment of cell wall thermal stability, nutritional parameters and antioxidant enzymatic activity. *Front. Plant Sci.* 16:1550131. doi: 10.3389/fpls.2025.1550131

Impact of methyl Jasmonate on blueberry ripening fruits: assessment of cell wall thermal stability, nutritional parameters and antioxidant enzymatic activity

Carlos Vasquez-Rojas[1,2], Marcelo Muñoz-Vera[3], Sebastián Flores[4], Mauricio Betancourt[1,5], Ricardo I. Castro[3], Patricio Ramos[4,6], Daniel Laporte[7], Carolina Parra-Palma[1]* and Luis Morales-Quintana[1]*

[1]Multidisciplinary Agroindustry Research Laboratory, Instituto de Ciencias Biomédicas, Facultad Ciencias de la Salud, Universidad Autónoma de Chile, Talca, Chile, [2]Programa de Doctorado en Ciencias Biomédicas, Facultad Ciencias de la Salud, Universidad Autónoma de Chile, Talca, Chile, [3]Multidisciplinary Agroindustry Research Laboratory, Instituto de Ciencias Químicas Aplicadas, Facultad de Arquitectura, Construcción y Medio Ambiente, Universidad Autónoma de Chile, Talca, Chile, [4]Plant Microorganism Interaction Laboratory, Instituto de Ciencias Biológicas, Universidad de Talca, Talca, Chile, [5]Carrera de Química y Farmacia, Facultad Ciencias de la Salud, Universidad Autónoma de Chile, Talca, Chile, [6]Vicerrectoría de Investigación y Postgrado, Universidad Católica del Maule, Talca, Chile, [7]Laboratory of Plant Physiology and Molecular Biology, Instituto de Ciencias Biomédicas, Facultad Ciencias de la Salud, Universidad Autónoma de Chile, Talca, Chile

Introduction: The blueberry (Vaccinium spp.), recognized as one of the most significant horticultural crops globally, is valued for its rich bioactive compounds. In this study, we examine the effects of methyl jasmonate (MeJA) on blueberry, focusing on cell wall composition, nutritional properties, and antioxidant enzyme activity across two seasons (2022–2023). The objective is to evaluate the impact of MeJA treatments on fruit ripening dynamics and quality attributes.

Methodology: Blueberry plants were treated with single (T1) and double (T2) MeJA applications. Thermogravimetric analysis (TGA) and differential scanning calorimetry (DSC) were used to assess thermal degradation patterns of cell wall polymers. Biochemical evaluations included phenolic content, antioxidant capacity (DPPH and FRAP assays), and anthocyanin accumulation during ripening. Enzymatic antioxidant activities (APX, CAT, SOD, and POD) were also analyzed to determine oxidative stress responses.

Results and discussion: Thermal degradation analysis revealed that green-stage fruits exhibited higher thermal stability than ripe fruits, with variations in pink-stage behavior between seasons. Biochemical assessments indicated a progressive decline in phenolic content and antioxidant capacity during ripening, whereas anthocyanin accumulation peaked in the blue stage, enhancing pigmentation. MeJA treatments significantly influenced antioxidant enzyme activity: T1 maximized APX, CAT, and SOD activities, while T2 amplified POD activity, contributing to oxidative stress tolerance and improved fruit quality.

Furthermore, the modulation of hemicellulose fractions in TGA profiles suggests that MeJA helps maintain cell wall integrity, potentially reducing fruit softening during storage.

Conclusion: These findings indicate that MeJA enhances fruit resilience during ripening while preserving key biochemical properties critical for postharvest management. The observed improvements in antioxidant capacity, enzymatic activity, and cell wall stability suggest that MeJA could be a valuable tool for optimizing postharvest handling, extending shelf life, and enhancing the marketability of blueberries. This work provides a preliminary framework for integrating MeJA into sustainable horticultural practices to meet consumer demand for high-quality functional fruits.

KEYWORDS

antioxidant capacity, blueberry fruit ripening, cell wall, hormonal treatment, methyl jasmonate, phenols

1 Introduction

Blueberries (*Vaccinium corymbosum*) are recognized as one of the top five healthy fruits recommended by the Food and Agriculture Organization of the United Nations (Huang et al., 2018). They are renowned for their rich nutritive composition, boasting a high concentration of biologically active components, including anthocyanins, polyphenols, and flavonoids. Blueberries fruits are among the most nutrient-dense berries, abundant in fiber, vitamins, and antioxidant compounds (Kalt et al., 2020; Neto, 2007; Silva et al., 2020; Zafra-Stone et al., 2007). These antioxidants, part of the broad group of flavonoids and phenolic acids, possess functional properties that contribute to reducing the risk of heart disease, diabetes, and neurodegenerative disorders (Kalt et al., 2020; Neto, 2007; Silva et al., 2020; Zafra-Stone et al., 2007). The chemical composition of blueberries varies significantly depending on factors such as cultivar, variety, growing location, environmental conditions, plant nutrition, ripeness stage, harvest time, and storage conditions (Bujor et al., 2016; Lohachoompol et al., 2004; Skrovankova et al., 2015). These variables influence the content of individual components, thereby impacting the corresponding antioxidant profiles. Thus, finding solutions that allow improving the antioxidant profile of blueberries in post-harvest seems to be a good idea, and in this sense, various authors have described that Methyl Jasmonate (MeJA) could be a good candidate. Understanding these variations is crucial for optimizing the health benefits and nutritional value of blueberries (Bujor et al., 2016; Skrovankova et al., 2015). But it is necessary to understand its mode of action and the time and number of applications.

Methyl jasmonate (MeJA) is considered an important plant hormone that mediates intra- and inter-plant communications, modulating plant defense responses, including antioxidant systems (Wasternack, 2007; Wasternack and Hause, 2013). Thus, MeJA can significantly influence the ripening process of blueberries, enhancing fruit quality, delaying decay, and improving resistance to environmental stressors (Huang et al., 2015). In different species, such as barley and cauliflower, MeJA application has been shown to enhance enzymatic antioxidant activity and reduce cellular membrane damage caused by water deficiency (Wu et al., 2012). For example, MeJA application can regulate the production of terpenes, as lactones and carotenoids, and esters (Li et al., 2006; Cai et al., 2020); other example, in MeJA postharvest treatment of olives, not only enhanced the concentration of phenolic acids, but also decreased the levels of unhealthy saturated fatty acids and increased the content of unsaturated fatty acids: such as oleic, linoleic and linolenic acids (Flores et al., 2017). Particularly, in blueberry studies have shown that exogenous application of MeJA can accelerate ripening by increasing anthocyanin biosynthesis, phenols and flavonoids accumulations, which enhances the fruit's color and antioxidant properties in the fruits during postharvest (Huang et al., 2015; Balbontín et al., 2025; Parra-Palma et al., 2025).

For this reason, it has been suggested that the application of MeJA reduces the activity of enzymes that hydrolyze glycosidic linkages among cell wall components, inducing cell wall softening in fruits. Consequently, the MeJA application improves fruit firmness and resistance to mechanical damage, reducing in an indirect manner the microbial attacks (Balbontín et al., 2025; Bari and Jones, 2009). These combined effects make MeJA a valuable tool in postharvest treatments to improve the marketability and shelf life of blueberries.

In other hand, the softening process is a crucial factor determining the quality and storage life of many fruits. The intricate interaction of elements and mechanisms, in plant cell walls underscores their changing nature and crucial significance in the growth and functioning of plants. Additionally, very little is known about cell wall remodeling during fruit development and the

softening process in blueberry fruits. Although the processes involved in polysaccharide solubilization and depolymerization have been extensively studied using various techniques across a wide range of fresh fruits, these processes can exhibit considerable variability in both extent and timing among different species and even among cultivars of the same species, resulting in differing rates of fruit softening. Despite the extensive research in this area, the application of a thermal approach to study the degradation of cell wall polymers remains relatively novel. The impact of MeJA on the quality of blueberry fruits and the components of the fruit's cell wall, following differential applications of MeJA directly on the plant in blueberry production farms, has yet to be explored (Castro et al., 2021a; Jara et al., 2019).

Therefore, the current investigation focuses on exploring the principal quality traits of blueberry fruits obtained from plants that were treated with exogenous MeJA at two different times. Additionally, we evaluated the degradation and thermal characteristics of the cell wall in blueberry fruits 'O'neal', one of the most cultivated in Chile (https://www.odepa.gob.cl/), and the effect of MeJA on the cell wall components of blueberries after exogenous application in commercial blueberry plants, using thermogravimetric analysis (TGA) and differential scanning calorimetry (DSC), in conjunction with various other relevant parameters related to fruit quality.

2 Materials and methods

2.1 Plant material

Fruits harvested from the *V. corymbosum* 'O´Neal' were obtained from 25-year-old shrubs cultivated in a commercial orchard located in Cauquenes, Maule Region, Chile (latitude 35° 58′02′′ S; longitude 72°18′56′′ W) in two productive season, December 2022 and December of 2023, from trees grown in fields of soils come from granitic and metamorphic rocks, highly clayey. The transportation of the fruits was carried out in containers with dry ice, ensuring cold storage conditions within a temperature range of 4 to 8°C until their arrival at the Multidisciplinary Agroindustry Research Laboratory of the Universidad Autónoma de Chile. Upon arrival, the fruits were categorized into three different stages of growth based on criteria such as weight and color, following the classification system proposed by (Gupta et al., 2015), which included green (G), pink (P), and ripe (R) stages, which correspond to 20 to 25 days post-anthesis, 35 and 45 days post-anthesis, and 50 and 60 days post-anthesis, respectively (Figure 1). To conduct the analyses, nine different plants per treatment MeJA (T1 and T2), and controls (C) were utilized, more other different nine plants to collect development state fruit were utilized to collect fruits representing each of the three ripening stages, with around thirty berries sampled from each stage and treated fruit per plant, and the blueberry fruits were collected from various parts of the tree, including the upper and lower sections, the central area, as well as from locations exposed to sunlight and those in shaded areas.

2.2 MeJA exogenous treatment

For MeJA treatments, nine plants organized in different random locations of the commercial orchard, were treated sprinkling with a water solution containing 0.1 mM MeJA and 0.05% Tween-20. In the case of nine control plants, a solution of distilled water and 0.05% Tween-20 was sprayed. The MeJA concentration (0.1 mM MeJA) was selected based on previous studies conducted by (Cocetta et al., 2015). The solution (100 mL per bush) was applied to the above-ground parts of the blueberry bushes. This was done either as a single when the berries began to develop color (turning point), or double application (with the second application was 7 days after the first application). Then, fruits from treated plants were harvested at the ripe (R) stage on the same day, one hour from the last MeJA application.

2.3 Physiological parameters evaluations

Firstly, the fruit size was evaluated using a digital caliper to measure the equatorial diameters. The means and standard deviations of thirty measurements were provided per treatment and controls. Soluble solids content in the entire fruit was measured using a portable refractometer (0–32°Brix). One millilitre of homogenised pulp, obtained by grinding five berries, was used for the measurement. The analysis was performed three times for each

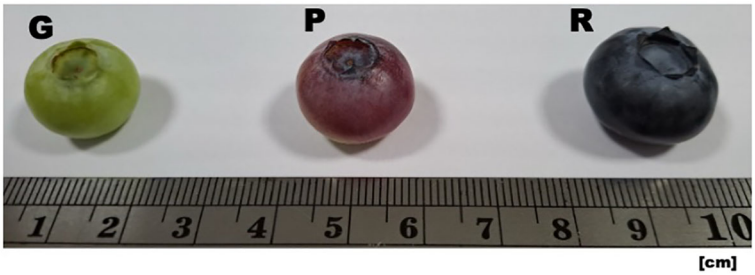

FIGURE 1
Different ripening stages of Blueberry fruits: G green fruit; P pink fruit or 50% Ripe fruit; and R ripe fruit, which correspond to 20 to 25 days post-anthesis, 35 and 45 days post-anthesis, and 50 and 60 days post-anthesis, respectively.

fruit stage, and the median and average deviation for the replicates were recorded and expressed as °Brix. Colour measurements were taken from ten random were obtained from the pool, using a Nix Pro 2 Color Sensor (Nix Sensor Ltd. Hamilton, ON, Canada), and the results were expressed using the Hunter scale (L*, a*, b*). Nix Color was used to generate a schematic representation of the CIELAB color system. Color changes were expressed as E* using the following formula (see Equation 1):

$$\Delta E* = (\Delta L^2 + \Delta a^2 + \Delta b^2)^{1/2} \quad (1)$$

where ΔL, Δa*, and Δb* represent the differences between the initial and final values for color change determination (Castro et al., 2023; Parra-Palma et al., 2024) (Supplementary Table S1).

2.4 Thermogravimetric analysis and differential scanning calorimetry

Thermogravimetric analysis (TGA) was performed in order to assess the stability of *V. corymbosum* fruits, in accordance with the methodology outlined by Castro et al. (Castro et al., 2021b). Following a drying period of 48 hours at 80°C, each sample cohort underwent homogenization through employment of a mortar. Subsequently, 5 mg of desiccated material from each sample group was subjected to scrutiny utilizing a Discovery SDT-Q650 simultaneous DSC-TGA instrument (manufactured by TA Instruments, based in New Castle, DE, USA). The specimens were subjected to a temperature range spanning from 50°C to 500° C, with a consistent escalation rate of 5°C/min, all conducted under a nitrogen gas stream maintaining a flow rate of 50 mL/min.

Differential scanning calorimetry (DSC) was conducted utilizing a Discovery SDT-Q650 simultaneous DSC-TGA instrument from TA Instruments, located in New Castle, DE, USA. The specimens were placed in an Al_2O_3 crucible and subjected to analysis within a temperature range spanning from room temperature (25°C) up to 500°C. Prior to the commencement of heating at a rate of 5°C per minute, the samples were allowed to stabilize at 25°C for one minute. The calibration of the equipment was carried out utilizing sapphire as the benchmark material, in accordance with the guidelines provided by the manufacturer. Each evaluation involved the utilization of 15 to 20 mg of desiccated fruit specimens. The computation of parameters such as transition enthalpy (H, expressed in J g^{-1}), onset temperature (T_o), peak temperature (T_p), and conclusion temperature (T_c) was conducted using the TRIOS TA-Instrument Thermal Analysis System Software, as outlined in the works of (Andler et al., 2023) and Morales-Quintana et al. (2022b).

2.5 Determination of the antioxidant compounds

Total phenolics and flavonoids were quantified in different developmental stages and treated fruits using well-established methodologies. Three independent extractions were performed on 10 g of each sample, representing the different treatments and developmental stages. These extracts were subsequently analyzed for total phenolic and flavonoid content following the procedures outlined by Parra-Palma et al. (2020). Firstly, the total phenolic content was evaluated diluted extracts were oxidized with the Folin–Ciocalteu reagent, neutralized with sodium carbonate, and the absorbance of the blue coloration was measured at 700 nm after 30 minutes using a Multiskan SkyHigh Microplate Spectrophotometer (Thermo Fisher Scientific). A standard curve of gallic acid was used for quantification, and results were expressed as grams of gallic acid equivalents per kilogram of fruit (g kg^{-1} GAE). Data represent the means ± standard errors (SEs) of three biological replicates, each with two technical replicates. Respect to the total flavonoid content, it was determined using the aluminum chloride colorimetric method adapted from Chang et al. (2002), with quercetin as the calibration standard. A 0.5 mL aliquot of each diluted extract was mixed with 1.5 mL of 95% ethanol, 0.1 mL of 10% aluminum chloride, 0.1 mL of 1 M potassium acetate, and 2.8 mL of distilled water. After 30 minutes of incubation at room temperature, absorbance was measured at 415 nm using the same microplate spectrophotometer. Results were expressed as grams of quercetin equivalents per kilogram of fruit (g kg^{-1} QE) and represent the means ± SEs of three biological replicates with two technical replicates. Finally, the total anthocyanin content was quantified using the differential pH method and expressed as cyanidin-3-O-glucoside equivalents per 100 mg of fresh fruit weight (C3GE/100 mg FW), following the methodology described by Parra-Palma et al. (2020).

2.6 Total antioxidant capacity of the fruits

The antioxidant capacity of the treated and developmental fruit stage extracts was assessed using the DPPH radical scavenging assay, following the method described by Cheel et al. (2007). Briefly, 20 µL of the extract was mixed with 0.5 mL of 0.5 mM DPPH solution and 0.5 mL of 100 mM acetate buffer (pH 5.5). The reaction mixtures were prepared in triplicate, and absorbance was measured at 517 nm using an Epoch 2 microplate spectrophotometer. Radical scavenging ability was calculated by comparing the samples to a methanol-DPPH negative control. The ferric reducing antioxidant power (FRAP) assay was also employed, based on the methodology of Parra-Palma et al. (2020). In this assay, methanol extracts were reacted with a ferric-tripyridyltriazine (Fe^{3+}-TPTZ) complex, which antioxidants reduce to the ferrous form (Fe^{2+}-TPTZ), resulting in a blue coloration measured spectrophotometrically, and using Trolox for the calibration curve. FRAP values provided a quantitative measure of reducing power and antioxidant potential.

2.7 Antioxidant enzyme activity

Ripe fruits (500 mg fresh weight) were ground in liquid nitrogen, and the resulting powder was homogenized in a pre-chilled 50 mM

phosphate buffer (pH 7.8) containing 1% polyvinylpyrrolidone (PVP). The homogenates were centrifuged at 10,000 rpm for 20 minutes at 4°C, and 5 mL of the supernatant was collected for enzymatic assays. Activities of superoxide dismutase (SOD), catalase (CAT), peroxidase (POD), and ascorbate peroxidase (APX) were determined following the protocols previously standardized by Morales-Quintana et al. (2022a). All determinations were conducted in biological triplicates to ensure reliability. Briefly, in the apoplastic fractions obtained from frozen cell samples were measured spectrophotometrically. The CAT activity was measured by monitoring the decrease in absorbance at 240 nm in 50 mM phosphate buffer (pH 7.5) containing 20 mM H_2O_2 (Erdogan et al., 2016). APX activity was determined by following the decrease in A290 (extinction coefficient 2.8 mM^{-1} cm^{-1}) for 1 min in 1 mL of a reaction mixture containing 50 mM potassium phosphate buffer (pH 7.0), 0.5 mM ascorbic acid, 0.1 mM H_2O_2 and 200 µl of enzyme extract (Erdogan et al., 2016). Respect to the POP activity, it was measured by monitoring the increase in absorbance at 470 nm in 50 mM phosphate buffer (pH 5.5) containing 1 mM guaiacol and 0.5 mM H_2O_2 (Guo et al., 2010; Erdogan et al., 2016). Finally, The SOD activity was estimated by recording the decrease in optical density of nitro-blue tetrazolium dye by the enzyme (Guo et al., 2010; Erdogan et al., 2016).

2.8 Statistical analysis and experimental design

The following experimental design was implemented, utilizing control groups composed of fruits at various stages examined in the research, alongside an experimental group exposed to MeJA at diverse stages of the fruits. The results, acquired in triplicate, were represented as average values ± standard deviation. The statistical analysis was conducted utilizing statistical software by SPSS Inc. (Chicago, IL, version 15). An ANOVA test was employed to compare the average values among groups, with a significance threshold established at $p < 0.05$.

3 Results

3.1 Fruits physiological evaluations

Firstly, a comprehensive analysis of blueberry (*V. corymbosum*) fruit characteristics reveals significant changes in color, weight, and diameter across the ripening stages (green, pink, blue) over two agronomic seasons (Table 1). The CIELAB color parameters (L*, a*, b*) indicate a progressive shift in fruit color as ripening advances. Specifically, the *L value** (lightness) decreases from the green to blue stage, suggesting that the fruit becomes darker as chlorophyll degrades and anthocyanins accumulate in the two seasons (Table 1). The *a value** transitions from negative (indicating green) in the green stage to positive in the pink and blue stages, highlighting the increase in red pigmentation associated with anthocyanin synthesis (Table 1). Meanwhile, the *b value** decreases, reflecting a reduction in yellow hues and a shift towards a blue-purplish tone, which is characteristic of mature blueberries (Table 1). The calculated ΔE* values, which indicate color change from the green stage, are highest between green and blue stages, confirming significant color transitions during ripening (Table 1).

Respect to the size of the fruit during the developmental stages, in 2022, fruits at the blue stage exhibit significantly higher weight and diameter (1.99 g and 16.57 mm) compared to the green (1.23 g and 14.28 mm) and pink (1.38 g and 14.28 mm) stages (Table 1). A similar trend is observed in 2023, with blue-stage fruits reaching 1.73 g in weight and 16.10 mm in diameter, confirming the physical enlargement and mass increase that typically accompany blueberry ripening (Table 1). The green-stage fruits in 2023 had lower average weight (0.64 g) and diameter (11.20 mm) compared to 2022, possibly reflecting environmental or agronomic factors affecting fruit development this season (Table 1). This form, the fruit transitions from green to blue-purple stage, reflecting chlorophyll degradation and pigment synthesis, while increasing in size and weight due to cell expansion. Simultaneously, the breakdown of hemicellulose and pectin leads to softening, enhancing fruit texture.

TABLE 1 Physiological parameter of the different fruit ripening stage of blueberry (*Vaccinium corymbosum*) evaluation during two agronomical seasons.

Season	Stage	CIELAB color space			ΔE*	Weight (g)	Diameter (mm)
		L*	a*	b*			
2022	Green	25.99 ± 9.53	-2.66 ± 4.53	23.47 ± 7.55	–	1.23 ± 0.20 ^{b}	14.28 ± 0.83 ^{b}
	Pink	12.81 ± 7.39	10.87 ± 8.92	6.64 ± 6.21	23.97	1.38 ± 0.30 ^{b}	14.28 ± 1.16 ^{b}
	Blue	18.55 ± 10.33	-3.13 ± 10.31	0.35 ± 5.17	24.26	1.99 ± 0.32 ^{a}	16.57 ± 1.17 ^{a}
2023	Green	11.52 ± 6.42	-3.03 ± 2.69	11.12 ± 7.77	–	0.64 ± 0.17 ^{b}	11.20 ± 1.10 ^{b}
	Pink	18.23 ± 9.92	10.13 ± 9.00	11.09 ± 10.21	14.77	1.48 ± 0.28 ^{b}	15.23 ± 1.43 ^{b}
	Blue	13.20 ± 7.09	7.67 ± 8.19	1.34 ± 4.73	14.59	1.73 ± 0.32 ^{a}	16.10 ± 1.27 ^{a}

Values indicate the mean of thirty replicates, and the standard deviations are also shown. Different superscript alphabets in a column represent a statistically significant difference between the means ($p < 0.05$).
*Values compared to the green stage in each season.

Seasonal variations in these traits highlight the influence of environmental factors, underscoring the importance of optimizing agronomic practices to ensure consistent fruit quality and yield.

Additionally, the cell wall stability was determined using a thermogravimetric analysis (TGA) and derivative thermogravimetry (DTG), according to Castro and Morales-Quintana (2019). The TGA and DTG results in Figure 2 show how different cell wall components in the samples degrade at specific temperature ranges, which can give us insights into how the structure of the cell wall changes and relates to fruit softening according to the development stage. As the temperature increases, we observe different stages of weight loss, which correspond to the breakdown of various parts of the cell wall, including water loss and the degradation of important polymers like cellulose and hemicellulose (Figure 2). These polymers provide rigidity and structure, so when they break down, the cell wall becomes softer (Castro and Morales-Quintana, 2019). As shown in Figure 2, in the temperature range of 200 to 330°C, the green stage exhibited greater firmness compared to the ripe (blue) stage. Notably, differences were observed in the behavior of the pink stage, where in the 2022 season, its thermal profile resembled that of the green stage, while in the 2023 season, it was more like the blue stage. This suggests that the blue stage is more depolymerized than the green stage, which demonstrated higher thermal stability of the cell wall (Figures 2A, C). According to the data described by Castro and Morales-Quintana (2019), the region corresponds to the decomposition of hemicellulose fractions between 200 and 300°C (Xiao et al., 2001) and shorter-chain pectin fractions at approximately 250°C (Ghaffari et al., 2007) (Figures 2B, D).

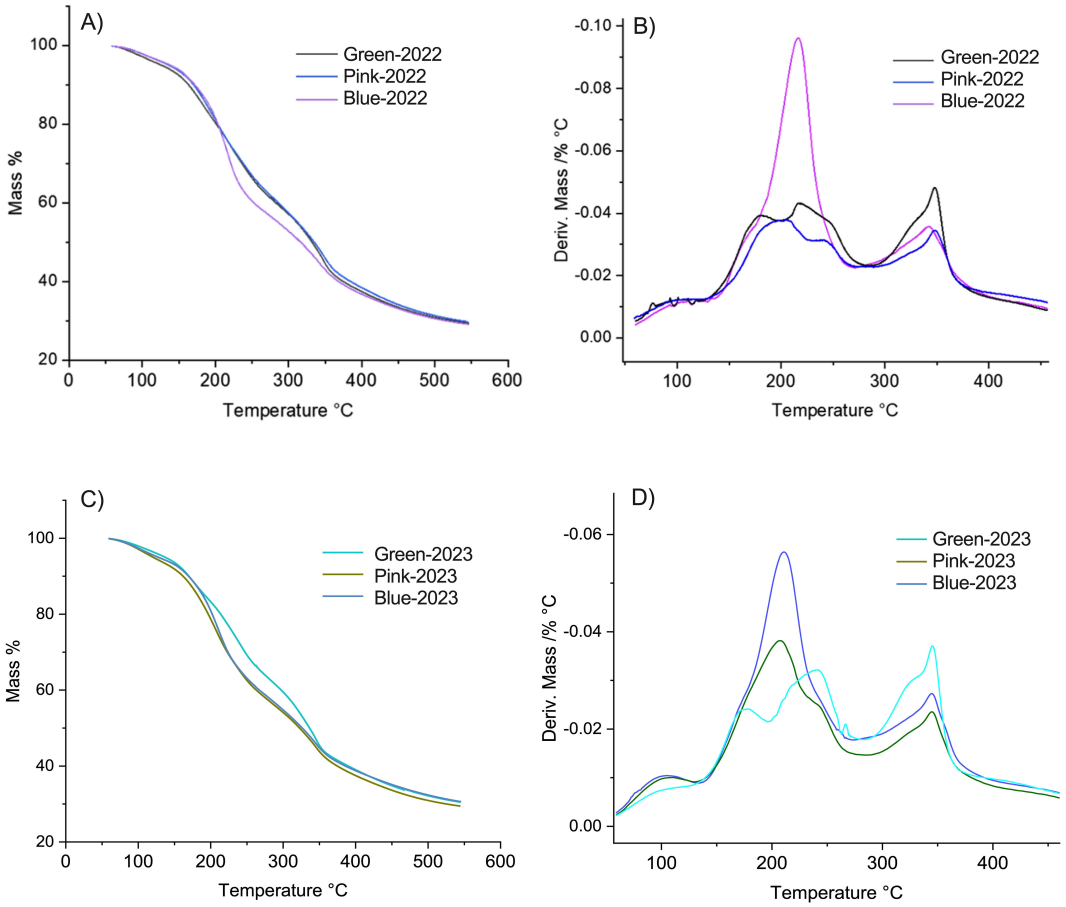

FIGURE 2
Thermogravimetric analysis (TGA) and derivative thermogravimetry (DTG) curves of blueberries at different developmental stages from the 2022 and 2023 seasons. **(A)** TGA thermograms representing mass loss (%) as a function of temperature (50–550°C) for blueberries harvested in 2022 at three different developmental stages (Green, Pink, and Blue). The thermal degradation profiles exhibit a continuous weight loss, indicative of different decomposition phases related to moisture evaporation, thermal degradation of organic components, and residual char formation. **(B)** DTG curves derived from **(A)**, showing the rate of mass loss as a function of temperature. The peaks indicate the maximum degradation rates, highlighting key thermal degradation events for each developmental stage in the 2022 season. A distinct peak is observed around 200°C, suggesting variations in the thermal stability of the fruit depending on its ripeness. **(C)** TGA thermograms for blueberries from the 2023 season, following the same developmental stages (Green, Pink, and Blue). The mass loss patterns are similar to those of 2022, with minor differences likely attributed to seasonal variations in fruit composition. **(D)** DTG curves corresponding to **(C)**, illustrating the temperature points at which the highest degradation rates occur. Compared to 2022, the degradation peaks in 2023 exhibit slight shifts, which may be associated with differences in biochemical composition, water content, or structural changes during fruit maturation.

3.2 Flavor, antioxidant, and enzymatic dynamics in blueberry across developmental stages

In terms of SSC (an indicator of sugar content described in °Brix), the blue stage shows the highest values, especially in 2022 where it measured 18.5 ± 0.1°Brix, aligning with the increased sweetness typically associated with fruit ripening (Supplementary Figure S1). TA decreases across the developmental stages, with 1.0 ± 0.015%TA in green stage of 2022 season to 1.7 ± 0.011%TA in blue stage of 2022, reflecting a reduction in acidity as the fruit ripe (Supplementary Figure S1). Consequently, the SSC/TA ratio—a critical measure of fruit taste quality—rises sharply, especially in the pink and blue stages (Supplementary Figure S1). This ratio increase suggests a shift from acidic to sweeter flavors, which are more desirable in ripe fruits.

The antioxidant capacity of blueberry fruits at different developmental stages (green, pink, and blue) was evaluated through DPPH radical scavenging activity and ferric reducing antioxidant power (FRAP) assays over two consecutive years (2022 and 2023) (Figure 3). The DPPH scavenging activity indicates a strong antioxidant potential at the green stage, with values near 100% in both years (Figure 3). This activity significantly declines as the fruit matures, particularly at the blue stage, where a notable decrease is observed in 2023 compared to 2022. These findings suggest that early-stage blueberries possess high radical-scavenging capacity, which diminishes as the fruit ripens,

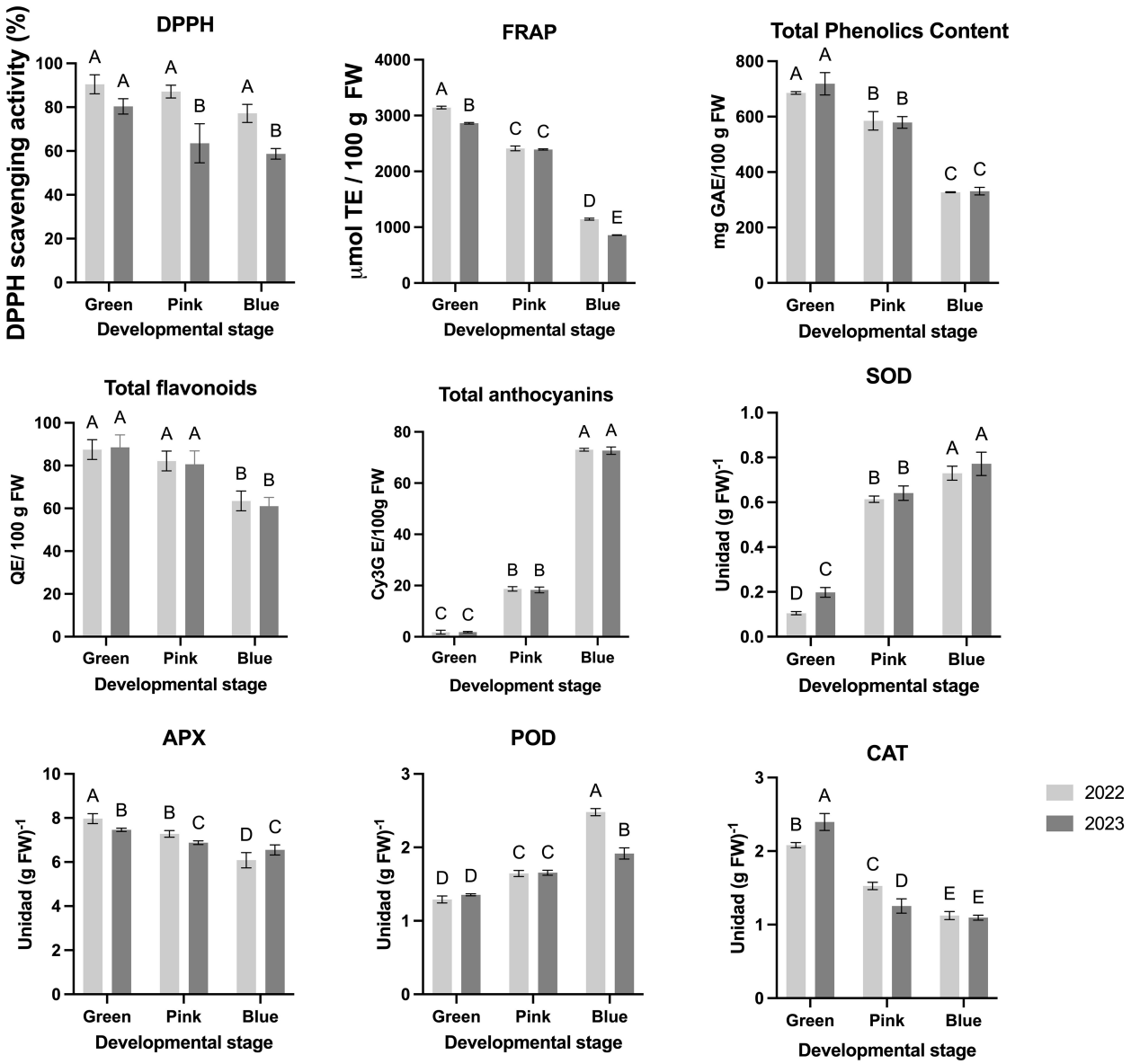

FIGURE 3
Nutritional and antioxidant parameters of the blueberry fruits during three different developmental stage and two different seasons. Different letters indicate significant differences ($P < 0.05$; two-way ANOVA). Bars represent means SE from three independent experiments.

potentially due to the degradation or transformation of phenolic compounds (Figure 3). Similarly, the FRAP results reveal a high antioxidant potential in the green stage, reaching values close to 3,000 μmol TE/100 g FW. As with DPPH, FRAP values decrease progressively through the pink and blue stages, with the lowest values recorded in the blue stage for both years (Figure 3). The significant decline in FRAP at later stages aligns with the ripening process, which is associated with reduced levels of antioxidant compounds as total phenols (Figure 3).

The total phenolic content demonstrates a clear decline as the fruit progresses from the green to the blue stage, with the highest concentration observed at the green stage for both years (Figure 3). Flavonoid Content remains relatively stable across stages in both years, with minor differences observed between developmental stages, indicating that flavonoid accumulation is less affected by ripening compared to phenolics (Figure 3). Respect to the total Anthocyanins exhibit a marked increase by the blue stage, reflecting anthocyanin accumulation (Figure 3) linked to the color change associated with ripening (Table 1). Anthocyanins are significantly more concentrated in the blue stage than in earlier stages, underscoring their role in late-stage pigmentation.

The enzymatic activity of antioxidant enzymes—ascorbate peroxidase (APX), catalase (CAT), peroxidase (POD), and superoxide dismutase (SOD)—was assessed across developmental stages (green, pink, and blue) in blueberry fruits for two consecutive years (2022 and 2023), highlighting the fruit's dynamic response to oxidative stress during ripening (Figure 3). APX activity is notably higher at the green stage, reaching approximately 8 units/g FW in both years, but statistically decreases progressively through the pink and blue stages (Figure 3). This trend suggests an early peak in APX activity as the fruit initiates protective mechanisms against oxidative stress during the initial stages of maturation. Similarly, CAT activity is highest at the green stage in both years (over 2 units/g FW), then declines significantly as the fruit transitions to the pink and blue stages, indicating a reduction in CAT-mediated hydrogen peroxide scavenging as ripening advances (Figure 3). In contrast, POD activity shows a peak at the blue stage, with a significant increase from the green and pink stages, especially in 2022. This late rise in POD activity suggests an adaptive response that may play a role in the final stages of fruit maturation and protection against oxidative degradation during full ripeness (Figure 3). SOD activity, essential for dismutation of superoxide radicals, increases as the fruit matures, reaching similarly high levels at the pink and blue stages in both years. The progressive rise in SOD aligns with the increased metabolic demands and potential oxidative stress encountered as the fruit reaches maturity (Figure 3).

3.3 Different number of the MeJA applications in the blueberry plants and the effect over the fruits obtained

MeJA applications influenced multiple physiological, biochemical, and enzymatic parameters in blueberry fruits across two consecutive seasons (2022 and 2023). While thermogravimetric analysis showed no significant differences between treatments, minor variations around 200°C (Figure 4), suggested changes in hemicellulose structure, according to Xiao et al. (2001) and validated by our laboratory in Castro and Morales-Quintana (2019).

Single MeJA (T1) led to a reduction in SSC in 2022, suggesting lower sugar accumulation (Figure 5). TA varied across years, increasing significantly in T1 during 2022 but showing a slight decline in T2 in 2023 (Figure 5). Consequently, the SSC/TA ratio, a key indicator of fruit sweetness, was lower in treated fruits, particularly in 2022 (Figure 5). For the color parameters in 2022, the control group displayed L*, a*, and b* values of 5.88 ± 3.40, 1.25 ± 2.36, and -0.55 ± 1.51, respectively. Treatment T1 showed increased L* and altered color attributes, with values of 15.98 ± 11.50 for L*, -0.46 ± 9.23 for a*, and -0.72 ± 5.55 for b*, corresponding to a color difference (ΔE*) of 10.24. In T2, these values were 7.48 ± 6.34, -0.40 ± 3.94, and -0.08 ± 2.31, with ΔE* at 2.35 (Table 2). The average fruit weight and diameter remained statistically consistent across treatments, with slight variances (e.g., 1.46 ± 0.39 g and 14.62 ± 1.42 mm in the control) (Table 2). In 2023, the control group values were 12.63 ± 3.55 for L*, 3.88 ± 5.44 for a*, and 0.62 ± 3.32 for b*. T1 had color parameters of 18.14 ± 5.22 (L*), 3.54 ± 5.93 (a*), and -1.76 ± 2.82 (b*), with ΔE* of 6.01, while T2 displayed L*, a*, and b* values of 12.70 ± 4.48, 1.83 ± 3.21, and 0.43 ± 2.24, with ΔE* of 2.06 (Table 2). Across both seasons, treatment effects on weight and diameter showed non-significant differences compared to the control group, with values in T1 and T2 generally within the range of 1.46–2.16 g and 14.62–17.40 mm, respectively (Table 2).

In terms of phenolic composition, total phenolic content remained stable across treatments in 2022 but increased in T1 during 2023 (Figure 5). Flavonoid content was higher in T2 in 2022, whereas no differences were observed in 2023 (Figure 5). Anthocyanin accumulation increased with MeJA applications, particularly in T2, suggesting enhanced pigmentation and antioxidant potential (Figure 5).

MeJA treatments also influenced antioxidant enzyme activities. Ascorbate peroxidase (APX) and catalase (CAT) increased significantly in T1, particularly in 2022, while T2 exhibited a slight decline, indicating a possible saturation effect with repeated applications (Figure 6). Peroxidase (POD) responded more strongly to T2, suggesting a role in cell wall reinforcement (Figure 6). Superoxide dismutase (SOD) was higher in T1 than in T2, implying that a single MeJA application may be sufficient to trigger an optimal antioxidative response (Figure 6).

Additionally, antioxidant capacity, measured through DPPH and FRAP assays, improved with MeJA treatments (Figure 7). While FRAP values were higher in T1 and T2 during 2023, no significant differences were detected in 2022 (Figure 7). DPPH scavenging activity showed a progressive increase with MeJA, particularly in T2, indicating enhanced free radical neutralization (Figure 7).

Overall, MeJA treatments modified fruit physiology, biochemical composition, and antioxidant activity, with T1 generally inducing stronger metabolic changes, while T2 resulted in more pronounced antioxidant responses, particularly in anthocyanin accumulation and peroxidase activity.

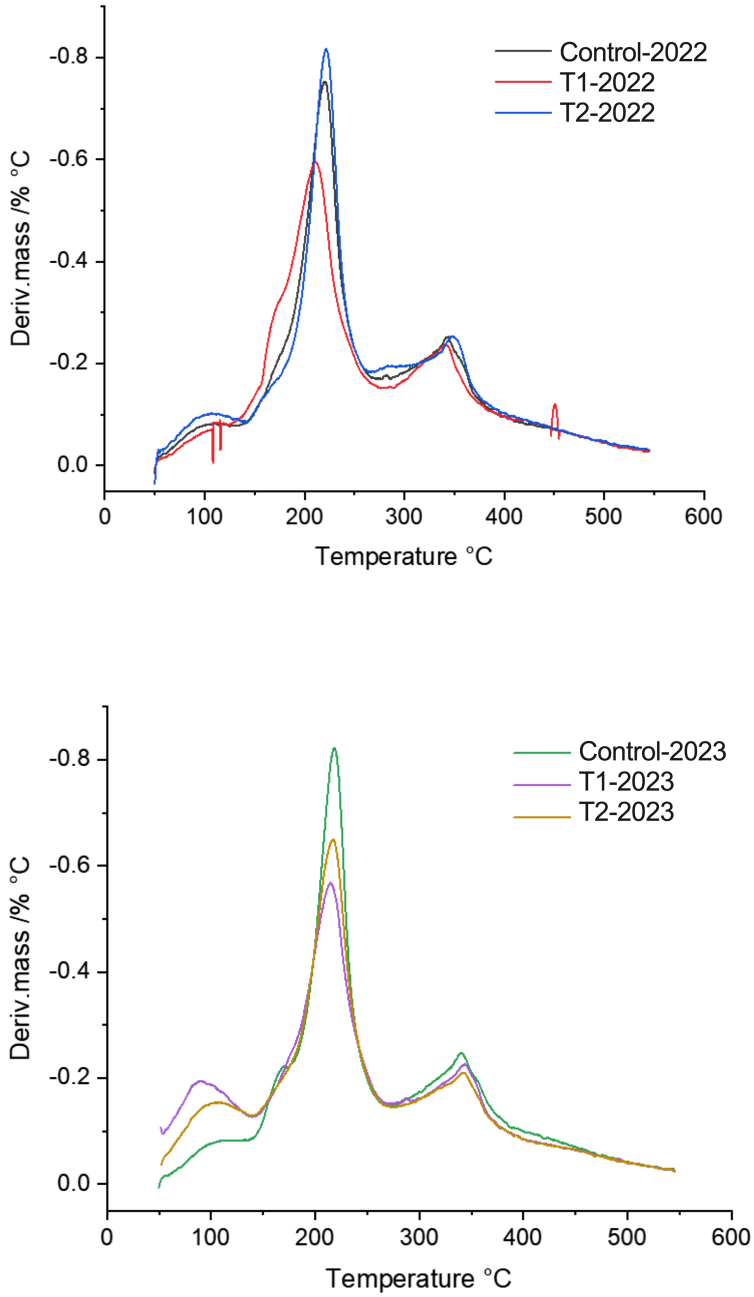

FIGURE 4
First derivative of the thermogram curves (TG/DTG thermogram) showing the maximum degradation temperatures from two different MeJA treatment (T1 and T2), during two season 2022 and 2023. DTG curves showing the rate of mass loss as a function of temperature. The peaks indicate the maximum degradation rates, highlighting key thermal degradation events for each developmental stage in the 2022 and 2023 seasons. A distinct peak is observed around 200°C, suggesting variations in the thermal stability of the fruit depending on its ripeness.

Finally, a Pearson's correlation analysis reveals key relationships among the measured parameters in MeJA-treated blueberry fruits across the two seasons. In the 2022 season, phenolics content showed strong negative correlations with CAT (-0.99) and APX (-1.00) activities, suggesting that higher phenolic levels may reduce the need for these antioxidant enzymes (Table 3). Total flavonoids were strongly positively correlated with POD activity (1.00) but negatively with DPPH (-0.99), indicating a potential trade-off between flavonoid accumulation and DPPH scavenging capacity (Table 3). In the 2023 season, phenolics content was strongly positively correlated with total anthocyanins (0.99), SSC (0.99), and FRAP (1.00), highlighting the role of phenolics in enhancing sugar content, anthocyanin accumulation, and overall antioxidant capacity (Table 3). These results underscore the complex interplay between phenolic compounds, antioxidant enzymes, and fruit quality parameters in response to MeJA treatment.

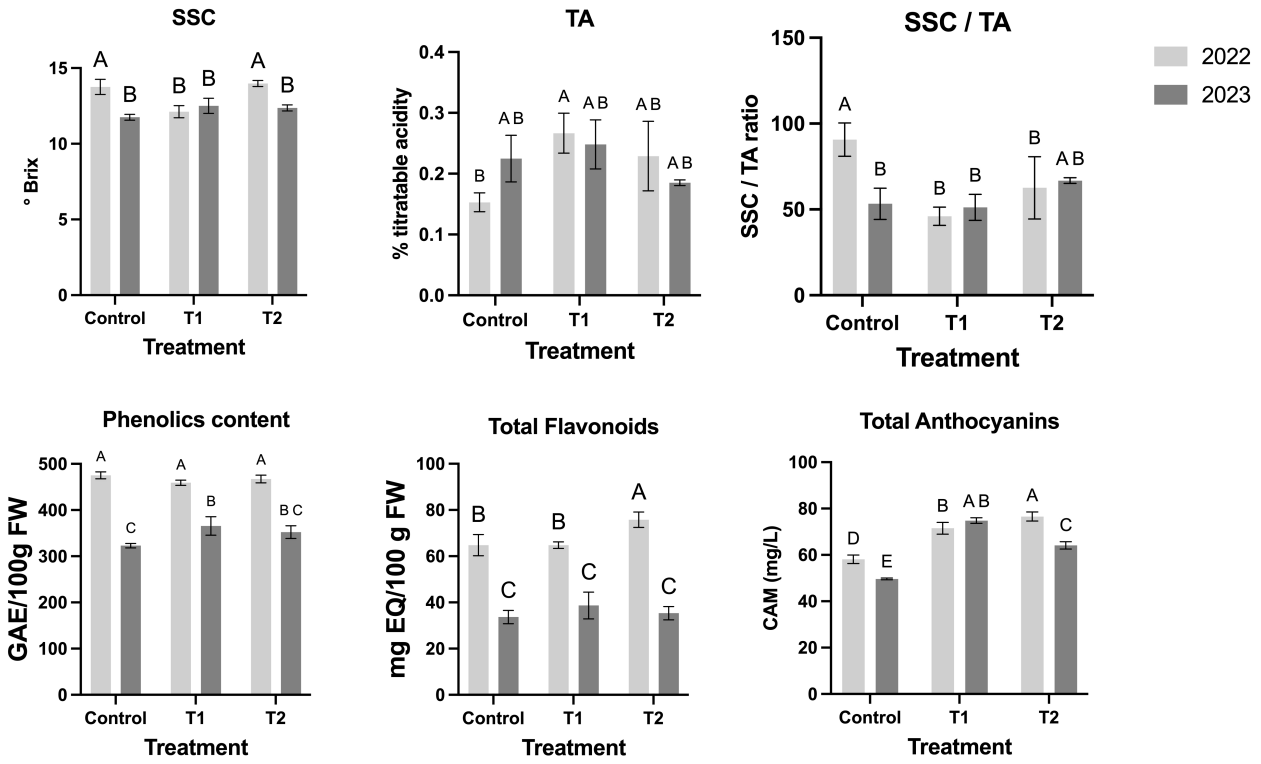

FIGURE 5
MeJA treatment over blueberry plants and the effect over the nutritional and physiological fruits parameters. Different letters indicate significant differences ($P < 0.05$; two-way ANOVA). Bars represent means SE from three independent experiments.

4 Discussion

The results of this study reveal the complex biochemical, physiological, and structural changes occurring in blueberry (*V. corymbosum*) fruits during ripening and following MeJA treatments. These findings significantly enhance our understanding of how hormonal treatments influence fruit quality, nutritional value, and cell wall integrity, offering valuable insights for both production and postharvest management during two productive seasons. In this line, when evaluating the effects of MeJA on blueberries over the 2022 and 2023 growing seasons, it's essential to consider environmental factors that may have influenced the observed differences in responses. Variations in climate conditions between these seasons can significantly impact plant physiology and the efficacy of treatments like MeJA, when these are carried out in open productive commercial orchard exposed to the environment. For instance, temperature fluctuations can affect the rate of plant metabolic processes, potentially altering the plant's response to MeJA. Differences in rainfall, with 480.2 mm of rainfall during 2022 and 678.4 mm of

TABLE 2 Physiological parameters of blueberry (*Vaccinium corymbosum*) fruits obtained from plants after different treatments with MeJA, during 2 agronomic harvests seasons.

Season	Stage	CIELAB color space			ΔE*	Weight (g)	Diameter (mm)
		L*	a*	b*			
2022	Control	5.88 ± 3.40	1.25 ± 2.36	-0.55 ± 1.51	–	1.46 ± 0.39 [a]	14.62 ± 1.42 [a]
	T1	15.98 ± 11.50	-0.46 ± 9.23	-0.72 ± 5.55	10.24	1.66 ± 0.35 [a]	15.65 ± 1.31 [a]
	T2	7.48 ± 6.34	-0.40 ± 3.94	-0.08 ± 2.31	2.35	1.46 ± 0.35 [a]	16.65 ± 11.28 [a]
2023	Control	12.63 ± 3.55	3.88 ± 5.44	0.62 ± 3.32	–	1.75 ± 0.24 [a]	16.00 ± 0.98 [a]
	T1	18.14 ± 5.22	3.54 ± 5.93	-1.76 ± 2.82	6.01	2.16 ± 0.33 [a]	17.40 ± 1.25 [a]
	T2	12.70 ± 4.48	1.83 ± 3.21	0.43 ± 2.24	2.06	1.93 ± 0.21 [a]	16.53 ± 0.97 [a]

Values indicate the mean of thirty replicates, and the standard deviations are also shown.
*In ΔE, the values compared to the control samples in each season.
In the weight and diameter column, the superscript 'a' indicates that there are no significant differences with a p<=0.95.

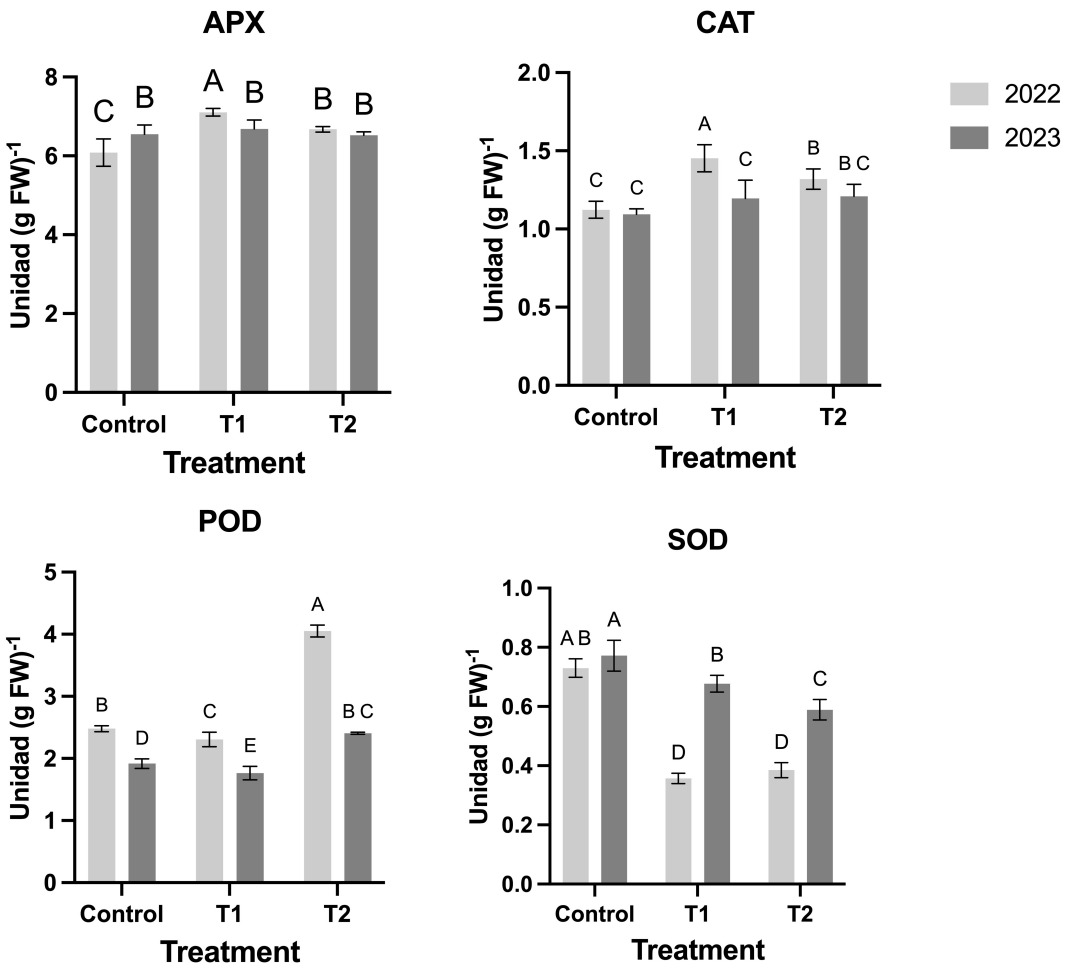

FIGURE 6
Effect of MeJA treatment on the activities of the antioxidant enzymes (CAT, POD, SOD, and APX) in the blueberry fruits. Different letters indicate significant differences ($P < 0.05$; two-way ANOVA). Bars represent means ± SE from three independent experiments.

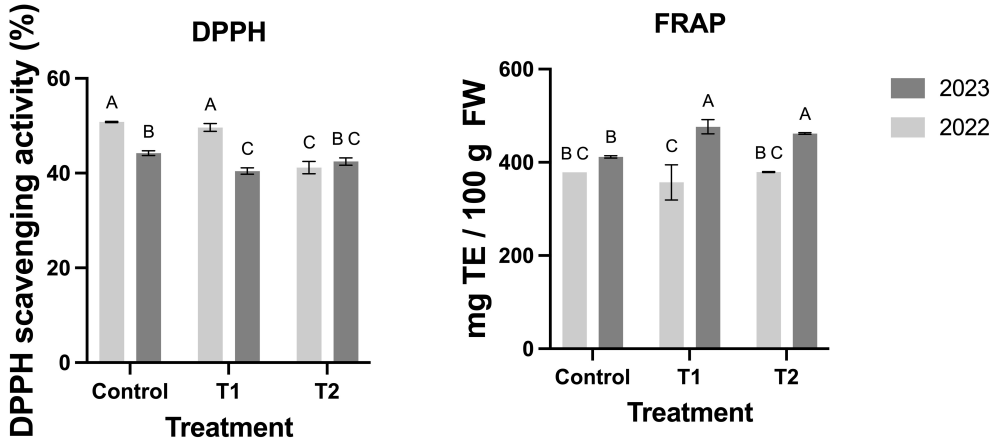

FIGURE 7
Effect of MeJA treatment on the activities of the antioxidant capacity in the blueberry fruits. Different letters indicate significant differences ($P < 0.05$; two-way ANOVA). Bars represent means ± SE from three independent experiments.

10.3389/fpls.2025.1550131

TABLE 3 Pearson's correlation analysis of phenolics content, total flavonoids, total anthocyanins, SSC, TA, SSC/TA, CAT, APX, POD, SOD, DPPH, and FRAP in four different MeJA treatment fruits samples.

2022	Phenolics content	Total Flavonoids	Total Anthocyanins	SSC	TA	SST/ TA	CAT	APX	POD	SOD	DPPH	FRAP
Phenolics content												
Total Flavonoids	0,00											
Total Anthocyanins	-0,70	0,71										
SSC	0,80	0,59	-0,14									
TA	-0,98	0,19	0,83	-0,67								
SSC/TA	0,99 *	-0,15	-0,80	0,71	-1,00 *							
CAT	-0,99 *	0,11	0,78	-0,73	1,00 *	-1,00 *						
APX	-1,00 *	0,09	0,76	-0,75	0,99 *	-1,00 *	1,00 *					
POD	0,09	1,00 *	0,65	0,67	0,10	-0,06	0,02	0,00				
SOD	0,90	-0,44	-0,94	0,46	-0,97 *	0,95	-0,94	-0,93	-0,36			
DPPH	0,11	-0,99 *	-0,79	-0,50	-0,30	0,26	-0,22	-0,20	-0,98 *	0,54		
FRAP	0,86	0,52	-0,23	1,00 *	-0,74	0,77	-0,79	-0,81	0,59	0,54	-0,42	
2023	Phenolics content	Total Flavonoids	Total Anthocyanins	SSC	TA	SST/ TA	CAT	APX	POD	SOD	DPPH	FRAP
Phenolics content												
Total Flavonoids	0,92											
Total Anthocyanins	0,99 *	0,96										
SSC	0,99 *	0,85	0,96									
TA	0,16	0,54	0,28	0,01								
SSC/TA	0,09	-0,31	-0,04	0,24	-0,97 *							
CAT	0,91	0,67	0,85	0,96	-0,27	0,50						
APX	0,62	0,88	0,71	0,50	0,88	-0,73	0,23					
POD	-0,02	-0,41	-0,14	0,13	-0,99 *	0,99 *	0,40	-0,80				
SOD	-0,69	-0,35	-0,59	-0,79	0,61	-0,78	-0,93	0,15	-0,71			
DPPH	-0,97	-0,99 *	-0,99 *	-0,92	-0,40	0,16	-0,78	-0,79	0,27	0,48		
FRAP	1,00 *	0,88	0,98	1,00 *	0,07	0,18	0,94	0,54	0,08	-0,75	-0,94	

*indicate significant at 0.01 p<value Fisher's least significant difference (LSD) test.

rainfall during 2023 in Cauquenes (Information available at https://agrometeorologia.cl/), its can influence disease prevalence and stress levels in plants, particularity during 2022 season which may interact with MeJA treatment outcomes. Additionally, the number of chilling hours (periods of cold temperatures) varies annually and is vital for blueberry bud development; insufficient chilling can lead to poor bud break and uneven ripening, which may alter the plant's responsiveness to MeJA treatments.

Now, respect to the thermogravimetric analysis (TGA), it's have been widely used in different investigations, including a study of the changes in the physiological properties of the cell wall during ripening of the commercial strawberry fruit, and showed a lower thermal stability at the ripe stage than at the green stage (Castro and Morales-Quintana, 2019). Additionally, a second work was published, when we evaluated the changes in cell wall thermal stability produced by the abscisic acid (ABA) hormone and showed that ABA treatment produced a lower thermal stability in strawberry fruit than the control treatment (Castro et al., 2021a). Now, we showed the thermal analysis (Figure 2), that provides further insights into structural changes in the cell wall during ripening in blueberries fruits. As the cell wall undergoes gradual degradation, the fruit softens, losing firmness. The degradation

patterns observed through temperature-based analysis highlight which components of the cell wall confer stability over time, offering a deeper understanding of the natural softening process in ripening fruits. This technique proves valuable for studying both thermal stability and the structural transformations associated with fruit texture, as well as providing evidence of the effect of MeJA on increasing the stability of the different polymers in the cell wall, which would serve as a starting point for further studies on post-processing and drying of fruits.

Table 1 highlights the intricate relationships between color, size, and developmental stages in blueberries, with each ripening stage exhibiting distinct physiological profiles that vary between seasons. MeJA application has been shown to promote anthocyanin biosynthesis (Figure 3), leading to intensified blue pigmentation in ripe fruits. In red-blushed pears, MeJA treatment increased anthocyanin content in the peels, resulting in enhanced coloration (Li et al., 2023). This effect is attributed to the upregulation of genes involved in the anthocyanin biosynthetic pathway, as evidenced by increased expression of both structural and regulatory genes following MeJA application (Li et al., 2023), while in terms of acceptability, it could generate greater consumer appeal.

Variations in phenolic content observed in the study respect to the different seasons, could be attributed to environmental factors, particularly sunlight exposure, which is a well-documented regulator of phenolic biosynthesis in plants. Sunlight, especially UV-B radiation, stimulates the phenylpropanoid pathway, leading to increased accumulation of flavonoids and other phenolic compounds as part of the plant's protective mechanisms against oxidative stress (Zoratti et al., 2014). In this study, fruits exposed to direct sunlight exhibited a 23.5% increase in total phenolic content compared to those grown in shaded conditions. This trend aligns with findings in blueberries, where in the control samples exist differences between two seasons, and according to the According to data obtained from the INIA experimental station, the average solar radiation value during 2022 was higher than in 2023, with values of 16.1 Mj/m² and 15.5 Mj/m², respectively (Information available at https://agrometeorologia.cl/).

These data emphasize the importance of monitoring such parameters for quality control in blueberry production, as they directly affect consumer preference and marketability. As the fruits progress from the green to the blue ripening stage, phenolic content and antioxidant capacity (DPPH and FRAP assays) decline, while anthocyanin content increases (Figure 3). This trend aligns with prior studies showing that ripening reduces antioxidant metabolites such as phenolics, whereas anthocyanins accumulate to enhance pigmentation. These findings underscore the metabolic trade-offs during maturation, where antioxidant defenses are balanced with physiological requirements such as fruit coloration and sweetness development. Early-stage fruits (green stage) demonstrate the highest radical scavenging activity, making them particularly advantageous for applications prioritizing health-promoting properties over sensory attributes. The increase in DPPH and FRAP activity observed in MeJA-treated fruits is likely associated with the activation of the phenylpropanoid pathway, which leads to the accumulation of bioactive compounds with strong radical-scavenging properties (Delgado et al., 2018; Zuñiga et al., 2020). MeJA has been shown to induce key enzymes such as phenylalanine ammonia-lyase (PAL), chalcone synthase (CHS), and peroxidase (POD), all of which contribute to enhanced antioxidant responses (Wasternack, 2007). Moreover, the consistently higher antioxidant activity in MeJA-treated fruits aligns with findings from similar studies in other crops. For instance, strawberries (*Fragaria* × *ananassa*) treated with MeJA exhibited increased total phenolic and flavonoid content, leading to improved antioxidant activity and delayed senescence (Zuñiga et al., 2020).

Biochemically, MeJA applications influenced key nutritional traits (Figure 5). While total phenolic and flavonoid contents showed year-dependent variability, T2 consistently enhanced anthocyanin accumulation, which correlated with the blue stage's pigmentation. These results align with the role of MeJA in activating the biosynthesis of secondary metabolites such as anthocyanins, which contribute to both fruit coloration and antioxidant properties. Additionally, MeJA-treated fruits displayed lower SSC/TA ratios compared to controls, indicating a subtle modulation of sugar and acid metabolism that could impact fruit flavor (Figure 5). Additionally, previously MeJA treatment has been shown to enhance the antioxidant capacity of blueberries, which has practical implications for extending their shelf life (Wang et al., 2019). Studies indicate that MeJA application increases the content of non-enzymatic antioxidants, such as phenolics and flavonoids, in blueberries (Wang et al., 2019). This is partially like what was observed for the O'neail cultivar that we have worked on in this study, because the results are like those described by Wang et al. (2019) but only in the case of phenols for the 2022 season, while flavonoids only in the 2023 season (Figure 5). This enhancement in antioxidant compounds helps in maintaining fruit quality during storage.

MeJA treatments significantly influenced enzymatic and antioxidant dynamics in blueberry fruits. Single (T1) and double (T2) applications enhanced the activity of antioxidant enzymes (APX, CAT, POD, and SOD), with T2 eliciting the strongest POD response. This aligns with MeJA's known role in modulating plant defense pathways and improving oxidative stress tolerance. Understanding oxidative stress as the product of the imbalance between the production of ROS and the plant's ability to detoxify naturally. Antioxidant capacities measured by DPPH and FRAP assays increased substantially with MeJA applications, particularly in T2, indicating that exogenous MeJA stimulates secondary metabolite biosynthesis. These results suggest that MeJA treatments can improve fruit resilience and nutritional quality, further supporting their use in horticultural practices. Specifically, the enzymatic response patterns suggest that single applications (T1) maximize APX, CAT, and SOD activities, while repeated applications (T2) amplify POD activity, contributing to improved oxidative stress tolerance and overall fruit quality during ripening (Figure 6). MeJA modulates antioxidant enzymes through the activation of the jasmonic acid signaling pathway (Fernández-Calvo et al., 2011). Previously, various authors demonstrated that exogenous MeJA treatment during postharvest of different fruits can increase the fruit antioxidant capacity. This result was mainly

observed by enhanced SOD, CAT, APX, and polyphenol oxidase (PPO) with cinnamyl-alcohol dehydrogenase (CAD) activities (Asghari and Hasanlooe, 2015, 2016; Li et al., 2017; Mustafa et al., 2018; Wang et al., 2019). Now we evaluate three of this five enzymes during fruit development to evaluate the effect over postharvest conditions.

The MeJA perception process begging by cell receptors, which activates transcription factors such as MYC2, that bind to the promoters of genes encoding these antioxidant enzymes, increasing their expression. MeJA promotes the accumulation of ROS, which, at controlled levels, act as signals to further activate the antioxidant response, enhancing the activity of these enzymes. The interaction of MeJA with other hormones such as ABA also strengthens the antioxidant response, particularly under abiotic stress conditions like drought. In this way, the increase in antioxidant enzyme activity helps mitigate cellular damage induced by oxidative stress, contributing to plant tolerance under various adverse conditions.

Elevated anthocyanin levels (Figure 3), in blueberries ripe fruits are associated with numerous health benefits due to their potent antioxidant properties. Anthocyanins have been shown to possess antidiabetic, anticancer, anti-inflammatory, antimicrobial, and anti-obesity effects, as well as prevention of cardiovascular diseases (Khoo et al., 2017).

Finally, Figure 7 demonstrates that the enhanced enzymatic activity and accumulation of antioxidant compounds induced by MeJA treatments translate into significant improvements in the antioxidant capacity of blueberry fruits. The observed interannual variability highlights the influence of environmental factors on fruit responses. Overall, these findings support the use of MeJA as a practical tool for enhancing the nutritional and functional quality of blueberries by modulating their antioxidant profiles and improving their resilience and marketability.

The evidence findings during the two seasons suggest that the enhanced enzymatic activity (Figure 6) and accumulation of antioxidant compounds induced by MeJA treatments (Figure 5) translate into significant improvements in the antioxidant capacity of blueberry fruits (Figure 7). Variations between the two years may reflect environmental influences on fruit responses. Overall, this evidence supports the use of MeJA as a practical tool to improve the nutritional and functional quality of blueberries by modulating their antioxidant profiles.

While MeJA and ABA have been studied for their roles in fruit ripening and quality enhancement, their effects can vary. For instance, MeJA has been shown to induce resistance to postharvest pathogens, whereas ABA does not significantly affect pathogen development during storage. Auxins, on the other hand, may delay ripening, which could be advantageous or detrimental depending on the desired outcome (Wang et al., 2018, 2020). In this line, recently we have recently published the effect of ABA and MeJA applications on 'legacy' blueberry plants and their ability to tolerate water deficit (Balbontín et al., 2025). However, these approaches have been carried out in greenhouse plants, like the large number of the extensive bibliography that can be found on ABA, MeJA and/or Auxin applications. For this reason, our work provides some new approaches to how MeJA can positively affect fruit development and its organoleptic properties.

5 Conclusions

This study provides a comprehensive evaluation of the biochemical, physiological, and structural changes occurring in blueberry (*V. corymbosum*) fruits during ripening and following methyl jasmonate (MeJA) treatments. The findings reveal that ripening is characterized by a decline in phenolic content and antioxidant capacity, coupled with an increase in anthocyanin accumulation and metabolic trade-offs that balance antioxidant defenses with pigmentation and sweetness development. Thermal analysis of cell wall components demonstrated a progressive softening process during ripening, highlighting the role of cell wall integrity in fruit texture and postharvest quality.

Importantly, MeJA treatments significantly enhanced enzymatic antioxidant activity (APX, CAT, POD, and SOD) and overall antioxidant capacity (DPPH and FRAP), with repeated applications (T2) eliciting the strongest responses. These treatments not only improved the nutritional profile of the fruit but also reinforced its resilience to oxidative stress, suggesting their potential as a practical tool in horticultural practices. Furthermore, the observed modulation of cell wall stability by MeJA highlights its role in delaying softening, thereby improving fruit firmness and extending shelf life.

The study underscores the dual role of MeJA in enhancing both the functional and marketable quality of blueberries. By modulating antioxidant enzyme activities and secondary metabolite biosynthesis, MeJA not only improves the fruit's nutritional value but also its resistance to oxidative stress, which is crucial for postharvest management. The findings suggest that MeJA can be integrated into sustainable horticultural practices to meet consumer demand for high-quality, functional fruits. However, the study also highlights the importance of considering environmental factors, such as seasonal variations in temperature and rainfall, which can influence the efficacy of MeJA treatments. This variability underscores the need for tailored application protocols that account for genotype-environment interactions.

While this study provides valuable insights into the effects of MeJA on blueberry ripening and quality, several limitations should be acknowledged. First, the research was conducted over two seasons, and while this provides some insight into interannual variability, longer-term studies are needed to fully understand the environmental impacts on MeJA efficacy. Future research should explore the molecular pathways involved in MeJA's effects, including the role of specific genes and transcription factors, to optimize application protocols for different cultivars and growing conditions.

Data availability statement

The original contributions presented in the study are included in the article/Supplementary Material. Further inquiries can be directed to the corresponding author/s.

Author contributions

CV: Conceptualization, Formal analysis, Investigation, Methodology, Visualization, Writing – original draft. MM: Conceptualization, Data curation, Investigation, Methodology, Validation, Writing – review & editing. SF: Investigation, Methodology, Visualization, Writing – review & editing. MB: Investigation, Methodology, Writing – review & editing. RC: Formal analysis, Investigation, Methodology, Visualization, Writing – review & editing. PR: Formal analysis, Funding acquisition, Investigation, Methodology, Project administration, Supervision, Writing – review & editing. DL: Conceptualization, Formal analysis, Validation, Writing – review & editing. CP: Conceptualization, Data curation, Formal analysis, Funding acquisition, Investigation, Methodology, Supervision, Writing – review & editing. LM: Conceptualization, Funding acquisition, Project administration, Resources, Supervision, Writing – original draft, Writing – review & editing.

Funding

The author(s) declare that financial support was received for the research and/or publication of this article. The Agencia Nacional de Investigación y Desarrollo (ANID, Chile) (FONDECYT; Grant No. 1220782, 1240771; ANILLO; Grant No. ATE220014; FONDECYT Postdoctoral; Grant No. 3240463). CV-R acknowledges Universidad Autónoma de Chile for a doctoral scholarship.

Conflict of interest

The authors declare that the research was conducted in the absence of any commercial or financial relationships that could be construed as a potential conflict of interest.

Generative AI statement

The author(s) declare that no Generative AI was used in the creation of this manuscript.

Publisher's note

Supplementary material

The Supplementary Material for this article can be found online at: https://www.frontiersin.org/articles/10.3389/fpls.2025.1550131/full#supplementary-material

References

Andler, R., Rojas, V., Pino, V., Castro, R. I., Valdés, C., Kumar, V., et al. (2023). Efficient production of a polyhydroxyalkanoate by *Azotobacter vinelandii* OP using apple residues as promising feedstock. *Int. J. Biol. Macromol.* 242, 124626. doi: 10.1016/j.ijbiomac.2023.124626

Asghari, M., and Hasanlooe, A. R. (2015). Interaction effects of salicylic acid and methyl jasmonate on total antioxidant content, catalase and peroxidase enzymes activity in "Sabrosa" strawberry fruit during storage. *Scientia Hortic.* 197, 490–495. doi: 10.1016/j.scienta.2015.10.009

Asghari, M., and Hasanlooe, A. R. (2016). Methyl jasmonate effectively enhanced some defense enzymes activity and total antioxidant content in harvested "Sabrosa" strawberry fruit. *Food Sci. Nutr.* 4, 377–383. doi: 10.1002/fsn3.2016.4.issue-3

Balbontín, C., Reyes, M., Yáñez, M. A., Parra-Palma, C., Morales-Quintana, L., and Ramos, P. (2025). Enhancing blueberry drought resilience: ABA and MeJA hormonal formulations unveil water-saving strategies. *Hortic. Environ. Biotechnol.* 66, 99–110. doi: 10.1007/s13580-024-00640-4

Bari, R., and Jones, J. D. G. (2009). Role of plant hormones in plant defence responses. *Plant Mol. Biol.* 69, 473–488. doi: 10.1007/s11103-008-9435-0

Bujor, O.-C., Le Bourvellec, C., Volf, I., Popa, V. I., and Dufour, C. (2016). Seasonal variations of the phenolic constituents in bilberry (Vaccinium myrtillus L.) leaves, stems and fruits, and their antioxidant activity. *Food Chem.* 213, 58–68. doi: 10.1016/j.foodchem.2016.06.042

Cai, H., Han, S., Yu, M., Ma, R., and Yu, Z. (2020). The alleviation of methyl jasmonate on loss of aroma lactones correlated with ethylene biosynthesis in peaches. *J. Food Sci.* 85, 2389–2397. doi: 10.1111/1750-3841.15339

Castro, R. I., Gonzalez-Feliu, A., Valenzuela-Riffo, F., Parra-Palma, C., and Morales-Quintana, L. (2021a). Changes in the cell wall components produced by exogenous abscisic acid treatment in strawberry fruit. *Cellulose.* 28, 1555–1570. doi: 10.1007/s10570-020-03607-7

Castro, R. I., and Morales-Quintana, L. (2019). Study of the cell wall components produced during different ripening stages through thermogravimetric analysis. *Cellulose* 26, 3009–3020. doi: 10.1007/s10570-019-02305-3

Castro, R. I., Muñoz-Vera, M., and Morales-Quintana, L. (2021b). Evaluation of cell wall modification in two strawberry cultivars with contrasted softness. *Agronomy* 11, 1100. doi: 10.3390/agronomy11061100

Castro, R. I., Vásquez-Rojas, C., Cortiella, M. G. I., Parra-Palma, C., Ramos, P., and Morales-Quintana, L. (2023). Evolution of the Volatile Organic Compounds, Phenols and Antioxidant Capacity during Fruit Ripening and Development of Rubus ulmifolius Schott Fruits. *Horticulturae* 9, 13. doi: 10.3390/horticulturae9010013

Chang, C. C., Yang, M. Y., Wen, H. M., and Chern, J. C. (2002). Estimation of total flavonoid content in propolis by two complementary colorimetric methods. *J. Food Drug Anal.* 10, 178–182. doi: 10.38212/2224-6614.2748

Cheel, J., Theoduloz, C., Rodríguez, J. A., Caligari, P. D. S., and Schmeda-Hirschmann, G. (2007). Free radical scavenging activity and phenolic content in achenes and thalamus from Fragaria chiloensis ssp. chiloensis, *F. vesca* and *F. x ananassa* cv. Chandler. *Food Chem.* 102, 36–44. doi: 10.1016/j.foodchem.2006.04.036

Cocetta, G., Rossoni, M., Gardana, C., Mignani, I., Ferrante, A., and Spinardi, A. (2015). Methyl jasmonate affects phenolic metabolism and gene expression in blueberry (*Vaccinium corymbosum*). *Physiol. Plant* 153, 269–283. doi: 10.1111/ppl.12243

Delgado, L. D., Zúñiga, P. E., Figueroa, N. E., Pastene, E., Escobar-Sepúlveda, H. F., Figueroa, P. M., et al. (2018). Application of a JA-ile biosynthesis inhibitor to methyl jasmonate-treated strawberry fruit induces upregulation of specific MBW complex-related genes and accumulation of proanthocyanidins. *Molecules* 23, 1433. doi: 10.3390/molecules23061433

Erdogan, Ü, Çakmakçi, R., Varmazyari, A., Turan, M., Erdogan, Y., and Kitir, N. (2016). Role of inoculation with multi-trait rhizobacteria on strawberries under water deficit stress. *Agriculture* 103, 67–76. doi: 10.13080/z-a.2016.103.009

Fernández-Calvo, P., Chini, A., Fernández-Barbero, G., Chico, J. M., Gimenez-Ibanez, S., Geerinck, J., et al. (2011). The Arabidopsis bHLH transcription factors MYC3 and MYC4 are targets of JAZ repressors and act additively with MYC2 in the activation of jasmonate responses. *Plant Cell* 23, 701–715. doi: 10.1105/tpc.110.080788

Flores, G., Blanch, G. P., and Ruiz del Castillo, M. L. (2017). Effect of postharvest methyl jasmonate treatment on fatty acid composition and phenolic acid content in olive fruits during storage. *J. Sci. Food Agric.* 97, 2767–2772. doi: 10.1002/jsfa.2017.97.issue-9

Ghaffari, A., Navaee, K., Oskoui, M., Bayati, K., and Rafiee-Tehrani, M. (2007). Preparation and characterization of free mixed-film of pectin/chitosan/Eudragit RS intended for sigmoidal drug delivery. *Eur. J. Pharm. Biopharm* 67, 175–186. doi: 10.1016/j.ejpb.2007.01.013

Guo, X. Y., Zhang, X. S., and Huang, Z. Y. (2010). Drought tolerance in three hybrid poplar clones submitted to different watering regimes. *J. Plant Ecol.* 3, 79–87. doi: 10.1093/jpe/rtq007

Gupta, V., Estrada, A. D., Blakley, I., Reid, R., Patel, K., Meyer, M. D., et al. (2015). RNA-Seq analysis and annotation of a draft blueberry genome assembly identifies candidate genes involved in fruit ripening, biosynthesis of bioactive compounds, and stage-specific alternative splicing. *GigaScience* 4, 5. doi: 10.1186/s13742-015-0046-9

Huang, X., Li, J., Shang, H., and Meng, X. (2015). Effect of methyl jasmonate on the anthocyanin content and antioxidant activity of blueberries during cold storage. *J. Sci. Food Agric.* 95, 337–343. doi: 10.1002/jsfa.6725

Huang, W., Yao, L., He, X., Wang, L., Li, M., Yang, Y., et al. (2018). Hypoglycemic activity and constituents analysis of blueberry (Vaccinium corymbosum) fruit extracts. *Diabetes Metab. Syndr. Obes. Targets Ther.* 11, 357. doi: 10.2147/DMSO.S166728

Jara, K., Castro, R. I., Ramos, P., Parra-Palma, C., Valenzuela-Riffo, F., and Morales-Quintana, L. (2019). Molecular Insights into FaEG1, a Strawberry Endoglucanase Enzyme Expressed during Strawberry Fruit Ripening. *Plants* 8, 140. doi: 10.3390/plants8060140

Kalt, W., Cassidy, A., Howard, L. R., Krikorian, R., Stull, A. J., Tremblay, F., et al. (2020). Recent research on the health benefits of blueberries and their anthocyanins. *Adv. Nutr.* 11, 224. doi: 10.1093/advances/nmz065

Khoo, H. E., Azlan, A., Tang, S. T., and Lim, S. M. (2017). Anthocyanidins and anthocyanins: colored pigments as food, pharmaceutical ingredients, and the potential health benefits. *Food Nutr. Res.* 61, 1361779. doi: 10.1080/16546628.2017

Li, H., Suo, J., Han, Y., Liang, C., Jin, M., Zhang, Z., et al. (2017). The effect of 1-methylcyclopropene, methyl jasmonate and methyl salicylate on lignin accumulation and gene expression in postharvest 'Xuxiang' kiwifruit during cold storage. *Postharvest Biol. Technol.* 124, 107–118. doi: 10.1016/j.postharvbio.2016.10.003

Li, D.-P., Xu, Y.-F., Sun, L.-P., Liu, L.-X., Hu, X.-L., Li, D.-Q., et al. (2006). Salicylic acid, ethephon, and methyl jasmonate enhance ester regeneration in 1-MCP-treated apple fruit after long-term cold storage. *J. Agric. Food Chem.* 54, 3887–3895. doi: 10.1021/jf060240j

Li, B., Zhang, X., Han, C., Duan, R., Yang, J., and Xue, H. (2023). Effects of methyl jasmonate on fruit coloration and quality improvement in pears (*Pyrus bretschneideri*). *Agronomy.* 13, 2409. doi: 10.3390/agronomy13092409

Lohachoompol, V., Srzednicki, G., and Craske, J. (2004). The change of total anthocyanins in blueberries and their antioxidant effect after drying and freezing. *BioMed. Res. Int.* 2004, 485873. doi: 10.1155/S1110724304406123

Morales-Quintana, L., Moya, M., Santelices-Moya, R., Cabrera-Ariza, A., Rabert, C., Pollmann, S., et al. (2022a). Improvement in the physiological and biochemical performance of strawberries under drought stress through symbiosis with Antarctic fungal endophytes. *Front. Microbiol.* 13. doi: 10.3389/fmicb.2022.939955

Morales-Quintana, L., Tapia-Valdebenito, D., Castro, R. I., Rabert, C., Larama, G., Gutiérrez, A., et al. (2022b). Characterization of the Cell Wall Component through Thermogravimetric Analysis and Its Relationship with an Expansin-like Protein in Deschampsia Antarctica. *Int. J. Mol. Sci.* 23, 5741. doi: 10.3390/ijms23105741

Mustafa, M. A., Ali, A., Seymour, G., and Tucker, G. (2018). Treatment of dragonfruit (Hylocereus polyrhizus) with salicylic acid and methyl jasmonate improves postharvest physico-chemical properties and antioxidant activity during cold storage. *Scientia Hortic.* 231, 89–96. doi: 10.1016/j.scienta.2017.09.041

Neto, C. C. (2007). Cranberry and blueberry: evidence for protective effects against cancer and vascular diseases. *Mol. Nutr. Food Res.* 51, 652–664. doi: 10.1002/mnfr.200600279

Parra-Palma, C., Morales-Quintana, L., and Ramos, P. (2020). Phenolic content, color development, and pigment related gene expression: A comparative analysis in different cultivars of strawberry during the ripening process. *Agronomy* 10, 588. doi: 10.3390/agronomy10040588

Parra-Palma, C., Ramos, P., and Morales-Quintana, L. (2025). Optimization of ultrasound-assisted extraction (UAE) of phenolics from blueberries by response surface methodology (RSM). *Analytical Lett.* 204, 1–19. doi: 10.1080/00032719.2025.2453592

Parra-Palma, C., Valdes, C., Muñoz-Vera, M., Morales-Quintana, L., and Castro, R. I. (2024). Assessing the modifications and degradation of cell wall polymers during the ripening process of Rubus ulmifolius Schott fruit. *J. Hortic. Sci. Biotechnol.* 99, 471–479. doi: 10.1080/14620316.2024.2302515

Silva, S., Costa, E. M., Veiga, M., Morais, R. M., Calhau, C., and Pintado, M. (2020). Health promoting properties of blueberries: a review. *Crit. Rev. Food Sci. Nutr.* 60, 181–200. doi: 10.1080/10408398.2018.1518895

Skrovankova, S., Sumczynski, D., Mlcek, J., Jurikova, T., and Sochor, J. (2015). Bioactive compounds and antioxidant activity in different types of berries. *Int. J. Mol. Sci.* 16, 24673–24706. doi: 10.3390/ijms161024673

Wang, H., Kou, X., Wu, C., Fan, G., and Li, T. (2020). Methyl jasmonate induces the resistance of postharvest blueberry to gray mold caused by Botrytis cinerea. *J. Sci. Food Agric.* 100, 4272–4281. doi: 10.1002/jsfa.10469

Wang, Y.-W., Malladi, A., Doyle, J. W., Scherm, H., and Nambeesan, S. U. (2018). The effect of ethephon, abscisic acid, and methyl jasmonate on fruit ripening in rabbiteye blueberry (Vaccinium virgatum). *Horticulturae* 4, 24. doi: 10.3390/horticulturae4030024

Wang, H., Wu, Y., Yu, R., Wu, C., Fan, G., and Li, T. (2019). Effects of postharvest application of methyl jasmonate on physicochemical characteristics and antioxidant system of the blueberry fruit. *Scientia Hortic.* 258, 108785. doi: 10.1016/j.scienta.2019.108785

Wasternack, C. (2007). Jasmonates: an update on biosynthesis, signal transduction and action in plant stress response, growth and development. *Ann. Bot.* 100, 681–697. doi: 10.1093/aob/mcm079

Wasternack, C., and Hause, B. (2013). Jasmonates: biosynthesis, perception, signal transduction and action in plant stress response, growth and development. *Ann. Bot.* 111, 1021–1058. doi: 10.1093/aob/mct067

Wu, H., Wu, X., Li, Z., Duan, L., and Zhang, M. (2012). Physiological evaluation of drought stress tolerance and recovery in cauliflower (*Brassica oleracea* L.) seedlings treated with methyl jasmonate and coronatine. *J. Plant Growth Regul.* 31, 113–123. doi: 10.1007/s00344-011-9224-x

Xiao, B., Sun, X., and Sun, R. (2001). Chemical, structural, and thermal characterizations of alkali-soluble lignins and hemicelluloses, and cellulose from maize stems, rye straw, and rice straw. *Polym Degrad Stab* 74, 307–319. doi: 10.1016/S0141-3910(01)00163-X

Zafra-Stone, S., Yasmin, T., Bagchi, M., Chatterjee, A., Vinson, J. A., and Bagchi, D. (2007). Berry anthocyanins as novel antioxidants in human health and disease prevention. *Mol. Nutr. Food Res.* 51, 675–683. doi: 10.1002/mnfr.200700002

Zoratti, L., Karppinen, K., Luengo Escobar, A., Häggman, H., and Jaakola, L. (2014). Light-controlled flavonoid biosynthesis in fruits. *Front. Plant Sci.* 5. doi: 10.3389/fpls.2014.00534

Zuñiga, P. E., Castañeda, Y., Arrey-Salas, O., Fuentes, L., Aburto, F., and Figueroa, C. R. (2020). Methyl Jasmonate Applications From Flowering to Ripe Fruit Stages of Strawberry (*Fragaria* × *ananassa* 'Camarosa') Reinforce the Fruit Antioxidant Response at Post-harvest. *Front. Plant Sci.* 11. doi: 10.3389/fpls.2020.00538

frontiers | Frontiers in Plant Science

TYPE Original Research
PUBLISHED 28 March 2025
DOI 10.3389/fpls.2025.1501545

OPEN ACCESS

EDITED BY
Hosam O. Elansary,
King Saud University, Saudi Arabia

REVIEWED BY
Yogesh K. Ahlawat,
Chandigarh University, India
Rajiv Ranjan,
Dayalbagh Educational Institute, India

*CORRESPONDENCE
Guangying Du
duguangying114@gzy.edu.cn
Jinqiang Zhang
552450374@qq.com

RECEIVED 25 September 2024
ACCEPTED 11 March 2025
PUBLISHED 28 March 2025

CITATION
Hou Y, Du G, Li J, Liu P and Zhang J (2025) Multidimensional evaluation of quality differences for *Dendrobium officinale* stems grown under different cultivation environments based on widely targeted metabolomics, network pharmacology, molecular docking, and cell experiments. *Front. Plant Sci.* 16:1501545. doi: 10.3389/fpls.2025.1501545

Multidimensional evaluation of quality differences for *Dendrobium officinale* stems grown under different cultivation environments based on widely targeted metabolomics, network pharmacology, molecular docking, and cell experiments

Yingyue Hou[1], Guangying Du[1*], Jing Li[1], Pei Liu[2] and Jinqiang Zhang[2*]

[1]School of Information Engineering, Guizhou University of Traditional Chinese Medicine, Guiyang, China, [2]Resource Institute for Chinese and Ethnic Materia Medica, Guizhou University of Traditional Chinese Medicine, Guiyang, China

Introduction: *Dendrobium officinale* is an endangered perennial epiphytic herbaceous plant. In the Chinese Pharmacopoeia, the dried stems of *D. officinale* are used medicinally and are commonly utilized as a medicinal and food homologous product. Notable variations in the quality of *D. officinale* stems are observed across different cultivation environments; however, the underlying mechanisms remain unclear.

Methods: Metabolites in *D. officinale* stems grown in stone epiphytic, tree epiphytic, and greenhouse environments were identified using UPLC-MS/MS-based widely targeted metabolomics. Differential metabolites from stems grown in different cultivation environments were selected for studies on quality differences. Network pharmacology was employed to investigate the core targets of these differential metabolites, and molecular docking validation was conducted with these metabolites to identify quality markers. Finally, a combination of network pharmacology and *in vitro* experimental results was used to explore the reasons behind the differences in therapeutic effects of *D. officinale* stems grown in various cultivation environments.

Results: A total of 1929 primary and secondary metabolites were identified. Compared to the tree epiphytic and greenhouse environments, 58 primary and secondary metabolites were up-regulated in the stone epiphytic environment. Among these, 7 amino acids and their derivatives were exclusively found as up-regulated primary metabolites, while 18 flavonoids constituted the main up-regulated secondary metabolites. The binding affinities of the 18 flavonoids to the core targets (MAOA and TNF) were superior to those of other up-regulated metabolites, and they can be utilized in quality difference studies, particularly nicotiflorin and isoquercitrin. Stems grown in the stone epiphytic environment

showed a superior protective effect on chronic atrophic gastritis cells compared to the other two environments. This was associated with increased binding of differential metabolites to targets such as MAOA and TNF and decreased binding to targets such as SRC and PTGS2.

Discussion: The composition and content of metabolites in *D. officinale* stems are influenced by the cultivation environment, which in turn affects the therapeutic effects of the stems. The change of the target preference could be the reason for the difference in drug efficacy. This study introduces a novel approach for distinguishing the quality of *D. officinale* stems grown under different cultivation environments and exploring the variations in their therapeutic effects.

KEYWORDS

***Dendrobium officinale*, metabolomics, network pharmacology, quality evaluation, molecular docking**

1 Introduction

Dendrobium is one of the three largest genera in the Orchidaceae family (Schuiteman, 2011). *Dendrobium officinale* Kimura et Migo, regarded as the most valuable species within the genus *Dendrobium*, is a perennial epiphytic plant commonly found across Southeast and South Asia. In the Chinese Pharmacopoeia (2020 edition), only the dried stems of *D. officinale* are used, with reported effects that include benefiting the stomach, generating fluids, nourishing *Yin*, and clearing heat (National Pharmacopoeia Commission, 2020). Modern pharmacological studies have also demonstrated that *D. officinale* stems are rich in active compounds (Yang et al., 2023a) and are widely utilized as a functional food (Luo et al., 2017). Notably, on November 9, 2023, the National Health Commission of China officially included *D. officinale* stems in the "Catalogue of Substances Traditionally Used as Both Food and Herbal Medicine," affirming their long-term safety for consumption (National Health Commission et al., 2023).

Numerous studies have shown that *D. officinale* stems possess various health benefits, including the improvement of gastrointestinal mucosa injury (Yang et al., 2020), anti-colitis effects (Liang et al., 2018), anticancer properties (Liu et al., 2023), anti-diabetes activity (Lv et al., 2023), immune regulation (Dong et al., 2022), anti-liver injury effects (Lei et al., 2019), and protection against metabolic hypertension (Li et al., 2021). These therapeutic effects are primarily attributed to the rich bioactive compounds found in the plant, such as polysaccharides, flavonoids, alkaloids, and free amino acids (Xu et al., 2022; Wu et al., 2020). In the Chinese Pharmacopoeia, moisture content, total ash, alcohol-soluble extract, polysaccharide content, and mannose content serve as quality standards for the dried stems of *D. officinale* (National Pharmacopoeia Commission, 2020). As a result, most current quality evaluations and pharmacological activity studies of *D. officinale* focus on the polysaccharides found in its stems. However, the chemical complexity and diversity of plants further suggest that relying on a single compound is insufficient to comprehensively assess the quality of medicinal plants (Luo et al., 2024; Qaderi et al., 2023). Secondary metabolites also play a vital role in the pharmacological activities of medicinal plants (Strzemski et al., 2019). Flavonoids, the main secondary metabolites in *D. officinale* stems, are significant contributors to its physiological activity (Zuo et al., 2020). These compounds exhibit a range of pharmacological properties, including antioxidant and hypoglycemic effects (Ross and Kasum, 2002; Luo et al., 2023). Therefore, it is necessary to conduct a comprehensive analysis of the primary and secondary metabolites of *D. officinale* stems.

Due to long-term overharvesting, the wild resources of *D. officinale* are nearing extinction. Currently, the market primarily relies on artificially cultivated *D. officinale*, with three main cultivation methods: Stone epiphytic cultivation (on black limestone with carbonate rock as the parent rock), Tree epiphytic cultivation (on the bark of Schima superba trees), and Greenhouse cultivation (on the bark of pine trees) (Cheng et al., 2019). Notably, classical texts emphasize that *D. officinale* stems grown in stone epiphytic cultivation environment are regarded as having the highest quality (Zheng et al., 2024). It is well known that the composition and content of secondary metabolites in plants are influenced by their growth environment (Hornyák et al., 2022). Research has shown that *D. officinale* stems grown in wild stone epiphytic cultivation environment have higher polysaccharide, total flavonoid, and total alkaloid content than those from greenhouse environment (Yuan et al., 2020). On the other hand, *D. officinale* stems grown in stone epiphytic cultivation have significantly higher levels of secondary metabolites compared to those grown in tree epiphytic and greenhouse environments (Yang et al., 2023b). Therefore, there are significant differences in the quality of

D. officinale stems grown in these three cultivation environments, with those grown in stone epiphytic cultivation environment potentially having higher quality. However, how to fully evaluate the quality of *D. officinale* stems in different cultivation environments is still a problem. The identification of suitable quality markers for controlling the quality of medicinal plants has become widely recognized as essential (Dong et al., 2020; Zeng et al., 2023). The widely targeted metabolomics, also known as second-generation targeted metabolomics, analysis based on liquid chromatography-tandem mass spectrometry (UPLC-MS/MS) is a fast and reliable method for detecting plant metabolites (Fraga et al., 2010). It overcomes the limitations of targeted metabolomics, which focuses on a narrow range of compounds, and addresses the shortcomings of untargeted metabolomics, such as reduced accuracy in both qualitative identification and quantitative analysis due to the lack of standardized references (Li et al., 2022). Based on UPLC-MS/MS, screening appropriate metabolites for quality evaluation of medicinal plants represents a viable direction (Tong et al., 2021).

On the other hand, the mechanism of action of a metabolite or the entire crude extract of *D. officinale* stems on its target is not yet fully understood. A promising direction for further research involves studying the mechanism of action by analyzing the interactions between multiple components and their target preferences (Zeng et al., 2023). By integrating metabolomics data with network pharmacology, a compound-target-disease network can be constructed, allowing for the exploration of the material basis and molecular mechanisms of traditional Chinese medicine in treating diseases from a systematic and holistic perspective. However, traditional network pharmacology analysis typically only quantifies compound-target-disease correlations without evaluating their strength (Li and Zhang, 2013). Therefore, in this study, the predicted target scores and Protein-Protein Interaction (PPI) network scores based on the metabolites of *D. officinale* stems were weighted to identify important targets.

This study collected samples of *D. officinale* stems from three cultivation environments: tree epiphytic cultivation, stone epiphytic cultivation, and greenhouse cultivation. Ultra Performance Liquid Chromatography-Tandem Mass Spectrometry (UPLC-MS/MS) technology was employed to analyze the metabolites of *D. officinale* stems, and weighted network pharmacology was constructed to investigate the bioactive components and mechanisms of action of *D. officinale* stems. Eighteen flavonoid types were selected as references for cultivating high-quality *D. officinale* stems, and the target preference mechanism of *D. officinale* stems was preliminarily explored. Additionally, the advantages and disadvantages of *D. officinale* stems under different cultivation environments for treating liver cancer and chronic atrophic gastritis were investigated through *in vitro* experiments. The experimental process is shown in Supplementary Figure S1. The research findings provide a foundational basis for the rational assessment of *D. officinale* stems quality across different cultivation environments and hold significant scientific importance for the high-quality development of the *D. officinale* forest understory ecological planting industry.

2 Materials and methods

2.1 Sampling and preparing

Fresh stems (2-year-old) of *D. officinale* were collected from Anlong County in Southwest Guizhou, China, in April 2023. Details of the sample collection are shown in Table 1. To ensure the accuracy and representativeness of the collected samples, nine stems were combined to form one sample, with three replicate samples per group. A total of nine sample groups were classified as SEC 1-3 (stone epiphytic culture environment, Figure 1A), TEC 1-3 (tree epiphytic culture environment, Figure 1B), and GC 1-3 (greenhouse culture environment, Figure 1C). The plant samples were identified by Guangying Du. The samples were placed into sampling bags and stored in a dry ice bucket on site. Upon returning to the laboratory, the samples were stored at -80°C for later use.

Using vacuum freeze-drying technology, place the biological samples in a lyophilizer (Scientz-100F), then grinding (30 Hz, 1.5 min) the samples to powder form by using a grinder (MM 400, Retsch). Next, weigh 50 mg of sample powder using an electronic balance (MS105Dμ) and add 1200 μL of -20°C pre-cooled 70% methanolic aqueous internal standard extract (less than 50 mg added at the rate of 1200 μL extractant per 50 mg sample). Vortex once every 30 min for 30 sec, for a total of 6 times. After centrifugation (rotation speed 12000 rpm, 3 min), the supernatant was aspirated, and the sample was filtered through a microporous membrane (0.22 μm pore size) and stored in the injection vial for UPLC-MS/MS analysis.

TABLE 1 The information of the selected samples.

Cultivation Environments	Epiphytic Substrates	Time of Harvesting	Growing Years	Elevation (m)	Climate Type
Tree epiphytic cultivation (TEC)	*Schima superba*	202304	2 years old	1135.6	Subtropical monsoon climate
Stone epiphytic cultivation (SEC)	Limestone	202304	2 years old	1152.2	Subtropical monsoon climate
Greenhouse cultivation (GC)	Pine bark	202304	2 years old	1119.5	–

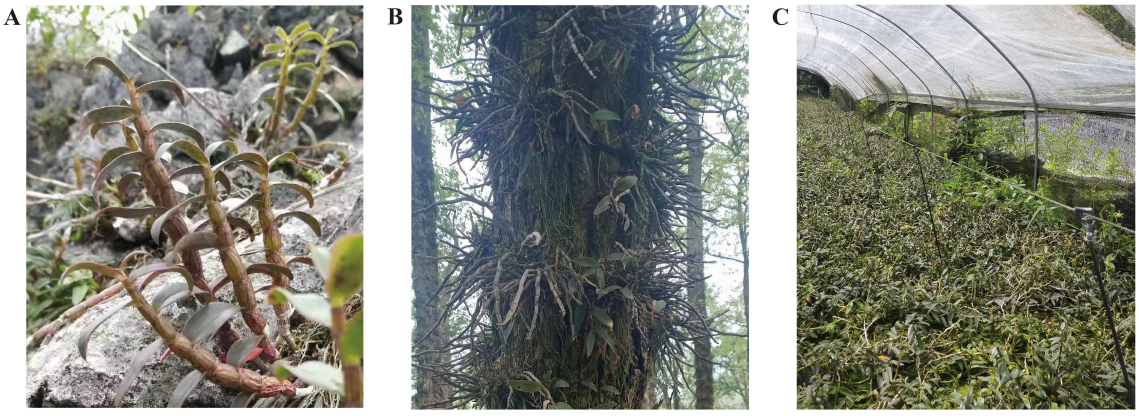

FIGURE 1
The three growth environments of *D. officinale*: **(A)** Stone epiphytic culture environment in the wild. **(B)** Tree epiphytic culture environment in the wild. **(C)** Greenhouse culture environment.

2.2 Metabolite identification and quantification

2.2.1 Widely targeted metabolomics

The widely targeted metabolomics employed in this study is based on the multiple reaction monitoring (MRM) mode of UPLC-MS/MS. UPLC: Utilizes ultra-high pressure and small particle size chromatographic columns to achieve efficient separation of metabolites, thereby minimizing co-elution of compounds; MS/MS: Employs a triple quadrupole mass spectrometer (QQQ), where the first quadrupole (Q1) screens for parent ions of target metabolites, the second quadrupole (Q2) fragments these parent ions into characteristic daughter ions through collision-induced dissociation (CID), and the third quadrupole (Q3) selectively monitors specific daughter ions; MRM mode: Based on the known molecular weights (m/z) of metabolites, specific parent ions are screened in Q1. In Q3, only the characteristic daughter ions generated from the fragmentation of parent ions via CID are monitored (Chen et al., 2013; Dunn et al., 2013).

2.2.2 UPLC conditions

The sample extracts were analyzed using an UPLC-ESI-MS/MS system (UPLC, ExionLC™ AD, *https://sciex.com.cn/*) and Tandem mass spectrometry system (*https://sciex.com.cn/*). The analytical conditions were as follows, UPLC: column, Agilent SB-C18 (1.8 μm, 2.1 mm * 100 mm); The mobile phase was consisted of solvent A, pure water with 0.1% formic acid, and solvent B, acetonitrile with 0.1% formic acid. Sample measurements were performed with a gradient program that employed the starting conditions of 95% A, 5% B. Within 9 min, a linear gradient to 5% A, 95% B was programmed, and a composition of 5% A, 95% B was kept for 1 min. Subsequently, a composition of 95% A, 5.0% B was adjusted within 1.1 min and kept for 2.9 min. The flow velocity was set as 0.35 mL per minute; The column oven was set to 40°C; The injection volume was 2 μL. The effluent was alternatively connected to an ESI-triple quadrupole-linear ion trap (QTRAP)-MS.

2.2.3 ESI-Q TRAP-MS/MS

The ESI source operation parameters were as follows: source temperature 500°C; ion spray voltage (IS) 5500 V (positive ion mode)/-4500 V (negative ion mode); ion source gas I (GSI), gas II (GSII), curtain gas (CUR) were set at 50, 60, and 25 psi, respectively; the collision-activated dissociation (CAD) was high. QQQ scans were acquired as MRM experiments with collision gas (nitrogen) set to medium. DP (declustering potential) and CE (collision energy) for individual MRM transitions was done with further DP and CE optimization. A specific set of MRM transitions were monitored for each period according to the metabolites eluted within this period.

2.2.4 Qualitative and quantitative analysis of metabolites

Mass spectrometry data were processed using Analyst 1.6.3 software. The total ion current (TIC), which represents the sum of all ion intensities in the mass spectrum plotted over time, was analyzed for the quality control (QC) samples from the mixed group. Additionally, multi-peak chromatograms from metabolite detection in MRM mode (ion chromatography spectrum for multi-substance extraction, XIC) were evaluated. The x-axis denotes the retention time (Rt) for metabolite detection, while the y-axis represents ion current intensity, measured in counts per second (CPS). The labels “N” and “P” correspond to negative and positive ion modes, respectively. The TIC and MRM chromatograms are presented in Supplementary Figures S2-Supplementary Figures S3. Qualitative and quantitative metabolite analysis was conducted using a local metabolic database (Metware database, Wuhan Metware Biotechnology Co., Ltd., Wuhan, 430070, China). The MRM multi-peak detection plot shows the metabolites identified in the samples, with each chromatographic peak assigned a distinct color corresponding to a specific metabolite. A triple quadrupole mass spectrometer was used to screen characteristic ions for each metabolite, and the signal intensity (CPS) of these ions was recorded by the detector. Raw mass spectrometry data files were processed using MultiQuant software for chromatographic peak integration and correction. The peak area (Area) of each

chromatographic peak was used to represent the relative abundance of the corresponding metabolite. All integrated chromatographic peak area data were exported and saved for further analysis. To evaluate differences in metabolite content across samples, chromatographic peaks for each metabolite were corrected based on retention time and peak shape information. This approach ensured accurate qualitative and quantitative results for all detected metabolites. The comparison results are shown in Supplementary Figure S4.

2.3 Statistical analysis and differential metabolites selected

2.3.1 Principal component analysis

Unsupervised principal component analysis (PCA) was performed by statistics function prcomp within R (*www.r-project.org*). The data was unit variance scaled before unsupervised PCA.

2.3.2 Hierarchical cluster analysis and pearson correlation coefficients

The HCA (hierarchical cluster analysis) results of samples and metabolites were presented as heatmaps with dendrograms, while pearson correlation coefficients (PCC) between samples were calculated by the cor function in R and presented as only heatmaps. Both HCA and PCC were carried out by R package ComplexHeatmap. For HCA, normalized signal intensities of metabolites (unit variance scaling) are visualized as a color spectrum.

2.3.3 Differential metabolites selected

The characteristics of metabolomics data are "high-dimensional and massive," necessitating the integration of both univariate and multivariate statistical analysis methods. These methods should be applied from multiple perspectives according to the data's properties to accurately identify differential metabolites. Univariate statistical analysis methods encompass hypothesis testing and fold change (FC) analysis. Multivariate statistical analysis methods include PCA, orthogonal partial least squares discriminant analysis (OPLS-DA), among others. Based on the variable importance in projection (VIP) values obtained from the OPLS-DA model (with biological replicates ≥ 3), preliminary screening of metabolites differing among different varieties or tissues can be conducted (Zeng et al., 2024). Simultaneously, the P-value/FDR obtained from univariate analysis (Li et al., 2023) or FC value (Sun et al., 2020b) can be combined to further filter out differential metabolites. In this study, for two-group analysis, differential metabolites were identified based on VIP > 1, $p < 0.01$, and $|\text{Log}_2\text{FC}| \geq 1.0$. VIP values were extracted from the OPLS-DA results, which also included score plots and permutation plots, generated using the R package MetaboAnalystR. Data were log-transformed and mean-centered before OPLS-DA. To avoid overfitting, a permutation test with 200 permutations was performed.

2.3.4 KEGG annotation and enrichment analysis

Identified metabolites were annotated using KEGG Compound database (*http://www.kegg.jp/kegg/compound/*), annotated metabolites were then mapped to KEGG Pathway database (*http://www.kegg.jp/kegg/pathway.html*). Pathways with significantly regulated metabolites mapped to were then fed into MSEA (metabolite sets enrichment analysis), their significance was determined by hypergeometric test's p-values.

2.4 Weighted network pharmacology analysis

2.4.1 Collection of differential metabolite targets and disease targets

The SMILES format files of differential metabolites were retrieved from the PubChem database (*https://pubchem.ncbi.nlm.nih.gov/*). The SMILES format files of the differential metabolites were input into the Swiss Target Prediction database (*https://www.swisstargetprediction.ch*) to predict the corresponding targets of these compounds. Targets with a probability greater than 0.12 were selected and summarized. Through a literature review, three diseases were identified where *D. officinale* stems may have therapeutic potential: type 2 diabetes, Alzheimer's disease, and liver cancer. Relevant disease targets were then searched for and downloaded from the GeneCards database (*https://www.genecards.org/*).

2.4.2 Weighted-targeted network analysis

The targets from the Swiss Target Prediction database were input into the protein-protein interaction network (PPI) of the STRING database (*https://www.string-db.org/*), with the interaction score set to greater than 0.4 (Supplementary Figure S5). Combined with the results of the Swiss Target Prediction and STRING analysis, a weighted-target network was constructed by Gephi 0.10.1, which can be downloaded from *https://gephi.org/users/download/*. The target degree was calculated using Cytoscape_v3.10.0 (Supplementary Table S1). To perform KEGG enrichment analysis on the targets of differential metabolites, the targets were entered into the DAVID database, with the identifier set to "SYMBOL" and the species selected as "Homo sapiens". After completing the analysis, the results were further visualized using a bioinformatics website (*https://www.bioinformatics.com.cn/*).

2.5 Collection of compound structures and receptor protein

The two-dimensional (2D) or three-dimensional (3D) structures of the compounds were downloaded from the PubChem database and saved in SDF format. The 2D structures of some compounds were provided by Wuhan Mateweier Biotechnology Co., Ltd. These compound structures are used as ligands. The SDF files were then converted to PDB format using Chem3D 2022, which served as small molecule ligands. The 3D structures of MAOA (Monoamine oxidase

A, PBD ID: 2Z5X), TNF (Tumor Necrosis Factor, PDB ID: 1NCF), SRC (SRC protein tyrosine kinase, PDB ID: 3D7T), and PTGS2 (Prostaglandin Endoperoxide Synthase 2, PDB ID: 5IKV) were obtained from the RCSB PDB database (*https://www.rcsb.org/*).

2.6 Molecular docking simulation

PyMOL 2.6 was used to remove water molecules and ligands from receptor proteins. AutoDockTools 1.5.6 was used to choose the torsions of ligands and add polar hydrogens of protein receptor molecules. Molecular docking simulation was performed using AutoDock Vina 1.1.2 (Liu et al., 2024; Zeng et al., 2023) (AutoDock Vina – molecular docking and virtual screening program (*https://vina.scripps.edu/*)). The accuracy of AutoDock Vina molecular docking simulations is approximately 80% (Trott and Olson, 2010; Eberhardt et al., 2021). In this study, each molecular docking was conducted over 20 times to improve reliability, with lower docking scores indicating more stable binding. The result files were visualized using PyMOL 2.6.

2.7 *In vitro* experiments

2.7.1 Liver cancer test

Human liver cancer cells (HepG2) were seeded uniformly at a density of 5000 cells per well in a 96-well plate and incubated for 24 hours in a 37°C, 5% CO_2 incubator. The ethanol extract of *D. officinale* stems was diluted to concentrations of 800 μg mL^{-1}, 400 μg mL^{-1}, 200 μg mL^{-1}, 100 μg mL^{-1}, and 50 μg mL^{-1}, with 100 μL of each concentration added per well. The control group received 100 μL of MEM medium only. The plates were then incubated for 24 hours. After incubation, the culture medium was discarded, and 100 μL of 10% CCK-8 solution was added to each well. The plates were incubated for an additional hour, and absorbance at 450 nm was measured using an enzyme-linked immunosorbent assay (ELISA) reader.

2.7.2 Chronic atrophic gastritis test

Human gastric mucosal cells (GES-1) were seeded uniformly at a density of 4000 cells per well in a 96-well plate and incubated for 24 hours in a 37°C, 5% CO_2 incubator. The ethanol extract of *D. officinale* stems was diluted to concentrations of 100 μg mL^{-1}, 50 μg mL^{-1}, 25 μg mL^{-1}, 12.5 μg mL^{-1}, and 6.25 μg mL^{-1}, with 100 μL of each concentration added per well. The control group and model group received 100 μL of DMEM medium only. The plates were incubated for 24 hours, after which the culture medium was discarded. To induce a chronic atrophic gastritis (CAG) model, 100 μL of 80 μmol/L 1-Methyl-3-nitro-1-nitrosoguanidine (MNNG) solution was added to each well, except for the control group, which received 100 μL of DMEM culture medium only. The plates were incubated for another 24 hours. Following incubation, the culture medium was discarded, and 100 μL of 10% CCK-8 solution was added to each well. The plates were incubated for 1 hour, and absorbance at 450 nm was measured using an enzyme-linked immunosorbent assay (ELISA) reader.

3 Results

3.1 Multivariate analysis of metabolomes

3.1.1 Widely targeted metabolome profiles

The UPLC-MS/MS results revealed that the types of metabolites present in *D. officinale* stems from the three different cultivation environments were generally similar. A total of 1929 metabolites were identified in the stems of *D. officinale* across the three cultivation environments (Supplementary Table S2, Figure 2A). These included 182 alkaloids (9.43%), 137 amino acids and derivatives (7.1%), 380 flavonoids (19.7%), 111 lignans and coumarins (5.75%), 190 lipids (9.85%), 65 nucleotides and derivatives (3.37%), 95 organic acids (4.92%), 302 other compounds (15.66%), 272 phenolic acids (14.1%), 58 quinones (3.01%), 2 tannins (0.1%), and 135 terpenes (7.0%). Notably, quercetin-3-O-(4''-O-glucosyl) rhamnoside and quercetin-3-O-rutinoside (rutin) were flavonoids uniquely detected in the stems of *D. officinale* cultivated in the SEC environment. Additionally, N1, N8-bis(sinapoyl)spermidine was detected exclusively in the stems of *D. officinale* cultivated in the TEC environment (Figure 2B). These 1,929 metabolites were further classified (Supplementary Figure S6).

Principal component analysis (PCA) revealed significant differences in the metabolites of *D. officinale* stems from the three cultivation environments (Figure 2C). When comparing the metabolite contents of *D. officinale* stems, 110 metabolites exhibited significant differences across the three environments (SEC_vs_other, $|Log_2FC| \geq 1.0$, $p < 0.01$, VIP > 1), with 58 metabolites being up-regulated and 52 metabolites down-regulated (Supplementary Table S3). These 110 differential metabolites were further categorized into primary and secondary metabolites (Figure 2E). Among them, 20 primary metabolites and 36 secondary metabolites were up-regulated in the SEC environment, while 23 primary metabolites and 27 secondary metabolites were down-regulated. Flavonoids (18/36) were the major category of up-regulated secondary metabolites, including dihydrocharcone-4'-O-glucoside, phloretin-4'-O-glucoside (Trilobatin), 6-C-methylkaempferol-3-glucoside, chrysoeriol-5-O-glucoside, chrysoeriol-7-O-(6''-malonyl) glucoside, diosmetin-7-O-galactoside, diosmetin-7-O-glucoside, diosmetin-8-C-(2''-O-arabinosyl)glucoside, isohyperoside, isorhamnetin-3-O-(6''-malonyl)glucoside-7-O-glucoside, kaempferol-3-O-(6'''-malonyl)sophorotrioside, kaempferol-3-O-(6''-O-acetyl)glucoside, kaempferol-3-O-rutinoside (nicotiflorin), myricetin-3-O-β-D-glucoside, quercetin-3-O-glucoside (isoquercitrin), quercetin-7-O-glucoside, hesperetin-5-O-glucoside, and homeriodictyol-7-O-β-O-glucoside. Additionally, amino acids and their derivatives (7/20) were found exclusively in the up-regulated primary metabolites, including (2S)-2-amino-4-methyl-4-pentenoic acid, cycloleucine, L-asparagine, L-glutamine, L-lysine, N-methyl-L-proline, and γ-glutamyl-L-valine.

3.1.2 Metabolic pathways

KEGG (metabolics) enrichment analysis of up-regulated differential metabolites (Figure 2D) revealed that up-regulated primary metabolites were predominantly enriched in the amino

10.3389/fpls.2025.1501545

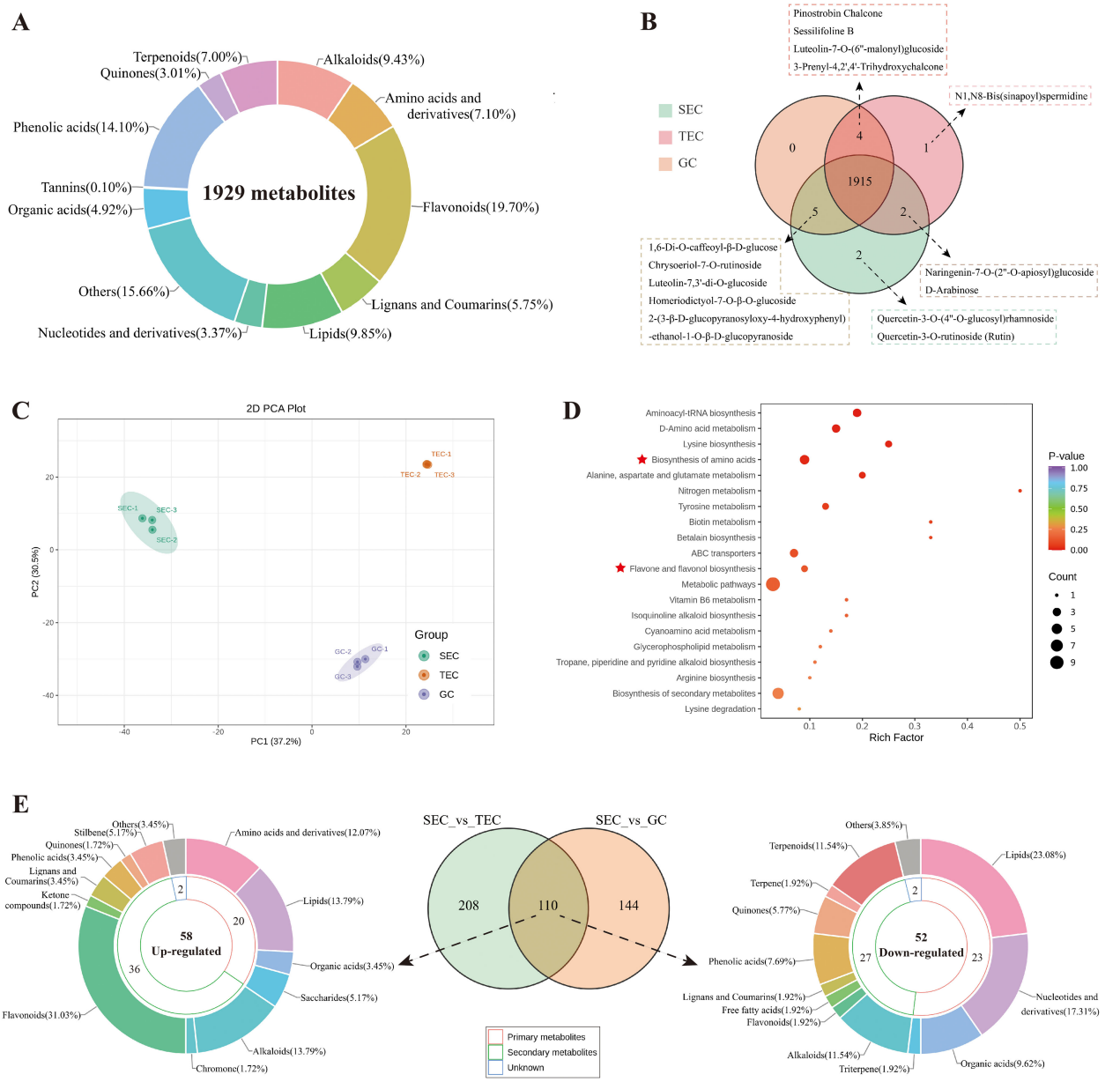

FIGURE 2
Widely targeted metabolome profiles of *D. officinale* stems in three cultivation environments. **(A)** Classification circular diagram of total metabolites in *D. officinale* stems from the three cultivation environments. **(B)** Venn diagram of total metabolites in *D. officinale* stems from the three cultivation environments. **(C)** PCA results of metabolites in *D. officinale* stems from the three cultivation environments. **(D)** KEGG (metabolics) enrichment analysis of up-regulated differential metabolites in *D. officinale* stems in different cultivation environments. **(E)** Venn diagram of differential metabolites in *D. officinale* stems and classification circular diagram of up-regulated and down-regulated metabolites.

acid biosynthesis pathway, while up-regulated secondary metabolites were primarily associated with the flavone and flavonol biosynthesis pathways. To further investigate, this study conducted heatmap analysis of the metabolic pathways of flavonoids, specifically the flavonoid biosynthetic pathway (ko00941, Figure 3A), the flavone and flavonol biosynthetic pathway (ko00944, Figure 3B), and the amino acid biosynthesis pathway (ko01230, Figure 3C).

The major metabolites in the flavonoid pathway of *D. officinale* stems included flavones, flavonols, flavanones, and chalcones. Interestingly, the results showed that 15 metabolites linked to the flavonoid biosynthesis pathway were more abundant in the TEC environment, while 8 metabolites had higher levels in the SEC environment, with phloretin and phlorizin showing a significant increase ($p < 0.05$) (Figure 3A). Additionally, 11 metabolites associated with the flavone and flavonol biosynthesis pathway were found to be more abundant in SEC compared to TEC (5 metabolites) and GC (6 metabolites). These included kaempferol and its derivatives (kaempferol-3-O-rutinoside [nicotiflorin], kaempferol-3-O-

10.3389/fpls.2025.1501545

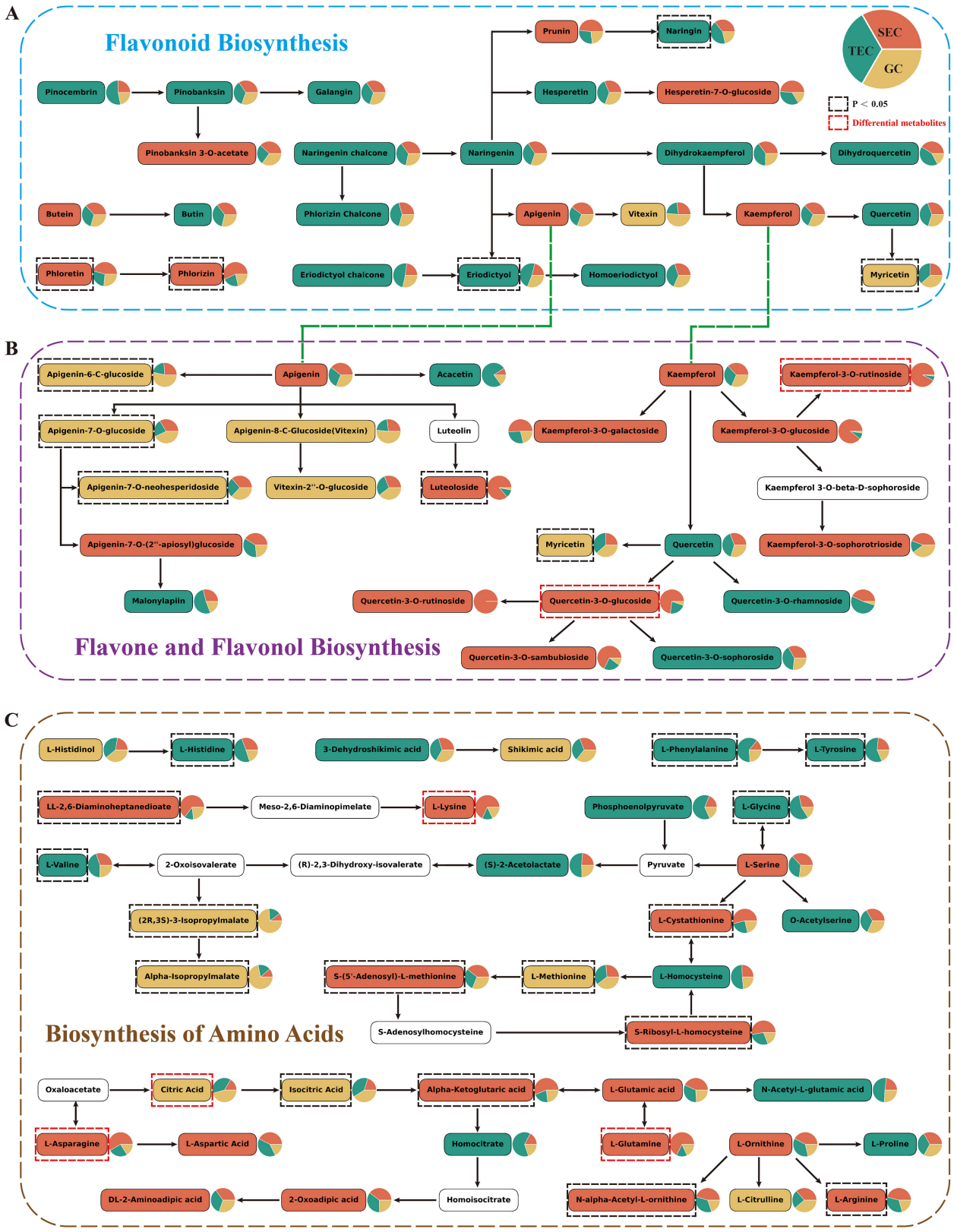

FIGURE 3
Metabolic pathways of *D. officinale* stems. The background colors of metabolites correspond to the group with higher content, and the red dashed box indicates differential metabolites. **(A)** Flavonoid Biosynthesis. **(B)** Flavone and Flavonol Biosynthesis. **(C)** Biosynthesis of Amino Acids.

galactoside, kaempferol-3-O-glucoside, kaempferol-3-O-sophorotrioside) as well as some quercetin derivatives (quercetin-3-O-glucoside [isoquercitrin], quercetin-3-O-rutinoside, quercetin-3-O-sambubioside). Notably, nicotiflorin and isoquercitrin were among the up-regulated differential metabolites. In contrast, the content of apigenin derivatives was higher in the GC environment (Figure 3B). Moreover, 16 metabolites associated with the amino acid biosynthesis pathway were more abundant in SEC compared to TEC (13 metabolites) and GC (8 metabolites), with 7 metabolites—LL-2,6-diaminoheptanedioate, L-cystathionine, S-(5'-adenosyl)-L-methionine, S-ribosyl-L-homocysteine, α-ketoglutaric acid, N-α-acetyl-L-ornithine, and L-arginine—showing a significant increase ($p < 0.05$). L-lysine, L-glutamine, and L-asparagine were among the up-regulated differential metabolites, while citric acid was a down-regulated differential metabolite (Figure 3C).

In conclusion, the flavone and flavonol biosynthesis pathway and the amino acid biosynthesis pathway are more active in the stems of *D. officinale* cultivated in the SEC environment compared to the other two cultivation environments.

3.1.3 KEGG (genes) enrichment analysis of targets of differential metabolites

The differential metabolite analysis revealed that, compared to the TEC and GC environments, 58 metabolites were up-regulated and 52 metabolites were down-regulated in the SEC environment. To explore the reasons behind the therapeutic differences in *D. officinale* stems grown under different cultivation environments, network pharmacology was applied to analyze the 58 up-regulated and 52 down-regulated metabolites. According to the Swiss Target Prediction database, a total of 163 targets (Probability ≥ 0.12) were identified for the differential metabolites (SEC_vs_other) in *D. officinale* stems, consisting of 110 targets for up-regulated metabolites and 66 targets for down-regulated metabolites. A Venn diagram was created to show the overlap between the three disease targets and the differential metabolite targets, revealing 25 common targets (Figure 4A).

All targets of the differential metabolites were selected for KEGG (genes) enrichment analysis. The KEGG pathway enrichment analysis identified 51 pathways (Supplementary Table S4), with the top 20

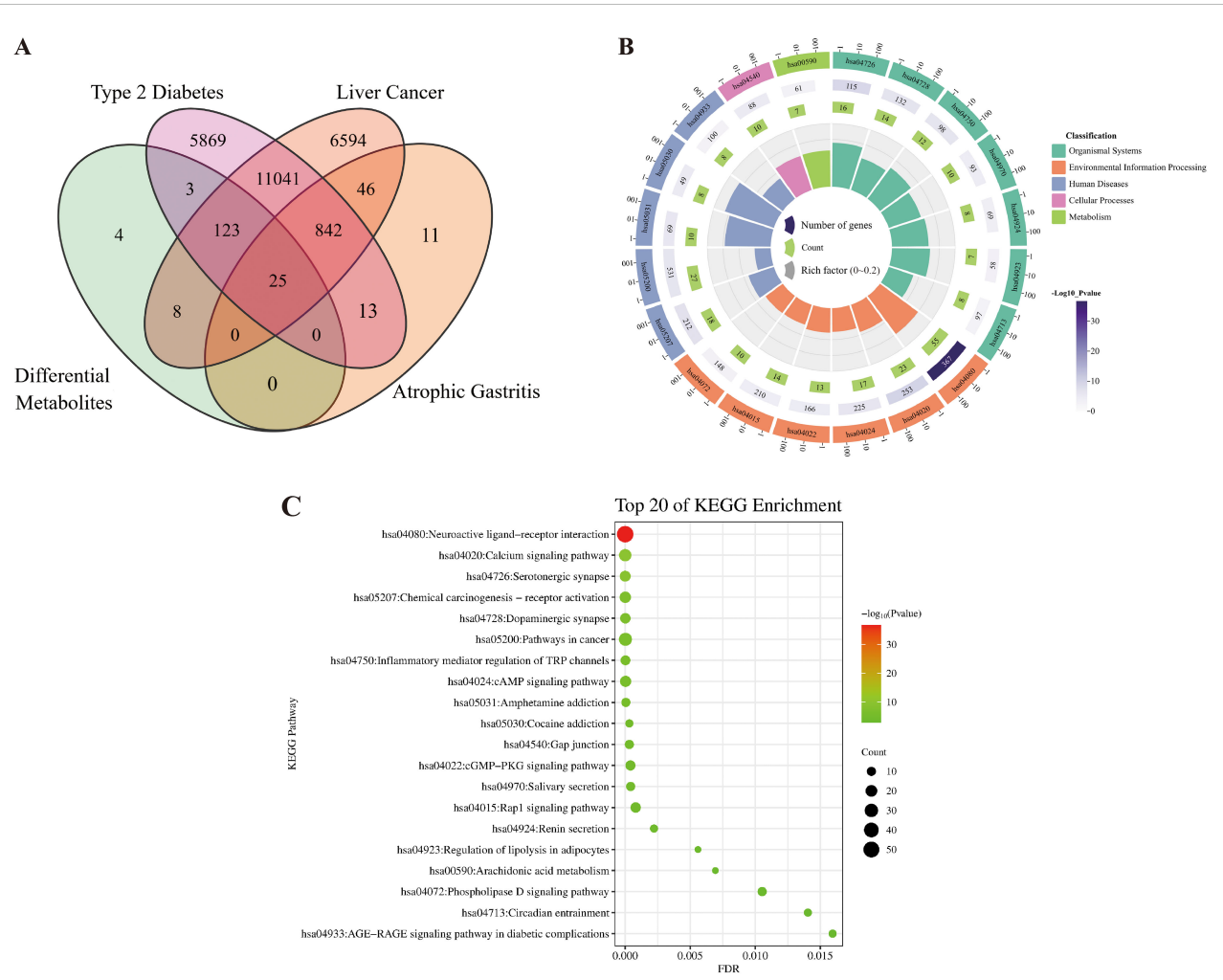

FIGURE 4
Target prediction and functional annotation in the stems of *D. officinale* across three cultivation environments. **(A)** Venn diagram showing the overlap of targets for differential metabolites in *D. officinale* stems across three cultivation environments and three diseases (Liver cancer, Type 2 diabetes, Chronic atrophic gastritis). **(B)** Circular plot of KEGG enrichment results. **(C)** Bubble chart of KEGG enrichment results.

10.3389/fpls.2025.1501545

pathways selected based on *p* values to generate KEGG enrichment circle plots and KEGG enrichment bubble plots. The analysis indicated that the targets of differential metabolites were mainly concentrated in organismal systems, environmental information processing, and human diseases. Significant pathways included the serotonergic synapse (organismal systems, hsa04726), neuroactive ligand-receptor interaction (environmental information processing, hsa04080), amphetamine addiction (human diseases, hsa05031), and cocaine addiction (human diseases, hsa05030). Other important pathways involved the calcium signaling pathway (environmental information processing, hsa04020), chemical carcinogenesis receptor activation (human diseases, hsa05207), dopaminergic synapse (organismal systems, hsa04728), inflammatory mediator regulation of TRP channels (organismal systems, hsa04750), and pathways in cancer (human diseases, hsa05200) (Figures 4B, C).

3.2 Weighted network pharmacology-based analysis of differential metabolites

3.2.1 Constructing a weighted network diagram for target points

The study identified 110 targets for up-regulated metabolites and 66 targets for down-regulated metabolites. To determine the core targets, a weighted analysis of the targets was conducted. Among the up-regulated differential metabolite (SEC_vs_other) targets, Monoamine Oxidase A (MAOA) and Tumor Necrosis Factor (TNF) emerged as the highest-weighted targets. In contrast, SRC protein tyrosine kinase (SRC) and Prostaglandin Endoperoxide Synthase 2 (PTGS2) were the highest-weighted targets among the down-regulated differential metabolite targets (Figure 5, Supplementary Table S1). This suggests that the benefits of the SEC environment, compared to the TEC and GC environments, might be attributed to alterations in the differential metabolite content in SEC, which increases binding to MAOA receptors and TNF, while reducing binding to SRC and PTGS2.

3.2.2 Molecular docking

Compared to the TEC and GC environments, the SEC environment led to the up-regulation of 58 differential metabolites and the down-regulation of 52 differential metabolites. To examine the binding capacity between these differential metabolites and core targets, the 58 up-regulated metabolites were docked with MAOA and TNF (Figure 6A), while the 52 down-regulated metabolites were docked with SRC and PTGS2 (Figure 6B). A docking energy value below -4.25 kcal·mol^{-1} suggests some binding activity between the molecules, a value below -5.0 kcal·mol^{-1} indicates good binding affinity, and a value below -7.0 kcal·mol^{-1} denotes strong binding affinity. The results showed that the up-regulated metabolites displayed binding activity with both MAOA and TNF, especially flavonoids, which exhibited docking energy values lower than -8.0 kcal·mol^{-1} with MAOA and lower than -7.8 kcal·mol^{-1} with TNF. Among these, kaempferol-3-O-(6”-malonyl) sophorotrioside demonstrated the lowest docking energy values with these two proteins (-9.9 and -9.2 kcal·mol^{-1}, respectively). Nicotiflorin and isoquercitrin, key components in the flavone and flavonol biosynthetic pathways (Figure 3B), also exhibited strong binding capacity. While amino acids and their derivatives showed some binding activity with MAOA and TNF (all below -4.8 kcal·mol^{-1}), they were not as potent. These 18 flavonoids can therefore be considered quality markers for differentiating the quality of *D. officinale* stems across the three cultivation environments and may also serve as potential targeted treatments for MAOA and TNF.

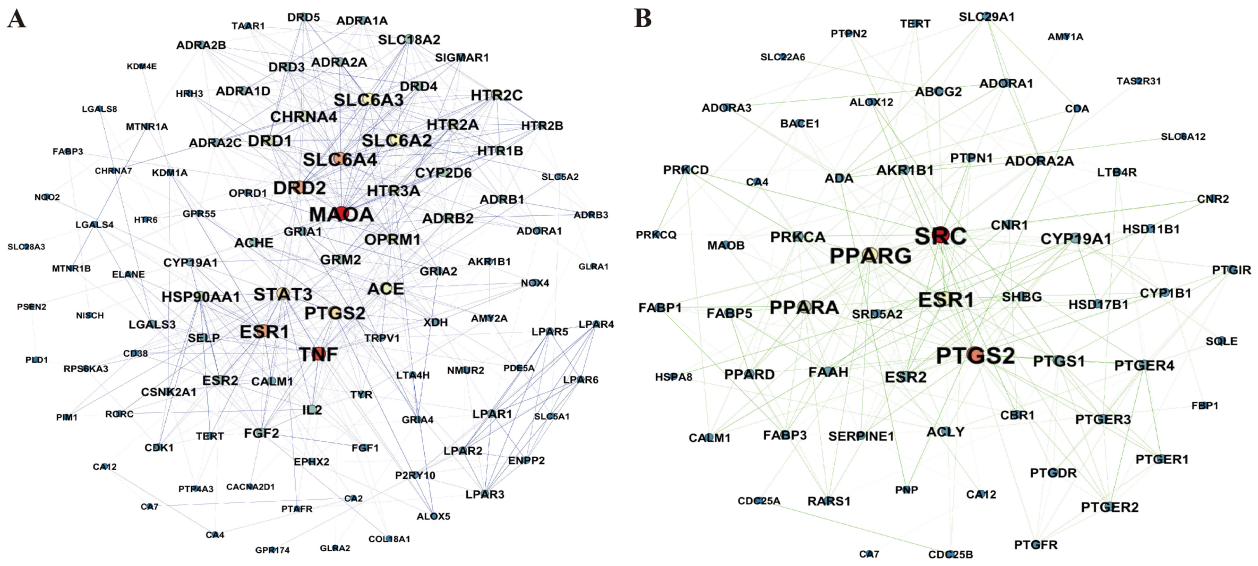

FIGURE 5
Weighted network pharmacology analysis of differential metabolites in the stems of *D. officinale* grown in a stone epiphytic culture environment compared to other cultivation environments. **(A)** Weighted network pharmacology analysis of up-regulated metabolites in the stems of *D. officinale* grown in a stone epiphytic culture environment *vs*. other environments. **(B)** Weighted network pharmacology analysis of down-regulated metabolites in the stems of *D. officinale* grown in a stone epiphytic culture environment *vs*. other environments.

10.3389/fpls.2025.1501545

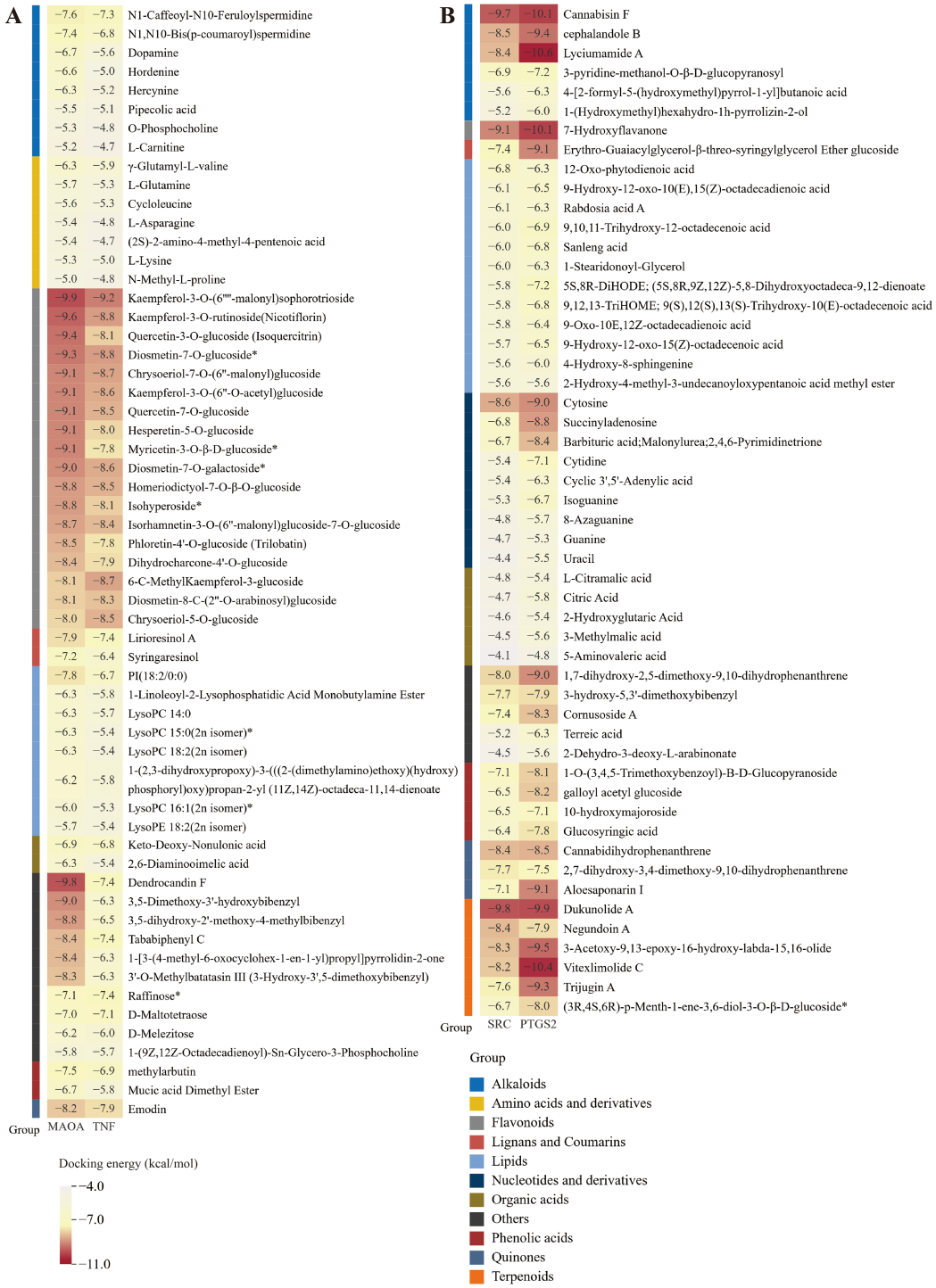

FIGURE 6
Molecular docking score results. **(A)** Molecular docking score results of up-regulated differential metabolites with MAOA and TNF. **(B)** Molecular docking score results of down-regulated differential metabolites with SRC and PTGS2.

Moreover, the down-regulated metabolites showed binding activity with SRC and PTGS2, with energy values below -4.25 kcal·mol^{-1} (except for 5-aminonovaleric acid). Dukunolide A had the lowest docking energy with SRC at -9.8 kcal·mol^{-1}, while lyciumumide A had the lowest docking energy with PTGS2 at -10.6 kcal·mol^{-1}. Eighteen up-regulated flavonoids were selected for molecular docking visualization with MAOA and TNF (Figure 7). Similarly, down-regulated metabolites with low binding energies were chosen for molecular docking visualization with SRC and PTGS2 (Supplementary Figure S7).

10.3389/fpls.2025.1501545

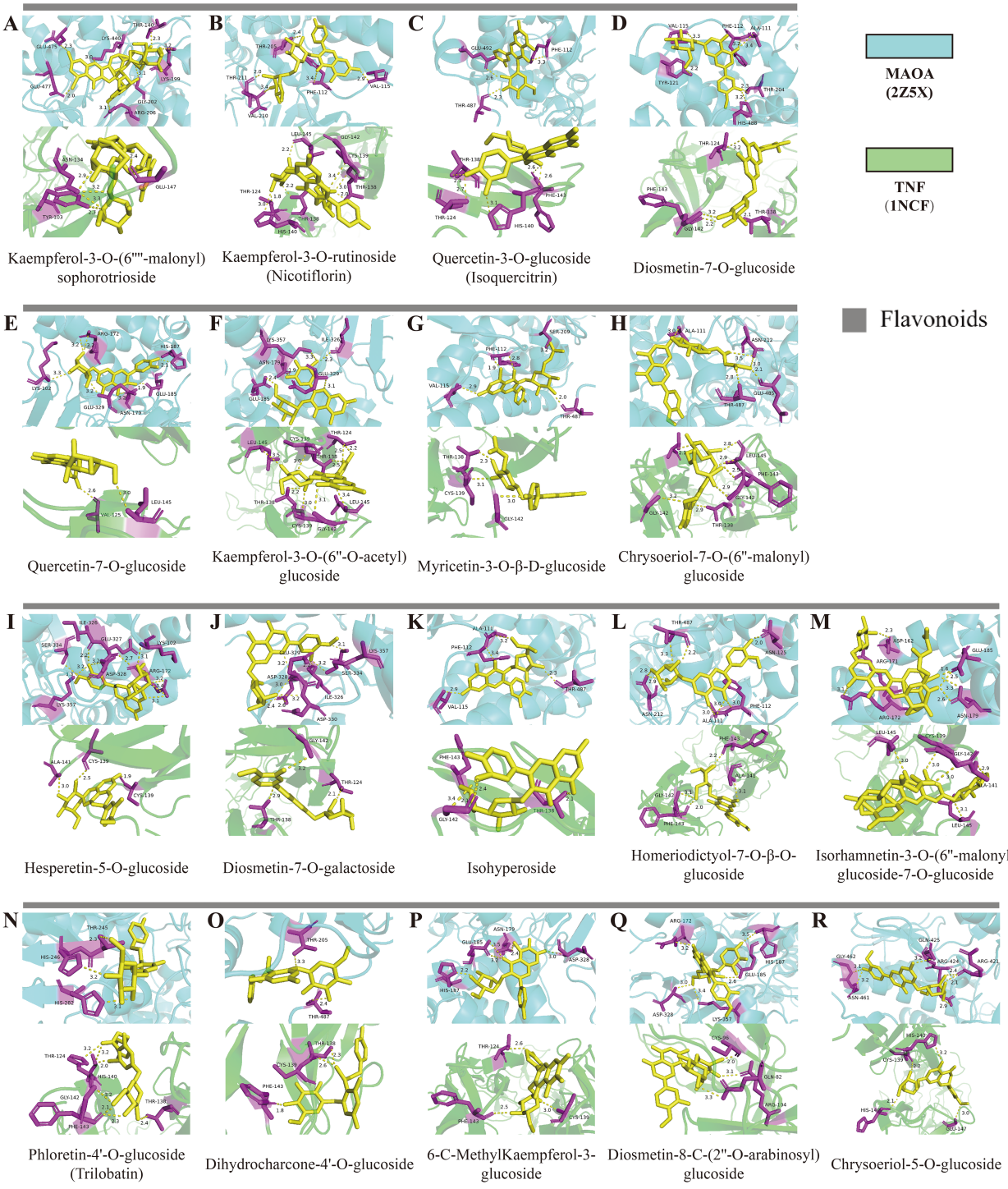

FIGURE 7
Molecular docking results of up-regulated flavonoids in *D. officinale* stems from different cultivation environments. **(A)** Predicted binding mode of Kaempferol-3-O-(6''-malonyl) sophorotrioside with MAOA and TNF. **(B)** Predicted binding mode of Kaempferol-3-O-rutinoside (Nicotiflorin) with MAOA and TNF. **(C)** Predicted binding mode of Quercetin-3-O-glucoside (Isoquercitrin) with MAOA and TNF. **(D)** Predicted binding mode of Diosmetin-7-O-glucoside with MAOA and TNF. **(E)** Predicted binding mode of Quercetin-7-O-glucoside with MAOA and TNF. **(F)** Predicted binding mode of Kaempferol-3-O-(6''-O-acetyl)glucoside with MAOA and TNF. **(G)** Predicted binding mode of Myricetin-3-O-β-D -glucoside with MAOA and TNF. **(H)** Predicted binding mode of Chrysoeriol-7-O-(6''-malonyl)glucoside with MAOA and TNF. **(I)** Predicted binding mode of Hesperetin-5-O-glucoside with MAOA and TNF. **(J)** Predicted binding mode of Diosmetin-7-O -galactoside with MAOA and TNF. **(K)** Predicted binding mode of Isohyperoside with MAOA and TNF. **(L)** Predicted binding mode of Homeriodictyol-7-O-β-O-glucoside with MAOA and TNF. **(M)** Predicted binding mode of Isorhamnetin-3-O-(6''-malonyl)glucoside-7-O-glucoside with MAOA and TNF. **(N)** Predicted binding mode of Phloretin-4'-O-glucoside (Trilobatin) with MAOA and TNF. **(O)** Predicted binding mode of Dihydrocharcone-4'-O-glucoside with MAOA and TNF. **(P)** Predicted binding mode of 6-C-MethylKaempferol-3-glucoside with MAOA and TNF.**(Q)** Predicted binding mode of Diosmetin-8-C-(2''-O-arabinosyl)glucoside with MAOA and TNF. **(R)** Predicted binding mode of Chrysoeriol-5-O-glucoside with MAOA and TNF.

3.3 *In vitro* experiments

To investigate the therapeutic differences of *D. officinale* stems grown in different cultivation environments for liver cancer and chronic atrophic gastritis, this study conducted HepG2 cell inhibition experiments and chronic atrophic gastritis cell protection experiments. The results showed that the inhibitory rate of *D. officinale* stem extracts on liver cancer cells increased with higher concentrations across all cultivation environments (Figure 8A). At 100 μg/mL, the SEC extract exhibited stronger inhibitory effects compared to TEC and GC ($p < 0.01$). However, at 800 μg/mL, SEC performed less effectively than the other two groups ($p < 0.05$). For other concentrations, the inhibitory effects of the different extracts on cancer cells varied, though SEC did not show a clear advantage overall. The extracts of *D. officinale* stems from different cultivation environments also exhibited protective effects on chronic atrophic gastritis cells. Among all concentration groups, the SEC extracts demonstrated better protective effects compared to TEC and GC (Figure 8B), with the highest performance observed at a concentration of 12.5 μg/mL ($p < 0.05$). This finding aligns with the stomach-benefiting properties outlined in the Chinese Pharmacopoeia (2020 edition).

4 Discussion

In this study, a total of 1929 metabolites, including flavonoids, amino acids, alkaloids, lipids, and phenolic acids, were identified in *D. officinale* stems cultivated in three distinct environments, consistent with previous research (Yang et al., 2023b). Differential analysis of metabolites revealed that, compared to the GC and TEC environments, 20 primary metabolites and 36 secondary metabolites were up-regulated in the SEC environment (SEC_vs_other, $|Log_2FC| \geq 1.0$, $p < 0.01$, VIP > 1). Primary metabolites were mainly enriched in the

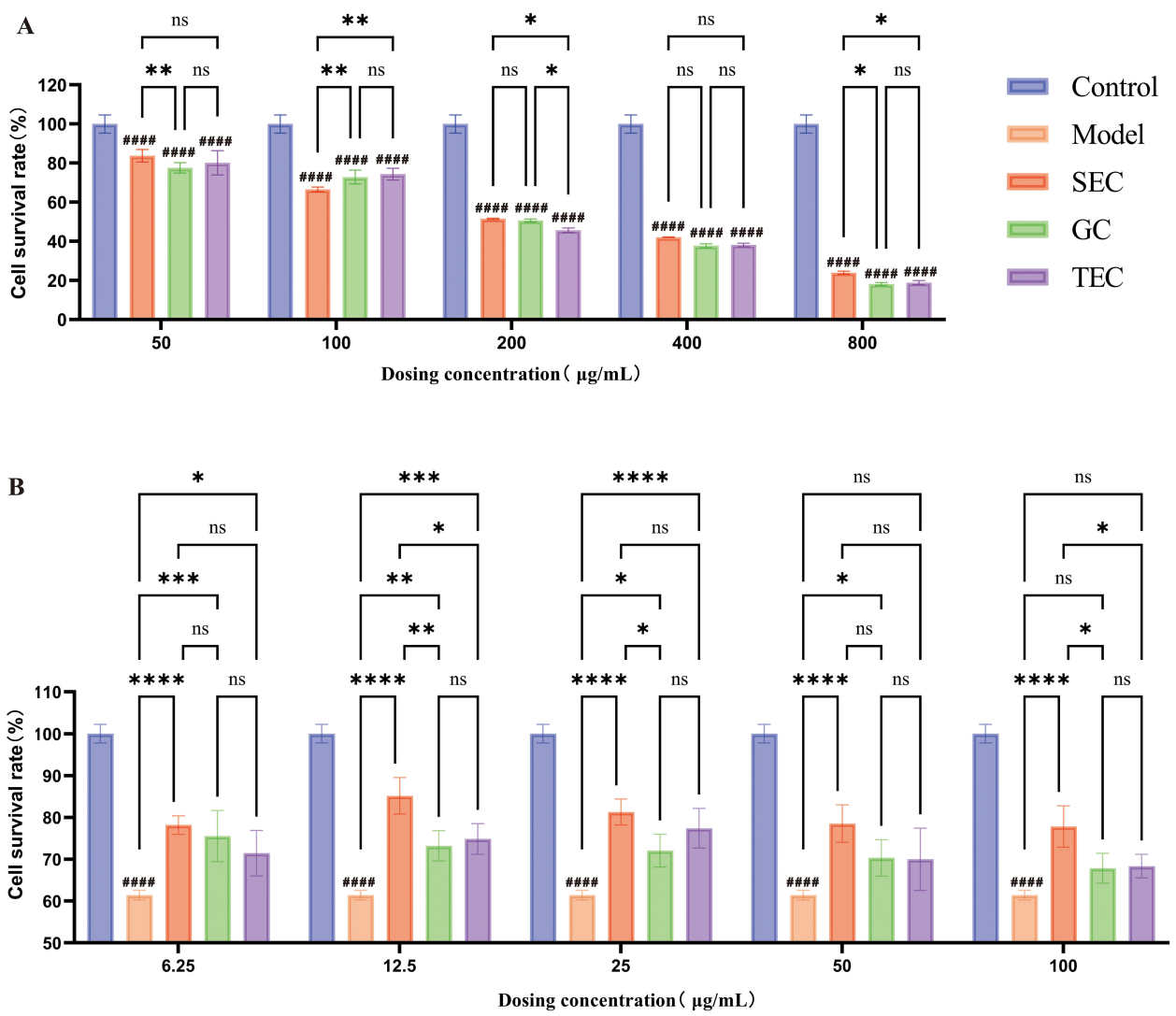

FIGURE 8
In vitro activity results of *D. officinale* stems extract at different concentrations. *$p < 0.05$; **$p < 0.01$; ***$p < 0.001$; ****$p < 0.0001$; $^{\#\#\#\#}p < 0.0001$, compared with the control group; ns, no significant difference. **(A)** Human liver cancer cell inhibition experiment. **(B)** Cell protection experiment for chronic atrophic gastritis.

biosynthesis of amino acids pathway, while secondary metabolites were primarily enriched in the flavone and flavonol biosynthesis pathway. Given that *D. officinale* stems in the SEC environment have long been exposed to high calcium, UV stress, and drought stress in natural settings, previous studies have indicated that kaempferol and quercetin in the flavonoid pathway play vital roles in plant resistance to UV, drought, and salt stress (Sun et al., 2020a; Xu et al., 2020). Additionally, amino acids, essential nutrients for plant growth and development, are critical for plant resistance to drought and other abiotic stresses (Mwadzingeni et al., 2016). Therefore, the enrichment of the flavonoid and amino acid pathways in the SEC environment may be associated with the increased resistance of *D. officinale* stems (cultivated on stones) to UV, drought, and salt stress.

The secondary metabolites up-regulated in the SEC environment were primarily flavonoids (18/36), including biologically active compounds such as homeriocitryol-7-O-β-O-glucoside, phloretin-4'-O-glucoside (phloridzin), nicotiflorin, and isoquercitrin. These compounds exhibit significant therapeutic effects, including in the treatment of acute myocardial infarction (Guan et al., 2000), anti-inflammatory properties (He et al., 2022), prevention of diabetic complications (Lu et al., 2023), antioxidant effects (Juan-Badaturuge et al., 2011), and hypoglycemic activity (Aimudula et al., 2020). Notably, quercetin-3-O-(4"-O-glucosyl) rhamnoside and rutin were two unique quercetin derivatives found specifically in the SEC environment. Rutin is known for its broad range of physiological and pharmacological activities, including anti-inflammatory (Liu et al., 2022), antidiabetic (Cai et al., 2023), and anticancer properties (Soosai et al., 2024). Additionally, 7 amino acids and their derivatives were found exclusively among the up-regulated primary metabolites in the SEC environment, with L-glutamine being particularly notable for its potential therapeutic effects in treating diabetes (Samocha-Bonet et al., 2011) and gastritis (Ren et al., 2013).

Network pharmacology involves utilizing databases such as proteomics, genomics, and bioinformatics to perform systematic analyses of medicinal plants at both molecular and holistic levels (Liu et al., 2024). In this study, metabolomics was employed to analyze the differential metabolites in *D. officinale* stems cultivated in different environments, and their corresponding targets were identified using databases. Through the construction of PPI networks and weighted analysis, two key up-regulated targets, MAOA and TNF, and two key down-regulated targets, SRC and PTGS2, were identified. To verify the binding capacity between the core targets and differential metabolites, molecular docking was conducted. Notably, flavonoids exhibited superior binding affinity with MAOA and TNF compared to other up-regulated compounds. These findings suggest that the collective action of these 18 flavonoids likely contributes to the stomach-benefiting and anti-inflammatory properties of *D. officinale* stems, highlighting their potential as targeted drugs for MAOA and TNF. Specifically, kaempferol-3-O-(6"-malonyl) sophorotrioside demonstrated the best binding capacity, while nicotiflorin and isoquercitrin, which are involved in the flavone and flavonol biosynthetic pathway (Figure 3B), also displayed excellent binding affinity. Previous studies have shown that nicotiflorin exhibits anti-inflammatory, hypoglycemic, and other biological activities (Juan-Badaturuge et al., 2011; Aimudula et al., 2020), while isoquercitrin can be used to prevent diabetic complications (Lu et al., 2023). Thus, the content of nicotiflorin and isoquercitrin serves as a key quality marker for assessing the therapeutic efficacy of *D. officinale* stems cultivated in different environments.

A study has shown that extracts from *D. officinale* stems can significantly inhibit the growth of human hepatocellular carcinoma cells (HepG2) (Xing et al., 2018). Additionally, granules made from *D. officinale* stems are currently undergoing clinical trials for the treatment of chronic atrophic gastritis (Yang et al., 2023a). To explore the therapeutic differences of *D. officinale* stems cultivated in various environments, this study conducted HepG2 cell inhibition experiments and chronic atrophic gastritis cell protection experiments. Simultaneously, network pharmacology was used to analyze the underlying causes of these differences in therapeutic efficacy. The results revealed that while no significant difference was observed in the inhibitory effects of *D. officinale* stems from different cultivation environments on HepG2 cells (Figure 8A), the SEC environment showed superior protective effects on chronic atrophic gastritis cells compared to the TEC and GC environments (Figure 8B). The traditional efficacy of *D. officinale* stems, known for nourishing the stomach and promoting the production of body fluid, aligns with our *in vitro* findings (Yang et al., 2023a). MAOA inhibits the metastasis of hepatocellular carcinoma cells by suppressing the adrenergic system and activating the epidermal growth factor receptor (EGFR) signaling pathway, showing a negative correlation with hepatocellular carcinoma progression (Li et al., 2014). TNF, typically referring to TNF-α, is recognized as a key regulatory factor in inflammatory responses (Croft, 2009). Meanwhile, SRC promotes the repair of inflammation-mediated intestinal mucosal damage by promoting cell proliferation and inhibiting apoptosis, while also activating related inflammatory pathways to drive inflammation's onset and progression (Dong et al., 2023). PTGS2 triggers inflammatory responses via the NF-κB pathway, with its expression, induced by cytokines and growth factors, being up-regulated during inflammation (Kunzmann et al., 2013). In the SEC environment, the up-regulated flavonoids in *D. officinale* stems compete with TNF-α for TNF receptors (Hayden and Ghosh, 2014; Sabio and Davis, 2014). Furthermore, the down-regulated metabolites bind less to SRC and PTGS2, decreasing inflammation production and thereby inhibiting inflammation (Roskoski, 2015). This provides an explanation for the superior protective effects of *D. officinale* stems in the SEC environment on chronic atrophic gastritis cells.

In summary, compared to the TEC and GC environments, the SEC environment exhibited 18 up-regulated flavonoids and 7 amino acids as key differential metabolites. Nicotiflorin and isoquercitrin not only demonstrated excellent binding affinity with the core targets MAOA and TNF, but also possess a broad range of biological activities, making them ideal as core quality markers. *In vitro* experiments further confirmed the superior protective effect of *D. officinale* stems from the SEC environment on cells with chronic atrophic gastritis, with changes in target preference being a crucial factor contributing to the observed differences in efficacy. However, despite the careful design of the experiments in this study, cellular models cannot fully replicate the complex *in vivo* environment of living organisms. Future research should prioritize further pharmacological studies on nicotiflorin and

isoquercitrin within the context of *D. officinale* stems from the SEC environment. Such studies, focusing on molecular pharmacology and *in vivo* experiments, will provide vital scientific insights into the medicinal value and quality assessment of *D. officinale* stems cultivated in natural environments.

5 Conclusions

In conclusion, this study selected 18 flavonoids as references for cultivating high-quality *D. officinale* stems through targeted metabolomics, weighted network pharmacology, and molecular docking. These flavonoids showed potential as targeted therapies for MAOA and TNF. In addition, modern pharmacological research highlighted nicotiflorin and isoquercitrin as the most important quality markers. *In vitro* experiments confirmed that *D. officinale* stems grown in SEC environment exhibited more significant protective effects on chronic atrophic gastritis cells. This was attributed to the combined effects of enhanced binding of differential metabolites to targets like MAOA and TNF, and reduced binding to targets like SRC and PTGS2. In the future, to fully enhance the medicinal quality of *D. officinale* stems, priority should be given to the development of the *D. officinale* cultivation industry under the SEC environment. Future research should consider conducting further pharmacological studies on the 18 flavonoid compounds, with a focus on molecular pharmacology and *in vivo* experiments. This study suggests that the simulated wild cultivation industry of medicinal plants should be fully developed to improve their quality. A combined approach involving widely targeted metabolomics, network pharmacology, molecular docking, and cellular experiments can be utilized to explore pharmacological differences among other medicinal plants.

Data availability statement

The original contributions presented in the study are included in the article/Supplementary Material. Further inquiries can be directed to the corresponding author.

Ethics statement

Ethical approval was not required for the studies on humans in accordance with the local legislation and institutional requirements because only commercially available established cell lines were used. The manuscript presents research on animals that do not require ethical approval for their study.

Author contributions

YH: Writing – original draft, Writing – review & editing, Data curation, Investigation, Methodology. GD: Formal analysis, Funding acquisition, Project administration, Supervision, Writing – original draft, Writing – review & editing. JL: Resources, Writing – original draft, Writing – review & editing. PL: Resources, Writing – original draft, Writing – review & editing. JZ: Formal analysis, Funding acquisition, Resources, Supervision, Writing – original draft, Writing – review & editing.

Funding

The author(s) declare that financial support was received for the research and/or publication of this article. This research was financially supported by the National Natural Science Foundation of China (82160717), the Research funding for scientific and technological projects in traditional Chinese medicine and ethnic medicine from Guizhou Provincial Administration of Traditional Chinese Medicine (QZYY-2024-110), the University Science and Technology Innovation Team of the Guizhou Provincial Department of Education (Qian-jiao-ji (2023)071), and National and Provincial Scientific and Technological Innovation Talent Team of Guizhou University of Traditional Chinese Medicine (Gui-zhong-yi TD he-zi (2022)003).

Acknowledgments

The authors sincerely thank the metabolome support by Metware Biotechnology Co., Ltd. (*www.metware.cn*, Wuhan, China).

Conflict of interest

The authors declare that the research was conducted in the absence of any commercial or financial relationships that could be construed as a potential conflict of interest.

Publisher's note

Supplementary material

The Supplementary Material for this article can be found online at: https://www.frontiersin.org/articles/10.3389/fpls.2025.1501545/full#supplementary-material

SUPPLEMENTARY TABLE 1
Degree values of differential metabolite targets.

SUPPLEMENTARY TABLE 2
Metabolomic raw data of *D. officinale* stems in different cultivation environments.

SUPPLEMENTARY TABLE 3
Fold change of differential metabolites from *D. officinale* stems.

SUPPLEMENTARY TABLE 4
KEGG pathways and related targets.

References

Aimudula, G., Zhang, S., Liu, T., Yao, Y., and Zhao, J. (2020). Protective Effect of Nicotiflorin from Nymphaea Candida on H2O2-Induced LO2 Cells Damage. *China Pharm.* 29, 42–46. doi: 10.3969/j.issn.1006-4931.2020.15.010

Cai, C., Cheng, W., Shi, T., Liao, Y., Zhou, M., and Liao, Z. (2023). Rutin alleviates colon lesions and regulates gut microbiota in diabetic mice. *Sci. Rep.* 13, 4897. doi: 10.1038/s41598-023-31647-z

Chen, W., Gong, L., Guo, Z., Wang, W., Zhang, H., Liu, X., et al. (2013). A novel integrated method for large-scale detection, identification, and quantification of widely targeted metabolites: application in the study of rice metabolomics. *Mol. Plant* 6, 1769–1780. doi: 10.1093/mp/sst080

Cheng, J., Dang, P., Zhao, Z., Yuan, L., Zhou, Z., Wolf, D., et al. (2019). An assessment of the Chinese medicinal *Dendrobium* industry: Supply, demand and sustainability. *J. Ethnopharmacol.* 229, 81–88. doi: 10.1016/j.jep.2018.09.001

Croft, M. (2009). The role of TNF superfamily members in T-cell function and diseases. *Nat. Rev. Immunol.* 9, 271–285. doi: 10.1038/nri2526

Dong, Y., Lin, M., Fang, X., Xie, Z., Luo, R., Teng, X., et al. (2022). Modulating effects of a functional food containing *Dendrobium officinale* on immune response and gut microbiota in mice treated with cyclophosphamide. *J. Funct. Foods.* 94, 105102. doi: 10.1016/j.jff.2022.105102

Dong, W., Zhang, Y., Yuan, X., Li, F., Zhang, S., Xu, H., et al. (2023). Mechanism of *Moringa oleifera* leaves in treating enteritis based on network pharmacology and molecular docking technology. *Chin. J. Anim. Nutr.* 35, 8053–8073. doi: 10.12418/CJAN2023.730

Dong, X., Zheng, F., Liu, X., Zhang, L., Hu, R., Wang, L., et al. (2020). Simultaneous quantitative analysis of Q-marker with one single reference in *Glycyrrhiza uralensis* Fisch. *J. Chromatogr Sci.* 58, 511–519. doi: 10.1093/chromsci/bmaa015

Dunn, W. B., Erban, A., Weber, R. J. M., Creek, D. J., Brown, M., Breitling, R., et al. (2013). Mass appeal: metabolite identification in mass spectrometry-focused untargeted metabolomics. *Metabolomics.* 9, 44–66. doi: 10.1007/s11306-012-0434-4

Eberhardt, J., Santos-Martins, D., Tillack, A. F., and Forli, S. (2021). AutoDock Vina 1.2.0: New docking methods, expanded force field, and python bindings. *J. Chem. Inf. Model.* 61, 3891–3898. doi: 10.1021/acs.jcim.1c00203

Fraga, C. G., Clowers, B. H., Moore, R. J., and Zink, E. M. (2010). Signature-discovery approach for sample matching of a nerve-agent precursor using liquid chromatography–mass spectrometry, XCMS, and chemometrics. *Anal. Chem.* 82, 4165–4173. doi: 10.1021/ac1003568

Guan, Z., Liu, X., Liu, H., and Cui, Y. (2000). A novel platelet-activating factor antagonist isolated from a Chinese herbal drug *Viscum coloratum*. *J. Chin. Pharm. Sci.* 9, 73–76. doi: CNKI:SUN:KXDH.0.2010-06-027

Hayden, M. S., and Ghosh, S. (2014). Regulation of NF-κB by TNF family cytokines. *Semin. Immunol.* 26, 253–266. doi: 10.1016/j.smim.2014.05.004

He, X., Liu, D., Liu, H., Wu, D., Li, H., Zhang, X., et al. (2022). Prevention of ulcerative colitis in mice by sweet tea (*Lithocarpus litseifolius*) via the regulation of gut microbiota and butyric-acid-mediated anti-inflammatory signaling. *Nutrients.* 14, 2208. doi: 10.3390/nu14112208

Hornyák, M., Dziurka, M., Kula-Maximenko, M., Pastuszak, J., Szczerba, A., Szklarczyk, M., et al. (2022). Photosynthetic efficiency, growth and secondary metabolism of common buckwheat (*Fagopyrum esculentum* Moench) in different controlled-environment production systems. *Sci. Rep.* 12, 257. doi: 10.1038/s41598-021-04134-6

Juan-Badaturuge, M., Habtemariam, S., and Thomas, M. J. K. (2011). Antioxidant compounds from a South Asian beverage and medicinal plant, *Cassia auriculata*. *Food Chem.* 125, 221–225. doi: 10.1016/j.foodchem.2010.08.065

Kunzmann, A. T., Murray, L. J., Cardwell, C. R., McShane, C. M., McMenamin, Ú.C., and Cantwell, M. M. (2013). PTGS2 (Cyclooxygenase-2) expression and survival among colorectal cancer patients: A systematic review. *Cancer Epidemiol. Biomarkers Prev.* 22, 1490–1497. doi: 10.1158/1055-9965.EPI-13-0263

Lei, S., Li, B., Chen, Y., He, X., Wang, Y., Yu, H., et al. (2019). *Dendrobii Officinalis*, a traditional Chinese edible and officinal plant, accelerates liver recovery by regulating the gut-liver axis in NAFLD mice. *J. Funct. Foods.* 61, 103458. doi: 10.1016/j.jff.2019.103458

Li, B., He, X., Jin, H., Wang, H., Zhou, F., Zhang, N., et al. (2021). Beneficial effects of *Dendrobium officinale* on metabolic hypertensive rats by triggering the enteric-origin SCFA-GPCR43/41 pathway. *Food Funct.* 12, 5524–5538. doi: 10.1039/D0FO02890H

Li, J., Yan, G., Duan, X., Zhang, K., Zhang, X., Zhou, Y., et al. (2022). Research progress and trends in metabolomics of fruit trees. *Front. Plant Sci.* 13. doi: 10.3389/fpls.2022.881856

Li, J., Yang, X., Wang, Y., Feng, M., Liu, X., Zhang, Y., et al. (2014). Monoamine oxidase A suppresses hepatocellular carcinoma metastasis by inhibiting the adrenergic system and its transactivation of EGFR signaling. *J. Hepatol.* 60, 1225–1234. doi: 10.1016/j.jhep.2014.02.025

Li, D., Ye, G., Li, J., Lai, Z., Ruan, S., Qi, Q., et al. (2023). High light triggers flavonoid and polysaccharide synthesis through DoHY5-dependent signaling in *Dendrobium officinale*. *Plant J.* 115, 1114–1133. doi: 10.1111/tpj.16284

Li, S., and Zhang, B. (2013). Traditional Chinese medicine network pharmacology: theory, methodology and application. *Chin. J. Nat. Med.* 11, 110–120. doi: 10.1016/S1875-5364(13)60037-0

Liang, J., Chen, S., Chen, J., Lin, J., Xiong, Q., Yang, Y., et al. (2018). Therapeutic roles of polysaccharides from *Dendrobium Officinaleon* colitis and its underlying mechanisms. *Carbohydr. Polym.* 185, 159–168. doi: 10.1016/j.carbpol.2018.01.013

Liu, Y., Huang, W., Ji, S., Wang, J., Luo, J., and Lu, B. (2022). *Sophora japonica* flowers and their main phytochemical, rutin, regulate chemically induced murine colitis in association with targeting the NF-κB signaling pathway and gut microbiota. *Food Chem.* 393, 133395. doi: 10.1016/j.foodchem.2022.133395

Liu, J., Li, Z., Zeng, M., Liang, Y., Liang, B., Ge, Q., et al. (2023). Rapid comparison of antitumor chemical constituents and mechanisms between *Dendrobium nobile* and *Dendrobium officinale* by UPLC-IT-TOF, network pharmacology and experimental verification. *Acta Chromatogr.* 35, 123–138. doi: 10.1556/1326.2022.01012

Liu, M., Zhao, X., Wen, J., Sun, L., Huang, R., Zhang, H., et al. (2024). A multidimensional strategy for uncovering comprehensive quality markers of *Scutellariae Radix* based on UPLC-Q-TOF-MS analysis, artificial neural network, network pharmacology analysis, and molecular simulation. *Front. Plant Sci.* 15. doi: 10.3389/fpls.2024.1423678

Lu, Z., Xu, L., Peng, C., Wang, P., Xie, Z., Xie, X., et al. (2023). Mechanism of action of quercetin-3-O-glucoside against the non-enzymatic glycosylation of alpha-Lactalbumin. *Food Science.* 44, 28–34. doi: 10.7506/spkx1002-6630-20221004-027

Luo, Z., Liu, L., Nie, Q., Huang, M., Luo, C., Sun, Y., et al. (2023). HPLC-based metabolomics of *Dendrobium officinale* revealing its antioxidant ability. *Front. Plant Sci.* 14. doi: 10.3389/fpls.2023.1060242

Luo, D., Qu, C., Zhang, Z., Xie, J., Xu, L., Yang, H., et al. (2017). Granularity and laxative effect of ultrafine powder of *Dendrobium officinale*. *J. Med. Food.* 20, 180–188. doi: 10.1089/jmf.2016.3827

Luo, Y., Yang, D., Xu, Y., Wu, D., Tan, D., Qin, L., et al. (2024). Hypoglycemic effects and quality marker screening of *Dendrobium nobile* Lindl. at different growth years. *Molecules.* 29, 699. doi: 10.3390/molecules29030699

Lv, M., Liang, Q., He, X., Du, X., Liu, Y., Liu, Y., et al. (2023). Hypoglycemic effects of *Dendrobium officinale* leaves. *Front. Pharmacol.* 14. doi: 10.3389/fphar.2023.1163028

Mwadzingeni, L., Shimelis, H., Tesfay, S., and Tsilo, T. J. (2016). Screening of bread wheat genotypes for drought tolerance using phenotypic and proline analyses. *Front. Plant Sci.* 7. doi: 10.3389/fpls.2016.01276

National Health Commission, and State Administration for Market Regulation (2023). *Announcement on 9 newly added substances, including* Codonopsis pilosula, *that are traditionally both food and traditional Chinese medicinal materials* (China: Food Safety Standards and Monitoring Evaluation Department). Available at: http://www.nhc.gov.cn/sps/s7892/202311/f0d6ef3033b54333a882e3d009ff49bf.shtml (Accessed July 30, 2024).

National Pharmacopoeia Commission (2020). *Chinese pharmacopoeia: volume 1* (Beijing: China Medical Science and Technology Press).

Qaderi, M. M., Martel, A. B., and Strugnell, C. A. (2023). Environmental factors regulate plant secondary metabolites. *Plants.* 12, 447. doi: 10.3390/plants12030447

Ren, W., Yin, J., Zhu, X., Liu, G., Li, N., Peng, Y., et al. (2013). Glutamine on intestinal inflammation: A mechanistic perspective. *Eur. J. Inflamm.* 11, 315–326. doi: 10.1177/1721727X1301100201

Roskoski, R. (2015). Src protein-tyrosine kinase structure, mechanism, and small molecule inhibitors. *Pharmacol. Res.* 94, 9–25. doi: 10.1016/j.phrs.2015.01.003

Ross, J. A., and Kasum, C. M. (2002). Dietary flavonoids: bioavailability, metabolic effects, and safety. *Annu. Rev. Nutr.* 22, 19–34. doi: 10.1146/annurev.nutr.22.111401.144957

Sabio, G., and Davis, R. J. (2014). TNF and MAP kinase signalling pathways. *Semin. Immunol.* 26, 237–245. doi: 10.1016/j.smim.2014.02.009

Samocha-Bonet, D., Wong, O., Synnott, E., Piyaratna, N., Douglas, A., Gribble, F. M., et al. (2011). Glutamine reduces postprandial glycemia and augments the glucagon-like peptide-1 response in type 2 diabetes patients. *J. Nutr.* 141, 1233–1238. doi: 10.3945/jn.111.139824

Schuiteman, A. (2011). *Dendrobium* (Orchidaceae): To split or not to split? *Gardens' Bull. Singapore.* 63, 245–257. doi: http://biostor.org/reference/140287

Soosai, D., Ramalingam, R., Perumal, E., Veeramani, K., Pancras, C., Almutairi, M. H., et al. (2024). Anticancer effects of rutin from *Fagopyrum tataricum* (tartary buckwheat) against osteosarcoma cell line. *Mol. Biol. Rep.* 51, 312. doi: 10.1007/s11033-024-09218-w

Strzemski, M., Dresler, S., Sowa, I., Czubacka, A., Agacka-Mołdoch, M., Płachno, B. J., et al. (2019). The impact of different cultivation systems on the content of selected secondary metabolites and antioxidant activity of *Carlina acaulis* plant material. *Molecules.* 25, 146. doi: 10.3390/molecules25010146

Sun, X., Li, L., Pei, J., Liu, C., and Huang, L. (2020b). Metabolome and transcriptome profiling reveals quality variation and underlying regulation of three ecotypes for *Cistanche deserticola*. Plant. *Mol. Biol.* 102, 253–269. doi: 10.1007/s11103-019-00944-5

Sun, J., Qiu, C., Ding, Y., Wang, Y., Sun, L., Fan, K., et al. (2020a). Fulvic acid ameliorates drought stress-induced damage in tea plants by regulating the ascorbate metabolism and flavonoids biosynthesis. *BMC Genomics* 21, 411. doi: 10.1186/s12864-020-06815-4

Tong, Y., Wang, P., Sun, J., Li, X., Wang, T., Zhou, Q., et al. (2021). Metabolomics and molecular networking approaches reveal differential metabolites of Radix *Scrophulariae* from different geographical origins: Correlations with climatic factors and biochemical compounds in soil. *Ind. Crops Prod.* 174, 114169. doi: 10.1016/j.indcrop.2021.114169

Trott, O., and Olson, A. J. (2010). AutoDock Vina: improving the speed and accuracy of docking with a new scoring function, efficient optimization, and multithreading. *J. Comput. Chem.* 31, 455–461. doi: 10.1002/jcc.21334

Wu, F., Zhang, Y., Liu, W., Zhu, N., Chen, J., and Sun, Z. (2020). Comparison of torrefied and lyophilized Dendrobii Officinalis Caulis (*Tiepishihu*) by fourier transform infrared spectroscopy and two-dimensional correlation spectroscopy. *J. Mol. Struct.* 1204, 127554. doi: 10.1016/j.molstruc.2019.127554

Xing, S., Zhang, X., Ke, H., Lin, J., Huang, Y., and Wei, G. (2018). Physicochemical properties of polysaccharides from *Dendrobium officinale* by fractional precipitation and their preliminary antioxidant and anti-HepG2 cells activities in *vitro*. *Chem. Cent. J.* 12, 100. doi: 10.1186/s13065-018-0468-4

Xu, X., Zhang, C., Wang, N., Xu, Y., Tang, G., Xu, L., et al. (2022). Bioactivities and mechanism of actions of *Dendrobium officinale*: a comprehensive review. *Oxid. Med. Cell. Longev.* 2022, 6293355. doi: 10.1155/2022/6293355

Xu, Z., Zhou, J., Ren, T., Du, H., Liu, H., Li, Y., et al. (2020). Salt stress decreases seedling growth and development but increases quercetin and kaempferol content in *Apocynum venetum*. *Plant Biol.* 22, 813–821. doi: 10.1111/plb.13128

Yang, J., Kuang, M., Yang, L., Huang, W., and Hu, J. (2023a). Modern interpretation of the traditional application of Shihu - A comprehensive review on phytochemistry and pharmacology progress of *Dendrobium officinale*. *J. Ethnopharmacol.* 302, 115912. doi: 10.1016/j.jep.2022.115912

Yang, K., Lu, T., Zhan, L., Zhou, C., Zhang, N., Lei, S., et al. (2020). Physicochemical characterization of polysaccharide from the leaf of *Dendrobium officinale* and effect on LPS induced damage in GES-1 cell. *Int. J. Biol. Macromol.* 149, 320–330. doi: 10.1016/j.ijbiomac.2020.01.026

Yang, D., Song, Y., Lu, A., Qin, L., Tan, D., Zhang, Q., et al. (2023b). Metabolomics-Based analysis of the effects of different cultivation strategies on metabolites of *Dendrobium officinale* Kimura et Migo. *Metabolites*. 13, 389. doi: 10.3390/metabo13030389

Yuan, Y., Tang, X., Jia, Z., Li, C., Ma, J., and Zhang, J. (2020). The effects of ecological factors on the main medicinal components of *Dendrobium officinale* under different cultivation modes. *Forests.* 11, 94. doi: 10.3390/f11010094

Zeng, L., Fu, Y., Gao, Y., Wang, F., Liang, S., Yin, J., et al. (2024). Dynamic changes of key metabolites in Longjing green tea during processing revealed by widely targeted metabolomic profiling and sensory experiments. *Food Chem.* 450, 139373. doi: 10.1016/j.foodchem.2024.139373

Zeng, T., Xiao, Q., Zhang, J., Sun, X., Guo, B., Pei, J., et al. (2023). Identification of a secondary Q-marker in high-quality ecotypes of *Carthamus tinctorius* L. and exploration of the target preference. *Food Funct.* 14, 2710–2726. doi: 10.1039/D2FO02596E

Zheng, Y., Zeng, H., Yu, J., Wang, X., and Yu, J. (2024). Research progress on the historical evolution and quality formation of *Dendrobium officinale*. *World Sci. Tech. -Mod. Trad. Chin. Med. Mater. Med.* 26, 502–510. doi: 10.11842/wst.20230130001

Zuo, S., Yu, H., Zhang, W., Zhong, Q., Chen, W., Chen, W., et al. (2020). Comparative metabolomic analysis of *Dendrobium officinale* under different cultivation substrates. *Metabolites.* 10, 325. doi: 10.3390/metabo10080325

frontiers | Frontiers in Plant Science

TYPE Original Research
PUBLISHED 01 May 2025
DOI 10.3389/fpls.2025.1537273

OPEN ACCESS

EDITED BY
Eman. A. Mahmoud,
Damietta University, Egypt

REVIEWED BY
Ahmed Noah Badr,
National Research Centre, Egypt
Archana Jain,
Zunyi Medical University, China

*CORRESPONDENCE
Liai Xu
20210035@zafu.edu.cn
Zupei Lei
leizupei2007@163.com
Yeqing Ying
yeqing@zafu.edu.cn

†These authors have contributed equally to this work and share first authorship

RECEIVED 30 November 2024
ACCEPTED 07 April 2025
PUBLISHED 01 May 2025

CITATION
Xu L, Liu X, Pan X, Xu S, Wu Q, Ma C, Lei Z and Ying Y (2025) Metabolomic profiles and health-promoting potential of *Euchresta japonica* tissues revealed by widely targeted metabolomics. *Front. Plant Sci.* 16:1537273. doi: 10.3389/fpls.2025.1537273

Metabolomic profiles and health-promoting potential of *Euchresta japonica* tissues revealed by widely targeted metabolomics

Liai Xu[1,2*†], Xi Liu[2†], Xiangdong Pan[2], Sinan Xu[1], Qinglian Wu[1], Chengyi Ma[1], Zupei Lei[2*] and Yeqing Ying[3*]

[1]Key Laboratory of Quality and Safety Control for Subtropical Fruit and Vegetable, Ministry of Agriculture and Rural Affairs, Collaborative Innovation Center for Efficient and Green Production of Agriculture in Mountainous Areas of Zhejiang Province, College of Horticulture Science, Zhejiang A&F University, Hangzhou, Zhejiang, China, [2]Wuyanling National Nature Reserve Management Center of Zhejiang, Wenzhou, Zhejiang, China, [3]State Key Lab Subtrop Silviculture, Zhejiang A&F University, Hangzhou, Zhejiang, China

Euchresta japonica, a medicinal plant in Chinese herbal medicine, lacks comprehensive metabolite data to explain its health benefits despite its long-standing use. Here, widely targeted metabolome at six different tissues of *E. japonica* was investigated, identifying 2,140 metabolites, including flavonoids, phenolic acids, amino acids, lipids, and alkaloids. Among them, 305 were annotated as key active ingredients, and 364 were active pharmaceutical ingredients for nine human disease-resistance, with 206 co-annotated. Metabolic profiles varied significantly across tissues, with medicinally active metabolites highly concentrated in lateral roots and inflorescences, indicating great medical potential. Notably, the lateral root, rather than the main root, was the primary source of root-derived bioactive metabolites. Additionally, KEGG analysis demonstrated that secondary metabolic pathways, especially "isoflavonoid biosynthesis" and "flavonoid biosynthesis" pathways, played important roles. Overall, lateral roots and inflorescences exhibit the strongest potential for disease treatment, particularly for chronic and multifactorial diseases. This study significantly advances our understanding of *E. japonica*'s chemical composition and underscores its potential as a valuable resource for novel therapeutic applications, providing a strong foundation for further investigation into its pharmacological properties and drug development prospects.

KEYWORDS

***Euchresta japonica*, UPLC-ESI-MS/MS, comparative metabolomics, KEGG analysis, health-promoting, pharmacological ingredients, differential metabolites**

1 Introduction

Metabolites, the intermediate and final products of biological processes, are particularly abundant in plants. It is estimated that there are approximately 200,000 distinct metabolites within the plant kingdom, though the majority remain unidentified (Razzaq et al., 2019). These metabolites play crucial roles not only in plant development, growth, and adaptation to biotic and abiotic stresses, but also serve as vital sources of nutrients and medicines for humans. Medicinal plants, which have preventive and therapeutic effects on diseases, are a prime example (Xiao et al., 2022). China boasts a rich diversity of medicinal plants, with over 10,000 species constituting approximately 87% of the total resources of Chinese medicinal materials. The 2020 edition of the Chinese Pharmacopoeia (ChP) has cataloged 499 categories of plant-derived Chinese medicinal materials. The pharmacological efficacy of these medicinal plants is primarily attributed to the biosynthesis of secondary metabolites, which exhibit a wide range of structures and activities (Li et al., 2023).

Plant metabolite profiles can vary greatly depending on species, habitat, growth stage, plant tissues, and other factors. Comprehensive analysis of these metabolites can help assess the quality of medicinal plants and identify health-promoting compounds, which is vital for clinical treatments and drug development. However, identifying plant metabolites is challenging due to the lack of methods capable of profiling the vast array of metabolites simultaneously. Recent rapid advancements in metabolomics technologies have enabled the qualitative and quantitative analysis of small molecular metabolites across different samples, revealing sample-specific differences. Widely targeted metabolomics has emerged as a prevalent method for metabolite analysis in numerous plant species, including medicinal plants such as black sesame (Wang et al., 2018), loquat (Zou et al., 2020), *Trichosanthis radix* (Kang et al., 2020), and citrus herbs (Cao et al., 2023).

The *Euchresta* J. Bonn, a small genus in the Fabaceae family, comprises four species worldwide: *E. japonica* Hook. F. ex Regel, *E. formosana* (Hayata) Ohwi, *E. horsfieldii* (Lesch.) Benn., and *E. tubulosa* Dunn (D). All these species are medicinal plants primarily found in eastern and southeast Asia (Li et al., 2014). The chemical constituents extracted from *Euchresta* species encompass a diverse array of compounds, including flavonoids, alkaloids, and steroids (Li et al., 2014, Li H. et al., 2019; Li W. H. et al., 2019). Modern pharmacological research has demonstrated that *Euchresta* species exhibit a spectrum of biological activities, such as anti-tumor, anti-HIV, anti-platelet aggregation, central nervous system inhibition, blood lipid regulation, and antibacterial properties (Lo et al., 2003; Toda and Shirataki, 2006; Hsu et al., 2007; Kim et al., 2011).

E. japonica is an evergreen shrub that grows in shady and humid areas of evergreen broad-leaved forests throughout southern China, Korea, and southwestern Japan. It is also known as Shandougen or Hudoulian in China, and has a rich history of use in traditional Chinese medicine for its pharmacological properties. For example, within the Wu-ling Mountains, the Tujia minority has traditionally employed *E. japonica* to alleviate sore throats and abdominal pain. In Japan, the roots of this species have been utilized for their anti-inflammatory, antiarrhythmic, anticancer, and antiulcer effects (Mizuno et al., 1989). However, due to its inherently low reproductive capacity and slow growth rate, compounded by ongoing habitat destruction and excessive human harvesting, *E. japonica* has been classified as an endangered species (Choi et al., 2013). It is now listed as a second-class protected species in China (2021) and is designated as vulnerable (VU) on the IUCN Red List.

Despite its significant medicinal potential, *E. japonica*'s rarity and endangered status have resulted in limited research, with most studies focusing primarily on its population distribution and genetic conservation (Choi et al., 2013). However, investigations into its metabolite constituents—critical for understanding its pharmacological properties—remain notably scarce. Li et al. (2014) cataloged the metabolites identified in *Euchresta* plants, reporting a total of 86 flavonoids, 14 alkaloids, 4 steroids, 9 other metabolites, and 40 volatile components. Of these, 38 flavonoids (Mizuno et al., 1988a, 1988b, 1992; Shirataki et al., 1980), 11 alkaloids (Ohmiya et al., 1978, 1980), and 1 steroid (Shirataki et al., 1980) were detected in *E. japonica*. Nevertheless, the identified metabolites represent only a small fraction of the thousands potentially present, and the quantities of each remain unknown. Furthermore, the specific metabolites responsible for *E. japonica*'s pharmacological properties have yet to be determined. It is therefore imperative to undertake large-scale metabolite identification in *E. japonica* and to discover the specific metabolites that contribute to its reputed health benefits. Moreover, while the root is the primary part exploited by humans for medicinal purposes, other tissues—such as leaves, stems, inflorescences, and fruits—have scant documentation regarding their use in disease treatment, and their metabolic composition and content remain poorly understood.

In this study, a widely targeted metabolomics approach based on ultra-performance liquid chromatography coupled to triple quadrupole mass spectrometry (UPLC-QQQ-MS) was used to systematically identify and quantify metabolites across various tissues of *E. japonica*. Additionally, we pinpointed the key ingredients within these tissues that possess health-promoting properties. More importantly, metabolite content comparison, hierarchical clustering, and metabolic pathway enrichment analyses were also performed to identify the differential functional components that may be associated with the bioactivity and health benefits specific to distinct tissues of *E. japonica*. This study significantly enhances our knowledge of the chemical components, metabolomic profiles, and health-promoting function of the entire *E. japonica* plant. Furthermore, it lays a robust theoretical foundation that can inform the future development and application of this medicinal species.

2 Materials and methods

2.1 Plant materials

The *E. japonica* plants used in this study were cultivated in a greenhouse for two years and then transplanted to the wild for one year. During the fruiting period, twelve healthy, mature plants of similar age and growth conditions were selected from Wuyanling Nature Reserve, Zhejiang Province (27°41′37.54″N, 119°40′48.52″ E), China. Fresh samples of main roots (MR), lateral roots (LR), stems (S), leaves (L) and black fruits (Fr) were collected from these plants. Inflorescences (Inf) were collected from three-year-old cultivated plants at full flowering stage. All samples were immediately frozen in liquid nitrogen and stored at –80°C for RNA and metabolic extraction. Experiments were conducted with four biological replicates.

2.2 Sample preparation and extraction

Metabolite extraction, detection, and quantitative analysis for the 24 samples were carried out using a widely targeted metabolomics approach by Metware Biotechnology Co., Ltd. (Wuhan, China). The samples were freeze-dried with a lyophilizer (Scientz-100F) and ground into fine powder with a grinder (MM400, Restc) at 30 Hz for 1.5 min. For each sample, 50 mg of powder was weighted and dissolved in 1.2 mL of pre-cooled (–20°C) 70% methanolic aqueous internal standard extract. The solution was vortexed every 30 min for 30 sec, repeated six times. After centrifugation at 12,000 rpm for 3 min, the extracts were filtrated through a 0.22 μm pore size microporous membrane and stored in injection vials for UPLC-MS/MS analysis.

2.3 Widely targeted metabolomic analysis

2.3.1 UPLC conditions and ESI-Q TRAP-MS/MS

Then, an UPLC-ESI-MS/MS system (UPLC, ExionLC™ AD, https://sciex.com.cn/) and Tandem mass spectrometry system (https://sciex.com.cn/) were used to analyze the sample extracts. Each parameter choice was carefully considered based on established scientific principles and previous research in the field (Li et al., 2022; Cao et al., 2023). The UPLC analytical conditions were set as follows: (1) Column: Agilent SB-C18 (1.8 μm, 2.1 mm * 100 mm); (2) Mobile phase: Solvent A, pure water with 0.1% formic acid; Solvent B, acetonitrile with 0.1% formic acid; (3) Gradient elution: The analysis began with 95% A and 5% B. Over 9 min, a linear gradient was applied to reach 5% A and 95% B, which was maintained for 1 min. Then, the composition was adjusted to 95% A and 5.0% B over 1.1 min and held for 2.9 min; (4) Flow velocity, 0.35 mL/min; column oven, 40°C; injection volume, 2 μL. The effluent was alternately connected to an ESI-triple quadrupole-linear ion trap (Q-TRAP)-MS.

The ESI source operation parameters were set as follows: Source temperature, 500°C; Ion spray voltage (IS), 5500 V (positive ion mode)/-4500 V (negative ion mode); Ion source gas I (GSI), II (GSII), and curtain gas (CUR) were set at 50, 60, and 25 psi, respectively; Collision-activated dissociation (CAD) was set to high. QQQ scans were acquired as multiple reaction monitoring (MRM) experiments with collision gas (nitrogen) set to medium. Declustering potential (DP) and collision energy (CE) for individual MRM transitions were optimized as needed. Specific MRM transitions were monitored based on the metabolites eluted during each period.

2.3.2 Qualitative and quantitative determination of metabolites

For qualitative analysis, the secondary mass spectrum data from UPLC-MS/MS were acquired and pre-processed using Analyst software (Version 1.6.3). To ensure the accurate metabolite annotation, isotopic signals, duplicate signals containing K^+, Na^+, and NH_4^+ ions, and repeated fragment ions from other larger molecular weight substances were excluded from the analysis. The data were then annotated using the self-built Metware database (MWDB, Metware Biotechnology Co., Ltd., Wuhan, China).

For quantitative analysis, the MRM mode of triple-quadrupole mass spectrometry was employed. Peak detection, integration and correction were performed using MultiaQuant™ software. The corrected peak area for each chromatographic peak was used as an indicator of the relative concentration of the metabolites.

2.4 Network pharmacology

2.4.1 Identification of the key active ingredients in traditional Chinese medicines in *Euchresta japonica*

All metabolites of *E. japonica* identified through widely targeted metabolomics were queried in the Traditional Chinese Medicine Systems Pharmacology Database and Analysis Platform (TCMSP, https://old.tcmsp-e.com/tcmsp.php). Metabolites meeting the criteria of oral bioavailability (OB) ≥ 5% and drug-likeness (DL) ≥ 0.14 (Li et al., 2022) were considered key bioactive ingredients in Traditional Chinese Medicines derived from *E. japonica*. The related-targets and related-diseases information of these identified metabolites were listed as the TCMSP database annotation.

2.4.2 Identification of the active pharmaceutical ingredients for human diseases-resistance

Based on the disease-related annotation in the TCMSP database, the active pharmaceutical ingredients in *E. japonica* with function of anti-cancer/tumor, anti-Alzheimer's disease, analgesics, anti-myocardial infarction, anti-inflammatory, anti-arthritis, anti-gestational hypertension, anti-stroke, and anti-cardiovascular disease were summarized. The identification process of these active pharmaceutical ingredients followed previous methodologies with some modifications (Li et al., 2022; Xia et al., 2023).

2.5 Differential metabolites analysis

Multivariate statistical analysis methods were employed to analyze the metabolic data of *E. japonica*. Unsupervised principal component analysis (PCA) was performed using prcomp function in R (www.r-project.org), with data scaled to unit variance before analysis. Hierarchical Cluster Analysis (HCA) and Pearson Correlation Coefficients (PCC) were conducted using the R package Complex-Heatmap. HCA results for samples and metabolites were displayed as heatmaps with dendrograms, while PCC between samples were presented heatmaps only.

To identify the differential metabolites, Orthogonal Partial Least Squares-Discriminant Analysis (OPLS-DA) was used to maximize the differences between metabolite profiles of two samples (Thévenot et al., 2015). The Variable Importance in Projection (VIP) scores from the OPLS-DA model were used for preliminary screening of differential metabolites. Significantly differentially expressed metabolites (DEMs) were determined by VIP (VIP ≥ 1) and absolute Log2 fold change (|Log2FC| ≥ 1.0, $p \leq 0.05$). To prevent overfitting, a permutation test with 200 permutations was conducted. Identified metabolites were annotated using KEGG Compound database (http://www.kegg.jp/kegg/compound/) and MetMap databases, and annotated metabolites were mapped to KEGG Pathway database (http://www.kegg.jp/kegg/pathway.html) and MetMap databases. Pathways with significantly regulated metabolites were subjected to metabolite sets enrichment analysis (MSEA), and significance was determined by *p*-values from the hypergeometric test.

3 Results and discussion

3.1 Identification and overview of metabolites in six tissues of *Euchresta japonica*

To investigate metabolites in *E. japonica*, we used a widely targeted metabolite method based on UPLC-ESI-MS/MS on samples from different tissues, including MR, LR, Fr, Inf, S, and L (Figure 1). The good reproducibility and reliability of UPLC-ESI-MS/MS analysis were demonstrated by the highly overlapping total ion current (TIC) chromatograms of the Quality Control (QC) samples (Supplementary Figure S1).

A total of 2,140 metabolites were identified from six tissues of *E. japonica*, which can be classified into twelve distinct categories: flavonoids (638, 29.81%), phenolic acids (280, 13.08%), amino acids and derivatives (220, 10.28%), lipids (205, 9.58%), alkaloids (186, 8.69%), organic acids (121, 5.65%), lignans and coumarins (103, 4.81%), nucleotides and derivatives (72, 3.36%), terpenoids (71, 3.32%), quinones (22, 1.03%), tannins (15, 0.7%), and others (207, 9.67%) (Figure 2A; Supplementary Table S1). Furthermore, several categories were further subdivided into subclasses (Supplementary Figure S2). Specifically, the 207 other compounds comprised eight subclasses: 86 saccharides, 21 vitamins, 20 ketone compounds, 14 aldehyde compounds, 12 chromones, 8 alcohol compounds, 4 lactones, and 42 others (Figure 2B). To our best knowledge, this is the first comprehensive identification of metabolites across different tissues of *E. japonica*. Overall, the number of metabolites

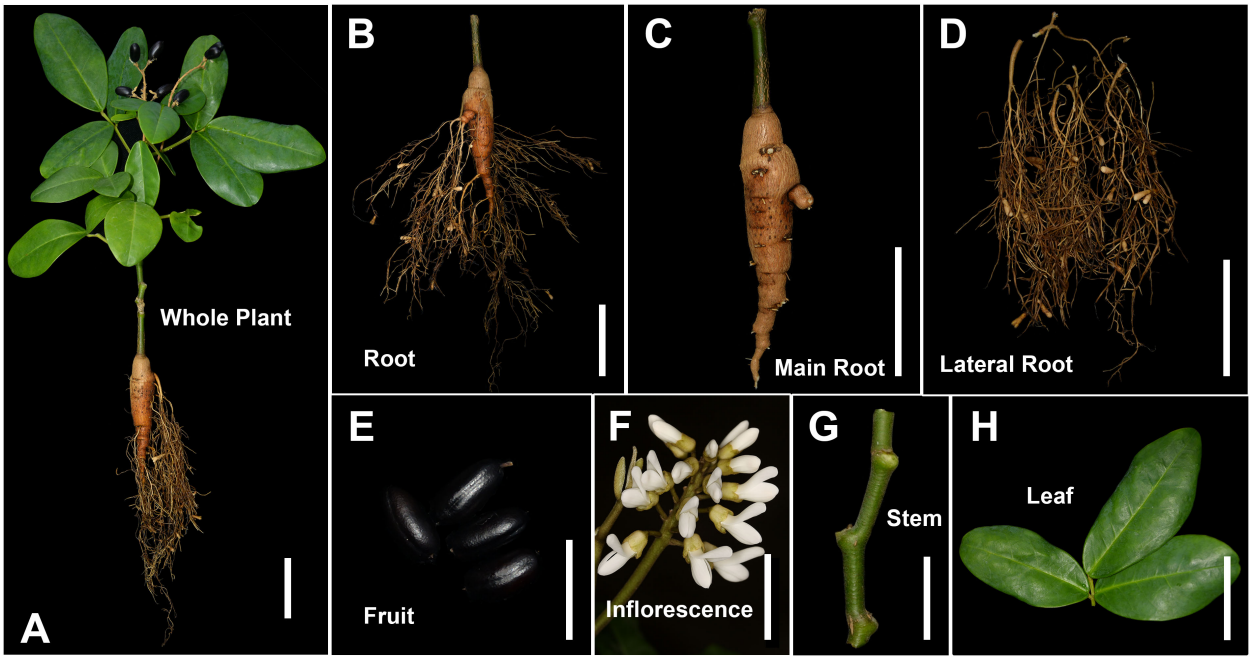

FIGURE 1
Different tissues of *Euchresta japonica* plant. **(A-H)** whole plant, root, main-root (MR), lateral-root (LR), fruit (Fr), inflorescence (Inf), stem (S), leaf (L). Scale bars, 5 cm in **(A-D)**, **(F, H)**, 2 cm in **(E, G)**.

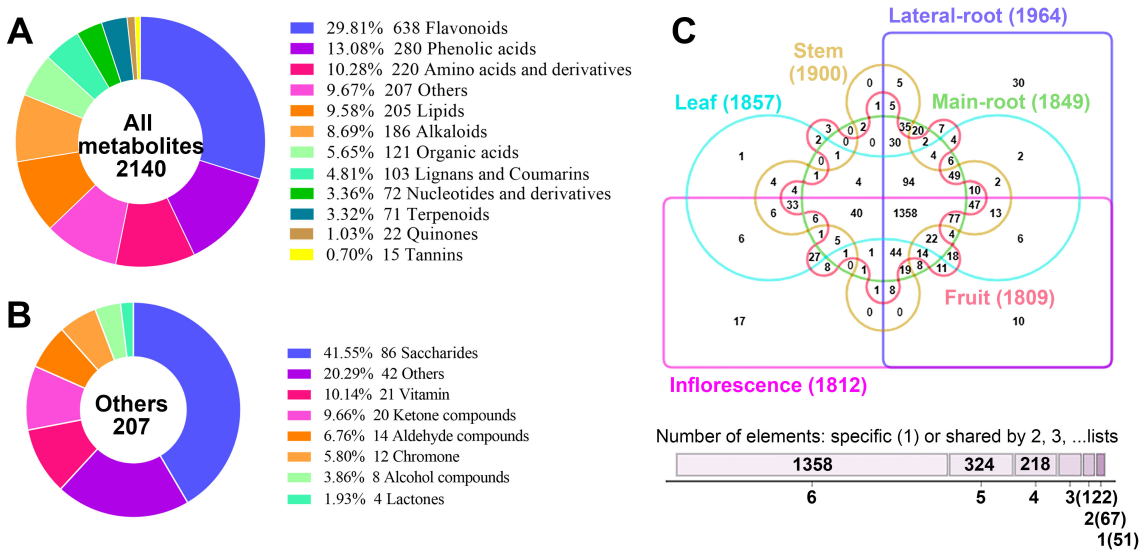

FIGURE 2
Analysis of the 2140 metabolites identified from the six tissues of *Euchresta japonica*. **(A)** Classification of the 2140 metabolites. **(B)** Classification of the 207 metabolites belonging to the "others" category. **(C)** Venn diagram showed the distribution of 2140 metabolites in the six tissues of *Euchresta japonica*.

was far greater than that detected in most other plants (Li et al., 2022; Cao et al., 2023; Xia et al., 2023). This finding underscores the efficacy of the UPLC-ESI-MS/MS-based widely targeted metabolomics approach for the comprehensive identification of metabolites in plants.

The metabolites in the six tissues were also categorized, revealing that the proportions of metabolites across twelve categories were broadly similar among different tissues, with the top five being flavonoids, phenolic acids, amino acids and derivatives, lipids, and alkaloids (Supplementary Figure S3). Although all twelve categories were detected in all six tissues, their relative levels varied significantly. Correlation analysis showed similar profiles between MR and LR ($0.42 \leq |r| \leq 0.49$), MR and S ($0.39 \leq |r| \leq 0.47$), L and Inf ($0.36 \leq |r| \leq 0.51$) (Supplementary Figure S4). Each tissue contained over 1800 metabolites, with LR having the most (1964) and Fr the least (1801) (Figure 2C). Any two tissues shared over 1600 metabolites, with the highest overlap (over 1750) between any pair of MR, LR, and S. A total of 1358 metabolites were identified across all six tissues, while 51 were tissue-specific. Notably, 30 of these were in LR and 17 in Inf. Furthermore, 18 of the 51 unique metabolites were alkaloids (35.29%), much higher than the proportion in total metabolites (186/2140, 8.69%). These findings indicate both conservation and diversity of metabolites across different tissues of *E. japonica*.

Additionally, we assessed which tissue had the highest accumulation of each metabolite. Results showed that LR and Inf contained the highest number of richest metabolites, 583 (27.24%) and 552 (25.79%), respectively, followed by L (416, 19.44%), Fr (270, 12.62%), MR (166, 7.76%) and S (153, 7.15%) (Supplementary Figure S5A, Supplementary Table S1). Statistical analysis of the distribution of richest metabolites across the six tissues also revealed notable differences in certain metabolites' accumulation patterns (Supplementary Figures S5B–M).

3.2 Screening the key active ingredients related to human health

For a long time, *E. japonica*, as a rare traditional Asian herbal medicine, has been used in folk remedies to treat conditions such as enteritis, diarrhea, pain (abdominal, stomach, toothache), and even cancers like throat and esophageal cancer (Mizuno et al., 1989). However, its potential health-promoting active components remain largely unclarified. To address this, we used the TCMSP database to screen the identified metabolites for key function-active components in *E. japonica*.

Among the 2,140 metabolites examined, 596 were identified as chemical constituents of traditional Chinese medicines. These included 219 flavonoids, 82 phenolic acids, 41 organic acids, 40 alkaloids, 33 lipids, 31 lignans and coumarins, 28 terpenoids, 25 amino acids and derivatives, 19 nucleotides and derivatives, 7 quinones, 7 tannins, and 64 other compounds (Supplementary Table S2). Among them, 402 were associated with at least one target protein and disease, 7 only with target proteins, and the remaining 187 had no corresponding target proteins or diseases.

To further characterize key active ingredients, we used OB ≥ 5% and DL ≥ 0.14 as screening criteria (Li et al., 2022). Consequently, 305 of 596 metabolites met these criteria (Figure 3A; Supplementary Table S2). Over half (176, 57.5%) were flavonoids. The rest included 25 lipids, 21 phenolic acids, 21 terpenoids, 20 lignans and coumarins, 11 alkaloids, 7 quinones, 6 nucleotides and derivatives, 4 tannins, 2 organic acids, and 12 others. Moreover,

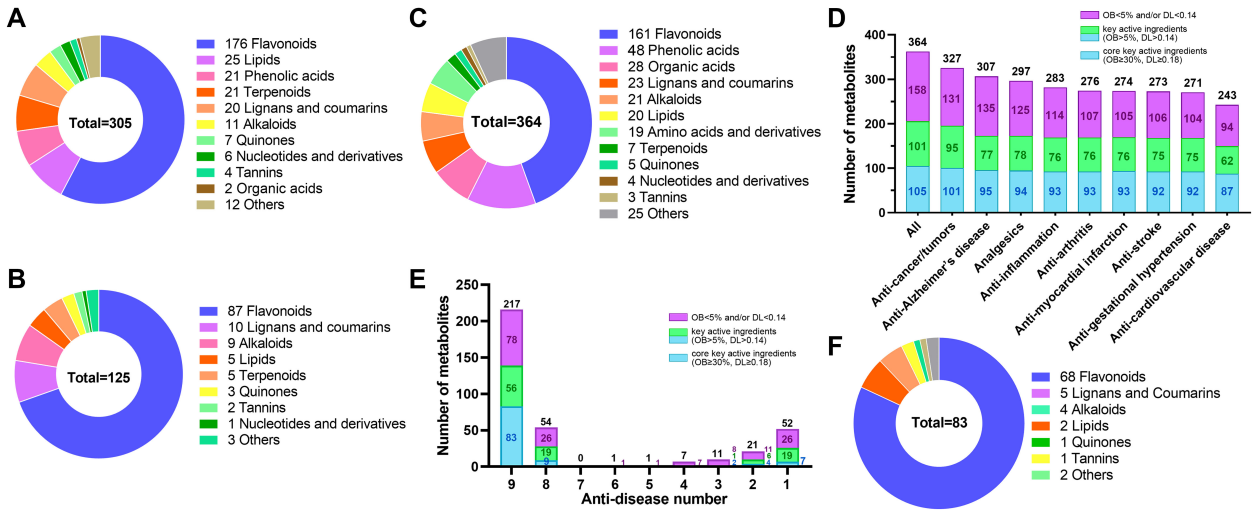

FIGURE 3
Identification of 305 key active ingredients, 125 core key active ingredients and 83 active pharmaceutical ingredients in *Euchresta japonica*. The ring chart showed the classification of the 305 key active ingredients **(A)** and 125 core key active ingredients **(B)**. **(C)** The ring chart showed the classification of the 364 metabolites that correspond to at least one of the nine diseases. **(D)** The number of metabolites corresponding to the nine diseases. **(E)** The bar chart showed the anti-disease number of the 364 metabolites. **(F)** The ring chart showed the classification of the 83 core key active pharmaceutical ingredients for nine major diseases resistance. OB, oral bioavailability; DL, drug-likeness. Key active ingredient, meet the criteria (OB ≥ 5% and DL ≥ 0.14); Core key active ingredient, meet the criteria (OB ≥ 30% and DL ≥ 0.18); Core key active pharmaceutical ingredient: core key active ingredient associated with at least one disease.

125 of the 305 key active ingredients met a stricter criterion (OB ≥ 30% and DL ≥ 0.18) for screening potential drug candidates (Jiang et al., 2021; Qu et al., 2021). These 125 metabolites were identified as core key active ingredients and composed of 87 flavonoids, 10 lignans and coumarins, 9 alkaloids, 5 lipids, 5 terpenoids, 3 quinones, 2 tannins, 1 nucleotides and derivatives, and 3 other compounds (Figure 3B). These results indicate that flavonoids are the primary chemical metabolites contributing to *E. japonica*'s health-promoting functions. However, other metabolites such as lipids, phenolic acids, terpenoids, lignans and coumarins, alkaloids, quinones may also make important roles.

Among the 305 key active ingredients, 212 were associated with at least one disease and/or target protein, while the remaining 93 were not. These 212 were found to play roles in interacting with 421 target proteins (Supplementary Table S3) and corresponded to 370 diseases (Supplementary Table S4). Additionally, 110 of the 125 core key active ingredients meeting potential drug-selection criteria were linked to 227 target proteins and corresponded to 313 diseases (Supplementary Tables S3, S4). The diseases primarily involved various cancers, e.g. breast, colorectal, lung, bladder, prostate, and ovarian cancers. Other diseases encompassed Alzheimer's disease, analgesics, tumors, inflammation, arthritis, gestational hypertension, myocardial infarction, stroke, cardiovascular disease, and so on (Supplementary Tables S3–S5). Together, these findings highlight that the identified metabolites are crucial or core key active ingredients for human health in *E. japonica*.

Furthermore, among the 291 non-key active ingredients not meeting the OB ≥ 5% and DL ≥ 0.14 criteria, 196 were associated with targets and/or diseases, corresponding to 126 different target proteins and 359 different target diseases. Many were related to the aforementioned diseases and additional diseases, e.g., depression, Parkinson's disease, Schizophrenia, alcoholism, anxiety disorders, and insomnia. (Supplementary Table S6). Notably, of the 187 metabolites with no identified corresponding target proteins or diseases, 93 met the OB ≥ 5% and DL ≥ 0.14 criteria. Among them, 15 (8 flavonoids, 2 alkaloids, 2 terpenoids, 2 lignans, and 1 lipid) satisfied the potential drug-candidate thresholds (Supplementary Table S2). These results suggest that some metabolites lacking identified target proteins and diseases in the TCMSP database may still play significant health-promoting roles and could be valuable for new drug development.

3.3 Identification of the active pharmaceutical ingredients for nine major diseases-resistance in *Euchresta japonica*

The nine human diseases—cancers/tumors, Alzheimer's disease, analgesics, inflammation, arthritis, myocardial infarction, stroke, gestational hypertension, and cardiovascular diseases—pose global health threats. Based on previous metabolite annotation, these diseases are key targets of *E. japonica* metabolites. To identify the active pharmaceutical ingredients against these nine major diseases in *E. japonica*, we queried 596 metabolites confirmed as traditional Chinese medicine chemical components in TCMSP. Among them, 364 were associated with at least one of the nine diseases (Supplementary Table S2), including 161 flavonoids, 48 phenolic acids, 28 organic acids, 23 lignans and coumarins, 21 alkaloids, 20 lipids, 19 amino acids and derivatives, etc. (Figure 3C; Supplementary Table S2). Specifically, 327 were related to anti-

cancer/tumors, 307 to anti-Alzheimer's disease, 297 to analgesics, 283 to anti-inflammation, 276 to anti-arthritis, 274 to anti-myocardial infarction, 273 to anti-stroke, 271 to anti-gestational hypertension, and 243 to anti-cardiovascular diseases (Figure 3D; Supplementary Table S2). Moreover,206 (56.59%) of the 364 were annotated as key active ingredients, including 105 (28.85%) core key active ingredients (Figure 3D; Supplementary Table S2). Notably, many metabolites were associated with multiple diseases. About 60% (217/364) were effective against all nine diseases, with 83 being core key active ingredients, 68 of which were flavonoids (Figures 3E, F; Supplementary Table S2). These findings partially explain why *E. japonica* is widely used in folk medicine for treating various diseases, from small ailments like stomach pain to intractable diseases such as various cancers. The extensive identification of metabolites with health-promoting potential highlight *E. japonica*'s promise for new herbal medicine development.

3.4 Identification of differential metabolites

3.4.1 Data quality assessment

To identify differential metabolites among different *E. japonica* tissues, the PCA and HCA were performed. The PCA results indicated clear separation among tissue groups. High aggregation of QC samples confirming the stability and reliability of the chromatography and quality detection system. As shown in Figure 4A, the two principal components (PC1 and PC2) explained 45.74% of the cumulative variance (PC1: 24.67%, PC2: 21.07%). Notably, PC1 and PC2 primarily differentiated the Inf and LR from the other four tissues. The remaining tissues, MR, S, L, and Fr were relatively clustered but still distinguishable along PC1 and PC2. These results suggest that the metabolites in *E. japonica* tissues differ significantly, with Inf and LR showing the most pronounced differences.

In line with the PCA results, HCA also demonstrated significant tissue-specific metabolite differences (Figure 4B). In PCA, the four biological replicates of each tissue clustered tightly, and the correlation analysis showed that the Pearson correlation coefficient |r| was close to 1 for all inter-group comparisons (Supplementary Figure S4), confirming high data reproducibility.

3.4.2 OPLS-DA analysis

OPLS-DA was used to screen differential metabolites among tissues. The OPLS-DA models exhibited high predictability ($Q^2 \geq 0.991$) and strong goodness of fit ($R^2X \geq 0.722$, $R^2Y = 1$) across all fifteen pairwise comparisons among the six tissues, indicating model stability and reliability (Supplementary Figure S6).

The OPLS-DA model score plots (Supplementary Figure S7) revealed significant separations among tissue groups, suggesting distinct metabolite profiles. The OPLS-DA S-plots, which graphically project specific metabolites, showed that red and green dots represent metabolites with VIP values ≥ 1 and < 1, respectively (Supplementary Figure S8). The top 20 metabolites with higher VIP values for each comparison were shown in Supplementary Figure S9. Notably, in LR comparisons (except LR vs. Inf), at least 15 of the top 20 metabolites were upregulated in LR compared to other tissues.

Fold change (FC) values were calculated to provide a clearer and more intuitive representation of overall metabolic differences. A dynamic distribution map of metabolite content differences was created, highlighting the top 10 up- and down-regulated metabolites (Supplementary Figure S10). Each pairwise comparison identified more than 1,100 metabolites meeting the criteria of $|\text{Log2FC}| \geq 1.0$, with the most (1,543) in LR vs. L and the fewest (1,127) in MR vs. S (Supplementary Table S7). Moreover, among the 15 comparisons, LR vs. MR/Fr/Inf/S/L exhibited a higher number of up-regulated metabolites, with 1,056, 974, 825, 843, and 885 metabolites, respectively (Supplementary Table S7).

To further explore tissue differences, DEMs were screened from the 2140 identified metabolites based on FC and VIP scores. Using the criteria (VIP ≥ 1; $|\text{Log2FC}| \geq 1.0$; $p \leq 0.05$), a total of 2045 DEMs were identified in at least one pairwise comparison, accounting for 97.2% of all detected metabolites. As shown in Figures 4C, Supplementary Figure S11 and Supplementary Tables S7, S8, over 40% of detected metabolites in all pairwise comparisons were DEMs, with the most (1,335) in MR vs. Inf and the fewest (873) in S vs. L. These results strongly suggest significant variations in metabolite composition and regulation among tissues.

3.4.3 K-means clustering algorithm analysis

To evaluate metabolite variations across tissues of *E. japonica*, we performed unit variance scaling on 2045 DEMs and clustered them into 10 subclasses using K-means analysis (Figure 5; Supplementary Table S7). This classification revealed tissue-specific metabolite accumulation patterns. For instance, subclass 1 to 6 exhibited high metabolite accumulation in MR, LR, Fr, Inf, S and L, respectively, with 145, 424, 254, 418,76 and 262 DEMs each (Figure 5; Table 1). Saccharides, though a minor fraction of all DEMs, were prominent in MR-specific subclass 1(Figure 5A). Flavonoids dominated subclasses 2 to 6, indicating their prevalence in LR, Fr, Inf, S, and L (Figures 5B–F; Table 1). Subclass 2 was distinguished by elevated alkaloids (35) and terpenoids (25), with lipids and phenolic acids ranking second to subclass 4. This indicates that flavonoids, phenolic acids, lipids, alkaloids, and terpenoids are the primary metabolites with high accumulation in the lateral roots of *E. japonica*. Subclass 3 was rich in flavonoids, amino acids and derivatives, and organic acids. Subclass 4, with 418 Inf-concentrated metabolites, included 104 flavonoids, 83 lipids, 65 phenolic acids, 45 amino acids and derivatives, and 32 organic acids, totally accounting for 78.7%. Subclass 5, with 76 stem-enriched metabolites, highlighted flavonoids, phenolic acids, and alkaloids. Subclass 6, boasting 262 leaf-enriched metabolites, featured flavonoids, phenolic acids, and saccharides. Subclasses 7 to 10 had elevated metabolite levels in tissue pairs: LR & Inf (99), LR & S (113), Inf & L (161), and S & L (93), with flavonoids being predominant. Overall, inflorescences and lateral roots of *E. japonica* had the highest number of metabolites at elevated levels, followed by leaves, stems, fruits, and main roots.

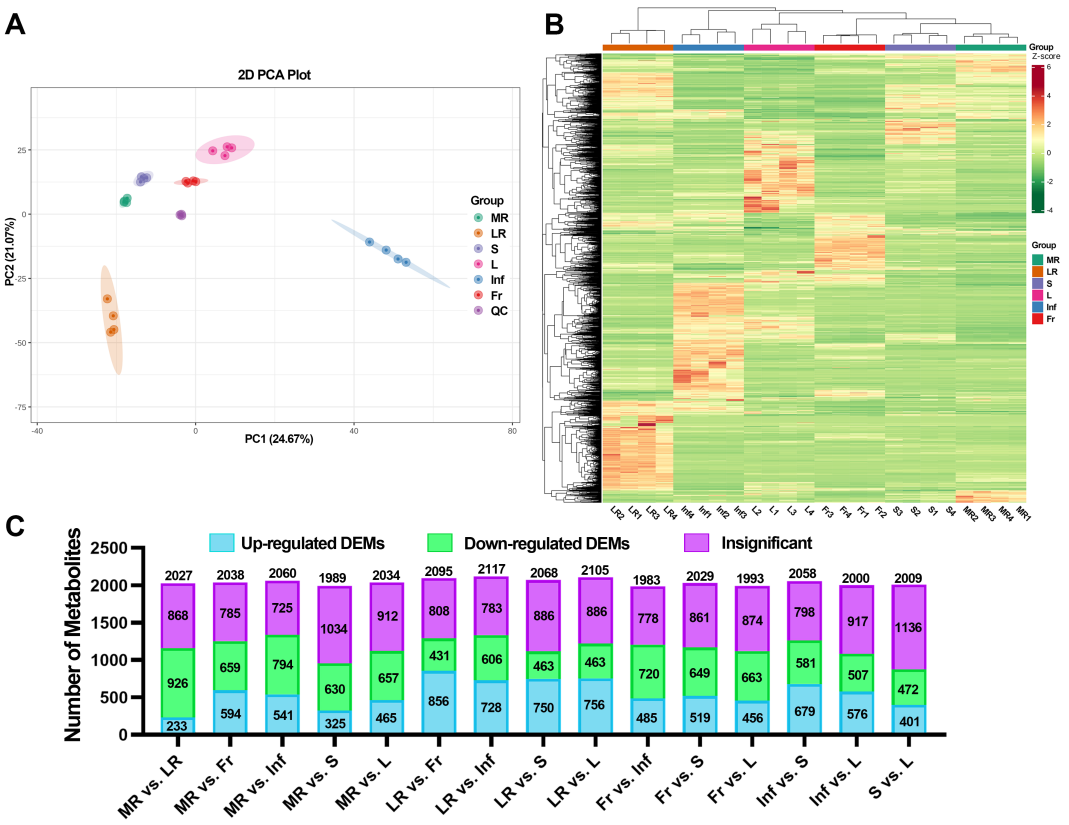

FIGURE 4
Different metabolome profiling of six tissues of *Euchresta japonica*. **(A)** The result of principal component analysis (PCA). **(B)** The hierarchical cluster analysis (HCA) of metabolites. **(C)** Statistical analysis of the numbers of up/down-regulated metabolites in 15 comparison groups. MR, LR, Fr, Inf, S, and L represent main-roots, lateral-roots, fruits, inflorescence, stems, and leaves of *E. japonica*, respectively.

3.5 Differences in the chemical constituents among the different tissues of *Euchresta japonica*

Among the 2045 DEMs, there were 629 flavonoids, 271 phenolic acids, 207 amino acids and derivatives, 190 lipids, 164 alkaloids, 116 organic acids, 99 lignans and coumarins, 85 saccharides, 71 nucleotides and derivatives, 70 terpenoids, 22 quinones, 12 tannins, and 194 others (Table 1; Supplementary Table S7). Detailed information on each metabolite category in the different comparisons was provided in Supplementary Table S8. The tissues with the richest metabolites were listed in Supplementary Table S1 and illustrated in Supplementary Figure S5. The characteristics and differences in the chemical composition were shown in Supplementary Figures S12–24.

3.5.1 Flavonoids

Flavonoids are the most abundant metabolites in *E. japonica*, with 638 identified across six tissues. They can be further categorized into nine subclasses: flavones, isoflavones, flavonols, flavanones, chalcones, dihydroisoflavones, flavanols, flavanonols, and others (Supplementary Figure S2A). Each tissue of *E. japonica* identified 82.1% to 87.9% of total flavonoids, with the highest proportion found in LR, followed by L, Inf, S, and MR (Supplementary Figure S12). Similarly, LR also contained the highest number of richest flavonoids (30.4%, 194), followed by L and Inf (Supplementary Figure S5B). Comparative analyses revealed more up-regulated flavonoids in LR, L, and Inf than in other tissues, while MR contained more down-regulated ones (Supplementary Table S8). In summary, although the number of detectable flavonoid metabolites varied little among the six tissues, the concentration of flavonoids in LR, L, and Inf was significantly higher than that in Fr, S, and MR, highlighting their potential in *E. japonica*'s medicinal value.

Flavonoids are well-documented for their significant role in managing chronic diseases by inhibiting oxidative damage and persistent inflammation (Ding et al., 2022). Pharmacological data further underscore the importance of flavonoids in disease resistance (Supplementary Table S9). Among the 87 core key active flavonoids, 68 were effective against nine major diseases, many highly accumulated in LR, Inf, and L (Supplementary Tables S2, S9). Many of these flavonoids are known for their antioxidant, anti-inflammatory, anti-arteriosclerotic, anti-tumor, and cancer therapeutic effects. For instance, wogonin, a flavone with notable antitumor activity and a potential chemosensitizer in cancer therapy (Huynh et al., 2017, 2020; Zhang et al., 2022), was highly concentrated in LR but low in MR/Inf and absent in Fr/S/L (Figure 6A). Calycosin and formononetin, isoflavones with strong

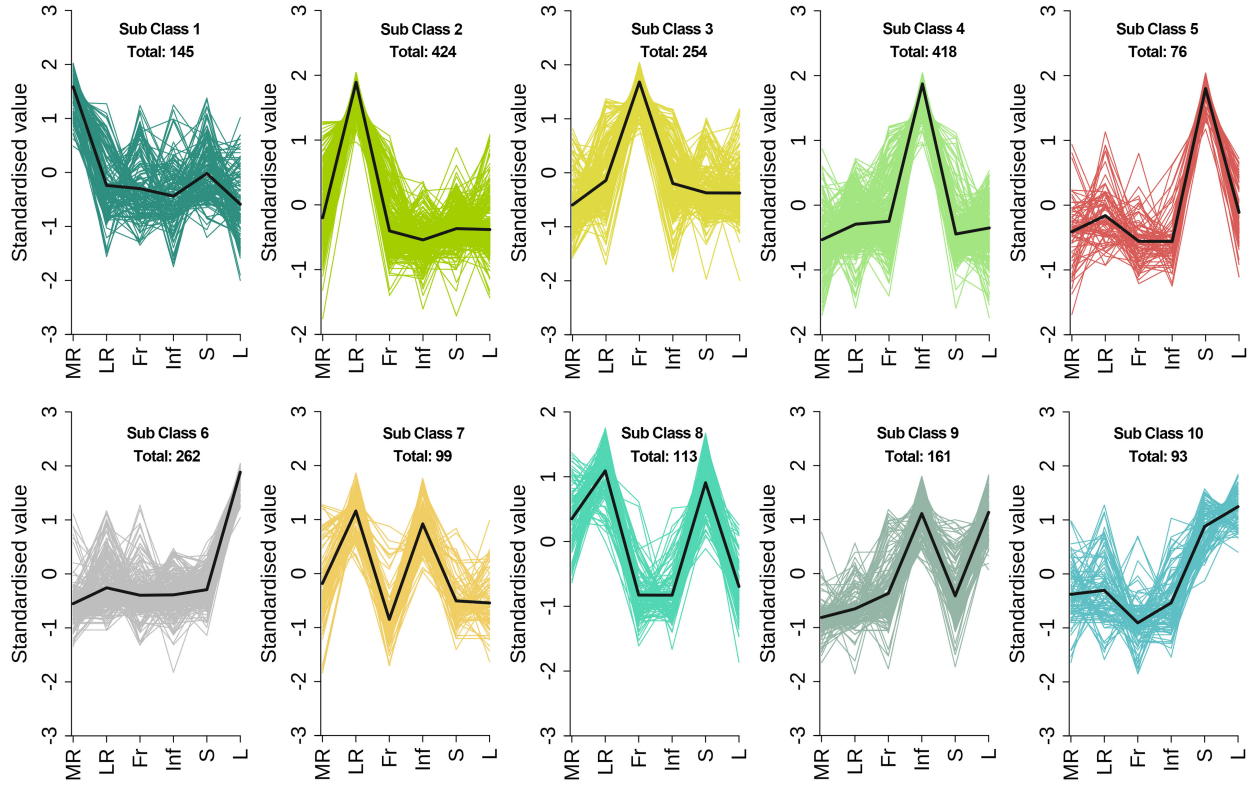

FIGURE 5
K-means clustering algorithm analysis of differential metabolites in different tissues of *Euchresta japonica*. The x axis represented the different tissues of *E. japonica*, and the y axis represented the standardized content of per metabolite. MR, LR, Fr, Inf, S, and L represent main-roots, lateral-roots, fruits, inflorescence, stems, and leaves, respectively. The total number of differential metabolites per subclass was shown.

TABLE 1 The number of different types of DEMs in the 10 subclasses of K-means clustering analysis.

Sub Class Types	Sub Class 1	Sub Class 2	Sub Class 3	Sub Class 4	Sub Class 5	Sub Class 6	Sub Class 7	Sub Class 8	Sub Class 9	Sub Class 10	Total
Alkaloids	17	35	23	21	10	16	14	6	13	9	164
Amino acids and derivatives	31	18	42	45	7	18	23	7	10	6	207
Flavonoids	8	160	59	104	24	121	8	30	78	37	629
Lignans and Coumarins	3	19	12	9	5	13	4	24	4	6	99
Lipids	11	47	13	83	0	6	20	2	7	1	190
Nucleotides and derivatives	8	9	15	16	2	3	12	5	1	0	71
Organic acids	5	12	30	32	4	12	2	2	12	5	116
Phenolic acids	16	61	21	65	18	27	9	27	7	20	271
Quinones	0	9	8	0	0	2	0	1	1	1	22
Tannins	0	6	0	0	2	1	0	1	1	1	12
Terpenoids	6	25	7	12	3	5	1	2	6	3	70
Saccharides	32	1	9	10	0	21	1	2	9	0	85
Others	8	22	15	21	1	17	5	4	12	4	109
Total	145	424	254	418	76	262	99	113	161	93	2045

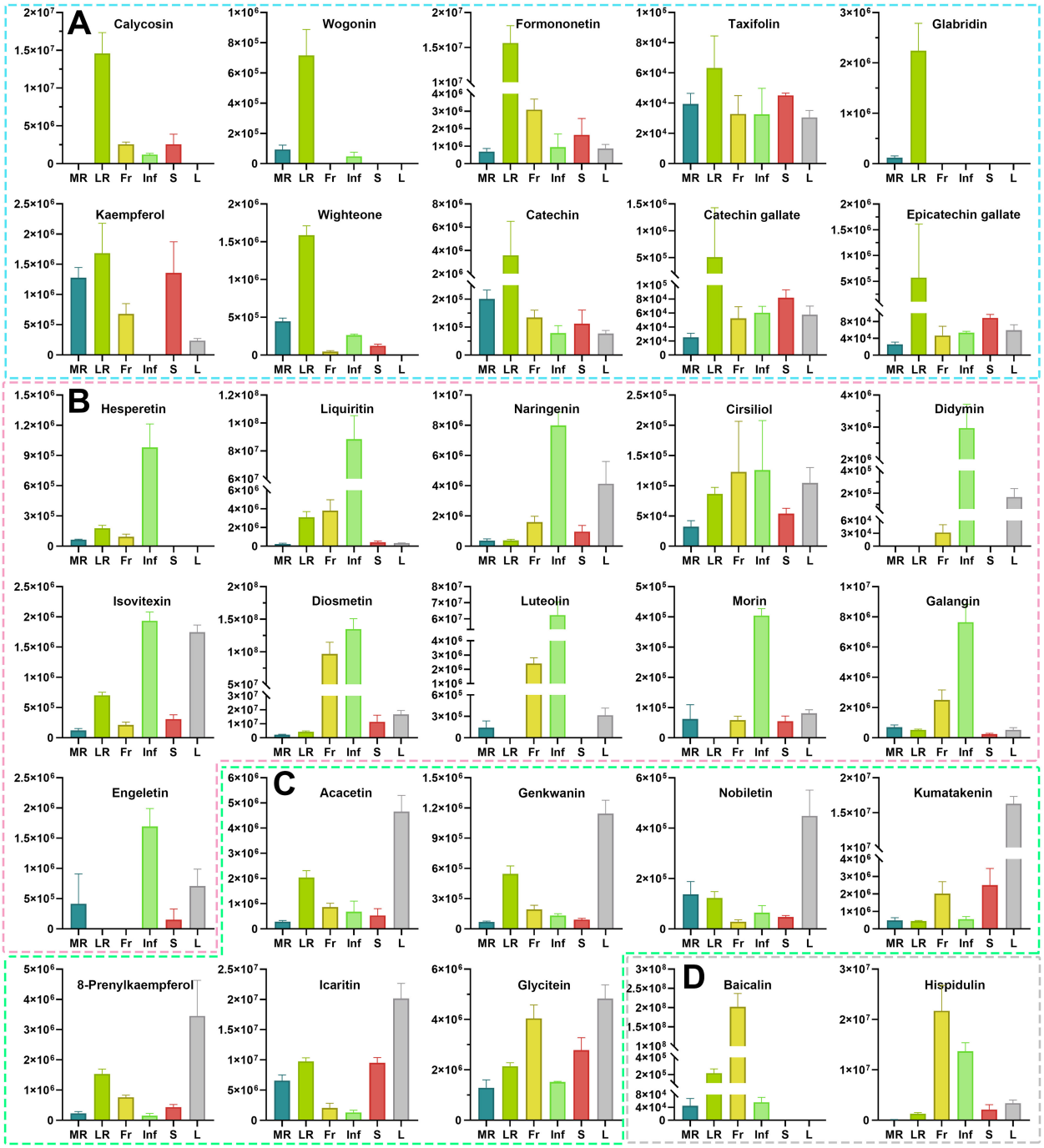

FIGURE 6
The relative contents of the 30 health-promoting flavonoids metabolites in different tissues of *Euchresta japonica*. More health-promoting flavonoid metabolites accumulate at high levels in the LR, Inf and L. Flavonoids accumulated the highest amount in LR **(A)** Calycosin; Wogonin; Formononetin; Taxifolin; Glabridin; Kaempferol; Wighteone; Catechin; Catechin gallate; Epicatechin gallate), Inf **(B)** Hesperetin; Liquiritin; Naringenin; Cirsiliol; Didymin; Isovitexin; Diosmetin; Luteolin; Morin; Galangin; Engeletin), L **(C)** Acacetin; Genkwanin; Nobiletin; Kumatakenin; 8-Prenylkaempferol; Icaritin; Glycitein), and Fr **(D)** Baicalin; Hispidulin). Each relative content value was mean (± SD) of four biological replicates. MR, LR, Fr, Inf, S, and L represent main-roots, lateral-roots, fruits, inflorescence, stems, and leaves, respectively.

cardiovascular protective effects (Chen et al., 2022; Ma et al., 2022; Qian et al., 2024), were most abundant in LR, followed by Fr or S (Figure 6A). Other flavonoids, such as taxifolin (Topal et al., 2016), glabridin (Parlar et al., 2020), kaempferol (Devi et al., 2015), wighteone (Wang et al., 2024), catechin, catechin gallate and epicatechin gallate (Musial et al., 2020), which exhibit excellent antioxidant and/or anti-inflammatory effects, were also highly accumulated in LR (Figure 6A). Similarly, several core key active flavonoids with the highest accumulation in Inf have also been reported to have diverse physiological and pharmacological effects.

These include four flavanones (hesperetin, liquiritin, naringenin, cirsiliol, and didymin), three flavones (isovitexin, diosmetin, and luteolin), two flavonols (morin and galangin), and one flavanonol (engeletin) (Figure 6B). Isovitexin is a potential inhibitor of multiple tumor cells, including colon, breast, ovarian, prostate, esophageal, and pancreatic cancer, demonstrating its capability for promoting apoptosis in tumor cells (Yang et al., 2013; Ganesan and Xu, 2017; Ghanbari-Movahed et al., 2023). Engeletin, with anti-inflammatory, antioxidant, and immunomodulatory properties (Zhong et al., 2023), is a promising drug candidate. Flavonoids with higher relative contents in L include acacetin, genkwanin, nobiletin, kumatakenin, 8-prenylkaempferol, icaritin, glycitein, etc. (Figure 6C). Acacetin has demonstrated anti-inflammatory, antiperoxidative, and anticancer activities, and is a promising potential drug for treating osteoarthritis (Kim et al., 2014; Chen et al., 2020). Icaritin possesses a wide range of pharmacological effects, including alleviating sexual dysfunction, osteoporosis, cardiovascular diseases (Reyes-Hernández et al., 2024), and showing efficacy against solid tumor, particularly advanced hepatocellular carcinoma (Luo et al., 2024). Among the 11 core key active flavonoids with the highest accumulation in Fr, baicalin and hispidulin (Figure 6D) are noted for their anti-diabetic, anti-inflammatory, antioxidant, and anticancer properties (Wang et al., 2020; Miao et al., 2024). The six core key active flavonoids with the highest accumulation in S include three flavanols (cinchonain Ic, cinchonain Id, and garbanzol), two isoflavones (flemiphilippinin C, and glycyroside), and one other flavonoid (kushenol O) (Supplementary Table S1). Taken together, many flavonoids with diverse pharmacological activities like anti-cancer/tumor, anti-inflammatory, etc., are predominantly concentrated in LR, Inf, and L, and those flavonoids can be used as lead compounds for the development of potential therapeutic agents. For example, wogonin with high anti-tumor activity can be structurally modified to develop new anti-cancer drugs (Banik et al., 2022). Calycosin and formononetin with cardiovascular-protective effects can be further studied for drug or health-products development.

3.5.2 Phenolic acids

A comprehensive analysis identified 280 phenolic acids in *E. japonica*, with LR exhibiting the highest accumulation, followed by S, MR, L, Inf, and Fr (Supplementary Figure S3). Comparative analyses revealed more up-regulated phenolic acids in LR, S, and Inf than in L, MR, and Fr, indicating higher concentrations in the former (Supplementary Table S8, Supplementary Figure S13). Among these, 21 were key active ingredients, and 12 were active pharmaceutical ingredients (Supplementary Table S2, S9). Four of these—grandidentatin, salidroside, syringin, and usnic acid—show resistance to nine major diseases (Supplementary Table S2). Salidroside, for instance, has been shown to reduce oxidative substances such as reactive oxygen species and malondialdehyde, thereby delaying the progression of aging-related diseases (Campisi et al., 2019). Though not meeting the criteria for key active ingredients, gallic and ferulic acids were predicted to resist all nine diseases (Supplementary Table S2). Gallic acid is known for its antioxidant, anti-inflammatory, antineoplastic activities, and therapeutic activities against gastrointestinal, neuropsychological, metabolic, and cardiovascular disorders (Kahkeshani et al., 2019). Ferulic acid is effective in treating diabetes, angina pectoris, heart stroke, coronary heart disease, and cardiovascular diseases (Liu et al., 2003; Guo et al., 2008). Of the six highlighted phenolic acids, except gallic acid (high in LR) and usnic acids (high in L), the other four were most abundant in Inf (Supplementary Figure S25). Given their significant antioxidant properties, the high levels of phenolic acids in *E. japonica*, especially in Inf, LR, and S, suggest its potential for improving human health.

3.5.3 Amino acids and derivatives

Over 200 amino acids and derivatives were found in each tissue of *E. japonica*, representing over 90% of the total 220 (Supplementary Figure S3). Notably, Inf, LR, and Fr had higher concentrations (Supplementary Table S8, Supplementary Figure S14). None were key active ingredients, but 19 were active pharmaceutical ingredients. Six were predicted to correspond to nine major diseases: L-valine, 5-hydroxy-L-tryptophan, L-tryptophan, L-histidine, 5-hydroxy-DL-tryptophan, and N-methylphenylalanine (Supplementary Table S2). L-valine and L-histidine were more prevalent in MR and Fr, respectively, while 5-hydroxy-DL-tryptophan and N-methylphenylalanine were particularly abundant in Inf (Supplementary Figure S26).

3.5.4 Lipids

In *E. japonica*, 205 lipids were detected across tissues, with LR containing the most (197) and Fr the least (168) (Supplementary Figure S3). Comparative analyses revealed more up-regulated lipids in Inf and LR, suggesting higher concentrations in these tissues (Supplementary Table S8; Supplementary Figure S15). Out of the total lipids, 25 were key active ingredients, and 16 were active pharmaceutical ingredients (Supplementary Tables S2, S9). Among these, 13 lipids were predicted to protect against nine major diseases, including nine most highly accumulated in Inf (9-hydroxy-10,12,15-octadecatrienoic acid, ethyl linoleate, linoleic acid, octadeca-9,12,15-trienoic acid, pinolenic acid, punicic acid, α-linolenic acid, and γ-linolenic acid, ricinoleic acid), two in LR (arachidonic acid, methyl linolenate), one in MR (elaidic acid) and one in Fr (stearic acid) (Supplementary Figure S27). Ricinoleic acid, linoleic acid, elaidic acid and stearic acid have also accumulated considerable amounts in other tissues (Supplementary Figure S27). Additionally, arachidonic acid and ethyl linoleate met criteria for potential drug candidates, with arachidonic acid playing a crucial role in cardiometabolic diseases (Hu et al., 2024), indicating its therapeutic potential in cardiovascular health. The higher relative content of these lipids in Inf and LR may enhance their value in protecting human health.

3.5.5 Alkaloids

Among the 186 alkaloid metabolites detected in *E. japonica*, LR had the highest number of alkaloids (163), as well as richest accumulated alkaloids (53, 28.49%) (Supplementary Figure S5F). Differential expression and heatmap cluster analysis indicated a higher relative content of alkaloids in LR, Inf and L (Supplementary

Table S8; Supplementary Figure S16). Nine alkaloids were core key active ingredients: lauroscholtzine, N-cis-feruloyltyramine, tetrahydroprotopapaverine, p-coumaroyltyramine, sophocarpine, sparteine, β-isosparteine, isomatrine, and moupinamide. Notably, the first four were core key active pharmaceutical ingredients, predicted to address nine major diseases, and significantly accumulated in LR (Supplementary Table S2; Supplementary Figure S28). Sophocarpine was also suggested to have anti-nociceptive, anti-inflammatory, neuroprotective, anti-tumor, and immune regulatory functions (Zhou et al., 2022), with higher relative content found in Fr and Inf. Additionally, sparteine and β-isosparteine were found to be significantly accumulated in S and were predicted to have anti-Alzheimer's and analgesic effects, while isomatrine was notably present in Fr, L and Inf, and moupinamide was concentrated in LR.

3.5.6 Organic acids

Of the 121 organic acids identified in *E. japonica*, the detectable quantities in each tissue ranged from 109 to 118 (Supplementary Figure S3). A high relative abundance of organic acids was also observed in Inf, Fr, and L, while MR and S exhibited lower levels (Supplementary Table S8; Supplementary Figure S17). Among the 41 organic acids recognized as components of traditional Chinese medicines in TCMSP, only two—anacardic acid and tianshic acid—were identified as key active ingredients (Supplementary Table S2). Anacardic acid, predicted to possess analgesic and anti-inflammatory properties, was found to be highly concentrated in Fr, whereas tianshic acid was relatively more abundant in Inf (Supplementary Figure S29).

3.5.7 Lignans and coumarins

In MR, all lignans and coumarins identified in *E. japonica* were detected, totaling 103, while Fr detected the fewest, with only 76 (Supplementary Figure S2). Notably, LR contained the largest number of the richest accumulated lignans and coumarins, totaling 33 (Supplementary Figure S5H). Moreover, LR, S, and L also contained relatively high levels of lignans and coumarins (Supplementary Table S8; Supplementary Figure S18). A total of 20 lignans and coumarins were identified as key active ingredients, among which 10 were further categorized as core key active ingredients with potential for drug development. This subset included six lignans (acanthoside B, diphyllin, fargesin, glycyrin, picraquassioside C, and sesamin) and four coumarins (coumestrol, dalbergin, fraxin, and stevenin) (Supplementary Table S2). Furthermore, diphyllin, glycyrin, sesamin, dalbergin, and stevenin were predicted to be effective against nine major diseases, while coumestrol and fraxin were found to confer resistance to eight major diseases, excluding cardiovascular disease (Supplementary Table S2). The pharmacological properties of these lignans and coumarins have been continuously validated; for example, sesamin is known for its antioxidative, anti-cancerogenic, anti-inflammatory, anti-proliferative, anti-hypertensive, anti-melanogenesis, and promoting effect in treating osteoporosis (Yang et al., 2022; Dossou et al., 2023), highlighting its potential for various therapeutic applications. Coumestrol has also demonstrated anti-tumor activity by facilitating apoptosis in colorectal cancer cells (Geng et al., 2024). Here, considerable accumulation of sesamin was detected in all six tissues of *E. japonica*. Additionally, fargesin, picraquassioside C, acanthoside B, and coumestrol exhibited relatively high levels in MR, LR, and S. Fraxin and dalbergin were notably concentrated in LR, while stevenin was found in both LR and Fr, and glycyrin and diphyllin were primarily present in S and L, respectively (Supplementary Figure S30). These findings suggest that lignans and coumarins in various tissues of *E. japonica* significantly contribute to its pharmacological efficacy.

3.5.8 Nucleotides and derivatives

A total of 72 nucleotides and derivatives were detected in *E. japonica*, with detectable quantities in each tissue ranging from 63 to 71 (Supplementary Figure S3). Inf and LR had higher levels of these compounds (Supplementary Table S8; Supplementary Figure S19). Six were identified as key active ingredients: 2'-deoxyadenosine, adenosine, cordycepin, guanosine, uridine 5'-diphosphate, and uridine 5'-monophosphate (Supplementary Tables S2, S9). Their concentrations across various tissues were presented in Supplementary Figure S31. Additionally, 2'-deoxyadenosine and cordycepin were predicted to be associated with nine major diseases (Supplementary Table S2). Existing studies have also confirmed that cordycepin, recognized as a potential anti-cancer/tumor agent, exhibits complementary therapeutic activities in promoting apoptosis, anti-proliferation, and anti-metastasis in cancer cells (Yoon et al., 2018; Schwenzer et al., 2021).

3.5.9 Terpenoids

The highest number of terpenoids was detected in LR (67), followed by MR (65) (Supplementary Figure S3). Differential metabolite analysis revealed that the relative contents of many terpenoids in LR were significantly higher than those in other tissues (Supplementary Table S8; Supplementary Figure S20). A total of 21 terpenoids were identified as key active ingredients, comprising 16 triterpenes, four diterpenoids, and one triterpene saponin (Supplementary Table S9). Among these, two triterpenes (asiatic acid, and mangiferonic acid) and three diterpenoids (gibberellin A3, isopimaric acid, and kaurenoic acid) met the criteria of core key active ingredients (Supplementary Table S2; Supplementary Figure S32). Asiatic acid, despite no TCMSP disease annotations, has shown anti-inflammatory, antioxidant, anti-fibrosis, and anti-tumor properties in diverse disease models (Lv et al., 2017; Chung et al., 2021), and was most abundant in LR, indicating the tissue's potential health benefits.

3.5.10 Quinones

A total of 22 quinones were detected in *E. japonica*, with approximately 21 detected in all tissues except for Inf, with only 13 identified in Inf (Supplementary Figure S2). LR and Fr contained more up-regulated quinones than down-regulated ones compared to other tissues, indicating higher overall quinone levels in LR and Fr (Supplementary Table S8; Supplementary Figure S21). Seven quinones were identified as key active ingredients, including three

highly accumulated quinones in LR (1,2,4-trihydroxyanthraquinone, physcion, and rheic acid), two highly accumulated quinones in Fr (emodin-8-O-glucoside, and helminthosporin), one quinone shared between LR and Fr (rubiadin-1-methyl ether), and one quinone (embelin) that was commonly found in all tissues (Supplementary Table S2; Supplementary Figure S33). Furthermore, embelin, emodin-8-O-glucoside, and rheic acid were classified as core key active ingredients. Additionally, 1,2,4-trihydroxyanthraquinone, physcion, rheic acid, and embelin were annotated as active pharmaceutical ingredients associated with nine or eight major diseases (Supplementary Table S2). The higher accumulation of these quinones in LR and/or Fr suggested that they significantly contribute to the health benefits attributed to these tissues.

3.5.11 Tannins

Tannins were predominantly detected in LR, where 14 out of 15 tannins were identified, with 10 exhibiting the highest relative content or accumulating exclusively in LR (Supplementary Figures S3, S5L, S22). Among the 15 tannins, only seven were annotated in TCMSP, of which four were annotated as key active ingredients: 3,3'-di-O-methylellagic acid 4'-glucoside, ellagic acid, procyanidin B1, and procyanidin B4 (Supplementary Tables S2, S9). Metabolite content analysis revealed that ellagic acid accumulated at comparable levels across all six tissues, while 3,3'-di-O-methylellagic acid 4'-glucoside mainly accumulated in high concentrations in S and L. In contrast, procyanidin B1 and procyanidin B4 were highly or exclusively accumulated in LR (Supplementary Figure S34).

3.5.12 Others

In addition to the aforementioned metabolites, a total of 207 metabolites from eight other categories were detected in *E. japonica* (Figure 2B), with quantities ranging from 191 to 200 in each tissue (Supplementary Figure S3). Besides saccharides being most abundant in MR, other types of metabolites were also mainly accumulated in LR and Inf (Supplementary Table S8; Supplementary Figures S23, S24). Of the 64 metabolites annotated in TCMSP, only 12 were annotated as key active ingredients, while 25 were identified as active pharmaceutical ingredients, with eight metabolites co-annotated (Supplementary Table S2). The 12 key active ingredients included three chromones, three saccharides, three vitamins, two ketone compounds, and 3'-O-methylorobol (Supplementary Table S2; Supplementary Figure S35). Among these metabolites, capillarisin, vitamin K1, and 3'-O-methylorobol met the criteria of OB ≥ 30% and DL ≥ 0.18, and were associated with nine or eight major diseases, indicating their potential for new drug development (Supplementary Table S2).

In summary, *E. japonica*'s tissues showed distinct metabolite profiles. LR had higher accumulations of most metabolite classes, especially flavonoids, phenolic acids, alkaloids, lignans and coumarins, terpenoids, quinones, and tannins. Inf was rich in many metabolite classes except lignans and coumarins, quinones, and tannins. In other tissues, the accumulation of certain metabolites was relatively abundant. For instance, the content of flavonoids, alkaloids and organic acids was relatively high in L; phenolic acids, lignans and coumarins were richly accumulated in S; organic acids and quinones were also abundant in Fr. However, except for saccharides that predominantly accumulated in MR, the content of other metabolites in MR was comparatively lower than that in other tissues. These findings indicate that for *E. japonica*, with its roots used as folk medicine, the medicinal efficacy likely derives mainly from LR, as LR generally contains a higher content of pharmacologically active components than MR.

Overall, the diverse chemical composition across *E. japonica* tissues points to its significant pharmacological potential. Notably, LR and Inf demonstrate the greatest application potential due to their rich profiles of bioactive compounds, suggesting they could serve as key sources for developing treatments for various diseases, particularly for treating chronic and multifactorial diseases. This study underscores the pharmacological promise of *E. japonica* in medicinal applications, warranting further investigation into these specific tissues for drug development.

3.6 KEGG annotation and enrichment analysis of DEMs

To explore *E. japonica*'s metabolic pathways across different tissues, the KEGG and MetMap databases were used to annotate and analyze 2045 DEMs. A total of 416 DEMs were annotated in KEGG, 276 in MetMap, with 43 co-annotated (Supplementary Table S1). These DEMs were assigned into 101 KEGG metabolic pathways and 16 MetMap metabolic pathways (Supplementary Figure S36). Subsequent enrichment analysis and mapping of DEMs across 15 comparisons among the six tissues revealed involvement in various metabolic pathways, with 101–113 pathways in each comparison. Notably, 153 DEMs were mapped to the biosynthesis of secondary metabolites. Furthermore, the number of DEMs associated with the biosynthesis of cofactors, biosynthesis of amino acids, ABC transporters, biosynthesis of isoflavones aglycones I, flavonoid biosynthesis, and isoflavonoid biosynthesis was particularly large, highlighting their significance in *E. japonica*'s metabolism (Supplementary Figure S36).

3.6.1 KEGG enrichment analysis of DEMs

KEGG pathway enrichment analysis was conducted based on the characteristics of the DEMs. In KEGG enrichment analysis, the rich factor reflects the degree of enrichment; a value closer to 1 indicates a higher proportion of annotated metabolites within a corresponding pathway that are classified as DEMs. The top 20 pathways identified via KEGG enrichment analysis were shown in Supplementary Table S10, Figure 7 and Supplementary Figures S37–39.

Among the top 20 pathways across the 15 comparisons, a total of 88 pathways were identified, with 32 pathways significantly enriched ($p < 0.05$) in at least one comparison (Supplementary Table S10; Supplementary Figure S37). Notably, six pathways—biosynthesis of isoflavones aglycones I, II, and III, and biosynthesis of flavones aglycones I, II, and III—ranked among the top 20 pathways in most comparisons and were significantly enriched in

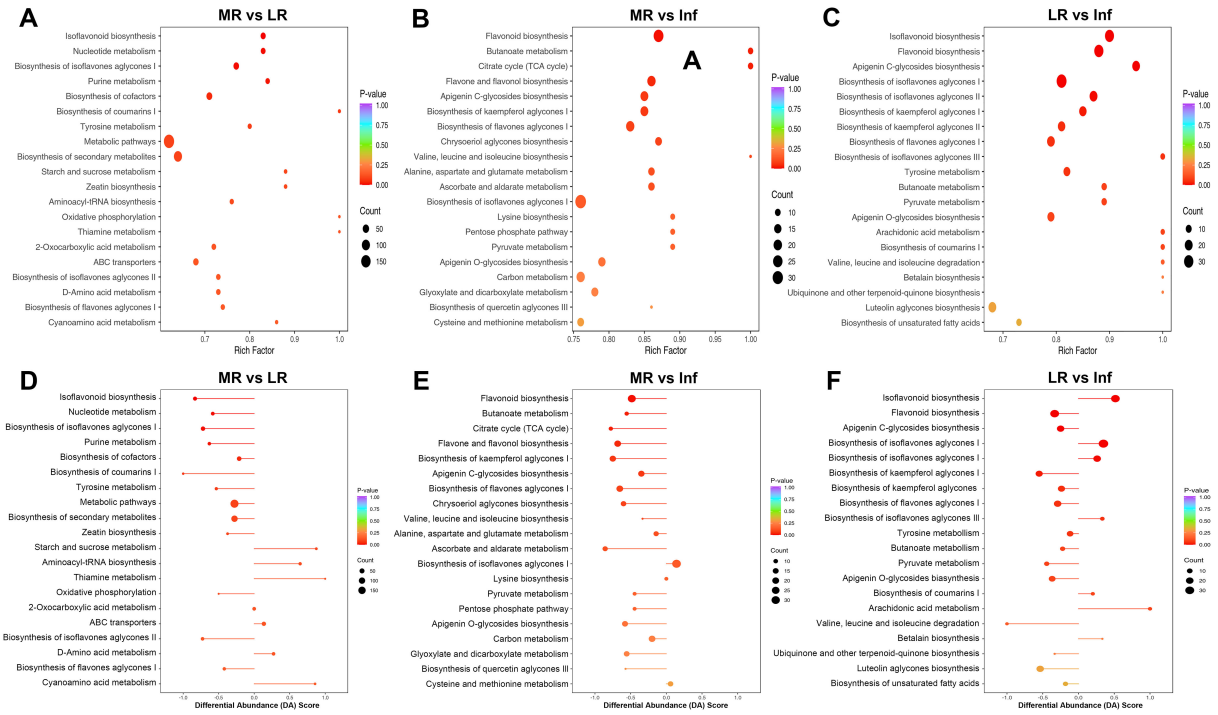

FIGURE 7
KEGG pathway enrichment analysis of differentially expressed metabolites (DEMs) of each pairwise comparison among MR, LR and Inf. KEGG annotations and enrichment of DEMs of MR vs. LR **(A)** MR vs. Inf **(B)** and LR vs. Inf **(C)**. Differential abundance (DA) score of DEMs of MR vs. LR **(D)** MR vs. Inf **(E)** and LR vs. Inf **(F)**. MR, LR, and Inf represent main-roots, lateral-roots, and inflorescence, respectively. The top 20 most significantly enriched pathways identified through KEGG enrichment analysis were presented.

several cases. Additionally, ten pathways, including starch and sucrose metabolism, flavonoid biosynthesis, isoflavonoid biosynthesis, galactose metabolism, pentose and glucuronate interconversions, biosynthesis of cofactors, ascorbate and aldarate metabolism, biosynthesis of kaempferol aglycones I, carbon fixation in photosynthetic organisms, and nucleotide metabolism, were significantly enriched in at least two comparisons (Supplementary Table S10; Supplementary Figure S37). Overall, the pathways mentioned above are likely responsible for the significant differences in chemical composition observed among the six tissues of *E. japonica*.

3.6.2 Overall changes in KEGG metabolic pathway

The DA score is a pivotal metric for metabolite changes within metabolic pathways, with values closer to 1 indicating more up-regulated DEMs and -1 indicating more down-regulated DEMs. The top 20 pathways, ranked by *p*-values, were detailed in Supplementary Table S10, yielding 300 records across 88 pathways from 15 comparisons (Supplementary Figure S37). Notably, the "biosynthesis of flavones aglycones I" and "biosynthesis of isoflavones aglycones I" pathways were most prominent, featuring in 12 of the 15 comparisons. Other notable pathways included "biosynthesis of isoflavones aglycones II," "biosynthesis of flavones aglycones II," "biosynthesis of flavones aglycones III," "isoflavonoid biosynthesis," and "flavonoid biosynthesis", which appeared in at least eight comparisons. This underscores the significant divergence in flavonoid and isoflavonoid biosynthesis across tissues. Up-regulated DEM distribution revealed that the expression of "flavonoid biosynthesis" pathway was most active in Inf, while "isoflavonoid biosynthesis" was most abundant in LR (Figure 8). In similar studies of *Astragalus membranaceus* and *Sophora flavescens*, flavonoids have also been confirmed as their main bioactive components, and these components are highly accumulated in the roots. The studies have also identified flavonoid and isoflavonoid biosynthesis as critical pathways, highlighting their conserved functions in medicinal legumes (Wu et al., 2020; Wei et al., 2021). Revealing flavonoid and isoflavonoid biosynthetic pathways and their regulation in medicinal legumes will provide a key theoretical basis for cultivating high-bioactivity plants in the future.

In the comparative analysis of each tissue against others, the top 20 pathways were selected, and DA scores for 100 pathways per tissue were statistically analyzed. Inf vs. MR/LR/Fr/S/L showed the most pathways (77) with DA scores above zero, indicating higher expression, followed by LR (52), Fr (46), L (42), S (34), and MR (21) (Figure 8C). These findings suggest that the expression of numerous pathways in Inf and LR was more abundant than in other tissues, whereas MR showed relatively fewer pathways expressed at higher levels compared to the other tissues.

In the MR vs. LR/Fr/Inf/S/L comparisons, only 6, 3, 2, 4, and 6 pathways exhibited DA scores greater than zero, respectively (Figures 7D, E; Supplementary Figures S39A–C). Additionally, only two pathways—"starch and sucrose metabolism" and

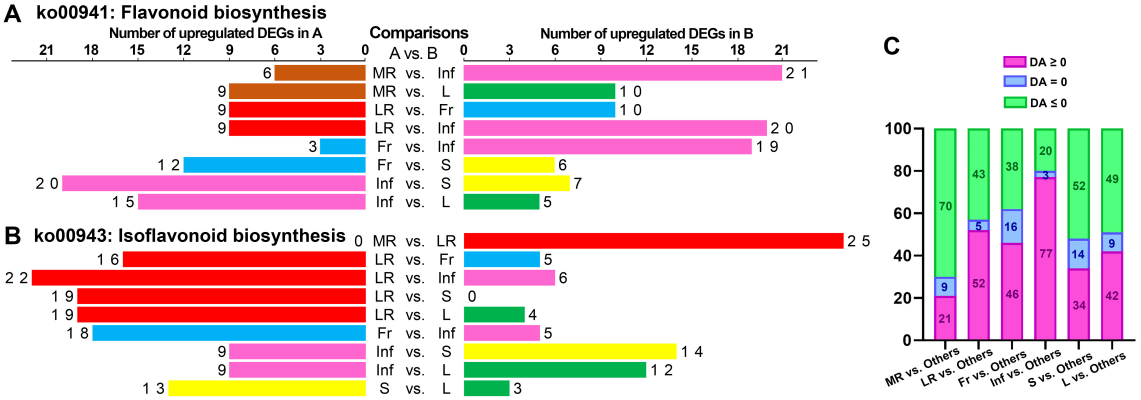

FIGURE 8
Statistical analysis of the number of up-regulated metabolites enriched in specific KEGG pathways in each tissue of each pairwise comparison. The number of up-regulated metabolites enriched in "flavonoid biosynthesis" (ko00941) **(A)** and "isoflavonoid biosynthesis" (ko00943) **(B)** in each tissue of each pairwise comparison. **(C)** Statistical analysis of differential abundance (DA) scores for the top 20 KEGG pathways in pairwise comparison between each tissue and five other tissues.

"galactose metabolism"—in the MR vs. L, were significantly enriched with DA scores above zero, indicating relatively high expression of these pathways in MR. In contrast, in the LR vs. MR/Fr/Inf/S/L comparisons, more pathways had DA scores greater than zero (Figures 7D, F; Supplementary Figures S39D–F). Besides those involved in isoflavonoid biosynthesis, metabolites related to "arachidonic acid metabolism," "biosynthesis of coumarins I," "biosynthesis of various alkaloids," "alpha-linolenic acid metabolism," and "benzoxazinoid biosynthesis" were also relatively abundant in LR. Inf vs. MR/LR/Fr/S/L comparisons highlighted a greater number of pathways with higher DA scores (Figures 7B, C; Supplementary Figures S39G, J, K), indicating that many pathways were expressed more abundantly in Inf than in other tissues. In addition to pathways associated with flavonoid biosynthesis, pathways with high expression in Inf also included "butanoate metabolism," "pyruvate metabolism," "apigenin O-glycosides biosynthesis," "apigenin C-glycosides biosynthesis," "alanine, aspartate and glutamate metabolism," and "biosynthesis of kaempferol aglycones I". In the comparisons of Fr vs. MR/LR/Inf/S/L, S vs. MR/LR/Fr/Inf/L, and L vs. MR/LR/Fr/Inf/L, the number of pathways with high DA scores varied (Supplementary Figure S39). The expression levels of several pathways in these tissues were also noteworthy. For example, the expression of "luteolin aglycones biosynthesis" in Fr was more abundant than in MR/LR/S, while "pentose and glucuronate interconversions" was expressed at higher levels in L compared to MR/LR/Inf/S. Conversely, the expression of "starch and sucrose metabolism" in L was significantly lower than in MR/Fr/Inf/S.

4 Conclusion

In this study, we conducted a UPLC-ESI-Q TRAP-MS/MS-based widely targeted metabolomics analysis to systematically identify metabolites across six tissues of *E. japonica* for the first time. Our findings provided firsthand comprehensive information on the composition and abundance of metabolites, revealing that flavonoids were the most abundant, followed by phenolic acids, amino acids and derivatives, lipids, and alkaloids. Distinct metabolite profiles were observed among the different tissues. Notably, LR and Inf exhibited higher concentrations for most metabolite categories compared to other tissues. L, S, and Fr also showed elevated levels in several metabolite categories, while the MR contained lower levels except for saccharides. This work also provided the information of the key and iconic health-promoting compounds in *E. japonica*, identifying 305 metabolites as key active ingredients and 364 metabolites as active pharmaceutical ingredients, of which 206 were co-annotated. Given the high concentration of these active pharmaceutical ingredients, *E. japonica* shows great promise in pharmaceutical applications. For instance, extracts rich in these metabolites could potentially be developed into drugs for treating chronic inflammatory diseases, considering the anti-inflammatory properties often associated with flavonoids and phenolic acids. Additionally, they might be used in the development of nutraceuticals to improve overall health and boost the immune system. Moreover, the comparative analysis of LR and MR indicates that the therapeutic efficacy of *E. japonica* roots, commonly utilized in folk medicine, is primarily attributed to the lateral roots rather than the main roots. These observations underscore the importance of prioritizing the application of lateral roots in future therapeutic strategies involving *E. japonica*. Overall, these findings highlight the strongest application potential of LR and Inf for disease treatment, particularly for addressing chronic and multifactorial diseases due to their high concentrations of bioactive compounds. The notable accumulation of therapeutic metabolites in *E. japonica* indicates its potential as a valuable resource for novel treatments, warranting further investigation into its pharmacological properties and applications in drug development.

Data availability statement

The original contributions presented in the study are included in the article/Supplementary Material. Further inquiries can be directed to the corresponding authors.

Author contributions

LX: Writing – original draft, Conceptualization, Formal Analysis, Methodology, Project administration, Supervision, Validation, Visualization. XL: Data curation, Formal Analysis, Funding acquisition, Investigation, Resources, Writing – review & editing. XP: Data curation, Resources, Writing – review & editing. SX: Formal Analysis, Writing – review & editing. QW: Formal Analysis, Writing – review & editing. CM: Formal Analysis, Writing – review & editing. ZL: Funding acquisition, Resources, Supervision, Writing – review & editing. YY: Project administration, Writing – review & editing.

Funding

The author(s) declare that financial support was received for the research and/or publication of this article. This work was supported by the project of Central Forestry Grassland Ecological Protection and Restoration Fund in 2024 (National Nature Reserve Subsidy) (TaiCaiJian (2024)81).

Conflict of interest

The authors declare that the research was conducted in the absence of any commercial or financial relationships that could be construed as a potential conflict of interest.

Generative AI statement

The author(s) declare that no Generative AI was used in the creation of this manuscript.

Publisher's note

Supplementary material

The Supplementary Material for this article can be found online at: https://www.frontiersin.org/articles/10.3389/fpls.2025.1537273/full#supplementary-material

References

Banik, K., Khatoon, E., Harsha, C., Rana, V., Parama, D., Thakur, K. K., et al. (2022). Wogonin and its analogs for the prevention and treatment of cancer: a systematic review. *Phytother. Res.* 36, 1854–1883. doi: 10.1002/ptr.v36.5

Campisi, J., Kapahi, P., Lithgow, G. J., Melov, S., Newman, J. C., and Verdin, E. (2019). From discoveries in ageing research to therapeutics for healthy ageing. *Nature* 571, 183–192. doi: 10.1038/s41586-019-1365-2

Cao, X., Shi, K., Xu, Y., Zhang, P., Zhang, H., and Pan, S. (2023). Integrated metabolomics and network pharmacology to reveal antioxidant mechanisms and potential pharmacological ingredients of citrus herbs. *Food Res. Int.* 174, 113514. doi: 10.1016/j.foodres.2023.113514

Chen, J., Wang, C., Huang, K., Chen, S., and Ma, Y. (2020). Acacetin suppresses IL-1β-induced expression of matrix metalloproteinases in chondrocytes and protects against osteoarthritis in a mouse model by inhibiting NF-κB signaling pathways. *BioMed. Res. Int.* 2020, 2328401. doi: 10.1155/2020/2328401

Chen, G., Xu, H., Xu, T., Ding, W., Zhang, G., Hua, Y., et al. (2022). Calycosin reduces myocardial fibrosis and improves cardiac function in post-myocardial infarction mice by suppressing TGFBR1 signaling pathways. *Phytomedicine* 104, 154277. doi: 10.1016/j.phymed.2022.154277

Choi, H.-J., Kaneko, S., Yokogawa, M., Song, G.-P., Kim, D.-S., Kang, S.-H., et al. (2013). Population and genetic status of a critically endangered species in Korea, *Euchresta japonica* (Leguminosae), and their implications for conservation. *J. Plant Biol.* 56, 251–257. doi: 10.1007/s12374-013-0106-6

Chung, J. Y.-F., Chan, M. K.-K., Tang, P. C.-T., Chan, A. S.-W., Chung, J. S.-Y., Meng, X.-M., et al. (2021). AANG: A natural compound formula for overcoming multidrug resistance via synergistic rebalancing the TGF-beta/Smad signalling in hepatocellular carcinoma. *J. Cell. Mol. Med.* 25, 9805–9813. doi: 10.1111/jcmm.v25.20

Devi, K. P., Malar, D. S., Nabavi, S. F., Sureda, A., Xiao, J., Nabavi, S. M., et al. (2015). Kaempferol and inflammantion: From chemistry to medicine. *Pharmacol. Res.* 99, 1–10. doi: 10.1016/j.phrs.2015.05.002

Ding, S., Wang, P., Pang, X., Zhang, L., Qian, L., Jia, X., et al. (2022). The new exploration of pure total flavonoids extracted from *Citrus maxima* (*Burm.*) *Merr.* as a new therapeutic agent to bring health benefits for people. *Frontier Nutr.* 9. doi: 10.3389/fnut.2022.958329

Dossou, S. S. K., Xu, F.-T., Dossa, K., Zhou, R., Zhao, Y.-Z., and Wang, L.-H. (2023). Antioxidant lignans sesamin and sesamolin in sesame (*Sesamum indicum* L.): A comprehensive review and future prospects. *J. Integr. Agric.* 22, 14–30. doi: 10.1016/j.jia.2022.08.097

Ganesan, K., and Xu, B. (2017). Molecular targets of vitexin and isovitexin in cancer therapy: a critical review. *Ann. New York Acad. Sci.* 1401, 102–113. doi: 10.1111/nyas.2017.1401.issue-1

Geng, J., Wang, Y., Lv, F., Yu, X., Gong, M., Zhang, J., et al. (2024). Coumestrol facilitates apoptosis in colorectal cancer cells by interacting with ZIP8 protein via the ferroptosis pathway. *J. Cancer* 15, 4656–4667. doi: 10.7150/jca.94628

Ghanbari-Movahed, M., Shafiee, S., Burcher, J. T., Lagoa, R., Farzaei, M. H., and Bishayee, A. (2023). Anticancer potential of apigenin and isovitexin with focus on oncogenic metabolism in cancer stem cells. *Metabolites* 13, 404. doi: 10.3390/metabo13030404

Guo, X., Chen, X., Cheng, W., Yang, K., Ma, Y., and Bi, K. (2008). RP-LC determination and pharmacokinetic study of ferulic acid and isoferulic acid in rat plasma after taking traditional chinese medicinal-preparation: guanxinning lyophilizer. *Chromatographia* 67, 1007–1011. doi: 10.1365/s10337-008-0614-6

Hsu, S.-C., Kuo, C.-L., Lin, J.-P., Lee, J.-H., Lin, C.-C., Su, C.-C., et al. (2007). Crude extracts of *Euchresta formosana* radix inhibit invasion and migration of human hepatocellular carcinoma cells. *Anticancer Res.* 27, 2377–2384.

Hu, Y., Li, W., Cheng, X., Yang, H., She, Z.-G., Cai, J., et al. (2024). Emerging roles and therapeutic applications of arachidonic acid pathways in cardiometabolic diseases. *Circ. Res.* 135, 222–260. doi: 10.1161/CIRCRESAHA.124.324383

Huynh, D. L., Ngau, T. H., Nguyen, N. H., Tran, G.-B., and Nguyen, C. T. (2020). Potential therapeutic and pharmacological effects of Wogonin: an updated review. *Mol. Biol. Rep.* 47, 9779–9789. doi: 10.1007/s11033-020-05972-9

Huynh, D. L., Sharma, N., Singh, A. K., Sodhi, S. S., Zhang, J.-J., Mongre, R. K., et al. (2017). Anti-tumor activity of wogonin, an extract from *Scutellaria baicalensis* through regulating different signaling pathways. *Chin. J. Natural Medicines* 15, 15–40. doi: 10.1016/S1875-5364(17)30005-5

Jiang, N., Li, H., Sun, Y., Zeng, J., Yang, F., Kantawong, F., et al. (2021). Network pharmacology and pharmacological evaluation reveals the mechanism of the

sanguisorba officinalis in suppressing hepatocellular carcinoma. *Front. Pharmacol.* 12. doi: 10.3389/fphar.2021.618522

Kahkeshani, N., Farzaei, F., Fotouhi, M., Alavi, S. S., Bahramsoltani, R., Naseri, R., et al. (2019). Pharmacological effects of gallic acid in health and diseases: A mechanistic review. *Iranian J. Basic Med. Sci.* 22, 225–237. doi: 10.22038/ijbms.2019.32806.7897

Kang, C., Lv, C., Yang, J., Kang, L., Ma, W., Zhang, W., et al. (2020). A practical protocol for a comprehensive evaluation of sulfur fumigation of trichosanthis radix based on both non-targeted and widely targeted metabolomics. *Frontier Plant Sci.* 11. doi: 10.3389/fpls.2020.578086

Kim, J.-H., Kim, D., Kim, J., and Hwang, J.-K. (2011). *Euchresta horsfieldii* Benn. activates peroxisome proliferator-activated receptor α and regulates expression of genes involved in fatty acid metabolism in human HepG2 cells. *J. Ethnopharmacol* 133, 244–247. doi: 10.1016/j.jep.2010.09.029

Kim, H. R., Park, C. G., and Jung, J. Y. (2014). Acacetin (5,7-dihydroxy-4'-methoxyflavone) exhibits *in vitro* and *in vivo* anticancer activity through the suppression of NF-κB/Akt signaling in prostate cancer cells. *Int. J. Mol. Med.* 33, 317–324. doi: 10.3892/ijmm.2013.1571

Li, H., Lv, Q., Liu, A., Wang, J., Sun, X., Deng, J., et al. (2022). Comparative metabolomics study of Tartary (*Fagopyrum tataricum* (L.) Gaertn) and common (*Fagopyrum esculentum* Moench) buckwheat seeds. *Food Chem.* 371, 131125. doi: 10.1016/j.foodchem.2021.131125

Li, W., Wang, H., and Dong, A. (2019). Preparative separation of alkaloids from stem of euchresta tubulosa dunn. by high-speed counter-current chromatography using stepwise elution. *Molecules* 24, 4602. doi: 10.3390/molecules24244602

Li, W.-X., Wang, H., and Dong, A.-W. (2019). Systematic separation and purification of alkaloids from euchresta tubulosa dunn. by various chromatographic methods. *Processes* 7, 924. doi: 10.3390/pr7120924

Li, Z., Wang, Y., Xu, M., Liu, H., Li, L., and Xu, D. (2023). Molecular mechanism overview of metabolite biosynthesis in medicinal plants. *Plant Physiol. Biochem.* 204, 108125. doi: 10.1016/j.plaphy.2023.108125

Li, C. H., Yuan, P. D., and Liu, Y. (2014). Research progress on chemical constituents in plants of *Euchresta J.* Benn and their biological activities. *Chin. Traditional Herbal Drugs* 45, 3486–3493. doi: 10.7501/j.issn.0253-2670.2014.23.024

Liu, I.-M., Chen, W.-C., and Cheng, J.-T. (2003). Mediation of beta-endorphin by isoferulic acid to lower plasma glucose in streptozotocin-induced diabetic rats. *J. Pharmacol. Exp. Ther.* 307, 1196–1204. doi: 10.1124/jpet.103.053900

Lo, W.-L., Wu, C.-C., Chang, F.-R., Wang, W.-Y., Khalil, A. T., Lee, K.-H., et al. (2003). Antiplatelet and anti-HIV constituents from *Euchresta formosana*. *Natural Prod. Res.* 17, 91–97. doi: 10.1080/1478641031000103669

Luo, P., An, Y., He, J., Xing, X., Zhang, Q., Liu, X., et al. (2024). Icaritin with autophagy/mitophagy inhibitors synergistically enhances anticancer efficacy and apoptotic effects through PINK1/Parkin-mediated mitophagy in hepatocellular carcinoma. *Cancer Lett.* 587, 216621. doi: 10.1016/j.canlet.2024.216621

Lv, H., Qi, Z., Wang, S., Feng, H., Deng, X., and Ci, X. (2017). Asiatic acid exhibits anti-inflammatory and antioxidant activities against lipopolysaccharide adn d-galactosamine-induced fulminant hepatic failure. *Front. Immunol.* 8, 785. doi: 10.3389/fimmu.2017.00785

Ma, C., Wu, H., Yang, G., Xiang, J., Feng, K., Zhang, J., et al. (2022). Calycosin ameliorates atherosclerosis by enhancing autophagy via regulating the interaction between KLF2 and MLKL in apolipoprotein E gene-deleted mice. *Br. J. Pharmacol.* 179, 252–269. doi: 10.1111/bph.15720

Miao, L., Zhang, X., Zhang, H., Cheong, M. S., Chen, X., Farag, M. A., et al. (2024). Baicalin ameliorates insulin resistance and regulates hepatic glucose metabolism via activating insulin signaling pathway in obese pre-diabetic mice. *Phytomedicine* 124, 155296. doi: 10.1016/j.phymed.2023.155296

Mizuno, M., Matsuura, N., Iinuma, M., and Tanaka, T. (1992). Coumaronochromones in the roots of *Euchresta japonica*. *Phytochemistry* 31, 643–645. doi: 10.1016/0031-9422(92)90052-R

Mizuno, M., Tamura, K.-I., and Tanaka, T. (1988a). A novel coumaronochromone from the stems of euchresta japonica and its antibacterial activity. *Heterocycles* 27, 2047–2050. doi: 10.3987/COM-88-4552

Mizuno, M., Tamura, K.-I., Tanaka, T., and Iinuma, M. (1988b). Three prenylflavanones from *Euchresta japonica*. *Phytochemistry* 27, 1831–1834. doi: 10.1016/0031-9422(88)80454-0

Mizuno, M., Tamura, K.-I., Tanaka, T., and Iinuma, M. (1989). Chemotaxonomy of the genus *euchresta*. III. Three new flavonoids in the roots of *euchresta japonica*. *Chem. Pharm. Bull.* 37, 195–196. doi: 10.1248/cpb.37.195

Musial, C., Kuban-Jankowska, A., and Gorska-Ponikowska, M. (2020). Beneficial properties of green tea catechins. *Int. J. Mol. Sci.* 21, 1744. doi: 10.3390/ijms21051744

Ohmiya, S., Otomasu, H., Haginiwa, J., and Murakoshi, I. (1978). (+)-5,17-dehydromatrine *N*-oxide, a new alkaloid in *Euchresta japonica*. *Phytochemistry* 17, 2021–2022. doi: 10.1016/S0031-9422(00)88755-5

Ohmiya, S., Otomasu, H., Haginiwa, J. J., and Murakoshi, I. (1980). The alkaloid constituents of *Euchresta japonica* and the stereochemical assignment of two isomeric sophoridine *N*-oxides. *Chem. Pharm. Bull.* 28, 546–551. doi: 10.1248/cpb.28.546

Parlar, A., Arslan, S. O., and Çamb, S. A. (2020). Glabridin alleviates inflammation and nociception in rodents by activating BK_{Ca} channels and reducing NO levels. *Biol. Pharm. Bull.* 43, 884–897. doi: 10.1248/bpb.b20-00038

Qian, L., Xu, H., Yuan, R., Yun, W., and Ma, Y. (2024). Formononetin ameliorates isoproterenol induced cardiac fibrosis through improving mitochondrial dysfunction. *Biomed. Pharmacother.* 170, 116000. doi: 10.1016/j.biopha.2023.116000

Qu, Y., Yang, X., Li, J., Zhang, S., Li, S., Wang, M., et al. (2021). Network pharmacology and molecular docking study of zhishi-baizhu herb pair in the treatment of gastric cancer. *Evidence-Based Complementary Altern. Med.* 2021, 2311486. doi: 10.1155/2021/2311486

Razzaq, A., Sadia, B., Raza, A., Khalid Hameed, M., and Saleem, F. (2019). Metabolomics: A way forward for crop improvement. *Metabolites* 9, 303. doi: 10.3390/metabo9120303

Reyes-Hernández, O. D., Figueroa-González, G., Quintas-Granados, L. I., Hernández-Parra, H., Peña-Corona, S. I., Cortés, H., et al. (2024). New insights into the anticancer therapeutic potential of icaritin and its synthetic derivatives. *Drug Dev. Res.* 85, e22175. doi: 10.1002/ddr.22175

Schwenzer, H., de Zan, E. D., Elshani, M., van Stiphout, R., Kudsy, M., Morris, J., et al. (2021). The novel nucleoside analogue proTide NUC-7738 overcomes cancer resistance mechanisms *in vitro* and in a first-in-human phase I clinical trial. *Clin. Cancer Res.* 27, 6500–6513. doi: 10.1158/1078-0432.CCR-21-1652

Shirataki, Y., Manaka, A., Yokoe, I., and Komatsu, M. (1980). Two prenylflavanones from *Euchresta japonica*. *Phytochemistry* 21, 2959–2963. doi: 10.1016/0031-9422(80)85077-1

Thévenot, E. A., Roux, A., Xu, Y., Ezan, E., and Junot, C. (2015). Analysis of the human adult urinary metabolome variations with age, body mass index, and gender by implementing a comprehensive workflow for univariate and OPLS statistical analyses. *J. Proteome Res.* 14, 3322–3335. doi: 10.1021/acs.jproteome.5b00354

Toda, S., and Shirataki, Y. (2006). Inhibitory Effect of Prenylated Flavonoid in *Euchresta japonica.* and *Artocarpus heterophyllus* on Lipid Peroxidation by Interaction of Hemoglobin and Hydrogen Peroxide. *Pharm. Biol.* 44, 261–263. doi: 10.1080/13880200600714095

Topal, F., Nar, M., Gocer, H., Kalin, P., Kocyigit, U. M., Gülçin, İ., et al. (2016). Antioxidant activity of taxifolin: an activity-structure relationship. *J. Enzyme Inhibition Medicinal Chem.* 31, 674–683. doi: 10.3109/14756366.2015.1057723

Wang, S., Li, Y., Lin, X., Fu, X., Zhong, H., Ren, K., et al. (2024). Rapid screening of phenolic compounds with anti-enteritis activity from *camellia oleifera* oil using a smurf drosophila model and molecular docking methods. *Molecules* 29, 76. doi: 10.3390/molecules29010076

Wang, Y., Wang, A., Alkhalidy, H., Luo, J., Moomaw, E., Neilson, A. P., et al. (2020). Flavone hispidulin stimulates glucagon-like peptide-1 secretion and ameliorates hyperglycemia in streptozotocin-induced diabetic mice. *Mol. Nutr. Food Res.* 64, e1900978. doi: 10.1002/mnfr.201900978

Wang, D., Zhang, L., Huang, X., Wang, X., Yang, R., Mao, J., et al. (2018). Identification of nutritional components in black sesame determined by widely targeted metabolomics and traditional chinese medicines. *Molecules* 23, 1180. doi: 10.3390/molecules23051180

Wei, G., Chen, Y., Guo, X., Wei, J., Dong, L., and Chen, S. (2021). Biosyntheses characterization of alkaloids and flavonoids in *Sophora flavescens* by combining metabolome and transcriptome. *Sci. Rep.* 11, 7388. doi: 10.1038/s41598-021-86970-0

Wu, X., Li, X., Wang, W., Shan, Y., Wang, C., Zhu, M., et al. (2020). Integrated metabolomics and transcriptomics study of traditional herb *Astragalus membranaceus Bge.* var. *mongolicus (Bge.) Hsiao* reveals global metabolic profile and novel phytochemical ingredients. *BMC Genomics* 21, 697. doi: 10.1186/s12864-020-07005-y

Xia, T., Xiong, Z., Sun, X., Chen, J., Wang, C., Chen, Y., et al. (2023). Metabolomic profiles and health-promoting functions of *Camellia drupifera* mature-seeds were revealed relate to their geographical origins using comparative metabolomic analysis and network pharmacology approach. *Food Chem.* 426, 136619. doi: 10.1016/j.foodchem.2023.136619

Xiao, Q., Mu, X., Liu, J., Li, B., Liu, H., Zhang, B., et al. (2022). Plant metabolomics: a new strategy and tool for quality evaluation of Chinese medicinal materials. *Chin. Med.* 17, 45. doi: 10.1186/s13020-022-00601-y

Yang, Z., Feng, L., Wang, M., Li, Y., Bai, S., Lu, X., et al. (2022). Sesamin promotes osteoporotic fracture healing by activating chondrogenesis and angiogenesis pathways. *Nutrients* 14, 2106. doi: 10.3390/nu14102106

Yang, S.-H., Liao, P.-H., Pan, Y.-F., Chen, S.-L., Chou, S.-S., and Chou, M.-Y. (2013). The novel p53-dependent metastatic and apoptotic pathway induced by vitexin in human oral cancer OC_2 cells. *Phytother. Res.* 27, 1154–1161. doi: 10.1002/ptr.v27.8

Yoon, S. Y., Park, S. J., and Park, Y. J. (2018). The anticancer properties of cordycepin and their underlying mechanisms. *Int. J. Mol. Sci.* 19, 3027. doi: 10.3390/ijms19103027

Zhang, T., Liu, M., Liu, Q., and Xiao, G. G. (2022). Wogonin increases gemcitabine sensitivity in pancreatic cancer by inhibiting Akt pathway. *Front. Pharmacol.* 13. doi: 10.3389/fphar.2022.1068855

Zhong, X., Huang, R., Chen, X., and Lei, Y. (2023). A review on the pharmacological aspects of engeletin as natural compound. *Drug Design Dev. Ther.* 17, 3833–3843. doi: 10.2147/DDDT.S437703

Zhou, W., Fu, Y., and Xu, J.-S. (2022). Sophocarpine alleviates isoproterenol-induced kidney injury by suppressing inflammation, apoptosis, oxidative stress and fibrosis. *Molecules* 27, 7868. doi: 10.3390/molecules27227868

Zou, S., Wu, J., Shahid, M. Q., He, Y., Lin, S., Liu, Z., et al. (2020). Identification of key taste components in loquat using widely targeted metabolomics. *Food Chem.* 323, 126822. doi: 10.1016/j.foodchem.2020.126822

frontiers | Frontiers in Plant Science

TYPE Original Research
PUBLISHED 30 May 2025
DOI 10.3389/fpls.2025.1488697

OPEN ACCESS

EDITED BY
Eman. A. Mahmoud,
Damietta University, Egypt

REVIEWED BY
Amardeep Singh Virdi,
Amity University Punjab, India
Pradeep Kumar Rai,
University of Agricultural Sciences and Technology, India

*CORRESPONDENCE
Ranjeet R. Kumar,
ranjeetranjaniari@gmail.com,
prashanthbabuh@gmail.com

RECEIVED 30 August 2024
ACCEPTED 16 April 2025
PUBLISHED 30 May 2025

CITATION
Kumar RR, Babu H P, Hasija S, Gampa M, Goswami S, T. V, Kumar S, Mishra GP, Mishra D, Rai GK, Jha GK, Kumar SN, Praveen S, Tyagi A and C. V (2025) Thiol-based redox sensing regulates the yellow pigment and antioxidant accumulation and improves the nutritional quality of wheat grains (*Triticum aestivum* L.). *Front. Plant Sci.* 16:1488697. doi: 10.3389/fpls.2025.1488697

Thiol-based redox sensing regulates the yellow pigment and antioxidant accumulation and improves the nutritional quality of wheat grains (*Triticum aestivum* L.)

Ranjeet R. Kumar[1]*, Prashant Babu H[2], Sumedha Hasija[1], Mallesh Gampa[1], Suneha Goswami[1], Vinutha T.[1], Sudhir Kumar[3], Gyan P. Mishra[4], Dwijesh Mishra[5], Gyanendra K. Rai[6], Girish K. Jha[7], Soora Naresh Kumar[7], Shelly Praveen[1], Aruna Tyagi[1] and Viswanathan C.[3]

[1]Division of Biochemistry, Indian Council of Agricultural Research (ICAR)-Indian Agricultural Research Institute, New Delhi, India, [2]Division of Genetics, Indian Council of Agricultural Research (ICAR)-Indian Agricultural Research Institute, New Delhi, India, [3]Division of Plant Physiology, Indian Council of Agricultural Research (ICAR)-Indian Agricultural Research Institute, New Delhi, India, [4]Division of Seed Technology, Indian Council of Agricultural Research (ICAR)-Indian Agricultural Research Institute, New Delhi, India, [5]CABin, ICAR-Indian Agricultural Statistics Research Institute, New Delhi, India, [6]Sher-e-Kashmir University of Agricultural Sciences and Technology, Jammu, India, [7]Centre for Environment Science and Climate Resilient Agriculture (CESCRA), Indian Agricultural Research Institute, New Delhi, India

Thiol-based redox sensing has been found to play diverse roles in regulating various metabolic pathways. Here, the thiol-based redox system of 16 diverse genotypes of wheat grains was characterized, and it correlated with the accumulation of macro-/micronutrients inside the grains. We observed significant variations in the thiol and disulfide content in the grains. An expression analysis of the genes responsible for thiol-based redox sensing, such as thioredoxin (*TRX*), glutaredoxin (*GRX*) and glutathione reductase (*GR*), showed maximum fold expression in wheat *cvs*. Halna and HD2985 (high thiol *cvs*.) during the seed hardening stage (G_2) of endosperm, as compared to low thiol-containing *cvs*. We retrieved the amino acid sequences of 11 genes linked with nutrient biosynthesis pathways and observed the highest cysteine (Cys) (2.25%) in Granule bound starch synthase (*GBSS;* involved in starch biosynthesis) and methionine (Met) (4.04%) in the *BCH* gene (involved in tannin synthesis). Genotypes with a Cys : Met ratio >1.0 were observed to be nutrient-rich and robust due to the high stability of key proteins and enzymes. The yellow pigment (shining factor) was observed to be the highest in the grains of wheat cv. NIAW34 (6.08 µg/g dry matter) with a Cys: Met ratio of 2.15. Antioxidants such as total phenolic content and tannin were observed to be significantly higher in *cvs*. (Halna, HI1544, etc.) with a ratio of Cys: Met ≥2.0. The highest level of polysaccharides (starch and resistant starch) was observed in the grains of wheat cv. HD1914 with a Cys : Met ratio of 4.0. The results of Pearson's correlation indicated a negative relationship between thiol content and nutrient-linked traits such as total protein, gluten, and phytic acid.

Micronutrients such as iron and zinc showed a weak positive correlation with thiol content. The role of thiol-based redox sensors needs to be further explored and utilized for manipulating the tolerance level and nutrient compositions of wheat grains. This will help in developing "nutrient-smart grain" and "climate-smart" crops with improved downstream processing and dough engineering.

KEYWORDS

thiol, redox sensor, grain quality, Trx, GRX, glutathione peroxidase, yellow pigment

Introduction

Cereals are the predominant grain crops, providing a major share of carbohydrates and calories in the diet. They have an adequate amount of nutrients required for the body, though they are poor in some of the important amino acids and micronutrients (Ciudad-Mulero et al., 2021). The bioavailability of most of the nutrients has been observed to be compromised in different cereals. Wheat is a staple grain crop utilized in a large part of the world as chapatti, bread, and many other formulations. Wheat grains are rich in carbohydrates, especially polysaccharides such as starch, and also contain protein, lipids, and other nutrients (Kumar et al., 2019). The protein content of the grains varies between 7%–22% (Wieser et al., 2023). The critical phases of grain filling, mainly the grain ripening and seed desiccation stages, decide the yield and quality of the wheat grains in terms of nutrient compositions (Zhang et al., 2021). Adverse environmental conditions during the grain-filling stage in wheat have a severe effect on the physical and chemical quality of the grains (Fernie et al., 2022). The nutrient composition of wheat flour has been reported to have wide diversity across the genotypes. The effect of agro-geo-climate conditions, fertilizers, heat, drought, salinity, and other biotic/abiotic stresses on the proximate composition of wheat is well elucidated. The regulation underlying the variations in the proximate composition has been observed to be related to different biochemical metabolites synthesizing and accumulating inside the grains (Kumar et al., 2019; Grace and Henry, 2020). The metabolic pathway-associated enzymes have been reported to show significant variation in activity with changes in the accumulation of different metabolites (Cañas et al., 2017).

Cells have an inherent potential to sense their environment and adapt themselves accordingly by regulating the networks of genes and proteins. Proteins have evolved with time and show remarkable features in sensing the environment and regulating the expression of genes and the activity of enzymes. The binding of cofactors provides more specificity to the proteins in sensing the cytoplasmic/environmental changes.

Starch is one of the predominant polysaccharides present in most cereals and millets (Kumar et al., 2019). It consists of amylose and amylopectin and determines the yield and quality of the grains. Currently, lifestyle diseases such as diabetes are more prevalent and have been reported to be due to diets rich in carbohydrates (Kumar and Pathak, 2014). Starch has different fractions present in the flour, and a few of them have been recommended for patients with diabetes (Bajka et al., 2021). Resistant starch (RS) is a fraction that is a slow-digestible starch, which takes time to be digested and releases glucose slowly into the blood upon feeding. There are different types of RS, and each has a different mode of synthesis. For example, RS1 is physically not accessible to the amylase enzyme and is present in = coarse grains; RS2 is granular starch extracted from raw potatos, bananas, etc.; RS3 is synthesized though heating and cooling of starch; RS4 is chemically modified starch; and RS5 is a amylose–lipid complex (Harris, 2019). Researchers have reported wide variations in the resistant starch content of different agriculturally important crops such as wheat, maize, rice, and millet (Zheng et al., 2020). Wheat has ~0.75% to 1.0% RS in the grains (Kumar et al., 2019). The mechanism underlying the variation in the proportion of RS is mostly enzymatically based and has not been much characterized. A high RS content in flour has been considered one of the desirable traits for good quality grains and flours. RS has been observed to enhance the texture, integrity, and quality of flour (Khan et al., 2020).

Antioxidants are considered one of the most important traits deciding the quality of the wheat grains. They have many health benefits, such as boosting the immune system, protecting from various pathogenic and auto-regulatory diseases (Ranjbar et al., 2019). They scavenge the free radicals present inside the cells and balance the redox system of the cells. The accumulation of antioxidants such as tannin, vitamin E, and total phenolic compounds is considered a desirable trait for good quality grain and flour (Goswami et al., 2020). Wheat *cvs.* have shown wide diversity in their antioxidant content (Yadav et al., 2021). Wheat grains have very significant amounts of phenolic and flavonoids with very high bioavailability, as compared to other nutrients (Ma et al., 2021). An increase in the accumulation of antioxidants above the optimum level causes bitterness and leads to compromised quality and taste (Bruno et al., 2019). Antioxidants in the wheat grains are good from a health point of view. Other than the health benefits, antioxidants have been reported to be used as food preservatives and play a very important role in enhancing the quality and shelf-life of the flour (Chen et al., 2021). Anti-nutritional factors, such as phytate in flour, have been reported to reduce the bioavailability of micronutrients such as iron and zinc, and are considered a nutrient

that reduces the quality of flour (Alkarawi et al., 2018). The activity of phytases has been reported to be reduced in wheat and is one of the reasons behind the significant accumulation of phytate in grains (Madsen and Brinch-Pedersen, 2020). Phytase activity was observed to be more stable in a ground sample of wheat than in whole grains (Schollenberger et al., 2022). The regulation underlying the phytase activity and accumulation of phytate is not well understood.

Protein thiols are present in the cytosol in their reduced state. In most cells, the cytoplasm is a reducing environment, and protein thiols are maintained in their reduced state. Thiol redox buffers maintain the reduced state of thiol in cells (Meyer and Hell, 2005). Reactive oxygen species (ROS) are highly reactive molecules containing oxygen, such as superoxide, hydrogen peroxide, and hydroxyl radicals. They are produced as byproducts of normal cellular metabolism, and also arise from different biotic and abiotic stresses. ROS are involved in damaging cellular components such as lipids, proteins, and DNA, leading to oxidative stress, which has an adverse effect on the growth and development of plants. ROS and other free radicals damage the cellular compartment, organelles, enzymes, nucleic acids, and proteins inside cells. In order to neutralize these free radicals, different defense mechanisms become active inside the cells and are triggered by redox-sensitive transcription factors and cysteine residues present in the respective proteins. Cysteine (Cys) thiol groups have been reported to have a acid dissociation constant (pKa) of 8, which causes more reactive thiolate (RS–) and anion formation at physiological pH. The modification of thiol causes up- or downregulation of TFs, which ultimately regulates the expression of different genes and proteins involved in various metabolic pathways (Li et al., 2023). Thiol has been reported to indirectly regulate the expression at the transcript and protein level, as evident from the changes in the cellular response and metabolites.

Active thiols are oxidized by ROS, especially H_2O_2, which is produced in response to different environmental and cellular conditions. Thiol has intrinsic pKa values of 8.4–8.6. The catalytic Cys groups in thiol have lower pKa values of 5.5–7.4, which in turn act as a H_2O_2-sensing center and react with H_2O_2 under physiological conditions (Chae et al., 2023). The thiol group undergoes oxidation at the H_2O_2 level and forms an inter or intramolecular disulfide bond (–S–S–), sulfenic acid (–SOH), sulfinic acid (–SO_2H), and sulfonic acid (–SO_3H), which alters the structure, activity, and interactions of different proteins and enzymes and ultimately changes their localization and regulates the metabolism and physiology of plants. Similarly, thiol peroxidases such as thioredoxin peroxidases (TPXs) and glutathione peroxidases (GPXs) are also oxidized by H_2O_2, especially the cys residue, and are oxidized into different forms and transfer their redox signal to target genes and proteins (Paulsen and Carroll, 2013). Thioredoxin (Trx) and glutaredoxin (Grx) proteins depend upon thiol peroxidase for their oxidizing potential and receive electrons from NADPH/GSH with the help of thiol reductases (Meyer and Hell, 2005). Trx/Grx proteins can act as redox sensors in both oxidized and reduced forms in response to different cellular and environmental conditions (Paulsen and Carroll, 2013).

Various enzymes have been reported to interplay in the spatiotemporal mode in carbon assimilatory processes, especially photosynthesis and starch biosynthesis. The developing endosperm has also been reported to have a diverse network of enzymes working in tandem to synthesize starch to be packed inside the endospermic tissues. The accumulation of macro- and micronutrients is influenced by the activities of pathway-associated enzymes, other than environmental factors, and is one of the decisive factors in the nutritional composition of grains (Zhang et al., 2021). Storage protein in seeds basically acts as a reservoir of nitrogen, carbon, and sulfur. The main objective of the plant when storing the SSPs is to use them during germination or in adverse conditions. Wide diversity has been reported in the nature and composition of SSPs in the grains of different plant species (Antonets et al., 2020).

Here, we have studied the effect of the regulation of thiol on the accumulation of macro- and micronutrients inside the grains of diverse genotypes of wheat. We have established a correlation between thiol and the proximate composition in the grains. The findings can be used to evaluate diverse genotypes of wheat for grain quality and for the development of nutrient-dense grains.

Materials and methods

Samples and growing conditions

We have used 16 diverse genotypes of wheat selected from the core set developed for improved grain quality at the ICAR-Indian Agricultural Research Institute (ICARI), New Delhi. The list of wheat genotypes used in the present investigation has been presented in the Supplementary Material (Supplementary Table S1). The pre-treated seeds were sown in pots (22.5 cm diameter) at the Nanaji Deshmukh Plant Phenomics Centre, Pusa, ICAR-IARI, New Delhi, and recommended intercultural operations were followed along with the timely application of fertilizers and irrigations. The pots were kept in a regulated glasshouse at a temperature of 22 ± 3°C (daytime) and 18 ± 3°C (nighttime) during the vegetative stage, and at 28 ± 3°C (daytime) and 32 ± 3°C (nighttime) during the pollination and grain-filling stages. Other parameters, such as light and RH, were maintained, as mentioned in our previous publication (Kumar et al., 2022). Only healthy plants were tagged and further used for sample collection at a specific stage based on the Feekes scale. Samples were collected in three biological replicates from the tagged plants and were packed in an airtight container and stored at -20°C for further downstream analysis.

Determination of free thiol content

The freshly harvested grains from different genotypes of wheat were further subjected to fine grinding using a mechanized mini-grinder machine (Kolar Mill Stores Pvt. Ltd. Karnataka, India), keeping the temperature constant in order to protect them from the

adverse effects of milling temperature on biochemical constituents. We used Ellman's test to estimate the free thiols in the ground sample (Ellman, 1959). In brief, 10 µL of powder extract (prepared by passing the slurry prepared in green solvent through a chromatographic column) was placed in a test tube along with 50 µL of Ellman's reagent [50 mM of sodium acetate (NaoAc), 2 mM of 5'5-Dithio-bis-(2-nitobenzoic acid) in water, and 1M of Tris solution (pH 8.0)], 100 µL of Tris solution, and 840 µL of distilled water. The absorbance of the solution was taken at 412 nm using a UV-Vis spectrophotometer. The thiol content was calculated using the following equations:

$$Abs_{sample} = (Total\ volume/Sample\ volume) \times (Abs_{412})$$

$$Free\ Thiol\ (mM) = Abs_{sample}/13600$$

The thiol content was expressed as µmol/g of the sample.

Expression analysis of thiol-reducing genes

The total RNA was extracted from the developing seeds (high thiol content - Halna, HD2985; Low thiol content - NIAW34, PBW443) collected during the button (G_0), milky-ripe (G_1), and seed hardening (G_2) stages using a RaFlex Total RNA Isolation Kit (GeNei, USA). The quality of the isolated total RNA was checked using a BioAnalyzer (Agilent, USA), and an OD 260 to 280 ratio of > than 1.9 was used for the expression analysis. We have selected the thiol-reducing genes [Thioredoxin (*TRX*, acc. no. AF438359.1), Glutaredoxin (*GRX*, acc. no. AF542185.1), and Glutathione reductase (*GR*, acc. no. XM_044564013)] for the oligo design using the Genefisher2 Primer design software (https://bibiserv.cebitec.uni-bielefeld.de/genefisher2/) and it was synthesized commercially (Table 1). cDNA was synthesized using the Revert^{Aid} H Minus First Strand cDNA Synthesis Kit (Thermo Fisher Scientific) following the protocol, as given by the manufacturer. The expression analysis was performed using the Bio-Rad CFX96 platform, and the steps were followed as mentioned in our previous publication (Kumar et al., 2022). We used the β-actin gene (acc. no. JQ004803.1) as the endogenous control gene for normalizing the C_t value. The relative fold expression ($2^{\wedge -ddCt}$ value) was calculated using the Pfaffl method (Pfaffl et al., 2002).

TABLE 1 List of primers used for the expression analysis of genes linked with thiol-based redox sensing in wheat.

Oligo's ID	Primer sequence (5'-3')	Tm (°C)
TRX-F	5'-GGCAAGGATCGTAGCATTGT-3'	58.3
TRX-R	5'-CGGCATAAACAGGTGCAATG-3'	58.0
GRX-F	5'-ATTGCACTGAACAAGGGAGG-3'	58.0
GRX-R	5'-GCCAAACACATCCAACTTCG-3'	57.9
GR-F	5'-GAAGATGCTCAAGGACAGGG-3'	57.9
GR-R	5'-CAATCCGAGCTGATAGGGTG-3'	57.8
Act-F	5'-CCTGGTATACACGAAGCGAC-3'	58.1
Act-R	5'-GGAAAGTGCTAAGAGAGGCC-3'	57.9

*TRX, thioredoxin gene; GRX, glutaredoxin gene; GR, glutathione reductase gene; Act, actin gene.

Cysteine and methionine estimation in regulatory genes associated with different metabolic pathways

In order to know the abundance of cysteine and methionine (Met) amino acids residues in regulatory genes linked with different metabolic pathways associated with the biosynthesis of yellow pigment and other proximate composition (macro- and micronutrients), we retrieved the amino acid sequences of the following genes from NCBI that are involved in different biosynthesis pathways and have been cloned from contrasting wheat *cvs.*: phytoene synthase gene (*PSY*, NCBI acc. no. FJ393546), which is involved in yellow pigment synthesis; ADP glucopyrophosphorylase gene (*AGPase-L*, acc. no. DQ406820), *Triticum aestivum* ADP glucopyrophosphorylase-1 gene (*TaAGPase-1*, acc. no. KC347594), starch synthase (*SS*, acc. no. AY050174), Starch synthase-III (*SS-III*, acc. no. AF258608), and pullulanase gene (acc. no. XM_044583776), which are involved in the starch biosynthesis pathway; phytoene desaturase (*PDS*, acc. no. FJ517553) and β-Carotene hydroxylase (*BCH*, acc. no. JX171675), which are involved in the tannin biosynthesis pathway; phenylalanine ammonia lyase gene (*PAL*, acc. no. XM_044557325), which is involved in the biosynthesis of phenolic compounds; chalcone synthase 2-like (*CHS*, acc. no. XM_044543986) and inositol hexakisphosphate kinase gene (*IP6K1*, acc. no. XM_044517289), which are involved in the biosynthesis of phytic acid. Further, the amino acid sequences were characterized using the Prot pi tool available online (https://www.protpi.ch/Calculator/ProteinTool). The abundance of Cys/Met was presented as a percentage of the amino acids.

Cys/Met estimation in the grains of contrasting wheat *cvs.* using high-performance liquid chromatography

We estimated the Cys/Met in the grains following the standardized method at our Nutrition Analysis Lab, ICAR-IARI, New Delhi. In brief, 50 µg of the sample was taken and transferred into a clean glass vial. To 50 mL broth tubes, 20 mL of 6N HCl was added, and the glass vial containing the sample was dipped into the tube and sealed with parafilm. The tube was placed in a dry bath at 60°C under N_2 gas for 15 min to maintain inertness. Further, the temperature was increased to 110°C and it was incubated for 24 h for complete hydrolysis of the protein sample (Marino et al., 2010). The filtrate was then evaporated in a vacuum flash evaporator and was made acid free by repeated washing with distilled water and subsequent evaporation. The hydrolyzed sample was further subjected to pre-column derivatization using O-phthalaldehyde in the presence of βxA7B5;-mercaptoethanol. Further, 80 µL of the

derivatized sample was injected in high-performance liquid chromatograph (HPLC) (Shimadzu, Model CBM 20 A) equipped with a C18 reverse phase (RP) column and a fluorescence detector. The amino acids were identified and quantified by comparing the retention times and peak areas with those of the Sigma standard. The concentration of amino acids was presented as the percentage of a mole.

Yellow pigment estimation

The estimation of yellow pigment (β-carotene) in the sample was carried out as per the modified method of Kumar et al (2022), published in the technical bulletin of ICAR-Indian Agricultural Research Institute, New Delhi, India. We used 1 kg of treated wheat grains (conditioned to 13% moisture and debranned to 6% using a fabricated peeling machine available at the Agricultural Engineering Workshop at ICAR-IARI, New Delhi, India). We used 40 g of fine powdered (100 mesh size particles) from each genotype prepared using a mini-miller machine (Kolar Mill Stores Pvt. Ltd. Karnataka, India). The fine powder was stored in air-tight bags in two groups for further downstream characterization. The estimation of total yellow pigment was carried out by using the cold percolation method. The fine powdered flour (40 g) was loaded onto the chromatograph column packed with cotton and sodium sulphate. Further, 75 mL of n-butanol was used for the extraction of the eluent from the bottom in a fresh test tube. The extract was packed in dark colored bottle and was used for the estimation of yellow pigment by measuring the absorbance at 412 nm. The yellow pigment was calculated using the extinction coefficient of 13,000 mM cm^{-1}.

Estimation of total starch and resistant starch

The collected samples (0.1 g) were fractionated in 80% ethanol (hot) as per the protocol of Thayumanavan and Sadasivam (1984). In brief, the residue retained after centrifugation was washed repeatedly until the absence of color formation by the anthrone reagent. The dried residue was mixed with 5.0 mL of water and 6.5 mL of perchloric acid (52%). The mixture was incubated at 0°C for 20 min followed by centrifugation at 12,000 rpm for 10 min. The extraction using fresh perchloric acid was repeated twice, and further volume was made up to 100 mL. An aliquot of 0.1 mL was taken, and the volume was made up to 1 mL with water. Further, 4 mL of anthrone reagent was added, and the reaction mixture was heated for 8 min in a boiling water bath, followed by rapid cooling. The intensity of the green to dark green color was read by measuring OD at 630 nm. The glucose standard was used to estimate the concentration of starch by multiplying it by a factor of 0.9.

RS in the grain was estimated using the Resistant Starch Assay kit (Megazyme) (Englyst et al., 1992). In brief, 50 g of grains were used for the estimation following the protocols as provided by the manufacturers. A mixture of 0.1 mL of aliquot and 3.0 mL of glucose oxidase/peroxidase (GOPOD) reagent was incubated at 50° C for 20 min, and the OD was read at 510 nm against the reagent blank. The RS was calculated using the D-glucose solution standard provided in the kit.

Estimation of total phenolic content

The total phenolic content was estimated using the method of Singleton et al. (1999). In brief, 0.5 mL of supernatant (extract from the slurry by passing the mixture through a chromatograph column) was mixed with 5 mL of 1 M Folin–Ciocalteu reagent (FCR). Further, the solution was neutralized by adding 4 mL of 75 g/L saturated sodium carbonate and the solution was kept at room temperature (RT) for at least 2 h. The solution was further used for measuring the absorbance at 765 nm. The total phenolic content (TPC) was measured using Gallic acid as a standard curve, and the result was presented in terms of Gallic acid equivalents (mg GAE/ g DW).

Estimation of total tannin content

The tannin content was estimated using the Folin–Ciocalteu reagent method (Everette et al., 2010). We used 0.1 mL of extract and a further reaction mixture was prepared by adding 0.5 mL of FCR, 1 mL of 35% sodium carbonate (Na_2CO_3), and 7.5 mL of double-distilled water, followed by incubation at RT for 30 min. The RM was further used to measure the absorbance at 700 nm against the blank. The total tannin content was calculated using the standard curve of tannic acid and expressed as mg/mL.

Estimation of micronutrients (iron and zinc)

The finely ground grains (1.0 g) were digested using 20 mL of the digestion mixture (consisting of HNO_3 and $HClO_4$ in the ratio of 9:4) using the digestion chamber. The mixture was evaporated until the volume was reduced to 3 to 5 mL. The flasks were then cooled at room temperature, and double-distilled water was added to make the volume 50 mL. The clear, digested solution in each flask was filtered using Whatman filter paper No. 42 and used to analyze the micronutrients. The micronutrients Zn and Fe were analyzed using an atomic absorption spectrophotometer (AAS, Electronics Corporation of India Limited, Hyderabad, India) by measuring the absorption at 213.9 nm and 248.3 nm for Zn and Fe, respectively. The concentration was estimated using the pure standard and the content was expressed as µg/g DW.

Estimation of anti-nutritional factor (phytic acid) and phosphorus

The finely ground grains (1 g) were used for the phytic acid estimation by digesting the powder using 20 mL of hydrochloric

acid (0.66 M) overnight. Further, 0.5 mL of the extract was neutralized by adding 0.5 mL of NaOH (0.75 M) and used for the enzymatic dephosphorylation reaction using the phytic acid assay kit (Megazyme). The supernatant was used for the colorimetric determination of phosphorus by measuring the absorbance at 655 nm and the calculation was conducted as given in the instruction manuals.

Estimation of total storage protein and gluten

The crude nitrogen present in the grain was estimated using the micro-Kjeldahl method (Miller and Houghton, 1945). In brief, the flour (100 mg) was digested in strong sulfuric acid (10 mL) along with 2 g of K_2SO_4 and $CuSO_4$ (in a ratio of 10:1) for 90 min at 420° C, followed by distillation using 40% NaOH and 4% Boric acid. The trapped ammonia was determined through titration with 0.1 N HCl and the burette reading was used to calculate the percentage of nitrogen using the formula -

$$\%\ N = 14.01 \times Burette\ reading \times 100 \times Normality\ (HCl)/1007 \times Volume\ of\ sample\ taken$$

The percentage of nitrogen calculated was used for the calculation of total protein content using the conversion factor of 5.81.

The gluten was estimated in the finely ground flour following the traditional method of washing the dough with water. We used 2 g of flour and added 1–2 mL of water for dough preparation. The prepared dough was wrapped in two layers of chicken cloth and washed with distilled water until a fine elastic layer was left over. The gluten leftover was dried in an oven at 72°C for overnight, and further weighed for the calculation of the percentage of gluten in the flour.

Statistical analysis

The samples were three biological replicates for the biochemical analysis, and we used the statistical tool of one-way ANOVA to analyze the variance of different parameters for statistically significant differences ($P \leq 0.05$). The correlation between the biochemical traits was analysed using Pearson's correlation coefficient (r, $p<0.01$).

Results and discussion

Total thiol and disulfide profiling in the grains of diverse genotypes of wheat

Thiol is a very important component of storage proteins, providing stability and strong networking in dough and many desirable rheological characteristics in flour. It is considered one of the desirable traits for analyzing the quality of flour. We have analyzed the thiol content in the grains of diverse genotypes of wheat and observed the highest thiol content in the grain of wheat *cvs*. Halna followed by HD2985 and Raj3765 (Figure 1a). The thiol content was observed to be th elowest in wheat cv. NIAW34.

In order to understand the effect of the changes in the thiol content on developing endosperm tissues, we collected samples at different grain-filling stages: button, milky-ripe, seed hardening, and mature grains, and used them for the thiol estimation (Figure 1b). Wheat cv. Halna had the highest thiol content at different sub-stages of endosperm development, as compared to other *cvs*., whereas the lowest was observed in PBW343 and NIAW34 during different sub-stages. We observed significant variations in the flour thiol content across the genotypes (*F*-values are significant at $p \leq 0.05$). Most of the wheat *cvs*., which are popular among consumers for flour and chapatti-making quality (HD2985, Raj3765, etc.), had very high thiol content, as compared to other genotypes. Manu and Rao (2008) reported that high thiol content in flour decreases the toughness of chapatti.

Disulfide bonds (SS) are formed by the oxidation of sulfhydryl groups (SH) and have been reported to be involved in stabilizing the folded conformation of gliadin (monomeric proteins). The polymeric structure of dough is also stabilized due to the presence of disulfide bonds. We analyzed the disulfide bonds in the grains of diverse genotypes of wheat. The disulfide content was observed to be the highest in the grains of wheat cv. HI1544 followed by Halna and PBW443 (Figure 2c). The lowest disulfide content was observed in wheat cv. UP-2506. Disulfide bonds are linked with the empirical rheology of flour and are considered one of the important traits.

We analyzed the pattern of increase in the disulfide content in the developing endosperm tissue in diverse *cvs*. and observed the highest disulfide content in wheat cv. HI1544 and the lowest in UP2506 at different sub-stages of endosperm growth and development (Figure 2b). Manu and Rao (2008) observed that protein disulfide content showed a positive correlation with dough hardness and the texture of chapatti. The thiol content has been observed to influence the formation of disulfide bonds in flour and helps in improving the rheological characteristics of dough. Various studies have shown that GSH-dependent protein-disulfide oxidoreductase (TPDO) present in the developing wheat kernels manipulate the quality matrix of dough, causing stiffness. Disulfide bond dynamics have been reported to enhance the dough extensibility in wheat (Osipova et al., 2007).

Expression analysis of genes responsible for thiol-based redox sensing

We selected three genes—*TRX* (acc. no. AF438359.1), *GRX* (acc. no. AF542185.1), and *GR* (acc. no. XM_044564013)—to assess the thiol-based redox sensing in developing endosperm (sub-stages G_0, G_1, and G_2) of Halna and HD2985 (high-thiol content genotypes) and NIAW34 and PBW443 (low-thiol content genotypes). *TRX* expression was observed to be higher (2.4-fold) in wheat cv. Halna during the G_2 stage compared to the G_0 stage

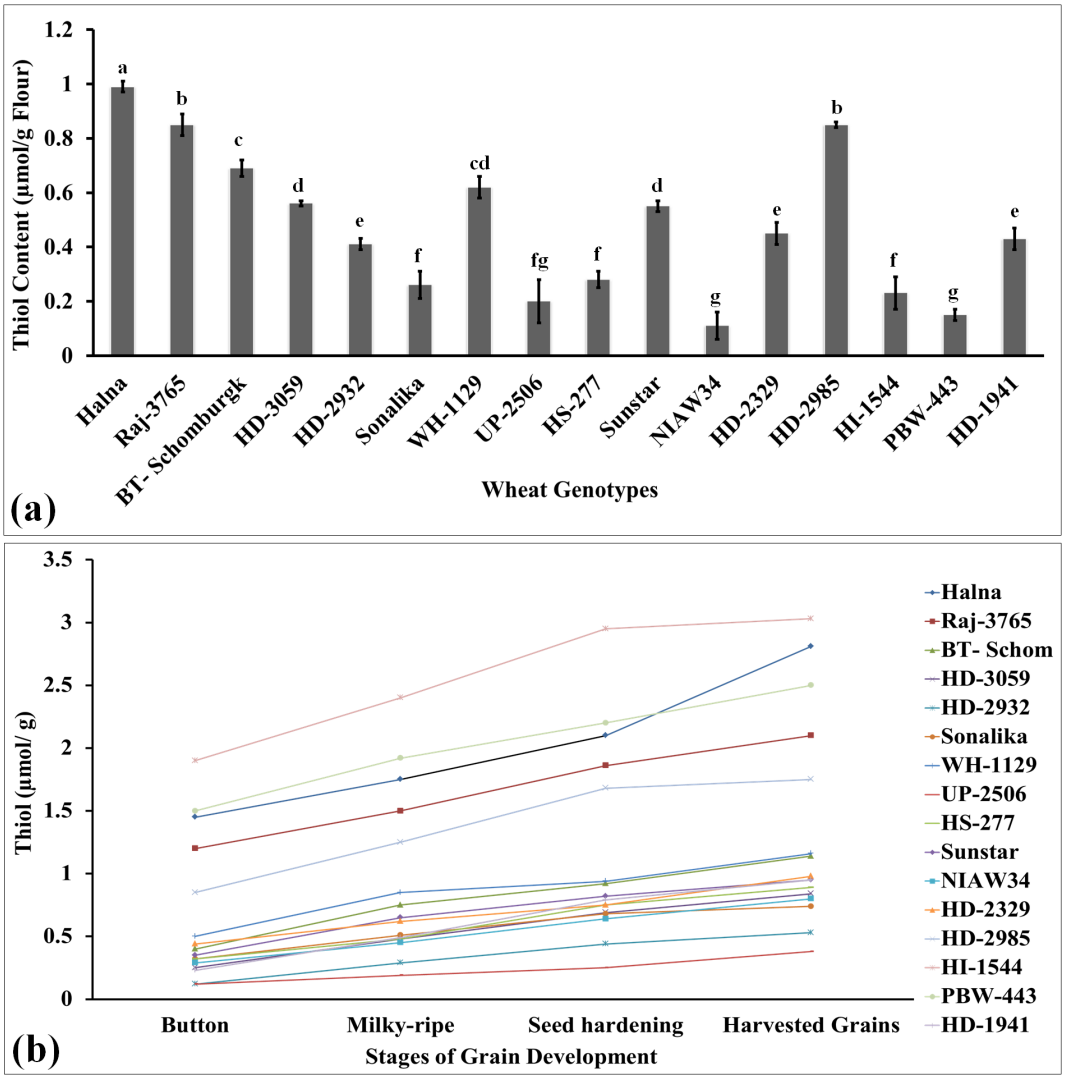

FIGURE 1
Thiol profiling in the developing endospermic tissues and harvested grains of diverse genotypes of wheat grown under regulated conditions. **(a)** Total thiol content in harvested grains. **(b)** Variations in the thiol content in developing endospermic tissue. Sub-stages of endosperm used for the estimation include the button, milky-ripe, seed hardening, and harvested grain stages. In total, 16 diverse genotypes of wheat were selected for the study. The vertical line above the bar denotes the *SEM* (n=3); a letter above a bar shows the significance level (P<0.05).

(Figure 3a). The expression was observed to be the lowest in wheat cv. PBW443 compared to other genotypes. Overall, we observed an abundance of *TRX* transcripts in the developing grains of genotypes with high thiol content (Halna and HD2985) compared to low thiol-containing genotypes (NIAW34 and PBW443).

We observed similar patterns of GRX expression in contrasting wheat genotypes (Figure 3b). The relative fold expression was observed to be the highest (4.9-fold) in wheat cv. Halna during the G_2 stage, whereas it was observed to be the lowest (3.1-fold) in cv. NIAW34 compared to G_o. Sainz et al. (2022) reported the differential expression of 12 *Trx* and 12 *Grx* genes in response to water deficit stress in soybean.

Similarly, expression analysis of GR showed a relatively higher expression (9.9-fold) in wheat cv. HD2985 during the G_2 stage compared to G_0 (Figure 3c). The GR expression was observed to be the lowest (4.1-fold) in wheat cv. PBW443 during the G_2 stage compared to G_o. We observed significant variations ($p \leq 0.05$) in the expression of *TRX*, *GRX*, and *GR* during different sub-stages of endosperm development in contrasting wheat *cvs*., with an abundance of transcripts in Halna and HD2985 compared to NIAW34 and PBW443. He et al. (2023) identified 85 GRX genes in common wheat using a bioinformatic method and reported differential upregulation of these genes under biotic and abiotic stresses in wheat.

Cys/Met estimation in regulatory genes associated with different metabolic pathways

The ratio of Cys: Met has been reported to play very important role in deciding the structural and thermal stability of protein under

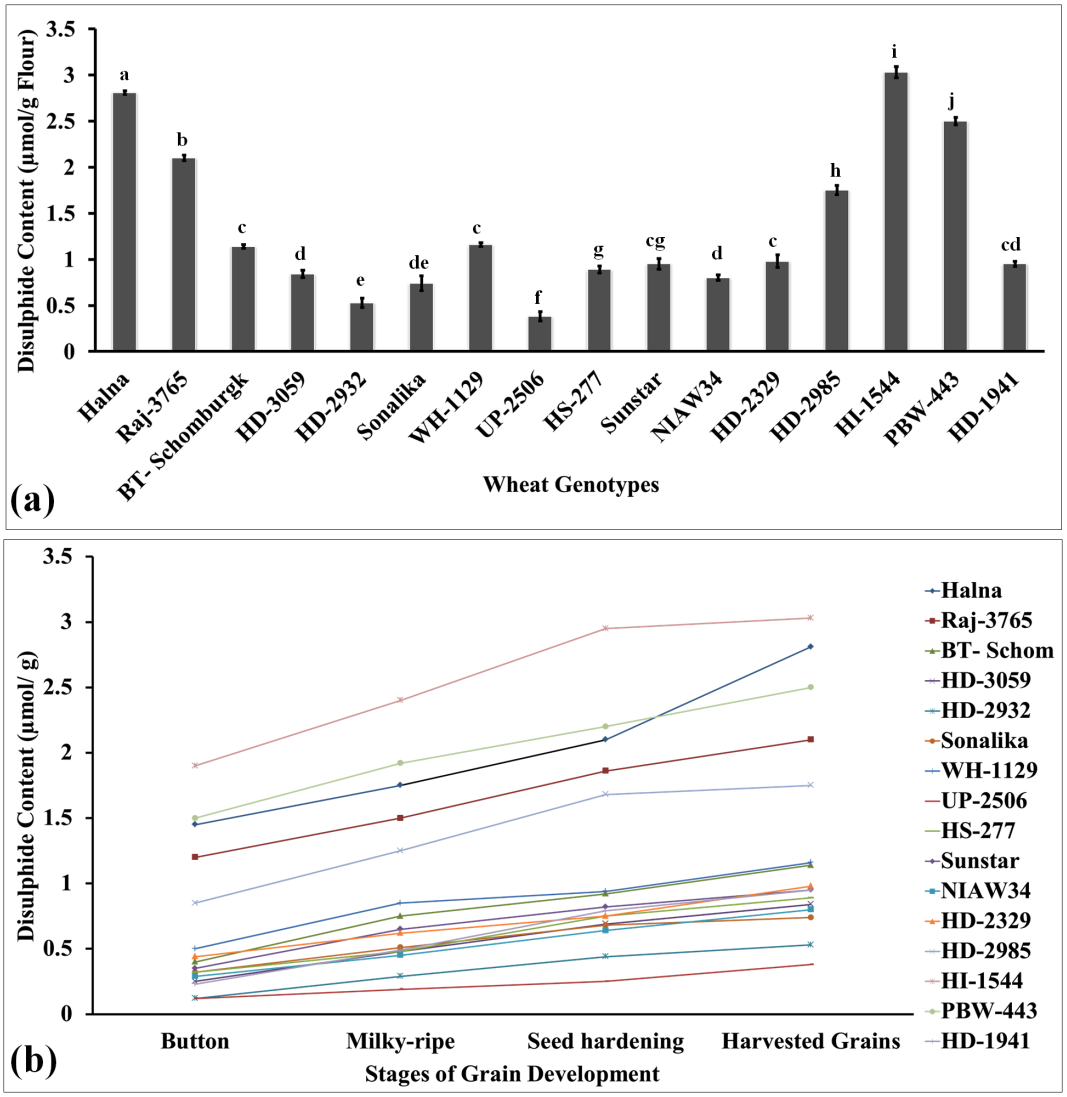

FIGURE 2
Disulfide profiling in the developing endospermic tissues and harvested grains of diverse genotypes of wheat grown under regulated conditions. **(a)** Total disulfide content in the harvested grains. **(b)** Variations in the disulfide content in the developing endospermic tissue. Sub-stages of endosperm used for the estimation include the button, milky-ripe, seed hardening, and harvested grain stages. In total, 16 diverse genotypes of wheat were selected for the study. The vertical line above the bar denotes the *SEM* (n=3); a letter above a bar shows the significance level (P<0.05).

oxidizing conditions (Bhopatkar et al., 2020). In order to analyze the Cys/Met ratio, we retrieved the amino acid sequences of some of the regulatory genes (cloned from *Triticum aestivum*) linked with different metabolic pathways associated with the biosynthesis of macro- and micronutrients in the grains, i.e., yellow pigment biosynthesis (*PSY*, acc. no. FJ393546), starch biosynthesis [*AGPase-L*, (acc. no. DQ406820), *TaAGPase-1* (acc. no. KC347594), *SS* (acc. no. AY050174), *SS-III* (acc. no. AF258608), and pullulanase gene (acc. no. XM_044583776)], tannin biosynthesis [*PDS* (acc. no. FJ517553) and *BCH* (acc. no. JX171675)], phenolic compound biosynthesis (*PAL*, acc. no. XM_044557325), and phytic acid biosynthesis [*CHS* (acc. no. XM_044543986) and *IP6K1*, (acc. no. XM_044517289)]. The amino acid sequences were characterized for the estimation of Cys/Met in the amino acid pool (Figure 4A). GBSS is considered one of the important enzymes involved in the starch biosynthesis pathway. We observed 2.25% Cys and 2.95% Met in the amino acid sequence of *GBSS* cloned from wheat (Figure 4A). Similarly, in the case of pullulanase, which is involved in RS synthesis, it had 0.98% Cys and 2.7% Met in the amino acid pool. The Cys content was observed to be the highest (2.25%) in *GBSS* and Met was observed to be the highest (4.04%) in the *BCH* gene involved in tannin synthesis. The ratio of Cys: Met was observed to be the highest in *GBSS* (0.77) and the lowest in *BCH* (0.08). Other genes also showed the same pattern of Cys and Met in their amino acid sequences. All these key genes were observed to have a high percentage of Cys and Met, which provide stability to the proteins against various factors. Walker et al. (2022) reported that S-containing amino acids protect the proteins from oxidation and correlated it with the folding stabilities of the proteins under stress.

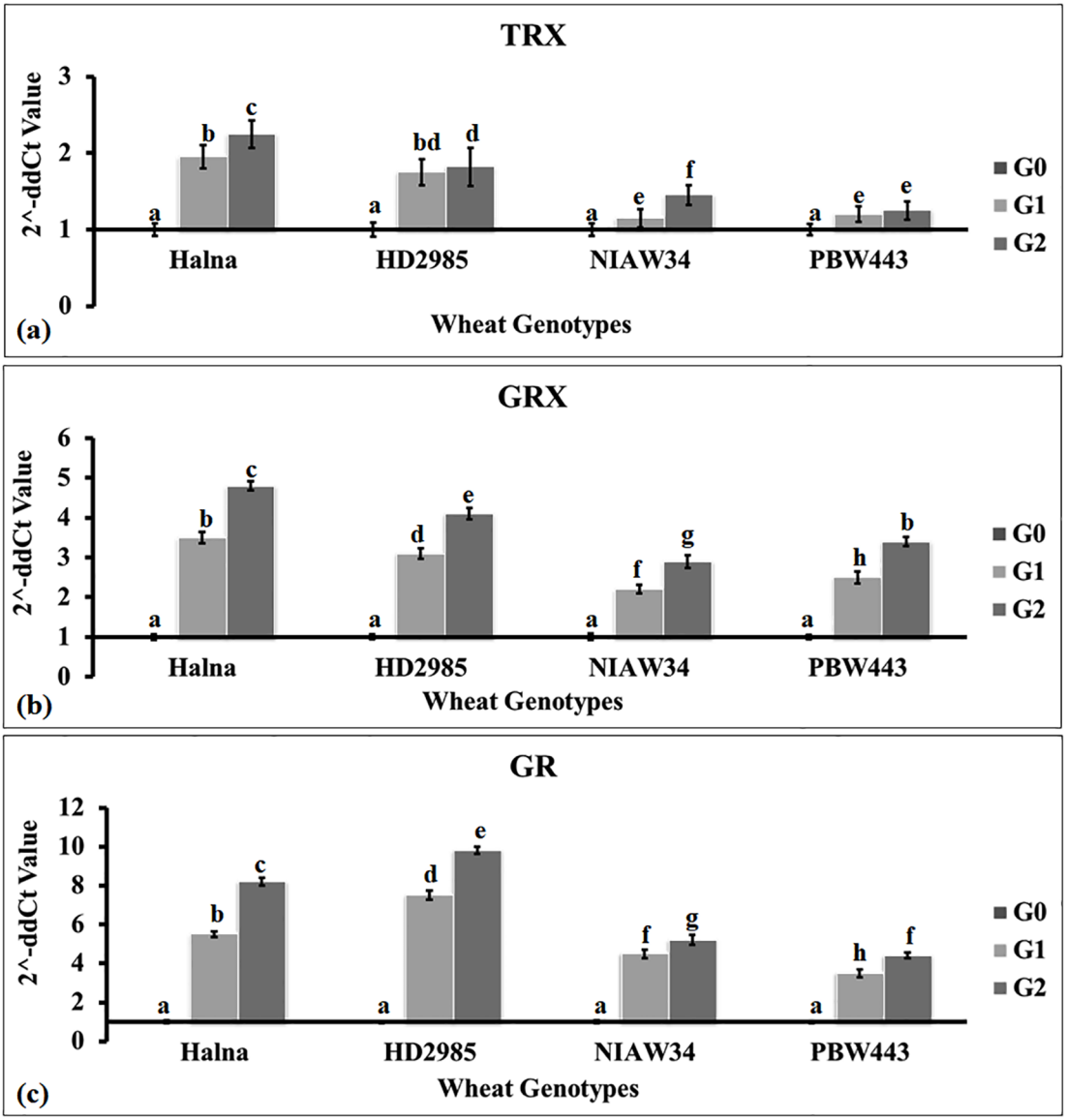

FIGURE 3
Expression profiling of genes linked with thiol-based redox sensors in developing endospermic tissue of wheat. **(a)** Expression of the thioredoxin (*TRX*) gene. **(b)** Expression of the glutaredoxin gene (*GRX*). **(c)** Expression of the glutathione reductase gene (*GR*). Four genotypes were selected for the expression profiling: high thiol content in grains: Halna and HD2985; low thiol content in grains: NIAW34 and PBW443. The sub-stages of endosperm tissue used for the expression analysis were the button (G_0), milky-ripe (G_1), and seed hardening (G_2) stages. The vertical line above the bar denotes *SEM* (n=3).

Cys/Met estimation in the grains of contrasting wheat *cvs* using HPLC

We estimated the Cys and Met concentration in the grains of diverse *cvs*. of wheat in order to understand its effect on different metabolic pathways linked with various macro- and micronutrients. The cysteine content was observed to be the highest (3.56% mole) in wheat cv. Halna (thermotolerant) followed by HD2985 (3.40% mole), whereas it was observed to be the lowest (1.25% mole) in NIAW34 (thermosusceptible) (Figure 4B). Similarly, the methionine content was observed to be the highest (2.20% mole) in wheat cv. HD2985 (thermotolerant) and to be the lowest (0.33% mole) in cv. HD1914 (thermosusceptible). We observed significant ($p \leq 0.05$) variations in the Cys and Met content in the grains among the diverse genotypes. Most of the genotypes that have been reported to be thermotolerant, such as HD2985, Halna, and HD2932, showed very high Cys and Met contents, whereas thermosensitive *cvs*., such as BT-Schomburgk, HD1914, and PBW343, showed low Cys and Met contents in the amino acid pool of the grains. The abundance of Cys and Met may be the reason behind the high stability of the proteins and tolerance level of the plant under heat stress, since it behaves as a strong antioxidant, enhancing the stability of the enzymes involved in various pathways responsible for the synthesis of many macro- and micromolecules. Liu et al. (2020) reported that higher concentrations of glutathione

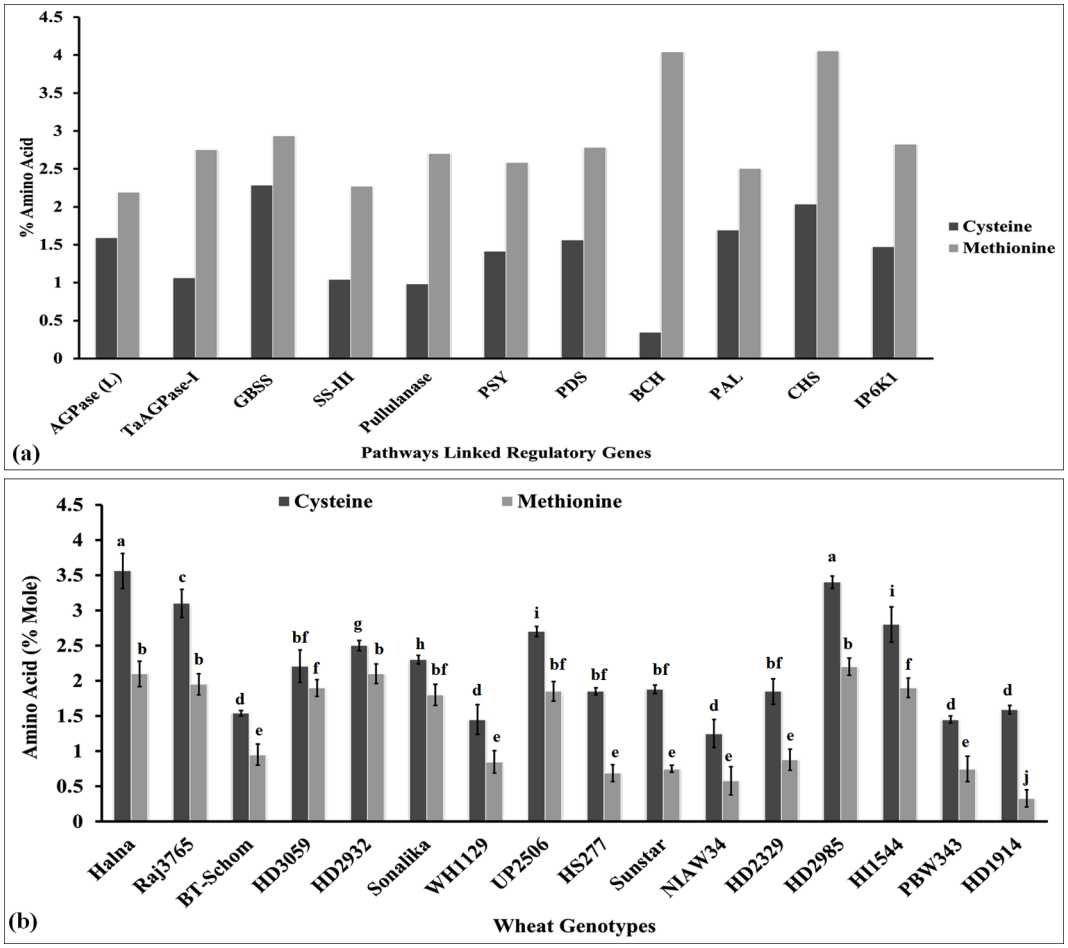

FIGURE 4
Characterization of sulfur-containing amino acids in the key regulatory genes linked with various metabolic pathways and in the grains of diverse genotypes of wheat. **(A)** Cys/Met estimation in regulatory genes associated with different metabolic pathways. **(B)** Cys/Met estimation in the grains of diverse genotypes of wheat. In total, 11 genes linked with key metabolic pathways were retrieved from NCBI, and their amino acid compositions were analyzed using the Prot pi tool. Moreover, 16 diverse genotypes of wheat were selected for the Cys/Met estimation in grains. The vertical line above the bar denotes *SEM* (n=3); a letter above a bar shows the significance level (P<0.05).

maintain the redox balance and enhance the accumulation of protein and S-containing amino acids in the grains of maize, which in turn improves the grain quality.

Yellow pigment is essentially carotenoids such as lutein and α/βxA7B5;-carotene, and these are considered potential natural antioxidants with many medical benefits. It also provides the shining color of the grains and is one of the traits used to decide the export value of wheat grains. This is one of the deciding factors in the popularization of wheat grains and consumer preference. Many processed products require wheat grains to have a very high content of yellow pigment. We also analyzed the yellow pigment in the grains of diverse genotypes of wheat to decide their quality. The yellow pigment content was observed to be the highest in the grains of wheat cv. NIAW34 (6.08 µg/g dry matter), followed by BT-Schomburgk (5.71 µg/g dry matter), whereas the content was observed to be the lowest in wheat cv. UP-2506 (1.01 µg/g dry matter) (Figure 5a). We observed significant variations ($p \leq 0.05$) in the total yellow pigment content in the diverse genotypes selected for the present study. Butler and Ghugre (2020) reported that β-carotene acts as a potential iron enhancer and limits the phytate-chelating mechanism. It causes an increase in the availability of ionizable iron, which is considered an indicator of the bioavailability index. Wheat genotypes with a high yellow pigment are recommended to be used in the pasta industry, and it is one of the desirable traits.

Variations in the grains' antioxidants

Accumulation of total phenolic content

Phenolic is considered one of the important antioxidants in the grains, which has many beneficial effects, such as helping in scavenging the free oxygen radicals inside the cells and protecting the proteins, enzymes, and organelles from disintegration. We analyzed the phenolic content in diverse wheat *cvs.* and observed the highest TPC in Halna (48.5 mg GAE/100g) and HI1544 (49.2 mg GAE/100g), whereas the lowest content was observed in HD2329 (20.2 mg GAE/100g) (Figure 5b). Most of the popular

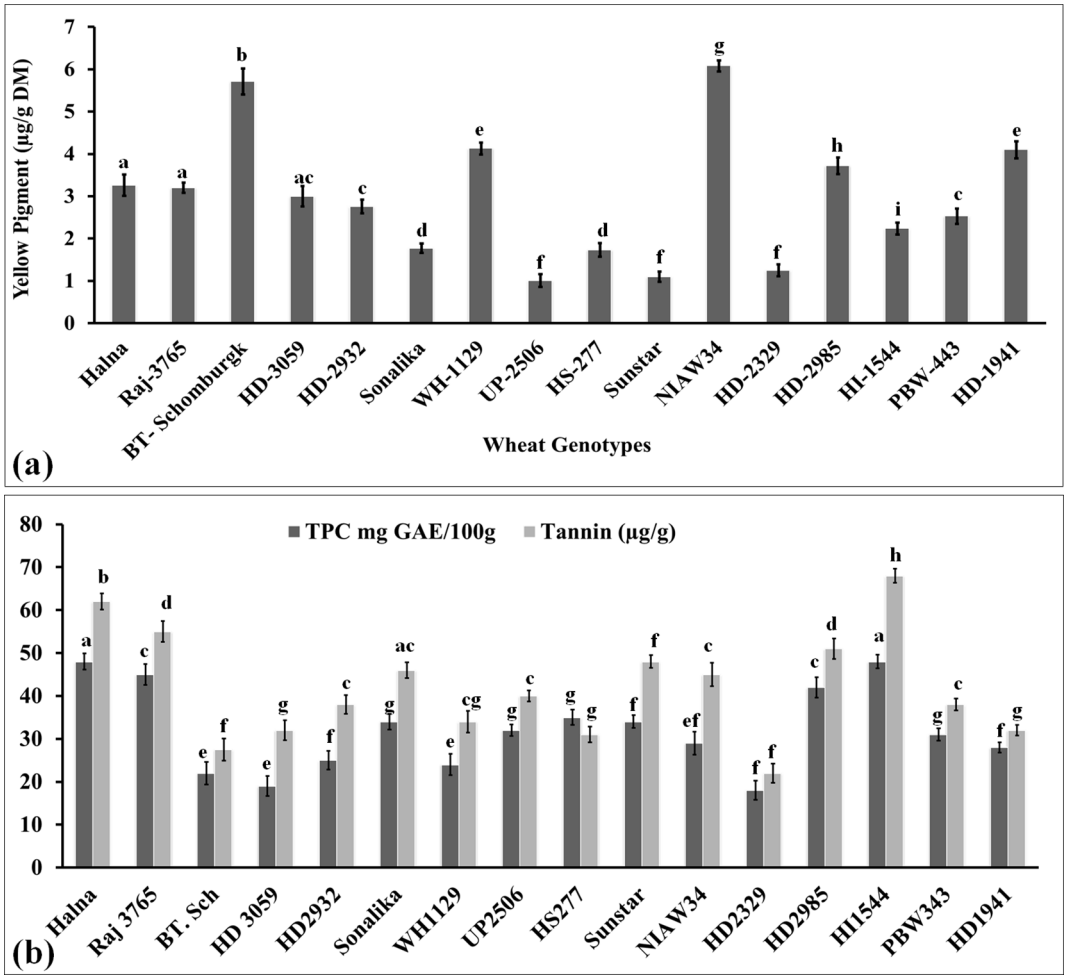

FIGURE 5
Yellow pigment and antioxidant estimation in the grains of diverse genotypes of wheat. **(a)** Yellow pigment content in the grains. **(b)** Total phenolic and tannin content in the grains. In total, 16 diverse genotypes of wheat were selected for the study. The vertical line above the bar denotes the *SEM* (n=3); a letter above a bar shows the significance level (P<0.05).

wheat *cvs*., such as Halna, HD2985, Raj3765, Sonalika, showed higher accumulation of TPC compared to other *cvs*. Ali et al. (2023) highlighted the importance of phenolics in improving the grain quality of pearl millet. Phenolics have also been reported to suppress the activity of many starch-degrading enzymes inside the human body and, in turn, provide a low spike of glucose and make it suitable for consumption by diabetic patients (Deka et al., 2022).

Accumulation of tannin content

Tannin is a water-soluble polyphenol and is considered one of the most effective antioxidants within the plant system. It provides the bitterness and astringency in the seeds and helps in protecting the grains from pests. It reduces cholesterol and lowers blood pressure inside the human body. Tannins play a very important role in modifying the protein rheology through non-covalent interactions. Girard et al. (2019) reported that gluten strength in wheat seeds is determined by the cross-linking of condensed tannins, which ultimately enhances the viscosity of the protein. Here, we analyzed the total tannin content in the grains of diverse genotypes of wheat and observed the highest tannin content in wheat cv. HI1544 (70.5 µg/g) and the lowest in wheat cv. HD2329 (21.8 µg/g) (Figure 5b). All the popular *cvs*. were observed to have higher tannin content compared to other genotypes. We observed a large positive correlation between the TPC and total tannin content [$r(16) = 0.904$, $p < .001$]. Wang et al (2017) observed an increase in the strength of wheat dough due to the presence of hydrolysable tannins. Khazaei and Vandenberg (2020) reported a negative effect of tannin on mineral accumulation and protein content of seeds in Faba beans. It also compromises the bioavailability of various nutrients present in the seeds, influencing the germination process. Ferulic acid (4-hydroxy-3-methoxycinnamic acid) has a very high radical scavenging capacity and is recommended due to its anti-ageing and anticancer properties (Wang et al., 2017). *p*-Coumaric and ferulic acid have been reported to be predominantly accumulated in the wheat bran/pericarp fraction, which shows very high antioxidant potential in grains (Boz, 2015).

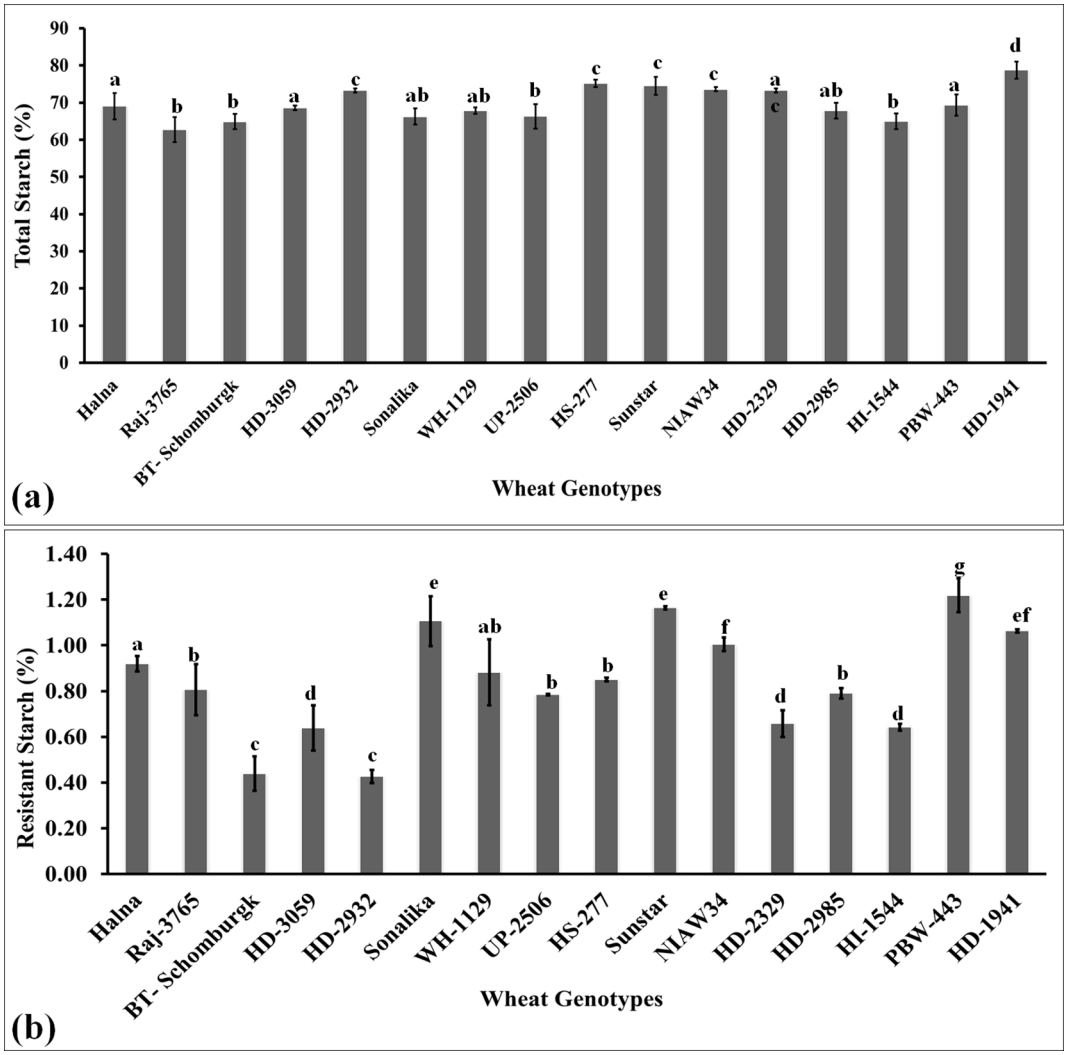

FIGURE 6
Variations in the polysaccharide (starch and resistant starch) content in the grains of diverse genotypes of wheat. **(a)** Total starch estimation in the grains. **(b)** Resistant starch content in the grains. In total, 16 diverse genotypes of wheat were selected for the study. The vertical line above the bar denotes the *SEM* (n=3).

Variations in the polysaccharide accumulation inside the grains

Total starch content in the grains

The total starch was estimated in the grains of diverse genotypes of wheat selected from the core set of wheat developed for their nutritional composition. Starch is a polysaccharide consisting of amylose and amylopectin and is predominant in the grains of cereals. The highest starch level was observed in the grains of wheat cv. HD1941 (79.2%) followed by HS-277 (76.8%) and Sunstar (75.9%) (Figure 6a). We observed significant variation in the accumulation of starch in the grains of diverse wheat genotypes. Popular wheat *cvs*., such as Raj3765, HD2329, BT-Schomburgk, and HD2320, also showed significant accumulation of starch in the grains. Wide diversity in the functionality of starch (composition, structure, and granule size) has been observed in different wheat *cvs*. across the world due to variations in genetic and environmental conditions. *Triticum aestivum* or bread wheat is widely grown all over the world with the highest starch content, followed by *T. durum* (Shevkani et al., 2017). Durum wheat is rich in yellow pigment and proteins and is used for making pasta. *T. monococcum*, *T. dicoccum*, and *T. spelta* are ancient species mainly grown in Ethiopia, Turkey, France, and Iran and have little starch, as compared to common wheat or durum wheat.

Resistant starch content in the grains

RS is one of the fractions of starch present in the endospermic tissue of the grains and is a slow-digestible starch. It is recommended in the diet of diabetic patients and is considered one of the desirable traits for analyzing the quality of the grains (Khan et al., 2020). We observed the highest RS content in the grains of wheat cv. PBW443 followed by Sunstar and Sonalika (Figure 6b). The variations in RS were observed to be significant across the genotypes. The lowest RS content was observed in the

wheat *cvs*. HD2932 and BT-Schomburgk. The mechanism underlying the synthesis of RS and significant variations across the genotypes is not known, though pullulanase and starch debranching enzymes have been reported to be associated with the synthesis of RS. RS has been reported to improve the viscoelasticity properties of dough in wheat (Xie et al., 2018). The results of Pearson's correlation indicated that there was a non-significant small positive relationship between starch and resistant starch, [$r(16) = 0.286$, $p = 0.283$]. This is the reason behind the high starch content in the grains of cereals, though the RS content is very low, as compared to millets. Recent studies have identified a positive correlation between starch and RS content in wheat, influenced by factors such as amylose content, starch molecular structure, and processing conditions. Research involving 129 wheat accessions found that RS content varied from 0.07% to 0.47%, with higher amylose content associated with increased RS levels (Liu et al., 2024).

Effect of thiol on the accumulation of anti-nutritional factors in the grains

Phytic acid and total phosphorus content in the grains of diverse wheat genotypes

Phytic acid is one of the anti-nutritional factors that compromises the quality of flour. It limits the bioavailability of micronutrients such as iron and zinc and has many effects on the health of humans. We also analyzed the phytic acid content in the grains of diverse genotypes of wheat. The phytic acid content was observed to be the lowest in the grains of wheat cv. WH-1129 (0.56 g/100g) followed by PBW443 (0.62 g/100g) and BT-Schomburgk (0.68 g/100g) (Figure 7a). The phytic acid content was observed to be the highest in wheat cv. HD3059 (1.48 g/100g) followed by Sonalika (1.38 g/100g). Most of the *cvs*. selected for the nutritional analysis in the present investigation showed a high content of phytic acid in the grains. A study involving 12 wheat genotypes reported

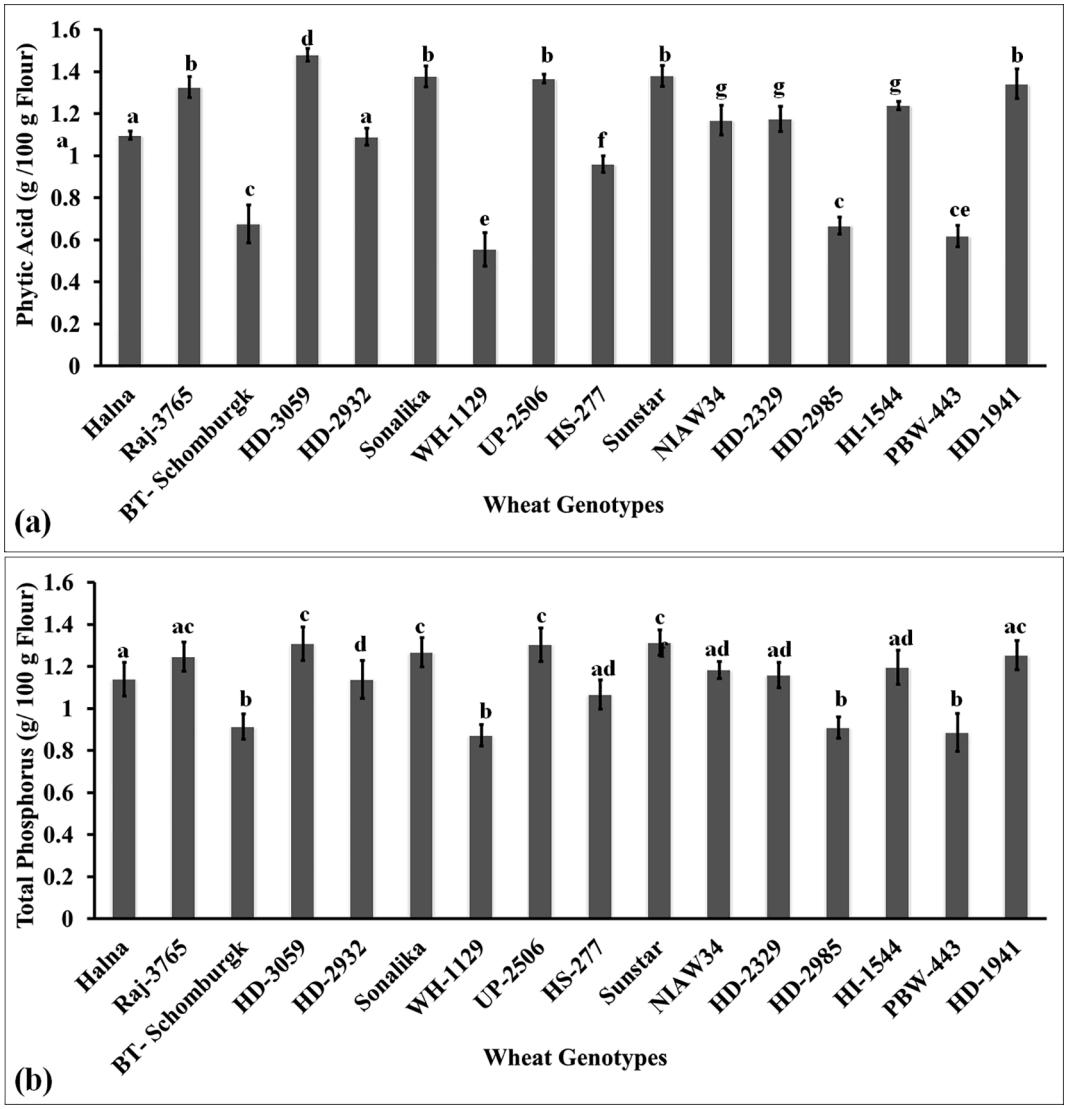

FIGURE 7
Characterizing the anti-nutritional factor (ANF) present in the grains of diverse genotypes of wheat. **(a)** Phytic acid content in the grains. **(b)** Total phosphorus content in the grains. In total, 16 diverse genotypes of wheat were selected for the study. The vertical line above the bar denotes the *SEM* (n=3); a letter above a bar shows the significance level (P<0.05).

significant variability in phytic acid content, ranging from 0.48% to 1.95%, with an average of 1.24%. This variation in phytic acid levels influenced the nutritional and physical parameters of the wheat grains, highlighting the importance of phytic acid in determining grain quality (Shujaat et al., 2024). The accumulation of high phytic acid has been reported to form complexes with micronutrients such as iron and zinc and restrict their bioavailability inside the body. The results of Pearson's correlation indicated that there was a non-significant, very small negative relationship between phytic acid and thiol content [$r(16) = -0.0552$, $p = 0.839$]. Phytic acid binds to metal ions and forms stable complexes. Thiol groups present in proteins coordinate with metal ions and maintain the structure and activity of proteins. In contrast to this, phytic acid restricts the availability of metal ions required by the thiol group to maintain the function of proteins in food. The stability and activity of the protein are ultimately compromised. Graminho et al. (2015) reported that the phytase enzyme requires thiol for its activity, acts on the breakdown of phytic acid, and is mainly responsible for the chelation of beneficial micronutrients.

Total phosphorus accumulation in grain is considered one of the desirable traits when analyzing the quality of flour. It has been reported that phosphorus accumulation in grains determines the appearance of grains. It is considered one of the desirable traits for deciding the quality of grains. We observed the highest P accumulation in the grains of wheat cv. HD3059 (1.3 g/100g) followed by UP2506 and Sunstar (Figure 7b). Most of the genotypes showed non-significant variations ($p<0.05$) in the accumulation of phosphorus in grains. The P accumulation was observed to be the lowest in wheat cv. WH1129 (0.872 g/100g). The phosphorus is utilized as a cofactor by different enzymes involved in various metabolic reactions. Lipid composition and fatty acid profile of the seeds were observed to be affected by P deficiency (Xie et al., 2018). Phosphorus in the endospermic tissue has been reported to enhance the synthesis of total storage proteins in the seeds. Phosphorus has been reported to enhance the biosynthesis of starch during the early stages and degradation of starch during the later stages of grain development by triggering the expression of enzymes responsible for starch synthesis and degradation (Zhang

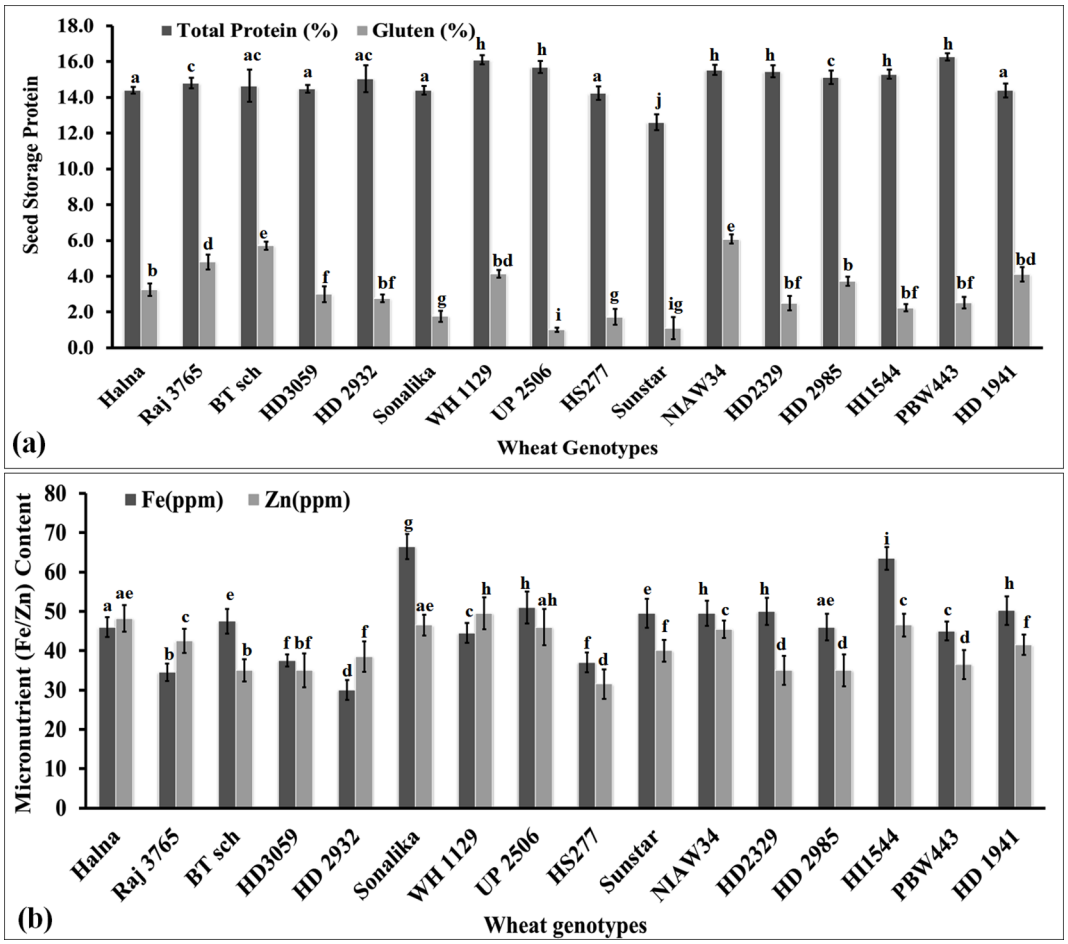

FIGURE 8
Variations in the seed storage proteins (SSPs) and micronutrient content in the grains of diverse genotypes of wheat. **(a)** Total seed storage proteins in the grains. **(b)** Iron and zinc content in the grains. In total, 16 diverse genotypes of wheat were selected for the study. The vertical line above the bar denotes the *SEM* (n=3).

et al., 2021). We observed a positive correlation between the starch and the phosphorus contents in flour/meal. Phosphorus enhances the synthesis of starch-bound lipids (phospholipids). Cereals have very little starch-bound phosphate compared to root and tuber crops.

We observed a significantly large positive relationship between phytic acid and total phosphorus [$r(16) = 0.995$, $p< 0.001$] and a negative correlation with thiol [$r(16) = -0.20$, $p< 0.001$].

Variations in the total protein and gluten content in grains

We analyzed the variations in the seed storage protein in terms of total protein and gluten content in the grains of diverse genotypes of wheat. The total protein content was observed to be the highest (16.1%) in wheat cv. PBW443 followed by WH1129 (15.8%), whereas it was observed to be the lowest (12.8%) in cv. Sunstar (Figure 8a). Most of the *cvs*. showed a non-significant difference in their total protein content. Pearson's correlation coefficient showed a negative correlation between the total protein and thiol content [$r(16) = -0.25$, $p< 0.001$]. Hussein and Alshammari (2022) reported that cysteine modulates amino nitrogen, total phenols, and the synthesis of new proteins in plants under adverse conditions.

Furthermore, we estimated the gluten content in the grains of diverse genotypes of wheat. The highest gluten content (6.2%) was observed in wheat cv. NIAW34 followed by BT-Schomburgk (5.9%), whereas the lowest (0.9%) gluten content was observed in cv. UP2506 (Figure 8a). We observed significant ($p<0.05$) differences in the gluten content among the diverse genotypes. However, we could not establish any correlation between the total protein and gluten content in the grains. The gluten content was observed to be the highest in thermosusceptible wheat *cvs*. with a low Cys/Met ratio. A non-significant negative correlation was established between the thiol and gluten contents in the wheat grains. We observed that the *cvs*. that are popular among consumers had a total protein content >14% and gluten content above 2%. Veraverbeke and Delcour (2002) observed a linear correlation between the total protein and gluten content in wheat grains. Tea et al. (2005) observed that the abundance of S-containing amino acids in the grains modifies the degree of polymerization of storage proteins and influences the rheological properties of dough.

Variations in the micronutrient content in diverse genotypes of wheat

We analyzed the Fe and Zn contents in the grains of diverse genotypes of wheat. Iron content was observed to be the highest (68.0 ppm) in wheat cv. Sonalika, followed by HI1544 (65.0 ppm), whereas Zn was observed to be the highest (52 ppm) in cv. WH1129 (Figure 8b). We observed significant variations ($p<0.05$) in the Fe and Zn content in the grains of diverse genotypes of wheat. Most of the sensitive *cvs*., such as BT-Schomburgk, HD3059, HS277, and NIAW34, were observed to have high Fe and Zn contents compared to the tolerant *cvs*., such as Halna, HD2985, and HD2932. Pearson's correlation coefficient showed a positive correlation between the Fe/Zn content and thiol content [$r(16) = 0.15$, $p< 0.023$; 0.35, $p< 0.001$]. The Fe/Zn variations among the genotypes were an inherited characteristic of the cv., which changes drastically under stress or adverse environmental conditions.

Based on the present findings and the literature available in the public domain, we modeled a simple pathway of activity of a thiol-based redox sensor. ROS produced inside the cells in response to different environmental and internal conditions act on active thiols and oxidize the catalytic Cys group and form inter- or intramolecular S–S–, –SOH, $–SO_2H$, and $–SO_3H$, which modify the structure and interactions of different proteins and enzymes involved in various metabolic pathways and ultimately regulate the accumulation of various metabolites inside the cells.

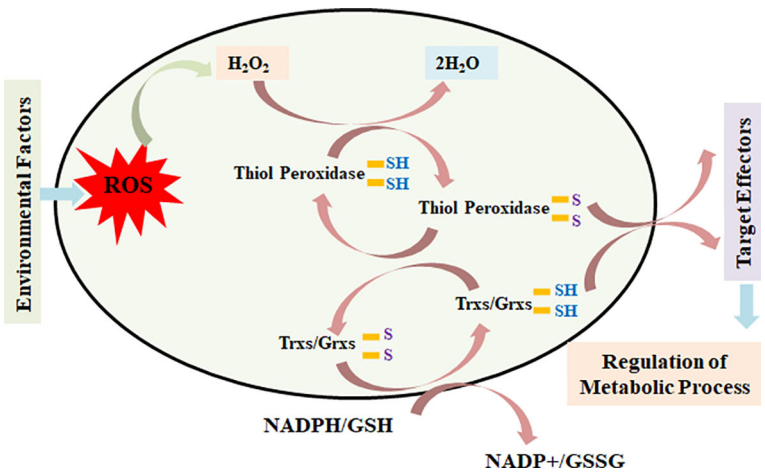

FIGURE 9
Model depicting the role of thiol-based redox sensors—thiol peroxidase, thioredoxin, glutaredoxin, and glutathione reductase—in transmitting the redox signal to effector target genes/proteins and, in turn, modulating the expression/activities of key genes/proteins linked with different metabolic pathways.

ROS also acts on thiol peroxidases such as TPXs and GPXs and oxidizes the Cys residue into different forms and transfers their redox signal to target genes and proteins linked to different metabolic processes (Figure 9). Similarly, Trx and Grx proteins are oxidized at the Cys center by thiol peroxidase and simultaneously are reduced by electrons received from NADPH/GSH with the help of thiol reductases. Trx/Grx proteins play the role of redox sensors through their conversion from the oxidized to reduced form and *vice versa* in response to different cellular and environmental conditions. This regulates the target effectors and, in turn, modulates the different metabolic processes operating inside the plants.

Thiol-based redox sensors can be used in wheat breeding programs to improve the stress tolerance and grain quality of the wheat and regulate antioxidant pathways, and can be integrated with advanced breeding techniques such as CRISPR and marker-assisted selection to accelerate the development of wheat varieties with desired traits.

Conclusions

Thiol-based redox sensors are essential in regulating various processes such as defense, growth, and the accumulation of metabolites within plant tissues. To explore their role, we characterized 16 diverse wheat genotypes and observed significant variations in thiol and disulfide contents in the grains. Wheat cultivar Halna exhibited the highest thiol content, followed by HD2985 and Raj3765. This pattern was confirmed through expression analysis of genes involved in thiol-based redox sensing, such as TRX, GRX, and GR, in the developing endosperm. The highest relative fold expression of these genes was observed in Halna, considered a tolerant cultivar, during the seed hardening stage of endosperm development, compared to sensitive cultivars. Amino acid analysis of 11 biosynthetic genes showed that GBSS, involved in starch biosynthesis, had the highest Cys content (2.25%), while BCH, involved in tannin synthesis, had the highest Met content (4.04%). The Cys: Met ratio was >1.5 in tolerant genotypes such as HD2985, Halna, and HD2932, whereas it was<1.5 in sensitive cultivars such as BT-Schomburgk and PBW343. Wheat cv. NIAW34, with a Cys: Met ratio >2.1, had the highest yellow pigment content (6.08 µg/g dry matter). Genotypes with higher Cys: Met ratios also had higher total TPC and tannins. A positive correlation was observed between polysaccharide (starch and resistant starch) accumulation and thiol content. This approach could contribute to the development of wheat with improved proximate compositions, addressing the challenges posed by global climate change and ensuring "Food for the Future."

Data availability statement

The original contributions presented in the study are included in the article/Supplementary Material. Further inquiries can be directed to the corresponding author.

Author contributions

RK: Conceptualization, Funding acquisition, Methodology, Validation, Writing – original draft. PH: Data curation, Investigation, Validation, Writing – review & editing. SH: Data curation, Formal Analysis, Methodology, Writing – review & editing. MG: Data curation, Methodology, Supervision, Writing – review & editing. SG: Conceptualization, Validation, Writing – review & editing. VT: Formal Analysis, Methodology, Project administration, Writing – review & editing. SK: Formal Analysis, Validation, Writing – review & editing. GM: Methodology, Validation, Writing – review & editing. DM: Data curation, Formal Analysis, Software, Writing – review & editing. GR: Formal Analysis, Methodology, Supervision, Writing – review & editing. GJ: Data curation, Investigation, Software, Writing – review & editing. SNK: Funding acquisition, Project administration, Validation, Writing – review & editing. SP: Resources, Validation, Visualization, Writing – review & editing. AT: Formal Analysis, Investigation, Methodology, Supervision, Writing – review & editing. VC: Funding acquisition, Resources, Visualization, Writing – review & editing.

Funding

The author(s) declare that financial support was received for the research and/or publication of this article. This work was supported by the Indian Council of Agricultural Research [grant number 12/115, TG3079]; and Center for Agricultural Bioinformatics project [grant number 21-56, TG3064].

Acknowledgments

The authors duly acknowledge the support received from In-charge, Nanaji Deshmukh Plant. Phenomics Centre, ICAR-IARI, Pusa, New Delhi for raising the crops under controlled conditions.

Conflict of interest

The authors declare that the research was conducted in the absence of any commercial or financial relationships that could be construed as a potential conflict of interest.

Publisher's note

Supplementary material

The Supplementary Material for this article can be found online at: https://www.frontiersin.org/articles/10.3389/fpls.2025.1488697/full#supplementary-material

References

Ali, A., Kumar, R. R., Vinutha, T., Bansal, N., Bollinedi, H., Singh, S. P., et al. (2023). Characterization of biochemical indicators and metabolites linked with rancidity and browning of pearl millet flour during storage. *J. Plant Biochem. Biotechnol.* 32. doi: 10.1007/s13562-022-00787-0

Alkarawi, H. H., Al-Musaifer, M. A., and Zotz, G. (2018). Phytate in seeds of wild plants. *Flora Morphol. Distrib. Funct. Ecol. Plants*, 244–245. doi: 10.1016/j.flora.2018.06.001

Antonets, K. S., Belousov, M. V., Sulatskaya, A. I., Belousova, M. E., Kosolapova, A. O., Sulatsky, M. I., et al. (2020). Accumulation of storage proteins in plant seeds is mediated by amyloid formation. *PloS Biol.* 18. doi: 10.1371/journal.pbio.3000564

Bajka, B. H., Pinto, A. M., Ahn-Jarvis, J., Ryden, P., Perez-Moral, N., van der Schoot, A., et al. (2021). The impact of replacing wheat flour with cellular legume powder on starch bioaccessibility, glycaemic response and bread roll quality: A double-blind randomised controlled trial in healthy participants. *Food Hydrocoll.* 114. doi: 10.1016/j.foodhyd.2020.106565

Bhopatkar, A. A., Ghag, G., Wolf, L. M., Dean, D. N., Moss, M. A., and Rangachari, V. (2019). Cysteine-rich granulin-3 rapidly promotes amyloid-β fibrils in both redox states. *Biochem. J.* 476 (5), 859–873.

Boz, H. (2015). Ferulic acid in cereals–a review. *Czech J. Food Sci.* 33. doi: 10.17221/401/2014-CJFS

Bruno, J. A., Konas, D. W., Matthews, E. L., Feldman, C. H., Pinsley, K. M., and Kerrihard, A. L. (2019). Sprouted and non-sprouted chickpea flours: Effects on sensory traits in pasta and antioxidant capacity. *Polish J. Food Nutr. Sci.* 69. doi: 10.31883/pjfns/109280

Butler, N., and Ghugre, P. (2020). Effect of beta carotene on the ionisable iron content of wheat. *Curr. Res. Nutr. Food Sci.* 8. doi: 10.12944/CRNFSJ.8.1.08

Cañas, R. A., Yesbergenova-Cuny, Z., Simons, M., Chardon, F., Armengaud, P., Quilleré, I., et al. (2017). Exploiting the genetic diversity of maize using a combined metabolomic, enzyme activity profiling, and metabolic modeling approach to link leaf physiology to kernel yield. *Plant Cell* 29. doi: 10.1105/tpc.16.00613

Chae, H. B., Bae, S., Bin, Paeng, S. K., Wi, S. D., Phan, K. A. T., Kim, M. G., et al. (2023). The physiological role of thiol-based redox sensors in plant defense signaling. *New Phytol.* 239. doi: 10.1111/nph.19018

Chen, K., Zhang, M., Bhandari, B., and Mujumdar, A. S. (2021). Edible flower essential oils: A review of chemical compositions, bioactivities, safety and applications in food preservation. *Food Res. Int.* 139. doi: 10.1016/j.foodres.2020.109809

Ciudad-Mulero, M., Matallana-González, M. C., Callejo, M. J., Carrillo, J. M., Morales, P., and Fernández-Ruiz, V. (2021). Durum and bread wheat flours. Preliminary mineral characterization and its potential health claims. *Agronomy* 11. doi: 10.3390/agronomy11010108

Deka, H., Choudhury, A., and Dey, B. K. (2022). An overview on plant derived phenolic compounds and their role in treatment and management of diabetes. *J. Pharmacopuncture* 25. doi: 10.3831/KPI.2022.25.3.199

Ellman, G. L. (1959). Tissue sulfhydryl groups. *Arch. Biochem. Biophys.* 82. doi: 10.1016/0003-9861(59)90090-6

Englyst, H. N., Kingman, S. M., and Cummings, J. H. (1992). Classification and measurement of nutritionally important starch fractions., in. *Eur. J. Clin. Nutrition*.doi: 10.1016/S0271-5317(97)00010-9

Everette, J. D., Bryant, Q. M., Green, A. M., Abbey, Y. A., Wangila, G. W., and Walker, R. B. (2010). Thorough study of reactivity of various compound classes toward the folin-Ciocalteu reagent. *J. Agric. Food Chem.* 58. doi: 10.1021/jf1005935

Fernie, E., Tan, D. K., Liu, S. Y., Ullah, N., and Khoddami, A. (2022). Post-anthesis heat influences grain yield, physical and nutritional quality in wheat: A review. *Agric.* 12, 886. doi: 10.3390/agriculture12060886

Girard, A. L., Teferra, T., and Awika, J. M. (2019). Effects of condensed vs hydrolysable tannins on gluten film strength and stability. *Food Hydrocolloids* 89, 36–43.

Goswami, S., Asrani, P., Ansheef Ali, T. P., Kumar, R. D., Vinutha, T., Veda, K., et al. (2020). Rancidity matrix: development of biochemical indicators for analysing the keeping quality of pearl millet flour. *Food Anal. Methods* 13. doi: 10.1007/s12161-020-01831-2

Grace, N. C. F., and Henry, C. J. (2020). The physicochemical characterization of unconventional starches and flours used in Asia. *Foods* 9. doi: 10.3390/foods9020182

Graminho, E. R., Takaya, N., Nakamura, A., and Hoshino, T. (2015). Purification, biochemical characterization, and genetic cloning of the phytase produced by Burkholderia sp. Strain a13. *J. Gen. Appl. Microbiol.* 61. doi: 10.2323/jgam.61.15

Harris, K. F. (2019). An introductory review of resistant starch type 2 from high-amylose cereal grains and its effect on glucose and insulin homeostasis. *Nutr. Rev.* 77, 748–764. doi: 10.1093/nutrit/nuz040

He, X., Chen, W., Sun, X., Gao, Y., He, Y., Xu, X., et al. (2023). Genome-wide identification and characterization of glutaredoxin family genes in common wheat. *Agronomy* 13. doi: 10.3390/agronomy13122985

Hussein, H. A. A., and Alshammari, S. O. (2022). Cysteine mitigates the effect of NaCl salt toxicity in flax (Linum usitatissimum L) plants by modulating antioxidant systems. *Sci. Rep.* 12. doi: 10.1038/s41598-022-14689-7

Khan, A., Siddiqui, S., Ur Rahman, U., Ali, H., Saba, M., Andleeb Azhar, F., et al. (2020). Physicochemical properties of enzymatically prepared resistant starch from maize flour and its use in cookies formulation. *Int. J. Food Prop.* 23. doi: 10.1080/10942912.2020.1742736

Khazaei, H., and Vandenberg, A. (2020). Seed mineral composition and protein content of faba beans (Vicia faba L.) with contrasting tannin contents. *Agronomy* 10. doi: 10.3390/agronomy10040511

Kumar, R. R., Ahuja, S., Rai, G. K., Kumar, S., Mishra, D., Kumar, S. N., et al. (2022). Silicon triggers the signalling molecules and stress-associated genes for alleviating the adverse effect of terminal heat stress in wheat with improved grain quality. *Acta Physiol. Plant* 44. doi: 10.1007/s11738-022-03365-y

Kumar, R. R., and Pathak, H. (2014). "Omics approaches for deciphering the mechanism of thermotolerance and development of climate smart wheat (Triticum aestivum L)," in *XVI Indian Agricultural Scientist and Farmers Congress on Nano-biotechnological approaches for sustainable agriculture and rural development* (SHUATS, Allahabad), 12.

Kumar, R. R., Tasleem, M., Jain, M., Ahuja, S., Goswami, S., Bakshi, S., et al. (2019). Nitric oxide triggered defense network in wheat: Augmenting tolerance and grain-quality related traits under heat-induced oxidative damage. *Environ. Exp. Bot.* 158. doi: 10.1016/j.envexpbot.2018.11.016

Li, X., Gluth, A., Zhang, T., and Qian, W. J. (2023). Thiol redox proteomics: Characterization of thiol-based post-translational modifications. *Proteomics* 23. doi: 10.1002/pmic.202200194

Liu, S., Cui, S., Zhang, X., Wang, Y., Mi, G., and Gao, Q. (2020). Synergistic regulation of nitrogen and sulfur on redox balance of maize leaves and amino acids balance of grains. *Front. Plant Sci.* 11. doi: 10.3389/fpls.2020.576718

Liu, X., Qiao, L., Kong, Y., Wang, H., and Yang, B. (2024). Characterization of the starch molecular structure of wheat varying in the content of resistant starch. *Food Chemistry: X* 21, 101103. doi: 10.1016/j.fochx.2023.101103

Ma, D., Wang, C., Feng, J., and Xu, B. (2021). Wheat grain phenolics: a review on composition, bioactivity, and influencing factors. *J. Sci. Food Agric.* 101, 6167–6185. doi: 10.1002/jsfa.v101.15

Madsen, C. K., and Brinch-Pedersen, H. (2020). Globoids and phytase: The mineral storage and release system in seeds. *Int. J. Mol. Sci.* 21. doi: 10.3390/ijms21207519

Manu, B. T., and Rao, U. J. S. (2008). Influence of size distribution of proteins, thiol and disulfide content in whole wheat flour on rheological and chapati texture of Indian wheat varieties. *Food Chem.* 110. doi: 10.1016/j.foodchem.2008.01.060

Marino, R., Iammarino, M., Santillo, A., Muscarella, M., Caroprese, M., and Albenzio, M. (2010). Rapid method for determination of amino acids in milk. *J. Dairy Sci.* 93, 2367–2370. doi: 10.3168/jds.2009-3017

Meyer, A. J., and Hell, R. (2005). Glutathione homeostasis and redox-regulation by sulfhydryl groups. *Photosynth. Res.* 86. doi: 10.1007/s11120-005-8425-1

Miller, L., and Houghton, J. A. (1945). The micro-kjeldahl determination of the nitrogen content of amino acids and proteins. *J. Biol. Chem.* 159. doi: 10.1016/s0021-9258(19)52798-3

Osipova, S., Permyakov, A., Mitrofanova, T., Trufanov, V., Ermakova, M., Chistyakova, A., et al. (2007). GSH-dependent proteindisulphide oxidoreductase of wheat grain: activity in maturing wheat kernels, and relationship with rheological properties of dough. *Cereal Res. Commun.* 35, 1477–1486. doi: 10.1556/CRC.35.2007.3.12

Paulsen, C. E., and Carroll, K. S. (2013). Cysteine-mediated redox signaling: Chemistry, biology, and tools for discovery. *Chem. Rev.* 113. doi: 10.1021/cr300163e

Pfaffl, M. W., Horgan, G. W., and Dempfle, L. (2002). Relative expression software tool (REST) for group-wise comparison and statistical analysis of relative expression results in real-time PCR. *Nucleic Acids Res.* 30, e36. Available at: http://www.ncbi.nlm.nih.gov/pubmed/11972351%5Cnhttp://www.pubmedcentral.nih.gov/articlerender.fcgi?artid=PMC113859.

Ranjbar, A., Heshmati, A., Momtaz, J. K., and Vahidinia, A. (2019). Effect of iron-enrichment on the antioxidant properties of wheat flour and bread. *J. Cereal Sci.* 87. doi: 10.1016/j.jcs.2019.03.010

Sainz, M. M., Filippi, C. V., Eastman, G., Sotelo-Silveira, J., Borsani, O., and Sotelo-Silveira, M. (2022). Analysis of thioredoxins and glutaredoxins in soybean: evidence of translational regulation under water restriction. *Antioxidants* 11. doi: 10.3390/antiox11081622

Schollenberger, M., Sommerfeld, V., Hartung, J., and Rodehutscord, M. (2022). Storage duration and conditions change the phytate content and phytase activity of wheat grains. *JSFA Rep.* 2, 100–106. doi: 10.1002/jsf2.v2.3

Shevkani, K., Singh, N., Bajaj, R., and Kaur, A. (2017). Wheat starch production, structure, functionality and applications—a review. *Int. J. Food Sci. Technol.* 52, 38–58. doi: 10.1111/ijfs.2017.52.issue-1

Shujaat, N., Ahmad, Y., Ikram, M., Shaheen, S., Ishaq, M., Hameed, T., et al. (2024). Phytic acid content variation among wheat grain lines and its impact on nutritional quality and growth. *Vegetos*, 1–7. doi: 10.1007/s42535-024-01150-5

Singleton, V. L., Orthofer, R., and Lamuela-Raventós, R. M. (1999). Analysis of total phenols and other oxidation substrates and antioxidants by means of folin-ciocalteu reagent. *Methods Enzymol.* 299. doi: 10.1016/S0076-6879(99)99017-1

Tea, I., Genter, T., Violleau, F., and Kleiber, D. (2005). Changes in the glutathione thiol-disulfide status in wheat grain by foliar sulphur fertilization: Consequences for the rheological properties of dough. *J. Cereal Sci.* 41. doi: 10.1016/j.jcs.2004.10.003

Thayumanavan, B., and Sadasivam, S. (1984). Physicohemical basis for the preferential uses of certain rice varieties. *Qual. Plant Plant Foods Hum. Nutr.* doi: 10.1007/BF01126554

Veraverbeke, W. S., and Delcour, J. A. (2002). Wheat protein composition and properties of wheat glutenin in relation to breadmaking functionality. *Crit. Rev. Food Sci. Nutr.* 42, 179–208. doi: 10.1080/10408690290825510

Walker, E. J., Bettinger, J. Q., Welle, K. A., Hryhorenko, J. R., Molina Vargas, A. M., O'Connell, M. R., et al. (2022). Protein folding stabilities are a major determinant of oxidation rates for buried methionine residues. *J. Biol. Chem.* 298. doi: 10.1016/j.jbc.2022.101872

Wang, H., Sun, X., Zhang, N., Ji, Z., Ma, Z., Fu, Q., et al. (2017). Ferulic acid attenuates diabetes-induced cognitive impairment in rats via regulation of PTP1B and insulin signaling pathway. *Physiol. Behav.* 182, 93–100. doi: 10.1016/j.physbeh.2017.10.001

Wieser, H., Koehler, P., and Scherf, K. A. (2023). Chemistry of wheat gluten proteins: Quantitative composition. *Cereal Chem.* 100, 36–55. doi: 10.1002/cche.v100.1

Xie, Y., Wang, C., and Hao, Z. (2018). The viscoelasticity properties of resistant starch and flour blends. *J. Chin. Cereal. Oils Assoc.* 33. doi: 10.1007/s42535-024-01150-5

Yadav, C. B., Tokas, J., Yadav, D., Winters, A., Singh, R. B., Yadav, R., et al. (2021). Identifying anti-oxidant biosynthesis genes in pearl millet [Pennisetum glaucum (L.) R. Br.] using genome—Wide association analysis. *Front. Plant Sci.* 12. doi: 10.3389/fpls.2021.599649

Zhang, S., Ghatak, A., Bazargani, M. M., Bajaj, P., Varshney, R. K., Chaturvedi, P., et al. (2021). Spatial distribution of proteins and metabolites in developing wheat grain and their differential regulatory response during the grain filling process. *Plant J.* 107. doi: 10.1111/tpj.15410

Zhang, X., Guo, D., Blennow, A., and Zörb, C. (2021). Mineral nutrients and crop starch quality. *Trends Food Sci. Technol.* 114, 148–157.

Zheng, Y., Wei, Z., Zhang, R., Deng, Y., Tang, X., Zhang, Y., et al. (2020). Optimization of the autoclave preparation process for improving resistant starch content in rice grains. *Food Sci. Nutr.* 8. doi: 10.1002/fsn3.1528

Frontiers in
Plant Science

Cultivates the science of plant biology and its applications

The most cited plant science journal, which advances our understanding of plant biology for sustainable food security, functional ecosystems and human health.

Discover the latest Research Topics

See more →

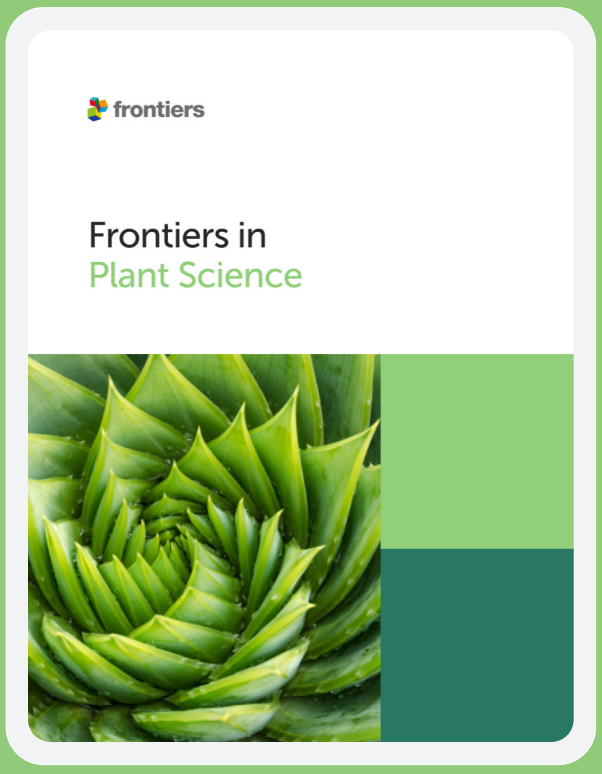

Frontiers

Avenue du Tribunal-Fédéral 34
1005 Lausanne, Switzerland
frontiersin.org

Contact us

+41 (0)21 510 17 00
frontiersin.org/about/contact